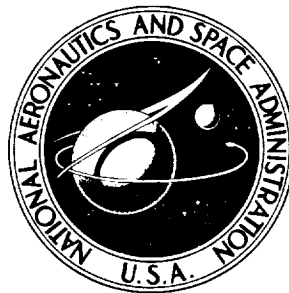


NASA TECHNICAL NOTE



NASA TN D-6800

NASA TN D-6800

**CASE FILE
COPY**

LONGITUDINAL AERODYNAMIC
CHARACTERISTICS OF LIGHT, TWIN-ENGINE,
PROPELLER-DRIVEN AIRPLANES

by Chester H. Wolowicz and Roxanah B. Yancey

Flight Research Center

Edwards, Calif. 93523

NATIONAL AERONAUTICS AND SPACE ADMINISTRATION • WASHINGTON, D. C. • JUNE 1972

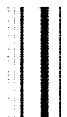
4. 10. 19

10. 10. 19

10. 10. 19

10. 10. 19

10. 10. 19



1. Report No. TN D-6800		2. Government Accession No.		3. Recipient's Catalog No.	
4. Title and Subtitle LONGITUDINAL AERODYNAMIC CHARACTERISTICS OF LIGHT, TWIN-ENGINE, PROPELLER-DRIVEN AIRPLANES				5. Report Date June 1972	
				6. Performing Organization Code	
7. Author(s) Chester H. Wolowicz and Roxanah B. Yancey				8. Performing Organization Report No. H-646	
				10. Work Unit No. 736-05-00-01-24	
9. Performing Organization Name and Address NASA Flight Research Center P. O. Box 273 Edwards, California 93523				11. Contract or Grant No.	
				13. Type of Report and Period Covered Technical Note	
12. Sponsoring Agency Name and Address National Aeronautics and Space Administration Washington, D. C. 20546				14. Sponsoring Agency Code	
15. Supplementary Notes					
16. Abstract <p style="text-align: center;">This report documents representative state-of-the-art analytical procedures and design data for predicting the longitudinal static and dynamic stability and control characteristics of light, propeller-driven airplanes. Procedures for predicting drag characteristics are also included.</p> <p style="text-align: center;">The procedures are applied to a twin-engine, propeller-driven airplane in the clean configuration from zero lift to stall conditions. The calculated characteristics are compared with wind-tunnel and flight data. Included in the comparisons are level-flight trim characteristics, period and damping of the short-period oscillatory mode, and windup-turn characteristics. All calculations are documented.</p>					
17. Key Words (Suggested by Author(s)) Light airplane Aerodynamic characteristics - prediction			18. Distribution Statement Unclassified - Unlimited		
19. Security Classif. (of this report) Unclassified		20. Security Classif. (of this page) Unclassified		21. No. of Pages 361	
				22. Price* \$6.00	

CONTENTS

	Page
TABLES RELATED TO SUBJECT AIRPLANE	vi
FIGURES COMPARING CALCULATED CHARACTERISTICS	ix
SUMMARY	1
1.0 INTRODUCTION	2
2.0 SCOPE OF THE STUDY	2
3.0 THE AIRPLANE	3
3.1 Center-of-Gravity Positions Used in the Analysis	6
3.2 Geometric Parameters of the Wing and Horizontal Tail Used in the Analysis	7
3.2.1 Symbols	7
4.0 PREDICTION OF PROPELLER-OFF AERODYNAMIC CHARACTERISTICS	13
4.1 Wing and Horizontal-Tail Airfoil Section Characteristics	13
4.1.1 Symbols	15
4.2 Lift Characteristics of the Wing and Horizontal Tail	27
4.2.1 Symbols	29
4.3 Lift Due to Fuselage and Nacelles	37
4.3.1 Symbols	38
4.4 Lift Due to Combined Wing-Fuselage-Nacelle	46
4.4.1 Symbols	48
4.5 C_{m_0} and Aerodynamic Center of the Wing and Horizontal Tail	55
4.5.1 Symbols	56
4.6 Wing-Fuselage Pitching Moment at Zero Lift	60
4.6.1 Symbols	60
4.7 Fuselage and Nacelle Pitching Moments	64
4.7.1 Symbols	64
4.8 Wing-Fuselage-Nacelle Pitching Moments	68
4.8.1 Contributing Factors to Wing-Fuselage-Nacelle Pitching Moments	68
4.8.2 Static Margin of Wing-Fuselage-Nacelles	71
4.8.3 Pitching-Moment Coefficient of Wing-Fuselage- Nacelles	72
4.8.4 Symbols	75
4.9 Downwash and Dynamic Pressure at the Horizontal Tail	87
4.9.1 Downwash	87
4.9.2 Dynamic-Pressure Ratio	90
4.9.3 Symbols	92
4.10 Lift of the Complete Airplane ($\delta_e = 0^\circ$)	109
4.10.1 Symbols	111
4.11 Pitching Moments of the Complete Airplane ($\delta_e = 0^\circ$)	117
4.11.1 Symbols	118
4.12 Drag of the Complete Airplane	122
4.12.1 Zero-Lift Drag of Wing, Horizontal Tail, and Vertical Tail	122
4.12.2 Zero-Lift Drag of Fuselage and Nacelles	123
4.12.3 Zero-Lift Interference Drag of Wing-Fuselage, Tail-Fuselage, and Wing-Nacelles	124

CONTENTS - Continued

	Page
4.12.4 Drag of Wing and Horizontal Tail at Angle of Attack	127
4.12.5 Drag of Fuselage and Nacelles at Angle of Attack	129
4.12.6 Wing-Fuselage Interference Drag at Angle of Attack	130
4.12.7 Cooling Drag	131
4.12.8 Summary Drag of the Complete Airplane	131
4.12.9 Symbols	132
4.13 Effect of Horizontal Tail and Tab Deflection on Lift and Pitching Moments	156
4.13.1 Lift of the Horizontal Tail in the Linear Range	156
4.13.2 Maximum Lift of the Horizontal Tail	160
4.13.3 Lift Curves of the Horizontal Tail Through Stall	161
4.13.4 Lift and Pitching-Moment Curves of the Airplane Including the Effect of Elevator Positions	162
4.13.5 Symbols	165
4.14 Horizontal-Tail Hinge Moments and Stick Forces	184
4.14.1 Horizontal-Tail Hinge Moments	184
4.14.2 Stick Forces	191
4.14.3 Symbols	192
5.0 PREDICTION OF POWER-ON AERODYNAMIC CHARACTERISTICS	215
5.1 Power Effects on Lift	216
5.1.1 Tail-Off Lift Characteristics With Power On	217
5.1.2 Horizontal-Tail Contribution to Lift	221
5.1.3 Net Characteristics of the Subject Airplane	223
5.1.4 Symbols	224
5.2 Power Effects on Pitching Moments	256
5.2.1 Symbols	262
5.3 Power Effects on Drag	282
5.3.1 Symbols	285
5.4 Power Effects on Horizontal-Tail Hinge Moments and Stick Forces	300
5.4.1 Symbols	301
6.0 DYNAMIC CHARACTERISTICS	310
6.1 Lift Due to Dynamic Motions	311
6.1.1 Lift Due to Pitch Rate, C_{L_q}	311
6.1.2 Lift Due to Vertical Acceleration, $C_{L_{\dot{\alpha}}}$	313
6.1.3 Symbols	315
6.2 Pitching Moments Due to Dynamic Motions	325
6.2.1 Pitching Moments Due to Pitch Rate, C_{m_q}	325
6.2.2 Pitching Moment Due to Vertical Acceleration, $C_{m_{\dot{\alpha}}}$	328
6.2.3 Pitching Moments Due to Pitch Rate and Vertical Acceleration in Short-Period Transient Oscillations, $(C_{m_q} + C_{m_{\dot{\alpha}}})$	330

CONTENTS - Concluded

	Page
6.2.4 Symbols	331
6.3 Short-Period Transient Oscillation Characteristics	340
6.3.1 Symbols	341
6.4 Windup-Turn Characteristics	346
6.4.1 Variation of α_{trim} and $\delta_{e_{trim}}$ With Load Factor	346
6.4.2 Variation of Hinge Moments and Stick Forces With Load Factor	349
6.4.3 Symbols	351
REFERENCES	359

TABLES RELATED TO SUBJECT AIRPLANE

	Page
3-1 MANUFACTURER'S PHYSICAL CHARACTERISTICS OF THE SUBJECT AIRPLANE	4
3.2-1 PERTINENT WING AND HORIZONTAL-TAIL GEOMETRIC PARAMETERS USED IN THE ANALYSIS	9
PREDICTION OF PROPELLER-OFF AERODYNAMIC CHARACTERISTICS	
4.1-1 AIRPLANE WING AND HORIZONTAL-TAIL AIRFOIL SECTION CHARACTERISTICS	16
4.2-1 LIFT CHARACTERISTICS OF AIRPLANE WING AND HORIZONTAL TAIL	31
4.3-1 CONTRIBUTION OF FUSELAGE AND NACELLES TO AIRPLANE LIFT COEFFICIENT	40
4.4-1 WING LIFT OF AIRPLANE INCLUDING MUTUAL WING- FUSELAGE INTERFERENCE	50
4.4-2 SUMMARY OF WING-FUSELAGE-NACELLE LIFT	51
4.5-1 C_{m_0} AND AERODYNAMIC CENTER OF WING AND HORIZONTAL TAIL	57
4.6-1 WING-FUSELAGE PITCHING MOMENTS OF AIRPLANE AT ZERO LIFT	62
4.7-1 FUSELAGE AND NACELLE PITCHING MOMENTS OF AIRPLANE	66
4.7-2 TABULAR INTEGRATION OF FUSELAGE PITCHING- MOMENT PARAMETERS	67
4.8.1-1 WING PITCHING MOMENTS OF THE AIRPLANE	80
4.8.1-2 "FREE MOMENTS" OF FUSELAGE AND NACELLES	81
4.8.3-1 PITCHING MOMENTS OF WING-FUSELAGE-NACELLES CONFIGURATION	83
4.9.1-1 PERTINENT PARAMETERS FOR COMPUTING AVERAGE DOWNWASH AT HORIZONTAL TAIL OF SUBJECT AIRPLANE	96
4.9.1-2 SUMMARY CALCULATION OF AVERAGE DOWNWASH AT HORIZONTAL TAIL OF SUBJECT AIRPLANE	97
4.9.2-2 DYNAMIC-PRESSURE RATIO AT THE HORIZONTAL TAIL OF THE SUBJECT AIRPLANE	99
4.10-1 LIFT OF HORIZONTAL TAIL IN THE PRESENCE OF THE FUSELAGE ($\delta_e = 0^\circ$)	113
4.10-2 LIFT OF THE COMPLETE AIRPLANE ($\delta_e = 0^\circ$)	114
4.11-1 PITCHING MOMENTS OF THE COMPLETE AIRPLANE ($\delta_e = 0^\circ$)	119
4.12.1-1 SURFACE ROUGHNESS HEIGHT k	137
4.12.1-2 ZERO-LIFT DRAG OF WING, HORIZONTAL AND VERTICAL TAILS	137
4.12.2-1 ZERO-LIFT DRAG OF FUSELAGE AND NACELLES	138
4.12.3-1 ZERO-LIFT DRAG OF THE COMPONENTS	139
4.12.4-1 DRAG OF WING AND HORIZONTAL TAIL DUE TO LIFT	140

TABLES - Continued

	Page
4.12.5-1 DRAG DUE TO LIFT OF FUSELAGE AND NACELLES	142
4.12.8-1 DRAG OF THE COMPLETE AIRPLANE ($\delta_e = 0^\circ$)	143
4.13.1-1 LIFT CONTRIBUTION OF THE HORIZONTAL TAIL WITH TAB-TO-ELEVATOR GEAR RATIO OF 1.5	170
4.13.2-1 MAXIMUM LIFT COEFFICIENTS OF THE HORIZONTAL TAIL	173
4.13.4-1 EFFECT OF ELEVATOR DEFLECTION ON LIFT AND PITCHING MOMENTS OF THE AIRPLANE	174
4.14.1-1 LIFT CHARACTERISTICS OF HORIZONTAL TAIL ALONE IN THE PRESENCE OF THE BODY AS A FUNCTION OF α_h AND δ_e , WITH TAB GEARED IN RATIO OF $\delta_{tab}/\delta_e = 1.5$	197
4.14.1-2 PERTINENT RELATIONS FOR HORIZONTAL-TAIL HINGE MOMENTS	198
4.14.1-3 HORIZONTAL-TAIL TAB CHARACTERISTICS	200
4.14.1-4 HORIZONTAL-TAIL HINGE-MOMENT CHARACTERISTICS . . .	202
PREDICTION OF POWER-ON CHARACTERISTICS	
5.1.1-1 LIFT DUE TO DIRECT ACTION OF THE PROPELLER FORCES	230
5.1.1-2 WING-LIFT INCREMENTS DUE TO PROPELLER SLIP- STREAM EFFECTS	232
5.1.1-3 TAIL-OFF LIFT CHARACTERISTICS WITH POWER ON	235
5.1.1-4 POWER EFFECTS ON MAXIMUM LIFT	236
5.1.2-1 EFFECT OF ELEVATOR DEFLECTION ON LIFT WITH POWER ON	237
5.2-1 PITCHING-MOMENT INCREMENTS DUE TO PROPELLER FORCES	267
5.2-2 ZERO-LIFT PITCHING-MOMENT INCREMENT DUE TO POWER	268
5.2-3 PITCHING-MOMENT INCREMENT DUE TO POWER- INDUCED CHANGE IN WING LIFT	270
5.2-4 PITCHING-MOMENT INCREMENT DUE TO POWER EFFECT ON NACELLE FREE MOMENTS	271
5.2-5 TAIL-OFF PITCHING-MOMENT CHARACTERISTICS WITH POWER ON	272
5.2-6 EFFECT OF ELEVATOR DEFLECTION ON PITCHING MOMENTS WITH POWER ON	273
5.3-1 ZERO-LIFT DRAG INCREMENTS DUE TO POWER	289
5.3-2 INDUCED-DRAG INCREMENT DUE TO POWER	290
5.3-3 CHANGE IN COOLING-SYSTEM DRAG DUE TO POWER	294
5.3-4 POWER-ON DRAG OF THE COMPLETE AIRPLANE	295
5.4-1 HORIZONTAL-TAIL TAB CHARACTERISTICS	304
5.4-2 HORIZONTAL-TAIL HINGE-MOMENT CHARACTERISTICS . . .	305
DYNAMIC CHARACTERISTICS	
6.1.1-1 LIFT DUE TO PITCH RATE, CL_q	319

TABLES - Concluded

		Page
6.1.2-1	LIFT DUE TO VERTICAL ACCELERATION, $C_{L\dot{\alpha}}$	321
6.2.1-1	PITCHING MOMENTS DUE TO PITCH RATE, C_{mq}	335
6.2.2-1	PITCHING MOMENT DUE TO VERTICAL ACCELERATION, $C_{m\dot{\alpha}}$	337
6.4.1-1	WINDUP-TURN VARIATION OF α_{trim} AND $\delta_{e_{trim}}$ WITH LOAD FACTOR	354
6.4.2-1	VARIATION OF HINGE MOMENTS AND STICK FORCES WITH LOAD FACTOR IN WINDUP TURN	356

FIGURES COMPARING CALCULATED CHARACTERISTICS

	Page
PROPELLER-OFF CHARACTERISTICS	
4.4-4 Comparison of predicted wing-fuselage-nacelles lift curve with wind-tunnel data. $S_w = 178$ sq ft.	54
4.8.3-2 Comparison of calculated tail-off pitching-moment character- istics with wind-tunnel data. $S_w = 178$ sq ft.	86
4.10-1 Comparison of predicted airplane lift curve with wind-tunnel data. $\delta_e = 0^\circ$; $S_w = 178$ sq ft.	115
4.11-1 Comparison of predicted airplane pitching moments with wind- tunnel data. $\delta_e = 0^\circ$; $S_w = 178$ sq ft; center of gravity = $0.10\bar{c}_w$	120
4.12.8-1 Comparison of predicted airplane drag characteristics with wind-tunnel data. $\delta_e = 0^\circ$; propellers off; $S_w = 178$ sq ft. . .	152
4.13.4-1 Comparison of predicted propeller-off lift and pitching- moment characteristics of the airplane with wind-tunnel data as a function of α_b and δ_e . $S_w = 178$ sq ft; $\delta_{tab}/\delta_e = 1.5$ (propeller-off wind-tunnel data obtained from propeller-on data at $T'_C = 0$ with propeller effects calculated out); center of gravity = $0.10\bar{c}_w$	182
4.14.1-10 Comparison of calculated and wind-tunnel-determined hinge- moment coefficients of the horizontal tail. $\delta_{tab}/\delta_e = 1.5$; wind-tunnel data at $T'_C = 0$ assumed equivalent to propeller- off condition.	214
POWER-ON CHARACTERISTICS	
5.1.2-4 Comparison of calculated and experimentally determined (ref. 2) downwash at the horizontal tail of the subject airplane at several power settings.	253
5.1.3-1 Comparison of calculated and wind-tunnel-determined variation of C_L with α_b at different power conditions and elevator deflections.	255
5.2-2 Comparison of calculated and wind-tunnel-determined tail-off lift and pitching-moment characteristics at $T'_C = 0.44$ and center of gravity = $0.10\bar{c}_w$	275
5.2-3 Comparison of calculated and wind-tunnel-determined variation of C_m with α_b at different power conditions and elevator deflections. Center of gravity = $0.10\bar{c}_w$	276
5.2-4 Comparison of calculated and wind-tunnel-determined variation of C_m with C_L at different power conditions and elevator deflections. Center of gravity = $0.10\bar{c}_w$	277

FIGURES - Concluded

		Page
5.2-5	Comparison of neutral-point characteristics determined from modified calculated and wind-tunnel pitching-moment characteristics. Center of gravity = $0.10\bar{c}_w$	278
5.2-6	Comparison of the variation of calculated and wind-tunnel-determined pitch-control effectiveness with thrust coefficient and angle of attack.	279
5.2-7	Comparison of calculated static pitch, C_{m_α} , and control effectiveness, $C_{m\delta_e}$, with wind-tunnel and flight-determined values as a function of angle of attack. Center of gravity = $0.12\bar{c}_w$	280
5.2-8	Comparison of calculated C_L , α_b , and δ_e characteristics for trim level flight conditions with those obtained from wind-tunnel and flight data as a function of calibrated airspeed. Center of gravity = $0.12\bar{c}_w$	281
5.3-4	Comparison of calculated and wind-tunnel-determined variation of C_D with α_b at different power conditions. $\delta_e = 0^\circ$	298
5.3-5	Comparison of calculated and wind-tunnel-determined variation of C_D with C_L at different power conditions. $\delta_e = 0^\circ$	299
5.4-1	Comparison of calculated and wind-tunnel-determined variation of hinge moment $C_{h_h(f)}$ with angle of attack at different power conditions and elevator deflections.	308
5.4-2	Comparison of calculated hinge-moment and stick-force characteristics in level flight with those obtained from wind-tunnel and flight data as a function of airspeed. Altitude = 6000 ft; center of gravity = $0.12\bar{c}_w$	309
6.2.3-1	Comparison of calculated $C_{m_q} + C_{m_{\dot{\alpha}}}$ with flight-determined values obtained from transient short-period pulse maneuvers. Center of gravity = $0.12\bar{c}_w$	339
6.3-1	Comparison of calculated short-period frequency and damping characteristics with flight-determined values as a function of airspeed. Center of gravity = $0.12\bar{c}_w$	344
6.3-2	Comparison of calculated and flight-determined time histories of airplane response to pulse-type input. Center of gravity = $0.12\bar{c}_w$	345
6.4.2-1	Comparison of calculated hinge-moment and stick-force characteristics in a windup turn with those obtained from wind-tunnel and flight data as a function of load factor. Altitude = 6000 ft; center of gravity = $0.12\bar{c}_w$; $V = 220$ ft/sec.	358

LONGITUDINAL AERODYNAMIC CHARACTERISTICS OF LIGHT, TWIN-ENGINE, PROPELLER-DRIVEN AIRPLANES

Chester H. Wolowicz and Roxanah B. Yancey
Flight Research Center

SUMMARY

Representative state-of-the-art analytical procedures and design data for predicting the subsonic longitudinal static and dynamic stability and control characteristics of light, propeller-driven airplanes are documented. Procedures for predicting drag characteristics are also included.

The procedures are applied to a twin-engine, propeller-driven airplane in the clean configuration to determine the lift, pitching-moment, and drag characteristics from zero lift to stall conditions. Also determined are level-flight trim characteristics, period and damping of the short-period oscillatory mode, and windup-turn characteristics. All calculations are documented.

The calculated lift characteristics correlated well with full-scale wind-tunnel data as a function of angle of attack, elevator settings, and power conditions.

The calculated drag characteristics also correlated well with full-scale wind-tunnel data as a function of angle of attack, lift coefficient, and power settings in the linear range at zero thrust conditions. With increasing thrust, the correlation was good at the lower angles of attack, but tended to deteriorate with increasing angle of attack. When the increment of induced drag due to power was omitted, good correlation resulted throughout the power range at the high angles of attack. It was surmised that the wide, built-in nacelles had a significant nullifying effect on the power-induced drag of the immersed portion of the wing.

Calculated propeller-off pitching-moment characteristics agreed well with wind-tunnel data for zero elevator deflection. When different elevator settings were included, slope correlation was good but larger calculated control effectiveness in pitch was indicated than was reflected by tunnel data. Study of this discrepancy indicated that tail lift-carryover effects onto the body are nil for the horizontal-tail and body configuration of the airplane investigated. Correlation of pitch control effectiveness would have been improved if this carryover effect had been eliminated from the calculations.

The addition of power effects to the calculated pitching-moment characteristics resulted in an increasing disparity between the calculated and the wind-tunnel-derived pitching-moment slopes with increasing power. It was deduced that the deterioration in correlation with increasing power was due to inadequate design data for the power-induced downwash increment at the tail. When the power-induced downwash was reduced by 40 percent, good correlation of slopes for all power conditions resulted. It

was concluded that the design data used to obtain the downwash due to power did not properly account for the slipstream-flow interference of wide, built-in nacelles of the type used on the airplane analyzed.

Using the modified power-induced downwash, the calculated elevator hinge moments correlated relatively well with wind-tunnel data. Calculated stick-force characteristics for level flight and windup turns agreed reasonably well with flight data.

1.0 INTRODUCTION

As part of a NASA program to enhance general aviation safety and utility, the NASA Flight Research Center has undertaken the documentation of analytical procedures and design data, oriented to the needs of the industry, for predicting the subsonic static and dynamic stability and control characteristics of propeller-driven aircraft. In partial fulfillment of this project, representative state-of-the-art methods have been compiled and, in some instances, extensions proposed. The results have been applied to a representative light, low-wing, twin-engine, propeller-driven airplane in the clean configuration, and the accuracy of the methods has been determined by comparing calculated characteristics with wind-tunnel and flight data.

This report summarizes methods and guidelines which should enable a designer to obtain improved estimates of the stability and control characteristics for propeller-off conditions in general and the power effects on twin-engine, propeller-driven designs in particular.

Axis systems, sign conventions, and definitions of stability and control derivatives are in accord with standard NASA practice and usage.

2.0 SCOPE OF THE STUDY

As a logical starting point for the study, use was made of the USAF Stability and Control Datcom handbook (ref. 1). This is a compendium of methods and design data for predicting the stability and control characteristics of jet and propeller-driven aircraft from subsonic through hypersonic regions of flight. It deals primarily with winged configurations with untwisted constant airfoil sections. A considerable portion of the material is based on NACA and NASA reports. In the present report, Datcom is listed as the reference when it provides a unique treatment of information from other sources. The basic source is referenced when Datcom repeats pertinent equations and design data from another source. During this study, it became necessary to supplement the Datcom methods and to provide some innovations.

The analysis of longitudinal characteristics in the clean configuration ranged from zero lift to stall and involved stall conditions of the elevator. Propeller-off and power-on conditions are considered in all instances. Included are analyses of the lift, pitching-moment, drag, and hinge-moment-coefficient characteristics as functions of angle of attack and elevator position. Elevator trim and stick-force characteristics for 1 g

flight and windup turns are also included, as well as short-period and damping characteristics. In the systematic buildup of the predicted longitudinal characteristics, procedures, design charts, calculations, and correlating figures used to illustrate the accuracy of the results are presented.

The report is divided into three phases: propeller-off static characteristics; effect of power on the static characteristics; and dynamic characteristics, both with the propeller off and with the power on. The propeller-off static characteristic buildup initially considers tail-off lift and pitching moments in sequence. This is followed by a consideration of the effects of the horizontal tail on the characteristics, drag buildup of the complete airplane, and, finally, the derivation of the horizontal-tail hinge-moment characteristics.

The effects of power on the lift, pitch, drag, and hinge moments are considered in the second phase. The third phase considers the derivation of the dynamic-stability derivatives.

Throughout the report, comparisons are made with wind-tunnel and flight data when appropriate data are available. Notations and symbols are defined in each section as they are used.

3.0 THE AIRPLANE

The airplane used in the analysis is representative of general-aviation, personal-owner aircraft. It is a six-place, low-wing, twin-engine, propeller-driven, all-metal airplane with an all-movable horizontal stabilizer. Pertinent physical characteristics, as provided by the manufacturer, are listed in table 3-1. A three-view drawing is presented in figure 3-1.

The all-movable horizontal tail (referred to herein as a stabilator or elevator) is equipped with a trailing-edge antiservo tab geared to move in the same direction as the tail with a gear ratio of 1.5° tab per degree of stabilator. The servo tab is geared to increase the elevator control-force gradient.

TABLE 3-1
MANUFACTURER'S PHYSICAL CHARACTERISTICS OF THE SUBJECT AIRPLANE

Wing -	
Location	Low
Loading, lb/sq ft	20.2
Airfoil section	NACA 64 ₂ , A215 (modified)
Area, sq ft	178.0
Span, ft	35.98
Mean aerodynamic chord, ft	5.00
Aspect ratio	7.30
Dihedral, deg	5.00
Incidence, deg	2.00
Aerodynamic twist	0
Power -	
Horsepower/engine	160.00
Loading, lb/hp	11.3
Engine	2 Lycoming IO-320-B
Propellers -	
Type	Hartzell HC-E2YL-2A constant speed full feathering
Blades	7663-4
Diameter, in.	72.00
Weight and balance -	
Maximum gross weight, lb	3600.00
Empty gross weight, lb	2160.00
Allowable center of gravity for maximum gross weight, percent mean aerodynamic chord	12.5 to 28.6
Allowable center of gravity for empty gross weight, percent mean aerodynamic chord	3.3 to 21.6
Control-surface deflection, deg -	
Aileron	18 up, 14 down
Elevator (stabilator).	14 up, 4 down
Rudder	22 right, 20 left
Flap (full)	27
Adjustable trim systems -	
Longitudinal	Tab
Directional	Bungee
Lateral	-----

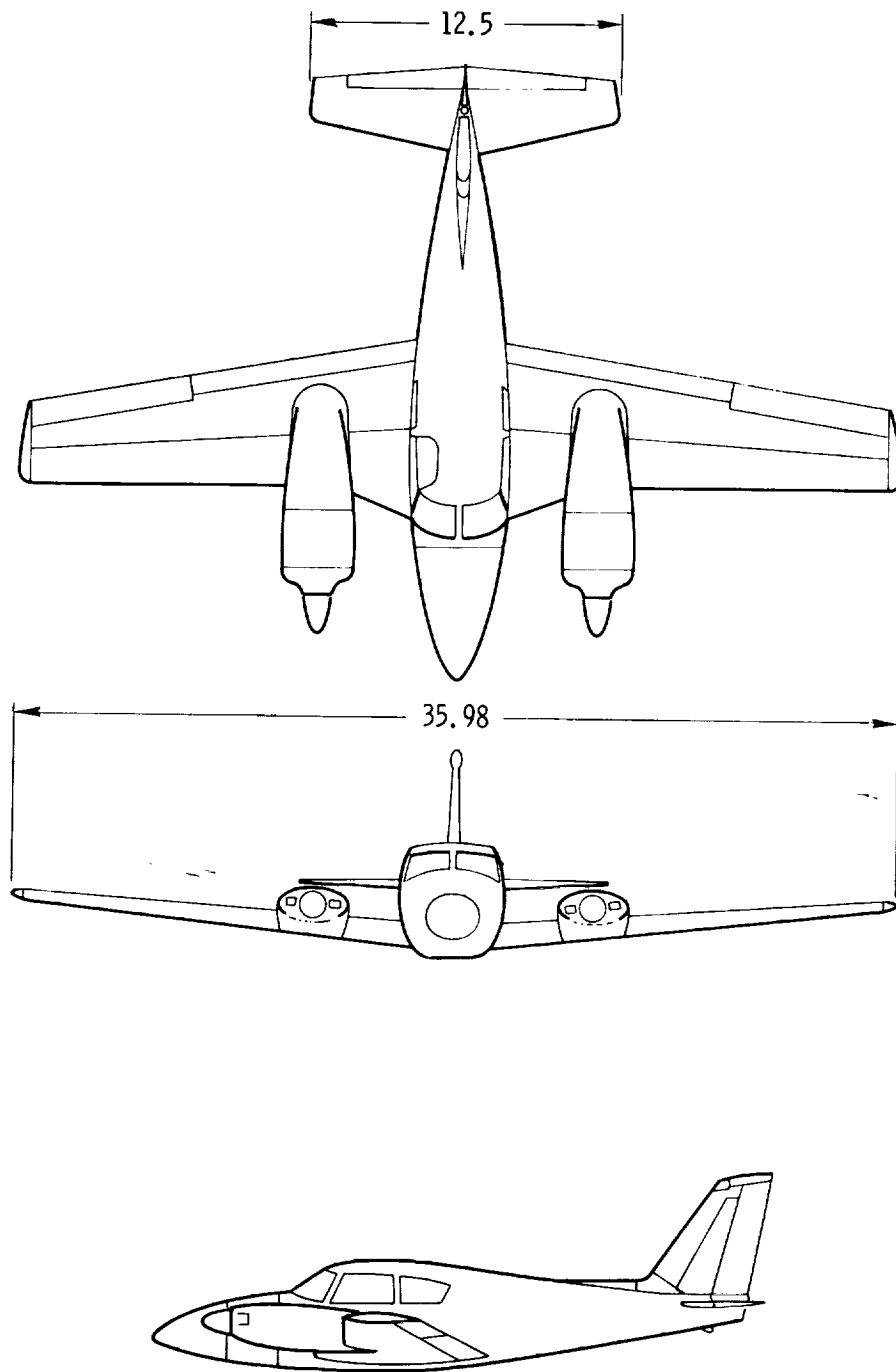


Figure 3-1. Three-view drawing of the test airplane. Dimensions in feet.

3.1 Center-of-Gravity Positions Used in the Analysis

The center of gravity of the airplane, for analytical purposes, was fixed at 10 percent of the wing mean aerodynamic chord and 12 inches below the X-body axis (located on the zero waterline) to conform with the full-scale wind-tunnel data (ref. 2) used in the correlation of analytically predicted characteristics. For preliminary design purposes, a more typical assumption of center-of-gravity position for the start of analysis would be 25 percent of the wing mean aerodynamic chord.

In correlations with flight data, both the analytically predicted characteristics and wind-tunnel data were modified to conform with the 12-percent mean aerodynamic chord center-of-gravity conditions of the flight data.

3.2 Geometric Parameters of the Wing and Horizontal Tail Used in the Analysis

In analytically predicting the longitudinal characteristics, the wing and horizontal tail were considered on the basis of total planform and exposed panel planform, depending on the characteristics being determined. Total planform was considered to extend through the nacelle and the fuselage; exposed panel planform terminated at the fuselage. Pertinent dimensions for the wing and tail are shown in figures 3.2-1 to 3.2-3.

The wing was considered to have zero leading-edge sweep, although there is actually some sweepback between the fuselage and the nacelle. As a result of the assumption of zero leading-edge sweep, the reference total planform area used in determining the characteristics was 172.3 square feet in contrast to the manufacturer's reference area of 178 square feet, based on a projection of the actual leading edge through the fuselage. Because wind-tunnel data and flight-determined characteristics were based on the 178-square-foot area, the predicted characteristics were ultimately referenced to this area for comparison purposes.

Table 3.2-1 lists the geometric parameters of the wing and horizontal tail pertinent to the analysis.

3.2.1 Symbols

A	aspect ratio, $\frac{b^2}{S}$
b	span, ft or in.
b _e	span of the exposed panels, ft or in.
b _{tab}	tab span, in.
\bar{c}	mean aerodynamic chord, in.
\bar{c}_e	mean aerodynamic chord of the exposed panel, in.
c _r	root chord, in.
(c _r) _e	root chord of the exposed panel, in.
c _t	tip chord, in.
c _{tab}	tab chord, in.
l _h	distance from the aircraft center of gravity to the quarter chord of the horizontal-tail mean aerodynamic chord, in.
S	area, sq ft
y \bar{c}	lateral distance to the mean aerodynamic chord from the root chord, in.
(y \bar{c}) _e	lateral distance to the mean aerodynamic chord of the exposed panel from the exposed panel root chord, in.

Γ	dihedral angle, deg
$\Lambda_{c/2}$	sweep of the half-chord line, deg
$\Lambda_{c/4}$	sweep of the quarter-chord line, deg
Λ_{le}	sweep of the leading edge, deg
λ	taper ratio, $\frac{c_t}{c_r}$

TABLE 3.2-1
PERTINENT WING AND HORIZONTAL-TAIL GEOMETRIC PARAMETERS
USED IN THE ANALYSIS

Symbol	Description	Wing		Horizontal tail		Vertical tail
		Total	Exposed	Total	Exposed	Exposed
S	Area, sq ft	^c 172.3	148.0	32.5	28.73	14.6
b	Span, ft	36.0	32.0	12.5	11.25	4.67
A	Aspect ratio, $\frac{b^2}{S}$	7.5	6.9	4.8	4.4	1.49
c_t	Tip chord, in.	39.0	39.0	21.4	21.4	24.0
c_r	Root chord, in.	76.0	71.9	41.5	39.3	51.0
λ	Taper ratio, $\frac{c_t}{c_r}$.513	.544	.515	.545	.471
\bar{c}	^a Mean aerodynamic chord, in.	59.50	57.10	32.45	31.2	^d 39.2
$y_{\bar{c}}$	^b Lateral position of mean aerodynamic chord, in.	96.48	86.58	33.10	30.10	24.6
Γ	Dihedral angle, deg	5	5	0	0	----
Λ_{le}	Leading-edge sweep, deg	0	0	12	12	35
$\Lambda_{c/4}$	Sweep of c/4 line, deg	-2.5	-2.5	8	8	30
$\Lambda_{c/2}$	Sweep of c/2 line, deg	-5	-5	5	5	25

$$^a \bar{c} = \frac{2}{3} c_r \left(\frac{1 + \lambda + \lambda^2}{1 + \lambda} \right)$$

$$^b y_{\bar{c}} = \frac{1}{3} \left(\frac{1 + 2\lambda}{1 + \lambda} \right) \frac{b}{2}$$

^cArea used as basic reference in theoretical determination of characteristics. The final values of calculated characteristics are based on 178 square feet, the reference area for the wind-tunnel and flight data.

^dFrom root chord of exposed vertical-tail panel as given in figure 3.2-3.

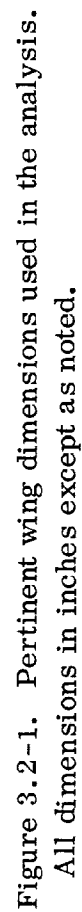


Figure 3.2-1. Pertinent wing dimensions used in the analysis.
All dimensions in inches except as noted.

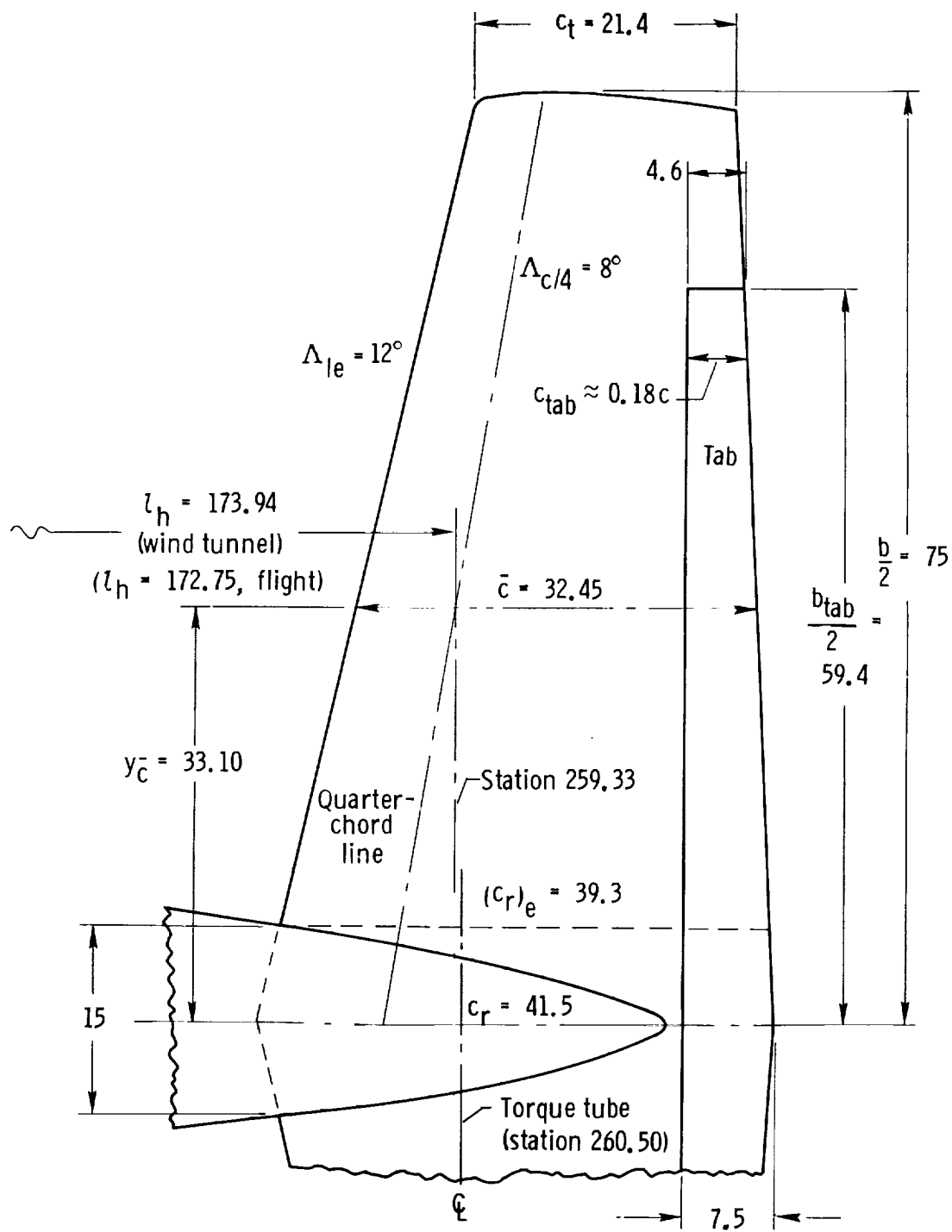


Figure 3.2-2. Pertinent horizontal-tail dimensions used in the analysis.
All dimensions in inches except as noted.

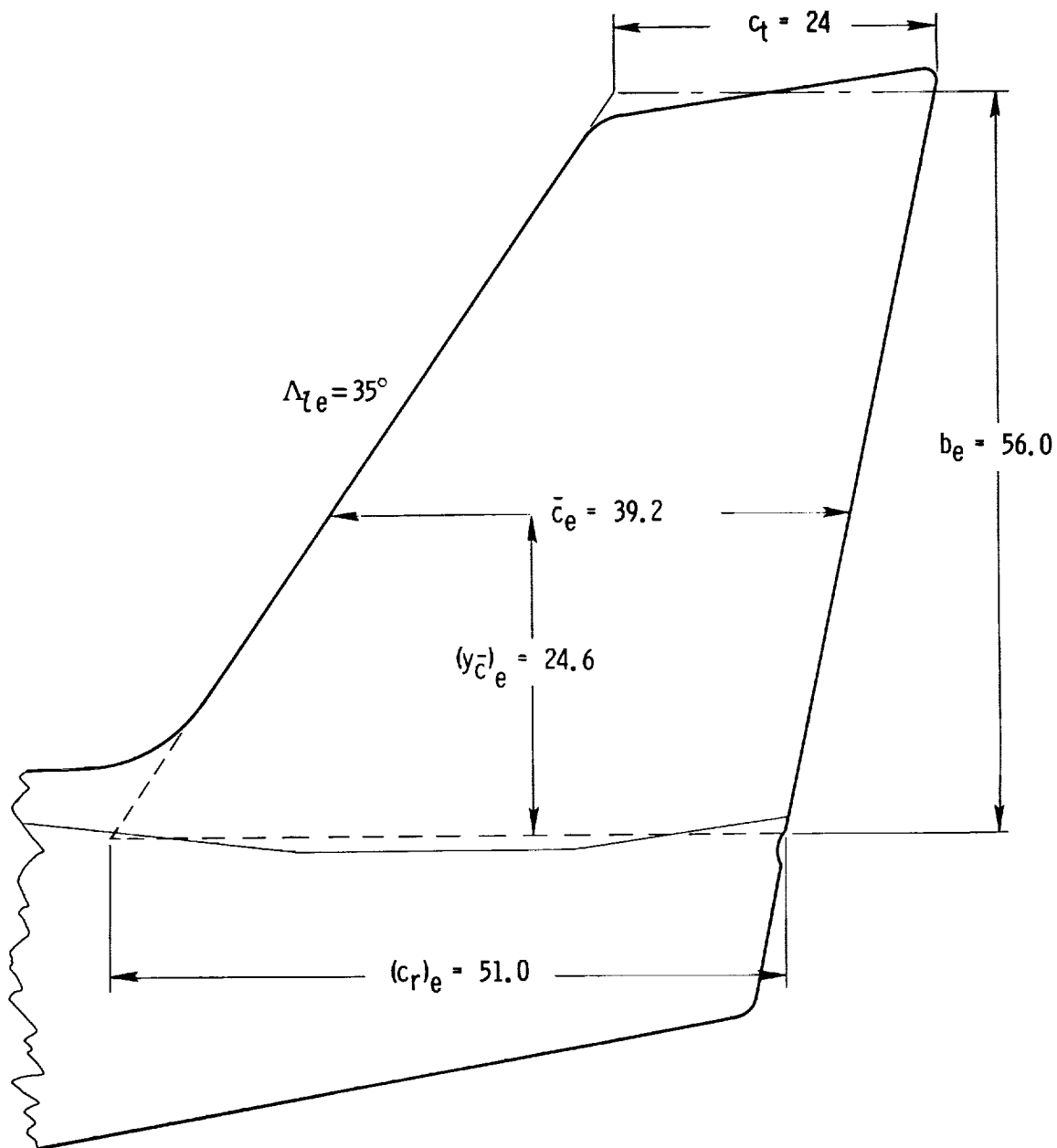


Figure 3.2-3. Pertinent dimensions of exposed vertical-tail panel used in drag calculations. All dimensions in inches except as noted.

4.0 PREDICTION OF PROPELLER-OFF AERODYNAMIC CHARACTERISTICS

4.1 Wing and Horizontal-Tail Airfoil Section Characteristics

Some success has been achieved in predicting airfoil section characteristics; however, where possible, section characteristics should be based on experimental data (ref. 3, for example) with the maximum lift coefficient corrected to the Reynolds number being considered. The discussion in this section is presented to show the trends created by the variation of pertinent section geometric characteristics.

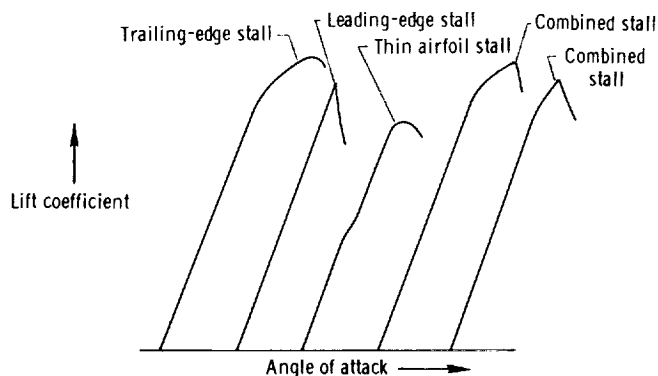
Theoretically, airfoil section lift-curve slopes for nonseparated, incompressible flow conditions are affected by airfoil thickness ratio, t/c , and to a much lesser extent by trailing-edge angle, ϕ_{te} (fig. 4.1-1), as shown by the following equation from reference 1:

$$c_{l_{\alpha}} = 6.28 + 4.7(t/c) (1 + 0.00375\phi_{te}) \text{ per radian} \quad (4.1-1)$$

where ϕ_{te} is in degrees. Practically, boundary layer (which is influenced by surface roughness, leading-edge sharpness, surface curvature, and pressure gradients) reduces the section lift-curve slope significantly. Leading-edge sharpness is normally expressed as a leading-edge-sharpness parameter, Δy (fig. 4.1-2). Effects of leading-edge sharpness and surface roughness are illustrated in this section. The variables ϕ_{te} and Δy are used as correlating parameters throughout the discussion of section characteristics.

Section zero-lift angle of attack cannot be predicted accurately. It is affected only slightly by Reynolds number and surface roughness (ref. 4); Mach number effects, however, can be significant in the higher subsonic regions as indicated in reference 5 and shown in figure 4.1-3 (from ref. 1).

Low-speed section stalling characteristics can be classified into three "pure" types of stall separation patterns and a fourth "impure" type (ref. 6) as shown in the adjacent sketch.



(a) Trailing-edge stall is characterized by a gradual turbulent boundary-layer separation starting at the section trailing edge and moving forward with increasing angle of attack. This type of stall occurs on wings having a thickness of 12 percent or greater. The stall is mild with a gradual rounding of the lift and moment curves near maximum lift coefficient.

(b) Leading-edge stall is characterized by an abrupt local (small bubble)

flow separation near the leading edge. For this separation pattern the lift and pitching-moment curves show little or no change in lift-curve slope prior to maximum lift and an abrupt, often large, change in lift and pitching moment after maximum lift is attained.

(c) Thin-airfoil stall is characterized by laminar flow separation from the leading edge, followed by a turbulent reattachment at a point along the chord which moves progressively downstream with increasing angle of attack. The stall is characterized by a rounded lift-curve peak, generally preceded by an inflection in the force and moment variation in the linear range for airfoils with rounded leading edges.

(d) Combined trailing-edge and leading-edge stall is characterized by either a semi-rounded or relatively sharp lift-curve peak and followed by either an abrupt or relatively rapid decrease in lift.

The type of leading-edge stall, (b) and (c), and the occurrence of trailing-edge and combined stall are dependent on leading-edge geometry and on the Reynolds number of the boundary layer at the point of separation and thus on the free-stream Reynolds number. This is reflected in figure 4.1-4, from reference 6, where the upper surface ordinate at the 0.0125 chord was used as a correlating parameter. The type of leading-edge stall affects the section maximum lift coefficient. This is reflected in figure 4.1-5, from reference 1, for an uncambered airfoil at a Reynolds number of 9×10^6 ; the leading-edge-sharpness parameter, Δy (fig. 4.1-2), is the correlating parameter.

The effect of Reynolds number on the maximum section lift coefficient can be accounted for by using figure 4.1-6, from reference 1, which uses the leading-edge-sharpness parameter, Δy , as the correlating parameter. The effects of surface roughness on maximum section lift coefficient are not so readily accounted for. Figure 4.1-7, from reference 3, shows the effects of Reynolds number and NACA standard roughness on an airfoil section. Figures 4.1-8 and 4.1-9, also from reference 3, show the effects of roughness at the leading edge and at various chordwise locations. It should be noted that NACA standard roughness is considered to be more severe than that caused by the usual manufacturing irregularities or deterioration in service.

The aerodynamic center of thin airfoil sections at subsonic conditions is theoretically located at the quarter-chord point. Experimentally, the aerodynamic center is a function of section thickness ratio and trailing-edge angle, as shown in figure 4.1-10.

For the subject airplane the section airfoil characteristics of the wing and horizontal tail, summarized in table 4.1-1, were determined from table 4.1-2 (from ref. 1), which is a summary of experimental data (at $N_{Re} = 9 \times 10^6$) for NACA four- and five-digit airfoils and NACA six-series airfoils reported in reference 3. The section characteristics of the wing airfoil (NACA 64₂A215) were obtained directly from table 4.1-2; the characteristics of the horizontal-tail airfoil (NACA 0008) were obtained from a linear interpolation of the characteristics listed for the NACA 0006 and 0009 airfoils.

The upper limit of linearity, α^* , indicated in table 4.1-2 is the upper angle-of-attack limit of the linear portion of the lift-curve slope.

4.1.1 Symbols

a.c.	aerodynamic center of an airfoil section, fraction or percent of chord
c	section chord, in. or ft
c_d	section drag coefficient
c_l	section lift coefficient
$c_{l_{\max}}$	section maximum lift coefficient
$(c_{l_{\max}})_{\text{base}}$	section maximum lift coefficient at reference Reynolds number of 9×10^6 based on section chord, ft
$\Delta c_{l_{\max}}$	correction of $c_{l_{\max}}$ for Reynolds number
$c_{l_{\alpha}}$	section lift-curve slope, rad or deg
c_{m_0}	section pitching-moment coefficient at zero lift
$c_{m_{c/4}}$	section pitching-moment coefficient about the quarter-chord point
M	Mach number
N_{Re}	Reynolds number, based on the chord in ft
t/c	maximum thickness ratio
x/c, y/c	section coordinate dimensions (fig. 4.1-7)
Δy	section leading-edge-sharpness parameter (fig. 4.1-2), percent of chord
α	angle of attack, rad or deg
α_0	angle of attack for zero lift
α^*	limit of linearity of $c_{l_{\alpha}}$
$\alpha_{c_{l_{\max}}}$	angle of attack at $c_{l_{\max}}$
$\Lambda_{c/4}$	sweep of the quarter-chord line, deg
φ_{te}	section trailing-edge angle (fig. 4.1-1), deg

TABLE 4.1-1
AIRPLANE WING AND HORIZONTAL-TAIL AIRFOIL SECTION CHARACTERISTICS

(a) Section geometric parameters

Symbol	Description	Reference	Wing	Reference	Horizontal tail
---	Airfoil section	-----	NACA 642A215	-----	NACA 0008
t/c	Thickness ratio	-----	0.15	-----	0.08
Δy	Leading-edge-sharpness parameter	Figure 4.1-2	3.16	Figure 4.1-2	2.1
ϕ_{te}	Trailing-edge angle, deg	Figure 4.1-1	15.8	Figure 4.1-1	11.0

(b) Section characteristics

Symbol	Description	Reference	Wing	Reference	Horizontal tail
α_0	Zero-lift α relative to chord line, deg	Table 4.1-2	-2.0	Table 4.1-2	0
$c_{l\alpha}$	Lift-curve slope, per deg	Table 4.1-2	.095	Table 4.1-2	.109
α^*	Limit of linearity of $c_{l\alpha}$ (relative to chord line)	Table 4.1-2	12.0	Table 4.1-2	10.6
$\alpha c_{l\max}$	α at $c_{l\max}$ (relative to chord line), deg	Table 4.1-2	15.0	Table 4.1-2	11.9
$(c_{l\max})_{base}$	Maximum lift coefficient at $N_{Re} = 9 \times 10^6$	Table 4.1-2	1.5	Table 4.1-2	1.19
$\Delta c_{l\max}$	Correction of maximum c_l from $N_{Re} = 9 \times 10^6$ to wind-tunnel $N_{Re} = 1.95 \times 10^6$	Figure 4.1-6	-.13	Figure 4.1-5	-.14
$c_{l\max}$	Maximum lift coefficient at wind-tunnel-test condition = $(c_{l\max})_{base} + \Delta c_{l\max}$	-----	1.37	-----	1.05
c_{m_0}	Zero-lift pitching-moment coefficient	Table 4.1-2	-.040	Table 4.1-2	0
a.c.	Aerodynamic center	Table 4.1-2	.252 c	Table 4.1-2	.250 c

TABLE 4.1-2
EXPERIMENTAL LOW-SPEED AIRFOIL SECTION AERODYNAMIC CHARACTERISTICS¹
[Ref. 1]

(a) 4- and 5-digit airfoils, $N_{Re} = 9 \times 10^6$, smooth leading edge

Airfoil	α_0 , deg	c_{m_0}	c_{l_α} per deg	a.c.	$\alpha_{c_{l_{max}}}$, deg	$c_{l_{max}}$	α^* , deg
0006	0	0	0.108	0.250	9.0	0.92	9.0
0009	0	0	.109	.250	13.4	1.32	11.4
1408	.8	-.023	.109	.250	14.0	1.35	10.0
1410	-1.0	-.020	.108	.247	14.3	1.50	11.0
1412	-1.1	-.025	.108	.252	15.2	1.58	12.0
2412	-2.0	-.047	.105	.247	16.8	1.68	9.5
2415	-2.0	-.049	.106	.246	16.4	1.63	10.0
2418	-2.3	-.050	.103	.241	14.0	1.47	10.0
2421	-1.8	-.040	.103	.241	16.0	1.47	8.0
2424	-1.8	-.040	.098	.231	16.0	1.29	8.4
4412	-3.8	-.093	.105	.247	14.0	1.67	7.5
4415	-4.3	-.093	.105	.245	15.0	1.64	8.0
4418	-3.8	-.088	.105	.242	14.0	1.53	7.2
4421	-3.8	-.085	.103	.238	16.0	1.47	6.0
4424	-3.8	-.082	.100	.239	16.0	1.38	4.8
23012	-1.4	-.014	.107	.247	18.0	1.79	12.0
23015	-1.0	-.007	.107	.243	18.0	1.72	10.0
23018	-1.2	-.005	.104	.243	16.0	1.60	11.8
23021	-1.2	0	.103	.238	15.0	1.50	10.3
23024	-.8	0	.097	.231	15.0	1.40	9.7

(b) 6-series airfoils, $N_{Re} = 9 \times 10^6$, smooth leading edge

Airfoil	α_0 , deg	c_{m_0}	c_{l_α} per deg	a.c.	$\alpha_{c_{l_{max}}}$, deg	$c_{l_{max}}$	α^* , deg
63-006	0	0.005	0.112	0.258	10.0	0.87	7.7
63-009	0	0	.111	.258	11.0	1.15	10.7
63-206	-1.9	-.037	.112	.254	10.5	1.06	6.0
63-209	-1.4	-.032	.110	.262	12.0	1.40	10.8
63-210	-1.2	-.035	.113	.261	14.5	1.56	9.6
63 ₁ -012	0	0	.116	.265	14.0	1.45	12.8
63 ₁ -212	-2.0	-.035	.114	.263	14.5	1.63	11.4
63 ₁ -412	-2.8	-.075	.117	.271	15.0	1.77	9.6
63 ₂ -015	0	0	.117	.271	14.5	1.47	11.0
63 ₂ -215	-1.0	-.030	.116	.267	15.0	1.60	8.8
63 ₂ -415	-2.8	-.069	.118	.262	15.0	1.68	10.0
63 ₂ -615	-3.6	-.108	.117	.266	15.0	1.67	8.6
63 ₃ -018	0	0	.118	.271	15.5	1.54	11.2
63 ₃ -218	-1.4	-.033	.118	.271	14.5	1.85	8.0
63 ₃ -418	-2.7	-.064	.118	.272	16.0	1.57	7.0
63 ₃ -618	-3.8	-.097	.118	.267	16.0	1.59	4.2
63 ₄ -021	0	0	.118	.273	17.0	1.38	9.0
63 ₄ -221	-1.5	-.035	.118	.269	15.0	1.44	9.2
63 ₄ -421	-2.8	-.062	.120	.275	16.0	1.48	6.7
63,4-420	-2.2	-.059	.109	.265	14.0	1.42	7.6
63,4-420 a = .3	-2.4	-.037	.111	.265	16.0	1.35	6.0
63(420)-422	-3.2	-.065	.112	.271	14.0	1.36	6.0
63(420)-517	-3.0	-.084	.108	.264	15.0	1.60	8.0
64-006	0	0	.109	.256	9.0	.8	7.2
64-009	0	0	.110	.262	11.0	1.17	10.0
64-108	0	-.015	.110	.255	10.0	1.10	10.0
64-110	-1.0	-.020	.110	.261	13.0	1.40	10.0
64-206	-1.0	-.040	.110	.253	12.0	1.03	8.0
64-208	-1.2	-.039	.113	.257	10.5	1.23	8.8
64-209	-1.5	-.040	.107	.261	13.0	1.40	8.9
64-210	-1.6	-.040	.110	.258	14.0	1.45	10.8
64 ₁ -012	0	0	.111	.262	14.5	1.45	11.0
64 ₁ -112	-.8	-.017	.113	.267	14.0	1.50	12.2
64 ₁ -212	-1.3	-.027	.113	.262	15.0	1.55	11.0
64 ₁ -412	-2.6	-.065	.112	.267	15.0	1.67	8.0

¹Lift coefficients used in these charts are based on chord.

TABLE 4.1-2 (Concluded)

Airfoil	α_0 , deg	c_{m_0}	c_{l_α} per deg	a.c.	$\alpha_{c_{l_{\max}}}$, deg	$c_{l_{\max}}$	α^* , deg
64 ₂ -015	0	0	0.112	0.267	15.0	1.48	13.0
64 ₂ -215	-1.6	-.030	.112	.265	15.0	1.57	10.0
64 ₂ -415	-2.8	-.070	.115	.264	15.0	1.65	8.0
64 ₃ -018	0	.004	.111	.266	17.0	1.50	12.0
64 ₃ -218	-1.3	-.027	.115	.271	16.0	1.53	10.0
64 ₃ -418	-2.9	-.065	.116	.273	14.0	1.57	8.0
64 ₃ -618	-3.8	-.095	.116	.273	16.0	1.58	5.6
64 ₄ -021	0	.005	.110	.274	14.0	1.30	10.3
64 ₄ -221	-1.2	-.029	.117	.271	13.0	1.32	6.8
64 ₄ -421	-2.8	-.068	.120	.276	13.0	1.42	6.4
65-006	0	0	.105	.258	12.0	.92	7.6
65-009	0	0	.107	.264	11.0	1.08	9.8
65-206	-1.6	-.031	.105	.257	12.0	1.03	6.0
65-209	-1.2	-.031	.106	.259	12.0	1.30	10.0
65-210	-1.6	-.034	.108	.262	13.0	1.40	9.6
65-410	-2.5	-.067	.112	.262	14.0	1.52	8.0
65 ₁ -012	0	0	.110	.261	14.0	1.36	10.0
65 ₁ -212	-1.0	-.032	.108	.261	14.0	1.47	9.4
65 ₁ -212 a = .6	-1.4	-.033	.108	.269	14.0	1.50	9.6
65 ₁ -412	-3.0	-.070	.111	.265	15.5	1.66	10.5
65 ₂ -015	0	0	.111	.257	15.0	1.42	11.2
65 ₂ -215	-1.2	-.032	.112	.269	15.5	1.53	10.0
65 ₂ -415	-2.6	-.060	.111	.268	16.0	1.61	8.7
65 ₂ -415 a = .5	-2.6	-.051	.111	.264	20.0	1.60	7.0
65(215)-114	-.7	-.019	.112	.265	15.0	1.44	10.5
65(216)-415 a = .5	-3.0	-.057	.106	.267	18.0	1.60	6.0
65,3-018	0	0	.100	.262	17.0	1.44	10.0
65-418 a = .8	-3.0	-.081	.112	.266	20.0	1.58	4.4
65-618	-4.0	-.100	.110	.273	20.0	1.60	4.9
65 ₃ -018	0	0	.100	.267	16.0	1.37	10.0
65 ₃ -218	-1.2	-.030	.100	.263	18.0	1.48	8.8
65 ₃ -418	-2.4	-.059	.110	.265	18.0	1.54	4.9
65 ₃ -418 a = .5	-2.8	-.055	.115	.267	18.0	1.50	6.0
65 ₃ -618	-4.0	-.102	.113	.276	18.0	1.64	5.2
65 ₃ -618 a = .5	-4.2	-.078	.104	.265	20.0	1.51	5.3
65 ₄ -021	0	0	.112	.267	18.5	1.40	7.4
65 ₄ -221	-1.3	-.029	.115	.274	20.5	1.46	6.0
65 ₄ -421	-2.8	-.066	.116	.272	22.0	1.56	5.0
65 ₄ -421 a = .5	-2.8	-.052	.116	.272	20.0	1.43	5.6
65(421)-420	-2.4	-.061	.116	.276	20.0	1.52	4.7
66-006	0	0	.100	.252	9.0	.80	6.5
66-009	0	0	.103	.259	10.0	1.05	10.0
66-206	-1.6	-.038	.108	.257	10.5	1.00	7.0
66-209	-1.0	-.034	.107	.257	11.0	1.17	9.0
66-210	-1.3	-.035	.110	.261	11.0	1.27	10.0
66 ₁ -012	0	0	.106	.258	14.0	1.25	11.2
66 ₁ -212	-1.2	-.032	.102	.259	15.0	1.46	11.6
66 ₂ -015	0	.005	.105	.265	15.5	1.35	12.0
66 ₂ -215	-1.3	-.031	.106	.260	16.0	1.50	11.4
66 ₂ -415	-2.6	-.069	.106	.260	17.0	1.60	10.0
66(215)-016	0	0	.105	.260	14.0	1.33	10.0
66(215)-216	-2.0	-.044	.114	.262	16.0	1.55	8.8
66(215)-216 a = .6	-1.2	-.030	.100	.257	16.0	1.46	7.0
66(215)-416	-2.6	-.068	.100	.265	18.0	1.60	4.0
63A010	0	.005	.105	.254	13.0	1.20	10.0
63A210	-1.5	-.040	.103	.257	14.0	1.43	10.0
64A010	0	0	.110	.253	12.0	1.23	10.0
64A210	-1.5	-.040	.105	.251	3.0	1.44	10.0
64A410	-3.0	-.080	.100	.254	15.0	1.61	10.0
64 ₁ A212	-2.0	-.040	.100	.252	14.0	1.54	11.0
64 ₂ A215	-2.0	-.040	.095	.252	15.0	1.50	12.0

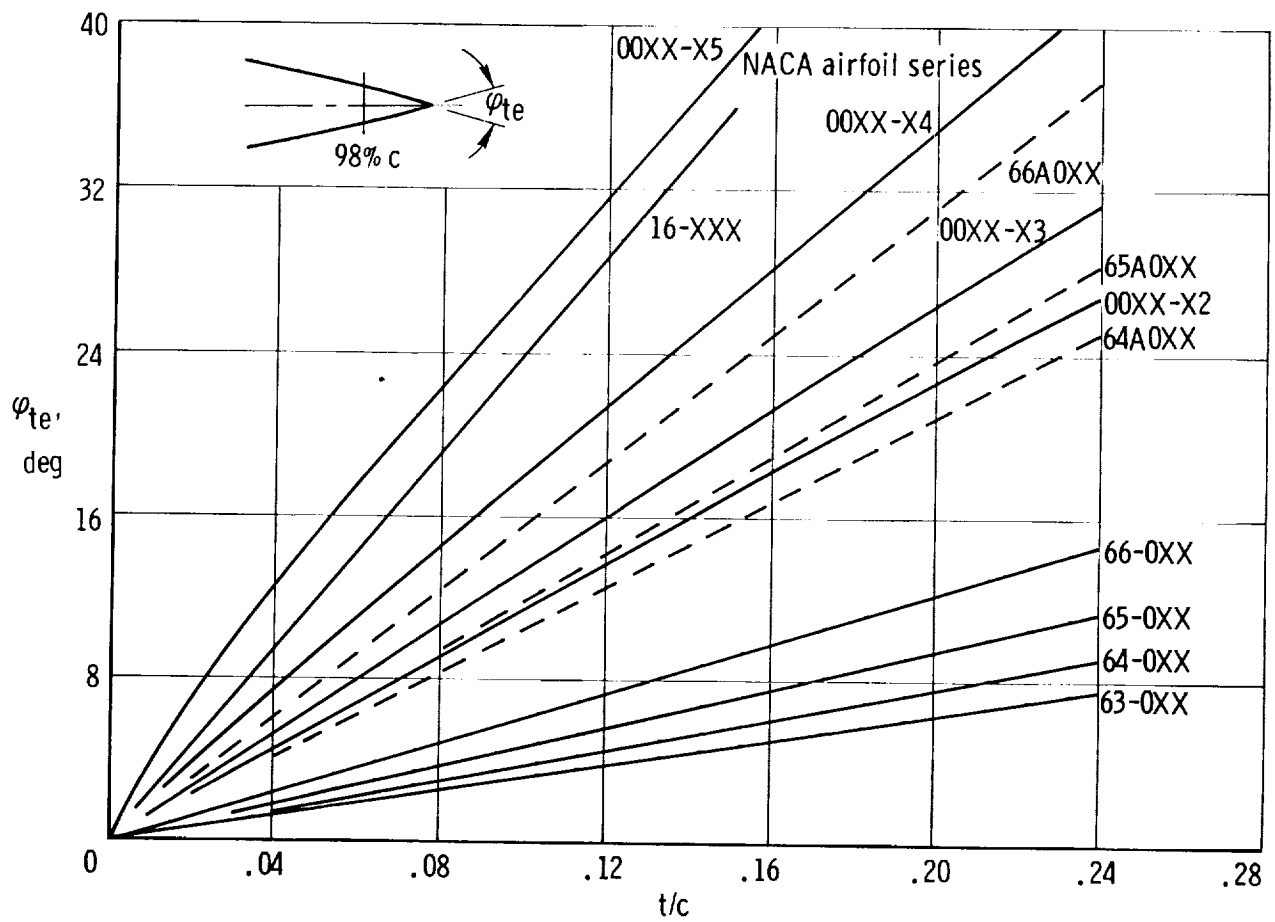


Figure 4.1-1. Variation of trailing-edge angle with airfoil thickness ratio (ref. 1).

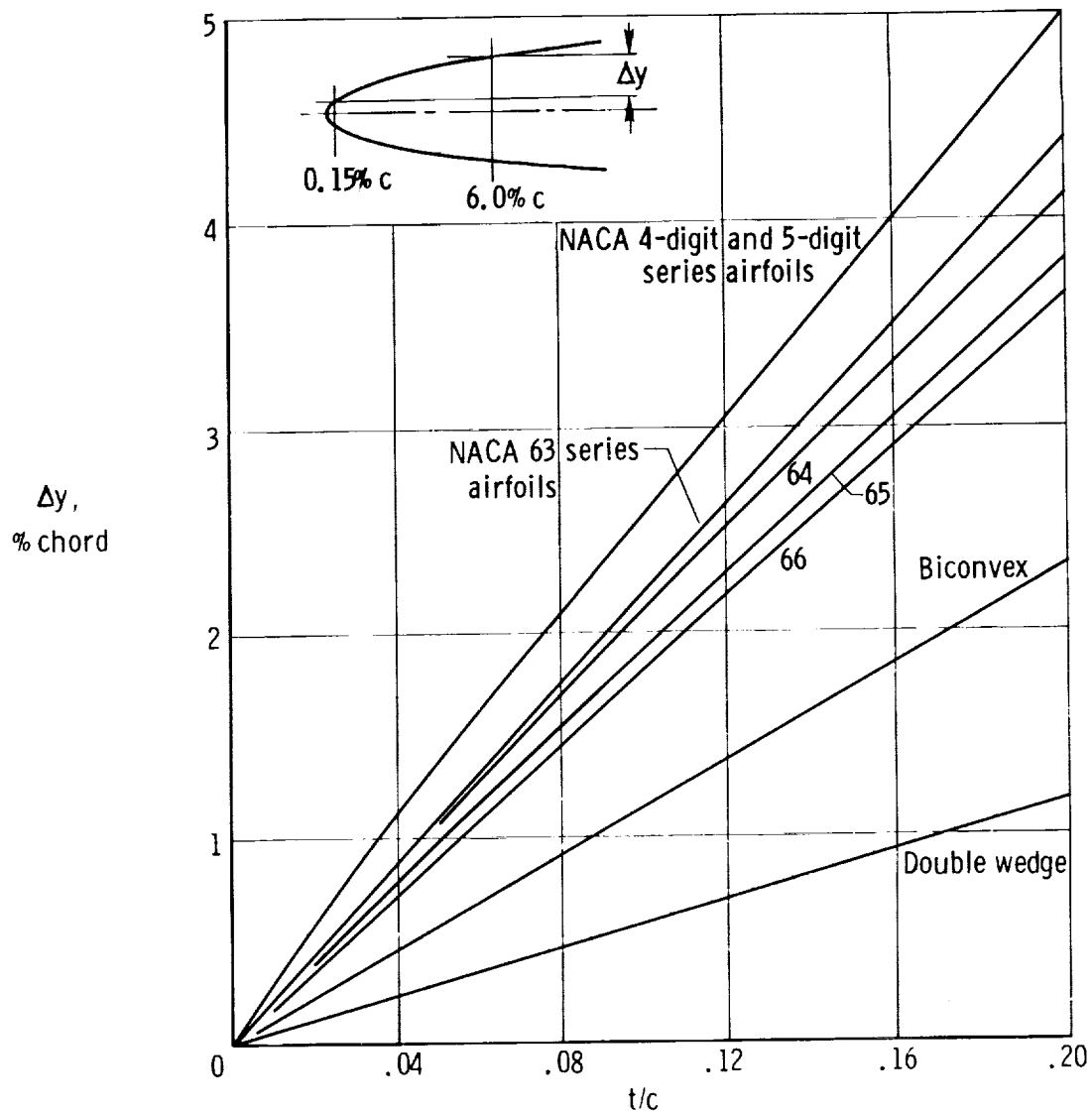


Figure 4.1-2. Variation of leading-edge sharpness parameter with airfoil thickness ratio (ref. 1).

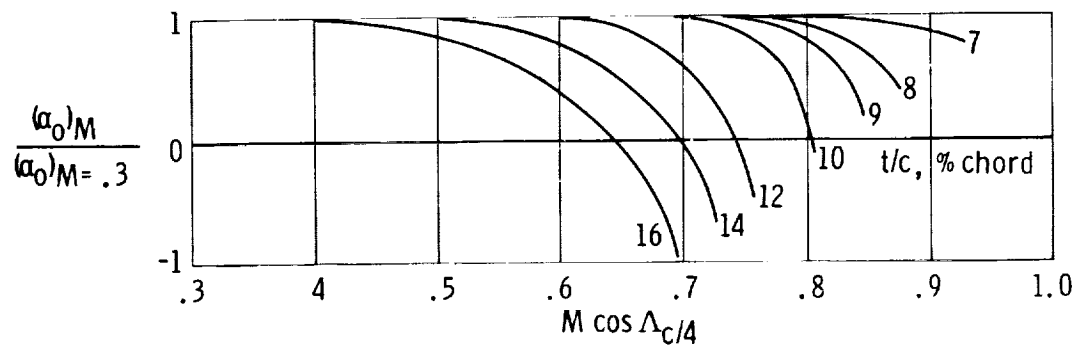


Figure 4.1-3. Mach number correction for zero-lift angle of attack (ref. 1).

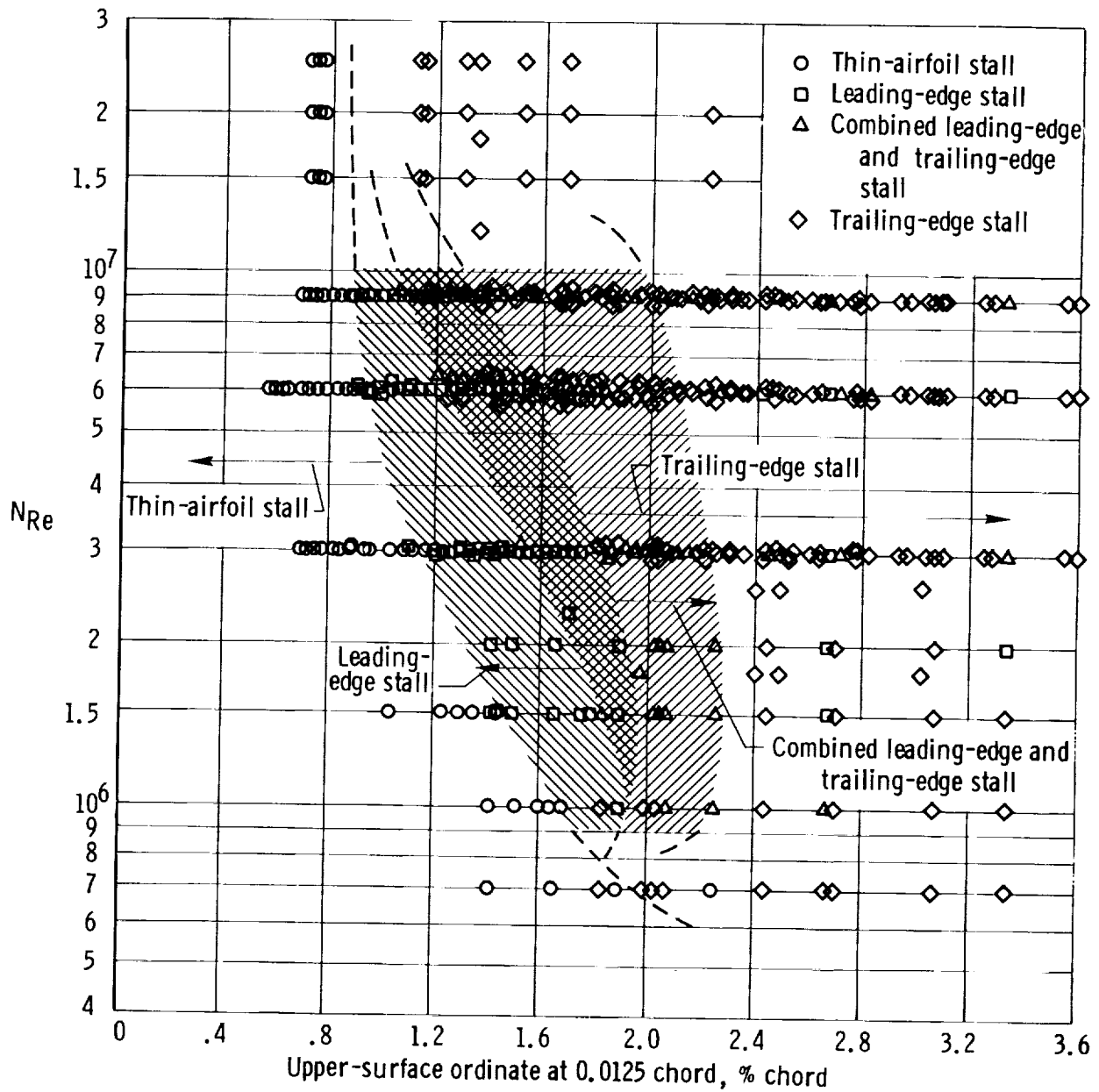


Figure 4.1-4. Low-speed stalling characteristics of airfoil sections correlated with Reynolds number and upper-surface ordinates of the airfoil sections at the 0.0125-chord station (ref. 6).

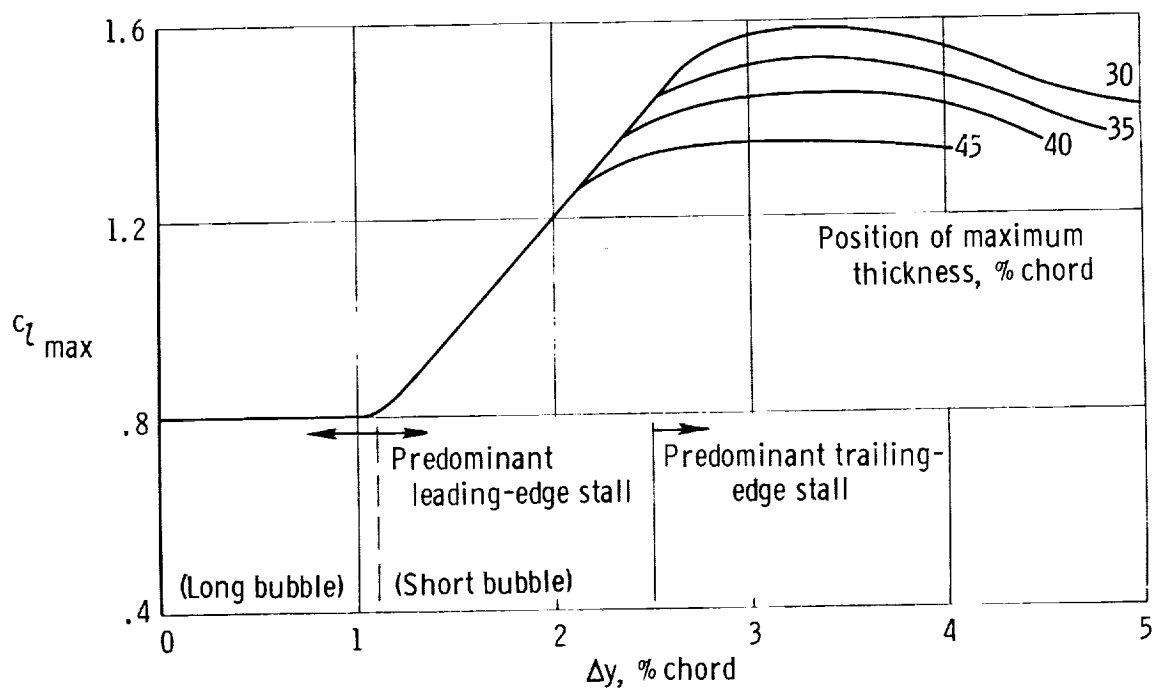


Figure 4.1-5. Airfoil section maximum lift coefficient of uncambered airfoils (ref. 1).
 $N_{Re} = 9 \times 10^6$.

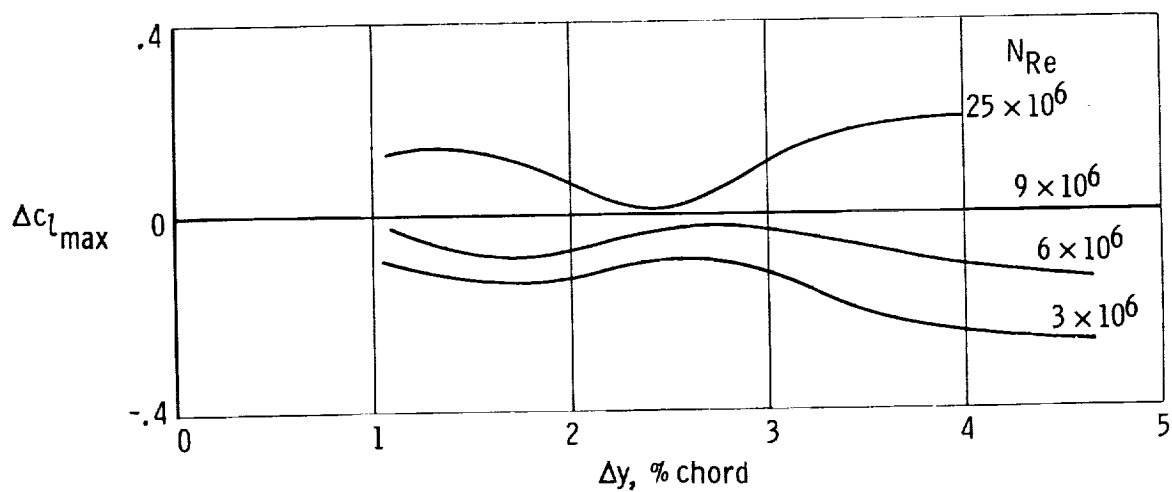


Figure 4.1-6. Effect of Reynolds number on section maximum lift (ref. 1).

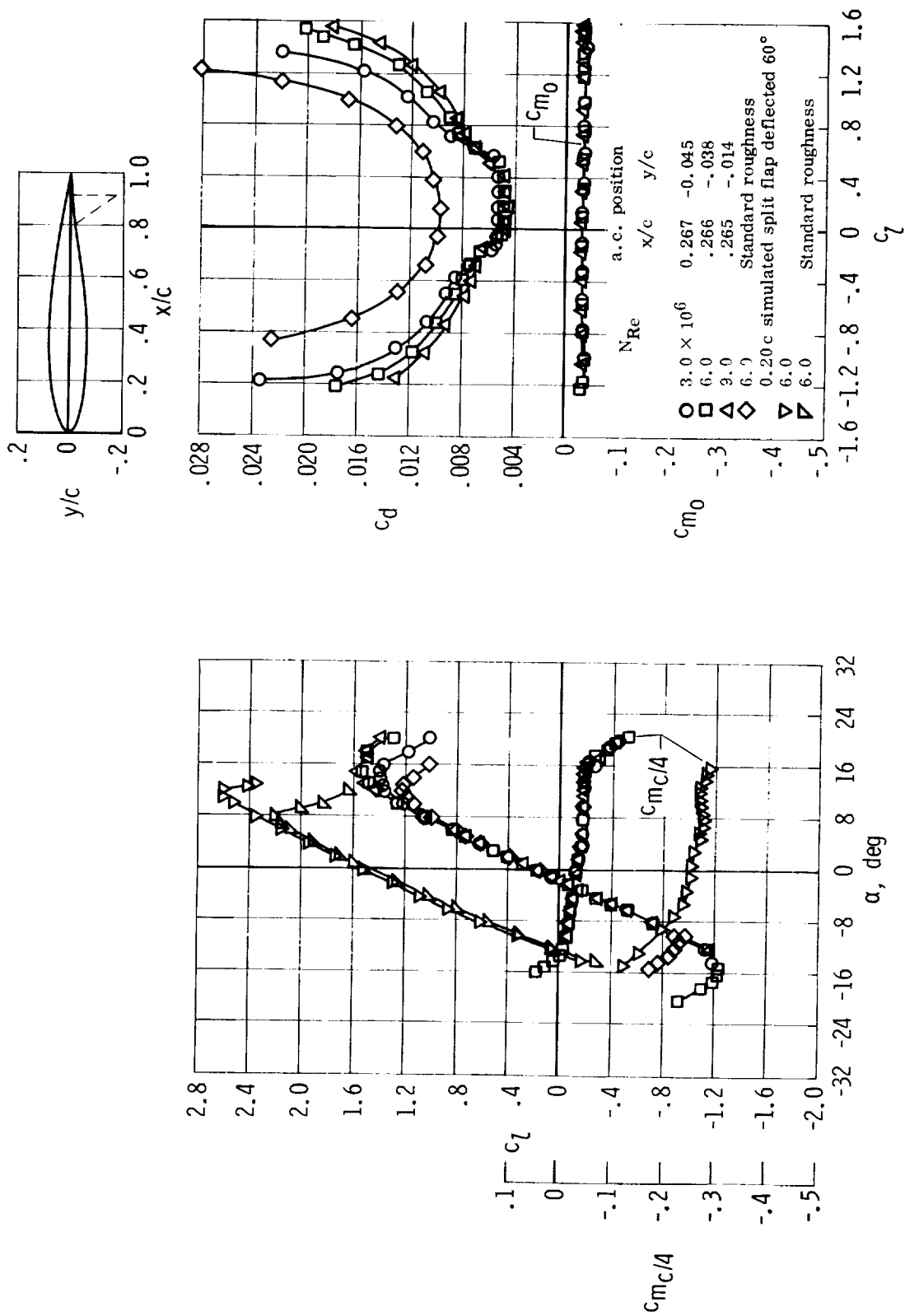


Figure 4.1-7. Aerodynamic characteristics of the NACA 64₂-215 airfoil section showing effects of Reynolds number and roughness (ref. 3).

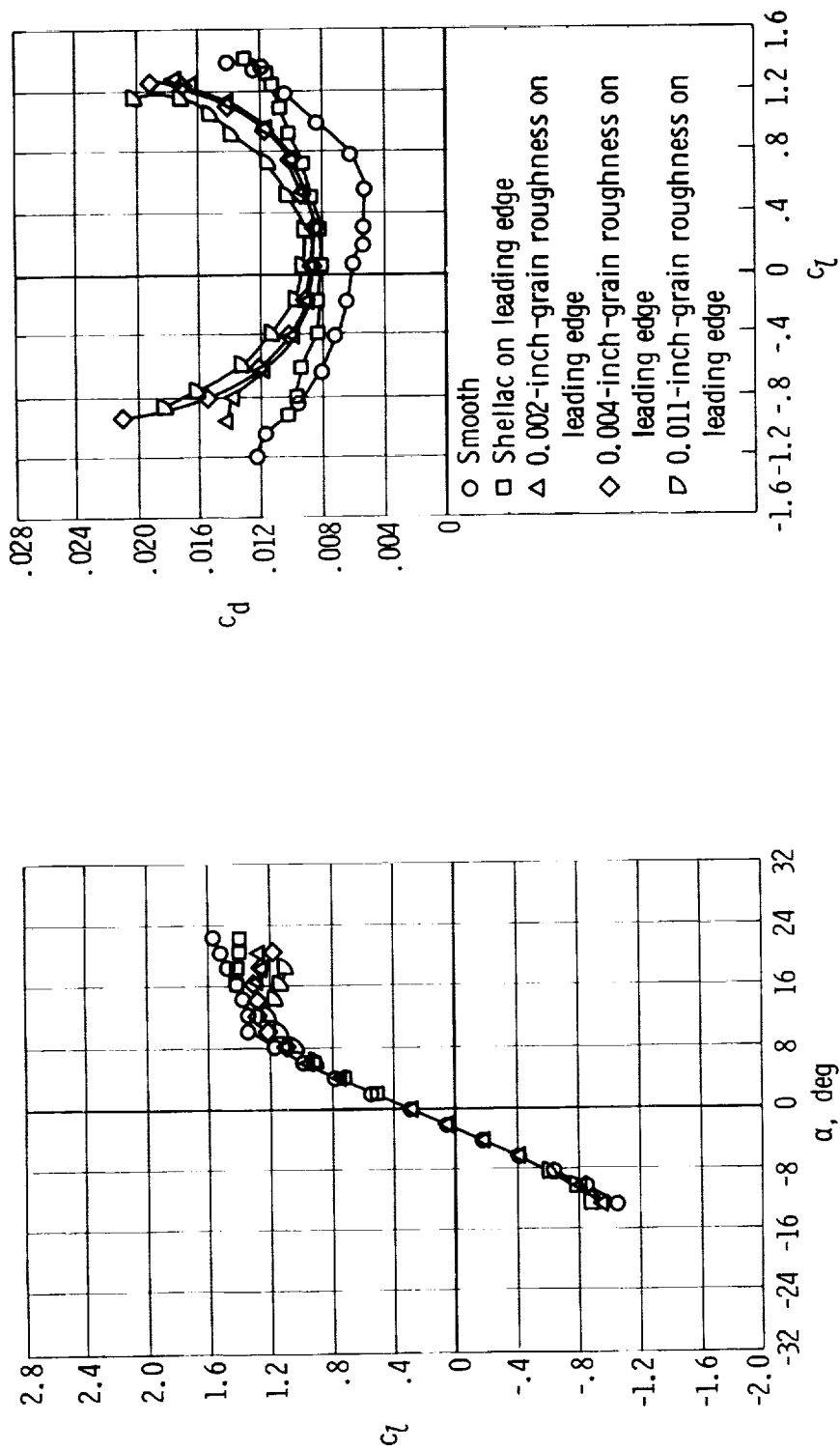


Figure 4.1-8. Lift and drag characteristics of an NACA 63(420)-422 airfoil with various degrees of roughness at the leading edge (ref. 3).

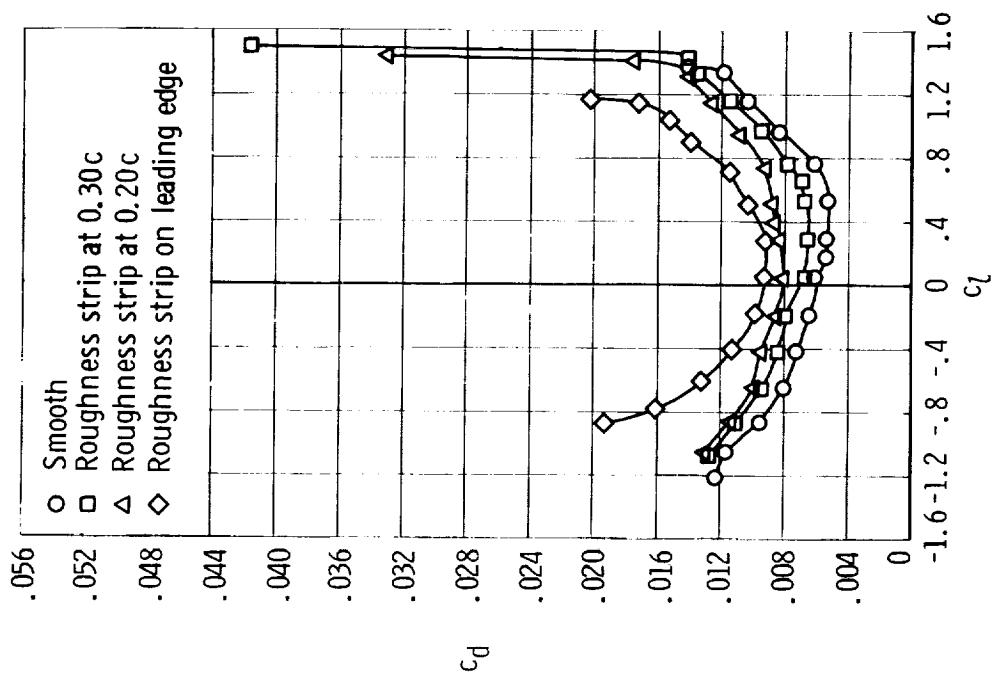
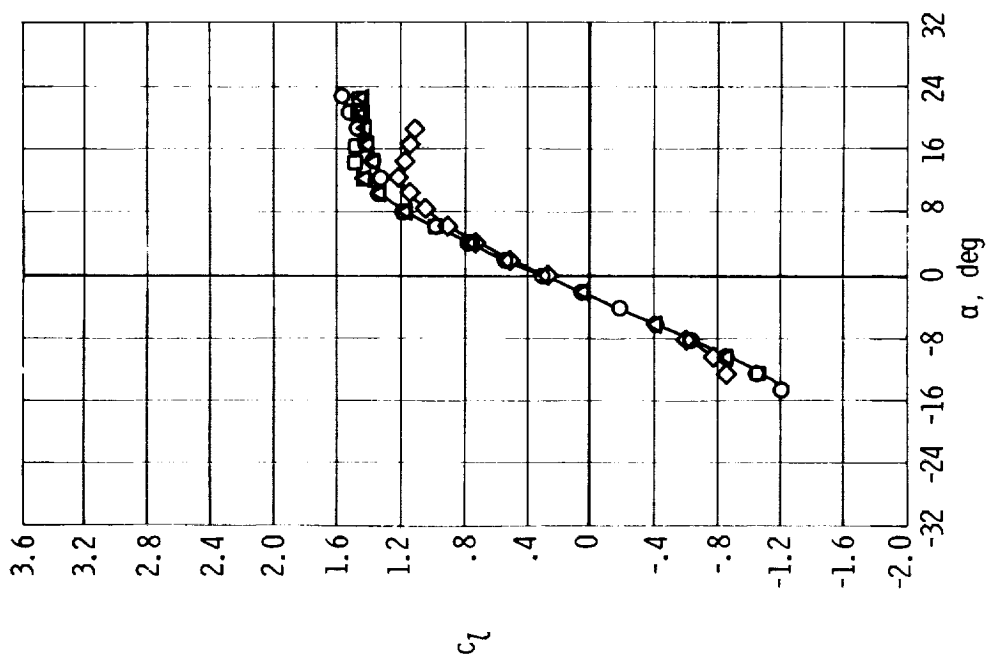


Figure 4.1-9. Lift and drag characteristics of an NACA 63(420)-422 airfoil with 0.011-inch-grain roughness at various chordwise locations (ref. 3).

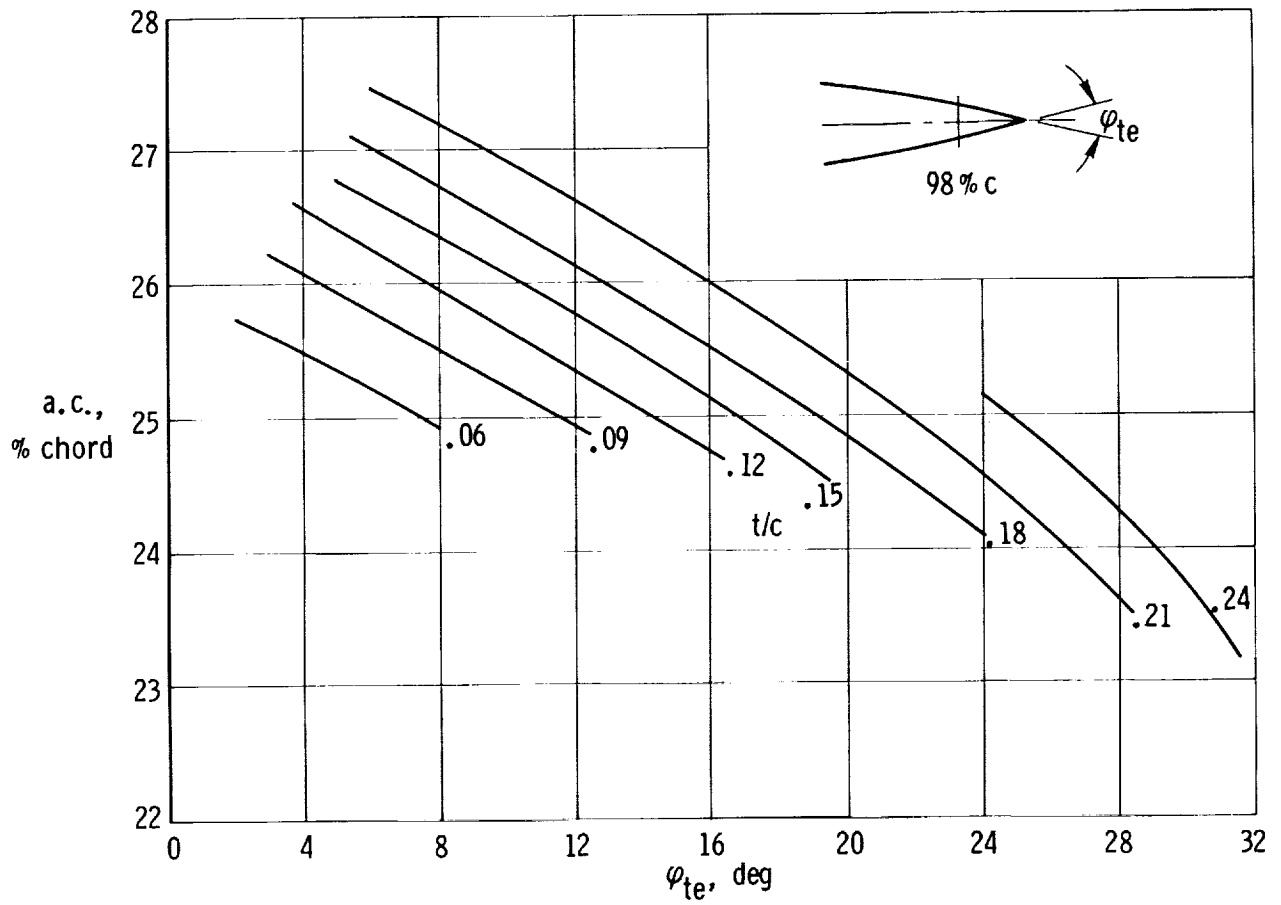


Figure 4.1-10. Effect of trailing-edge angle on section aerodynamic-center location (ref. 1). Subsonic speed.

4.2 Lift Characteristics of the Wing and Horizontal Tail

Lift characteristics of the wing and horizontal tail are considered in terms of total (which includes the portion covered by the body) and exposed areas of the respective surfaces (section 3.2). Body in this context includes fuselage and nacelles. The exposed panel concept is used in obtaining the net propeller-off lift and pitching-moment characteristics of the airplane; the total wing concept is used in determining maximum lift coefficient, drag, and power effects on the lift and pitching moment. The procedures of this section are restricted to untwisted wings; lift characteristics of twisted wings are considered in reference 7. In the following discussion the expression "wing" is used as a general term and applied to both wings and tail surfaces. The wing and horizontal-tail lift curves of the subject airplane, as determined by the following procedures, are shown in figure 4.2-1.

Zero-lift angle of attack for untwisted, constant section airfoil wings is relatively unaffected by wing planform geometry. It is primarily a function of section geometry (section 4.1). Therefore, the section zero-lift angle can be assumed to be the value for the overall wing.

Lift-curve slopes of tapered wings, in the subsonic region up to $M = 0.6$, can be determined by the modified lifting-line theory method of reference 8. The method is simple and does not require the use of the taper ratio as a parameter because the mid-chord sweep angle, rather than the quarter chord, is used as the sweep angle. The lift-curve slope is determined as a function of aspect ratio, A , midchord sweep angle, $\Lambda_{c/2}$, Mach number, M , and section lift-curve slope, $c_{l\alpha}$, by the following equation developed in reference 8:

$$\frac{C_{L\alpha}}{A} = \frac{2\pi}{2 + \sqrt{\frac{A^2}{k^2} (\beta^2 + \tan^2 \Lambda_{c/2}) + 4}} \text{ per radian} \quad (4.2-1)$$

where $\beta^2 = 1 - M^2$ and $k = \frac{c_{l\alpha}}{2\pi}$. Figure 4.2-2 is the graphical equivalent of the equation.

The upper limit of linearity of the wing lift-curve slope is considered to be equal to the section airfoil limit of linearity, α^* (section 4.1 and fig. 4.2-1).

The maximum lift coefficient and angle of attack for the maximum lift of wings at subsonic conditions (up to $M = 0.6$) may be determined by the empirical method of reference 1. The reference considered procedures for both high- and low-aspect-ratio wings; however, because general aviation aircraft are concerned with high-aspect-ratio wings as defined by

$$A > \frac{3}{(C_1 + 1) \cos \Lambda_{le}} \quad (4.2-2)$$

where C_1 is given in figure 4.2-3 as a function of taper ratio, only the high-aspect-ratio data are presented.

For high-aspect-ratio, untwisted, constant section wings,

$$C_{L_{\max}} = \frac{C_{L_{\max}}}{c_{l_{\max}}} c_{l_{\max}} + \Delta C_{L_{\max}} \quad (4.2-3)$$

$$\alpha_{C_{L_{\max}}} = \frac{C_{L_{\max}}}{C_{L_{\alpha}}} + \alpha_0 + \Delta \alpha_{C_{L_{\max}}} \quad (4.2-4)$$

where, as functions of leading-edge sweep, Λ_{1e} , and leading-edge sharpness ratio, Δy (fig. 4.1-2),

$\frac{C_{L_{\max}}}{c_{l_{\max}}}$ is obtained from figure 4.2-4 for $M = 0.2$

$\Delta \alpha_{C_{L_{\max}}}$ is the angle-of-attack correction at $C_{L_{\max}}$ for flow separation from figure 4.2-5

$\Delta C_{L_{\max}}$ is the Mach number correction from figure 4.2-6

and where

$C_{L_{\alpha}}$ is the lift-curve slope obtained from equation (4.2-1) or figure 4.2-2

$c_{l_{\max}}$ is the section airfoil maximum lift coefficient obtained from section 4.1

α_0 is the zero-lift angle obtained from section 4.1

It should be noted that, on the basis of equation (4.2-3) and figures 4.2-4 and 4.2-6, $C_{L_{\max}}$ is not a function of wing area or aspect ratio.

Pertinent aspects of the calculation for the lift characteristics of the wing and horizontal tail of the subject airplane at wind-tunnel Mach conditions are summarized in table 4.2-1. The results were applied to the lift curves shown in figure 4.2-1. The fairings of the curves in figure 4.2-1 from the upper limits of linearity, α^* , to the stall angle of attack, $\alpha_{C_{L_{\max}}}$, were based on the stall characteristics of section

airfoils (section 4.1). Regardless of where the separation first appears on three-dimensional wings (inboard or tips), it is the type of separation on the section airfoil that determines the lift-curve shape near maximum lift. In figure 4.2-1, it is evident that rounding of the lift curves occurs near $C_{L_{\max}}$.

The shape of the lift curve beyond stall is not so easily approximated. Although reference 1 provided a technique for estimating the shape of the lift curve beyond stall, the technique could not be applied satisfactorily to the subject airplane. Thus, for the wing, the lift curve was terminated at maximum lift. However, because a study of the pitch characteristics of the subject airplane involved stalled regions of the tail, the shape of the horizontal-tail lift curve in the stalled region was estimated on the basis of a study of the stall characteristics of various tails in reference 9.

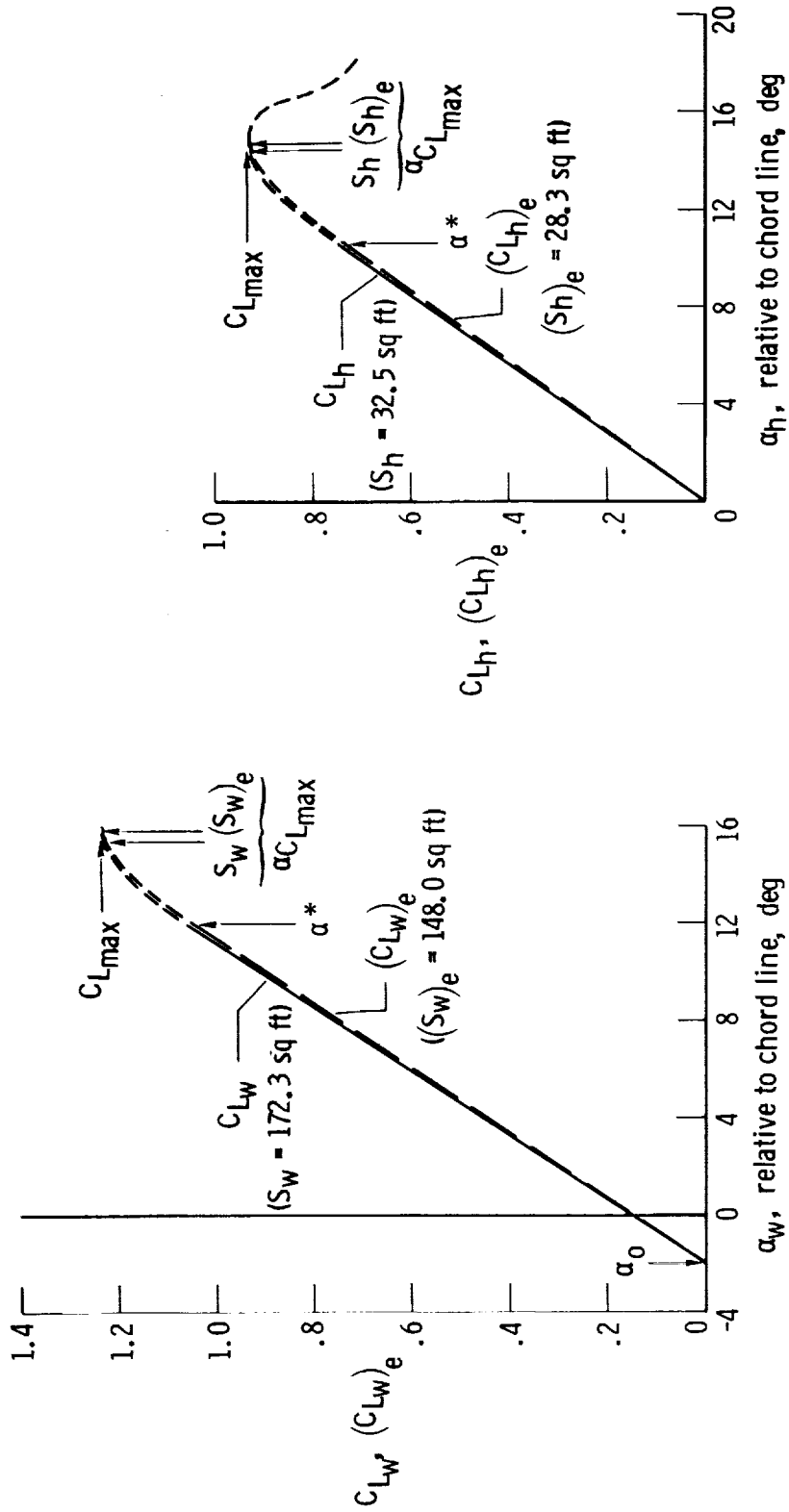
4.2.1 Symbols

A	aspect ratio
C_1	constant (from fig. 4.2-3) used in equation (4.2-2) defining high aspect ratio
C_L	lift coefficient of a finite surface at the subsonic Mach number considered
$C_{L_{\max}}$	maximum lift coefficient of a finite surface at the Mach number considered, obtained from equation (4.2-3)
$\frac{C_{L_{\max}}}{c_{l_{\max}}}$	maximum-lift-coefficient factor at $M = 0.2$, obtained from figure 4.2-4
$\Delta C_{L_{\max}}$	Mach number correction of the incompressible maximum lift coefficient, obtained from figure 4.2-6
$C_{L_{\alpha}}$	lift-curve slope of a finite surface at the Mach number considered, obtained from equation (4.2-1) or figure 4.2-2, per rad
$c_{l_{\max}}$	maximum section lift coefficient at incompressible ($M < 0.2$) conditions, obtained from section 4.1
$c_{l_{\alpha}}$	section lift-curve slope at incompressible ($M < 0.2$) conditions, obtained from section 4.1, per rad
$k = \frac{c_{l_{\alpha}}}{2\pi}$	
M	Mach number
S	planform surface area, sq ft
Δy	leading-edge-sharpness parameter as defined in section 4.1.1
α	angle of attack, rad or deg
α_0	angle of attack of surface for zero lift, deg

α^*	limit of linearity of the lift curve of a surface, deg
$\alpha_{C_{L_{\max}}}$	angle of attack of a surface at its $C_{L_{\max}}$, obtained from equation (4.2-4)
$\Delta\alpha_{C_{L_{\max}}}$	angle-of-attack correction at $C_{L_{\max}}$ for flow separation, obtained from figure 4.2-5, deg
$\beta = (1 - M^2)^{1/2}$	
Λ_{le}	sweep of the surface leading edge, deg
$\Lambda_{c/2}$	sweep of the surface midchord line, deg
λ	taper ratio of surface
Subscripts:	
e	exposed panel
h	horizontal tail
w	wing

TABLE 4.2-1
LIFT CHARACTERISTICS OF AIRPLANE WING AND HORIZONTAL TAIL

Symbol	Description	Reference	Wing		Horizontal tail	
			Total	Exposed panels	Total	Exposed panels
M β^2	Mach number $1 - M^2$	Wind-tunnel Mach number -----	0.083 .993	0.083 .993	0.083 .993	0.083 .993
A Λ_{le} Δy	Aspect ratio Leading-edge sweep, deg Leading-edge-sharpness parameter	Table 3.2-1 Table 3.2-1 Table 4.1-1	7.5 0 .0316	6.9 0 .0316	4.8 12 .021	4.4 12 .021
$c_{l\alpha}$ k $\frac{A}{k}(\beta^2 + \tan^2 \Lambda_{le})^{1/2}$ $\left(\frac{C_{L\alpha}}{A}\right)$ $C_{L\alpha}$	Section airfoil lift-curve slope, rad $c_{l\alpha}$ $\frac{2\pi}{A}$ Abscissa of figure 4.2-2 Ordinate of figure 4.2-2 $\left(\frac{C_{L\alpha}}{A}\right)$ A = slope at $M = 0.083$	Table 4.1-1 ----- Equation (4.2-1) Equation (4.2-1) -----	5.44 .865 8.68 .58 4.35 per rad .0759 per deg	5.44 .865 7.98 .62 4.28 per rad .0747 per deg	6.25 .995 4.85 .85 4.08 per rad .0711 per deg	6.25 .995 4.43 .91 4.01 per rad .0700 per deg
$c_{l_{max}}$ $\left(\frac{C_{L_{max}}}{c_{l_{max}}}\right)$ $\Delta C_{L_{max}}$ $C_{L_{max}}$	Section-airfoil maximum lift coefficient Maximum-lift-coefficient factor at $M = 0.2$ Mach number correction to $M = 0.083$ Maximum lift coefficient at $M = 0.083$	Table 4.1-1 Figure 4.2-4 Figure 4.2-6 Equation (4.2-3)	1.37 .90 0 1.23	1.37 .90 0 1.23	1.05 .89 0 .935	1.05 .89 0 .935
α_0 α^* $\left(\frac{C_{L_{max}}}{C_{L\alpha}}\right)$ $\Delta \alpha C_{L_{max}}$ $\alpha C_{L_{max}}$	Zero-lift angle of attack, deg Limit of linearity of lift curve, deg Maximum α for extended linearity conditions Correction for flow separation Angle of attack at $C_{L_{max}}$ at $M = 0.083$	Table 4.1-1 Table 4.1-1 ----- Figure 4.2-5 Equation (4.2-4)	-2.0 12.0 16.20° 1.30 15.5° relative to chord	-2.0 12.0 16.47° 1.30 15.77° relative to chord	0 10.6 13.14° 1.30 14.44° relative to chord	0 10.6 13.34° 1.30 14.64 relative to chord



(a) Wing.

(b) Horizontal tail.

Figure 4.2-1. Lift-curve slopes of wing and horizontal tail of the subject airplane.

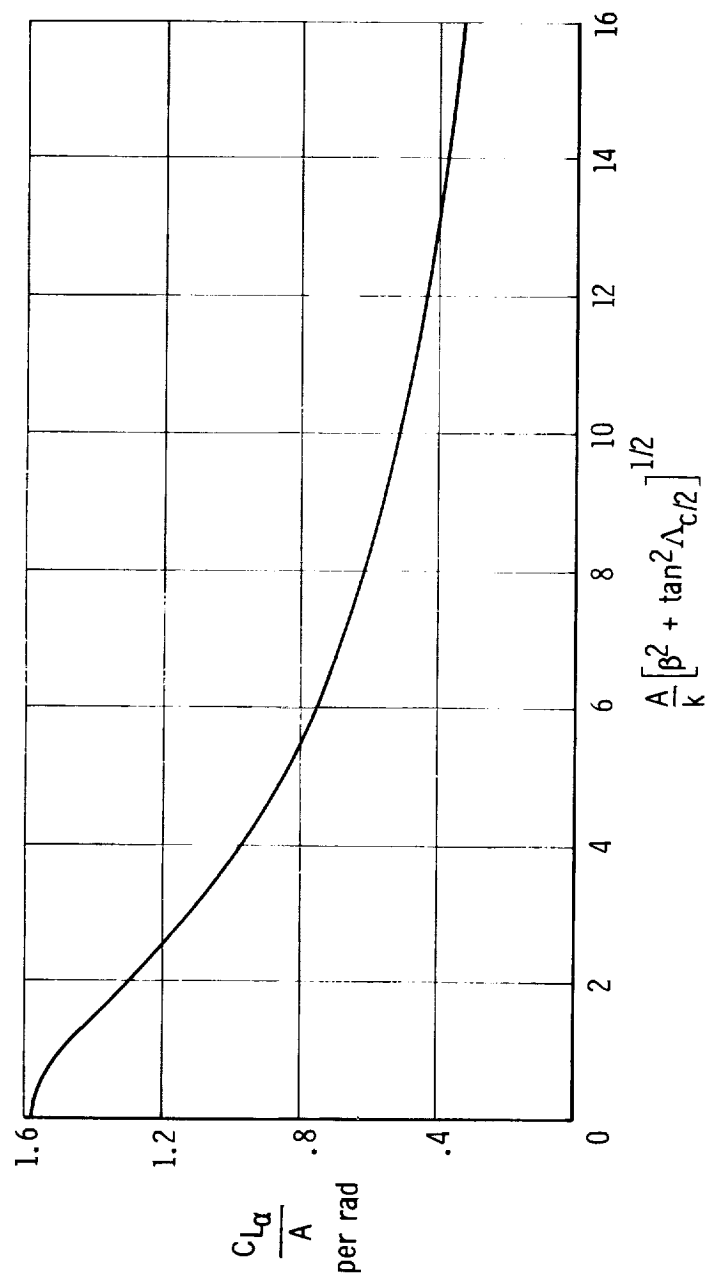


Figure 4.2-2. Subsonic wing lift-curve slope.

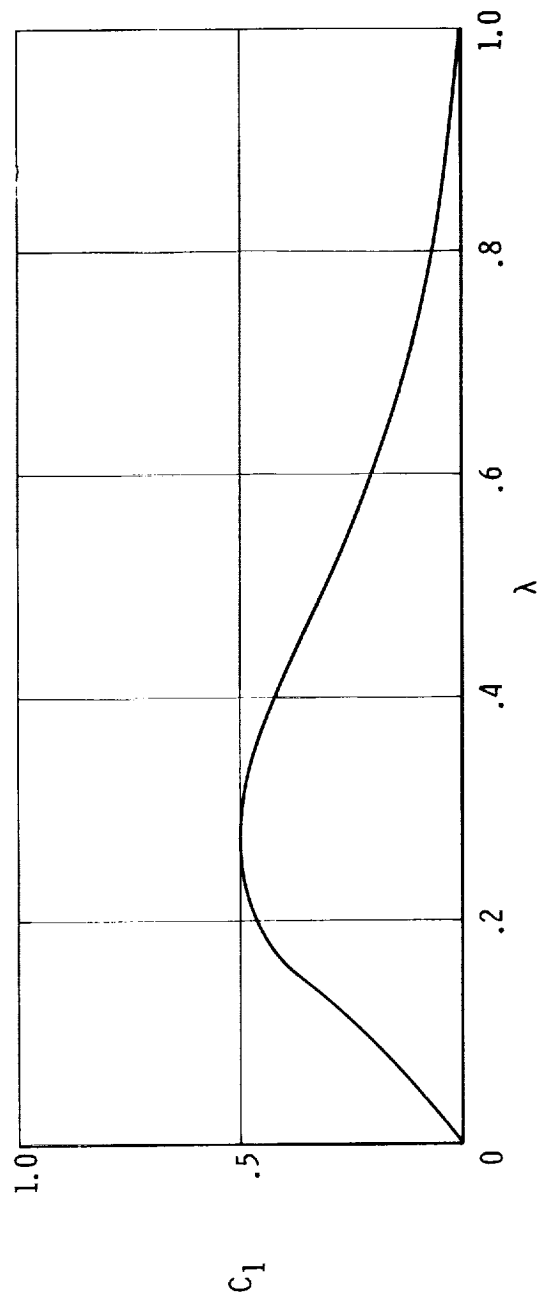


Figure 4.2-3. Taper ratio correction factor (ref. 1).

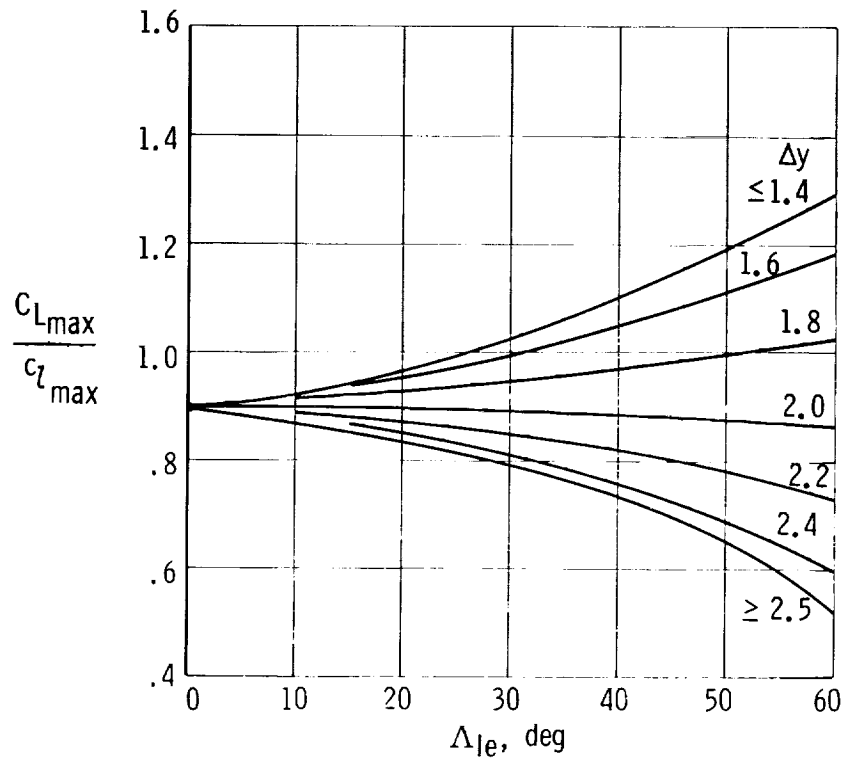


Figure 4.2-4. Subsonic maximum lift of high-aspect ratio, untwisted, constant airfoil section wings (ref. 1). $M \approx 0.2$.

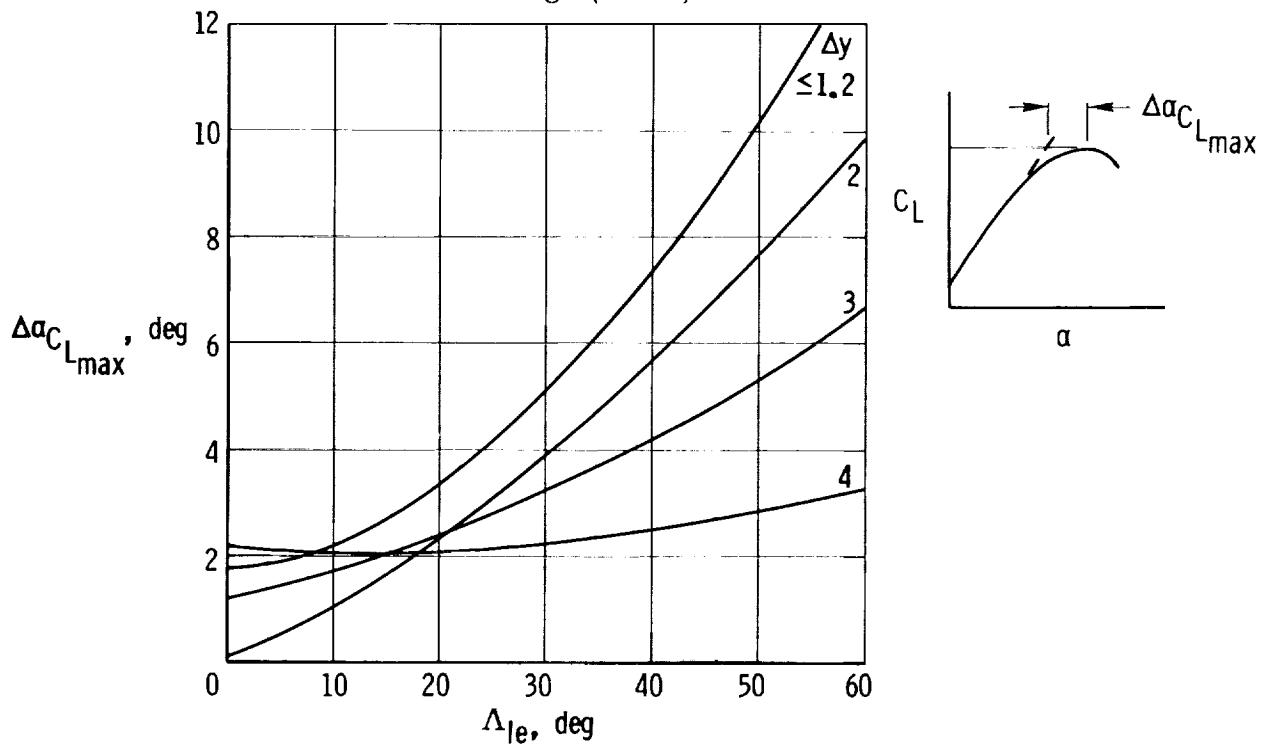


Figure 4.2-5. Angle-of-attack increment for subsonic maximum lift of high-aspect-ratio, untwisted, constant airfoil section wings (ref. 1). $M \approx 0.2$ to 0.6 .

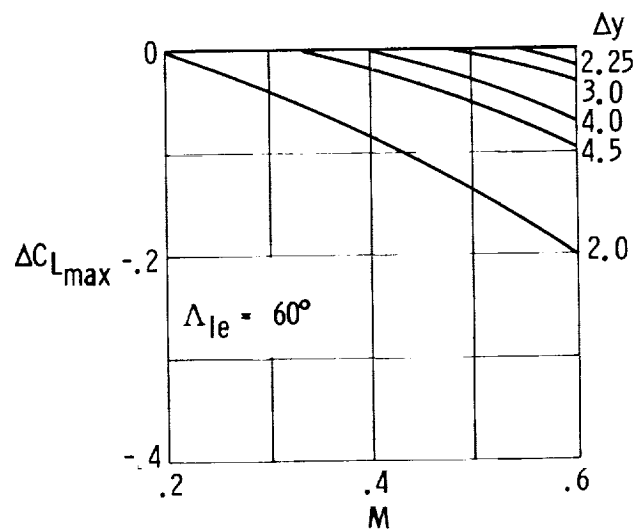
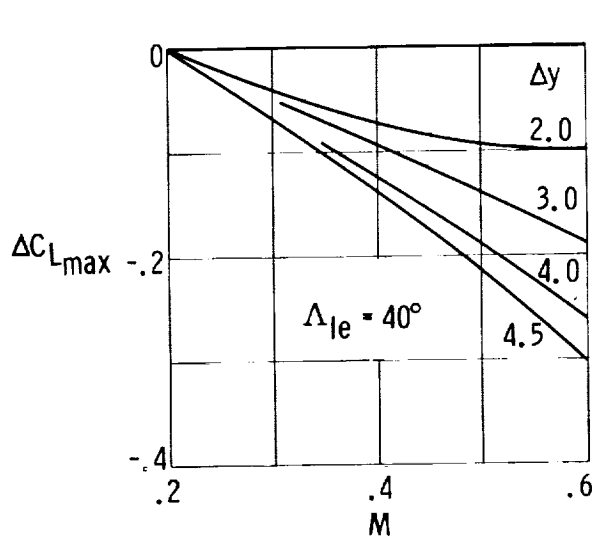
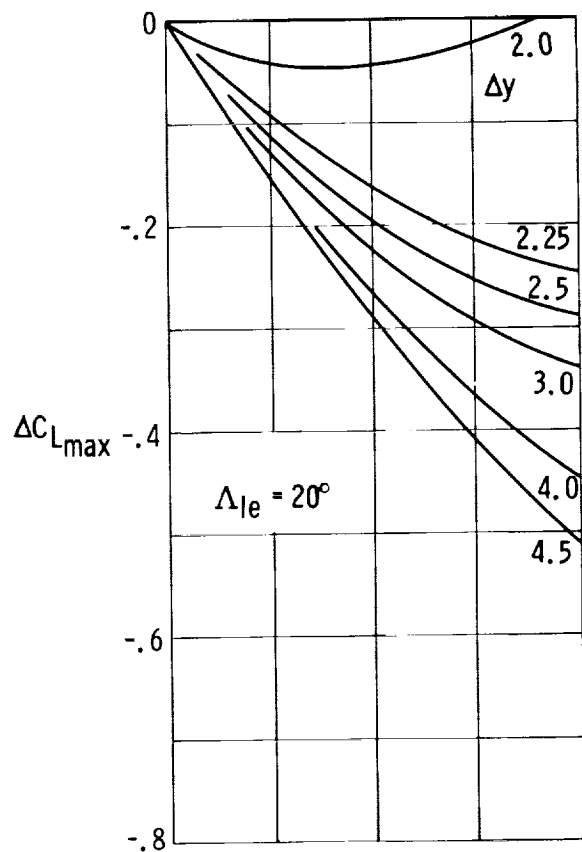
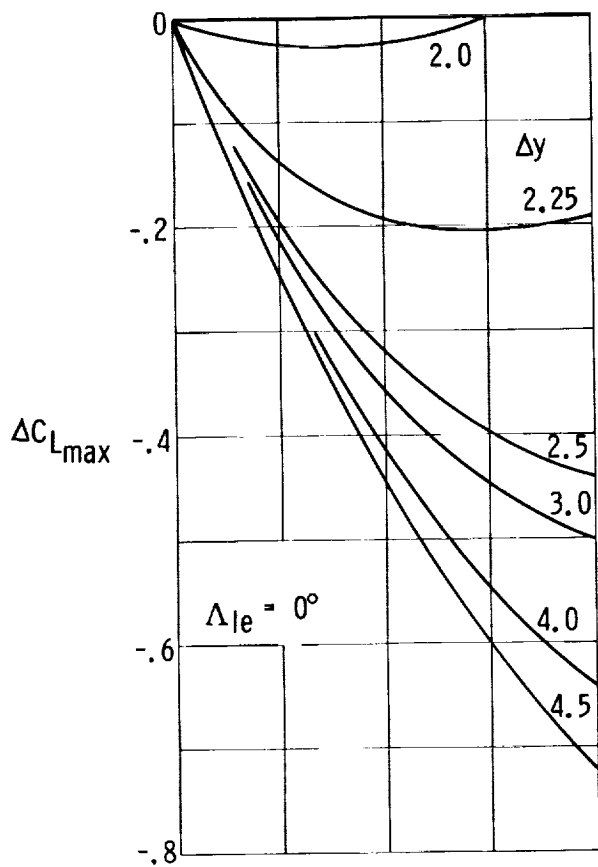


Figure 4.2-6. Mach number correction for subsonic maximum lift of high-aspect-ratio, untwisted, constant airfoil section wings (ref. 1).

4.3 Lift Due to Fuselage and Nacelles

Techniques for predicting the lift contribution of bodies assume that the normal forces acting on bodies of revolution at angles of attack consist of a linear combination of potential flow and viscous crossflow contributions. As indicated by reference 10, the normal forces acting on the forward or expanding portions of the bodies agree well with those predicted by potential theory, whereas poor agreement occurs for the aft or contracting portions where viscosity effects become more important. By assuming potential flow over only a forward portion of the body and viscous flow for the remainder of the body, reference 10 arrived at equations for lift, pitching moment, and drag of bodies which showed good correlation with experimental data for a number of bodies of revolution up to 16° to 18° angle of attack. The method of reference 10 is empirical only to the extent of the definition of the arbitrary longitudinal boundary between potential and viscous flow.

On the basis of reference 10, the lift coefficient of a body of revolution, based on the two-thirds power of the body volume, V_B , is obtained from the expression

$$C_{LB} = \overbrace{\frac{2\alpha_{B_{eff}}(k_2 - k_1)}{57.3(V_B)^{2/3}} \int_0^{x_0} \frac{dS_0}{dx} dx}^{\text{Potential flow}} + \overbrace{\frac{2\alpha_{B_{eff}}^2}{(57.3)^2(V_B)^{2/3}} \int_{x_0}^{l_B} \eta r c_{dc} dx}^{\text{Viscous flow}} \quad (4.3-1)$$

where

$(k_2 - k_1)$ is the apparent mass factor, and η is the drag proportionality factor, obtained from figures 4.3-1 and 4.3-2, respectively, as a function of body fineness ratio, $\frac{d_{max}}{l_B}$

c_{dc} is the steady-state crossflow drag coefficient for circular cylinders, a function of crossflow Mach number, M_c , obtained from figure 4.3-3

$\alpha_{B_{eff}}$ is the angle of attack of the equivalent body relative to its zero-lift line, degrees

x_0 is the limit of integration in feet (the arbitrary boundary between the two flows) determined from figure 4.3-4 as a function of $\frac{x_1}{l_B}$, where x_1 is the point at which the rate of change of the cross-section area, S_0 , with x , $\frac{dS_0}{dx}$, is a negative maximum

To simplify the application of equation (4.3-1), reference 1 considered the limit of integration, x_0 , to be determined by $\frac{x_1}{l_B}$, but with x_0 assumed to be the point at

which $\frac{dS_o}{dx}$ is a minimum, that is, x_1 is the point of maximum cross section. As a result of this simplifying assumption which results in slightly optimistic contributions of bodies,

$$C_{LB} \approx \frac{2\alpha_{B\text{eff}}(k_2 - k_1) S_{o\text{max}}}{57.3 (V_B)^{2/3}} + \frac{2\alpha_{B\text{eff}}^2}{(57.3)^2 (V_B)^{2/3}} \int_{x_0}^{l_B} \eta_{rc} d_c dx \quad (4.3-2)$$

which is the equation used in this report.

Because the equation for lift of bodies is based on bodies of revolution, it is necessary to replace the actual body of the airplane by an approximate equivalent body of revolution to serve as a mathematical model for analysis. This requires study of the profile as well as the plan-view outline of the body to arrive at the shape, based on judgment, which will provide the same lift characteristics. For the subject airplane, figure 4.3-5(a) shows the estimated equivalent circular fuselage in relation to the actual fuselage. It should be noted that the equivalent fuselage has a zero-lift angle 3° below the reference X-body axis. The nacelle, shown in figure 4.3-5(b), does not lend itself to such a simple estimate of equivalence because of its wide rectangular shape and irregular profile. As an approximation for equivalence, the cross-sectional area of an equivalent circular nacelle at any one point, x , was assumed to be equal to the actual cross-sectional area. The axis of the equivalent nacelle was assumed to be parallel to the X-body axis (reference axis of the airplane).

Table 4.3-1 lists the pertinent aspects of the calculations for the lift contributions of the fuselage and nacelles of the subject airplane as summarized by the following in terms of wing area ($S_w = 172.3$):

$$C_{L_f} + C_{L_n} = \left[\overbrace{0.00218(\alpha_B - 3) + 0.0000309(\alpha_B - 3)^2}^{\text{Fuselage}} \right] + \left[\overbrace{0.00160\alpha_B + 0.000010\alpha_B^2}^{\text{Nacelles}} \right] \quad (4.3-3)$$

where

α_B is the angle of attack of the airplane, relative to the body X-axis, deg

4.3.1 Symbols

C_{LB}	lift coefficient of the body (where body is a general term) referred to two-thirds power of the body volume or to the wing area as noted
C_{L_f}, C_{L_n}	lift coefficient of the body, C_{LB} , applied specifically to the fuselage and nacelle, respectively
c_{d_c}	steady-state crossflow drag coefficient, a function of crossflow Mach number, M_c , obtained from figure 4.3-3

d_{\max}	maximum diameter of an equivalent circular body, in.
$k_2 - k_1$	reduced mass factor from potential flow theory as listed in figure 4.3-1
l_B	body length, ft or in. as noted
l_f, l_n	body length, l_B , applied specifically to the fuselage and nacelle, respectively
M	Mach number
M_c	$M \sin \alpha_{B_{\text{eff}}}$
r	radius of an equivalent circular body at the body cross section being considered, in. or ft
S_o	cross-section area of an equivalent circular body, sq ft
$S_{o_{\max}}$	maximum cross-section area of an equivalent circular body, sq ft
S_w	reference wing area, sq ft
V_B	volume of an equivalent circular body, cu ft
V_f, V_n	body volume, V_B , applied specifically to the fuselage and nacelle, respectively
x_o	distance from the nose of the body to the point where potential flow ceases, in. or ft
x_1	distance from the nose of the body to the point of maximum negative rate of change of body cross-sectional area with body length, in. or ft
$dx, \Delta x$	increment length of the body, in. or ft
α_B	angle of attack of the actual body, synonymous to airplane angle of attack, α , using X-body axis as reference, deg
$\alpha_{B_{\text{eff}}}$	effective angle of attack of an equivalent circular body, $\alpha_B + \alpha_{o_B}$, deg
$\alpha_{f_{\text{eff}}}, \alpha_{n_{\text{eff}}}$	effective angle of attack, $\alpha_{B_{\text{eff}}}$, applied specifically to the fuselage and nacelle, respectively
α_{o_B}	zero-lift angle of an equivalent circular body relative to the reference X-body axis of the airplane, deg
α_{o_f}	zero-lift angle, α_{o_B} , applied specifically to the fuselage
η	drag proportionality factor from figure 4.3-2

TABLE 4.3-1

CONTRIBUTION OF FUSELAGE AND NACELLES TO AIRPLANE LIFT COEFFICIENT

Symbol	Description	Reference	Two nacelles	
			Fuselage	Nacelle
$C_{L_f} + C_{L_n}$	$= \left[\frac{2(k_2 - k_1)(S_o)_{\max}}{57.3 V_f^{2/3}} \alpha_{\text{eff}} + \frac{2\alpha_{\text{eff}}^2 \pi c_{d_c}}{(57.3)^2 V_f^{2/3} x_o} \right] \frac{l_f}{r\Delta x} \frac{V_f^{2/3}}{S_w} + 2 \left[\frac{2(k_2 - k_1)(S_o)_{\max}}{57.3 V_n^{2/3}} \alpha_{\text{eff}} + \frac{2\alpha_{\text{eff}}^2 \pi c_{d_c}}{(57.3)^2 V_n^{2/3} x_o} \right] \frac{l_n}{r\Delta x} \frac{V_n^{2/3}}{S_w}$			
M	Mach number	Wind-tunnel Mach number		
d_{\max}	Maximum diameter of equivalent circular body, in.	Figure 4.3-5	0.083	0.083
$S_{o_{\max}}$	$\frac{4(144)}{\pi d_{\max}^2}$, sq ft	-----	49.0	31.0
x_1	Location of $S_{o_{\max}}$ from nose of body, in.	Figure 4.3-5	12.56	5.25 per nacelle
l_B	Body length, in.	Figure 4.3-5	109	40
V_B	Volume of equivalent circular body, cu ft	-----	290	106
$(V_B)^{2/3}$	-----	-----	≈ 172	≈ 21.3 per nacelle
l_B	-----	-----	31	7.8 per nacelle
$\frac{l_B}{d_{\max}}$	Fineness ratio	-----	5.92	3.42
$(k_1 - k_2)$	Reduced mass factor	Figure 4.3-1	.86	.75
η	Ratio of drag coefficient of finite to infinite length cylinders	Figure 4.3-2	.635	.590
$\frac{x_1}{l_B}$	-----	-----		
x_o	Location, from nose, where potential flow ceases	Figure 4.3-4	0.376	0.378
$\frac{l_B}{l_B}$	$\left(\frac{x_o}{l_B} \right) l_B$, in.	-----	.575	.575
$\frac{1}{144} \int_{x_o}^{l_B} r dx$	$\frac{1}{144} \sum_{x_o}^{l_B} r \Delta x$ = half of projected area of equivalent circular body from x_o to end, sq ft	-----	167	61
α_{o_B}	Zero-lift angle of equivalent circular body relative to airplane x_B reference axis, deg	Figure 4.3-5	≈ 11.5	≈ 2.0 per nacelle
$\alpha_{B_{\text{eff}}}$	Angle of attack of equivalent body, $\alpha_B + (\alpha_o)_B$, deg	-----	-3.0	≈ 0
M_C	$M \sin \alpha_{B_{\text{eff}}}$	-----	$\alpha_B - 3$	α_B
c_{d_c}	Crossflow drag coefficient of infinite length cylinder	Figure 4.3-3	.083 $\sin (\alpha_B - 3)$ $a_{1.2}$.083 $\sin \alpha_B$ $a_{1.2}$
Summary (based on $S_w = 172.3$ sq ft): $C_{L_f} + C_{L_n} = \left[0.00218 (\alpha_B - 3) + 0.0000309(\alpha_B - 3)^2 \right] + \left[0.00160\alpha_B + 0.000010\alpha_B^2 \right]$				

^a c_{d_c} is constant for the M_C range involved.

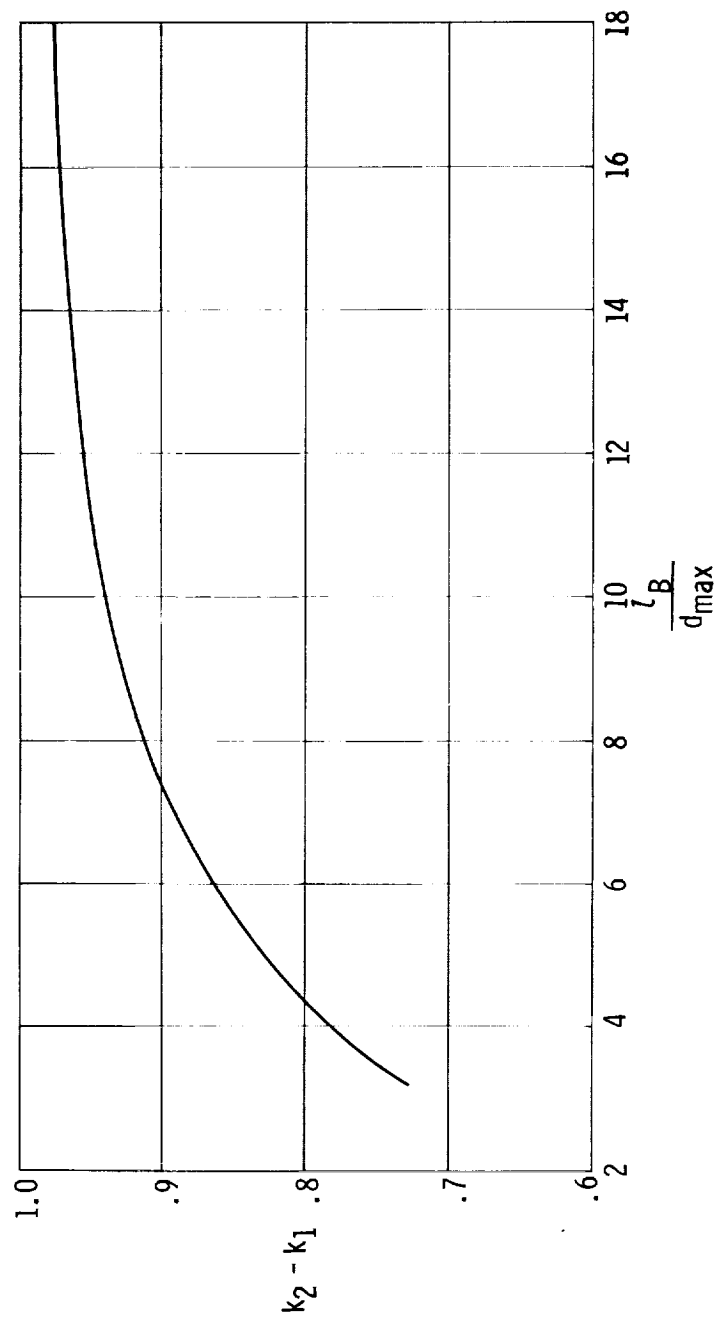


Figure 4.3-1. Apparent mass factor to be used in calculating the forces and moments of bodies of revolution (ref. 10).

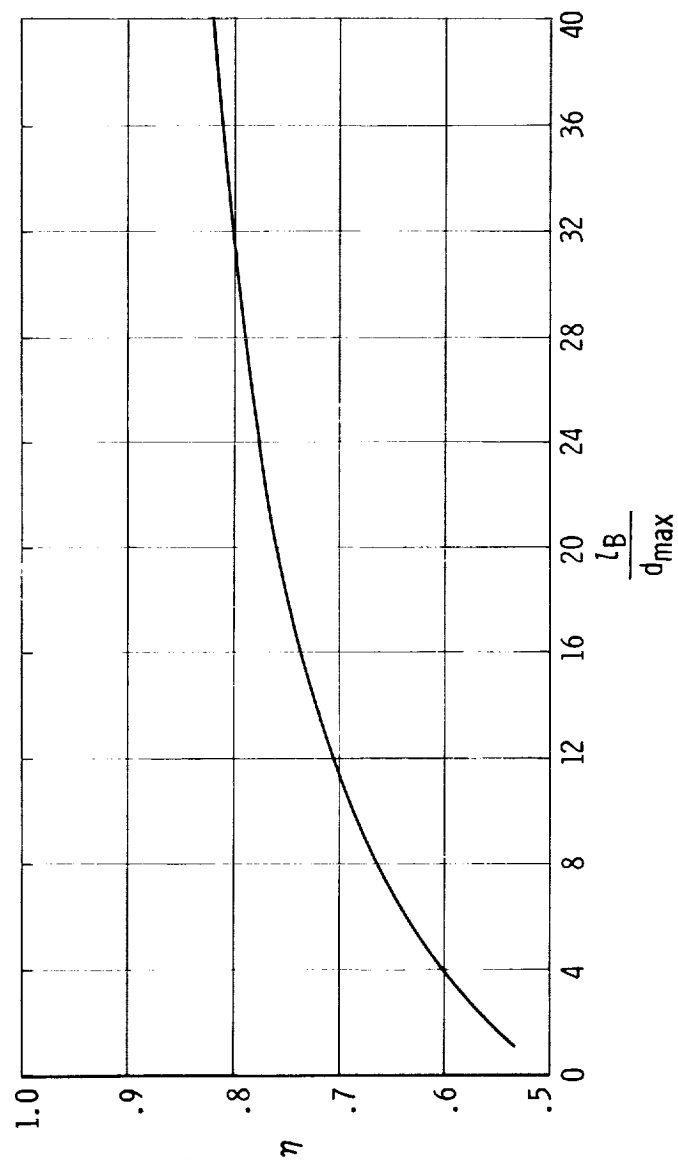


Figure 4.3-2. Ratio of the drag coefficient of a circular cylinder of finite length to that of a cylinder of infinite length as a function of the fineness ratio (ref. 10).

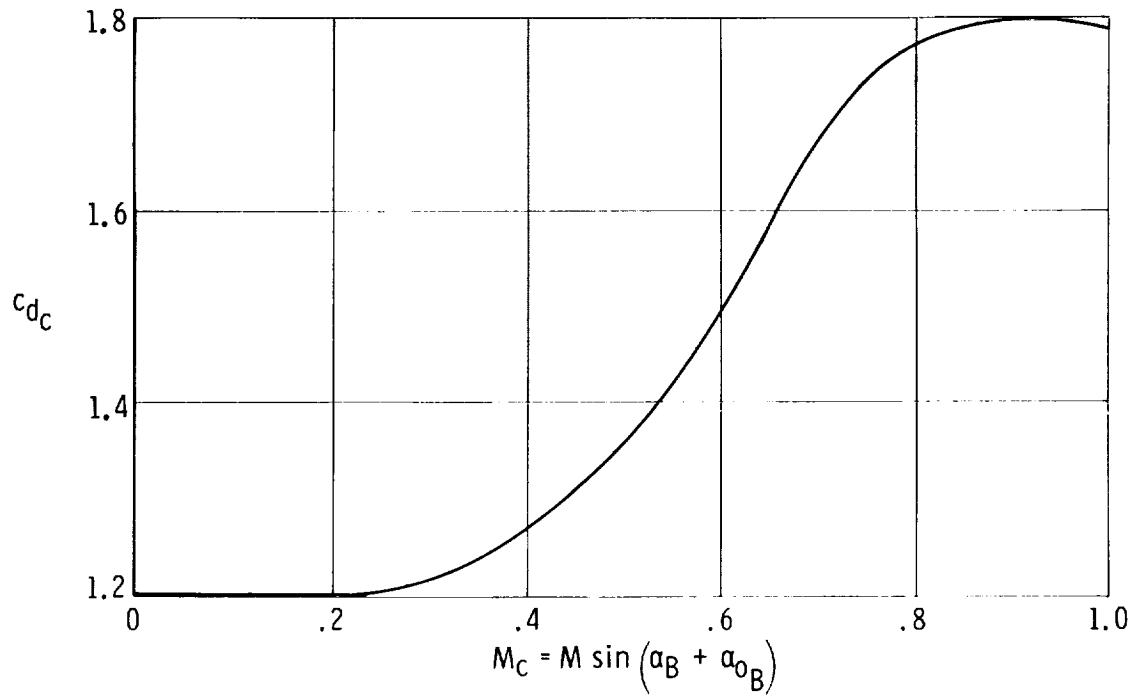


Figure 4.3-3. Steady-state crossflow drag coefficient for circular cylinders (two dimensional).

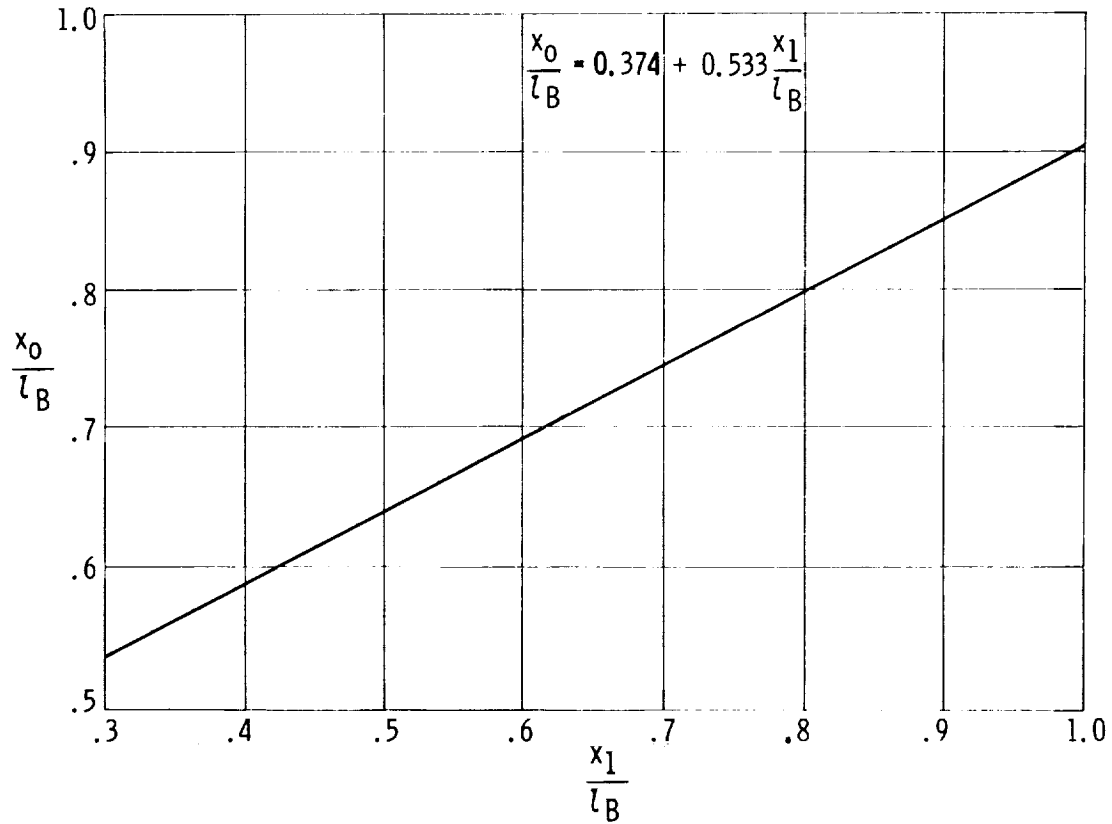
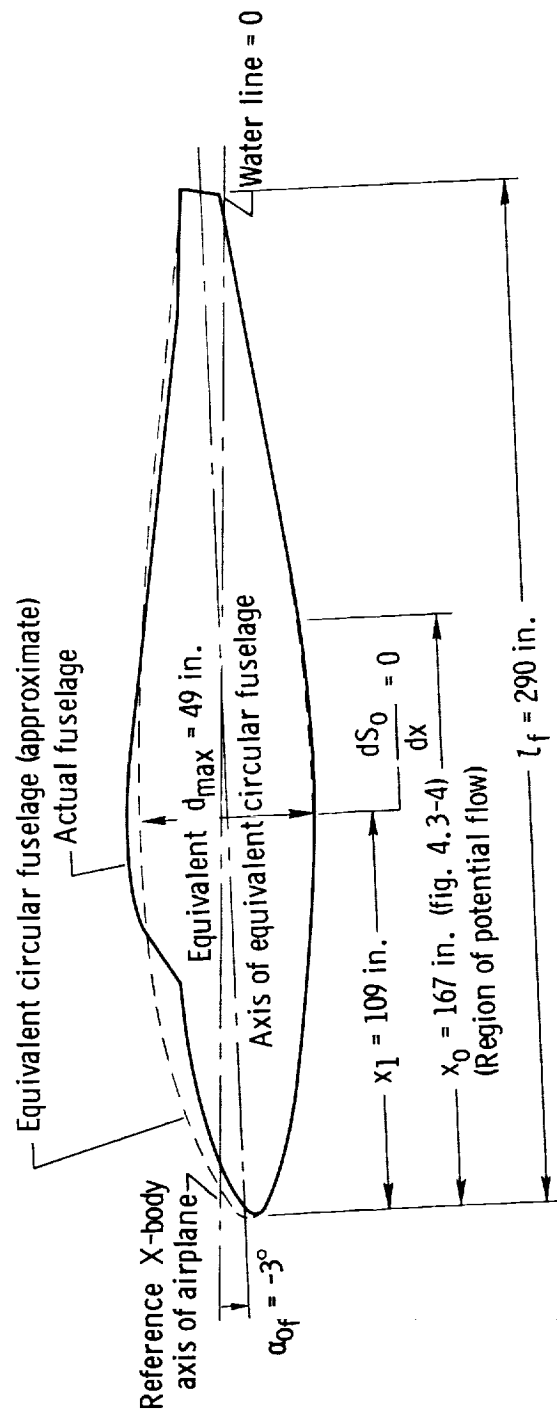
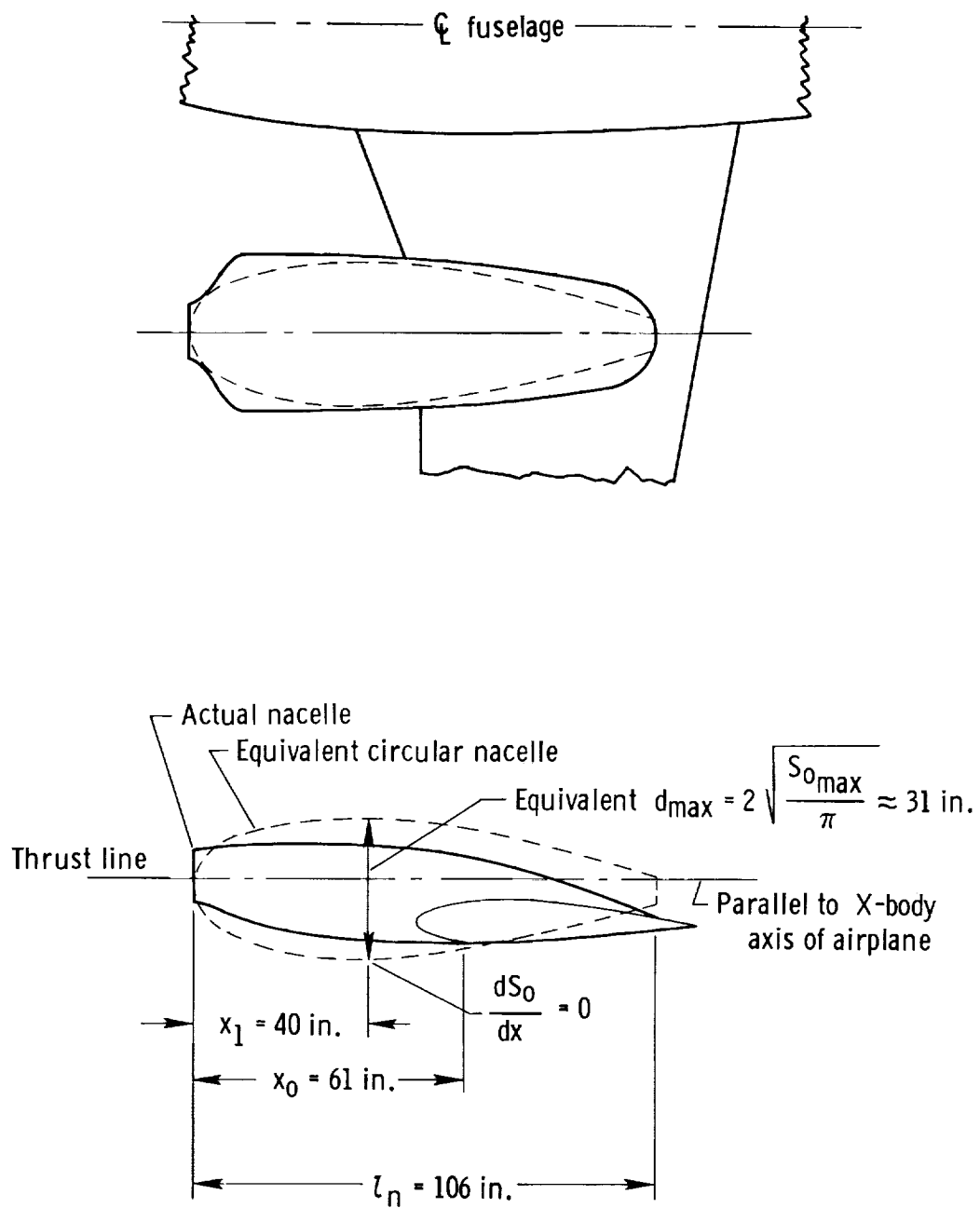


Figure 4.3-4. Extent of applicability of potential theory as a function of the maximum negative rate of change of body cross-sectional area with body length (ref. 10).



(a) Fuselage.

Figure 4.3-5. Pertinent geometric parameters of approximated equivalent circular fuselage and nacelles for estimating lift of the bodies.



(b) Nacelle.

Figure 4.3-5. Concluded.

4.4 Lift Due to Combined Wing-Fuselage-Nacelle

The addition of a body to a wing results in mutual interference effects. Lift of the wing-body combination is influenced by the body upwash effect on wing lift and the lift carryover of wing panel loading onto the body. Net wing upwash and downwash effects on the body influence body pitching moments primarily. Symmetrical body vortices which result from flow separation just behind or above the area of minimum pressure along the side of the body near the nose are normally negligible for most airplane types of wing-body combinations.

The lift of the wing-fuselage-nacelle combination accounting for the mutual interference effects of wing and fuselage may be estimated from

$$C_{L_{wfn}} = C_{L_f} + C_{L_n} + [K_{w(f)} + K_{f(w)}] (C_{L_\alpha})_{w_e} \alpha_{w_{abs}} \frac{S_{w_e}}{S_w} \quad (4.4-1)$$

where

C_{L_f} is the fuselage lift from equation (4.3-3)

C_{L_n} is the nacelle lift from equation (4.3-3)

$K_{w(f)}$ is the ratio of the lift on the wing in the presence of the body to the lift on an isolated wing, obtained from figure 4.4-1 and reference 11

$K_{f(w)}$ is the ratio of wing lift carryover onto the body to wing lift alone, obtained from figure 4.4-1

$(C_{L_\alpha})_{w_e}$ is the lift-curve slope of the exposed wing panels, obtained from table 4.2-1

$\alpha_{w_{abs}}$ is the absolute angle of attack of the wing, equal to $\alpha + i_w - \alpha_{O_w}$

Because of the lack of suitable data, the interference effects of the nacelles are not accounted for.

The use of the interference factors, $K_{w(f)}$ and $K_{f(w)}$, from reference 11 is restricted to wings which do not have sweptback trailing edges or sweptforward leading edges. The factors were obtained for wings mounted as midwings on bodies of revolution but have been used for other configurations.

For the subject airplane, the lift of the wing in the presence of the body and the carryover of the wing lift onto the body is calculated in table 4.4-1(a) to be equal to

$$C_{L_{w(f)+f(w)}} = 0.079(\alpha + 4) \text{ (referenced to } S_w = 172.3 \text{ sq ft)} \quad (4.4-2)$$

The net lift of the wing, fuselage, and nacelle combination in the linear lift range is obtained by summarizing the fuselage and nacelle contributions as obtained from table 4.3-1 and the lift of the wing in the presence of the body as obtained from table 4.4-1(a). Thus

$$C_{L_{wfn}} = C_{L_f} + C_{L_n} + C_{L_{w(f)+f(w)}} \\ = [0.00218(\alpha - 3) + 0.0000309(\alpha - 3)^2] + [0.00160\alpha + 0.000010\alpha^2] + 0.079(\alpha + 4) \quad (4.4-3)$$

The addition of a body to the wing in most airplane configurations tends to decrease the maximum lift coefficient and corresponding angle of attack, although an increase in the geometric stall angle is possible in some circumstances. The wing planform is a primary consideration. In the absence of theoretical methods, reference 1 devised empirical relations for predicting maximum lift coefficient, $(C_{L_{max}})_{wf}$,

and corresponding stall angle, $(\alpha C_{L_{max}})_{wf}$, for wing-body combinations up to

$M = 0.6$. The method uses an empirical taper ratio correction factor, c_2 (fig. 4.4-2), in determining, in the following equations, the empirical correction factors,

$\frac{(C_{L_{max}})_{wf}}{(C_{L_{max}})_w}$ and $\frac{(\alpha C_{L_{max}})_{wf}}{(\alpha C_{L_{max}})_w}$, from figure 4.4-3 as functions of $(c_2 + 1)A \tan \Lambda_{le}$

and the ratio of the fuselage diameter to the wing span, $\frac{d}{b}$:

$$(C_{L_{max}})_{wf} = \left[\frac{(C_{L_{max}})_{wf}}{(C_{L_{max}})_w} \right] (C_{L_{max}})_w \quad (4.4-4)$$

and

$$(\alpha C_{L_{max}})_{wf} = \left[\frac{(\alpha C_{L_{max}})_{wf}}{(\alpha C_{L_{max}})_w} \right] (\alpha C_{L_{max}})_w \quad (4.4-5)$$

where

$(C_{L_{max}})_w$ and $(\alpha C_{L_{max}})_w$ (the absolute stall angle from zero lift) are for total wing alone from section 4.2

Pertinent aspects of the calculations for $(C_{L_{max}})_{wf}$ and $(\alpha C_{L_{max}})_{wf}$ for the subject airplane are listed in table 4.4-1(b).

The net lift of the wing-fuselage-nacelle combination for the subject airplane in terms of a reference wing area of 172.3 square feet (reference area of analysis) and

178.0 square feet (reference area of wind-tunnel data) is summarized in table 4.4-2. The results for a wing area of 178.0 square feet are plotted and compared with wind-tunnel data in figure 4.4-4. The fairing from the limit of linearity to the maximum lift coefficient was performed in the same manner as for the wing alone (section 4.2).

In summary, the lift contributions attributed to the fuselage and nacelle crossflow effects are insignificant. The contributions due to the potential-flow effects on the fuselage and nacelles are negligible for preliminary estimates but are large enough to be significant for refined estimates. Although these fuselage contributions may be negligible or small for lift considerations, they are not necessarily negligible with regard to pitching-moment considerations, as discussed in section 4.8.

4.4.1 Symbols

A	wing aspect ratio
b	wing span, ft
C_{L_f}	lift coefficient of the fuselage based on the wing area
$(C_{L_{\max}})_w$	maximum lift coefficient of the wing alone, obtained from table 4.2-1
$(C_{L_{\max}})_{wf}$	maximum lift coefficient of the wing-fuselage combination, obtained from figure 4.4-3
C_{L_n}	lift coefficient of the nacelles based on wing area
$C_{L_{w(f)+f(w)}}$	lift coefficient of the wing including mutual wing-fuselage interference effects
$C_{L_{wfn}}$	lift coefficient of the wing-fuselage-nacelle assembly
$(C_{L_\alpha})_{w_e}$	lift-curve slope of the exposed wing panels, obtained from table 4.2-1, per deg
c_2	taper ratio correction factor from figure 4.4-2
d	fuselage width at the wing, ft
i_w	wing incidence, angle between the wing chord and reference X-body axis, deg
$K_{f(w)}$	ratio of wing lift carryover on the fuselage to the wing alone, obtained from figure 4.4-1
$K_{w(f)}$	ratio of the lift on the wing in the presence of the fuselage to the wing alone, obtained from figure 4.4-1
M	Mach number

S_w	reference wing area, sq ft
S_{we}	area of the exposed wing panels, sq ft
α	angle of attack relative to the reference X-body axis, deg
$\left(\alpha_{C_{L_{\max}}}\right)_w$	stall angle of attack of the wing alone relative to the zero-lift line of the wing, deg
$\left(\alpha_{C_{L_{\max}}}\right)_{wf}$	stall angle of attack of the wing-fuselage combination relative to the zero-lift line of wing, deg
α_{ow}	wing zero-lift angle of attack relative to the wing chord, deg
$\alpha_{w_{abs}}$	wing angle of attack relative to the wing zero-lift line, $\alpha - \alpha_{ow} + i_w$, deg
Λ_{le}	sweep of the wing leading edge, deg
λ	wing taper ratio

TABLE 4.4-1
WING LIFT OF AIRPLANE INCLUDING MUTUAL WING-FUSELAGE INTERFERENCE

(a) In linear range

$$C_{L_{W(f)+f(w)}} = \left[K_{W(f)} + K_{f(w)} \right] (C_{L_{\alpha}})_{w_e} \alpha_{w_{abs}} \frac{S_{w_e}}{S_w}$$

Symbol	Description	Reference	Magnitude
d	Fuselage width at wing, ft	Figure 3.2-1	4.0
b	Wing span, ft	Figure 3.2-1	36.0
S_w	Reference wing area, sq ft	Table 3.2-1	172.3
S_{w_e}	Area of exposed wing panels, sq ft	Table 3.2-1	148.0
α_{0w}	Zero-lift angle of attack relative to wing chord, deg	Table 4.2-1	-2.0
i_w	Wing incidence relative to X-body axis, deg	Table 3-1	2.0
$\alpha_{w_{abs}}$	Wing angle of attack relative to zero lift, $\alpha - \alpha_{0w} + i_w$, deg	-----	$\alpha + 4$
$(C_{L_{\alpha}})_{w_e}$	Lift-curve slope of exposed wing panels per deg	Table 4.2-1	.0747
$\frac{d}{b}$	Fuselage-width to wing-span ratio	-----	0.111
$K_{W(f)}$	Ratio of lift on wing in presence of fuselage to wing alone	Figure 4.4-1	1.09
$K_{f(w)}$	Ratio of wing lift carryover on fuselage to wing alone	Figure 4.4-1	.14
Summary: $C_{L_{W(f)+f(w)}} = 0.079(\alpha + 4)$			

(b) Maximum lift of wing with mutual wing-body interference

$$(C_{L_{max}})_{wf} = \left[\frac{(C_{L_{max}})_{wf}}{(C_{L_{max}})_w} \right] (C_{L_{max}})_w ; (\alpha C_{L_{max}})_{wf} = \left[\frac{(\alpha C_{L_{max}})_{wf}}{(\alpha C_{L_{max}})_w} \right] (\alpha C_{L_{max}})_w$$

Symbol	Description	Reference	Magnitude
λ	Wing taper ratio	Table 3.2-1	0.513
c_2	Taper ratio correction factor	Figure 4.4-2	.103
Λ_{le}	Leading-edge sweep of wing, deg	Table 3.2-1	0
A	Wing aspect ratio	Table 3.2-1	7.5
$(c_2 + 1)A \tan \Lambda_{le}$	-----	-----	0
$\frac{d}{b}$	-----	-----	.111
$\left[\frac{(C_{L_{max}})_{wf}}{(C_{L_{max}})_w} \right]$	Ratio of $C_{L_{max}}$ of wing-fuselage to wing alone	Figure 4.4-3	1.0
$\left[\frac{(\alpha C_{L_{max}})_{wf}}{(\alpha C_{L_{max}})_w} \right]$	Ratio of stall angle of wing-fuselage to wing alone	Figure 4.4-3	1.025
$(C_{L_{max}})_w$	Maximum lift coefficient of wing alone	Table 4.2-1	1.23
$(\alpha C_{L_{max}})_w$	Stall angle of wing alone relative to zero lift, deg	Table 4.2-1	$15.5 + 2 = 17.5$
Summary: $(C_{L_{max}})_{wf} = 1.23$; $(\alpha C_{L_{max}})_{wf} = 17.8$			

TABLE 4.4-2
SUMMARY OF WING-FUSELAGE-NACELLE LIFT

$$C_{L_{wfn}} = [0.00218(\alpha - 3) + 0.0000309(\alpha - 3)^2] + [0.00160\alpha + 0.000010\alpha^2] + 0.079(\alpha + 4)$$

①	②	③	④	⑤	⑥	⑦	⑧	⑨
α relative to body X-axis, deg	α_{wabs} relative to wing zero lift = $\alpha + 4$, deg	C_{L_f} (eq. (4.4-3) based on $S_w = 172.3$ sq ft) Potential flow = $0.00218(1 - 3.0)$	C_{L_n} (eq. (4.4-3) based on $S_w = 172.3$ sq ft) Potential flow = $0.00160(1)$	C_{L_n} (eq. (4.4-3) based on $S_w = 172.3$ sq ft) Crossflow = $0.000031(1 - 3.0)^2$	C_{L_n} (eq. (4.4-3) based on $S_w = 172.3$ sq ft) Crossflow = $0.000010(1)^2$	$[K_{w(f)} + K_{r(w)}](C_{L_n})_{w_e} \frac{\alpha_{wabs}}{S_w}$ = $0.079(2)$ (eq. (4.4-2) based on $S_w = 172.3$ sq ft)	$C_{L_{wfn}}$ = $(3) + (4) + (5)$ + $(6) + (7)$ on basis of $S_w = 172.3$ sq ft	$C_{L_{wfn}}$ = $0.968(9)$ on basis of $S_w = 178$ sq ft
-4	0	-0.01526	0.00152	-0.00640	0.00016	0	-0.01998	-0.0194
-2	2	-0.01090	0.000775	-0.00320	0.00004	.158	.147	.140
0	4	-0.00654	0.000279	0	0	.316	.310	.300
2	6	-0.00218	0.000031	.00320	.00004	.474	.475	.460
4	8	.00218	0.000031	.00640	.00016	.632	.641	.620
6	10	.00654	0.000279	.00960	.00036	.790	.807	.781
8	12	.01090	0.000775	.01280	.00064	.949	.973	.942
10	14	.01526	0.00152	.01600	.00100	1.106	1.140	1.104
12	16	.01962	0.00251	.01920	.00144	----- (nonlinear range)	-----	-----
13.8	17.8	.02354	.00366	.02210	.00190	a 1.23	1.281	b 1.280

^a $(\alpha_{C_{L_{max}}})_{wf} = 17.8^\circ$ relative to zero-lift line of wing (table 4.4-1(b)); $C_{L_{max}}$ of wing with mutual wing-body interference = 1.23 (table 4.4-1(b)).

^b $(C_{L_{max}})_{wfn}$ on basis of ($S_w = 178$ sq ft) = $[C_{L_f} + C_{L_n}] \left(\frac{S_w = 172.3}{S_w = 178.0} \right) + [C_{L_{max}} \text{ in column (7)}]$

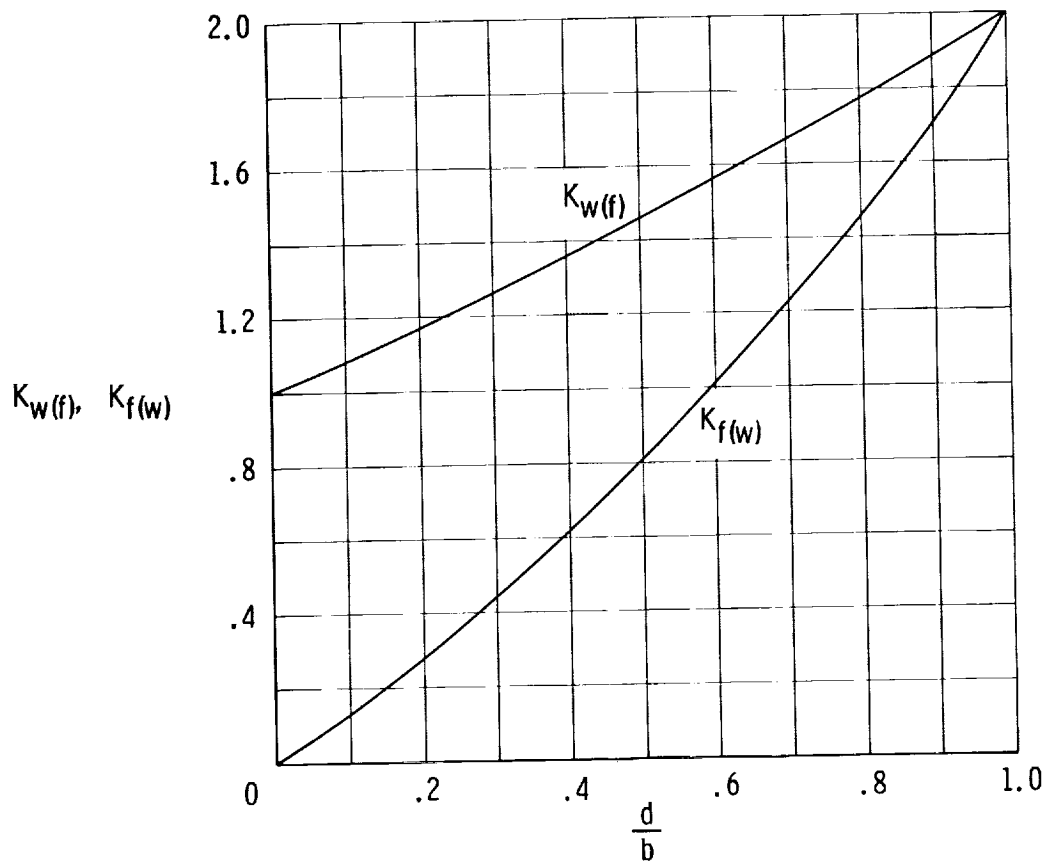


Figure 4.4-1. Lift ratios $K_{w(f)}$ and $K_{f(w)}$ based on slender-body theory with the wing at fixed incidence relative to the fuselage (ref. 11). Applicable at all speeds.

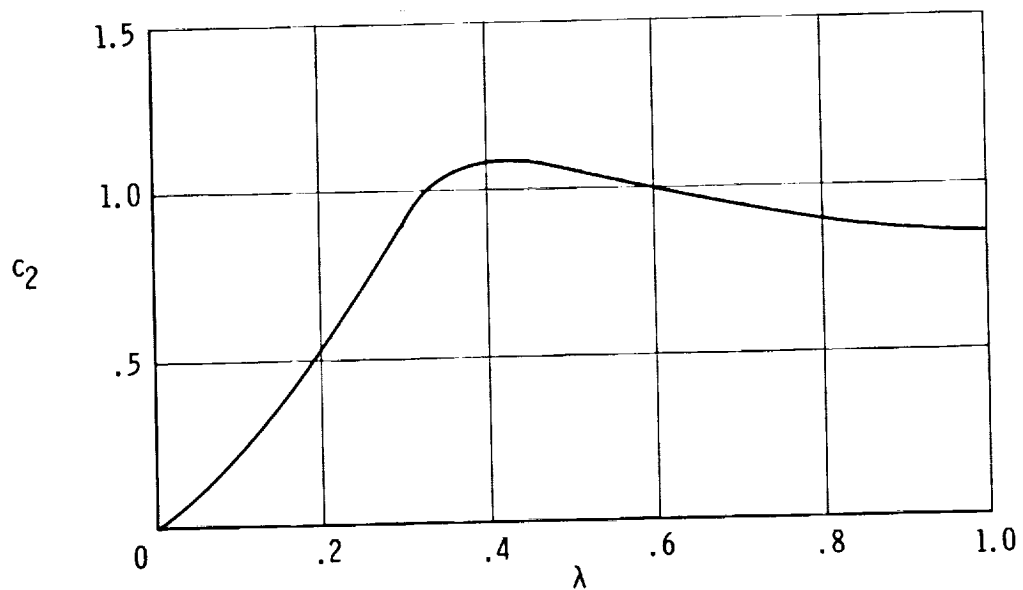


Figure 4.4-2. Taper ratio correction factors (ref. 1).

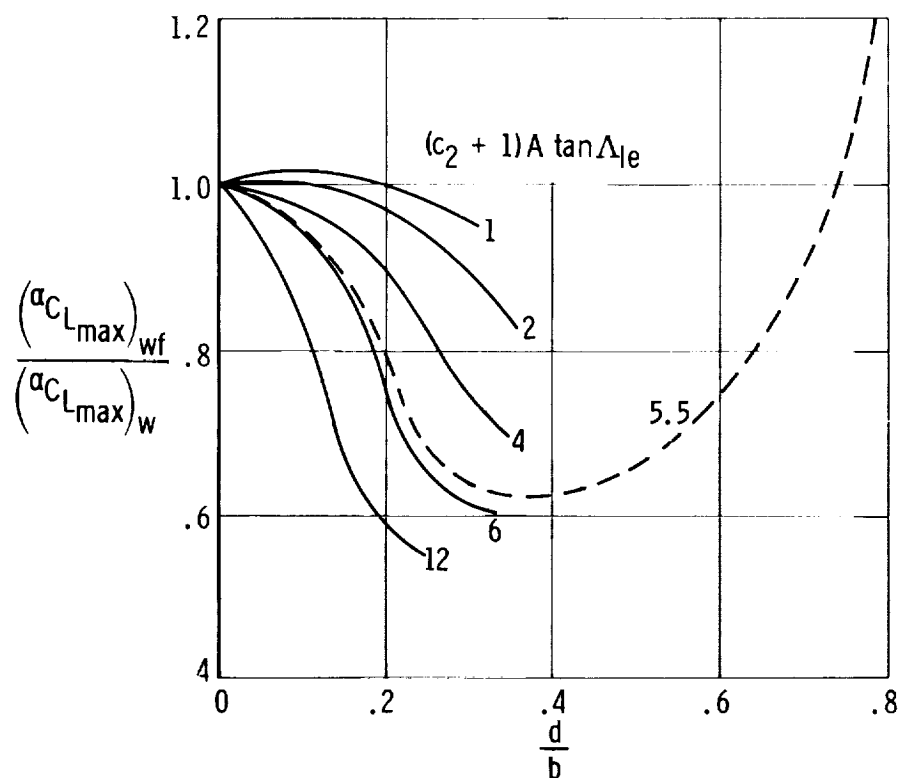
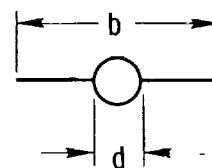
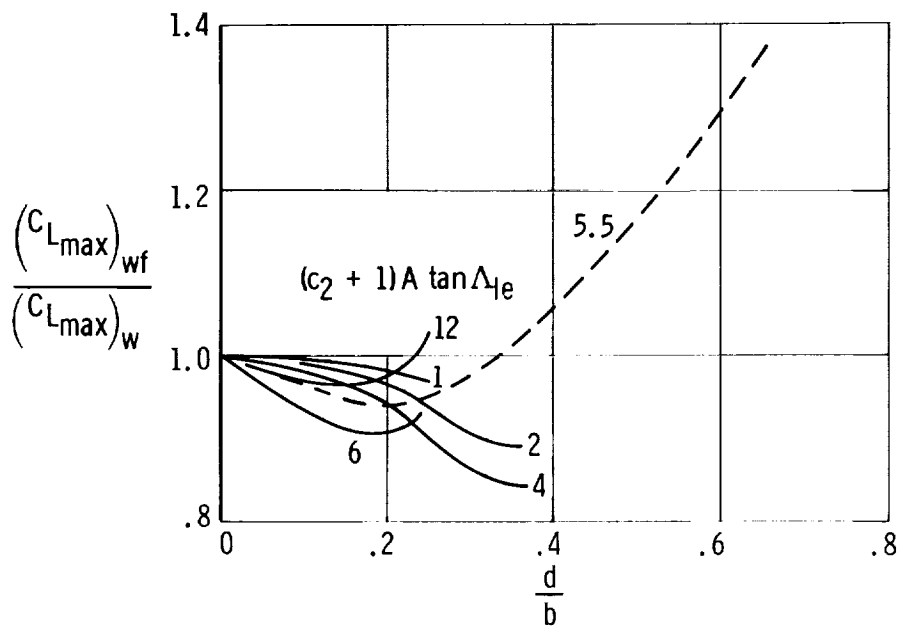


Figure 4.4-3. Wing-body maximum lift and angle of attack for maximum lift below $M = 0.6$ (ref. 1).

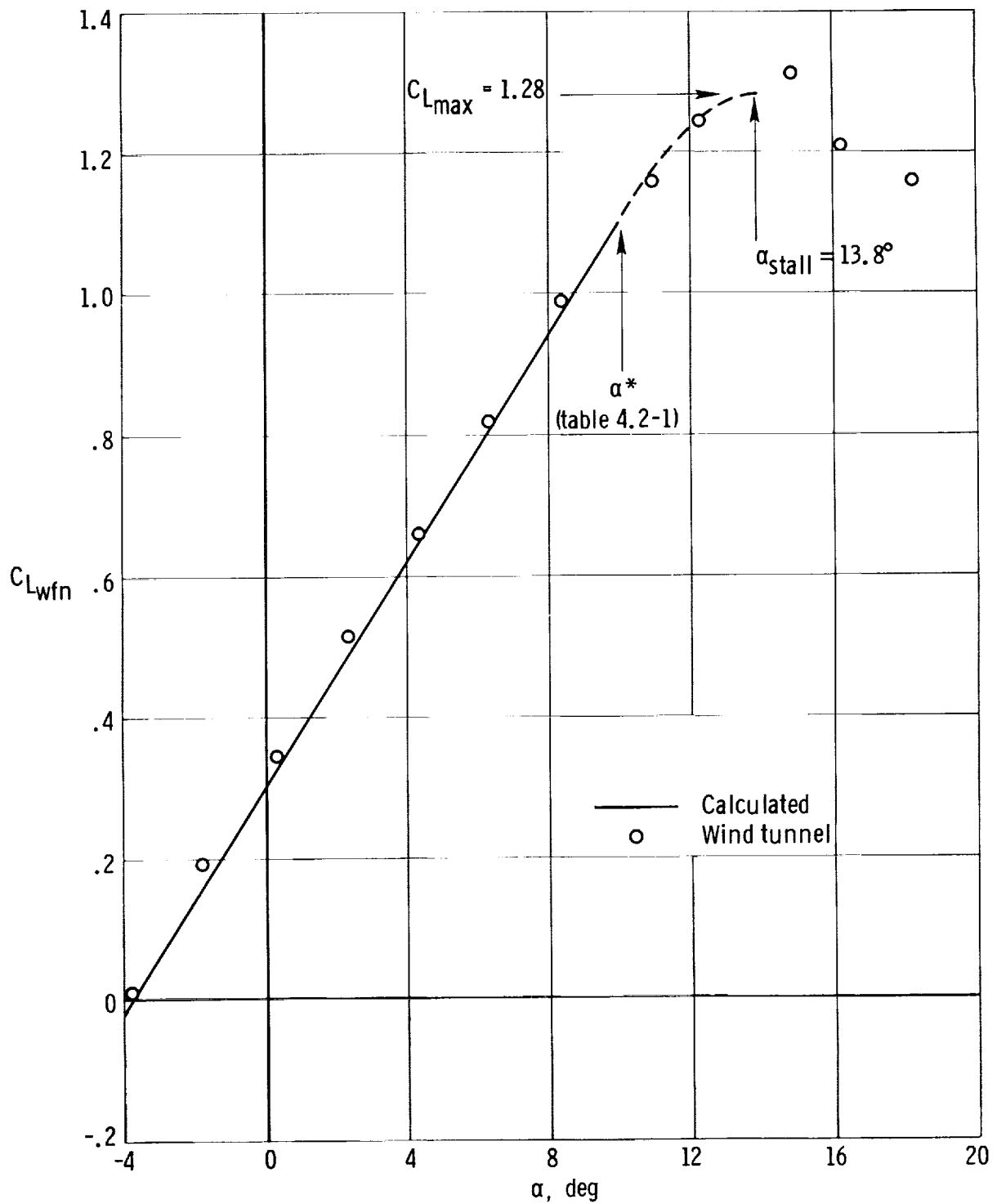


Figure 4.4-4. Comparison of predicted wing-fuselage-nacelle lift curve with wind-tunnel data. $S_w = 178$ sq ft.

4.5 C_{m_0} and Aerodynamic Center of the Wing and Horizontal Tail

Subsonic zero-lift pitching-moment coefficients for untwisted, constant section air-foil lifting surfaces can be determined approximately from the following empirical equation from reference 1:

$$C_{m_0} = c_{m_0} \frac{A \cos \Lambda_{c/4}}{A + 2 \cos \Lambda_{c/4}} \frac{1 + \lambda}{2} \cos \Lambda_{c/4} \quad (4.5-1)$$

where c_{m_0} is the section zero-lift pitching-moment coefficient (section 4.1).

The aerodynamic center, the point about which the lifting surface pitching-moment coefficient is invariant with lift, may be determined relative to a desired reference center on and as a ratio of the lifting surface mean aerodynamic chord by using figure 4.5-1 (from ref. 1) and the equation

$$-\frac{dC_m}{dC_L} = -\left(\frac{x_n}{c_r} - \frac{x_{ac}}{c_r}\right) \frac{c_r}{\bar{c}} \quad (4.5-2)$$

where

$-\frac{dC_m}{dC_L}$ is the static margin, the distance from the reference center on the mean aerodynamic chord of the lifting surface to the aerodynamic center of the surface as a ratio of the mean aerodynamic chord

$\frac{x_n}{c_r}$ is the distance from the lifting surface apex to the desired reference center in terms of root chord of the surface, positive rearward

$\frac{x_{ac}}{c_r}$ is the distance from the apex of the lifting surface to the aerodynamic center of the surface in terms of its root chord, positive aft, obtained from figure 4.5-1 as a function of λ , $A \tan \Lambda_{le}$, and $\frac{\tan \Lambda_{le}}{\beta}$

$\frac{c_r}{\bar{c}}$ is the ratio of the root chord to the mean aerodynamic chord of the surface

Care is required in using figure 4.5-1 to determine $\frac{x_{ac}}{c_r}$. In this study the best results were obtained by crossplotting, at the desired $\frac{\tan \Lambda_{le}}{\beta}$, to obtain a family of $A \tan \Lambda_{le}$ curves as functions of $\frac{x_{ac}}{c_r}$ versus λ , and crossplotting again to obtain a curve for the desired λ as a function of $\frac{x_{ac}}{c_r}$ versus $A \tan \Lambda_{le}$.

Table 4.5-1 summarizes the calculations made to determine the C_{m_0} of the wing and horizontal tail of the subject airplane and the location of the aerodynamic centers of the surfaces relative to the leading edges of the mean aerodynamic chords of the surfaces.

4.5.1 *Symbols* - The following symbols are related to the particular lifting surface under consideration, that is, the wing or the horizontal tail.

A	aspect ratio
ac	aerodynamic center relative to the leading edge of the mean aerodynamic chord as a ratio of the mean aerodynamic chord
C_L	lift coefficient of the surface
C_m	pitching-moment coefficient about the reference center on the mean aerodynamic chord of the surface
C_{m_0}	zero-lift pitching-moment coefficient of the surface
\bar{c}	mean aerodynamic chord, in.
c_{m_0}	section zero-lift pitching-moment coefficient
c_r	root chord of the surface, in.
M	Mach number
x_{ac}	distance from the lifting-surface apex to the aerodynamic center of the surface, obtained from figure 4.5-1 as a ratio of the root chord, in.
x_n	distance from the lifting surface apex to the desired reference center, in.
$y_{\bar{c}}$	lateral distance from the root chord of the surface to its mean aerodynamic chord, in.
β	$(1 - M^2)^{1/2}$
$\Lambda_{c/4}$	sweep of the quarter-chord line, deg
Λ_{le}	sweep of the leading edge, deg
λ	taper ratio

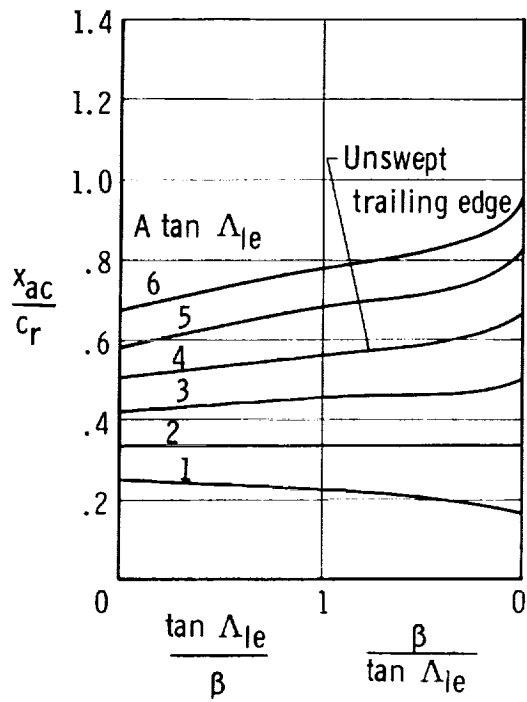
TABLE 4.5-1
 C_{m_0} AND AERODYNAMIC CENTER OF WING AND HORIZONTAL TAIL

$$(a) \quad C_{m_0} = c_{m_0} \frac{A \cos \Lambda_c/4}{A + 2 \cos \Lambda_c/4} \frac{1 + \lambda}{2} \cos \Lambda_c/4$$

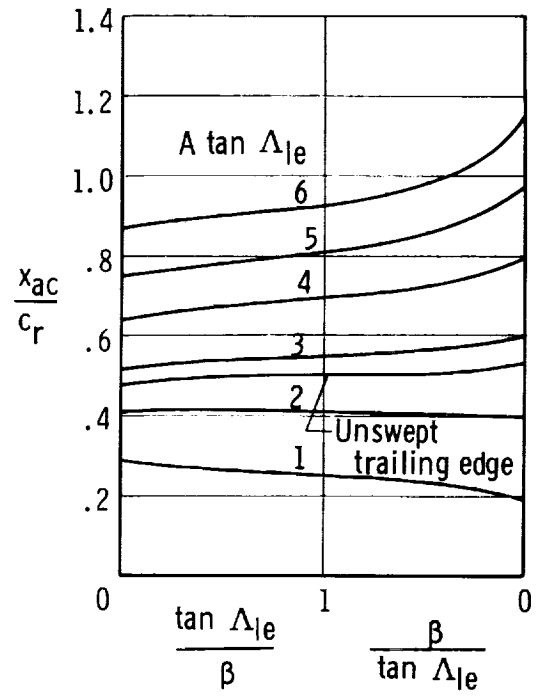
Symbol	Description	Reference	Wing		Horizontal tail	
			Total	Exposed panels	Total	Exposed panels
A	Aspect ratio	Table 3.2-1	7.5	6.9	4.8	4.4
$\Lambda_c/4$	Sweep of quarter-chord line, deg	Table 3.2-1	-2.5	-2.5	8.0	8.0
λ	Taper ratio	Table 3.2-1	.513	.544	.515	.545
c_{m_0}	Section airfoil zero-lift pitching-moment coefficient	Table 4.1-1	-.040	-.040	0	0
C_{m_0}	Zero-lift pitching-moment coefficient of surface	Equation (4.5-1)	-.0240	-.0212	0	0

$$(b) \quad -\frac{dC_m}{dC_L} = -\left(\frac{x_n}{c_r} - \frac{x_{ac}}{c_r}\right) \frac{c_r}{\bar{c}}$$

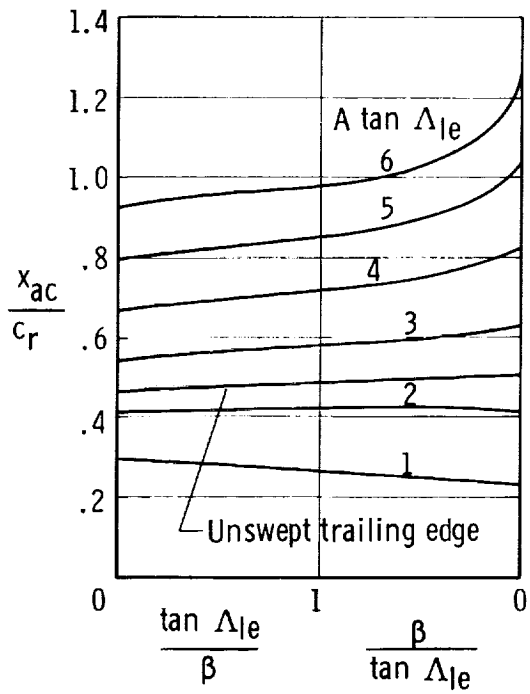
Symbol	Description	Reference	Wing		Horizontal tail	
			Total	Exposed panels	Total	Exposed panels
M	Mach number	Wind-tunnel Mach number	0.083	0.083	0.083	0.083
β	$(1 - M^2)^{1/2}$	-----	.997	.997	.997	.997
c_r	Root chord of surface, in.	Table 3.2-1	76.0	71.9	41.5	39.3
\bar{c}	Mean aerodynamic chord of surface, in.	Table 3.2-1	59.5	57.1	32.45	31.20
$y_{\bar{c}}$	Lateral position of \bar{c} , from root chord, in.	Table 3.2-1	96.48	86.58	33.10	30.10
Λ_{le}	Sweep of leading edge, deg	Table 3.2-1	0	0	12.0	12.0
$A \tan \Lambda_{le}$	Calculated parameter required in figure 4.5-1	-----	0	0	1.06	0.976
$\frac{\tan \Lambda_{le}}{\beta}$	Calculated parameter required in figure 4.5-1	-----	0	0	.222	.222
$\frac{x_{ac}}{c_r}$	Distance from apex of surface to aerodynamic center as ratio of c_r	Figure 4.5-1	.192	.198	.366	.360
x_n	Distance from apex of surface to leading edge of mean aerodynamic chord, $y_{\bar{c}} \tan \Lambda_{le}$	-----	0	0	7.055	6.406
$ac = -\left(\frac{dC_m}{dC_L}\right)_{le}$	Aerodynamic center relative to leading edge of mean aerodynamic chord, as ratio of \bar{c}	Equation (4.5-2)	.247	.249	.250	.249



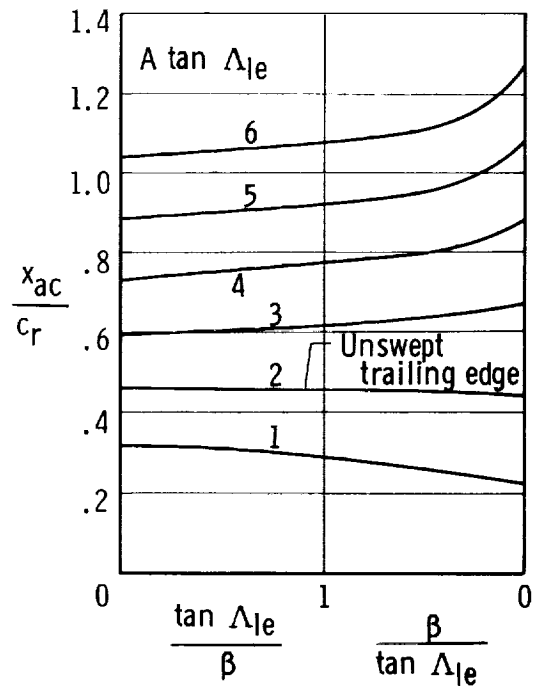
(a) $\lambda = 0$.



(b) $\lambda = 0.2$.

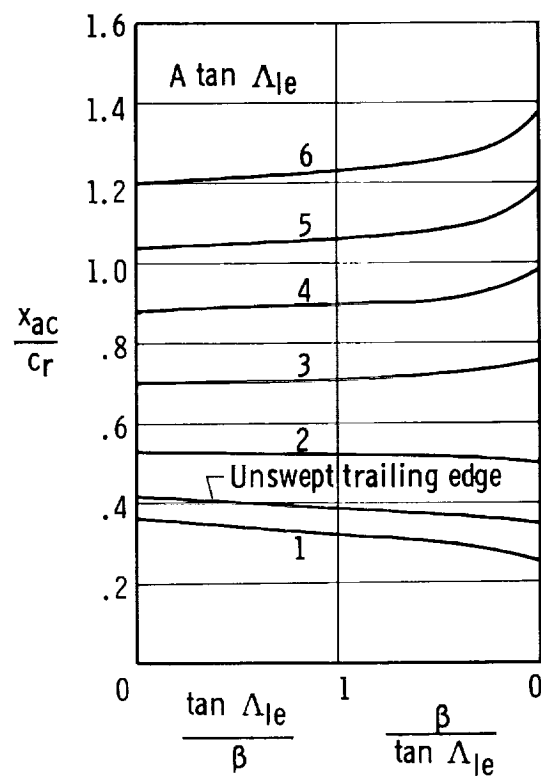


(c) $\lambda = 0.25$.

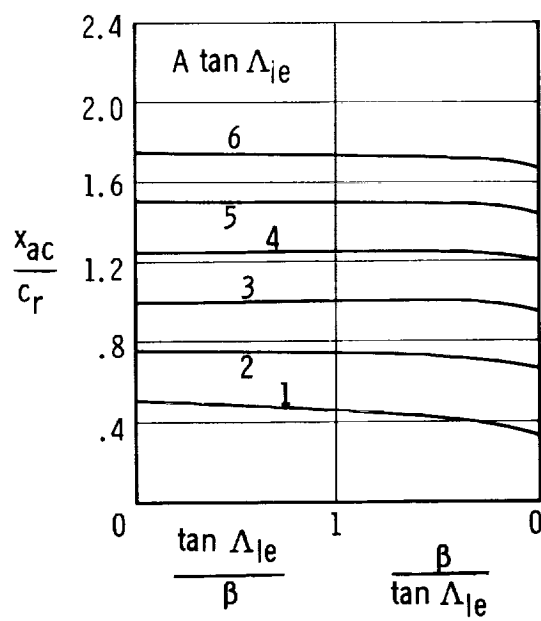


(d) $\lambda = 0.33$.

Figure 4.5-1. Wing aerodynamic-center position for subsonic conditions (ref. 1).



(e) $\lambda = 0.5$.



(f) $\lambda = 1$.

Figure 4.5-1. Concluded.

4.6 Wing-Fuselage Pitching Moment at Zero Lift

The addition of a fuselage to a wing results in a fuselage contribution to the pitching moment at zero lift. This contribution, $(C_{m_o})_f$, may be estimated from figure 4.6-1

(from ref. 12) which is based on streamline bodies of circular or near circular cross section for midwing conditions. For high- or low-wing configurations a positive or negative increment, $(\Delta C_{m_o})_f$, of 0.004 is added, respectively, to the value obtained

from the figure. In the absence of suitable data, the effects of the nacelles on C_{m_o} are considered to be zero.

The wing-fuselage pitching moment at zero lift for the subject airplane is determined in table 4.6-1. The summary results, on the basis of a reference wing area of 172.3 square feet, show the fuselage effect to be significant:

$$\begin{aligned}(C_{m_o})_{wfn} &= (C_{m_o})_w + (C_{m_o})_f + (\Delta C_{m_o})_f \\ &= -0.0240 - 0.0183 - 0.004 \\ &= -0.0463\end{aligned}\tag{4.6-1}$$

4.6.1 Symbols

C_{m_o}	zero-lift pitching-moment coefficient
$(C_{m_o})_f$	fuselage contribution to the zero-lift pitching-moment coefficient for the midwing configuration from figure 4.6-1
$(C_{m_o})_w$	zero-lift pitching-moment coefficient of the wing from table 4.5-1
$(C_{m_o})_{wfn}$	net zero-lift pitching-moment coefficient for the wing-fuselage-nacelles assembly
\bar{c}	wing mean aerodynamic chord, ft
i_w	incidence of the wing chord line relative to the X-body axis, deg
$(i_w)_o$	incidence of the zero-lift line of the wing relative to the reference X-body axis, $-\alpha_{o_w} + i_w$, rad
l_f	fuselage length, ft
\bar{l}_f	distance from the nose of the fuselage to the quarter chord of the wing, ft
S_f	planform area of the fuselage, sq ft

planform area of the fuselage forward of the quarter chord of the wing mean aerodynamic chord, sq ft

reference wing area, sq ft

width of the fuselage at the wing, ft

zero-lift angle of attack of the wing relative to the wing chord line, deg

correction to $(C_{m_o})_f$ for the non-midwing configuration equal to 0.004 and -0.004 for high- and low-wing configurations, respectively

TABLE 4.6-1
WING-FUSELAGE PITCHING MOMENTS OF AIRPLANE AT ZERO LIFT

$$\left[(C_{m_o})_{wf} = (C_{m_o})_w + (C_{m_o})_f + (\Delta C_{m_o})_f \right]$$

(a) Wing contribution

Symbol	Description	Reference	Magnitude
$(C_{m_o})_w$	C_{m_o} of wing	Table 4.5-1	-0.0240

(b) Effect of fuselage on C_{m_o}

$$(C_{m_o})_f + (\Delta C_{m_o})_f = \left[\frac{(C_{m_o})_f S_w \bar{c}}{(i_w)_o S_f l_f} \right] \frac{(i_w)_o S_f l_f}{S_w \bar{c}} + (\Delta C_{m_o})_f$$

Symbol	Description	Reference	Magnitude
w	Width of fuselage at the wing, ft	Figure 3.2-1	4.0
l_f	Fuselage length, ft	Figure 4.3-5	24.2
\bar{l}_f	Distance from nose of fuselage to $\bar{c}/4$ of wing, ft	Figure 3.2-1	9.01
S_w	Reference wing area, sq ft	Table 3.2-1	172.3
S_f	Planform area of fuselage, sq ft	From drawings	≈ 65.8
\bar{S}_f	Planform area of fuselage forward of $\bar{c}/4$ of wing, sq ft	From drawings	≈ 26.3
\bar{c}	Wing mean aerodynamic chord, ft	Table 3.2-1	4.96
$(i_w)_o$	Incidence of zero-lift line of wing = $-\alpha_{ow} + i_w$, rad	Table 4.4-1	$4/57.3 = .0698$
$\frac{w^2}{S_f}$	Parameter used in figure 4.6-1	-----	0.239
$\frac{\bar{S}_f \bar{l}_f}{S_f l_f}$	Parameter used in figure 4.6-1	-----	.149
$\left[\frac{(C_{m_o})_f S_w \bar{c}}{(i_w)_o S_f l_f} \right]$	-----	Figure 4.6-1	-.141
$(\Delta C_{m_o})_f$	Correction for low-wing configuration of airplane	Section 4.6	-0.004
Summary: $(C_{m_o})_f + (\Delta C_{m_o})_f = -0.0183 - 0.004 = -0.0223$			

(c) Summary

$$(C_{m_o})_{wf} = -0.0240 - 0.0183 - 0.004 = -0.0463 \text{ on basis of } S_w = 172.3 \text{ sq ft}$$

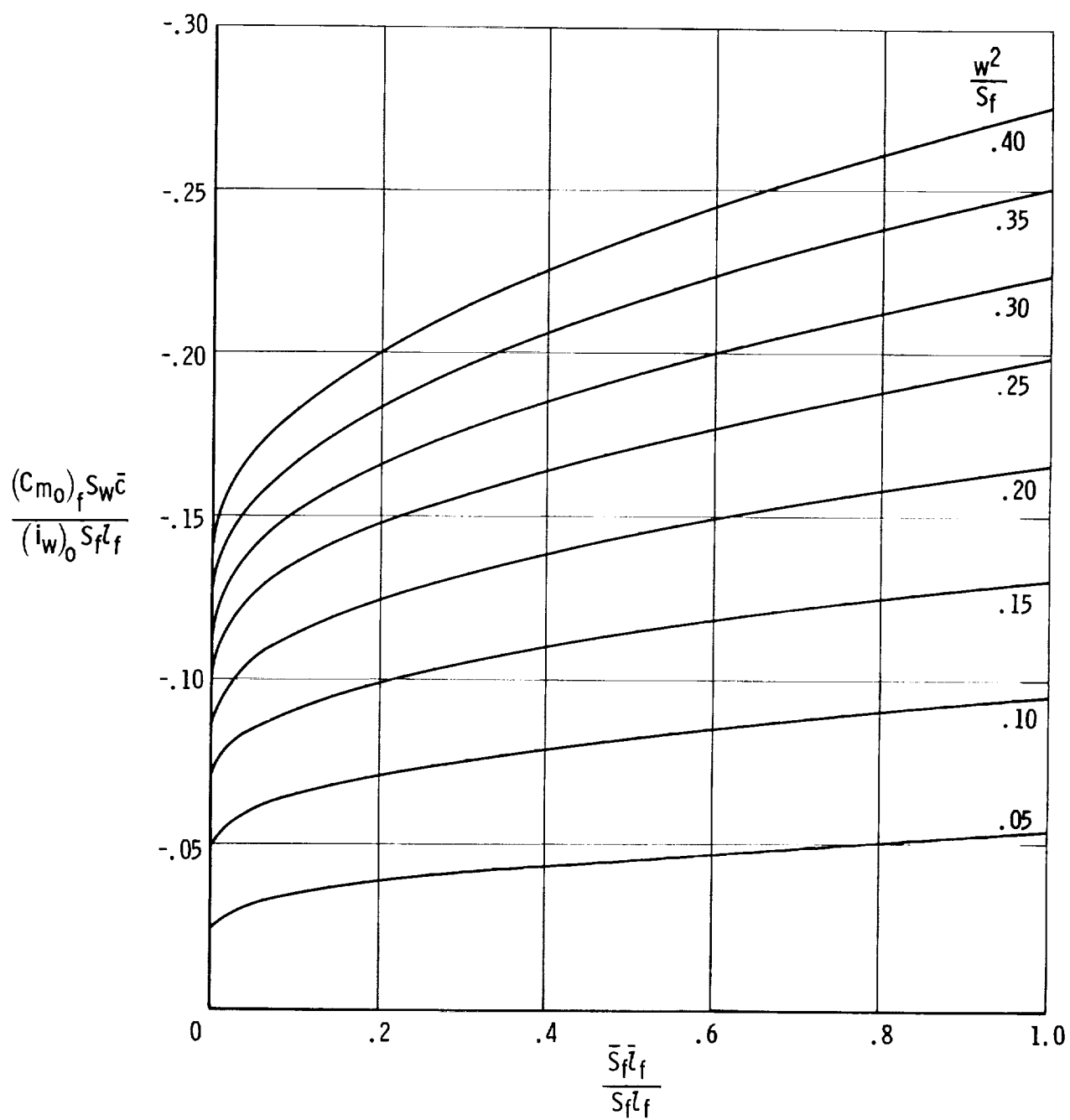


Figure 4.6-1. Effect of a fuselage on C_{m0} . Midwing configuration (ref. 12).

4.7 Fuselage and Nacelle Pitching Moments

The slope of the pitching-moment curve of the fuselage and nacelles at subsonic Mach numbers may be determined from the following equation, from reference 10, based on potential-flow lift effects on the forebody and on viscous-flow lift effects on the afterbody, which were discussed in section 4.3:

$$(C_{m\alpha})_B = \left[\overbrace{\frac{2(k_2 - k_1)}{(57.3)V_B} \int_0^{x_0} (x_m - x) dS_x}^{\text{Potential flow}} + \overbrace{\frac{4\eta c_{dc} \alpha}{(57.3)^2 V_B} \int_{x_0}^{l_B} r(x_m - x) dx}^{\text{Viscous crossflow}} \right] \frac{V_B}{S_w \bar{c}} \quad (4.7-1)$$

where

$(C_{m\alpha})_B$ is based on the reference wing area about a chosen moment center x_m distance from the nose of the body, per deg

S_x is the cross-section area of the body at distance x from the body nose, sq ft

x_m is the distance from the nose of the body to the chosen moment center, ft

V_B is the total volume of the body, cu ft

α is angle of attack, deg

The remaining symbols are defined below and also in table 4.7-1, which summarizes the calculation of the slope of the pitching-moment curve of the fuselage and nacelles of the subject airplane about the leading edge of the total wing mean aerodynamic chord. Table 4.7-2 shows the tabular integration procedure used to obtain the values of the integrals for the fuselage. The same procedure was used for the nacelles when x_m was taken to be 53 inches from the nose of the nacelles (propellers off).

The slope of the pitching-moment curve of the fuselage and nacelles of the subject airplane about the leading edge of the total wing mean aerodynamic chord, as summarized in table 4.7-1, is accounted for by

$$(C_{m\alpha})_{fn} = 0.00375 - 0.000128\alpha \quad (4.7-2)$$

4.7.1 Symbols

$(C_{m\alpha})_B$	variation of the body pitching-moment coefficient (based on reference wing area) with angle of attack
$(C_{m\alpha})_f, (C_{m\alpha})_n$	variation of the body pitching-moment coefficient with angle of attack, $(C_{m\alpha})_B$, applied specifically to the fuselage and nacelles, respectively

$$(C_{m\alpha})_{fn} = (C_{m\alpha})_f + (C_{m\alpha})_n$$

\bar{c}	wing mean aerodynamic chord, ft
c_{dc}	steady-state crossflow drag coefficient, obtained from table 4.3-1
$k_2 - k_1$	reduced mass factor, from potential-flow theory, obtained from table 4.3-1
l_B	body length, ft or in.
l_f, l_n	body length, l_B , applied specifically to the fuselage and nacelles, respectively
r	effective body radius of Δx segment of the afterbody length, ft or in.
S_w	reference wing area, sq ft
S_x	cross-section area of an equivalent circular body at the foregoing station being considered, sq ft
V_B	volume of an equivalent circular body, cu ft
V_f, V_n	body volume, V_B , applied specifically to the fuselage and nacelle, respectively
w	width (diameter) of an equivalent circular body at the foregoing station being considered, in.
x	distance from the nose of the body to the centroid of ΔS_x for the forebody, and to the centroid of Δx for the afterbody, ft or in.
x_m	distance from the nose of the body to the chosen moment center (leading edge of the mean aerodynamic chord in this instance), ft or in.
x_o	distance from the nose of the body to the point (demarcation of forebody and afterbody in this instance) where the potential flow ceases, ft or in.
α	angle of attack, deg
ΔS_x	change in the cross-section area of the body across the Δx segment of the body length being considered, sq ft
Δx	incremental length of the body, ft or in.
η	drag proportionality factor from table 4.3-1

TABLE 4.7-1
FUSELAGE AND NACELLE PITCHING MOMENTS OF AIRPLANE

Two nacelles

$$(C_{m\alpha})_{fn} = \left[\frac{2(k_2 - k_1)}{12} \frac{V_f}{(57.3)V_f} \int_0^{x_0} (x_m - x) dS_x + \frac{4\pi c_{d_c} \alpha}{1728} \frac{V_f}{(57.3)^2 V_f} \int_{x_0}^{l_f} r(x_m - x) dx \right] \left[\frac{2(k_2 - k_1)}{12} \frac{V_n}{(57.3)V_n} \int_0^{x_0} (x_m - x) dx + \frac{4\pi c_{d_c} \alpha}{1728} \frac{V_n}{(57.3)^2 V_n} \int_{x_0}^{l_n} r(x_m - x) dx \right] \frac{V_n}{S_w \bar{c}}$$

Fuselage

Nacelle

Symbol	Description	Reference	Fuselage	Nacelle
M	Mach number	Wind-tunnel Mach number	0.083	0.083
S_w	Reference wing area, sq ft	Table 3.2-1	172.3	172.3
V_B	Body volume, cu ft	Table 4.3-1	≈ 172	≈ 21.3 per nacelle
S_x	Equivalent body cross-section area, sq ft	Figure 4.3-5	Variable (see table 4.7-2)	Variable
l_B	Length of body, in.	Table 4.3-1	290	106
x_0	Location, from body nose, where potential flow ceases, in.	Table 4.3-1	167	61
x_m	Distance from body nose to leading edge of wing mean aerodynamic chord, in.	Figure 3.2-1	93.2	53.0
x	Distance from body nose to centroid of Δ quantity, in.	Figure 4.3-5	Variable (see table 4.7-2)	Variable
r	Effective body radius of Δx segment, in.	-----	Variable (see table 4.7-2)	Variable
\bar{c}	Wing mean aerodynamic chord, ft	Table 3.2-1	4.96	4.96
$(k_2 - k_1)$	Reduced mass factor	Table 4.3-1	0.86	0.75
η	Ratio of drag coefficient of finite to infinite length cylinders	Table 4.3-1	.635	.590
c_{d_c}	Crossflow drag coefficient of infinite length cylinder	Table 4.3-1	1.2	1.2
$\frac{1}{12} \int_0^{x_0} (x_m - x) dS_x$	$\frac{1}{12} \sum_0^{x_0} (x_m - x) \Delta S_x$, cu ft	-----	63.8 (see table 4.7-2)	25.0 per nacelle
$\frac{1}{1728} \int_{x_0}^{l_B} r(x_m - x) dx$	$\frac{1}{1728} \sum_0^{l_B} r(x_m - x) \Delta x$, cu ft	-----	-117.6 (see table 4.7-2)	Negligible

Summary: $(C_{m\alpha})_{fn} = 0.00223 - 0.000128\alpha + 0.00152 + 0$
 $= 0.00375 - 0.000128\alpha$ (with α in degrees)

TABLE 4.7-2
TABULAR INTEGRATION OF FUSELAGE PITCHING-MOMENT PARAMETERS

$$(a) \frac{1}{12} \int_0^{x_0} (x_m - x) dS_x = \sum_{x_0=167}^{x_0=167} \frac{(93.2 - x)}{12} \Delta S_x$$

Distance from nose to area S_x , in.	x, in.	w, in.	$S_x = \frac{\pi w^2}{4(144)}$, sq ft	ΔS_x , sq ft	$(93.2 - x)$, in.	$(93.2 - x)\Delta S_x$
0	6	0	0	1.39	87.2	121
9	19	16	1.396	2.59	74.2	192
25	37	27	3.98	3.50	56.2	197
44	55	37	7.47	2.15	38.2	82.1
63.5	72	42	9.62	1.42	21.2	30.1
80	87	45	11.04	1.26	6.2	7.8
94.5	106.5	47.5	12.3	0.8	-13.3	-10.6
119	123	49.0	13.1	-0.3	-29.8	8.9
127.5	139	48.5	12.8	-0.2	-45.8	9.16
150	157	48	12.6	-2.0	-63.8	127.6
167		44	10.6			
$\frac{1}{12} \int_0^{x_0} (x_m - x) dS_x = \frac{765.5}{12} = 63.8$ cu ft						$\Sigma = 765.5$

$$(b) \frac{1}{1728} \int_{x_0}^{l_f} r(x_m - x) dx = \sum_{x_0=167}^{l_f=287} \frac{r(93.2 - x)\Delta x}{1728}$$

Distance from nose, in.	Δx , in.	r, in.	x, in.	$(93.2 - x)$, in.	$r(93.2 - x)\Delta x$, cu in.
167	20	21	177	-83.8	-35,200
187	20	18	197	-103.8	-37,400
207	20	15	217	-123.8	-37,140
227	20	12	237	-143.8	-34,510
247	20	9	257	-163.8	-29,480
267	20	8	277	-183.8	-29,400
287					
$\frac{1}{1728} \int_{x_0}^{l_f} r(x_m - x) dx = \frac{-203,130}{1728} = -117.6$ cu ft					$\Sigma = -203,130$

4.8 Wing-Fuselage-Nacelle Pitching Moments

The wing-fuselage-nacelle pitching-moment characteristics are considered in terms of pitching-moment slopes, aerodynamic center, and pitching-moment coefficient. A first-order approximation of the variation of the pitching-moment coefficient beyond the limit of linearity of the lift-curve slope up to the stall is also considered.

4.8.1 Contributing Factors to Wing-Fuselage-Nacelle Pitching Moments

Zero-lift pitching moments: The zero-lift pitching moments of the wing, fuselage, nacelles, and wing-fuselage interference were accounted for in section 4.6. For the subject airplane, from table 4.6-1(c),

$$(C_{m_0})_{wfn} = -0.0463 \quad (4.6-1)$$

Fuselage and nacelle pitching moments: The fuselage and nacelle pitching moments due to potential- and viscous-flow lift effects were accounted for in section 4.7. For the subject airplane, with the moment center about the leading edge of the total wing mean aerodynamic chord, the results of table 4.7-1 indicate that

$$(C_{m_\alpha})_{fn} = 0.00375 - 0.000128\alpha \quad (4.7-2)$$

Wing pitching moments: The wing pitching moments due to effective wing lift, which includes the effects of body upwash on the wing and wing lift carryover onto the fuselage, can be accounted for (on the basis of relations in ref. 11) by equation (4.8.1-1) for a moment center about the leading edge of the root chord of the exposed wing panels. For the subject airplane, because of the zero sweep of the leading edge, this is synonymous to the moment center about the leading edge of the reference mean aerodynamic chord of the wing.

$$(C_{m_\alpha})_{w(f)+f(w)} = - \left[\left(\frac{x_{ac}}{c_{re}} \right)_{w(f)} K_{w(f)} + \left(\frac{x_{ac}}{c_{re}} \right)_{f(w)} K_{f(w)} \right] \left(\frac{c_{re}}{\bar{c}_w} \right) \left(\frac{S_{we}}{S_w} \right) (C_{L_\alpha})_{we} \quad (4.8.1-1)$$

where

$(C_{m_\alpha})_{w(f)+f(w)}$ is in terms of total wing area and mean aerodynamic chord about the leading edge of the total wing mean aerodynamic chord

$\left(\frac{x_{ac}}{c_{re}} \right)_{w(f)}$ is the aerodynamic center of the wing in the presence of the fuselage as a fraction of and about the leading edge of the root chord of the exposed wing panels,

obtained from figure 4.5-1

and

$\left(\frac{x_{ac}}{c_{re}}\right)_{f(w)}$ is the contribution to the aerodynamic center due to the lift carryover of the wing on the fuselage

For $A_w \sqrt{1 - M^2} \geq 4$ and body-width-to-wing-span ratios, $k = \frac{d}{b}$, less than 0.5, which is normal for general aviation airplanes, the contribution to the aerodynamic center due to lift carryover of the wing onto the body is

$$\left(\frac{x_{ac}}{c_{re}}\right)_{f(w)} = \frac{1}{4} + \frac{b-d}{2c_{re}} \tan \Lambda_{c/4} \left[-\frac{k}{1-k} + \frac{\frac{b}{2}\sqrt{1-2k} \ln\left(\frac{1-k}{k} + \frac{1}{k}\sqrt{1-2k}\right) - \frac{b}{2}(1-k) + \frac{\pi b}{4}k}{\frac{b}{2}\frac{k(1-k)}{\sqrt{1-2k}} \ln\left(\frac{1-k}{k} + \frac{1}{k}\sqrt{1-2k}\right) + \frac{b}{2}\frac{(1-k)^2}{k} - \frac{\pi b}{4}(1-k)} \right] \quad (4.8.1-2)$$

The wing pitching-moment slope for the subject airplane about the leading edge of the mean aerodynamic chord due to the effective wing lift in the presence of the body is summarized in table 4.8.1-1(a) in terms of the reference wing area of 172.3 square feet, or

$$(C_{m\alpha})_{w(f)+f(w)} = -0.0195 \text{ per deg} \quad (4.8.1-3)$$

Wing pitching moment due to wing drag: The wing pitching moment due to wing drag can be accounted for by the following relationship:

$$\begin{aligned} \left(\frac{dC_m}{dC_L}\right)_{w(D)} &= -\frac{z_w}{\bar{c}_w} \left(\frac{dC_D}{dC_L}\right)_w \\ &\approx -C_{Lw} \left[\frac{2}{\pi e A_w}\right] \frac{z_w}{\bar{c}_w} \end{aligned} \quad (4.8.1-4)$$

where

z_w is the vertical distance from the X-axis to the $\bar{c}/4$ of the wing, positive down

\bar{c}_w is the wing mean aerodynamic chord, feet

A_w is the wing aspect ratio

e is the wing efficiency factor for induced drag

C_{Lw} is the wing lift coefficient

After converting and expressing C_{L_w} in terms of $C_{L_{wfn}}$,

$$(C_{m_\alpha})_{w(D)} = -C_{L_{wfn}} \left[\frac{(C_{L_\alpha})_w}{(C_{L_\alpha})_{wfn}} \right] \left[\frac{2 (C_{L_\alpha})_w}{\pi e A_w} \right] \frac{z_w}{\bar{c}_w} \quad (4.8.1-5)$$

Wing pitching-moment slope due to drag for the subject airplane is summarized in table 4.8.1-1(b) in terms of wing area equal to 172.3 square feet, or

$$(C_{m_\alpha})_{w(D)} = 0.000197 C_{L_{wfn}} \text{ per deg} \quad (4.8.1-6)$$

Fuselage and nacelle "free moments": The fuselage and nacelle "free moments" due to induced flow from the wing can be estimated by the technique developed by Multhopp in reference 13. Multhopp indicates that, in considering wing lift carryover onto the body, there remains an essentially free moment (or couple) of the body due to wing upwash ahead of the wing and downwash behind the wing. This wing interference contribution was accounted for by the following equation, which indicates the free moment to be a function of angle of attack:

$$\begin{aligned} (C_{m_\alpha})_{B(\epsilon)} &= \frac{1}{36.5 S_w \bar{c}_w} \frac{\int_0^l w_B^2 \frac{d\beta}{d\alpha} dx}{1728} \\ &= \frac{1}{36.5 S_w \bar{c}_w} \sum_0^l \frac{w_B^2 \Delta x}{1728} \frac{d\beta}{d\alpha} \end{aligned} \quad (4.8.1-7)$$

where

w_B is the mean width of the body planform segment, Δx

$\frac{d\beta}{d\alpha}$ is the variation of local flow with α (considered to be zero in the body planform area overlapped by the wing)

Curves of $\frac{d\beta}{d\alpha}$ are shown in figure 4.8.1-1 as a function of Δx segment position ahead of the wing leading edge, $\frac{x_1}{c_w}$, where c_w is the root chord of the wing for the fuselage, and the chord at the centerline of the nacelle for the nacelle. For Δx segments immediately ahead of the wing leading edge, $\frac{d\beta}{d\alpha}$ rises so abruptly that integrated values, $\frac{d\bar{\beta}}{d\alpha}$, are given based on the length of the segment adjacent to the wing leading edge. For segments aft of the trailing edge of the wing, $\frac{d\beta}{d\alpha}$ is assumed

to vary linearly and is obtained from

$$\frac{d\beta}{d\alpha} = \frac{x'_1}{l_h} \left(1 - \frac{\partial \epsilon_w}{\partial \alpha} \right) \quad (4.8.1-8)$$

where

$\frac{\partial \epsilon_w}{\partial \alpha}$ is considered to be similar to $\left(\frac{\partial \bar{\epsilon}_h}{\partial \alpha} \right)_M$, from table 4.9.1-2, column 24

l_h is the distance from the wing trailing edge to the last Δx segment

x'_1 is the distance from the wing trailing edge to the Δx segment

Fuselage and nacelle "free moments" for the subject airplane are summarized in table 4.8.1-2 in terms of a wing area of 172.3 square feet, or

$$\begin{aligned} (C_{m\alpha})_{f(\epsilon)+n(\epsilon)} &= (C_{m\alpha})_{f(\epsilon)} + (C_{m\alpha})_{n(\epsilon)} \\ &= 0.00558 + 0.0053 \\ &= 0.0109 \text{ per deg} \end{aligned} \quad (4.8.1-9)$$

4.8.2 Static Margin of Wing-Fuselage-Nacelles

The pitching-moment characteristics in terms of the static margin, the distance from the center of gravity to the aerodynamic center, are obtained from the expression

$$-\left(\frac{dC_m}{dC_L} \right)_{cg} = -\frac{x_{cg}}{\bar{c}_w} - \frac{\sum (C_{m\alpha})_{le}}{\sum C_{L\alpha}} \quad (4.8.2-1)$$

where

$\frac{x_{cg}}{\bar{c}_w}$ is the distance to the center of gravity from the leading edge of the total wing mean aerodynamic chord as a ratio of the mean aerodynamic chord

$\left(\sum C_{m\alpha} \right)_{le}$ is the pitching-moment slope about the leading edge of the mean aerodynamic chord

For the wing-fuselage-nacelle configuration of this analysis,

$$-\left(\frac{dC_m}{dC_L} \right)_{cg} = -\frac{x_{cg}}{\bar{c}} - \frac{\left[(C_{m\alpha})_{fn} + (C_{m\alpha})_{w(f)+f(w)} + (C_{m\alpha})_{w(D)} + (C_{m\alpha})_{f(\epsilon)+n(\epsilon)} \right]_{le}}{(C_{L\alpha})_{fn} + (C_{L\alpha})_{w(f)+f(w)}} \quad (4.8.2-2)$$

The static margin of the subject airplane, relative to the center of gravity at $0.10\bar{c}$ (which corresponds to the reference center of the wind-tunnel data), is thus estimated to be

$$-\left(\frac{dC_m}{dC_L}\right)_{.10\bar{c}_w} = -0.10 - \frac{(0.00375 - 0.000128\alpha) - 0.0195 + 0.000197 C_{L_{wfn}} + 0.0109}{0.0831} \quad (4.8.2-3)$$

The preceding C_{m_α} quantities in the numerator were obtained from section 4.8.1. The net C_{L_α} quantity in the denominator was obtained from equation (4.4-3), with the higher order α terms considered to be negligible.

To express the static margin as a function of $C_{L_{wfn}}$ only, replace α in the above equation by

$$\alpha = \frac{C_{L_{wfn}}}{(C_{L_\alpha})_{wfn}} + \alpha_o = \frac{C_{L_{wfn}}}{0.0831} - 3.7^\circ \quad (4.8.2-4)$$

where -3.7° is the zero-lift angle of attack from figure 4.4-4.

Thus, on the basis of a 172.3-square-foot reference wing area, the static margin of the subject airplane in the linear range of the lift-curve slope is

$$-\left(\frac{dC_m}{dC_L}\right)_{.10\bar{c}_w} = -0.0456 + 0.0162 C_{L_{wfn}} \quad (4.8.2-5)$$

4.8.3 Pitching-moment coefficient of wing-fuselage-nacelles

Linear lift range: The pitching-moment coefficient in the linear range of the lift-curve slope is determined from

$$(C_{m_{wfn}})_{.10\bar{c}_w} = - \int \left(-\frac{dC_m}{dC_L}\right)_{.10\bar{c}_w} dC_{L_{wfn}} + (C_{m_o})_{wfn} \quad (4.8.3-1)$$

For the subject airplane, with $-\left(\frac{dC_m}{dC_L}\right)_{.10\bar{c}_w}$ obtained from equation (4.8.2-5) and

$(C_{m_o})_{wfn}$ from table 4.6-1(c) or equation (4.6-1), the pitching-moment coefficient about $0.10\bar{c}$, on the basis of the reference wing area of 172.3 square feet, is determined to be

$$(C_{m_{wfn}})_{.10\bar{c}_w} = 0.0456 C_{L_{wfn}} - 0.0081 C_{L_{wfn}}^2 - 0.0463 \quad (4.8.3-2)$$

The calculation of $(C_{m_{wfn}})_{.10\bar{c}_w}$ for the linear lift range is summarized in table 4.8.3-1, which also includes the results for the nonlinear range to be discussed.

Nonlinear lift range: No methods appeared to be available for determining the pitching-moment coefficient in the lift region between the upper limit of linearity of the lift-curve slope and stall. The apparent need to account for the pitching-moment characteristics in this region resulted in an empirical approach to the problem to provide a first approximation of the variation of C_m with C_L for the wing-fuselage-nacelle configuration.

The empirical approach takes into consideration equations (4.8.2-2) and (4.8.2-3). The equations were simplified by eliminating the pitching-moment contributions of the wing-induced drag effects. Because the stall characteristics of the wing-fuselage-nacelle configuration are generally governed by the stall characteristics of the wing, it was assumed that the potential flow and crossflow contributions of the fuselage and nacelles were unaffected. It was also assumed that the free moment contributions of the fuselage and nacelles were not significantly affected through most of the nonlinear range of the lift-curve slope approaching stall. This assumption is based on the fact that most of the free moment contributions are from the upwash of the wing.

As a result of the preceding assumptions and the fact that the stall characteristics of the wing-fuselage-nacelle characteristics are generally governed by wing stall characteristics, the format of equation (4.8.2-2) was modified to that of equation (4.8.3-3). The equation is restricted to the region extending from the upper limit of linearity of the lift-curve slope to stall.

$$\left(\frac{dC_m}{dC_L}\right)_{S, 10\bar{c}_w} \approx 0.10 + \frac{(C_{m\alpha})_{fn} + (C_{m\alpha})_{ws} + (C_{m\alpha})_{f(\epsilon)+n(\epsilon)}}{(C_{L\alpha})_{wfn} - (\Delta C_{L\alpha})_{ws}} \quad (4.8.3-3)$$

For the subject airplane, with data substituted from equation (4.8.2-3),

$$\left(\frac{dC_m}{dC_L}\right)_{S, 10\bar{c}_w} = 0.10 + \frac{(0.00375 - 0.000128\bar{\alpha}_s) + (C_{m\alpha})_{ws} + 0.0109}{0.0831 - (\Delta C_{L\alpha})_{ws}} \quad (4.8.3-4)$$

where

$\bar{\alpha}_s$ is the average α in the nonlinear range

$(C_{m\alpha})_{ws}$ is the average value of total wing $C_{m\alpha}$ in the nonlinear range to stall

$(\Delta C_{L\alpha})_{ws}$ is a correction to reduce $(C_{L\alpha})_{wfn}$ to an average slope in the non-

linear range

Because the aerodynamic center of the wing is normally at $0.25\bar{c}_w$ in the linear range of the lift curve and moves aft with increasing α in the nonlinear range to $0.50\bar{c}$ at stall, an average value of the aerodynamic center in the nonlinear range, $(ac)_{ws}$, is assumed to be $0.375\bar{c}$.

An average value of $(C_{L\alpha})_w$ of the total wing in the nonlinear range approaching stall, used to obtain $(\Delta C_{L\alpha})_{ws}$, is considered to be the average of the sum of $(C_{L\alpha})_w$ in the linear range and the slope of the line connecting the upper limit of linearity of the C_{Lw} versus α curve and the C_{Lmax} point. This average slope, referred to as $(C_{L\alpha})_{ws}$, may be determined from

$$(C_{L\alpha})_{ws} = \frac{1}{2} \left[(C_{L\alpha})_w + \frac{(C_{Lmax})_w - (C_{L\alpha})_w(\alpha^* - \alpha_0)}{\alpha_{C_{Lmax}} - \alpha^*} \right] \quad (4.8.3-5)$$

$$= 0.063$$

for the subject airplane using the total wing lift characteristics in table 4.2-1.

The difference in linear and nonlinear lift-curve slopes is determined from

$$\begin{aligned} (\Delta C_{L\alpha})_{ws} &= (C_{L\alpha})_w - (C_{L\alpha})_{ws} \\ &= 0.0759 - 0.063 \\ &= 0.0129 \text{ per deg for the subject airplane} \end{aligned} \quad (4.8.3-6)$$

An average value of $(C_{m\alpha})_w$ of the total wing in the nonlinear range is determined from

$$\begin{aligned} (C_{m\alpha})_{ws} &= -(ac)_{ws} (C_{L\alpha})_{ws} \\ &= -0.375 (0.063) \\ &= -0.0236 \text{ per deg for the subject airplane} \end{aligned} \quad (4.8.3-7)$$

The average value of α in the nonlinear range was determined from figure 4.4-4 to be

$$\begin{aligned} \bar{\alpha}_s &= \frac{1}{2} (\alpha^* + \alpha_{C_{Lmax}}) \\ &= \frac{1}{2} (10 + 13.8) \\ &\approx 12^\circ \end{aligned} \quad (4.8.3-8)$$

Substituting the determined values of $(C_{m\alpha})_{ws}$, $(\Delta C_{L\alpha})_{ws}$, and $\bar{\alpha}_s$ for the subject

airplane into equation (4.8.3-4) results in the pitching-moment slope

$$\left(\frac{dC_m}{dC_L} \right)_{S_{.10}\bar{c}_w} = -0.0496 \quad (4.8.3-9)$$

This slope is drawn, as in figure 4.8.3-1, from the point on the pitching-moment curve representing the upper limit of linearity, $C_{L_{wfn}}^*$, to $(C_{L_{max}})_{wfn}$. Finally, a reasonably flat curve is drawn from, and tangent to, the $C_{L_{wfn}}^*$ point to $(C_{L_{max}})_{wfn}$.

Summary: The pitching-moment characteristics of the subject airplane, including the nonlinear region, are summarized in table 4.8.3-1. The results, referenced to a wing area of 178 square feet, are compared with full-scale wind-tunnel data in figure 4.8.3-2. The lift coefficients for the $C_{m_{wfn}}$ versus $C_{L_{wfn}}$ plot were obtained from figure 4.4-4. The agreement between predicted and wind-tunnel-measured pitching-moment data is good. All contributions were pertinent.

4.8.4 Symbols

A_w	wing aspect ratio
$(ac)_{ws}$	average value of the aerodynamic center of the wing in the non-linear range of the wing lift-curve slope to stall expressed as a fraction of the wing mean aerodynamic chord
b	wing span, in.
C_L	lift coefficient
$C_{L_{max}}$	maximum lift coefficient
C_{L_w}	lift coefficient of the wing alone
$C_{L_{wfn}}$	lift coefficient of the wing-fuselage-nacelle configuration
$C_{L_{wfn}}^*$	magnitude of the lift coefficient, $C_{L_{wfn}}$, at the upper limit of linearity of the lift-curve slope, $(C_{L_\alpha})_{wfn}$
$(C_{L_{max}})_w$	lift coefficient of the wing at stall
$(C_{L_{max}})_{wfn}$	lift coefficient of the wing-fuselage-nacelle configuration at stall
$(C_{L_\alpha})_{fn}$	lift-curve slope of the fuselage and nacelles, per deg
$(C_{L_\alpha})_{w(f)+f(w)}$	variation of the lift of the wing in the presence of the fuselage, including the wing lift carryover onto the fuselage, with angle of attack, per deg

$(C_{L\alpha})_w$	lift-curve slope of the isolated wing, per deg
$(C_{L\alpha})_{we}$	lift-curve slope of the exposed wing panels, per deg
$(C_{L\alpha})_{wfn}, \Sigma C_{L\alpha}$	lift-curve slope of the wing-fuselage-nacelle configuration, per deg
$(C_{L\alpha})_{ws}$	average lift-curve slope of $(C_{L\alpha})_{wfn}$ in the nonlinear range approaching stall, per deg
$(\Delta C_{L\alpha})_{ws}$	correction to reduce $(C_{L\alpha})_{wfn}$ to an average slope in the nonlinear range approaching stall, per deg
C_m	pitching-moment coefficient
$(C_{m0})_{wfn}$	zero-lift pitching-moment coefficient of the wing-fuselage-nacelle configuration
$(C_{mwfn}), 10\bar{c}_w$	pitching-moment coefficient of the wing-fuselage-nacelle configuration relative to the 10-percent mean-aerodynamic-chord point
$(C_{m\alpha})_{B(\epsilon)}$	slope of the "free moment" coefficient of the body, per deg
$(C_{m\alpha})_{f(\epsilon)}, (C_{m\alpha})_{n(\epsilon)}$	"free moment" slope, $(C_{m\alpha})_{B(\epsilon)}$, applied specifically to the fuselage and nacelle, respectively
$(C_{m\alpha})_{f(\epsilon)+n(\epsilon)} = (C_{m\alpha})_{f(\epsilon)} + (C_{m\alpha})_{n(\epsilon)}$	
$(C_{m\alpha})_{fn}$	slope of the pitching-moment coefficient of the fuselage and nacelles about the leading edge of the wing mean aerodynamic chord as obtained from section 4.7 (does not include "free moments"), per deg
$(C_{m\alpha})_{w(D)}$	slope of the pitching-moment coefficient due to the wing drag, per deg
$(C_{m\alpha})_{w(f)+f(w)}$	slope of the pitching-moment coefficient about the leading edge of the wing mean aerodynamic chord due to the effective wing lift, including the effects of the fuselage upwash on the wing and wing lift carryover onto the fuselage, per deg
$(C_{m\alpha})_{ws}$	average slope of the wing pitching-moment coefficient about the leading edge of the wing mean aerodynamic chord in the nonlinear lift range to stall, per deg

$\Sigma(C_{m\alpha})_{le}$	summation of the contributions of the wing, fuselage, nacelles, and interacting effects to the slope of the pitching moment about the leading edge of the wing mean aerodynamic chord, per deg
$\left(\frac{dC_D}{dC_L}\right)_w$	rate of change of the wing drag with wing lift
$-\left(\frac{dC_m}{dC_L}\right)_{cg}$	static margin relative to the center of gravity as a fraction of the wing mean aerodynamic chord
$-\left(\frac{dC_m}{dC_L}\right)_{.10\bar{c}_w}$	static margin relative to the center of gravity as a fraction of the wing mean aerodynamic chord with the center of gravity at $0.10\bar{c}_w$
$-\left(\frac{dC_m}{dC_L}\right)_{S.10\bar{c}_w}$	average static margin in the nonlinear region to stall relative to the center of gravity at $0.10\bar{c}_w$
$\left(\frac{dC_m}{dC_L}\right)_{w(D)}$	rate of change of the pitching-moment coefficient, due to wing drag, with the wing lift coefficient
c_n	chord of the wing at the centerline of the nacelle, in.
c_r	root chord of the wing at the centerline of the fuselage, in.
c_{re}	root chord of the exposed wing panel, in.
c_w	wing chord, in.
\bar{c}_w	wing mean aerodynamic chord, in. or ft
d	width of the fuselage at the wing, in.
e	wing efficiency factor for induced drag (assumed equal to 1.0)
$K_{f(w)}$	ratio of the wing lift carryover onto the fuselage to the wing alone, obtained from table 4.4-1(a)
$K_{w(f)}$	ratio of the wing lift in the presence of the fuselage to the wing alone, obtained from table 4.4-1(a)
$k = \frac{d}{b}$	
l	upper limit of integration in equation (4.8, 1-7); the distance from the leading edge of the wing at the body to the nose of the body, in.

l_h	distance from the wing trailing edge to the centroid of the last aft Δx segment of the fuselage length (table 4.8.1-2), in.
M	Mach number
S_w	reference wing area, sq ft
S_{we}	area of the exposed wing panels, sq ft
w_B	mean width of the body planform segment, Δx , in.
w_f, w_n	mean width, w_B , specifically applied to the fuselage and nacelle, respectively
x_1	distance from the wing leading edge to the centroid of the forward Δx segment of the body planform area, in.
\bar{x}_1	length of the Δx segment of the body planform area adjacent to and forward of the wing leading edge, in.
x'_1	distance from the wing trailing edge to the centroid of the aft Δx segment of the body planform area, in.
Δx	length of the segment of the body planform area, in.
$\left(\frac{x_{ac}}{c_{re}}\right)_{f(w)}$	contribution to the aerodynamic center due to the lift carryover of the wing onto the fuselage, as a fraction of the root chord of the exposed wing panels
$\left(\frac{x_{ac}}{c_{re}}\right)_{w(f)}$	aerodynamic center of the wing with the wing in the presence of the fuselage, as a fraction of and about the leading edge of the root chord of the exposed wing panels
$\frac{x_{cg}}{\bar{c}_w}$	distance to the center of gravity from the leading edge of and as a ratio of the wing mean aerodynamic chord
z_w	vertical distance from the center of gravity to the quarter-chord point of the wing mean aerodynamic chord, in.
α	angle of attack, deg
α^*	angle of attack at the upper limit of linearity of the lift-curve slope, deg
α_0	angle of attack for zero lift, deg
$\alpha_{C_{L_{max}}}$	angle of attack at maximum lift, deg
$\bar{\alpha}_s$	average value of angle of attack from α^* to $\alpha_{C_{L_{max}}}$

$$\frac{\partial \beta}{\partial \alpha}$$

variation of upwash and downwash with angle of attack at the Δx segment of the body forward of the wing leading edge and aft of the wing trailing edge, respectively

$$\frac{\partial \bar{\beta}}{\partial \alpha}$$

variation of upwash with angle of attack of the Δx segment of the body forward of and adjacent to the wing leading edge

$$\left(\frac{\partial \bar{\epsilon}_h}{\partial \alpha} \right)_M$$

average downwash gradient at and across the horizontal tail with compressibility accounted for

$$\frac{\partial \epsilon_w}{\partial \alpha}$$

rate of change of downwash, behind the wing, with angle of attack

$$\Lambda_{c/4}$$

sweep of the quarter-chord line of wing, deg

TABLE 4.8.1-1
WING PITCHING MOMENTS OF THE AIRPLANE

(a) Due to wing lift including mutual wing-fuselage interaction

$$(C_{m\alpha})_{w(f)+f(w)} = - \left[\left(\frac{x_{ac}}{c_{re}} \right)_{w(f)} K_{w(f)} + \left(\frac{x_{ac}}{c_{re}} \right)_{f(w)} K_{f(w)} \right] \left(\frac{c_{re}}{\bar{c}_w} \right) \left(\frac{S_{we}}{S_w} \right) (C_{L\alpha})_{we}$$

Symbol	Description	Reference	Magnitude
\bar{c}_w	Total wing mean aerodynamic chord, in.	Table 3.2-1	59.5
c_{re}	Root chord of exposed wing panels, in.	Table 3.2-1	71.9
S_w	Reference wing area, sq ft	Table 3.2-1	172.3
S_{we}	Exposed panel wing area, sq ft	Table 3.2-1	148.0
$(C_{L\alpha})_{we}$	Lift-curve slope of exposed wing panels per deg	Table 4.2-1	.0747
$K_{w(f)}$	Ratio of lift of wing in presence of fuselage to wing alone	Table 4.4-1(a)	1.09
$K_{f(w)}$	Ratio of wing lift carryover onto fuselage to wing alone	Table 4.4-1(a)	.14
$\left(\frac{x_{ac}}{c_{re}} \right)_{w(f)}$	Aerodynamic center of wing with wing in presence of fuselage, as fraction of and about leading edge of c_{re}	Table 4.5-1(b)	.198
d	Fuselage width at wing, in.	Figure 3.2-1	48.0
b	Wing span, in.	Figure 3.2-1	432.0
k	$\frac{d}{b}$	-----	.0555
$\Lambda_{c/4}$	Sweep of wing quarter-chord line, deg	Table 3.2-1	-2.5
$\left(\frac{x_{ac}}{c_{re}} \right)_{f(w)}$	Contribution to the aerodynamic center due to lift carryover of wing onto fuselage, as fraction of c_{re}	Equation (4.8.2-1)	.25
Summary: $(C_{m\alpha})_{w(f)+f(w)} = -0.0195$ per deg			

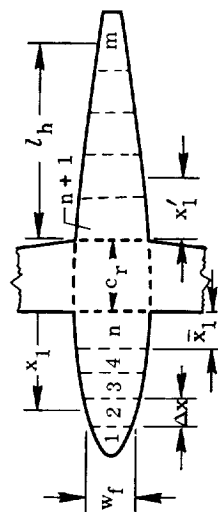
(b) Due to wing drag

$$(C_{m\alpha})_{w(D)} = -(C_L)_{wfn} \left[\frac{(C_{L\alpha})_w}{(C_{L\alpha})_{wfn}} \right] \left[\frac{2 (C_{L\alpha})_w}{\pi e A_w} \right] \frac{z_w}{\bar{c}_w}$$

Symbol	Description	Reference	Magnitude
A_w	Aspect ratio of total wing	Table 3.2-1	7.5
\bar{c}_w	Mean aerodynamic chord of total wing, in.	Table 3.2-1	59.5
z_w	Vertical distance from wind-tunnel center of gravity to $\bar{c}_w/4$, positive down, in.	From drawings	≈ -2.0
$(C_{L\alpha})_w$	Total wing lift-curve slope, based on $S_w = 172.3$ square feet per deg	Table 4.2-1	.0759
$(C_{L\alpha})_{wfn}$	Tail-off lift-curve slope, based on $S_w = 172.3$ square feet per deg	From columns 1 and 8 of table 4.4-2	.0831
e	Wing efficiency factor	-----	1.0 (assumed)
Summary: $(C_{m\alpha})_{w(D)} = 0.000197 C_{Lwfn}$ per deg			

TABLE 4.8.1-2
"FREE MOMENTS" OF FUSELAGE AND NACELLES

(a) Basic parameters



Segments 1 \rightarrow (n - 1), obtain $\frac{\partial \beta}{\partial \alpha}$ from $\frac{x_1}{c_r}$ versus $\frac{\partial \beta}{\partial \alpha}$

Segment n, obtain $\frac{\partial \beta}{\partial \alpha}$ from $\frac{\bar{x}_1}{c_r}$ versus $\frac{\partial \beta}{\partial \alpha}$

Segments (n + 1) \rightarrow m, $\frac{\partial \beta}{\partial \alpha} = \frac{x'_1}{l_h} (1 - \frac{\partial \epsilon}{\partial \alpha})$

Symbol	Description	Reference	Magnitude
w_B	Mean width of body planform segment Δx , in.	From drawing	$f(x_1), f(x'_1)$
x_1	Distance from wing leading edge to centroid of forward Δx segments	From drawing	Variable
x'_1	Distance from wing trailing edge to centroid of aft Δx segment	From drawing	Variable
c_r	Root chord of wing at centerline of fuselage, in.	Table 3.2-1	76.0
c_n	Chord of wing at centerline of nacelle, in.	Table 3.2-1	64.0
l_h	Distance from wing trailing edge to centroid of last aft Δx segment, in.	From drawings	116.0
$\frac{\partial \epsilon_w}{\partial \alpha}$	Rate of change of downwash, behind wing, with angle of attack	Table 4.9.1-2, column 24	$\approx .48$
$\frac{\partial \beta}{\partial \alpha}$	For Δx segments forward of the wing leading edge: the variation of upwash at the segment, with angle of attack; a function of $\frac{x_1}{c_r}$ for fuselage, a function of $\frac{x_1}{c_n}$ for nacelle For Δx segments aft of wing trailing edge: the variation of downwash at the segment with angle of attack	Figure 4.8.1-1	$f(\frac{x_1}{c})$
S_w	Reference wing area, sq ft	Equation (4.8.1-8)	$f(x'_1, h, \frac{\partial \epsilon_w}{\partial \alpha})$
\bar{c}_w	Reference mean aerodynamic chord, ft	Table 3.2-1	172.3
		Table 3.2-1	4.96

TABLE 4.8.1-2 (Concluded)

(b) Fuselage

$$(C_{m\alpha})_{f(c)} = \frac{1}{36.5S_w \bar{c}_w} \sum \frac{w_f^2 \Delta x}{1728} \frac{d\beta}{d\alpha}$$

Segment	Δx , in.	w_f	w_f^2	$\frac{w_f^2 \Delta x}{1728}$	x_1 , in.	$\frac{x_1}{c_r}$	$\frac{x_1}{l_h}$	$\frac{d\beta}{d\alpha}$ (fig. 4.8.1-1)	$\frac{x_1}{l_h} \left(1 - \frac{\partial c}{\partial \alpha}\right)$	$\frac{w_f^2 \Delta x}{1728} \frac{d\beta}{d\alpha}$
1	9.0	8.0	64	0.33	88.7	1.17	----	1.15	----	0.38
2	16.0	21.25	450	4.17	76.2	1.00	----	1.20	----	5.00
3	18.5	32.0	1020	10.90	58.9	.78	----	1.23	----	13.40
4	18.5	39.25	1540	16.50	40.4	0.53	----	1.32	----	21.78
5=n	31.2	44.5	1980	35.80	15.6	.21	----	3.50	----	125.3
6=n+1	5.1	44.0	1936	5.7	2.8	----	0.02	----	0.01	0.06
7	27.5	38.25	1463	23.3	18.0	----	0.15	----	0.08	1.86
8	41.0	27.75	770	18.3	52.0	----	.45	----	.23	4.21
9	35.4	16.0	256	5.24	88.0	----	0.76	----	0.40	2.10
10=m	17.0	5.0	25	.25	116.0	----	1.00	----	.52	.13
Summary: $(C_{m\alpha})_{f(c)} = 0.00558$ per deg based on $S_w = 172.3$ sq ft										$\sum \frac{w_f^2 \Delta x}{1728} \frac{d\beta}{d\alpha} = 174.22$

(c) Nacelles

$$(C_{m\alpha})_{n(c)} = (2 \text{ nacelles}) \frac{1}{36.5S_w \bar{c}_w} \sum \frac{w_n^2 \Delta x}{1728} \frac{d\beta}{d\alpha}$$

Segment	Δx , in.	w_n	w_n^2	$\frac{w_n^2 \Delta x}{1728}$	x_1 , in.	$\frac{x_1}{c_n}$	$\frac{d\beta}{d\alpha}$ (fig. 4.8.1-1)	$\frac{w_n^2 \Delta x}{1728} \frac{d\beta}{d\alpha}$
1	7	16.0	256	1.04	48.0	0.75	1.25	1.29
2	3	32.5	1055	1.83	44.0	0.69	1.27	2.32
3	10	35.0	1225	7.09	38.0	.59	1.32	9.36
4	10	35.5	1260	7.29	28.0	0.44	1.38	10.06
5=n	23	35.0	1225	16.30	11.5	.18	3.65	59.50
Summary: $(C_{m_\alpha})_{n(\epsilon)} = 0.0053$ per deg based on $S_w = 172.3$ sq ft								$\sum \frac{w_n^2 \Delta x}{1728} \frac{d\beta}{d\alpha} = 82.53$

(d) Summary

$$(C_{m\alpha})_{f(c)+n(c)} = (C_{m\alpha})_{f(c)} + (C_{m\alpha})_{n(c)} = 0.0109 \text{ per deg}$$

TABLE 4.8.3-1
PITCHING MOMENTS OF WING-FUSELAGE-NACELLES CONFIGURATION

$$(C_{m_{wfn}})_{.10\bar{c}_w} = -0.0463 + 0.0456 C_{L_{wfn}}^2 - 0.0081 C_{L_{wfn}}^3$$

①	②	③	④	⑤	⑥	⑦	⑧
α relative to X-axis, deg	$C_{L_{wfn}}$ (table 4.4-2, $S_w = 172.3$ sq ft)	$C_{L_{wfn}}^2$ $= \textcircled{2}^2$	$(C_{m_o})_{wfn}$	$0.0456 C_{L_{wfn}}$ $= 0.0456 \textcircled{2}$	$-0.0081 C_{L_{wfn}}^2$ $= 0.0081 \textcircled{3}$	$(C_{m_{wfn}})_{.10\bar{c}_w}$ $= \textcircled{4} + \textcircled{5} + \textcircled{6}$ on basis of $S_w = 172.3$ sq ft	$(C_{m_{wfn}})_{.10\bar{c}_w}$ on basis of $S_w = 178$ sq ft
-4	-0.020	0.0004	-0.0463	-0.0009	≈ 0	-0.0472	-0.0457
-2	.147	.0207	-.0463	.0065	-.0002	-.0399	-.0386
0	0.310	0.0961	-0.0463	0.0141	-0.0006	-0.0328	-0.0318
2	.475	.226	-.0463	.0217	-.0018	-.0264	-.0255
4	0.641	0.411	-0.0463	0.0292	-0.0033	-0.0204	-0.0198
6	.807	.653	-.0463	.0368	-.0053	-.0148	-.0143
8	0.973	0.949	-0.0463	0.0444	-0.0077	-0.0095	-0.0093
10	1.140	1.304	-.0463	.0520	-.0106	-.0049	-.0048
12	-----	-----	-----	-----	-----	-0.0045 ^c	-0.0044
13.8	1.281	-----	-----	-----	-----	-.0115 ^c	-.0111

^aLimit of linearity of lift-curve slope from figure 4.4-4.

^b $a_{C_{L_{max}}}$ from figure 4.4-4.

^cIn nonlinear range of lift-curve slope, determined from figure 4.8.3-1.

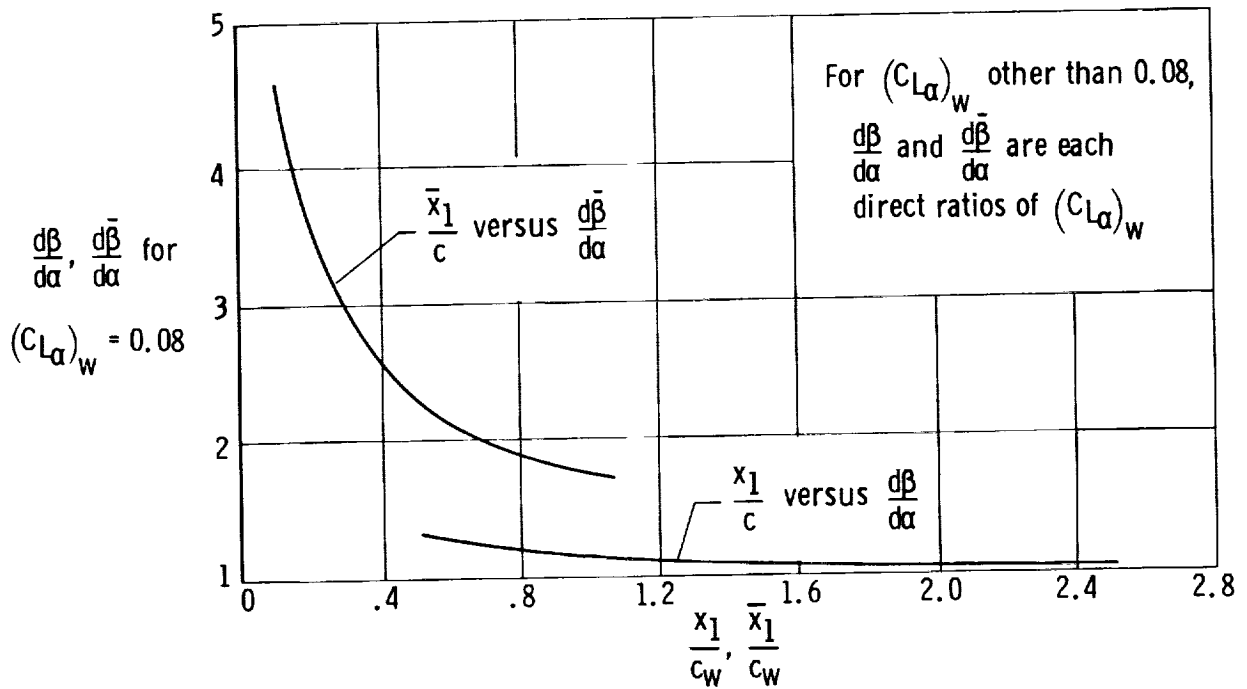


Figure 4.8.1-1. Variation of the wing upwash derivative with position along the body from the leading edge of the wing. For use in determining "free moments" of the body (ref. 13).

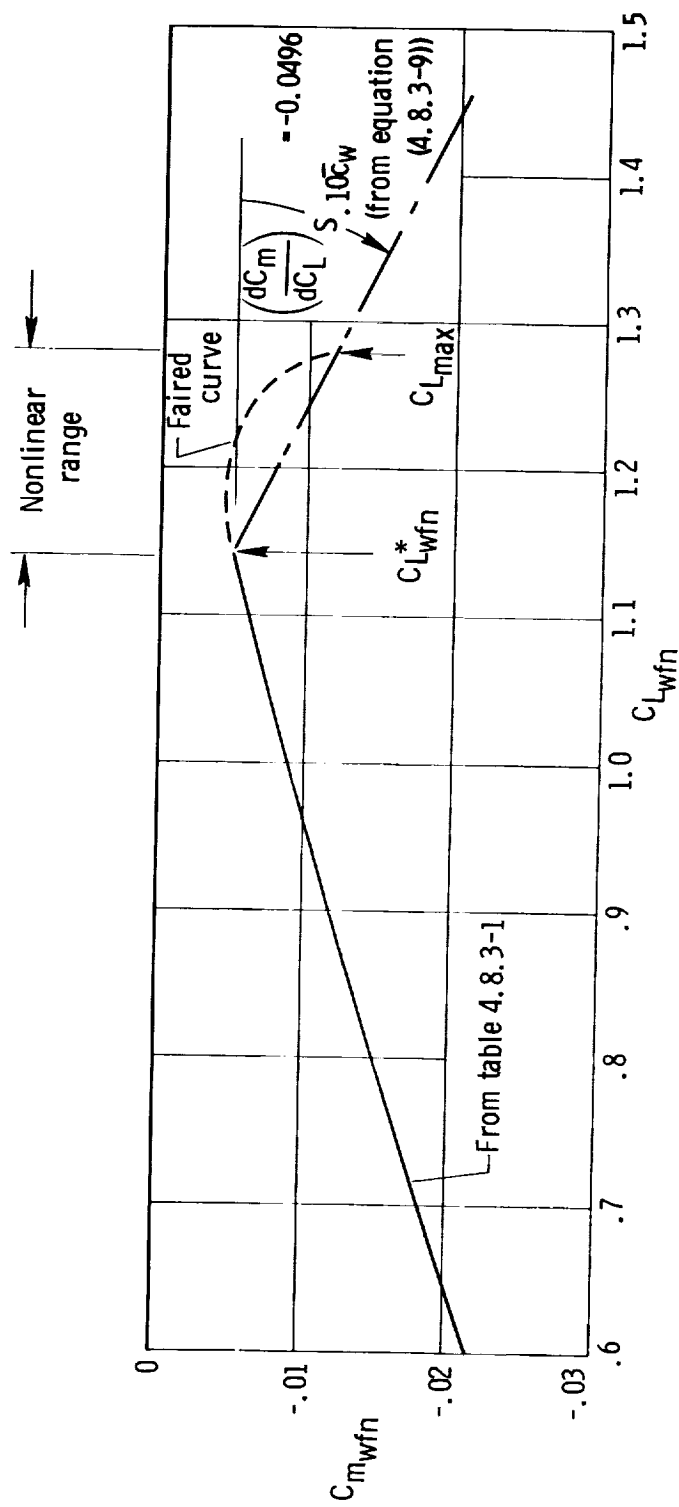


Figure 4.8.3-1. Approximate graphical determination of pitching-moment coefficient in nonlinear range for wing-fuselage-nacelle configuration. $S_w = 172.3$ sq ft; center of gravity $= 0.10 \bar{c}$.

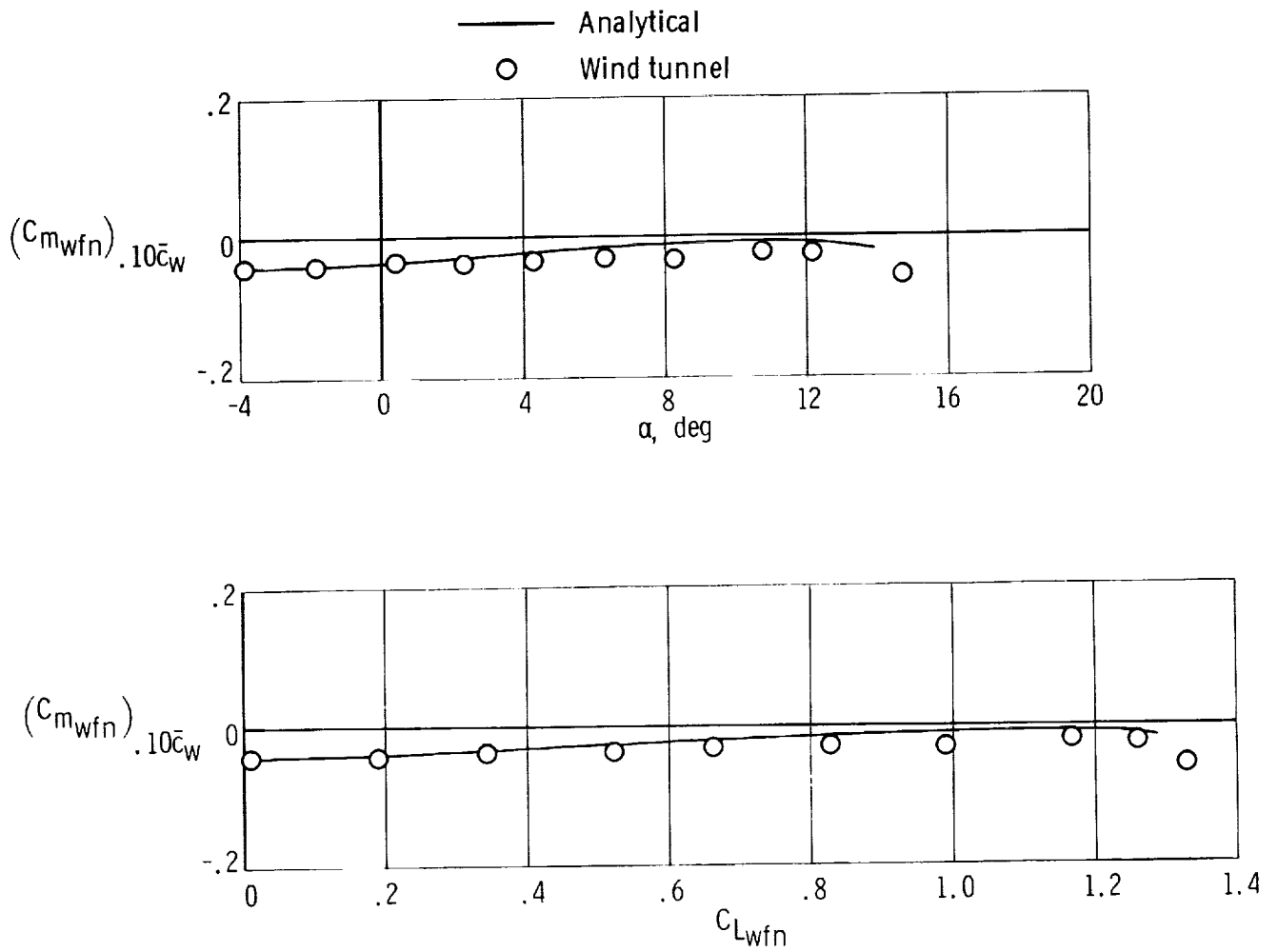


Figure 4.8.3-2. Comparison of calculated tail-off pitching-moment characteristics with wind-tunnel data. $S_w = 178$ sq ft.

4.9 Downwash and Dynamic Pressure at the Horizontal Tail

The methods presented for predicting the subsonic downwash and dynamic pressure in the region of the tail plane for preliminary design purposes were developed for the linear lift region for swept- and unswept-wing airplanes. Their use in the nonlinear region below stall, however, provides reasonable approximations. The total downwash picture is complex, as the following discussion illustrates.

A limitation of the method for downwash determination is its neglect of the interference from fuselage and nacelles. Also neglected is the small effect of the tail itself on the flow ahead of it. For conventional configurations of general aviation aircraft, and propeller-off conditions at least, the interference effects do not appear to be significant.

4.9.1 Downwash

The downwash behind a wing at subsonic flow conditions is the result of the wing's vortex system. A vortex sheet, shed by the lifting wing as in figure 4.9.1-1, is deflected downwind by the bound (lifting) and trailing (tip) vortices. The curvature of the vortex sheet is relatively small in the plane of symmetry for straight wings with reasonably large aspect ratios. Wings with large trailing-edge sweepback produce a vortex sheet that is bowed upward in the plane of symmetry.

The vortex sheet does not extend unaltered indefinitely downstream but, as it is displaced vertically, distends rapidly and rolls up like a volute about the tip-vortex cores. The tip vortexes have a relatively small vertical displacement from free-stream direction as they tend to move inboard. When all the vorticity is transferred from the sheet to the tip vortexes, the vortex system is considered to be rolled up.

Rational tail-plane design depends on a knowledge of the velocity and direction of the airflow in the region behind the wing. The shape of the vortex sheet significantly influences the downwash experienced by the tail in the flow field of the wing. For a complete rollup the spanwise downwash distribution is dependent upon the spanwise lift distribution of the wing. When the rollup is complete, however, the downwash angles for all wings of equal lift and equal effective span at the tail are identical. Since the tip vortexes are somewhat above the vortex sheet, the downwash above the sheet is somewhat greater than the downwash below the sheet.

The tip vortexes originate at the wing tips at angles of attack for which the flow is unseparated. Certain thin, highly swept wings have a significantly different flow pattern in the higher angle-of-attack range. These wings are characterized by a leading-edge separation vortex that lies above the surface of the wing. From its inception near the plane of symmetry, it moves outboard in the approximate direction of the wing leading edge and is finally shed in a streamwise direction near the wing tip.

For wings stalled at the tip—a characteristic of highly tapered, untwisted, straight wings and highly swept wings—the downwash in the region of the tail will be greater for a stalled wing than for an unstalled wing for a given lift coefficient. Wings with low taper ratio, or with washout, stall first at the center, and the wake does not leave the wing at the trailing edge but at a point $\frac{c}{2} \sin \alpha$ above the trailing edge. In general, when the wing stalls at the center, the center of the wake moves upward and

the vortexes rolling off the edge of the stalled portion reduce the downwash.

Several methods are available for predicting downwash at subsonic conditions. Reference 14 considers wings with zero sweep of the quarter-chord line and presents design charts for various taper ratios and aspect ratios for incompressible flow conditions. The design charts are for flapped as well as unflapped configurations and include load distribution, downwash displacement, and downwash angles. Reference 15 considers unflapped swept wings and compressible flow conditions. Reference 16 uses graphical procedures and considers unflapped wings of various sweeps at compressible flow conditions. Because of its relative simplicity and versatility, the method of reference 16 (also considered in ref. 1) is presented and applied to the subject airplane.

The method of reference 16 is for configurations in which the tail span is less than two-thirds of the wing span. The basic approach of the method is to:

(1) Determine the downwash in the plane of symmetry at the height of the tip vortexes at the longitudinal station of the horizontal tail mean aerodynamic chord quarter chord.

(2) Correct this value for tail height above the vortexes.

(3) Evaluate the effect of tail span by relating the average downwash at the tail to the downwash determined from step 2.

Details of the development of the method are included in reference 16. It should be noted, however, that the method assumes the vortexes to be essentially rolled up at the longitudinal-tail station. Thus it is fortunate that the vortexes roll up in a shorter distance as the angle of attack increases, because downwash effects become increasingly important at the higher angles of attack.

The procedural steps in applying the method are as follows (pertinent dimensions defined in fig. 4.9.1-1):

(1) The effective aspect ratio, $\frac{A_{w\text{eff}}}{A_w}$, and effective span ratio, $\frac{b_{w\text{eff}}}{b_w}$, are determined from figure 4.9.1-2 as functions of wing angle-of-attack ratio, $\frac{\alpha_w - \alpha_0}{\alpha_{C_{L\text{max}}} - \alpha_0}$, taper ratio, λ_w , and sweep of the quarter chord, $(\Lambda_{c/4})_w$.

(2) The low-speed downwash gradient, $\left(\frac{\partial \epsilon_{vc}}{\partial \alpha}\right)_{v_{\text{low speed}}}$, in the plane of symmetry at the height of the vortex core is obtained from figure 4.9.1-3 as a function of tail length $\frac{2l_2}{b_w}$, effective aspect ratio, $A_{w\text{eff}}$, quarter-chord sweep, $(\Lambda_{c/4})_w$, and downwash gradient at infinity obtained from

$$\frac{\partial \epsilon_{\infty}}{\partial \alpha} = \frac{2(57.3)}{\pi A_w} (C_{L\alpha})_w \quad (4.9.1-1)$$

where $(C_{L\alpha})_w$ is in degrees. At the wing trailing edge, $\frac{\partial \epsilon}{\partial \alpha} = 1$.

(3) The vertical position, a , of the horizontal-tail quarter-chord point relative to the vortex core depends upon the type of wing separation as determined from figure 4.9.1-4 as a function of leading-edge-sharpness parameter, Δy (from section 4.1), and quarter-chord sweep, $(\Lambda_c/4)_w$. For trailing-edge separation,

$$a = z_h - l_{\text{eff}} \left(\frac{\alpha_w}{57.3} - \frac{0.41 C_{Lw}}{\pi A_{w\text{eff}}} \right) - \frac{b_{w\text{eff}}}{2} \tan \Gamma \quad (4.9.1-2)$$

where l_{eff} is the distance in the wing-chord plane from the vortex tip of the quarter chord of $b_{w\text{eff}}$ to the quarter chord of the tail mean aerodynamic chord, and Γ is the dihedral angle of the wing. For leading-edge separation,

$$a = z'_h - (l_2 + l_3) \left(\frac{\alpha_w}{57.3} - \frac{0.41 C_{Lw}}{\pi A_{w\text{eff}}} \right) \quad (4.9.1-3)$$

where l_3 is the distance from the leading edge of the wing mean aerodynamic chord to the trailing edge of the wing root chord, and l_2 is as defined in figure 4.9.1-1.

(4) The span, b_{vor} , of the vortexes at the longitudinal location of the quarter chord of the tail mean aerodynamic chord is determined from the following equation originally obtained from reference 16 but also included in reference 1:

$$b_{\text{vor}} = b_{w\text{eff}} - (b_{w\text{eff}} - b_{\text{ru}}) \left(\frac{2l_{\text{eff}}}{b_w l_{\text{ru}}} \right)^{1/2} \quad (4.9.1-4)$$

where b_{ru} , the span of the completely rolled up vortexes, is obtained from

$$b_{\text{ru}} = [0.78 + 0.10(\lambda_w - 0.4) + 0.003(\Lambda_c/4)_w] b_{w\text{eff}} \quad (4.9.1-5)$$

and

$$l_{\text{ru}} = \frac{0.56 A_w}{C_{Lw}} \quad (4.9.1-6)$$

(5) The average downwash gradient acting on the tail is obtained from

$$\left(\frac{\partial \bar{\epsilon}_h}{\partial \alpha} \right)_{\text{low speed}} = \left[\frac{\frac{\partial \bar{\epsilon}_h}{\partial \alpha}}{\frac{\partial \epsilon_{vc}}{\partial \alpha}} \right]_{\text{low speed}} \left(\frac{\partial \epsilon_{vc}}{\partial \alpha} \right)_{\text{low speed}} \quad (4.9.1-7)$$

where the $[\]$ quantity is obtained from figure 4.9.1-5 (ref. 17) as a function of $\frac{2a}{b_{vor}}$ and $\frac{b_h}{b_{vor}}$.

(6) Because the preceding result is for low-speed conditions, an adjustment to higher subsonic Mach numbers is made, on the basis of reference 1, by

$$\left(\frac{\partial \bar{\epsilon}_h}{\partial \alpha}\right)_M = \left(\frac{\partial \bar{\epsilon}_h}{\partial \alpha}\right)_{\text{low speed}} \frac{(C_{L\alpha})_{w_M}}{(C_{L\alpha})_{w_{\text{low speed}}}} \quad (4.9.1-8)$$

Figure 4.9.1-6, from reference 16, compares the calculated and experimentally determined downwash variation with α for several airplanes and provides a qualitative index for the accuracy of the prediction procedure for propeller-off conditions.

Figure 4.9.1-7 shows the calculated downwash characteristics for the subject airplane. No test data were available for comparison. However, on the basis of the correlation of calculated and experimentally determined propeller-off pitching-moment characteristics presented in section 4.11, the calculated downwash characteristics appear to be accurate. Tables 4.9.1-1 and 4.9.1-2 list the pertinent parameters and summary calculations, respectively, for the subject airplane.

4.9.2 Dynamic-Pressure Ratio

A horizontal tail operating in the wake of a wing experiences a loss in effectiveness due to the decrease in dynamic pressure in the wake. This decrease is caused by the loss in flow energy in the form of friction and separation drag of the wing; the greater the drag, the greater the pressure loss.

The wake, usually thin and intense near the trailing edge, spreads and decays with increasing downstream distance from the trailing edge in a manner such that the integrated momentum across the wake is constant and not a function of longitudinal distance. The centerline of the wake coincides with the centerline of the trailing vortex sheet. The wake occurs in all speed regions.

A basic method for predicting the dynamic pressure at the horizontal tail in the linear lift range up to a Mach number of approximately 0.65 is given in reference 14. This method, which was applied to the subject airplane, neglects fuselage interference effects and was developed on the basis of wings with zero sweep of the quarter chord. Reference 18 extends the application of the method to nonlinear conditions approaching stall. A modification of the basic method, to account for fuselage interference and wing sweep, is presented in reference 19. The procedures of the basic method are considered at this time.

On the basis of reference 14, the half-width of the wake, Δz_{wake} , at distance x from the wing-root trailing edge to the horizontal-tail mean-aerodynamic-chord quarter chord (fig. 4.9.2-1) is given by

$$\frac{\Delta z_{\text{wake}}}{\bar{c}_w} = 0.68 \sqrt{C_{Df} \left(\frac{x}{\bar{c}_w} + 0.15 \right)} \quad (4.9.2-1)$$

where, in accordance with references 14 and 1, C_{Df} is the wing zero-lift drag coefficient. Curves of this equation are shown in figure 4.9.2-2 for different values of C_{Df} .

The maximum loss of dynamic pressure in the wake at the tail which occurs at the wake centerline is obtained from

$$\left(\frac{\Delta \bar{q}}{\bar{q}_\infty}\right)_o = \frac{2.42 C_{Df}^{1/2}}{\frac{x}{\bar{c}_w} + 0.3} \quad (4.9.2-2)$$

or its graphical representation, figure 4.9.2-3.

The dynamic-pressure loss at any point in the wake normal to and from the wake centerline is obtained from

$$\left(\frac{\Delta \bar{q}}{\bar{q}_\infty}\right)_h = \left(\frac{\Delta \bar{q}}{\bar{q}_\infty}\right)_o \cos^2 \left(\frac{\pi}{2} \frac{z_h''}{\Delta z_{wake}}\right) \quad (4.9.2-3)$$

or its graphical representation, figure 4.9.2-4. When $\frac{z_h''}{\Delta z_{wake}}$ is greater than 1, the dynamic-pressure loss is zero.

The vertical distance, z_h'' , is given by the equation

$$z_h'' = x \tan (\gamma + \epsilon_h - \alpha_w) \quad (4.9.2-4)$$

where ϵ_h is the downwash in the plane of symmetry and is given by

$$\epsilon_h = 57.3 \frac{1.62 C_{Lw}}{\pi A_w} = \frac{92.83 C_{Lw}}{\pi A_w} \text{ in degrees} \quad (4.9.2-5)$$

and where γ is defined in figure 4.9.2-1.

The dynamic pressure is then determined to be

$$\frac{\bar{q}_h}{\bar{q}_\infty} = 1 - \left(\frac{\Delta \bar{q}}{\bar{q}_\infty}\right)_h \quad (4.9.2-6)$$

Although the preceding relations were developed from results obtained at lifts below the stall, reference 18 indicates that they apply with reasonable accuracy above the stall if the profile drag coefficient of the stalled wing is known.

The accuracy of the procedure, developed on the basis of unswept wings, may be estimated from table 4.9.2-1 (from ref. 1) which includes swept as well as unswept configurations. The table compares calculated dynamic-pressure ratios with the low-speed model test data of references 20 and 21.

The foregoing procedures for determining the dynamic-pressure ratios at the horizontal tail were applied to the subject airplane. Basic pertinent parameters and a summary of the calculations are listed in table 4.9.2-2. The results indicated that the horizontal tail is outside the wake and thus the dynamic-pressure loss is zero in the linear and incipient stall region. At full stall, in the absence of an applicable profile-drag coefficient, the dynamic-pressure ratio was assumed to be equal to 1.00, although a more realistic value would probably have been closer to 0.80. The results are included in figure 4.9.1-7.

Although not used, a modification of the preceding method which considers wing sweep and combined wing-body profile drag was given in reference 19. The procedure is in the form of a nomograph (fig. 4.9.2-5). The accuracy of the method may be estimated from figure 4.9.2-6 (from ref. 19) which uses data from references 21 to 26.

4.9.3 Symbols

A_w	wing aspect ratio
$A_{w\text{eff}}$	effective aspect ratio of the wing (from fig. 4.9.1-2)
a	vertical position of the horizontal-tail quarter-chord point relative to the vortex core (fig. 4.9.1-1), in.
b_h	horizontal-tail span, ft
b_{ru}	span of the completely rolled up tip vortexes, ft
b_{vor}	span of the tip vortexes at the longitudinal location of the quarter chord of the horizontal-tail mean aerodynamic chord (fig. 4.9.1-1), ft
b_w	wing span, ft
$b_{w\text{eff}}$	effective span of the wing (from fig. 4.9.1-2), ft
C_{Df}, \bar{C}_{Df}	wing and wing-body zero-lift drag coefficient, respectively
C_{Lw}	wing lift coefficient
$(C_{L\alpha})_w$	wing lift-curve slope, per deg
$(C_{L\alpha})_{w\text{low speed}}, (C_{L\alpha})_{wM}$	wing lift-curve slope with compressibility unaccounted and accounted for, respectively
c	chord, ft

\bar{c}	mean aerodynamic chord, ft
\bar{c}_w	mean aerodynamic chord of the wing, ft
i_w	incidence of the wing relative to the X-body axis, deg
l_{eff}	distance, in the wing root-chord plane, from the tip vortex at the quarter chord of the $b_{w_{eff}}$ to the quarter chord of the horizontal-tail mean aerodynamic chord (fig. 9.4.1-1), ft
l_{ru}	distance required for the complete rollup of the wing-tip vortices, ft
l_2	tail length in the wing root-chord plane from the root-chord trailing edge to the quarter chord of the horizontal-tail mean aerodynamic chord (fig. 4.9.1-1), ft
l_3	distance from the leading edge of the wing mean aerodynamic chord to the trailing edge of the wing root chord, ft
M	Mach number
\bar{q}_∞	free-stream dynamic pressure, lb/sq ft
$\frac{\bar{q}_h}{\bar{q}_\infty}$	ratio of the horizontal-tail to free-stream dynamic pressure
$\left(\frac{\Delta \bar{q}}{\bar{q}_\infty}\right)_h$	dynamic-pressure loss at the horizontal tail as a ratio of \bar{q}_∞
$\left(\frac{\Delta \bar{q}}{\bar{q}_\infty}\right)_o$	dynamic-pressure loss at the wake centerline as a ratio of \bar{q}_∞
S_w	wing area, sq ft
V	airspeed, ft/sec
x	distance, parallel to the centerline of the wake, from the trailing edge of the wing root chord to the quarter chord of the horizontal-tail mean aerodynamic chord (fig. 4.9.2-1), ft
Δy	leading-edge-sharpness parameter
z'_h	vertical distance from the root-chord plane of the wing to the quarter-chord point of the horizontal-tail mean aerodynamic chord (fig. 4.9.1-1), ft

z_h''	vertical distance from the centerline of the wake to the quarter chord of the horizontal-tail mean aerodynamic chord (fig. 4.9.2-1)
Δz_{wake}	half-width of the wake at a distance x from trailing edge of the wing root chord (fig. 4.9.2-1), ft
α	angle of attack, deg
α_b	angle of attack relative to the X-body axis, deg
$\alpha_{C_{L\text{max}}}$	angle of attack of the wing, relative to the chord, at $C_{L\text{max}}$
α_o	wing zero-lift angle relative to the wing chord, deg
α_w	wing angle of attack relative to the wing chord, $\alpha_b + i_w$, deg
$(\alpha_w)_{\text{abs}}$	absolute angle of attack of the wing, $\alpha_w - \alpha_o$
γ	angle between the wing chord plane and the line connecting the trailing edge of the wing root chord and the quarter chord of the horizontal-tail mean aerodynamic chord (fig. 4.9.2-1), deg
ϵ	downwash, deg
ϵ_h	downwash in the plane of symmetry at the vortex sheet (fig. 4.9.2-1), deg
$\bar{\epsilon}_h$	average downwash across the horizontal tail, deg
$\frac{\partial \epsilon_{vc}}{\partial \alpha}$	rate of change of downwash, in the plane of symmetry at the height of the vortex core, with the absolute angle of attack
$\frac{\partial \epsilon_{\infty}}{\partial \alpha}$	downwash gradient at infinity
$\left(\frac{\partial \bar{\epsilon}_h}{\partial \alpha}\right)_{\text{low speed}}, \left(\frac{\partial \bar{\epsilon}_h}{\partial \alpha}\right)_M$	average downwash gradient at and across the horizontal tail with compressibility unaccounted and accounted for, respectively
λ_w	wing taper ratio
$(\Lambda_{le})_w$	sweep of the wing leading edge, deg
$(\Lambda_{c/4})_w$	sweep of the wing quarter-chord line, deg
$\mu = \gamma + \epsilon_h - \alpha_w$, deg	

Γ

wing dihedral angle, deg

TABLE 4.9.1-1
PERTINENT PARAMETERS FOR COMPUTING AVERAGE DOWNWASH AT
HORIZONTAL TAIL OF SUBJECT AIRPLANE

Symbol	Description	Reference	Magnitude
α_0	Wing zero-lift angle relative to chord, deg	Table 4.2-1	-2
$\alpha_{C_{L_{\max}}}$	Wing angle of attack at maximum lift coefficient, relative to chord, deg	Table 4.2-1	15.4
$(\Lambda_{c/4})_w$	Wing sweep along $c/4$ line, deg	Table 3.2-1	-2.5
Δy	Wing leading-edge-sharpness parameter, chord lengths	Table 4.1-1	.0316c
λ_w	Wing taper ratio	Table 3.2-1	.513
A_w	Wing aspect ratio	Table 3.2-1	7.5
b_w	Wing span, ft	Table 3.2-1	36.0
Γ	Wing dihedral, deg	Table 3.2-1	5.0
z'_h	Perpendicular distance from wing-chord plane to $\bar{c}/4$ of horizontal tail, ft	Scaled from drawings	2.5
l_2	Tail length in wing root-chord plane from wing-root trailing edge to $\bar{c}/4$ of horizontal tail, ft	Figure 3.2-1 and 3.2-2	8.68
l_3	Distance from leading-edge wing mean aerodynamic chord to trailing edge of wing root chord, ft; used only if flow separation is at leading edge (fig. 4.9.1-4)	Figure 3.2-1	6.33
$\frac{A_{weff}}{A_w}$	Ratio of effective to geometric aspect ratio	Figure 4.9.1-2	1.00
$\frac{b_{weff}}{b_w}$	Ratio of effective to geometric wing span	Figure 4.9.1-2	1.00
l_{eff}	Tail length in root-chord plane from vortex tip of $c/4$ of b_{weff} to $\bar{c}/4$ of horizontal tail, ft; function of b_{weff}	Scaled from drawings	14.18
$(C_{L\alpha})_w$	Lift-curve slope of wing, deg	Table 4.2-1	0.0759
$\frac{\partial \epsilon_\infty}{\partial \alpha}$	Downwash gradient at infinity = $\frac{114.6}{\pi A} (C_{L\alpha})_w$	Equation (4.9.1-1)	.369
$\frac{2l_2}{b_w}$	-----	-----	.482
$\left(\frac{\partial \epsilon_{vc}}{\partial \alpha}\right)_{\text{low speed}}$	Downwash gradient in plane of symmetry at height of vortex core	Figure 4.9.1-3	.472
b_{ru}	Span of completely rolled up wing-tip vortexes, $[0.78 + 0.10(\lambda_w - 0.4) + 0.003(\Lambda_{c/4})_w] b_{eff}$, ft	Equation (4.9.1-5)	$0.7836 b_{weff}$
l_{ru}	Distance required for complete rollup of wing-tip vortexes in chord plane, $\frac{0.56 A_w}{C_{L_w}}$, semispans	Equation (4.9.1-6)	$4.20/C_{L_w}$
b_{vor}	Span of vortexes at longitudinal location of $\bar{c}/4$ of horizontal tail, $b_{weff} - (b_{weff} - b_{ru}) \left(\frac{2l_{eff}}{b_w l_{ru}} \right)^{1/2} = 36 - [36 - b_{ru}] \left(\frac{0.786}{l_{ru}} \right)^{1/2}$, ft	Equation (4.9.1-4)	Variable
a	Vertical distance from horizontal-tail root chord to vortex core, $z'_h - l_{eff} \left(\frac{\alpha_w}{57.3} - \frac{0.41 C_{L_w}}{\pi A_{weff}} \right) - \frac{b_{weff}}{2} \tan \Gamma$ if separation is at trailing edge, ft	Equation (4.9.1-2)	Variable
$\left[\frac{\partial \bar{\epsilon}_h}{\partial \alpha} \right]_{\text{low speed}}$	Ratio of average downwash acting on horizontal tail to downwash at vortex-core height, $f \left(\frac{2a}{b_{vor}}, \frac{b_h}{b_{vor}} \right)$	Figure 4.9.1-5	Variable
$\left(\frac{\partial \bar{\epsilon}_h}{\partial \alpha} \right)_M$	Downwash gradient at horizontal tail at Mach number, $\left(\frac{\partial \bar{\epsilon}_h}{\partial \alpha} \right)_{\text{low speed}} \left[\frac{(C_{L\alpha})_{wM}}{(C_{L\alpha})_w} \right]_{\text{low speed}}$	Equation (4.9.1-8)	$\approx \left(\frac{\partial \bar{\epsilon}_h}{\partial \alpha} \right)_{\text{low speed}}$ at wind-tunnel Mach number

TABLE 4.9.1-2
SUMMARY CALCULATION OF AVERAGE DOWNWASH AT HORIZONTAL TAIL OF SUBJECT AIRPLANE

①	②a	②b	③	④	⑤	⑥	⑦	⑧	⑨	⑩	⑪	⑫	⑬	⑭	⑮
α_b , relative to X-axis, deg	α_w , relative to		$(\alpha_w)_{abs}$ $\alpha_w - \alpha_b$, deg	$\frac{\alpha_w - \alpha_b}{C_{L_{max}}}$ $(3)/17.4$	Figure 4.9.1-2 $\frac{A_{weff}}{A_w}$		A_{weff} 7.5 (5)	b_{weff} 36 (6)	Table 4.9.1-1, l_{eff} , ft	Figure 4.9.1-3, $\left(\frac{\partial \epsilon_{vc}}{\partial \alpha}\right)_{low\ speed}$	b_{ru} 0.7836 (8)	Figure 4.2-1, $S_w = 172.3\ ft^2$, C_{L_w}	$0.41 C_{L_w} = \frac{\pi A_{weff}}{0.0174}$ (12)	$(21) - (13)$	$(9) \times (14)$
	deg	rad			$\frac{b_{weff}}{b_w}$										
-2	0	0	2	0.115	1.00	1.00	7.5	36.0	14.18	0.472	28.2	0.152	0.00264	-0.00264	-0.0374
2	4	.0698	6	.344	1.00	1.00	7.5	36.0	14.18	.472	28.2	.455	.00792	.0619	.878
6	8	.1396	10	.575	1.00	1.00	7.5	36.0	14.18	.472	28.2	.755	.01314	.1265	1.794
10	12	.209	14	.804	1.00	1.00	7.5	36.0	14.18	.472	28.2	1.060	.01844	.191	2.71
13.4	15.4	.268	17.4	1.00	1.00	1.00	7.5	36.0	14.18	.472	28.2	1.23	.0214	.2476	3.51

①	⑩b	⑩c	⑩d	⑬	⑭	⑮	⑯	⑰	⑱	㉑	㉒	㉓	㉔	㉕	㉖
α_b , relative to X-axis, deg	$\frac{b_{weff} \tan \Gamma}{2}$ 0.0436 (8)	a 2.5 - (15) - (19), in.	l_{ru} 4.20/ (12), ft	$\left(\frac{2l_{eff}}{b_w/r_u}\right)^{1/2}$ (9)/18 (18) ^{1/2}	b_{vor} (8) - (8) - (11)(19), ft	$\frac{2a}{b_{vor}}$ 2 (17) (20)	$\frac{b_h}{b_{vor}}$ 12.5/ (21)	Figure 4.9.1-5, $\left(\frac{\partial \epsilon_h}{\partial \alpha}\right)_{low\ speed}$	$\left(\frac{\partial \epsilon_h}{\partial \alpha}\right) M$ $\approx (19) \times (23) \times 1$ (a)	$\frac{(C_{L_{\alpha}})_{wM}}{(C_{L_{\alpha}})_{wlow\ speed}}$	ϵ_h (3) \times (24), deg	(a)	(a)	(a)	(a)
-2	1.57	0.967	27.63	0.169	34.68	0.0558	0.360	1.02	0.481	0.481	0.96				
2	1.57	.052	9.23	.292	33.72	.0031	.371	1.036	.489	.489	2.93				
6	1.57	-.864	5.56	.376	33.07	-.0523	.378	1.030	.485	.485	4.86				
10	1.57	-1.780	3.96	.446	32.52	-.1095	.384	1.00	.472	.472	6.61				
13.4	1.57	-2.580	3.41	.481	32.25	-.160	.386	.98	.463	.463	8.00				

^aAt $M = 0.083$, the Mach number of wind-tunnel data, $\frac{(C_{L_{\alpha}})_{wM}}{(C_{L_{\alpha}})_{wlow\ speed}} \approx 1.0$.

TABLE 4.9.2-1
COMPARISON OF CALCULATED AND TEST-DETERMINED DYNAMIC-PRESSURE RATIOS AT
THE HORIZONTAL TAIL (FROM REF. 1)

[Calculations based on the procedures of reference 14]

Source	A_w	$(\Lambda_{le})_w$, deg	λ_w	$\frac{x}{c_w}$	$\frac{z_h''}{c_w}$	α_w , deg	$\left(\frac{\bar{q}_h}{\bar{q}_\infty}\right)_{\text{calculated}}$	$\left(\frac{\bar{q}_h}{\bar{q}_\infty}\right)_{\text{test}}$	Percent error
Reference 20	3	0	1.0	2	0	0	0.88	0.90	-2.2
						1	.89	.92	-3.3
Figure 27	---	---	---	---	---	2	0.92	0.94	-2.1
						3	.95	.95	0
						4	.98	.96	2.1
						6	1.0	.96	4.2
Figure 12	6	0	1.0	2	0	0	0.88	0.87	1.1
						1	.89	.89	0
						2	.93	.92	1.1
						3	.97	.93	4.3
						4	.99	.95	4.2
						6	1.0	.97	3.1
Figure 12	6	0	1.0	2	0.28	6	1.0	0.97	3.1
						8	.98	.96	2.1
						10	.91	.93	-2.2
Figure 30	4.5	30	1.0	2	0	0	0.88	0.96	-8.3
						1	.89	.96	-7.3
						2	.92	.95	-3.2
						3	.95	.95	0
						4	.98	.94	4.3
						6	1.0	.98	2.0
Figure 15	5.2	30	1.0	2	0	0	0.88	0.95	-7.4
						1	.89	.94	-5.3
						2	.92	.94	-2.1
						3	.96	.94	2.1
						4	.99	.94	5.3
						6	1.0	.96	4.2
Figure 15	5.2	30	1.0	2	0.28	6	1.0	1.01	-1.0
						8	.996	1.02	-2.4
						10	.94	1.02	-7.8
						12	.88	1.01	-13.0
Figure 36	1.5	60	1.0	2	0	0	0.89	0.95	-6.3
						1	.895	.95	-5.8
						2	.91	.95	-4.2
						3	.93	.94	-1.1
						4	.96	.94	2.1
						6	.99	.97	4.1
Figure 24	3	60	1.0	3	0	0	0.92	0.92	0
						1	.93	.93	0
						2	.96	.95	1.1
						3	.99	.97	2.1
Reference 21	3.5	47.5	0.5	1.213	0	4	1.0	.99	1.0
						0	0.85	----	----
						1	.86	----	----
						2	.89	----	----
						3	.93	0.86	8.1
						4	.96	.88	9.1
						6	1.0	.92	8.7

TABLE 4.9.2-2
DYNAMIC-PRESSURE RATIO AT THE HORIZONTAL TAIL OF THE SUBJECT AIRPLANE

(a) Pertinent parameters

Symbol	Description	Reference	Magnitude
α_w	Wing angle of attack relative to chord line = $\alpha_b + i_w$, deg	Table 3-1	$\alpha_b + 2$
γ	Angle between wing chord plane and line connecting trailing edge of wing root chord and $\bar{c}/4$ of horizontal tail, deg	-----	15
\bar{c}_w	Wing mean aerodynamic chord, ft	Table 3.2-1	4.96
A_w	Wing aspect ratio	Table 3.2-1	7.5
x	Distance from trailing edge of wing root chord to $\bar{c}/4$ of horizontal tail measured along centerline of wake, ft	-----	≈ 8.68
C_{Df}	Wing zero-lift drag coefficient of total wing per procedure of table 4.12-1	Section 4.12	.0097
ϵ_h	Downwash in plane of symmetry at vortex sheet $\approx \frac{1.62 C_{Lw}}{57.3 \pi A_w}$	Equation (4.9.2-5)	$3.94 C_{Lw}$
z_h''	Vertical distance from vortex sheet to $\bar{c}/4$ of horizontal tail = $x \tan(\gamma - \alpha_w + \epsilon_h)$, ft	Equation (4.9.2-4)	$8.68 \tan [15 - (\alpha_w - \epsilon)]$
Δz_{wake}	Half-width of wake = $0.68 \bar{c} \sqrt{C_{Df}(x/\bar{c}_w + 0.15)}$, ft	Equation (4.9.2-1) (fig. 4.9.2-2)	.458
$\left(\frac{\Delta \bar{q}}{\bar{q}_\infty}\right)_o$	Dynamic-pressure loss at wake centerline = $\frac{2.42 (C_{Df})^{1/2}}{x/\bar{c}_w + 0.3}$	Equation (4.9.2-2) (fig. 4.9.2-3)	.116
$\left(\frac{\Delta \bar{q}}{\bar{q}_\infty}\right)_h$	Dynamic-pressure loss at horizontal tail = $\left(\frac{\Delta \bar{q}}{\bar{q}_\infty}\right)_o \cos^2 \left(\frac{\pi}{2} \frac{z_h''}{\Delta z_{wake}} \right)$	Equation (4.9.2-3)	$.116 \cos^2 \left(\frac{\pi}{2} \frac{z_h''}{0.458} \right)$
$\frac{\bar{q}_h}{\bar{q}_\infty}$	Dynamic-pressure ratio at horizontal tail = $1 - \left(\frac{\Delta \bar{q}}{\bar{q}_\infty}\right)_h$	Equation (4.9.2-6)	Variable

(b) Summary calculations

(1)	(2)	(3)	(4)	(5)	(6)	(7)	(8)	(9)	(10)	(11)	(12)
α_b , relative to X-axis, deg	$\alpha_w = \alpha_b + 2$, deg	Figure 4.2-1, $S_w = 172.3 \text{ ft}^2$, C_{Lw}	$\epsilon_h = 3.94$ (3), deg	$\gamma - \alpha_w + \epsilon_h$, deg	\tan (5)	$z_h'' = 8.68$ (6)	$\frac{z_h''}{\Delta z_{wake}} = \frac{z_h''}{0.458}$ (7)	90 (8), deg	\cos^2 (9)	$\left(\frac{\Delta \bar{q}}{\bar{q}_\infty}\right)_h = 0.116$ (10)	$\frac{\bar{q}_h}{\bar{q}_\infty} = 1 -$ (11)
-4	-2	0	0	17.0	0.3057	2.65	5.78	Since $\frac{z_h''}{\Delta z_{wake}}$ is greater than 1.0, the horizontal tail is outside of the wake. Thus $\frac{\bar{q}_h}{\bar{q}_\infty} = 1$			
0	2	.300	1.182	14.18	.2527	2.19	4.78				
4	6	.604	2.380	11.38	.2013	1.75	3.81				
8	10	.910	3.585	8.58	.1509	1.31	2.85				
10	12	1.060	4.176	7.18	.1260	1.09	2.38				
12	14	1.190	4.689	5.69	.0996	0.86	1.88				
13.4	15.4	1.23	4.846	4.45	.0778	.68	1.47				

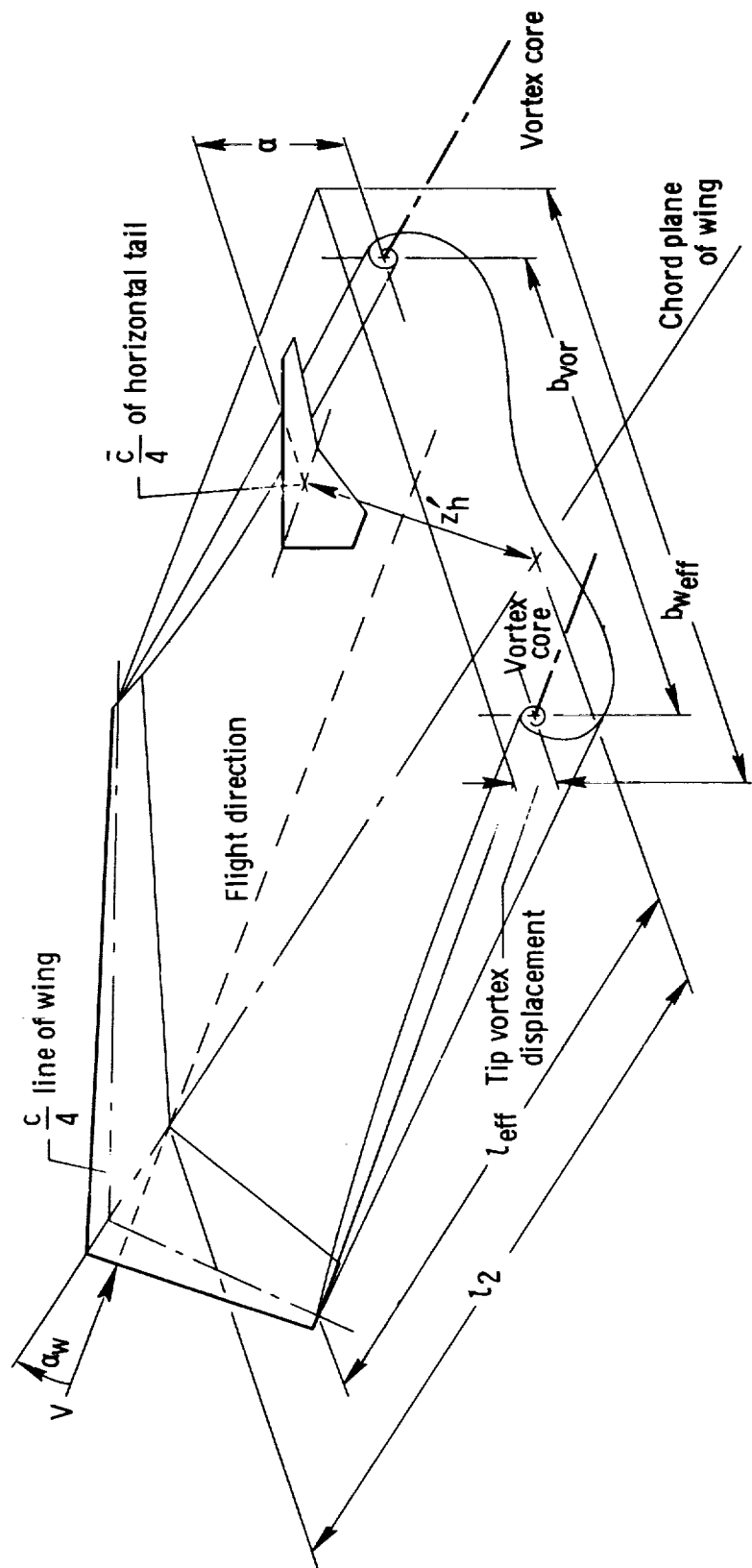


Figure 4.9.1-1. Wing vortex system.

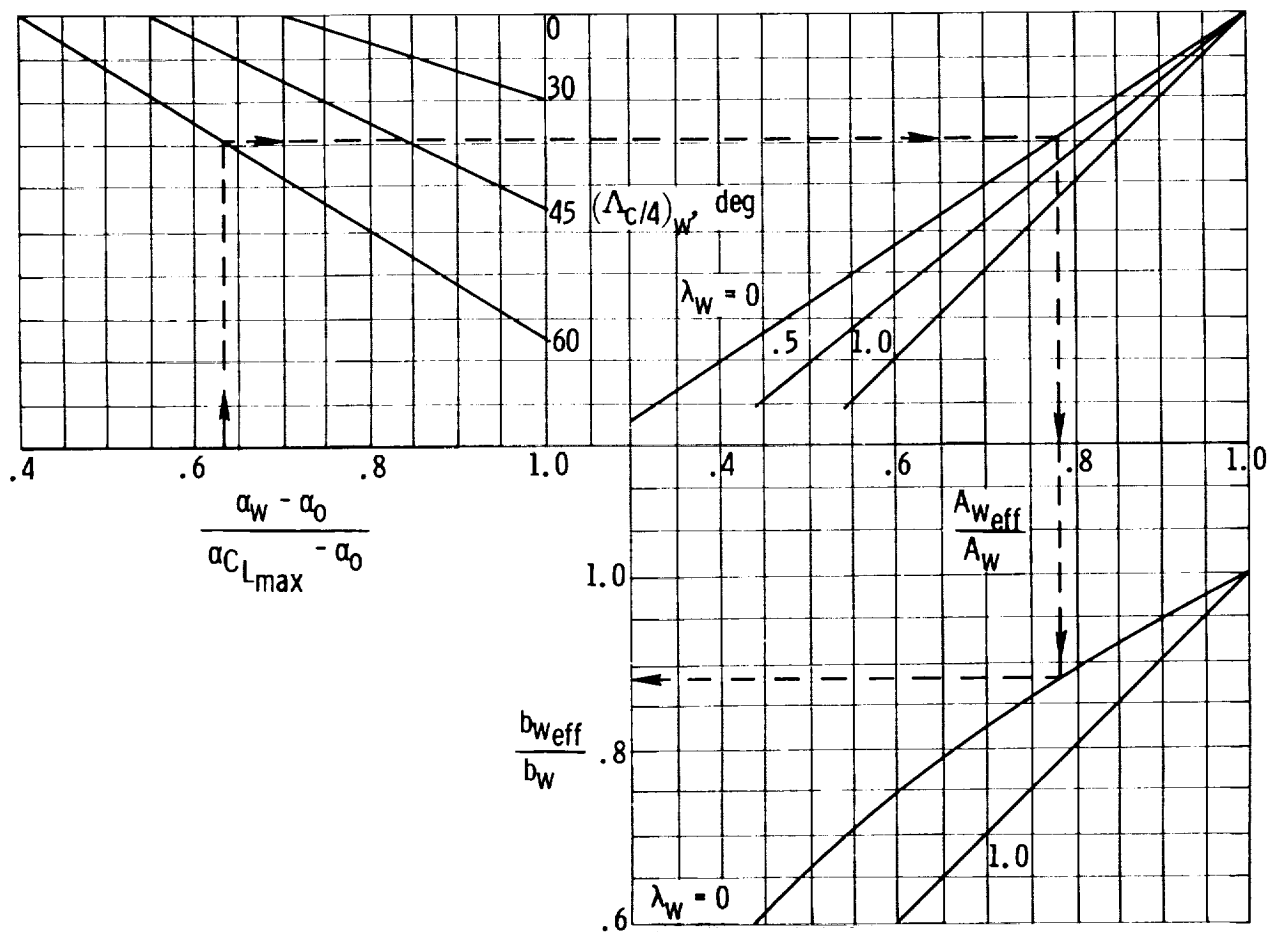


Figure 4.9.1-2. Effective wing aspect ratio and span for low speeds (from ref. 19).

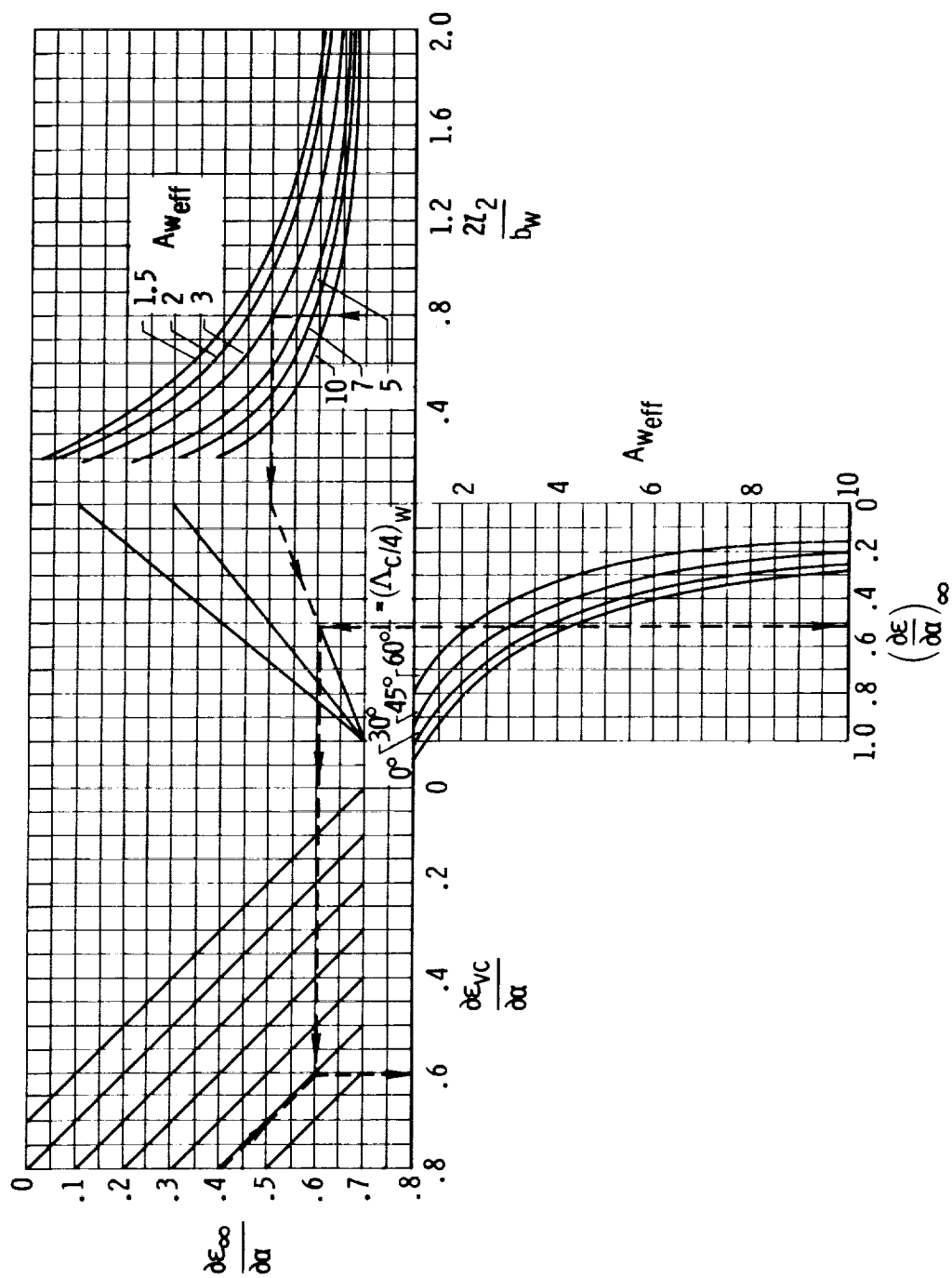


Figure 4.9.1-3. Downwash at the plane of symmetry and height of vortex core for low speeds (from ref. 19).

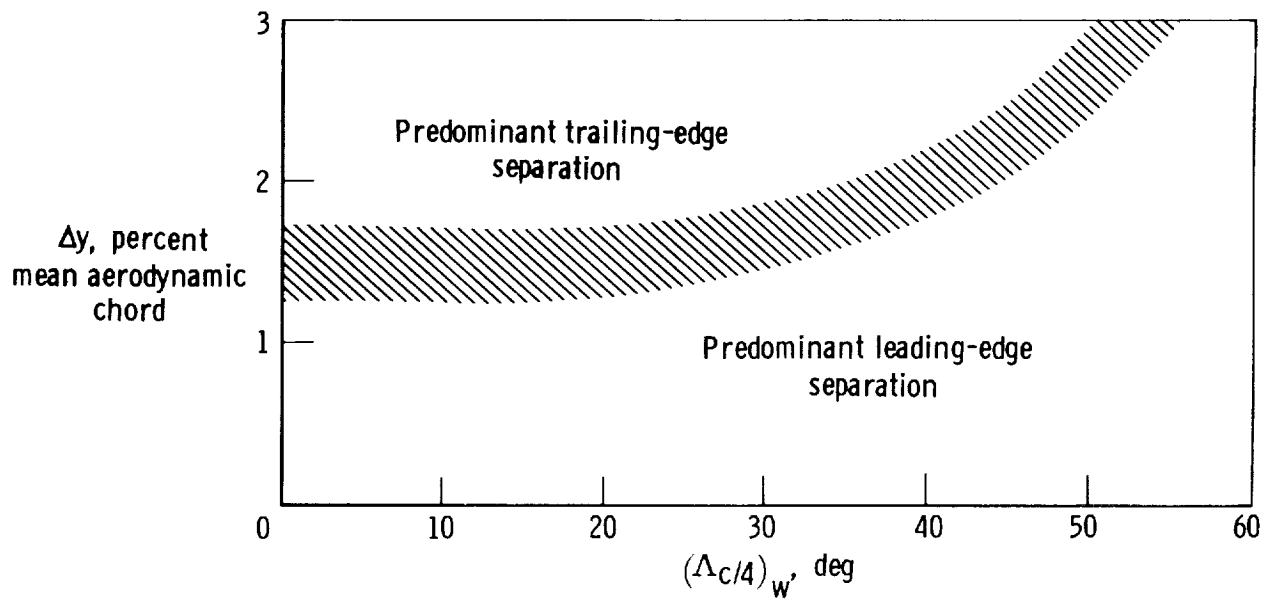


Figure 4.9.1-4. Type of flow separation as a function of airfoil and wing sweep for subsonic speeds (ref. 1).

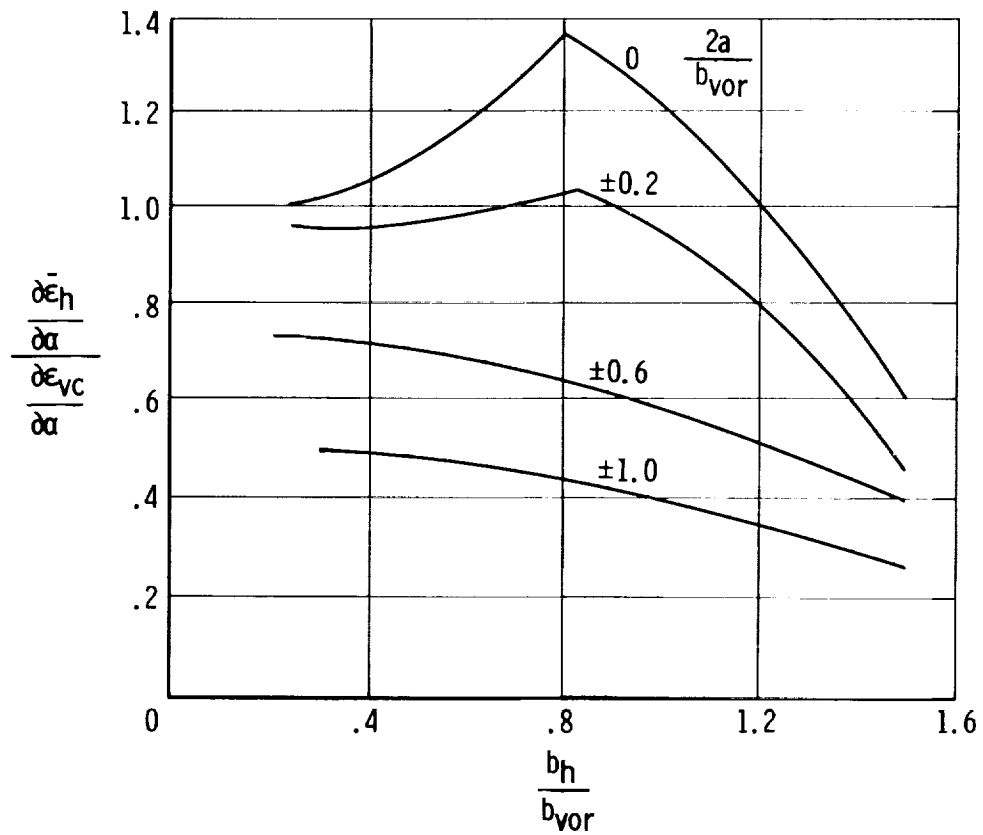
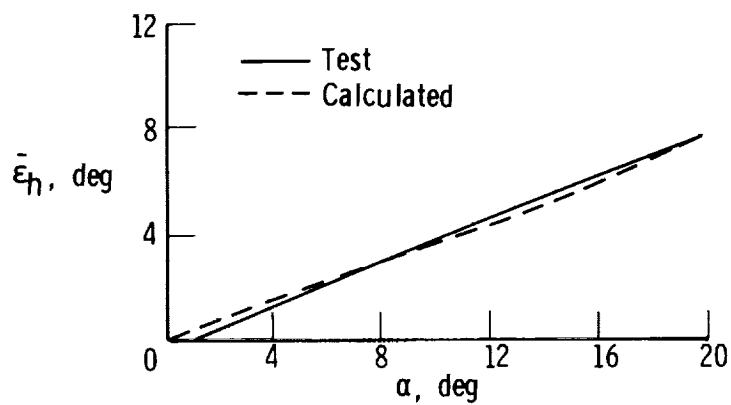
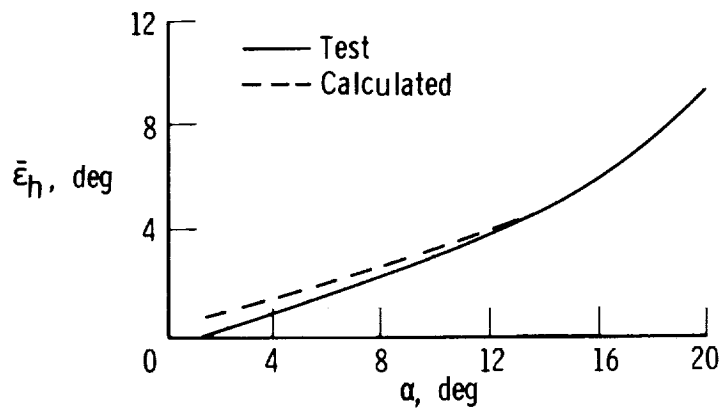


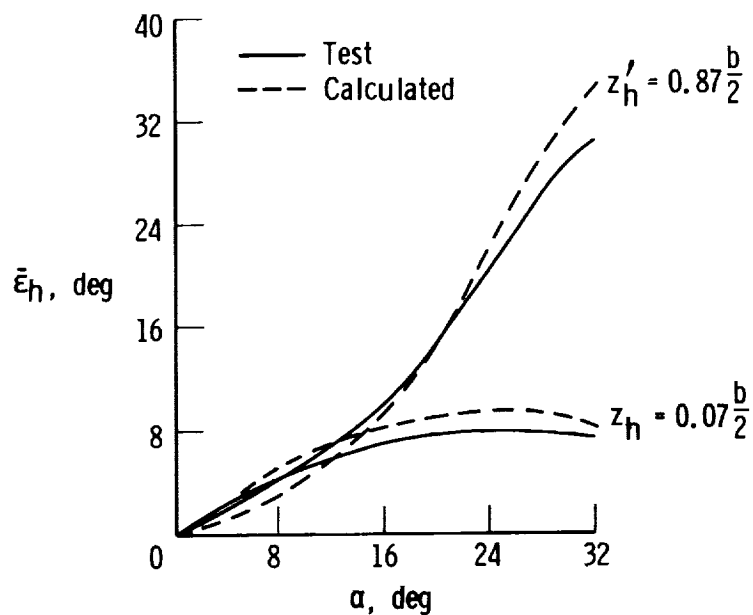
Figure 4.9.1-5. Average downwash acting on aft lifting surface for low speeds (ref. 17).



$$\begin{aligned} A_w &= 10.0 \\ l_2 &= 0.50 \frac{b_w}{2} \\ z'_h &= 0.13 \frac{b_w}{2} \\ (\Lambda_{c/4})_w &= 0^\circ \\ \lambda_w &= 0.40 \\ \frac{b_h}{b_w} &= 0.32 \end{aligned}$$



$$\begin{aligned} A_w &= 5.26 \\ l_2 &= 1.31 \frac{b_w}{2} \\ z'_h &= 0.40 \frac{b_w}{2} \\ (\Lambda_{c/4})_w &= 40^\circ \\ \lambda_w &= 0.33 \\ \frac{b_h}{b_w} &= 0.30 \end{aligned}$$



$$\begin{aligned} A_w &= 2.31 \\ l_2 &= 1.16 \frac{b_w}{2} \\ (\Lambda_{c/4})_w &= 56^\circ \\ \lambda_w &= 0 \\ \frac{b_h}{b_w} &= 0.36 \end{aligned}$$

Figure 4.9.1-6. Comparison of calculated and test downwash angles (ref. 16).

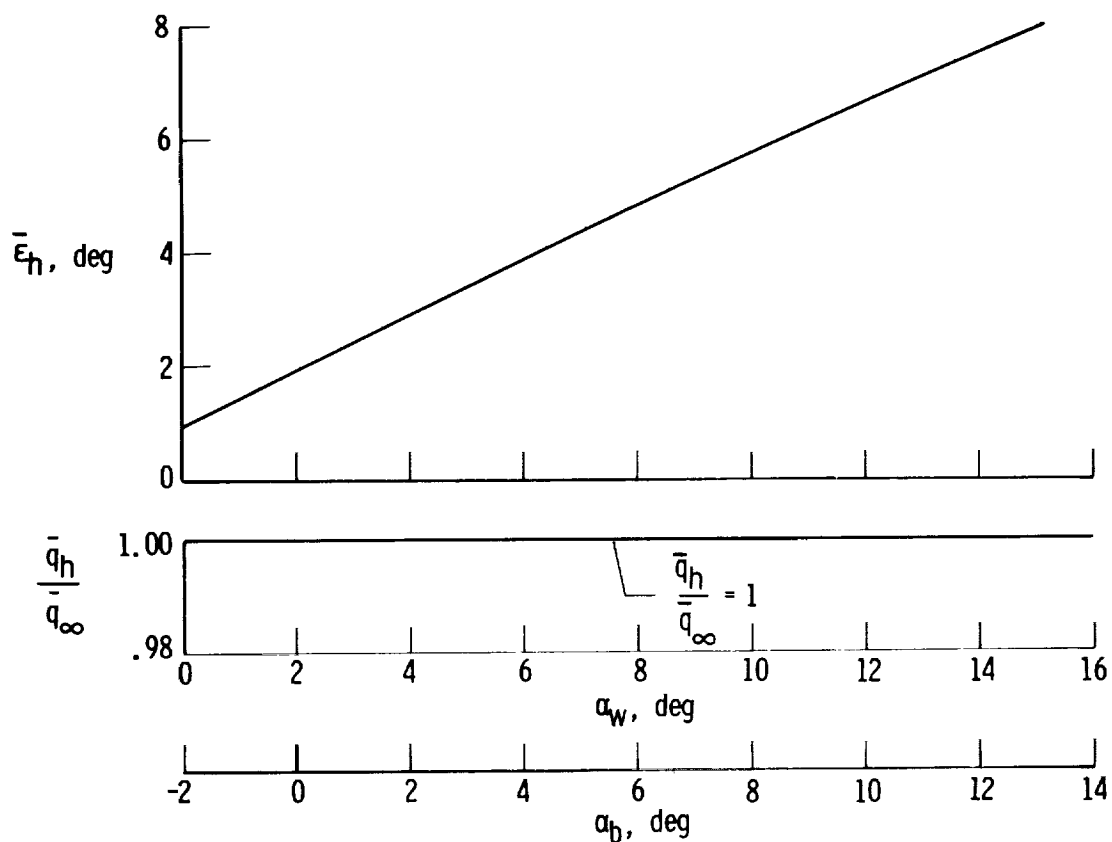


Figure 4.9.1-7. Calculated downwash and dynamic-pressure ratio at the horizontal tail of the subject airplane.

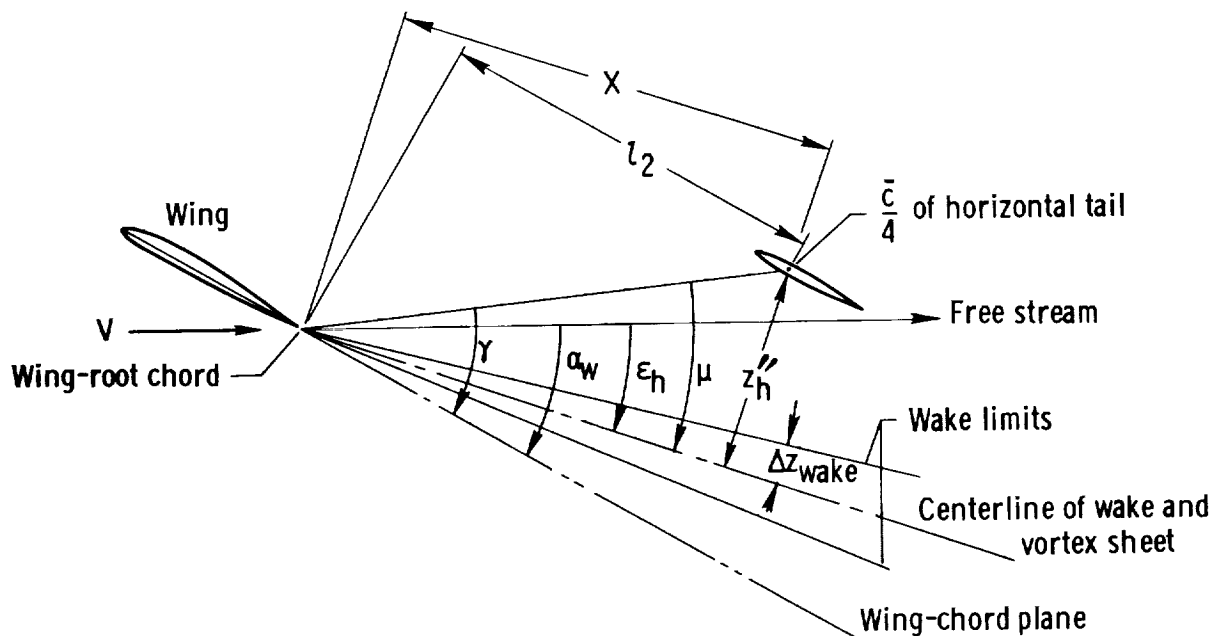


Figure 4.9.2-1. Relative positions of horizontal tail, wing wake, and wing-chord plane.

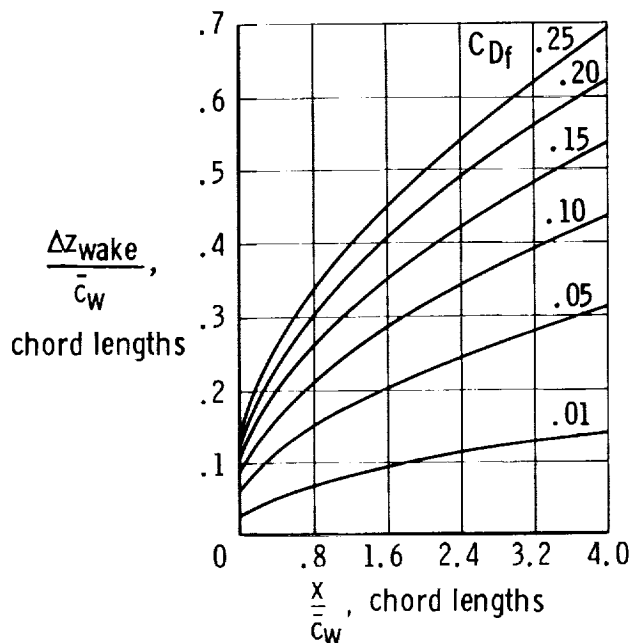


Figure 4.9.2-2. Relation between wake width and distance from trailing edge

(ref. 14). $\frac{\Delta z_{wake}}{\bar{c}_w} = 0.68 \left[C_{Df} \left(\frac{x}{\bar{c}_w} + 0.15 \right) \right]^{1/2}.$

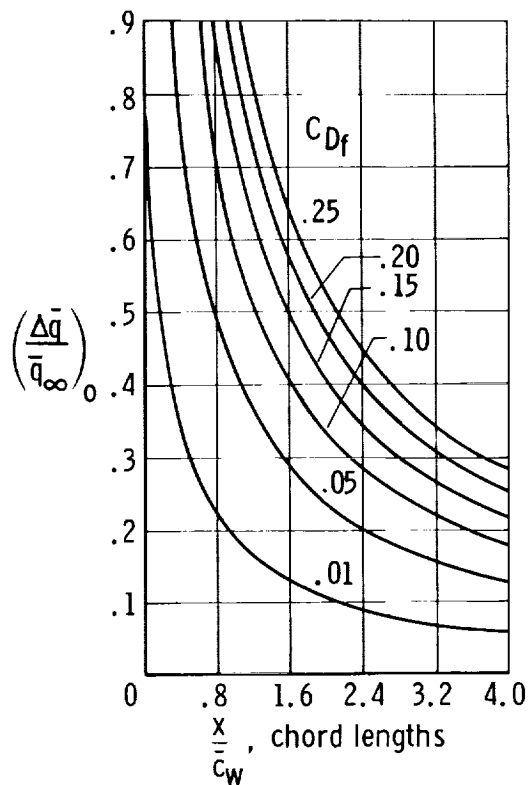


Figure 4.9.2-3. Relation between maximum loss of dynamic pressure in the wake and distance from the trailing edge (ref. 14).

$$\left(\frac{\Delta \bar{q}}{\bar{q}_\infty} \right)_0 = \frac{2.42 C_{Df}^{1/2}}{\frac{x}{\bar{c}_w} + 0.03}.$$

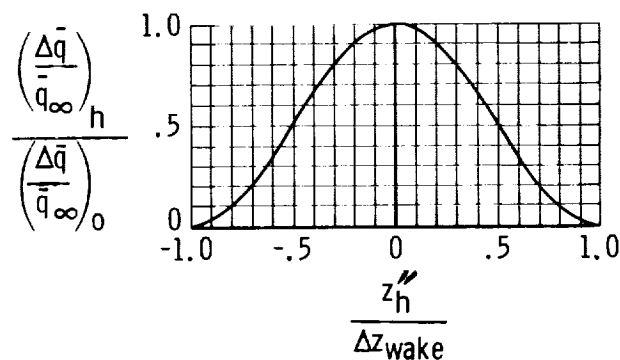


Figure 4.9.2-4. Variation of dynamic-pressure loss across the wake (ref. 14).

$$\frac{\left(\frac{\Delta \bar{q}}{\bar{q}_\infty} \right)_h}{\left(\frac{\Delta \bar{q}}{\bar{q}_\infty} \right)_0} = \cos^2 \left(\frac{\pi}{2} \frac{z_h''}{\Delta z_{wake}} \right).$$

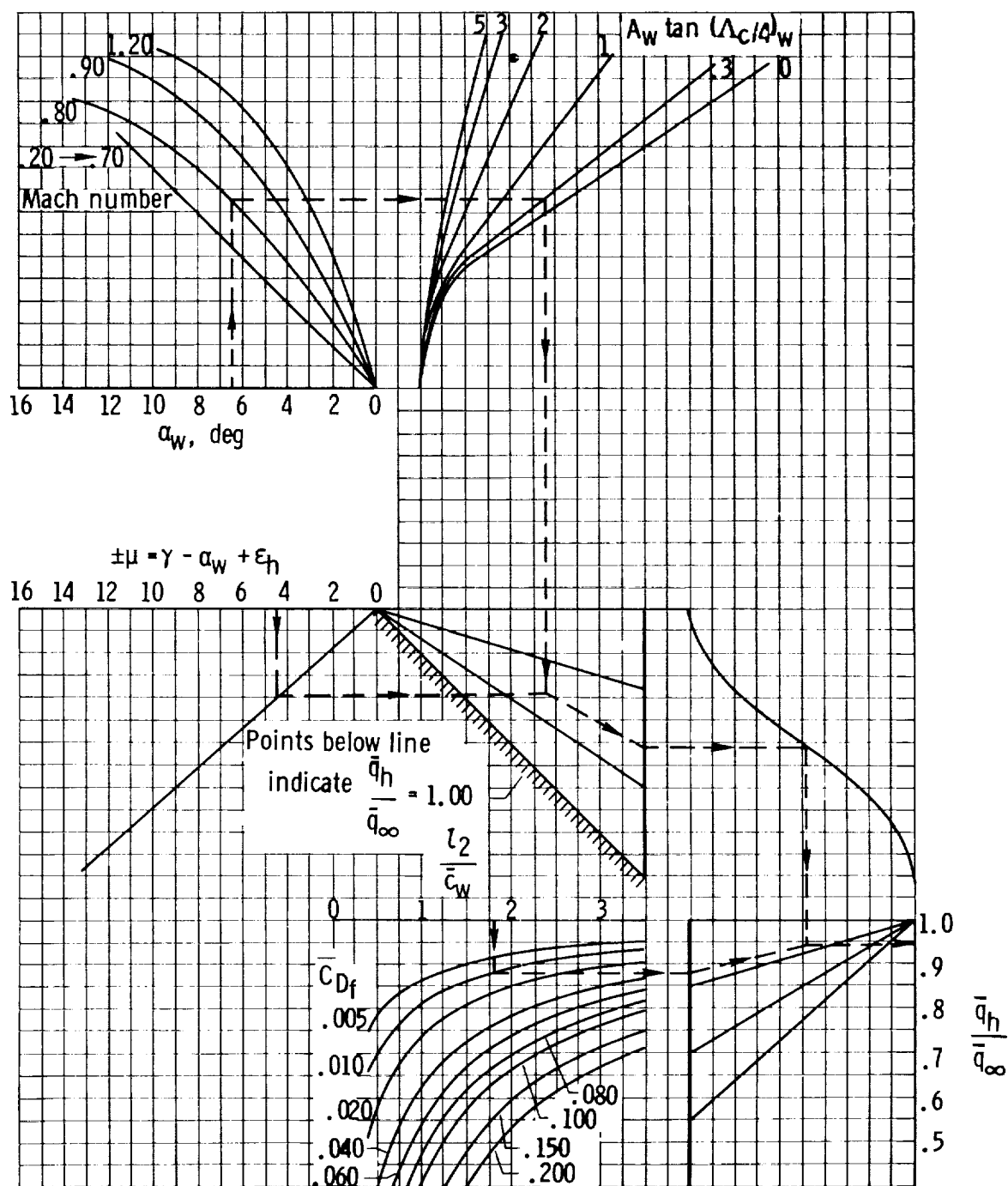


Figure 4.9.2-5. Nomograph for determining dynamic pressure at the horizontal tail by the method of reference 19, which is a modification of the basic method of reference 14.

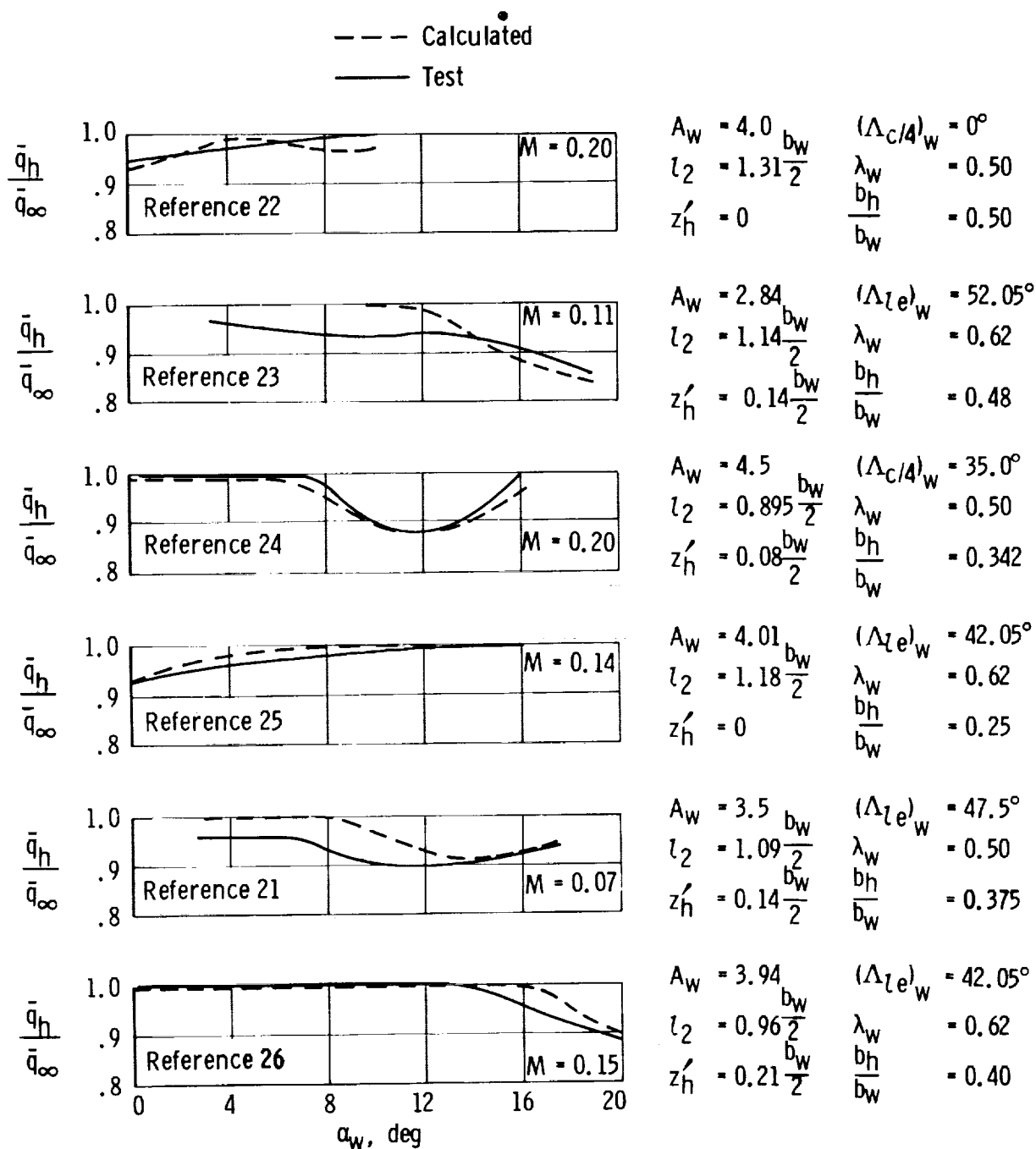


Figure 4.9.2-6. Comparison of calculated dynamic-pressure ratios, using the nomograph of figure 4.9.2-5, with wind-tunnel data (from ref. 19).

4.10 Lift of the Complete Airplane ($\delta_e = 0^\circ$)

The tail-off lift characteristics were previously considered in section 4.4. The tail contribution to lift is considered in this section in order to obtain the lift of the complete airplane. The net lift of the complete airplane in the linear range of the lift curve may be summarized by

$$C_L = C_{L_{wfn}} + C_{L_h(hf)} + (\Delta C_L)_{h(fv)} \quad (4.10-1)$$

where

$(C_L)_{wfn}$ is the tail-off lift coefficient considered in section 4.4 (4.4-1)

$C_{L_h(hf)}$ is the lift contribution of the horizontal tail including tail-fuselage interactions, wing downwash, and dynamic-pressure effects

$(\Delta C_L)_{h(fv)}$ is the effect of fuselage vortexes on the lift coefficient of the horizontal tail

The maximum or stall lift coefficient of the horizontal tail in the presence of the fuselage is determined in a manner synonymous to that used to determine the wing-fuselage maximum lift considered in section 4.4.

The lift contribution, $C_{L_h(hf)}$, of the horizontal tail in the presence of the fuselage, due to angle of attack at the tail, is given by equation (4.10-2) from reference 11. This equation, as noted in section 4.4, accounts for body-interference effects on the lifting surface and lift carryover from the lifting surface onto the fuselage. It should be noted that in the derivation of the equation, reference 11 considered a midwing configuration on a cylindrical body. The horizontal-tail and fuselage configuration of the subject airplane does not represent this idealized condition. The tail is near the top surface and at the end of the fuselage; also, there is an air gap between the tail surface and the body. Thus the application of the equation represents an approximation, and the amount of lift carryover from the tail to the fuselage may be questioned. The magnitude of this carryover would be of more concern in considering tail contributions to pitching moments than to lift. On the basis of the principles of reference 11,

$$C_{L_h(hf)} = (C_{L_\alpha})_{h_e} \left[K_{h(f)} + K_{f(h)} \right] \alpha_h \left(\frac{S_{h_e}}{S_w} \right) \left(\frac{\bar{q}_h}{\bar{q}_\infty} \right) \quad (4.10-2)$$

where

$(C_{L_\alpha})_{h_e}$ is the lift-curve slope of the exposed panels of the tail (section 4.2)

$K_{h(f)}$ is the ratio of the lift on the horizontal tail due to the local angle of attack, in the presence of the body to tail alone, obtained from figure 4.4-1

$K_{f(h)}$ is the ratio of the tail-lift carryover onto the body to tail alone due to local angle of attack, obtained from figure 4.4-1

$(\alpha)_h$ is the angle of attack at the tail, equal to $(\alpha_b - \bar{\epsilon}_h)$

$\bar{\epsilon}_h$ is the average downwash acting on the tail (section 4.9.1)

$\frac{\bar{q}_h}{\bar{q}_\infty}$ is the dynamic-pressure ratio at the tail (section 4.9.2)

Pertinent parameters and summary calculations for $C_{Lh(hf)}$ of the subject airplane are listed in table 4.10-1(a).

The effect of body vortices on the lift of the horizontal tail can be considered negligible when the tail span is greater than three times the body diameter at the tail. This ratio is exceeded in general aviation aircraft; therefore, the effect of body vortices is neglected.

The maximum lift coefficient of the tail in the presence of the fuselage, $C_{Lmax\ h(hf)}$, and the corresponding angle of attack, $(\alpha_{C_{Lmax}})_{h(hf)}$, are determined by the methods used in section 4.4 (eqs. (4.4-3) and (4.4-4)) to obtain the stall characteristics of the wing in the presence of the fuselage.

Pertinent parameters and summary calculations for $(C_{Lmax})_{h(hf)}$ and $(\alpha_{C_{Lmax}})_{h(hf)}$ of the subject airplane are listed in table 4.10-1(b).

At airplane stalled conditions, the lift contribution of the tail is dependent upon its position relative to the wing wake. The wake of the stalled wing can be considered, in accordance with reference 1, to be bounded by the lines emanating from the leading and trailing edges of the wing parallel to the free-stream direction. For tails outside the wake $\frac{\partial \bar{\epsilon}_h}{\partial \alpha}$ and $\bar{\epsilon}_h$ can be assumed to be equal to zero.

For tails inside the wake, reference 1 recommends that the lift contribution of the tail be assumed to be equal to zero at airplane stall. This does not appear to be a realistic assumption because it implies complete loss of pitch effectiveness of the tail, which is in contradiction with the statement on downwash in section 4.9.1 at stall: "For wings stalled at the tip... the downwash in the region of the tail will be greater for a stalled wing than for an unstalled wing for a given lift coefficient.... when the wing stalls at the center, the center of the wake moves upward and the vortices rolling off the edge of the stalled portion reduce the downwash."

In the absence of specific quantitative procedures to estimate the downwash at the tail at stall conditions, when the tail is inside the wake, the downwash as determined from figure 4.9.1-7 was assumed, as a first approximation, to be fully effective up to stall.

The summary calculations for the lift of the subject airplane are presented in tables 4.10-1 and 4.10-2. The resulting lift curve is compared with wind-tunnel data in figure 4.10-1. The shape of the curve from the limit of linearity to the stall was obtained in the same manner as for wings alone (section 4.2).

As a matter of interest, a buildup of calculated lift characteristics, from wing alone to the complete airplane, is shown in figure 4.10-2.

4.10.1 Symbols

A_h	horizontal-tail aspect ratio
b_h	horizontal-tail span, ft
C_L	lift coefficient
$C_{Lh(hf)}$	lift coefficient of the horizontal tail with tail-fuselage interaction effects included, referred to the wing area and free-stream dynamic pressure unless noted otherwise
C_{Lwfn}	tail-off lift coefficient
$(C_{Lmax})_h$	maximum lift coefficient of the isolated horizontal tail referred to the tail area and a dynamic-pressure ratio of 1
$(C_{Lmax})_{h(hf)}$	maximum value of $C_{Lh(hf)}$
$(\Delta C_L)_{h(fv)}$	increment lift coefficient of the horizontal tail due to the effect of fuselage vortexes, referred to the wing area and free-stream dynamic pressure
$(C_{L\alpha})_{wfn}$	tail-off lift-curve slope, per deg
$(\Delta C_{L\alpha})_{he}$	lift-curve slope of the exposed panels of the tail, per deg
c_2	taper-ratio correction factor
$(df)_h$	fuselage width at the horizontal tail, ft
i_h	incidence of the horizontal tail, equal to 0
$K_h(f)$	ratio of the lift on the tail in the presence of the fuselage to the tail alone
$K_f(h)$	ratio of the tail-lift carryover onto the fuselage to the tail alone
$\bar{q}_h, \bar{q}_\infty$	dynamic pressure at the horizontal tail and in the free stream, respectively, lb/sq ft
S_h	area of the horizontal tail, sq ft
S_{he}	area of the exposed horizontal-tail panels, sq ft

S_w	wing area, sq ft
α_b	airplane angle of attack relative to the X-body axis, deg
$(\alpha_{C_{Lmax}})_h$	stall angle of the isolated horizontal tail, deg
$(\alpha_{C_{Lmax}})_{h(hf)}$	stall angle of the horizontal tail in the presence of the fuselage, deg
α_h	horizontal-tail angle of attack, $\alpha_b + i_h - \bar{\epsilon}_h$, deg
α_h^*	horizontal-tail angle of attack at the limit of linearity of the tail lift-curve slope, deg
δ_e	elevator deflection, equal to 0 in the present analysis, deg
$\bar{\epsilon}_h$	average downwash across the horizontal tail, deg
$\frac{\partial \bar{\epsilon}_h}{\partial \alpha}$	downwash gradient at the horizontal tail
$(\Lambda_{le})_h$	sweep of the horizontal-tail leading edge, deg
λ_h	horizontal-tail taper ratio

TABLE 4.10-1

LIFT OF HORIZONTAL TAIL IN THE PRESENCE OF THE FUSELAGE ($\delta_e = 0^\circ$)(a) Lift of the horizontal tail in the linear range, $C_{Lh(hf)}$

$$C_{Lh(hf)} = (C_{L\alpha})_{he} [K_{h(f)} + K_{f(h)}] (\alpha_b - \bar{\epsilon}_h) \left(\frac{q_h}{q_\infty} \right) \left(\frac{S_{he}}{S_w} \right)$$

Symbol	Description	Reference	Magnitude
α_h^*	Limit of linearity of horizontal tail, relative to tail chord, deg	Table 4.2-1	10.6
$(df)_h$	Fuselage width at horizontal tail, ft	Figure 3.2-2	1.25
b_h	Horizontal-tail span, ft	Table 3.2-1	12.5
$\frac{(df)_h}{b_h}$	-----	-----	.10
$K_{h(f)}$	Ratio of lift on tail in presence of fuselage to tail alone	Figure 4.4-1	1.075
$K_{f(h)}$	Ratio of tail-lift carryover on fuselage to tail alone	Figure 4.4-1	.13
$(C_{L\alpha})_{he}$	Lift-curve slope of exposed horizontal-tail panels, per deg	Table 4.2-1	0.070
S_{he}	Area of exposed horizontal-tail panels, sq ft	Table 3.2-1	28.73
S_w	Reference wing area, sq ft	Table 3.2-1	172.3
$\frac{q_h}{q_\infty}$	Dynamic-pressure ratio at the horizontal tail	Figure 4.9.1-1	1.0 (constant)
Summary: $C_{Lh(hf)} = 0.01406(\alpha_b - \bar{\epsilon}_h)$ on basis of $S_w = 172.3$ sq ft up to $\alpha_h^* = 10.6^\circ$			

(b) Maximum lift and stall angle of horizontal tail

$$(C_{Lmax})_{h(hf)} = (C_{Lmax})_h \left[\frac{(C_{Lmax})_{h(hf)}}{(C_{Lmax})_h} \right] \quad (\alpha_{C_{Lmax}})_{h(hf)} = (\alpha_{C_{Lmax}})_h \left[\frac{(\alpha_{C_{Lmax}})_{h(hf)}}{(\alpha_{C_{Lmax}})_h} \right]$$

Symbol	Description	Reference	Magnitude
$(\Lambda_{le})_h$	Horizontal-tail leading-edge sweep, deg	Table 3.2-1	12.0
A_h	Horizontal-tail aspect ratio	Table 3.2-1	4.8
λ_h	Horizontal-tail taper ratio	Table 3.2-1	.515
$\frac{(df)_h}{b_h}$	Ratio of body width to tail span at the tail	Table 4.10-1(a)	.10
$(C_{Lmax})_h$	Horizontal-tail maximum lift coefficient (based on $S_h = 32.5$ sq ft)	Table 4.2-1	.935
$(\alpha_{C_{Lmax}})_h$	Horizontal-tail stall angle, deg	Table 4.2-1	14.45
c_2	Taper-ratio correction factor	Figure 4.4-2	1.06
$(c_2 + 1) A_h \tan (\Lambda_{le})_h$	-----	-----	2.10
$\left[\frac{(C_{Lmax})_{h(hf)}}{(C_{Lmax})_h} \right]$	-----	Figure 4.4-3	.99
$\left[\frac{(\alpha_{C_{Lmax}})_{h(hf)}}{(\alpha_{C_{Lmax}})_h} \right]$	-----	Figure 4.4-3	1.00
Summary: $(C_{Lmax})_{h(hf)} = 0.926$ based on $S_h = 32.5$ sq ft $(C_{Lmax})_{h(hf)} = 0.175$ based on $S_w = 172.3$ sq ft $(\alpha_{C_{Lmax}})_{h(hf)} = 14.45^\circ$			

TABLE 4.10-2
LIFT OF THE COMPLETE AIRPLANE ($\phi_e = 0^\circ$)

Reference $S_w = 172.3 \text{ sq ft}$						
①	②	③	④	⑤	⑥	⑦
α_b , deg	$\bar{\epsilon}_h$, deg, figure 4.9, 1-7	α_h = ① - ②, deg	$C_{Lh(hf)} =$ 0.01406 ③, table 4.10-1(a)	$C_{L_{wfn}}$, table 4.5-2	$C_L =$ ④ + ⑤ ($S_w = 172.3 \text{ sq ft}$)	$C_L =$ ($S_w = 178 \text{ sq ft}$)
-4	0	-4.00	-0.056	-0.020	-0.076	-0.074
-2	.962	-2.96	-.042	.144	.102	.099
0	1.90	-1.90	-.027	.310	.283	.274
2	2.93	-.93	-.013	.475	.462	.447
4	3.87	.13	.002	.641	.643	.622
6	4.86	1.14	.016	.807	.823	.797
8	5.77	2.23	.031	.973	1.004	.972
a_{10}	6.69	3.31	.047	1.140	1.187	1.149
12	7.55	4.45	.063	1.27	1.333	1.290
$b_{13.8}$	8.3	5.5	0.077, $S_w = 172.3 \text{ ft}^2$ 0.075, $S_w = 178 \text{ ft}^2$	1.281, $S_w = 172.3 \text{ ft}^2$ 1.280, $S_w = 178 \text{ ft}^2$	1.358	1.355

^aLimit of linearity of $(C_{L_{cl}})_{wfn}$ (fig. 4.4-4).

^bStall angle (table 4.4-2 or fig. 4.4-4).

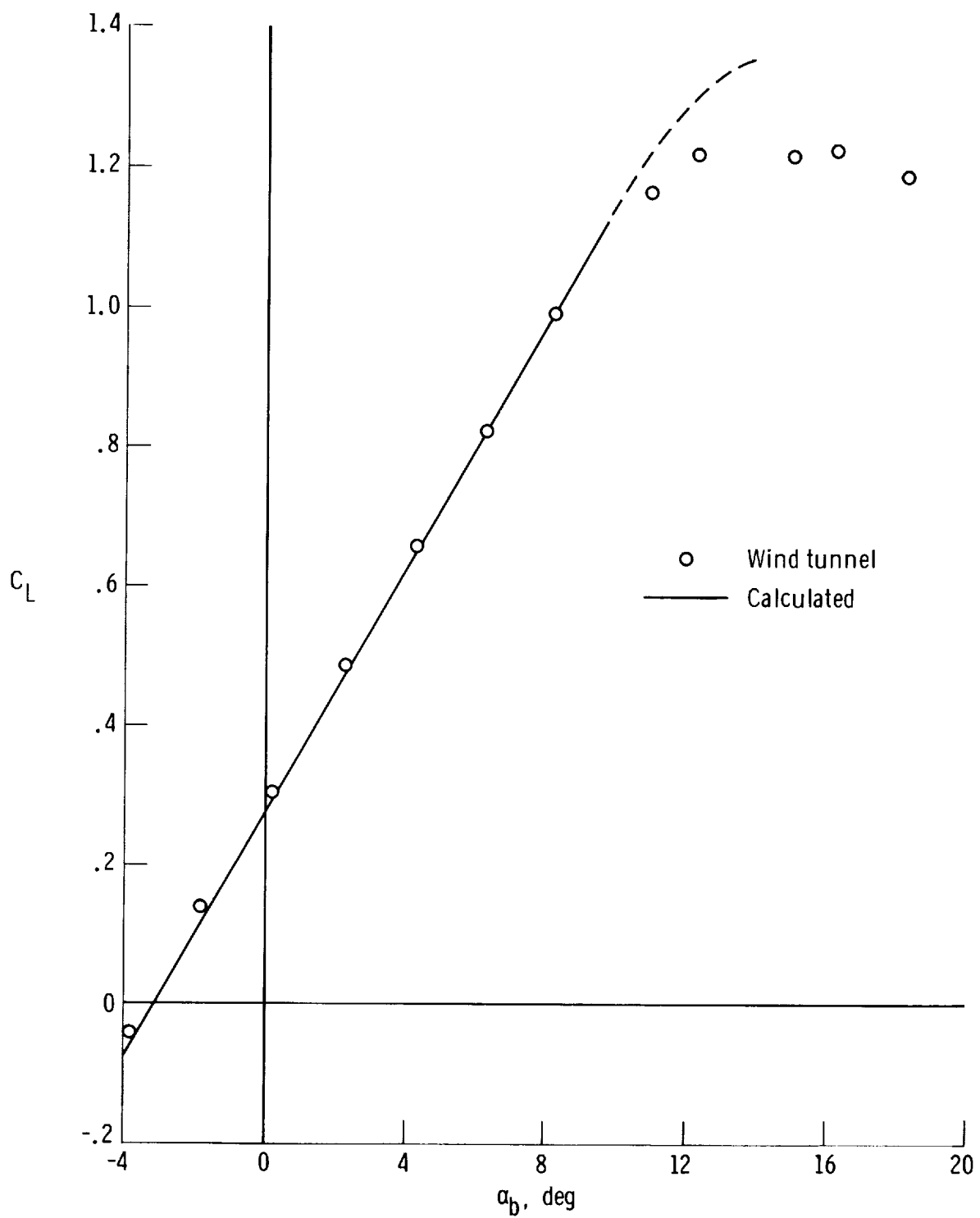


Figure 4.10-1. Comparison of predicted airplane lift curve with wind-tunnel data. $\delta_e = 0^\circ$; $S_w = 178$ sq ft.

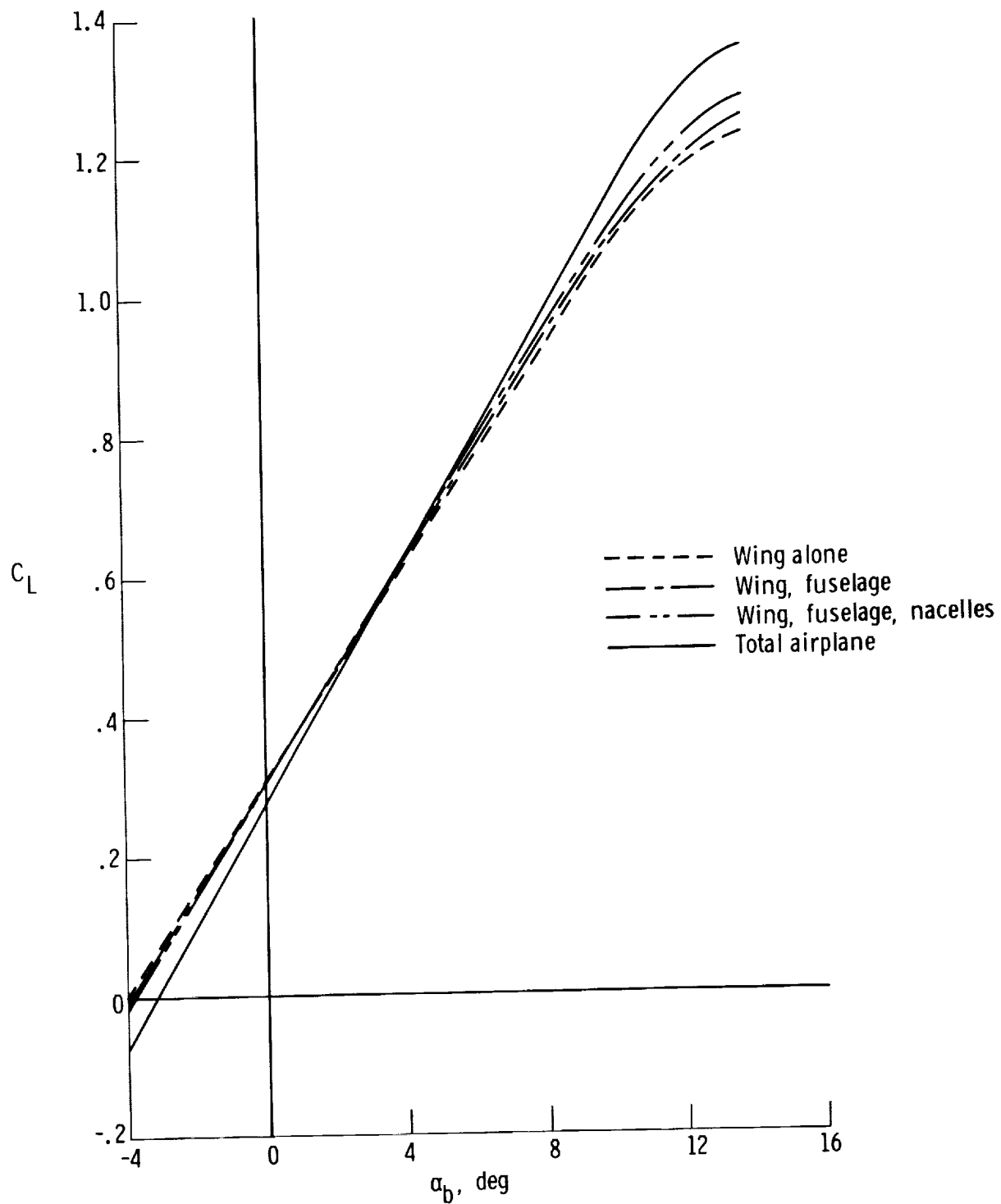


Figure 4.10-2. Predicted buildup of the lift characteristics of the airplane. $\delta_e = 0^\circ$; $S_w = 178$ sq ft.

4.11 Pitching Moments of the Complete Airplane ($\delta_e = 0^\circ$)

The pitching moments of the complete airplane ($\delta_e = 0^\circ$) are determined by synthesizing previously determined information in the following equation:

$$C_m = C_{m_{wfn}} + C_{m_h(hf)} \quad (4.11-1)$$

where

$C_{m_{wfn}}$ is the tail-off pitching-moment coefficient considered in section 4.8

$C_{m_h(hf)}$ is the contribution of the horizontal tail (including tail-fuselage interference effects) to the pitching-moment coefficient of the airplane

The pitching moments due to the horizontal tail are determined from

$$C_{m_h(hf)} = \left(\frac{x_{cg}}{\bar{c}_w} - \frac{x_h}{\bar{c}_w} \right) C_{L_h(hf)} \quad (4.11-2)$$

where, parallel to the X-body axis,

$\frac{x_{cg}}{\bar{c}_w}$ is the airplane center-of-gravity location from the wing leading edge

$\frac{x_h}{\bar{c}_w}$ is the distance to the $\frac{\bar{c}}{4}$ of the horizontal tail from the wing leading edge

$C_{L_h(hf)}$ is the lift of the tail in the presence of the fuselage, considered in section 4.10

Summary calculations for the pitching moments of the subject airplane relative to the center of gravity of the wind-tunnel data ($0.10\bar{c}_w$) are presented in table 4.11-1.

The resulting pitching-moment characteristics are compared with wind-tunnel data in figure 4.11-1. Although the correlation appears to be good, it should be noted that the slope of the calculated C_m versus α_b curve is slightly more negative than in the corresponding wind-tunnel data. Considering that the calculated tail-off C_m versus α_b curve (fig. 4.8.3-2) had slightly more positive slope than the wind-tunnel data, it is evident that the calculated pitch effectiveness of the tail is greater than reflected by the wind-tunnel data.

For the geometric fuselage-tail configuration of the subject airplane it appears that the lift carryover from the tail to the fuselage may be insignificant not only because of its location on the fuselage (see section 4.10) but also because of the gap between the horizontal tail and the fuselage. This implies that the $K_{f(h)}$ factor in the tail-lift equation (eq. (4.10-2)) should have been assumed to be equal to zero. It is suggested that $K_{f(h)}$ be considered negligible for tail-fuselage configurations similar

to that of the subject aircraft.

Another contributing factor to the discrepancy between calculated and wind-tunnel pitching moments is the neglect of the thickness of the boundary layer of the fuselage at the tail. This neglect affects the effective fuselage diameter used in obtaining the factor $K_h(f)$ from figure 4.4-1 for use in tail-lift equation (4.10-2).

The buildup of the calculated pitching-moment characteristics is shown in figure 4.11-2.

4.11.1 Symbols

C_L	lift coefficient
$C_{Lh(hf)}$	lift coefficient of the horizontal tail with tail-fuselage interaction effects included, referred to the wing area and free-stream dynamic pressure
C_{Lmax}	maximum lift coefficient
$(C_L\alpha)_{wfn}$	tail-off lift-curve slope
C_m	pitching-moment coefficient
$C_{mh(hf)}$	horizontal-tail contribution to the pitching-moment coefficient based on $C_{Lh(hf)}$
C_{mwfn}	tail-off pitching-moment coefficient
\bar{c}	mean aerodynamic chord, ft
\bar{c}_w	wing mean aerodynamic chord, ft
$K_f(h)$	ratio of the tail-lift carryover onto the fuselage to the tail alone
$K_h(f)$	ratio of the lift on the tail in the presence of the fuselage to the tail alone
S_w	wing area, sq ft
x_{cg}, x_h	distance, parallel to the X-body axis, from the airplane center of gravity and quarter chord of the horizontal-tail mean aerodynamic chord, respectively, to the leading edge of the wing mean aerodynamic chord, ft
α_b	airplane angle of attack relative to the X-body axis, deg
$\alpha_{C_{Lmax}}$	stall angle of attack, deg
δ_e	elevator deflection, equal to zero in the present analysis, deg

TABLE 4.11-1
PITCHING MOMENTS OF THE COMPLETE AIRPLANE ($\delta_e = 0^\circ$)

(a) Contribution of the horizontal tail, $C_{mh(hf)}$

$$C_{mh(hf)} = \left(\frac{x_{cg}}{\bar{c}_w} - \frac{x_h}{\bar{c}_w} \right) C_{Lh(hf)}$$

Symbol	Description	Reference	Magnitude
$\frac{x_{cg}}{\bar{c}_w}$	Airplane center-of-gravity location from wing leading edge/wing mean aerodynamic chord	Wind-tunnel test conditions	0.10
$\frac{x_h}{\bar{c}_w}$	Distance to $\bar{c}/4$ of the horizontal tail from wing leading edge, ft	Figures 3.2-1 and 3.2-2	15.0
\bar{c}_w	Wing mean aerodynamic chord, ft	Table 3.2-1	4.96
$\frac{x_h}{\bar{c}_w}$	-----	-----	3.024
$C_{Lh(hf)}$	Lift coefficient of horizontal tail on basis of $S_w = 172.3$ sq ft	Figure 4.10-1	Variable
Summary: $C_{mh(hf)} = -2.924 C_{Lh(hf)}$ on basis of $S_w = 172.3$ sq ft			

(b) Summary

$$C_m = C_{m_{wfn}} + C_{mh(hf)}$$

①	②	③	④	⑤	⑥	⑦
α_b , deg	Airplane C_L on basis of $S_w = 178$ sq ft, table 4.10-2	$C_{Lh(hf)}$, table 4.10-2	On basis of $S_w = 172.3$ sq ft		$C_m =$ ④ + ⑤	C_m on basis of $S_w = 178$ sq ft
			$C_{mh(hf)} =$ -2.924 ③	$C_{m_{wfn}}$, table 4.8.3-1		
-4	-0.074	-0.056	0.1637	-0.0472	0.1165	0.1128
-2	.099	-.042	.1228	-.0399	.0829	.0802
0	.274	-.027	.0789	-.0330	.0459	.0444
2	.447	-.013	.0380	-.0264	.0116	.0113
4	.622	.002	-.0058	-.0204	-.0262	-.0254
6	.797	.016	-.0468	-.0148	-.0616	-.0596
8	.972	.031	-.0906	-.0096	-.1002	-.097
^a 10	1.149	.047	-.1374	-.0049	-.1423	-.1377
12	1.290	.063	-.1842	-.0045	-.1887	-.1827
^b 13.8	1.355	.077	-.2251	-.0115	-.2366	-.2290

^aLimit of linearity of $(C_{L_a})_{wfn}$ (fig. 4.4-4).

^bStall angle (table 4.4-2 or fig. 4.4-4).

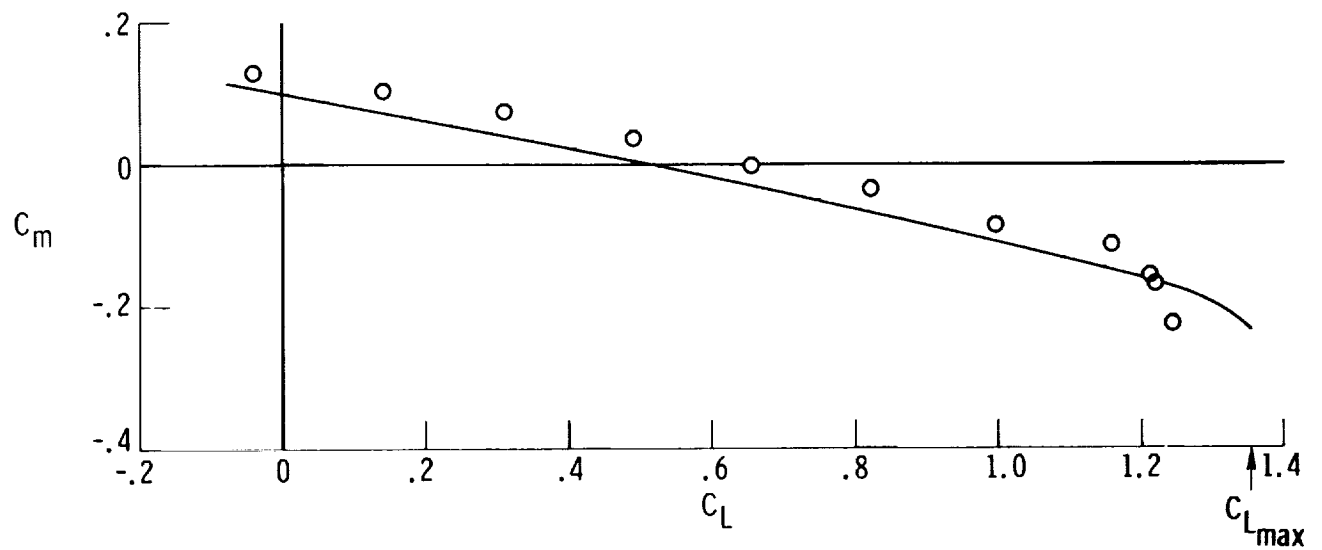
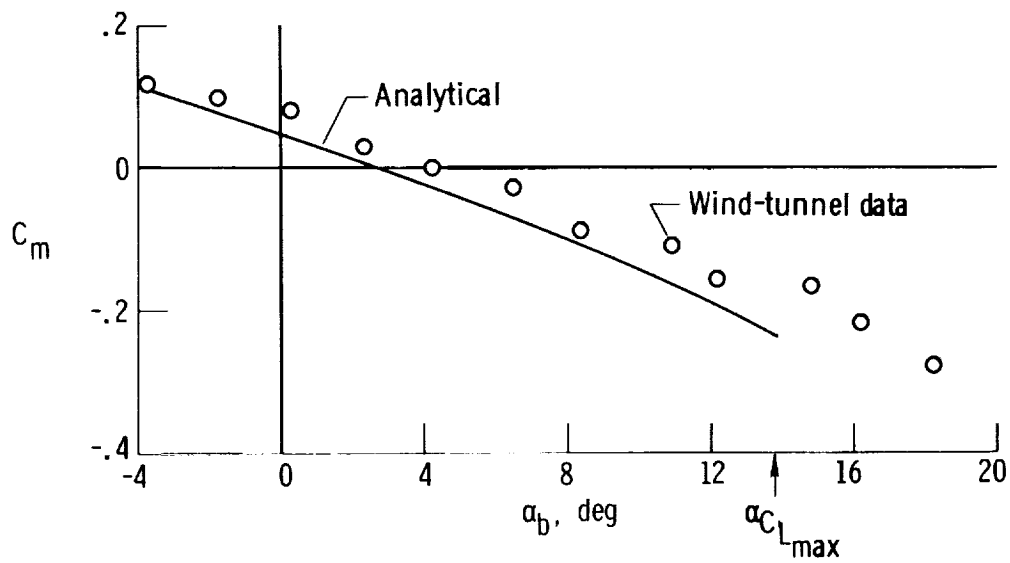


Figure 4.11-1. Comparison of predicted airplane pitching moments with wind-tunnel data. $\delta_e = 0^\circ$; $S_w = 178$ sq ft; center of gravity = $0.10\bar{c}_w$.

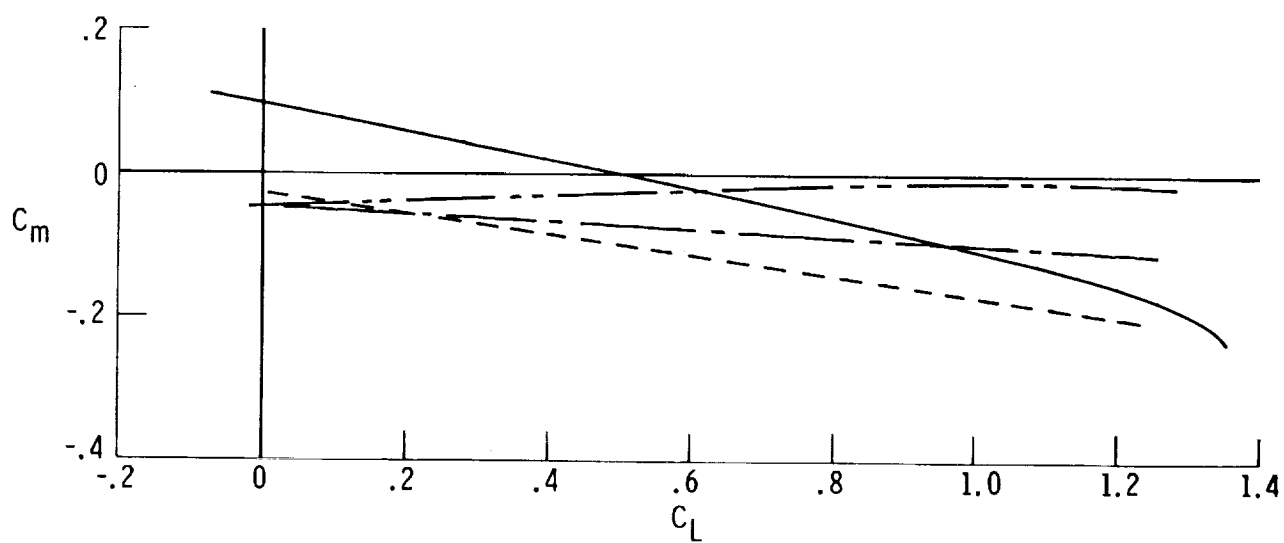
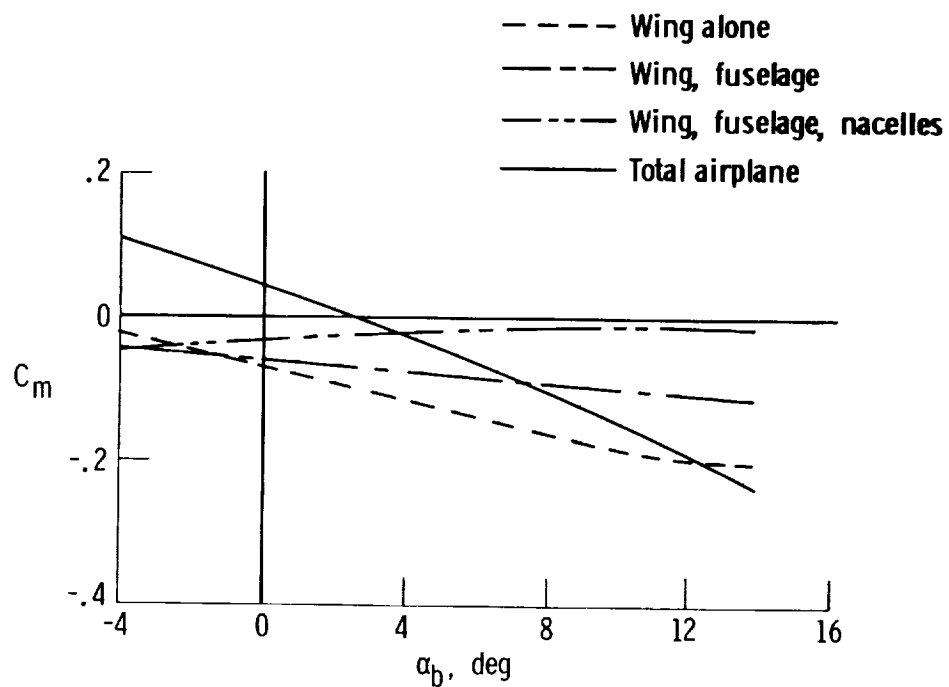


Figure 4.11-2. Predicted buildup of the pitching-moment characteristics of the airplane. $\delta_e = 0^\circ$; $S_w = 178$ sq ft; center of gravity $= 0.10\bar{c}_w$.

4.12 Drag of the Complete Airplane

The contributions to the drag of the complete airplane are as follows:

- (1) Zero-lift drag of the wing, horizontal tail, and vertical tail
- (2) Zero-lift drag of the fuselage and nacelles
- (3) Zero-lift interference drag of the wing-fuselage, tail-fuselage, and wing-nacelles
- (4) Drag of the wing and horizontal tail at angle of attack
- (5) Drag of the fuselage and nacelles at angle of attack
- (6) Wing-fuselage interference drag at angle of attack
- (7) Cooling drag due to nacelle inlets and cooling flaps

Each of these contributing factors is considered at this time and applied to the subject airplane.

4.12.1 Zero-Lift Drag of Wing, Horizontal Tail, and Vertical Tail

The zero-lift or profile drag is composed of a skin-friction drag and a pressure drag caused by the boundary layer, which prevents full pressure recovery at the trailing edge. For subsonic conditions the pressure drag is usually small.

The magnitude of the skin-friction drag, caused by shearing stresses within the boundary layer, depends upon the roughness of the surface and upon whether the flow in the boundary layer is laminar or turbulent. According to reference 1, transition from laminar to turbulent flow on a straight wing can be assumed to occur at a Reynolds number of approximately 1 million, based on the distance from the leading edge. Transition occurs at a lower Reynolds number on a swept wing. Thus, for all practical purposes, the boundary layer is considered to be turbulent for the subsonic conditions of general aviation airplanes.

For subsonic conditions ($M \leq 0.6$), the profile drag coefficient of a lifting surface may be accurately determined by using the following empirical equation (ref. 27) based on the lifting surface area under consideration:

$$(C_{D_o})_{ls} = 2C_f \left[\underbrace{1 + 2\left(\frac{t}{c}\right)}_{\text{Skin friction terms}} + \underbrace{120\left(\frac{t}{c}\right)^4}_{\text{Pressure drag term}} \right] \quad (4.12.1-1)$$

where

C_f is the skin-friction coefficient of a flat plate, obtained from figure 4.12.1-1 as a function of Reynolds number, N_{Re} , and the parameter $\frac{l}{k}$

l is the reference length in inches, the mean aerodynamic chord of the lifting surface

k is the surface-roughness height, estimated from table 4.12.1-1 on the basis of surface finish, inches

$\frac{t}{c}$ is the thickness ratio of the wing

It should be noted that only the exposed panels of the lifting surfaces are considered in arriving at the zero-lift drag of the surfaces to avoid overlap with the fuselage surface areas.

On the basis of equation (4.12.1-1) and the summary calculations of table 4.12.1-2, the contributions of the exposed panels of the wing, horizontal tail, and vertical tail of the subject airplane to the zero-lift drag of the airplane were determined, based on a reference wing area of 172.3 square feet, to be as follows:

$$\left. \begin{array}{ll} \text{Wing} & (C_{D_o})_w = (C_{D_o})_{w_e} \frac{S_{w_e}}{S_w} = 0.00853 \\ \text{Horizontal tail} & (C_{D_o})_h = (C_{D_o})_{h_e} \frac{S_{h_e}}{S_w} = 0.00159 \\ \text{Vertical tail} & (C_{D_o})_v = (C_{D_o})_{v_e} \frac{S_{v_e}}{S_w} = 0.00077 \end{array} \right\} \quad (4.12.1-2)$$

4.12.2 Zero-Lift Drag of Fuselage and Nacelles

The zero-lift drag of an isolated body may be estimated by using the following empirical equation from reference 1 based on axisymmetric bodies of revolution. It can be applied to non-body-of-revolution configurations by treating the actual body as an equivalent body of revolution having an axially distributed circumferential area similar to that of the actual body. For subsonic conditions ($M \leq 0.6$), on the basis of the frontal area, S_B ,

$$\begin{aligned} (C_{D_o})_B &= C_{D_f} + C_{D_b} \\ &= C_f \left[1 + \frac{60}{\left(\frac{l_B}{d_B}\right)^3} + 0.0025 \left(\frac{l_B}{d_B}\right) \right] \frac{S_{wet}}{S_B} + C_{D_b} \end{aligned} \quad (4.12.2-1)$$

$\underbrace{\left[1 + \frac{60}{\left(\frac{l_B}{d_B}\right)^3} + 0.0025 \left(\frac{l_B}{d_B}\right) \right]}_{\text{Pressure-drag terms}}$
 $\underbrace{\frac{S_{wet}}{S_B}}_{\text{Skin-friction term}}$
 $\underbrace{C_{D_b}}_{\text{Base drag}}$

where

C_{D_f} is the skin-friction and pressure-drag coefficient of the body

C_f is the skin-friction coefficient of a flat plate, obtained from figure 4.12.1-1 as a function of Reynolds number, N_{Re} , based on actual body length, l_B , and the parameter $\frac{l_B}{k}$ where k is obtained from table 4.12.1-1

d_B is the diameter of a circle having a perimeter equal to the perimeter of the maximum frontal area of the body

S_B is the maximum frontal area of an axisymmetric body having a diameter, d_B , equal to $\frac{\pi d_B^2}{4}$

S_{wet} is the wetted surface area of the body, and may be approximated from figure 4.12.2-1 as a ratio of S_B

From reference 27

$$C_{D_b} = 0.029 \left(\frac{d_b}{d_B} \right)^3 \sqrt{C_{D_f}} \quad (4.12.2-2)$$

where

d_b is the diameter of the equivalent circular perimeter of the base area

The preceding equations were applied to the estimation of the zero-lift drag of the fuselage and nacelles of the subject airplane, as isolated bodies. The summary calculations in table 4.12.2-1 show, on the basis of a reference wing area of 172.3 square feet, the zero-lift drags to be as follows:

$$\begin{aligned} \text{Fuselage } (C_{D_o})_f &= 0.00780 \\ \text{Nacelles } (C_{D_o})_n &= 0.00374 \text{ per nacelle} \end{aligned} \quad (4.12.2-3)$$

4.12.3 Zero-Lift Interference Drag of Wing-Fuselage, Tail-Fuselage, and Wing-Nacelles

Zero-lift interference drag of wing-fuselage combinations is at a minimum and tends toward zero at low subsonic speeds when the wing is at the nose or tail of the fuselage. It is at a maximum when the wing is at approximately midlongitudinal position on the body. This is substantiated by limited low-speed wind-tunnel data in reference 27. When these data were applied to the subject airplane, the wing-fuselage zero-lift interference drag was approximately 5 percent of the zero-lift fuselage drag.

A more up-to-date and substantial procedure to account for wing-fuselage zero-lift interference drag for conventional orientation of a wing relative to a fuselage is provided by the use of the correlation factor, R_{wf} , from figure 4.12.3-1, which is the ratio of fuselage drag in the presence of the wing to fuselage alone with base drag omitted. Thus the zero-lift drag of the fuselage in the presence of the wing, relative to wing area, is obtained from

$$(C_{D_o})_{f(w)} = \left[(C_{D_f})_f R_{wf} + C_{D_b} \right] \frac{S_B}{S_w} \quad (4.12.3-1)$$

where

$(C_{D_f})_f$ is the zero-lift drag of the fuselage (section 4.12.2)

R_{wf} is the ratio of the wing-fuselage to the fuselage-alone zero-lift drag, with base drag omitted, as a function of Mach number and Reynolds number based on fuselage length in figure 4.12.3-1.

The correlation factor was developed in reference 28 by determining the ratio of test values of minimum drag coefficient to values predicted on the basis of $R_{wf} = 1$ for several wing-body combinations. The scarcity of quality test data required that data for all classes of composite planforms be used in the correlation effort. No distinction was made in planform type.

When the correction factor, R_{wf} , technique was applied to the subject airplane, the net zero-lift wing-fuselage drag was (table 4.12.3-1(a))

$$\begin{aligned} (\bar{C}_{D_o})_{wf} &= (C_{D_o})_w + \left[(C_{D_f})_f R_{wf} + C_{D_b} \right] \frac{S_B}{S_w} \\ &= 0.01688 \end{aligned} \quad (4.12.3-2)$$

Zero-lift interference drag of tail-fuselage or tail-tail junctures: The zero-lift interference of tail-fuselage or tail-tail junctures may be estimated from empirical relations based on subsonic experimental data. When a tail panel intersects the fuselage, the subsonic interference drag at the junction of the two surfaces may be approximated by equation (4.12.3-3), which was formulated in reference 27 for the interference drag at the junction of a lifting surface (or strut) with a plane wall in turbulent flow conditions. On the basis of a reference wing area, S_w , the increment of tail drag due to fuselage interference is approximately

$$(\Delta C_{D_o})_{t(f)} = n_1 \left[0.8 \left(\frac{t}{c} \right)^3 - 0.0005 \right] \frac{c_{re}^2}{S_w} \quad (4.12.3-3)$$

where

n_1 is the number of junctures of the tail surface with the fuselage

c_{re} is the root chord of the exposed panel

$\left(\frac{t}{c} \right)$ is the thickness ratio of the section at c_{re}

When the vertical tails intersect the horizontal tail, the interference drag due to

each corner of the intersection may be approximated from the following empirical equation from reference 27, based on the experimental data of intersecting stream-lined struts:

$$(\Delta C_{D_o})_{v(h)} = \frac{n_2}{2} \left[17 \left(\frac{t}{c} \right)_{int}^4 - 0.05 \left(\frac{t}{c} \right)_{int}^2 \right] \frac{c_{int}^2}{S_w} \quad (4.12.3-4)$$

where

n_2 is the number of corners (a cruciform intersection would have four corners)

$\left(\frac{t}{c} \right)_{int}$ is the average thickness ratio of the intersecting surfaces at the intersection

c_{int} is the chord at the intersection

For the subject airplane, the horizontal and vertical tails intersect the fuselage in an area where the fuselage contour is changing. In the absence of pertinent information on the effects of surface contour, the zero-lift interference drag due to the juncture of the tail surfaces with the fuselage was conservatively estimated on the basis of equation (4.12.3-3), the equation for the juncture of a lifting surface with a plane wall. On the basis of the summary calculations in table 4.12.3-1(b), the net zero-lift vertical-tail-fuselage and horizontal-tail-fuselage interference drags are approximately

$$(\overline{C_{D_o}})_h = (C_{D_o})_h + (\Delta C_{D_o})_{h(f)} = 0.00159 \quad (4.12.3-5)$$

$$(\overline{C_{D_o}})_v = (C_{D_o})_v + (\Delta C_{D_o})_{v(f)} = 0.00077$$

Zero-lift interference drag of nacelle-wing combinations: The zero-lift interference drag of nacelle-wing combinations in which a relatively slender nacelle is faired into the wing was considered in reference 27. The study concluded that the interference drag of nacelles faired into the wing may be roughly accounted for by the increment of zero-lift wing drag due to the wing area covered by the nacelle. Thus, for one nacelle

$$(\Delta C_{D_o})_{n(w)} = (C_{D_o})_w \frac{(\Delta S_w)_n}{S_w} \quad (4.12.3-6)$$

where

$(C_{D_o})_w$ is the zero-lift drag of the exposed wing panels, based on equation (4.12.1-1), in terms of the reference wing area

S_w is the reference wing area, square feet

$(\Delta S_w)_n$ is the wing area overlapped by one nacelle, square feet

When applied to the subject airplane, the summary calculations of table 4.12.3-1(c) show the net zero-lift drag of the two nacelles to be, on the basis of the reference wing area, S_w ,

$$(\overline{C_{D_o}})_{n(w)} = 2 \left[(C_{D_o})_n + (\Delta C_{D_o})_{n(w)} \right] = 0.00854 \quad (4.12.3-7)$$

Summary: The zero-lift drag of the components plus the interference drags between mating components is

$$C_{D_o} = (\overline{C_{D_o}})_{wf} + (\overline{C_{D_o}})_h + (\overline{C_{D_o}})_v + (\overline{C_{D_o}})_{n(w)} \quad (4.12.3-8)$$

For the subject airplane, as summarized in table 4.12.3-1(d),

$$C_{D_o} = 0.02778 \quad (4.12.3-9)$$

based on a reference wing area of 172.3 square feet. When this is converted to the reference area (178 sq ft) of the wind-tunnel data, $C_{D_o} = 0.02681$.

4.12.4 Drag of Wing and Horizontal Tail at Angle of Attack

The drag due to lift of a wing is made up of the induced drag due to vortex system downwash and a viscous drag caused primarily by the upper-surface boundary layer which increases in thickness as the angle of attack increases.

On the basis of simple theory the induced drag of a wing at subsonic conditions is conventionally represented by

$$C_{D_i} = \frac{C_L^2}{\pi A_w e} \quad (4.12.4-1)$$

where e is the Oswald span-efficiency factor which is equal to 1 for elliptic wings and can be calculated for wings having other shapes. The equation has limited utility. It provides reasonable values for straight wings below the angle of attack for maximum $\frac{L}{D}$. Above this angle, separation of flow at the trailing edge usually causes the drag to increase significantly above the theoretical value obtained from the equation. The equation becomes invalid for swept and low-aspect-ratio wings because the shedding of the vortex inboard of the wing tips reduces the effective aspect ratio of the wing.

Many attempts have been made to develop empirical methods for predicting the subsonic span-efficiency factor, e , over the parabolic-induced-drag region. Development of empirical relations for predicting viscous drag has been handicapped by lack of full-scale correlation data. Substantiation of proposed techniques for calculating

the drag due to lift has been hindered by the need to refer to small-scale wind-tunnel data.

Several methods were considered for application to general aviation aircraft. These included the method of reference 29, which was refined in reference 28, and a method presented in reference 1. A spot check of the results of applying the two methods to the subject airplane and correlating them with the full-scale wind-tunnel data of the airplane indicated that the former method predicted wing drag which appeared to be excessive with increasing angle of attack. Predictions by the latter method, which is used in this report, appeared to be more reasonable.

The drag of the untwisted wing (and horizontal tail) due to lift can be determined from

$$(C_{Di})_w = \frac{\overbrace{C_{Lw}^2}^{\text{Induced}}}{\pi A_w} (1 + \delta_1 \delta_2) + \overbrace{k_3 \Delta}^{\text{Viscous}} \quad (4.12.4-2)$$

where

C_L is the lift coefficient of the lifting surface being considered and referenced to its own lifting surface area

δ_1 is a theoretically determined correction factor for the taper ratio of the surface being considered, obtained from figure 4.12.4-1 as a function of taper ratio, λ_w , and aspect ratio, A_w

δ_2 is a theoretically determined correction factor for the sweep angle of the surface being considered, obtained from figure 4.12.4-2 as a function of sweep angle, $\Lambda_c/4$, and aspect ratio, A_w

k_3 is an empirically determined sweep-angle correction factor for the viscous drag of the surface being considered, obtained from figure 4.12.4-3 as a function of sweep angle, Λ_{le} , and a parameter, J , defined in equation (4.12.4-3)

Δ is an empirical viscous drag increment factor for the surface being considered, obtained from figure 4.12.4-4 as a function of $\frac{\tan \alpha_{abs}}{\tan(\alpha_{abs}) C_{Lmax}}$ and the parameter J

and where

$$J = 0.3(c_1 + 1) \frac{A_w}{\beta'} \cos \Lambda_{le} \left\{ (c_1 + 1)(c_2 + 1) - \left[\frac{(c_2 + 1) \tan \Lambda_{le}}{7} \right]^3 \right\} \quad (4.12.4-3)$$

with the taper ratio constants c_1 and c_2 obtained from figures 4.2-3 and 4.4-2, respectively.

Applied to the subject aircraft, the summary calculations of table 4.12.4-1(a)

show that the lift-drag contributions of the wing and horizontal tail can be represented by

$$(C_{Di})_w = 0.0432C_{L_w}^2 + \Delta_w \text{ on the basis of } S_w = 172.3 \text{ sq ft} \quad (4.12.4-4)$$

$$(C_{Di})_h = 0.0669C_{L_h}^2 + \Delta_h \text{ on the basis of } S_h = 32.5 \text{ sq ft}$$

These equations are applied in tables 4.12.4-1(b) and 4.12.4-1(c) to determine the lift-drag contributions of the two surfaces as functions of α_b and $S_w = 172.3$ square feet to be applied in the drag summation in section 4.12.7.

4.12.5 Drag of Fuselage and Nacelles at Angle of Attack

The drag of a body at angle of attack is related to its lift. By assuming that the flow is potential over the forebody and is entirely viscous over the afterbody, as was done for the lift of the body in section 4.3, the following equation for the subsonic drag of a body due to angle of attack (in effect, due to lift) was arrived at in reference 10:

$$(C_{Di})_B = \left[\frac{2\alpha^2(k_2 - k_1)S_B}{V_B^{2/3}} + \frac{2\alpha^3}{V_B^{2/3}} \int_{x_0}^{l_B} \eta r c_{dc} dx \right] \frac{V_B^{2/3}}{S_w} \quad (4.12.5-1)$$

where

α is the angle of attack of the equivalent body of revolution relative to its zero-lift line, radians

S_B is the maximum cross-section area of the equivalent circular body, square feet

V_B is the volume of the equivalent circular body, cubic feet

$(k_2 - k_1)$ is a reduced mass factor, obtained from figure 4.3-1

η is the ratio of drag coefficients of finite to infinite length cylinders, obtained from figure 4.3-2

c_{dc} is a crossflow drag coefficient of an infinite length cylinder, obtained from figure 4.3-3

l_B is the length of the body, feet

x_0 is the location from the nose of the body where potential flow ceases, obtained from figure 4.3-4, feet

$\int r dx$ is half of the projected area of the equivalent circular body from x_0 to the end, square feet

A comparison of equation (4.12.5-1) with the equation for the lift of a body in section 4.3 indicates that

$$(C_{Di})_B = C_{LB} \alpha \quad (4.12.5-2)$$

where

C_{LB} is the lift of the body per equation (4.4-2)

α is the angle of attack of the body, radians

Because the subsonic drag of a body due to lift is simply a matter of multiplying its lift by the angle of attack, the drag due to lift of the fuselage and nacelles of the subject airplane, on the basis of the treatment of these components in section 4.3 for the lift of the components, is obtained from

$$(C_{Di})_{fn} = \overbrace{C_{Lf} \frac{(\alpha_b - 3)}{57.3}}^{\text{Fuselage}} + \overbrace{C_{Ln} \frac{\alpha_b}{57.3}}^{\text{Two nacelles}} \quad (4.12.5-3)$$

where

C_{Lf} is the sum of columns 3 and 4 in table 4.4-2

C_{Ln} is the sum of columns 5 and 6 in table 4.4-2

α_b is the reference angle of attack relative to the body axis

Table 4.12.5-1 summarizes the calculation of the drag of the fuselage and nacelles of the subject airplane due to lift. The calculations are based on a reference wing area.

4.12.6 Wing-Fuselage Interference Drag at Angle of Attack

Little appears to be known about wing-fuselage interference drag at angle of attack. There is undoubtedly some increase in parasitic drag at the juncture of the lifting surface and the body. There is also some modification of the induced drag of the wing due to the upwash from the body acting on the wing. This upwash modifies the loading across the span and, for an elliptic wing, could increase the induced drag. For a rectangular wing, the resulting load across the span is made "more elliptic" (tending toward lift distribution of an elliptic wing) and could result in some decrease in induced drag.

In the absence of applicable representative data, no attempt is made to account for wing-fuselage interference drag at angle of attack. However, it is believed that the

omission of this factor would affect the total drag of the subject airplane by less than 5 percent at the angle of attack of incipient stall.

4.12.7 Cooling Drag

The discussion of nacelle drag in the previous section did not take into account the effect of drag due to the cooling system, which could be a significant factor. An analytical treatment of cooling drag is beyond the scope of this paper because of the complexity and uncertainties in its determination. Some general considerations in its analytical determination may be obtained from reference 27. To account for the cooling drag in the predicted drag characteristics, which were to be compared with wind-tunnel data, consideration was given to the fact that the wind-tunnel tests of the subject airplane were conducted with the inlet and cooling flaps open and that unpublished, propeller-off, wind-tunnel data were available for the increment of drag due to the cooling system. These data, shown in figure 4.12.7-1, were used to account for the cooling drag. It should be noted that this cooling drag has a characteristic reversal in trends which would be difficult, if not impossible, to predict. The relatively sharp increase in cooling drag above an angle of attack of approximately 8.5° is particularly significant in providing improved correlation of predicted drag characteristics with wind-tunnel data at high angles of attack, as is shown in the next section.

4.12.8 Summary Drag of the Complete Airplane

The net drag of the subject airplane is summarized in table 4.12.8-1 in the following format. The data for the contributing factors, with the exception of the cooling drag, were obtained from the tables noted above the individual terms. The cooling drag data were obtained from figure 4.12.7-1.

Table

$$C_D = C_{D_0} + (C_{D_i})_w + (C_{D_i})_h + (C_{D_i})_f + (C_{D_i})_n + (C_D)_{\text{cooling system}} \quad (4.12.8-1)$$

The above result is for a reference wing area of 172.3 square feet. To permit a direct comparison of the calculated drag with wind-tunnel data, the results are converted to a reference wing area of 178 square feet in the last column of table 4.12.8-1.

The calculated drag characteristics with the cooling drag increments omitted and included are compared with wind-tunnel data in figures 4.12.8-1(a), 4.12.8-1(b), and 4.12.8-1(c) as functions of α_b , C_L , and C_L^2 , respectively. Although the calculated drag with cooling drag increments omitted correlates well with the wind-tunnel data through the angle-of-attack range of -4° to 12° in figure 4.12.8-1(a) (and a corresponding C_L range in fig. 4.12.8-1(b)), the addition of the cooling drag increment resulted in excellent correlation up to 4° angle of attack. Whereas the C_D versus α_b plot (fig. 4.12.8-1(a)) shows a slight decrease in correlation over the remainder of the angle-of-attack range, the C_D versus C_L plot (fig. 4.12.8-1(b)) shows excellent correlation at the limit of linearity (at $C_L = 1.15$, which corresponds to $\alpha_b = 10^\circ$). It should be noted that the appreciable, and important, increase in cooling drag increment at high angles of attack is difficult to predict analytically.

The predicted buildup of the drag characteristics shown in figure 4.12.8-2 indicates that all contributing factors considered were important.

4.12.9 Symbols

The following list of symbols constitutes the basic symbols used. In several instances, such as in the equation in table 4.12.1-2, a subscript "i" is applied to parenthesized quantities, with an identifying notation on the left side of the equation (such as $i = w, h, v$), to signify that the equation applies to the surfaces thus identified. If the wing is being considered, $i = w$ and all parenthesized quantities having an i subscript apply to the wing; for example, $S_{ie} = S_{we}$, the area of the exposed wing panels.

A_w	wing aspect ratio
C_D	drag coefficient
C_{D_b}	base drag coefficient referred to the maximum frontal (cross section) area of the body involved
$(C_D)_{\text{cooling system}}$	contribution of the cooling system to the airplane drag coefficient
C_{D_f}	skin friction and pressure drag coefficient referred to the maximum frontal area of the body involved
$(C_{D_f})_f$	fuselage C_{D_f}
C_{D_i}	induced drag coefficient referred to the wing area unless noted otherwise
$(C_{D_i})_B$	C_{D_i} of the body (fuselage or nacelle)
$(C_{D_i})_f, (C_{D_i})_h, (C_{D_i})_n, (C_{D_i})_w$	contribution of the fuselage, horizontal tail, nacelles, and wing, respectively, to C_{D_i}
$(C_{D_i})_{fn}$	net contribution of the fuselage and nacelles to C_{D_i}
C_{D_o}	zero-lift drag coefficient referred to the wing area unless noted otherwise
$(C_{D_o})_B$	zero-lift drag coefficient of a body referenced to the frontal area
$(C_{D_o})_f, (C_{D_o})_n$	C_{D_o} of the isolated fuselage and one isolated nacelle, respectively, referenced to the wing area
$(C_{D_o})_{f(w)}$	C_{D_o} of the fuselage with wing-fuselage interference accounted for, referenced to the wing area

$(C_{D_o})_h, (C_{D_o})_w, (C_{D_o})_v$	C_{D_o} of the exposed panels of the horizontal tail, wing, and vertical tail, respectively, referenced to the wing area
$(C_{D_o})_{h_e}, (C_{D_o})_{w_e}, (C_{D_o})_{v_e}$	C_{D_o} of the respective exposed panel surface areas
$(C_{D_o})_{ls}$	zero-lift drag coefficient of the exposed panels of a lifting surface, referenced to the exposed panel area
$(\overline{C_{D_o}})_h, (\overline{C_{D_o}})_n, (\overline{C_{D_o}})_v$	net contribution of the horizontal tail, nacelles, and vertical tail, respectively, to the zero-lift drag coefficient with interference effects accounted for, referenced to the wing area
$(\overline{C_{D_o}})_{hv} = (\overline{C_{D_o}})_h + (\overline{C_{D_o}})_v$	
$(\overline{C_{D_o}})_{wf} = (C_{D_o})_w + (C_{D_o})_{f(w)}$	
$(\Delta C_{D_o})_{h(f)}, (\Delta C_{D_o})_{v(f)}$	increment of the zero-lift drag coefficient of the horizontal and vertical tail, respectively, due to fuselage interference, referenced to the wing area
$(\Delta C_{D_o})_{n(w)}$	increment of the zero-lift drag coefficient of one nacelle due to wing interference, referenced to the wing area
$(\overline{C_{D_o}})_{n(w)}$	net zero-lift drag coefficient of the nacelles in the presence of the wing
$(\Delta C_{D_o})_{t(f)}$	generalized expression representing $(\Delta C_{D_o})_{h(f)}$ or $(\Delta C_{D_o})_{v(f)}$, referenced to the wing area
$(\Delta C_{D_o})_{v(h)}$	increment of the zero-lift drag coefficient of the vertical tail due to the horizontal-tail interference when the vertical tail intersects the horizontal tail, referenced to the wing area
C_f	skin-friction coefficient of a flat plate, based on a wet surface area, obtained from figure 4.12.1-1
C_L	lift coefficient referred to the wing area unless noted otherwise
C_{LB}	lift coefficient of the body (fuselage or nacelle), referenced to the wing area
C_{Lf}, C_{Ln}, C_{Lw}	lift coefficient of the fuselage, nacelles, and wing, respectively, referenced to the wing area

C_{Lh}	lift coefficient of the horizontal tail referred to the tail area
c_{dc}	two-dimensional steady-state crossflow drag coefficient for circular cylinders, obtained from figure 4.3-3
c_{int}	chord at the intersection of the vertical and horizontal tails when the horizontal tail is mounted on the vertical tail or vice versa, ft
c_{re}	root chord of the exposed portion of the tail surface intersecting the fuselage, ft
c_1, c_2	taper ratio correction factors, used in calculating the parameter J , as obtained from figures 4.2-3 and 4.4-2, respectively
d_B	diameter of the equivalent circular perimeter of the maximum frontal area of the body (fuselage or nacelle), ft
d_b	diameter of the equivalent circular perimeter of the base area, ft
e	Oswald span-efficiency factor used in the induced-drag equation (4.12.4-1)
J	parameter, defined by equation (4.12.4-3), used in obtaining the viscous drag increment, Δ , of a lifting surface
J_h, J_w	the parameter J applied to the horizontal tail and wing, respectively
k	equivalent sand roughness of a surface (table 4.12.1-1), in.
$k_2 - k_1$	apparent mass factor, obtained from figure 4.3-1
k_3	sweep-angle correction drag factor for the viscous drag increment, Δ
$\frac{L}{D}$	lift-to-drag ratio of the wing
l	reference length, for lifting surfaces, equal to the mean aerodynamic chord of the individual surface, for bodies, equal to the length of the body, in.
l_B	reference length of the body (fuselage or nacelle), in.
l_f	reference length of the fuselage, in.

M	Mach number
N_{Re}	Reynolds number
n_1	number of junctures of the tail surface with the fuselage
n_2	number of corners in the juncture of the vertical tail with the horizontal tail (cruciform intersection would have four corners)
R_{wf}	ratio of the wing-fuselage to fuselage-alone zero-lift drag with the base drag omitted
r	radius of the body, ft
S_B	maximum frontal area of the body (fuselage or nacelle), sq ft
S_h, S_w	horizontal tail and wing area, respectively, sq ft
S_{he}, S_{we}, S_{ve}	exposed-panel surface area of the horizontal tail, wing, and vertical tail, respectively, sq ft
S_{wet}	wetted surface area, sq ft
$(\Delta S_w)_n$	wing area overlapped by one nacelle, sq ft
$\frac{t}{c}$	airfoil section thickness ratio
$\left(\frac{t}{c}\right)_{int}$	average thickness ratio of intersecting vertical- and horizontal-tail surfaces
V_B	body volume (fuselage or nacelle), cu ft
x_o	distance from the nose of the body to the point of maximum cross-section area, ft
α	angle of attack, deg
α_{abs}	angle of attack relative to the zero-lift line, deg
α_b	airplane angle of attack relative to the X-body axis, deg
α_f, α_n	angle of attack of the fuselage and nacelle, respectively, deg
$\alpha_{habs}, \alpha_{wabs}$	absolute angle of attack of the horizontal tail and wing, respectively, deg
$(\alpha_{abs})_{CL_{max}}$	absolute stall angle of attack, deg

$(\alpha_{habs})_{CL_{max}}, (\alpha_{wabs})_{CL_{max}}$	absolute stall angle of attack of the horizontal tail and wing, respectively, deg
$\beta' = (1 - M^2)^{1/2}$	
Δ	viscous drag increment
Δ_h, Δ_w	viscous drag increment of the horizontal tail and wing, respectively
δ_e	elevator deflection, deg
δ_1, δ_2	correction factor for the taper ratio and sweep angle of the quarter-chord line, respectively, in calculating the induced-drag coefficient of the wing and horizontal tail
$\bar{\epsilon}_h$	net downwash at the horizontal tail
η	ratio of the drag coefficient of finite to infinite length cylinders
$\Lambda_{c/4}, \Lambda_{le}$	sweep of the quarter-chord line and leading edge, respectively, deg
λ_w	taper ratio of the wing

TABLE 4.12.1-1
SURFACE ROUGHNESS HEIGHT k
[ref. 1]

Type of surface	k , in.
Aerodynamically smooth	0
Polished metal or wood	.02 to .08 $\times 10^{-3}$
Natural sheet metal	.16 $\times 10^{-3}$
Smooth matte paint, carefully applied	.25 $\times 10^{-3}$
Standard camouflage paint, average application	.40 $\times 10^{-3}$
Camouflage paint, mass production spray	1.20 $\times 10^{-3}$
Dip galvanized metal surface	6.0 $\times 10^{-3}$
Natural surface of cast iron	10.0 $\times 10^{-3}$

TABLE 4.12.1-2
ZERO-LIFT DRAG OF WING, HORIZONTAL AND VERTICAL TAILS

$$(C_{D_o})_{i=w,h,v} = 2(C_f)_i \left[1 + 2\left(\frac{t}{c}\right)_i + 120\left(\frac{t}{c}\right)_i^4 \right] \frac{S_{i_e}}{S_w} \text{ on basis of } S_w = 172.3 \text{ sq ft}$$

Symbol	Description	Reference	Magnitude		
			Exposed wing panels	Exposed horizontal tail	Exposed vertical tail
k_i	Surface roughness height, in.	Table 4.12.1-1	0.25 $\times 10^{-3}$ smooth matte paint		
l_i	Reference length, mean aerodynamic chord of surfaces, in.	Table 3.2-1	57.1	31.2	39.2
$\frac{l_i}{k_i}$	-----	-----	2.28×10^5	1.25×10^5	1.57×10^5
$N_{Re,i}$	Reynolds number at 63.4 mph, sea level $= \frac{l}{12} (0.65 \times 10^6)$	Wind-tunnel test condition	3.09×10^6	1.69×10^6	2.12×10^6
C_{f_i}	Skin-friction coefficient of flat plate	Figure 4.12.1-1	3.65×10^{-3}	4.08×10^{-3}	3.9×10^{-3}
$\left(\frac{t}{c}\right)_i$	Thickness ratio of surface	Table 4.1-1	.15	.08	.08
$2(C_f)_i \left[\quad \right]$	Zero-lift drag of component on basis of exposed panel area, S_{i_e}	Equation (4.12.1-1)	0.00993	0.00951	0.00909
S_{i_e}	Exposed panel area of component surface	Table 3.2-1	148.0	28.73	14.6
$(C_{D_o})_i$	Zero-lift drag of component on basis of reference wing area, $(C_{D_o})_i = 2(C_f)_i \left[\quad \right] \frac{S_{i_e}}{S_w}$	-----	$(C_{D_o})_w = .00853$	$(C_{D_o})_h = .00159$	$(C_{D_o})_v = .00077$

TABLE 4.12.2-1
ZERO-LIFT DRAG OF FUSELAGE AND NACELLES

[On basis of reference wing area, $S_w = 172.3$ sq ft]

$$(C_{Do})_{i=f,n} = (C_{Df} + C_{Db})_i \frac{S_{Bi}}{S_w} = \left\{ (C_f)_i \left[1 + \frac{60}{\left(\frac{l}{d_B}\right)_i^3} + 0.0025 \left(\frac{l}{d_B}\right)_i \right] \frac{(S_{wet})_i}{S_{Bi}} + 0.029 \left(\frac{d_b}{d_B}\right)_i^3 \sqrt{(C_{Df})_i} \right\} \frac{S_{Bi}}{S_w}$$

Symbol	Description	Reference	Magnitude	
			Fuselage	Nacelle
d_{Bi}	Diameter of equivalent perimeter of maximum frontal area, ft	Airplane drawing	5.41	3.0
S_{Bi}	Frontal area of equivalent perimeter body, $\frac{\pi d_{Bi}^2}{4}$, sq ft	-----	23.0	7.07 per nacelle
l_i	Length of body, ft	Figure 4.3-5	24.2	8.82
d_{bi}	Diameter of base of equivalent body of revolution, ft	-----	≈ 0.79	≈ 1.0
$\left(\frac{l}{d_B}\right)_i$	$\frac{l_i}{d_{Bi}}$	-----	4.47	2.94
$\left(\frac{d_b}{d_B}\right)_i$	$\frac{d_{bi}}{d_{Bi}}$	-----	.15	.33
$\frac{(S_{wet})_i}{S_{Bi}}$	Ratio of wetted surface area to S_{Bi}	Figure 4.12.2-1	12.4	8.2
$(S_{wet})_i$	Wetted surface area of isolated body, $\left[\frac{(S_{wet})_i}{S_{Bi}}\right] S_{Bi}$, sq ft	-----	285	58 per nacelle
k_i	Surface roughness height (smooth matte finish)	Table 4.12.1-1	0.25×10^{-3} in.	0.25×10^{-3}
$\frac{l_i}{k_i}$	Ratio in common units	-----	1.16×10^6	4.24×10^6
$(N_{Re})_i$	Reynolds number at 63.4 mph (sea level); $(N_{Re})_i = (0.65 \times 10^6) l_i$	Wind-tunnel test condition	1.57×10^7	5.73×10^6
$(C_f)_i$	Skin friction of flat plate	Figure 4.12.1-1	2.8×10^{-3}	3.3×10^{-3}
$(C_{Df})_i$	$(C_f)_i \left[1 + \frac{60}{\left(\frac{l}{d_B}\right)_i^3} + 0.0025 \left(\frac{l}{d_B}\right)_i \right] \frac{(S_{wet})_i}{S_{Bi}}$	Equation (4.12.2-1)	0.0584	0.0912 per nacelle
$(C_{Db})_i$	$0.029 \left(\frac{d_b}{d_B}\right)_i^3 \sqrt{(C_{Df})_i}$	Equation (4.12.2-2)	≈ 0	≈ 0
$(C_{Do})_i$	$\left[(C_{Df})_i + (C_{Db})_i \right] \frac{S_{Bi}}{S_w}$, on basis of reference $S_w = 172.3$ sq ft	-----	$(C_{Do})_f = .00780$	$(C_{Do})_n = .00374$ per nacelle

TABLE 4.12.3-1
ZERO-LIFT DRAG OF THE COMPONENTS

(a) Net zero-lift drag of wing-fuselage combination

$$(\overline{C_{D_0}})_{wf} = (\overline{C_{D_0}})_w + \left[(C_{D_f})_f R_{wf} + C_{D_b} \right] \frac{S_B}{S_w}$$

Symbol	Description	Reference	Magnitude
$(\overline{C_{D_0}})_w$	Zero-lift drag of isolated exposed wing panels	Table 4.12.1-2	0.00853
C_{D_b}	Base drag of fuselage	Table 4.12.2-1	0
$(C_{D_f})_f$	Zero-lift drag of isolated fuselage with base drag omitted	Table 4.12.2-1	.0584
M	Mach number	Wind-tunnel condition	0.083
S_B	Frontal area of fuselage, sq ft	Table 4.12.2-1	23.0
l_f	Length of the fuselage, ft	Figure 4.3-5	24.2
S_w	Reference wing area, sq ft	Table 3.2-1	172.3
N_{Re}	Reynolds number = $0.65 \times 10^6 \times l_f$	Wind-tunnel test condition	1.57×10^7
R_{wf}	Wing-body interference correlation factor	Figure 4.12.3-1	1.071
Summary: $(\overline{C_{D_0}})_{wf} = 0.01688$			

(b) Net zero-lift drag of tail surfaces in presence of fuselage

$$(\overline{C_{D_0}})_{hv} = (\overline{C_{D_0}})_h + (\overline{C_{D_0}})_v = (C_{D_0})_h + (\Delta C_{D_0})_{h(f)} + (C_{D_0})_v + (\Delta C_{D_0})_{v(f)}$$

Symbol	Description	Reference	Magnitude	
			Horizontal tail	Vertical tail
$(C_{D_0})_h$	Zero-lift drag of isolated exposed horizontal-tail panels	Table 4.12.1-2	0.00159	-----
$(C_{D_0})_v$	Zero-lift drag of isolated exposed vertical-tail panel	Table 4.12.1-2	-----	0.00077
n_1	Number of junctures of tail with fuselage	-----	2	1
$\frac{t}{c}$	Thickness ratio of tail surface at juncture	Table 4.1-1	.08	.08
c_{re}	Root chord of exposed tail surface, ft	Table 3.2-1	3.275	4.25
S_w	Reference wing area, sq ft	Table 3.2-1	172.3	172.3
$(\Delta C_{D_0})_{h(f)}$	Interference drag of horizontal-tail surface due to fuselage	Equation (4.12.3-3)	≈ 0	-----
$(\Delta C_{D_0})_{v(f)}$	Interference drag of vertical-tail surface due to fuselage	Equation (4.12.3-3)	-----	≈ 0
Summary: $(\overline{C_{D_0}})_{hv} = 0.00159 + 0 + 0.00077 + 0 = 0.00236$				

(c) Net zero-lift drag of nacelles in presence of wing

$$(\overline{C_{D_0}})_n = 2 \left[(C_{D_0})_n + (C_{D_0})_w \frac{(\Delta S_w)_n}{S_w} \right]$$

Symbol	Description	Reference	Magnitude
$(C_{D_0})_n$	Zero-lift drag of one isolated nacelle	Table 4.12.2-1	0.00374 per nacelle
$(\Delta S_w)_n$	Wing area overlapped by one nacelle, sq ft	Figure 3.2-1	10.7
S_w	Reference wing area, sq ft	Table 3.2-1	172.3
Summary: $(\overline{C_{D_0}})_{n(w)} = 2 \left[0.00374 + 0.00853 \frac{10.7}{172.3} \right] = 0.00854$			

(d) Summary zero-lift drag of the components; on basis of reference
 $S_w = 172.3$ sq ft

$$C_{D_0} = (\overline{C_{D_0}})_{wf} + (\overline{C_{D_0}})_{hv} + (\overline{C_{D_0}})_{n(w)} = 0.01688 + 0.00236 + 0.00854 = 0.02778$$

TABLE 4.12.4-1
DRAG OF WING AND HORIZONTAL TAIL DUE TO LIFT

(a) Determination of functional equations

$$C_{Di} = \left(\frac{C_L^2}{\pi A} \right) (1 + \delta_1 \delta_2) + k_3 \Delta$$

Symbol	Description	Reference	Magnitudes	
			Wing, $S_w = 172.3$ sq ft	Horizontal tail, $S_{ht} = 32.5$ sq ft
Λ_{le}	Sweep of leading edge, deg	Table 3.2-1	0	12
$\Lambda_{c/4}$	Sweep of c/4 line, deg	Table 3.2-1	-2.5	8
A	Aspect ratio	Table 3.2-1	7.5	4.8
λ	Taper ratio	Table 3.2-1	.513	.515
$(\alpha_{abs})' C_{Lmax}$	Stall angle relative to zero lift, deg	Table 4.2-1	17.4	14.45
β'	$\sqrt{1 - M^2}$ at $M = 0.083$	Wind-tunnel test condition	.997	.997
c_1	Taper ratio correction factor	Figure 4.2-3	0.3	0.25
c_2	Taper ratio correction factor	Figure 4.4-2	1.06	1.05
J	Wing shape parameter	Equation (4.12.4-3)	7.86	4.52
δ_1	Taper ratio correction factor for induced drag	Figure 4.12.4-1	.0175	.0085
δ_2	Sweep angle correction factor for induced drag	Figure 4.12.4-2	1.0	1.0
k_3	Sweep angle correction factor for viscous drag	Figure 4.12.4-3	1.0	1.0
Δ	Viscous drag increment factor, function of J and $\left(\frac{\tan \alpha_{abs}}{\tan (\alpha_{abs})' C_{Lmax}} \right)$	Figure 4.12.4-4	$f(\alpha_{wabs})$	$f(\alpha_{habs})$
<p>Summary: Wing - $(C_{Di})_w = 0.0432 C_{Lw}^2 + \Delta_w$ on basis of $S_w = 172.3$ sq ft</p> <p>Horizontal tail - $(C_{Di})_h = 0.0669 C_{Lh}^2 + \Delta_h$ on basis of $S_h = 32.5$ sq ft</p>				

TABLE 4.12.4-1 (Concluded)

(b) Drag of wing due to lift = $0.0432 C_{L_w}^2 + \Delta_w$

$$J_w = 7.86 \text{ (from (a))}; (\alpha_{wabs})_{C_{L_{max}}} = 17.4^\circ \text{ (from (a))}; \tan(\alpha_{wabs})_{C_{L_{max}}} = 0.3134$$

①	②	③ (*)	④	⑤	⑥	⑦	⑧	⑨ (a)
α_b , deg	α_{wabs} = $\alpha_b + 4$ = $\alpha_w + 2$, deg	C_{L_w} , figure 4.2-1	$C_{L_w}^2$ = ③ ²	$0.0432 C_{L_w}^2$ = 0.0432 ④	$\tan \alpha_{wabs}$ = \tan ②	$\frac{\tan \alpha_{wabs}}{\tan(\alpha_{wabs})_{C_{L_{max}}}}$ = ⑥/0.3134	Δ_w , figure 4.12.4-4	$(C_{Di})_w$ = ⑤ + ⑧
-4 -2	0 2	0 .150	0 .0225	0 .00972	0 .0349	0 .1114	0 0	0 .0010
0 2	4 6	0.305 .450	0.0930 .2025	0.0402 .0875	0.0699 .1051	0.223 .335	0 .0025	0.0040 .01125
4 6	8 10	0.605 .759	0.366 .576	0.158 .249	0.1405 .1763	0.449 .562	0.008 .016	0.0238 .0409
8 10	12 14	0.910 1.055	0.828 1.113	0.688 .0481	0.2126 .2493	0.678 .796	0.026 .0395	0.0618 .0876
12 13.4	16 17.4	1.190 1.23	1.416 1.513	0.0612 .0654	0.2868 .3134	0.915 1.000	0.058 .077	0.1192 .1424

*On basis of $S_w = 172.3$ sq ft.(c) Drag of horizontal tail due to lift = $0.0669 C_{L_h}^2 + \Delta_h$

$$J_h = 4.50 \text{ (from (a))}; (\alpha_{habs})_{C_{L_{max}}} = 14.45^\circ \text{ (from (a))}; \tan(\alpha_{habs})_{C_{L_{max}}} = 0.2577$$

①	②	③	④ (a)	⑤	⑥	⑦	⑧	⑨	⑩ (a)	⑪
α_b , deg	$\bar{\epsilon}_h$, figure 4.9.1-7	α_{habs} $\alpha_b - \bar{\epsilon}_h$ = ① - ②, deg	C_{L_h} , figure 4.2-1	$C_{L_h}^2$ = ④ ²	$0.0669 C_{L_h}^2$ = 0.0669 ⑤	$\tan \alpha_{habs}$ = \tan ③	$\frac{\tan \alpha_{habs}}{\tan(\alpha_{habs})_{C_{L_{max}}}}$ = ⑦/0.2577	Δ_h , figure 4.12.4-4	$(C_{Di})_h$ = ⑥ + ⑨	$(C_{Di})_h$, on basis of $S_w = 172.3$ sq ft
-4 -2	0 .96	-4 -2.96	-0.284 -.210	0.0807 .0441	0.00540 .00295	-0.0699 -.0517	-0.271 -.201	0.001 .0002	0.0064 .0032	0.0012 .00060
0 2	1.90 2.93	-1.90 -.93	-0.135 -.066	0.0182 .0044	0.00122 .00029	-0.0332 -.0162	-0.129 -.0629	≈ 0 ≈ 0	0.00122 .0003	0.0002 .0001
4 6	3.87 4.86	0.13 1.14	0.009 .081	0.0001 .0066	≈ 0 .00044	0.0023 .0199	0.0089 .0772	≈ 0 ≈ 0	≈ 0 .0004	0 .0001
8 10	5.77 6.61	2.23 3.39	0.159 .241	0.0253 .0581	0.00169 .00389	0.0389 .0592	0.151 .230	0.0001 .0004	0.0018 .0043	.0003 .0008
12 13.4	7.55 -----	4.45 -----	0.317 -----	0.1005 -----	0.00672 -----	0.0778 -----	0.302 -----	0.0017 -----	0.0084 -----	0.0016 -----

*On basis of $S_h = 32.5$ sq ft.

TABLE 4.12.5-1
 DRAG DUE TO LIFT OF FUSELAGE AND NACELLES

$$(C_{Di})_{fn} = C_{Lf} \frac{\alpha_b - 3}{57.3} + C_{Ln} \frac{\alpha_b}{57.3}$$

①	②	③	④	⑤	⑥	⑦	⑧
α_b , deg	$C_{Lf} =$ ③ + ④ (table 4.4-2)	$\alpha_f =$ $\alpha_b - 3 =$ ① - 3, deg	$(C_{Di})_f =$ ② × ③ / 57.3	$C_{Ln} =$ ⑤ + ⑥ (table 4.4-2)	$\alpha_n =$ $\alpha_b =$ ①, deg	$(C_{Di})_n$ ⑤ × ⑥ / 57.3	$(C_{Di})_{fn} =$ ④ + ⑦ on basis of $S_w = 172.3$ sq ft
-4	-0.01374	-7	0.00168	-0.00624	-4	0.00044	0.00212
-2	-.01012	-5	.00088	-.00316	-2	.00011	.00099
0	-0.00626	-3	0.00033	0	0	0	0.00033
2	-.00215	-1	.00004	.00324	2	.00011	.00015
4	0.00221	1	0.00004	0.00656	4	0.00046	0.00050
6	.00682	3	.00036	.00996	6	.00104	.00140
8	0.01168	5	0.00102	0.01344	8	0.00188	0.00290
10	.01678	7	.00205	.01700	10	.00297	.00502
12	0.02213	9	0.00348	0.02064	12	0.00432	0.00780
13.8	.02720	10.8	.00513	.02400	13.8	.00578	.01091

TABLE 4.12.8-1
DRAG OF THE COMPLETE AIRPLANE ($\delta_e = 0^\circ$)

①	②	③ (a)	④ (a)	⑤ (a)	⑥ (a)	⑦ (a)	⑧ (a)	⑨ (a)	⑩
α_b , deg	C _L of airplane relative to $S_w = 178$ sq ft, table 4.10-2	C _{D0} , table 4.12.9-1	(C _D) _w , table 4.12.4-1(b)	(C _D) _h , table 4.12.4-1(c)	(C _D) _f , table 4.12.5-1	(C _D) _A , table 4.12.5-1	(C _D) cooling system, figure 4.12.7-1	(3) + (4) + (5) + (6) + (7) + (8)	C _D = ⑩ 174.3 178.0 (based on $S_w = 178$ sq ft)
-4	-0.074	0.02778	0	0.0012	0.00168	0.00044	0.00200	0.0331	0.0320
-2	.099	.02778	.0010	.0006	.00088	.00011	.00340	.0338	.0327
0	0.274	0.02778	0.0040	0.0002	0.00033	0	0.00333	0.0356	0.0345
2	.447	.02778	.01125	.0001	.00004	.00011	.00280	.0421	.0408
4	0.622	0.02778	0.0238	0	0.00004	0.00046	0.00224	0.0543	0.0526
6	.797	.02778	.0409	.0001	.00036	.00104	.00185	.0720	.0697
8	0.972	0.02778	0.0618	0.0003	0.00102	0.00188	0.00166	0.0944	0.0914
10	1.149	.02778	.0876	.0008	.00205	.00297	.00310	.1243	.1203
12	1.290	0.02778	0.1192	0.0016	0.00348	0.00432	≈0.00740	0.1638	0.1586
13.6	1.355	.02778	.1424	-----	.00513	.00578	≈.0090 (assumed)	.1901	.1840

*Values in this column based on reference wing area of $S_w = 172.3$ sq ft.

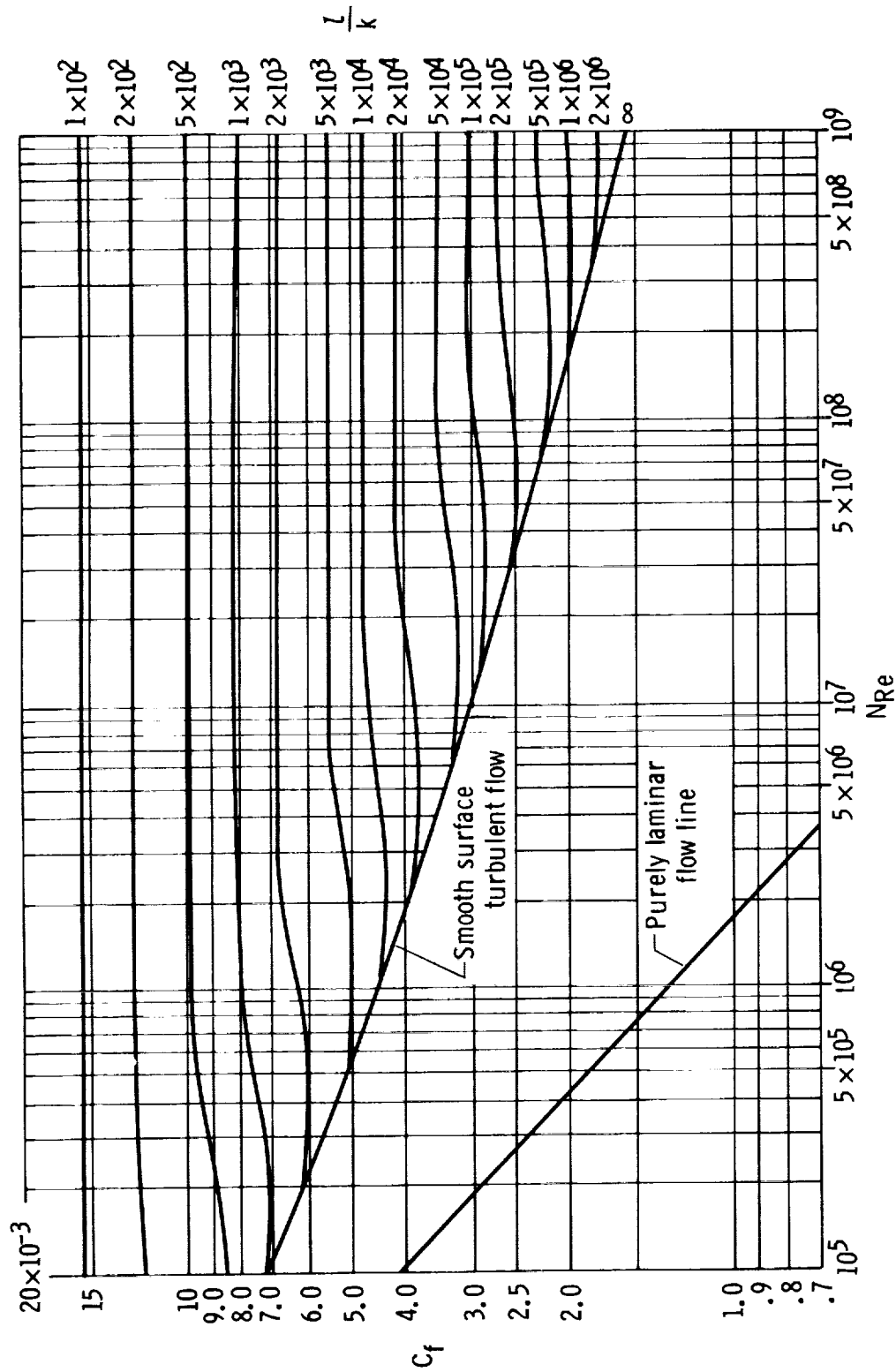


Figure 4.12.1-1. Incompressible skin-friction coefficient (ref. 1).
Transition at leading edge; $M = 0$.

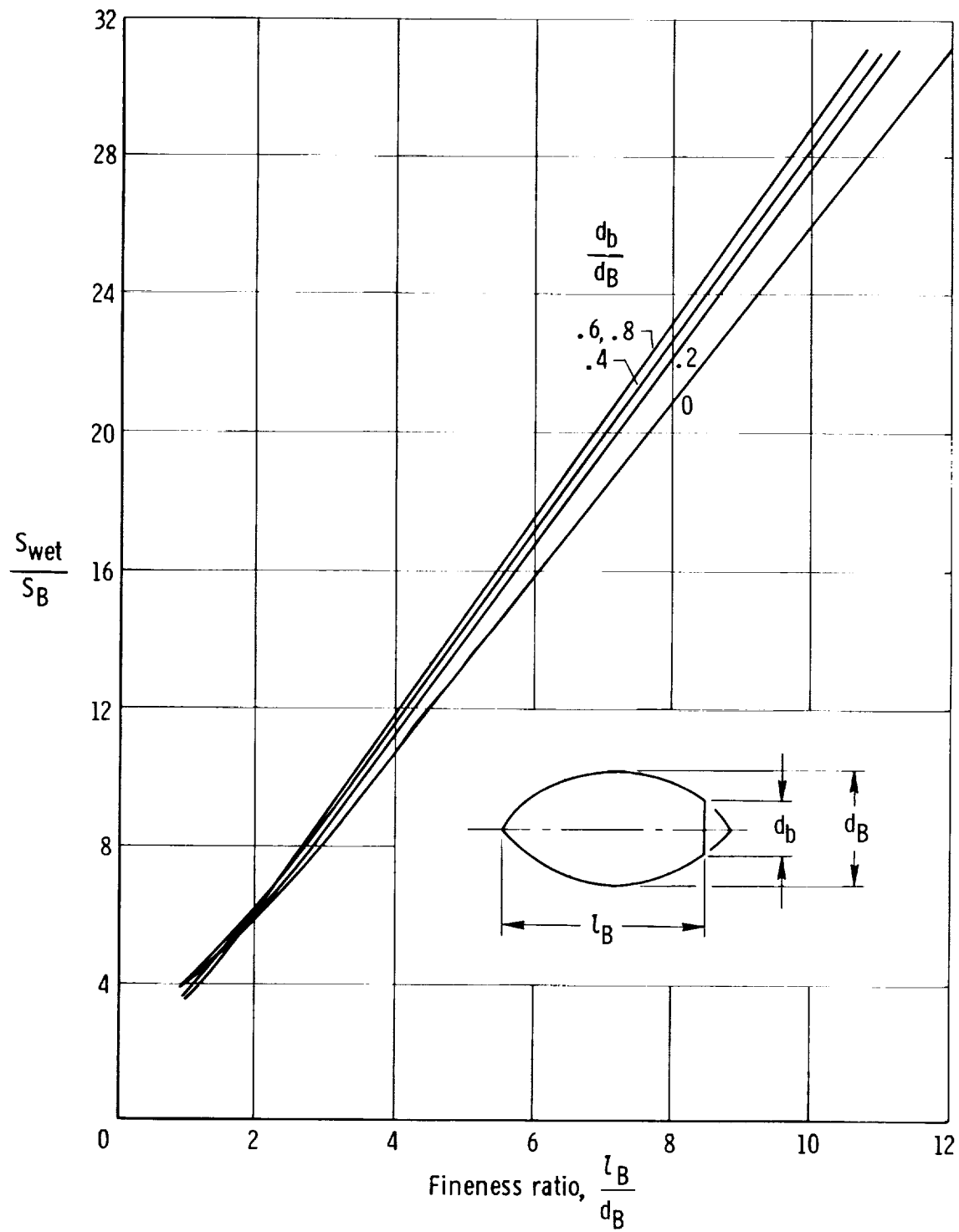


Figure 4.12.2-1. Wetted area of blunt-base ogive bodies (ref. 1).

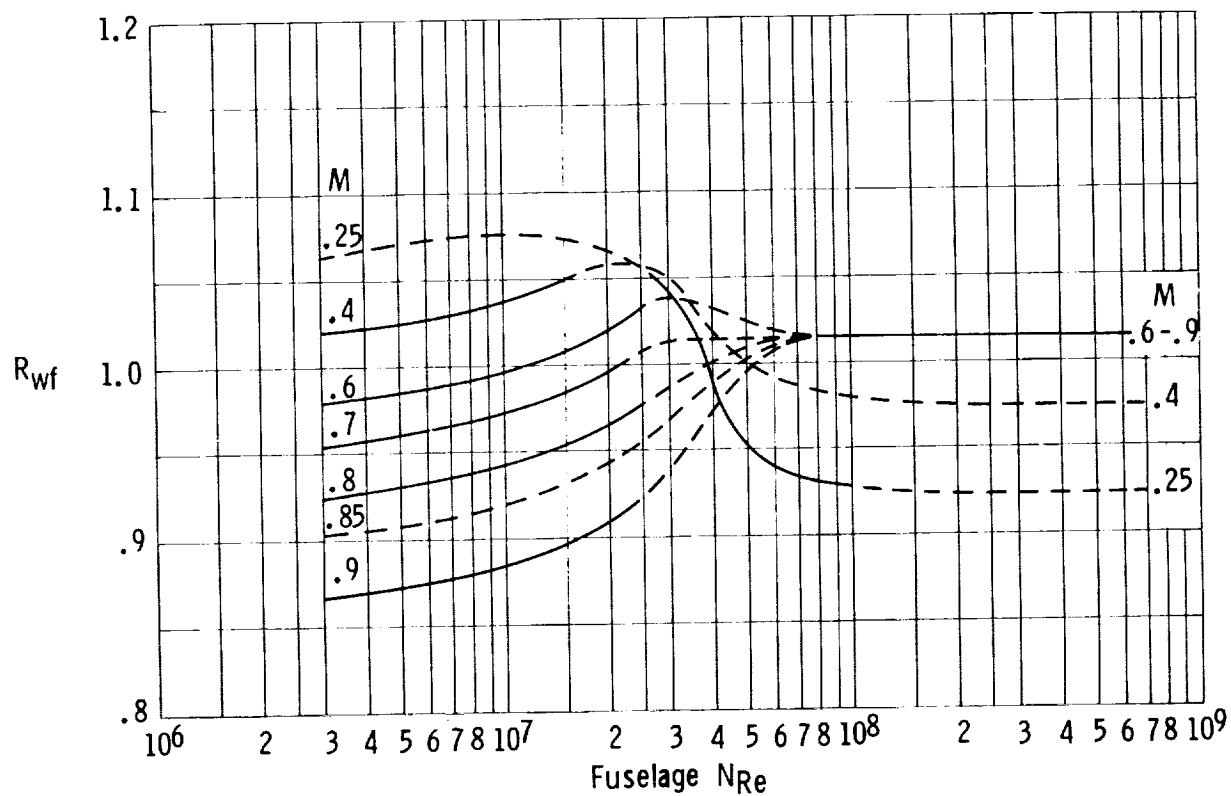


Figure 4.12.3-1. Wing-body interference correlation factor (ref. 1).

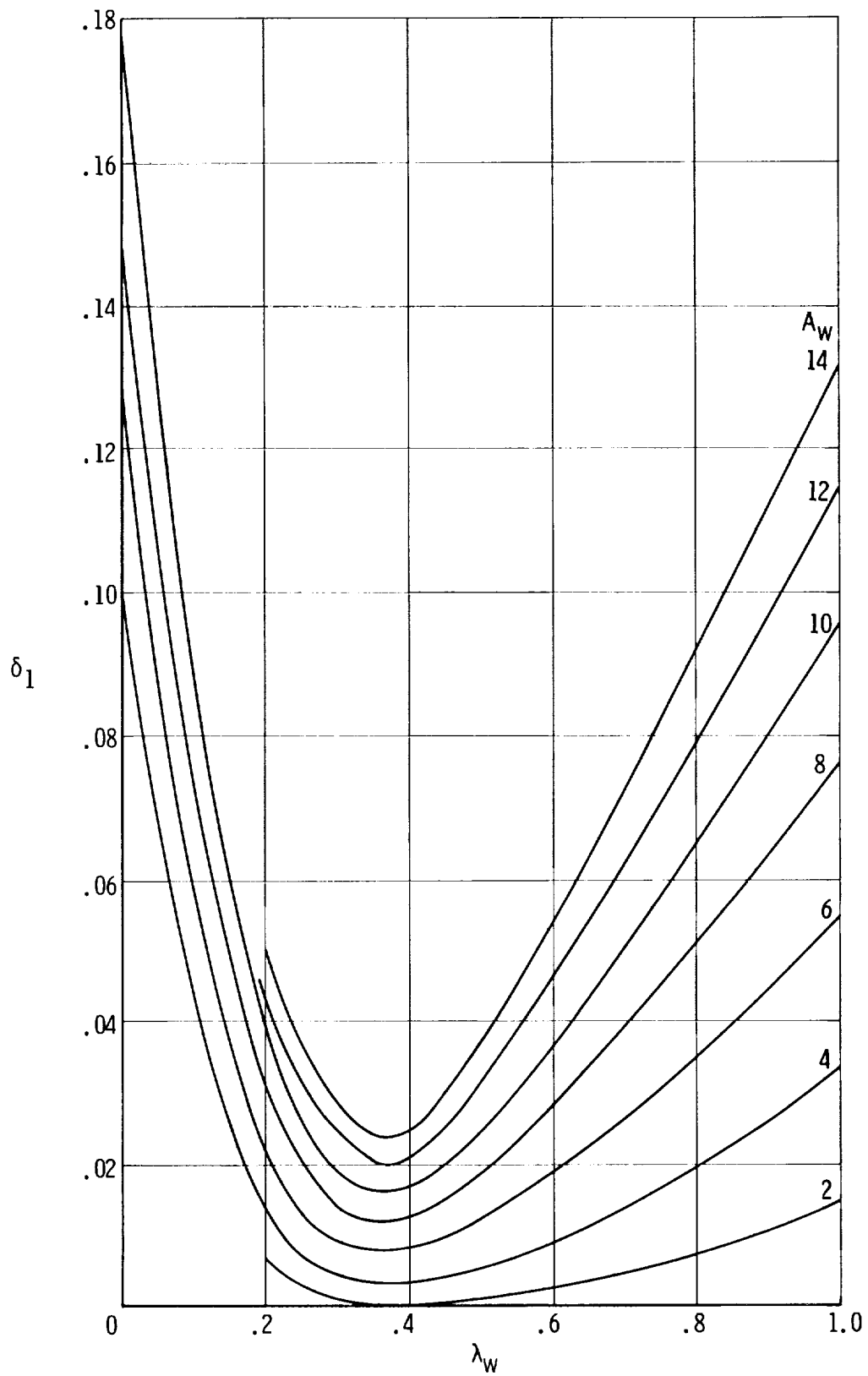


Figure 4.12.4-1. Taper ratio correction factor (from ref. 1).
Subsonic speeds; $\Lambda_{c/4} = 0$.

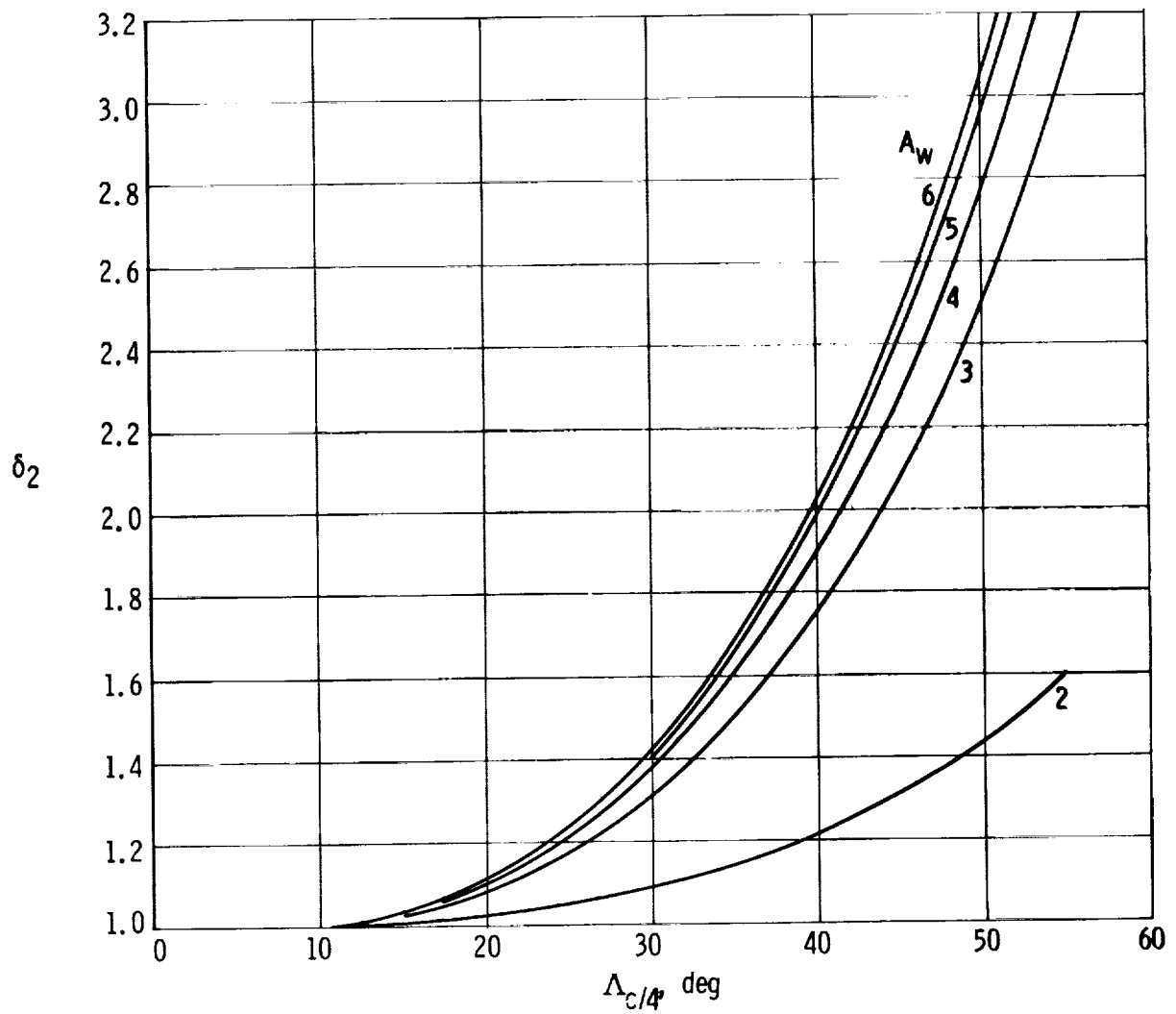


Figure 4.12.4-2. Sweep angle correction factor for δ_2 (from ref. 1).

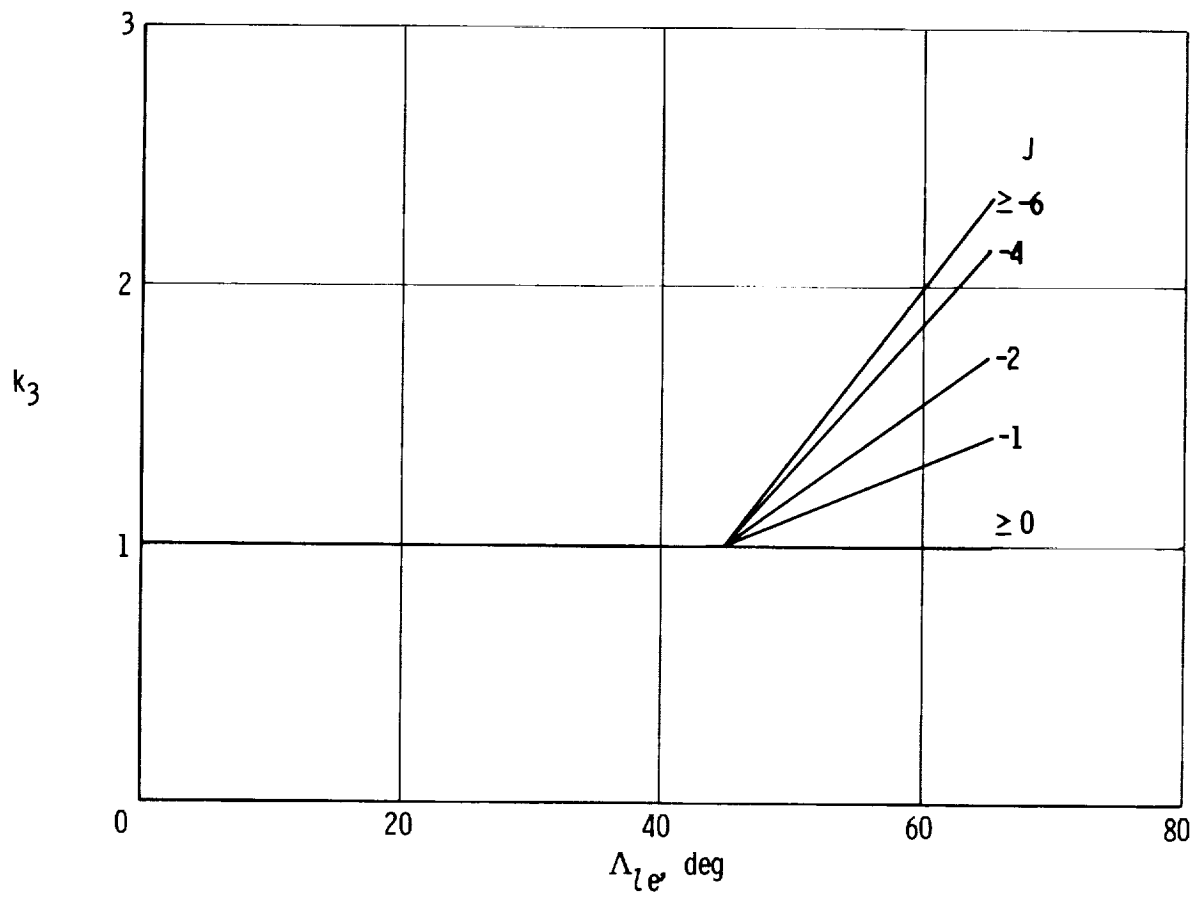


Figure 4.12.4-3. Sweep angle correction factor for k_3 (from ref. 1).

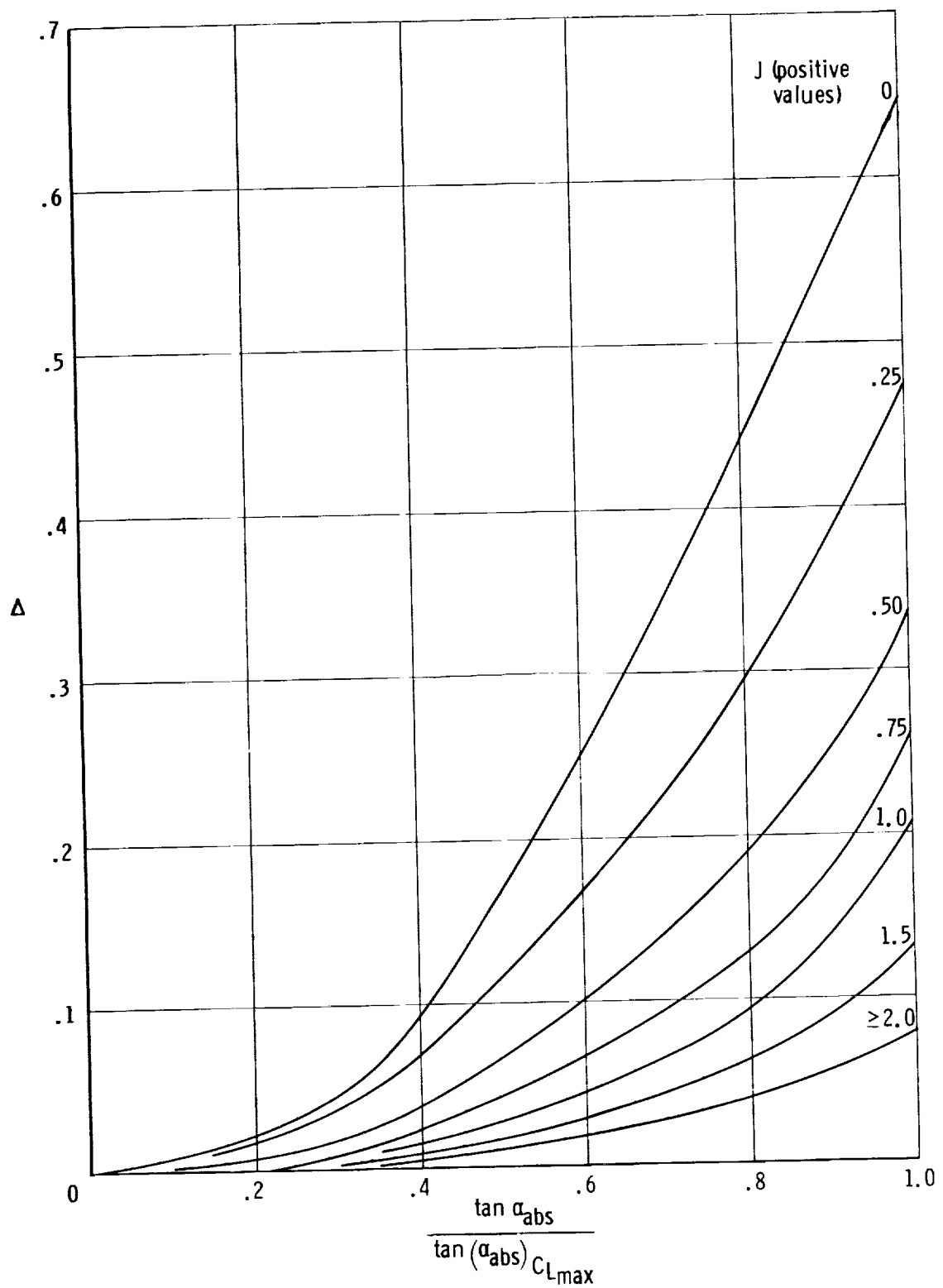


Figure 4.12.4-4. Variation with angle of attack of drag increment due to wing shape (from ref. 1). $\Lambda_{le} \leq 65^\circ$; $A_w \geq 2$.

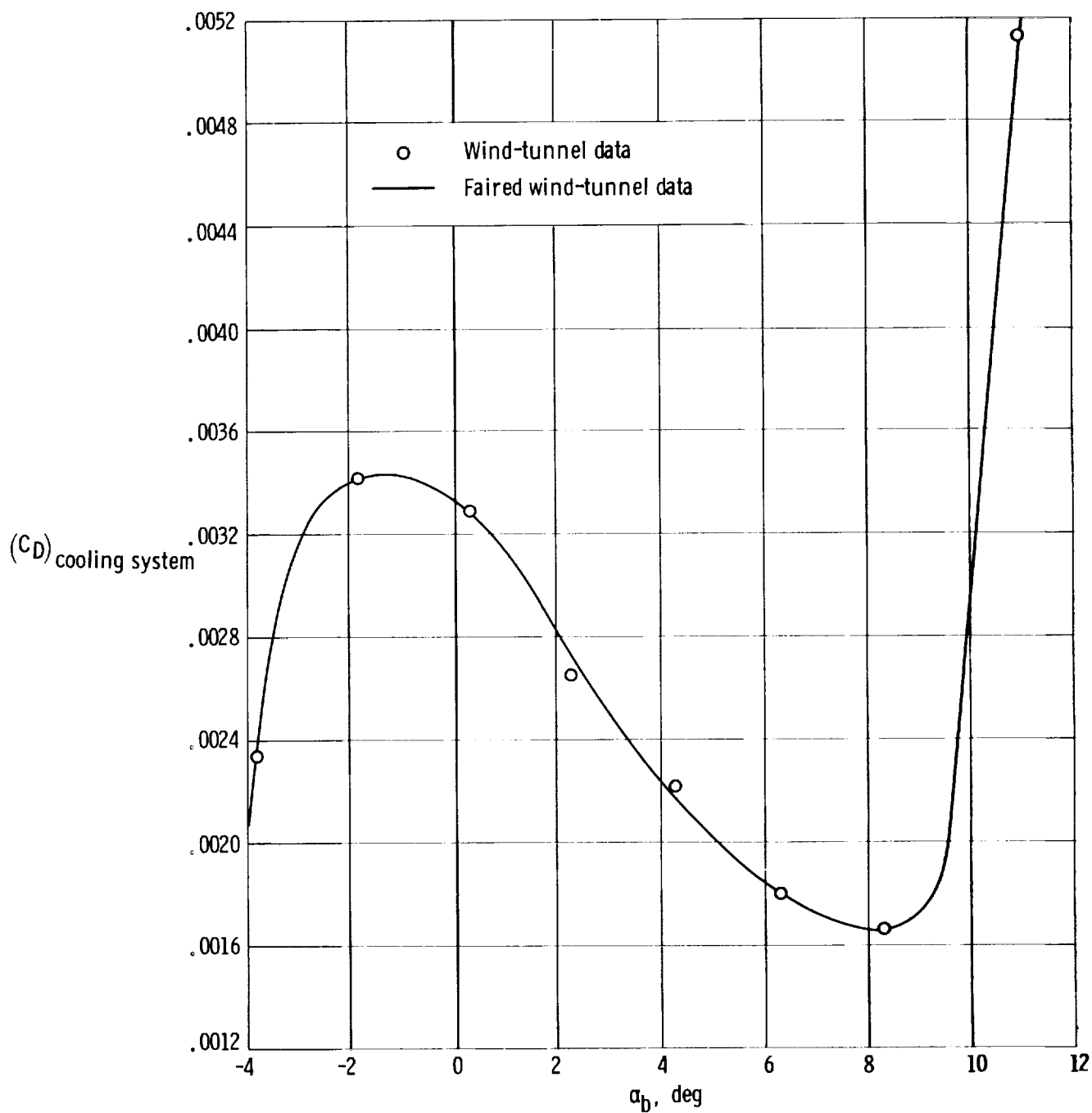
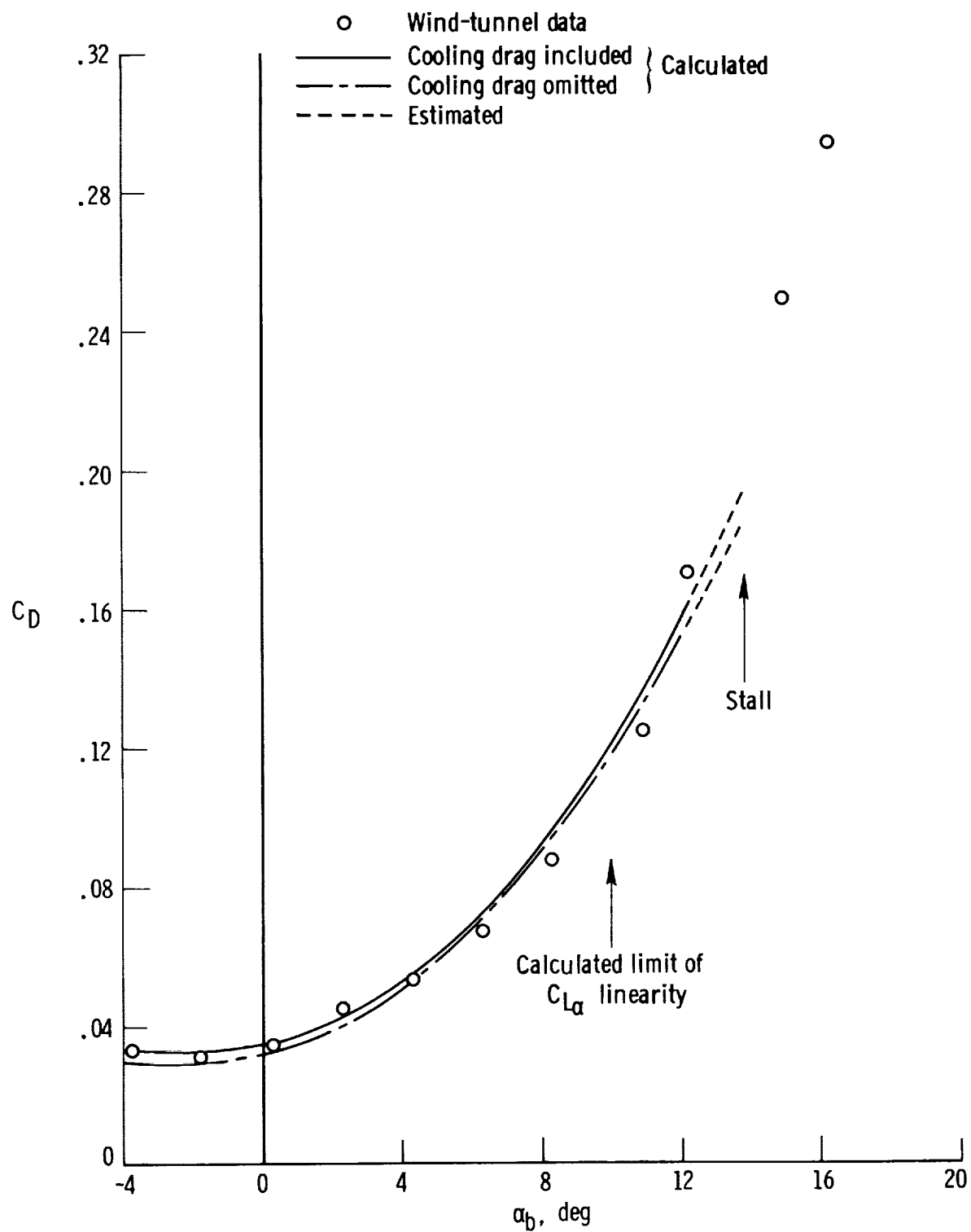
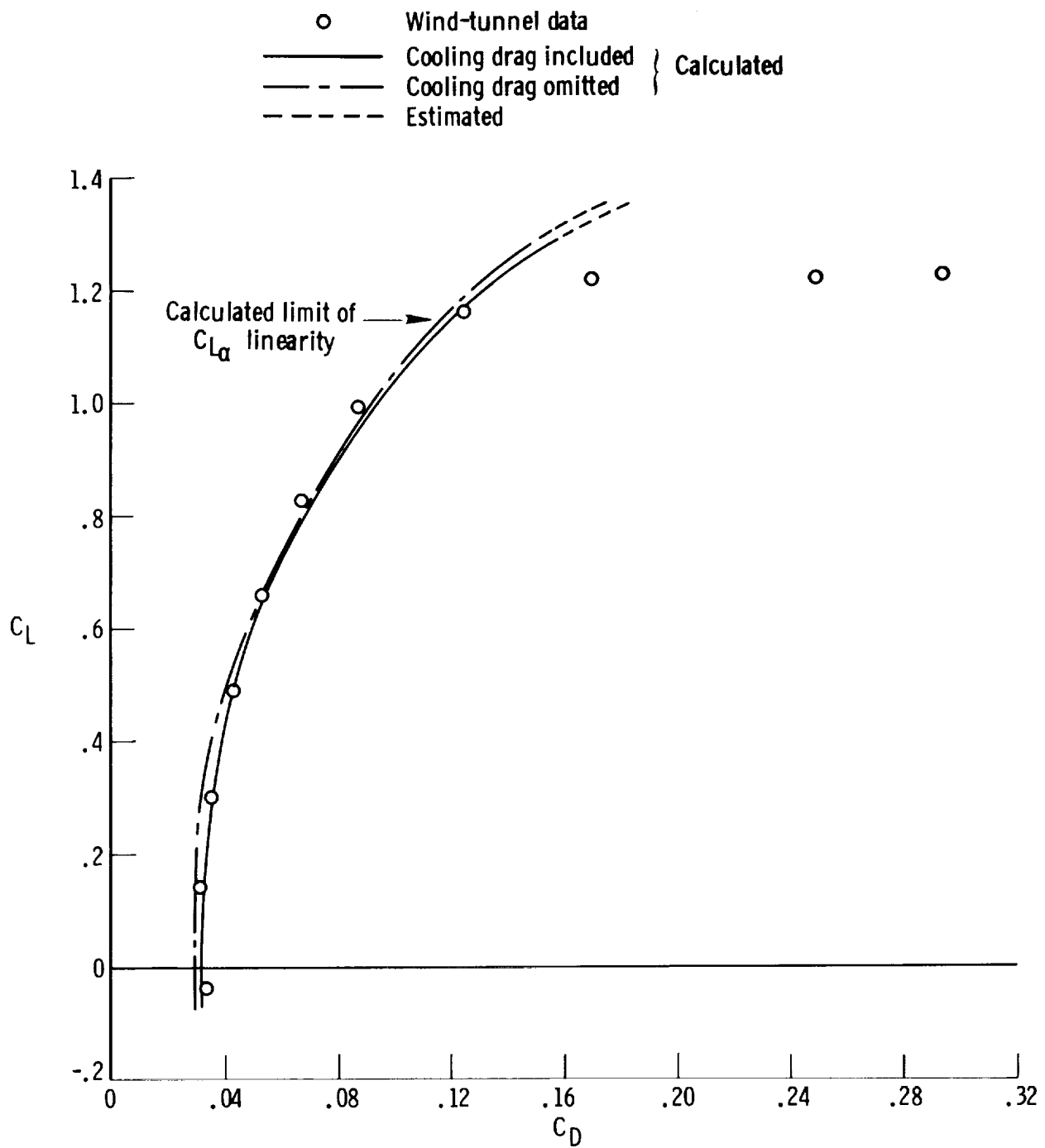


Figure 4.12.7-1. Unpublished propeller-off, full-scale wind-tunnel data of increment of drag of the subject airplane due to inlets and flaps of cooling system being open. $S_w = 172.3$ sq ft.



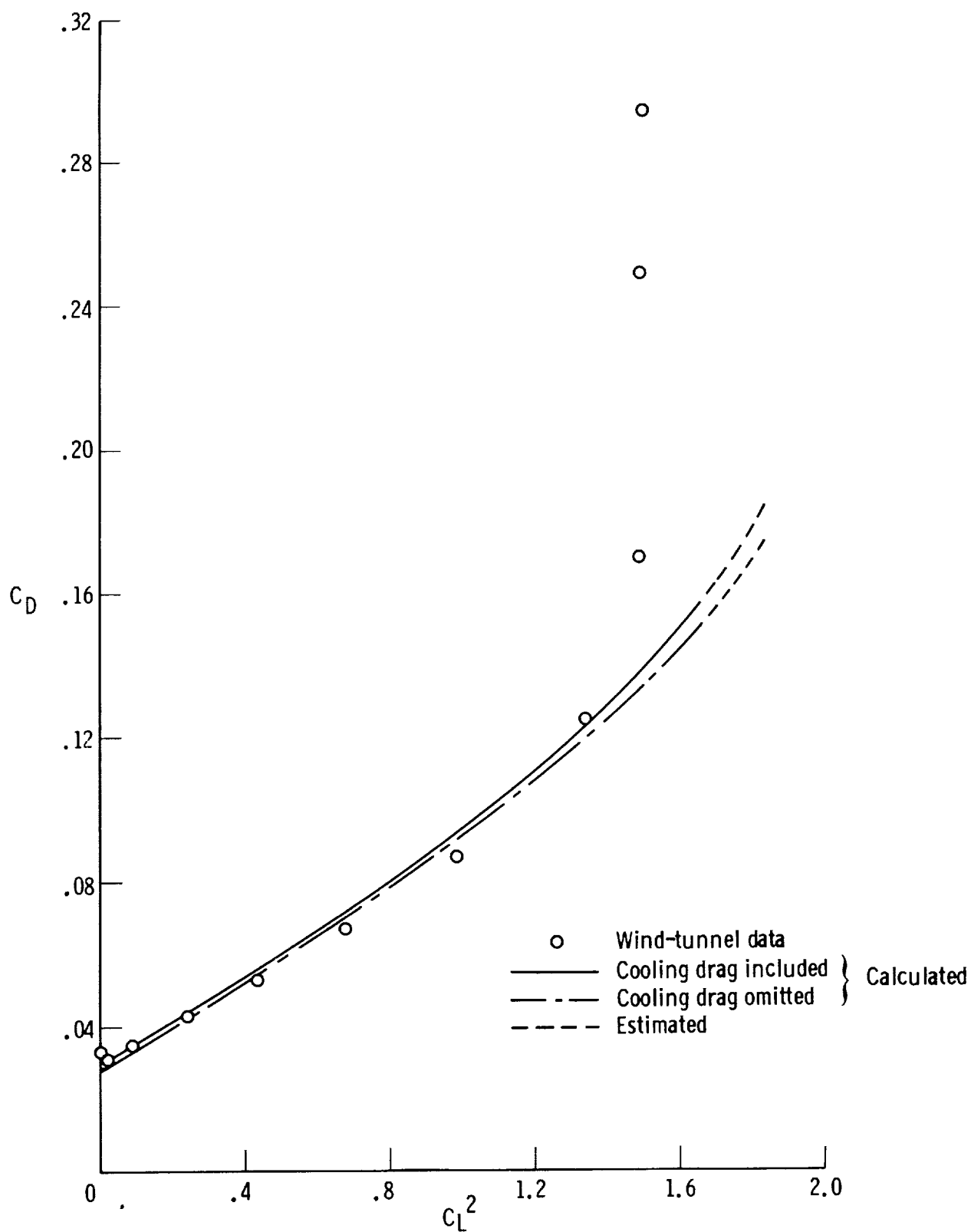
(a) C_D versus α_b .

Figure 4.12.8-1. Comparison of predicted airplane drag characteristics with wind-tunnel data. $\delta_e = 0^\circ$; propellers off; $S_w = 178$ sq ft.



(b) C_L versus C_D .

Figure 4.12.8-1. Continued.



(c) C_D versus C_L^2 .
Figure 4.12.8-1. Concluded.

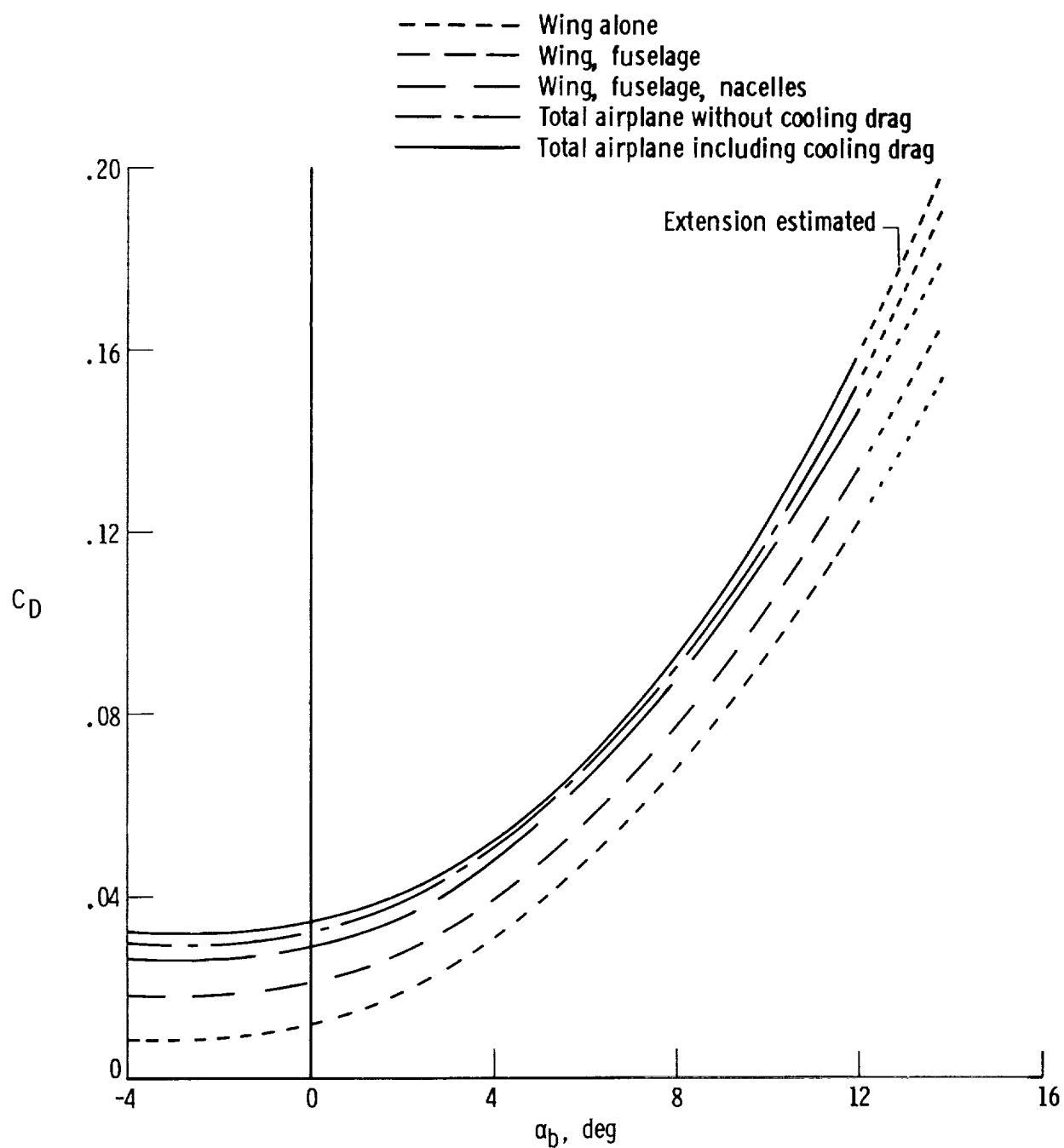


Figure 4.12.8-2. Predicted buildup of the drag characteristics of the airplane.
 $\delta_e = 0^\circ$; $S_w = 178$ sq ft.

4.13 Effect of Horizontal Tail and Tab Deflection on Lift and Pitching Moments

The contributions of the horizontal tail to the lift and pitching moments were considered in sections 4.10 and 4.11 on the basis of a fixed tail at zero incidence setting. In this section the tail is considered as an all-moving surface with a geared tab. Inasmuch as the results from this section are to be used also in obtaining horizontal-tail hinge moments, the tail lift is initially obtained referenced to the tail area.

4.13.1 Lift of the Horizontal Tail in the Linear Range

The lift of an all-moving horizontal tail equipped with a tab is attributed to three superimposed sources: (1) lift due to angle of attack of the tail, with the tail at zero incidence, (2) lift due to stabilizer deflection, δ_e , from zero incidence position, and (3) lift due to the tab. The tail lift in the presence of the fuselage, including carryover effects onto the fuselage, is accounted for by the following equation referenced to the horizontal-tail area, S_h :

$$\bar{C}_{Lh(hf)} = \left[(C_{L\alpha})_{h(hf)} (\alpha_b - \bar{\epsilon}_h) + (C_{L\delta_e})_{\delta_{tab}=0} \delta_e + C_{L\delta_{tab}} \left(\frac{\delta_{tab}}{\delta_e} \right) \delta_e \right] \frac{\bar{q}_h}{\bar{q}_\infty} \quad (4.13.1-1)$$

The three contributing sources for lift of the tail are considered separately.

Lift due to angle of attack of the tail, with the tail at zero incidence: On the basis of tail area, the lift due to the angle of attack of the tail, α_h , relative to the zero incidence setting of the tail, is represented by

$$(C_{Lh(hf)})_{\delta_e=0, \delta_{tab}=0} = (C_{L\alpha})_{h(hf)} (\alpha_b - \bar{\epsilon}_h) \frac{\bar{q}_h}{\bar{q}_\infty} \quad (4.13.1-2)$$

This contribution, which includes the lift of the tail in the presence of the fuselage and the lift on the fuselage due to lift carryover of the tail onto the fuselage, is accounted for in section 4.10 by equation (4.10-2), referenced to the wing area. When applied to the subject airplane and referenced to the tail area, S_h , table 4.13.1-1(a) shows that

$$(C_{Lh(hf)})_{\delta_e=0, \delta_{tab}=0} = 0.0746 (\alpha_b - \bar{\epsilon}_h) \quad (4.13.1-3)$$

for a dynamic-pressure ratio, $\frac{\bar{q}_h}{\bar{q}_\infty}$, equal to 1.0.

Lift due to stabilizer deflection from zero incidence position: The lift due to stabilizer deflection, δ_e , with $\delta_{tab} = 0$ was obtained in a manner synonymous to that used to obtain the lift due to angle of attack of the tail from equation (4.10.2). In this equation the tail (abutting the fuselage) was considered to be fixed ($\delta_e = 0^\circ$) relative to

the fuselage, and the lift of the tail due to angle of attack was considered on the basis of the combined tail-fuselage movement relative to the local flow vector and consequent interaction of lift effects. In accord with the principles developed in reference 11, this interaction of lift effects was accounted for by the use of the factors $K_{h(f)} + K_{f(h)}$. In the present instance where the lift due to the deflection, δ_e , of the tail surface is desired, the tail is moving relative to the abutting fuselage which is considered to be fixed and the interaction effects are accounted for by the factors $k_{h(f)} + k_{f(h)}$ on the basis of reference 11. Thus, when the stabilizer is abutting the fuselage, the lift due to stabilizer deflection, δ_e , relative to the fuselage is accounted for by the following equation, which is subject to the same cautionary remarks as were made for equation (4.10-2), which accounted for the tail lift due to the angle of attack at the tail, referenced to the tail area:

$$(\Delta C_L)_{\delta_e} = (C_{L\alpha})_{h_e} (k_{h(f)} + k_{f(h)}) \delta_e \frac{S_{h_e}}{S_h} \left(\frac{\bar{q}_h}{\bar{q}_\infty} \right) \quad (4.13.1-4)$$

where

$(C_{L\alpha})_{h_e}$ is the lift-curve slope of the exposed tail panels (section (4.2))

S_{h_e} is the area of the exposed tail panels

$k_{h(f)}$ is the ratio, due to stabilizer deflection, δ_e , of the lift on the stabilizer in the presence of the fuselage to stabilizer alone, obtained from figure 4.13.1-1

$k_{f(h)}$ is the ratio, due to stabilizer deflection, of the stabilizer lift carryover onto the fuselage to stabilizer alone, obtained from figure 4.13.1-1

$\frac{\bar{q}_h}{\bar{q}_\infty}$ is the dynamic-pressure ratio of the tail (section 4.9.2)

Applied to the subject airplane and referenced to the tail area, S_h , table 4.13.1-1(b) shows that

$$(\Delta C_L)_{\delta_e} = (C_{L\delta_e})_{\delta_{tab}=0} \delta_e \left(\frac{\bar{q}_h}{\bar{q}_\infty} \right) = 0.0662 \delta_e \quad (4.13.1-5)$$

for a dynamic-pressure ratio, $\frac{\bar{q}_h}{\bar{q}_\infty}$, equal to 1.0.

Lift due to the tab: The lift on the horizontal tail due to tab deflection in the linear lift range of the tail can be obtained by using the following equation which was developed in reference 8 to obtain the lift increment of high lift flaps:

$$\Delta C_L = \Delta c_l \left(\frac{C_{L\alpha}}{c_{l\alpha}} \right) \left[\frac{(\alpha \delta) C_L}{(\alpha \delta) c_l} \right] K_b \quad (4.13.1-6)$$

When applied to the horizontal tail equipped with a tab, as for the subject airplane, the lift contribution of the tab in terms of lift effectiveness (for $\frac{\bar{q}_h}{\bar{q}_\infty} = 1.0$) is obtained from

$$C_{L\delta_{\text{tab}}} = c_{l\delta_{\text{tab}}} \frac{(C_{L\alpha})_{h(f)}}{(c_{l\alpha})_h} \left[\frac{(\alpha_{\delta_{\text{tab}}})_{C_L}}{(\alpha_{\delta_{\text{tab}}})_{c_l}} \right] K_b \quad (4.13.1-7)$$

where

$(C_{L\alpha})_{h(f)}$ is the lift-curve slope of the horizontal-tail surface alone in the presence of the fuselage and is obtained from the following equation in which the terms have the same definition as for equation (4.13.1-4):

$$(C_{L\alpha})_{h(f)} = (C_{L\alpha})_{h_e} k_{h(f)} \frac{S_{h_e}}{S_h} \quad (4.13.1-8)$$

and

$(c_{l\alpha})_h$ is the section lift-curve slope of the untabbed tail ($\delta_{\text{tab}} = 0$), obtained from section 4.1

$\frac{(\alpha_{\delta_{\text{tab}}})_{C_L}}{(\alpha_{\delta_{\text{tab}}})_{c_l}}$ is the tab-chord factor, obtained from figure 4.13.1-2 as a function of aspect ratio, A_h , and $(\alpha_{\delta_{\text{tab}}})_{c_l}$

The required $(\alpha_{\delta_{\text{tab}}})_{c_l}$ may be obtained from $-\frac{c_{l\delta_{\text{tab}}}}{(c_{l\alpha})_h}$ based on experimental data, or from the insert in figure 4.13.1-2, based on theory.

When $(\alpha_{\delta_{\text{tab}}})_{c_l}$ varies along the span, as for a constant-chord tab on a tapered surface, an average value of $(\alpha_{\delta_{\text{tab}}})_{c_l}$, based on an average $\frac{c_{\text{tab}}}{c_h}$, may be used with good accuracy in most instances. Otherwise, as in accordance with reference 8, the effective $(\alpha_{\delta_{\text{tab}}})_{c_l}$ may be found by determining the value of $(\alpha_{\delta_{\text{tab}}})_{c_l}$ at each

of several locations across the tab span and plotting these values against corresponding values of K_b . The area under the curve divided by the change in K_b is the effective value of $(\alpha_{\delta_{\text{tab}}})_{c_l}$. The quantity K_b is the tab-span factor, obtained from fig-

ure 4.13.1-3 as a function of taper ratio, λ_h , and span ratio, η , as defined in the figure.

The section lift effectiveness of the tab, $c_{l\delta_{\text{tab}}}$, is obtained from the following equation from reference 1:

$$c_{l\delta_{\text{tab}}} = \frac{1}{\beta'} \left[\frac{c_{l\delta_{\text{tab}}}}{(c_{l\delta_{\text{tab}}})_{\text{theory}}} \right] (c_{l\delta_{\text{tab}}})_{\text{theory}}^{K'} \quad (4.13.1-9)$$

where

β' is the Prandtl-Glauert correction factor for subcritical Mach numbers, equal to $\sqrt{1 - M^2}$

$(c_{l\delta_{\text{tab}}})_{\text{theory}}$ is the theoretical lift effectiveness of the tab, obtained from figure 4.13.1-4 as a function of $\frac{c_{\text{tab}}}{c_h}$ and thickness ratio

$\frac{c_{l\delta_{\text{tab}}}}{(c_{l\delta_{\text{tab}}})_{\text{theory}}}$ is an empirical correction factor based on experimental data, obtained from figure 4.13.1-5 as a function of $\frac{c_{\text{tab}}}{c_h}$ and $\frac{(c_{l\alpha})_h}{(c_{l\alpha})_{\text{theory}}}$

$(c_{l\alpha})_{\text{theory}}$ is the section lift curve of the untabbed tail, obtained from section 4.1

$$(c_{l\alpha})_{\text{theory}} = \frac{1}{57.3} \left[6.28 + 4.7 \left(\frac{t}{c} \right) (1 + 0.00375 \phi_{\text{te}}) \right] \quad (4.1-1)$$

K' is an empirical correction for lift effectiveness of the tab at large deflections, obtained from figure 4.13.1-6 which was derived from extensive unpowered-model wind-tunnel data

Upon applying the preceding relations to the subject airplane, the lift effectiveness of the tab, referenced to the horizontal-tail area, S_h , and a dynamic-pressure ratio of 1.0, is shown in table 4.13.1-1(c) to be as follows:

$$\left. \begin{aligned} C_{L\delta_{\text{tab}}} &= 0.0279 \text{ per deg for } \delta_{\text{tab}} = 6^\circ, 0^\circ, -7.5^\circ \\ C_{L\delta_{\text{tab}}} &= 0.0273 \text{ per deg for } \delta_{\text{tab}} = -15^\circ \\ C_{L\delta_{\text{tab}}} &= 0.0231 \text{ per deg for } \delta_{\text{tab}} = -21^\circ \end{aligned} \right\} \quad (4.13.1-10)$$

The tab settings shown correspond to elevator settings of 4° , 0° , -5° , -10° , and -14° used in this report with the tab-to-elevator gear ratio of 1.5.

Summary: The net lift of the horizontal tail in the linear range as a function of α_h , δ_e , and δ_{tab} with the tab geared to the elevator was accounted for by equation (4.13.1-1). This equation, regrouped slightly and referenced to a dynamic-pressure ratio of 1.0, becomes

$$\bar{C}_{Lh(hf)} = (C_{L\alpha})_{h(hf)} (\alpha_b - \bar{\epsilon}_h) + \left[(C_{L\delta_e})_{\delta_{tab}=0} + C_{L\delta_{tab}} \left(\frac{\delta_{tab}}{\delta_e} \right) \right] \delta_e \quad (4.13.1-11)$$

This equation may be abbreviated to the following format, which is applied to the subject airplane in the summary calculations of table 4.13.1-1(d):

$$\bar{C}_{Lh(hf)} = (C_{L\alpha})_{h(hf)} (\alpha - \bar{\epsilon}_h) + C_{L\bar{\delta}_e} \delta_e \quad (4.13.1-12)$$

4.13.2 Maximum Lift of the Horizontal Tail

The maximum lift and corresponding angle of attack of the horizontal tail untabbed, $\delta_{tab} = 0^\circ$, was considered in section 4.2. The inclusion of the tab makes the determination of maximum lift somewhat more approximate than without the tab. The stall may begin at the tail, tips, or at the tabbed (or flapped) sections, depending on the amount of sweep, taper ratio, and difference in stall angle between the tabbed and untabbed sections.

The increment of maximum lift coefficient due to trailing-edge flaps can be determined to a first order of approximation by using semiempirical equation (4.13.2-1) developed in reference 1 on the basis of tabulated values of maximum lift coefficients and stall angles for many planforms with and without flaps (ref. 30). The equation applies to wings and tail surfaces with plain flaps or tabs. For convenience, the nomenclature of the following equation has been changed from a wing designation to a horizontal-tail designation. On the basis of tail area,

$$(\Delta C_{Lmax})_{\delta_{tab}} = (\Delta c_{lmax})_{tab} \frac{(S_h)_{tab}}{S_h} K_\Lambda \quad (4.13.2-1)$$

where

$(\Delta C_{Lmax})_{\delta_{tab}}$ is the increment of C_{Lmax} due to tab position

$(S_h)_{tab}$ is the tail area in front of and including the tab

K_Λ is an empirically derived correction factor to account for the effects of wing planform, obtained from figure 4.13.2-1 as a function of $(\Lambda_{c/4})_h$

The increment in airfoil maximum-lift coefficient due to the tab, $(\Delta c_{lmax})_{tab}$, is

obtained from the following empirically derived equation (from ref. 1):

$$(\Delta c_{l \max})_{\text{tab}} = k_1 k_2 k_3 (\Delta c_{l \max})_{\text{base}} \quad (4.13.2-2)$$

where

$(\Delta c_{l \max})_{\text{base}}$ is the section maximum lift increment for 25-percent-chord flaps at a reference flap-deflection angle, 60° for plain flaps or tabs, obtained from figure 4.13.2-2

k_1 is a factor accounting for $\frac{c_{\text{tab}}}{c}$ other than 0.25, obtained from figure 4.13.2-3

k_2 is a factor accounting for tab angle other than the reference value, obtained from figure 4.13.2-4

k_3 is a factor accounting for tab motion as a function of $\frac{\delta_{\text{tab}}}{(\delta_{\text{tab}})_{\text{reference}}}$, equal to 1 for plain flaps or tabs

The maximum lift coefficient for any one tab setting may now be determined, on the basis of tail area, S_h , from the relation

$$(\bar{C}_{L \max})_{h(hf)} = \left[(C_{L \max})_{h(hf)} \right]_{\delta_{\text{tab}=0}} + (\Delta C_{L \max})_{\delta_{\text{tab}}} \quad (4.13.2-3)$$

where

$\left[(\bar{C}_{L \max})_{h(hf)} \right]_{\delta_{\text{tab}=0}}$ is the maximum lift coefficient of the untabbed tail in the presence of the fuselage, obtained from section 4.10

The summary calculations for the maximum lift coefficient of the tail of the subject airplane for each of several elevator deflections in which the tab is geared to the elevator in the ratio, $\frac{\delta_{\text{tab}}}{\delta_e} = 1.5$, are presented in table 4.13.2-1(b).

4.13.3 Lift Curves of the Horizontal Tail Through Stall

Because the net lift and pitching moments of an airplane for different elevator positions are dependent upon the tail lift characteristics and could involve the stall region of the tail, operational tail lift curves for the subject airplane are plotted in figure 4.13.3-1 for several elevator positions through the stall region of the tail.

The following procedure was used in constructing the lift-curve plots in figure 4.13.3-1 for the subject airplane on the basis of the horizontal-tail area (32.5 sq ft for the subject airplane) and a dynamic-pressure ratio of 1. The resulting curves

are the graphical representation of equation (4.13.1-12) for the linear range and extend through the stall.

(1) Using the information in table 4.13.1-1(a), draw the slope of the basic lift curve ($\delta_e = \delta_{tab} = 0^\circ$) up to the limit of linearity.

(2) Spot the stall point for $\delta_e = 0^\circ$ using $\left[(C_{Lmax})_{h(hf)} \right]_{\delta_{tab}=0}$ and

$\left[(\alpha C_{Lmax})_{h(hf)} \right]_{\delta_{tab}=0}$ as listed in table 4.13.2-1(a). Fair a curve, similar to the

fairing for the isolated tail in figure 4.2-1(b), from the limit of linearity through the stall point. The shape of the curve in the stall region should now correspond to the shape in figure 4.10-1 as well as in figure 4.2-1(b).

(3) On the ordinate at $\alpha_h = 0^\circ$, spot the values of $C_{L\bar{\delta}_e}$ for $\delta_e = 4^\circ, 0^\circ, -5^\circ, -10^\circ$, and -14° using $C_{L\bar{\delta}_e}$ obtained from table 4.13.1-1(d). Draw lift curves through these points parallel to the basic lift curve.

(4) Using the $(\bar{C}_{Lmax})_{h(hf)}$ values determined in table 4.13.2-1(b), for the selected values of δ_e , draw horizontal lines to denote C_{Lmax} .

(5) Make a plot, to be used as an underlay in tracing, of the nonlinear portion (through and beyond the stall) of the basic lift curve ($\delta_e = 0^\circ$). Translate this underlay plot relative to the basic lift curve to the selected elevator settings and their corresponding C_{Lmax} and complete the curves for the stall regions.

4.13.4 Lift and Pitching-Moment Curves of the Airplane Including the Effect of Elevator Positions

The lift and pitching-moment characteristics of the complete airplane may now be determined as a function of $\alpha_b - \bar{\epsilon}_h$ and δ_e from the following relations:

$$C_L = C_{L_{wfn}} + \bar{C}_{Lh(hf)} \left(\frac{S_h}{S_w} \right) \frac{\bar{q}_h}{\bar{q}_\infty} \quad (4.13.4-1)$$

$$C_m = C_{m_{wfn}} + \frac{x_{cg} - x_h}{\bar{c}_w} \left(\bar{C}_{Lh(hf)} \right) \frac{S_h}{S_w} \frac{\bar{q}_h}{\bar{q}_\infty} \quad (4.13.4-2)$$

where

$C_{L_{wfn}}$ and $C_{m_{wfn}}$ are the tail-off coefficients, obtained from section 4.8.3

$\frac{x_{cg} - x_h}{\bar{c}_w}$ is the distance from the center of gravity to the quarter-chord mean

aerodynamic chord of the horizontal tail in chord lengths of the wing mean aerodynamic chord

The lift and pitching-moment characteristics of the subject airplane are calculated in table 4.13.4-1 as a function of α_b and δ_e with the tab geared to the elevator in the ratio of 1.5. At stall conditions, the horizontal tail is at and in the lower edge of the wake, and its effectiveness at stall was considered as suggested in section 4.10 for propeller-off and zero-thrust propeller-on conditions. The results, referenced to a wing area of 178 square feet, are compared with full-scale wind-tunnel data in figure 4.13.4-1. In the absence of appropriate propeller-off wind-tunnel data, propeller-on data for $T'_C = 0$ were used with calculated normal-force propeller effects subtracted. Such use of $T'_C = 0$ data is not normally recommended for comparison with propeller-off predictions. It was used in the present instance only after a preliminary comparison of pitching-moment slopes at $\delta_e = 0^\circ$ showed correlation and implied zero thrust power effects at the tail.

The calculated lift characteristics (fig. 4.13.4-1(a)) show generally good correlation with wind-tunnel data. The divergence between the calculated and wind-tunnel lift at α_b above 6° for $\delta_e = 4^\circ$, which is also reflected in the pitching-moment characteristics (fig. 4.13.4-1(b)), is attributed to flow separation on the horizontal tail. The design data used took into account flow separation as a function of tab deflection only (fig. 4.13.1-4). There is a need for design data which account for flow separation as a function of both angle of attack and tab deflection.

At low angles of attack, the horizontal tail is in the stall region when $\delta_e = -10^\circ$ and -14° . Both the calculated and wind-tunnel-determined lift characteristics reflect the tail stall. It should be noted that the subject airplane does not operate in regions involving large negative elevator deflections at low angles of attack and thus is not normally subject to tail stall.

The calculated pitching-moment characteristics (fig. 4.13.4-1(b)) show good slope correlation with wind-tunnel data up to an angle of attack of approximately 8° . Above this angle the calculated and wind-tunnel data diverge for all indicated elevator deflections except $\delta_e = 0^\circ$. The increasing divergence with increasing elevator deflection indicates progressive flow separation. As mentioned, design data are needed which account for flow separation as a function of both angle of attack and tab deflection. It is evident that the use of design data which take into account flow separation as a function of tab deflection only (fig. 4.13.1-4) is not sufficient.

Calculated pitch-control effectiveness, $C_{m\bar{\delta}_e}$, as obtained from figure 4.13.4-1(b) is approximately 20 percent higher than indicated by the wind-tunnel data. In an effort to locate the sources of the discrepancy, wind-tunnel control-effectiveness data (ref. 2) for $\delta_{tab} = 0^\circ$ and geared conditions were used. These data were available only for a total T'_C power condition of 0.2; however, because only incremental δ_e effects were desired at constant angle of attack, the data were satisfactory for the purpose. The following schedule shows the representative data, from reference 2, used in the study.

Figure (in ref. 2)	α_b , deg	δ_e , deg	δ_{tab} , deg	ΔC_m	$C_{m\bar{\delta}_e}$	$C_{m\delta_e}$
6(b)	5	-5	Geared	0.29	-0.058	-----
9	5	-5	0	.17	-----	-0.034

From this schedule

$$C_{m\delta_{tab}} = \frac{C_{m\bar{\delta}_e} - C_{m\delta_e}}{\left(\frac{\delta_{tab}}{\delta_e}\right)} = \frac{-0.024}{1.5} = -0.016$$

The calculated dynamic-pressure ratio for $T'_c = 0.2$ (section 5.1.2) was used to reduce $C_{m\delta_e}$, $C_{m\delta_{tab}}$, and $C_{m\bar{\delta}_e}$ to a dynamic-pressure ratio of 1.00, which was the ratio used for calculated propeller-off conditions. The wind-tunnel data, thus reduced, are compared in the following table with calculated values excluding and including lift carryover onto the body. The values are referenced to a wing area of 178 square feet and a dynamic-pressure ratio of 1.00.

	$C_{m\delta_e}$	$C_{m\delta_{tab}}$	$C_{m\bar{\delta}_e}$
From wind-tunnel data	-0.0298	-0.0141	-0.0510
Calculated, based on $k_{h(f)}$ only (carryover factor neglected)	-.0318	-.0145	-.0543
As calculated for this report	-.0355 (carry- over included)	-.0145 (carry- over not included)	-.0580

A comparison of the wind-tunnel data with the calculated values of $C_{m\delta_e}$, $C_{m\delta_{tab}}$, and $C_{m\bar{\delta}_e}$, which excluded the carryover effects, showed the calculated values to be approximately 6 percent higher than wind-tunnel data in each instance. This indicates that the factor $k_{h(f)}$ is about 6 percent too high for the tail-body configuration of the subject airplane. A comparison of the wind-tunnel value of $C_{m\delta_e}$ with the calculated value, including the carryover effect, showed the calculated value to be approximately 18 percent higher. The calculated value of $C_{m\bar{\delta}_e} = -0.0580$ used in this report, which included carryover effect, for corresponding δ_e conditions is approximately 14 percent higher than the wind-tunnel value of -0.0510.

On the basis of the preceding comparisons, for the tail-body configuration of the subject airplane it appears that the lift carryover from the tail to the body, due to

stabilizer deflection, is insignificant because of the location of the tail on the body and the gap between the tail and the body. This implies that the $k_{f(h)}$ factor in equation (4.13.1-4) should have been assumed to be equal to zero.

Although the lift carryovers from the tail to the body are included in the calculations and plots for the subject airplane, it is suggested that $k_{f(h)}$ be considered negligible for tail-body configurations similar to that of the subject airplane. This should result in calculated values of control effectiveness which would be within approximately 6 percent of the actual values.

4.13.5 Symbols

A_h	horizontal-tail aspect ratio
b_h	horizontal-tail span, ft
C_L	lift coefficient
$\bar{C}_{Lh(hf)}$	lift coefficient of the horizontal tail, referenced to the tail area, with tail-fuselage interaction effects, angle of attack, elevator deflection, and tab deflection accounted for
$(C_{Lh(hf)})_{\delta_e=0, \delta_{tab}=0}$	same as $\bar{C}_{Lh(hf)}$ with the elevator and tab settings at zero-deflection positions
$C_{L_{max}}$	maximum lift coefficient
$(\bar{C}_{L_{max}})_{h(hf)}$	maximum value of $\bar{C}_{Lh(hf)}$
$[(C_{L_{max}})_{h(hf)}]_{\delta_{tab}=0}$	maximum value of $\bar{C}_{Lh(hf)}$ with the tab at zero setting
$C_{L_{wfn}}$	airplane tail-off lift coefficient, referenced to wing area
ΔC_L	increment of lift
$(\Delta C_L)_{\delta_e}$	increment of lift coefficient due to the elevator deflection, referenced to tail area
$(\Delta C_{L_{max}})_{\delta_{tab}}$	increment of maximum lift coefficient due to the tab, referenced to tail area
C_{L_α}	lift-curve slope, per deg
$(C_{L_\alpha})_{h_e}$	lift-curve slope of the exposed portion of the horizontal-tail panels, referenced to the effective area of the exposed panels, per deg

$(C_{L\alpha})_{h(f)}$	lift-curve slope of the horizontal tail alone with fuselage effects on the tail accounted for, referenced to the tail area, per deg
$(C_{L\alpha})_{h(hf)}$	lift-curve slope of the horizontal tail with interacting tail-fuselage effects accounted for, referenced to the tail area, per deg
$(C_{L\delta_e})_{\delta_{tab}=0}$	elevator effectiveness, $\frac{\partial C_L}{\partial \delta_e}$, with the tab fixed at zero setting, referenced to the tail area, per deg
$C_{L\bar{\delta}_e}$	elevator effectiveness, $(C_{L\delta_e})_{\delta_{tab}=0} + C_{L\delta_{tab}}\left(\frac{\delta_{tab}}{\delta_e}\right)$, with the tab geared to the elevator to deflect in the ratio of $\frac{\delta_{tab}}{\delta_e}$, referenced to the tail area, per deg
$C_{L\delta_{tab}}$	tab effectiveness, $\frac{\partial C_L}{\partial \delta_{tab}}$, referenced to the tail area, per deg
C_m	pitching-moment coefficient
ΔC_m	increment of pitching-moment coefficient
$C_{m_{wfn}}$	tail-off pitching-moment coefficient, referenced to the wing area
$C_{m\delta_e}$	elevator effectiveness in pitch, $\frac{\partial C_m}{\partial \delta_e}$, with the tab fixed, referenced to the wing area, per deg
$C_{m\bar{\delta}_e}$	elevator effectiveness in pitch with the tab geared to the elevator to deflect in the ratio of $\frac{\delta_{tab}}{\delta_e}$, referenced to the wing area, per deg
$C_{m\delta_{tab}}$	tab effectiveness in pitch, $\frac{\partial C_m}{\partial \delta_{tab}}$, referenced to the wing area, per deg
c	chord
c_f	flap chord, synonymous to the tab chord, c_{tab} , in this section, ft or in.
c_h	horizontal-tail chord, ft or in.

c_l	airfoil-section lift coefficient
Δc_l	change in the airfoil-section lift coefficient
$(\Delta c_{l_{\max}})_{\text{base}}$	section maximum lift increment for the 25-percent-chord flaps at a reference flap-deflection angle (60° for plain flaps or tabs when obtained from fig. 4.13.2-2)
$(\Delta c_{l_{\max}})_{\text{tab}}$	section maximum lift increment due to the tab
c_{l_α}	airfoil-section lift-curve slope, per deg
$(c_{l_\alpha})_h$	horizontal-tail c_{l_α}
$c_{l_{\delta_{\text{tab}}}}$	section effectiveness of the tab, $\frac{\partial c_l}{\partial \delta_{\text{tab}}}$, per rad or deg
c_{tab}	tab chord, ft or in.
\bar{c}_w	wing mean aerodynamic chord, ft or in.
$(d_f)_h$	width of the fuselage at the horizontal tail (fig. 3.2-2), ft
K'	correction factor for the lift effectiveness of the tab at large tab deflections
K_b	span factor for the inboard flaps (or tabs)
$K_{f(h)}$	ratio of the tail-lift carryover onto the fuselage, with the tail fixed, to the tail alone
$K_{h(f)}$	ratio of the lift on the tail in the presence of the fuselage, with the tail fixed, to the tail alone
K_Λ	correction factor to account for the effects of the wing planform on the increment of maximum lift coefficient due to the tab position
$k_{f(h)}$	ratio of the lift carryover, due to stabilizer deflection, onto the fuselage to the lift of the stabilizer alone, obtained from figure 4.13.1-1
$k_{h(f)}$	ratio of the lift on the stabilizer, due to stabilizer deflection, in the presence of the fuselage to stabilizer alone, obtained from figure 4.13.1-1

k_1, k_2, k_3	factors used in obtaining $\left(\Delta c_{l_{\max}}\right)_{\text{tab}}$ to account for $\frac{c_{\text{tab}}}{c}$ other than 0.25, tab angle other than the reference value, and tab motion, respectively
M	Mach number
$\bar{q}_h, \bar{q}_\infty$	dynamic pressure at the horizontal tail and in the free stream, respectively, lb/sq ft
S_h, S_{he}	area of the horizontal tail and exposed panels of the horizontal tail, respectively, sq ft
$(S_h)_{\text{tab}}$	horizontal-tail area in front of and including the tab, sq ft
S_w	wing area, sq ft
T'_c	thrust coefficient of the propellers, $\frac{\text{Thrust}}{\bar{q}_\infty S_w}$
$\left(\frac{t}{c}\right)_h$	horizontal-tail thickness ratio
$\frac{x_{cg} - x_h}{\bar{c}_w}$	distance, parallel to the X-body axis, from the center of gravity to the quarter-chord point of the horizontal-tail mean aerodynamic chord as a ratio of the wing mean aerodynamic chord
α	angle of attack, deg
α_b	airplane angle of attack relative to the X-body axis, deg
$\left[\left(\alpha C_{L_{\max}}\right)_{h(hf)}\right]_{\delta_{\text{tab}}=0}$	angle of attack of the horizontal tail, relative to its chord line, for the maximum lift coefficient of the tail when the tab deflection is zero, deg
$\alpha_h = \alpha_b - \bar{\epsilon}_h$, deg	
α_h^*	limit of linearity of the horizontal-tail lift-curve slope, deg
$(\alpha_\delta)_{c_l}, (\alpha_\delta)_{C_L} = \frac{\frac{\partial c_l}{\partial \delta}}{\frac{\partial c_l}{\partial \alpha}}$ and $\frac{\frac{\partial C_L}{\partial \delta}}{\frac{\partial C_L}{\partial \alpha}}$, respectively	

$$(\alpha\delta_{\text{tab}})_{C_L}, (\alpha\delta_{\text{tab}})_{c_l} = \frac{\frac{\partial c_l}{\partial \delta_{\text{tab}}}}{\frac{\partial c_l}{\partial \alpha}} \text{ and } \frac{\frac{\partial C_L}{\partial \delta_{\text{tab}}}}{\frac{\partial C_L}{\partial \alpha}}, \text{ respectively}$$

$$\beta = (1 - M^2)^{1/2}$$

δ deflection, deg

δ_e elevator deflection, deg

$\delta_f, \delta_{\text{tab}}$ flap and tab deflection, respectively, used synonymously, deg

$\bar{\epsilon}_h$ average downwash across the horizontal tail, deg

η tab span, as a ratio of the tail semispan, for the tab extending from the centerline of the horizontal tail

η_i, η_o distance from the centerline of the tail to the inboard and outboard edge, respectively, as a ratio of the tail semispan

$$\Delta\eta = \eta_o - \eta_i$$

$(\Lambda_{c/4})_h$ sweep of the horizontal-tail quarter-chord line, deg

λ_h horizontal-tail taper ratio

φ_{te} trailing-edge angle, deg

TABLE 4.13.1-1

LIFT CONTRIBUTION OF THE HORIZONTAL TAIL WITH TAB-TO-ELEVATOR GEAR RATIO OF 1.5

$$\bar{C}_{Lh(hf)} = \left[(C_{L\alpha})_{h(hf)} (\alpha_b - \bar{\epsilon}_h) + (C_{L\delta_e})_{\delta_{tab}=0} \delta_e + (C_{L\delta_{tab}}) \left(\frac{\delta_{tab}}{\delta_e} \right) \delta_e \right] \frac{\bar{q}_h}{\bar{q}_\infty}$$

(a) Lift due to angle of attack, $(C_{Lh(hf)})_{\delta_e=0, \delta_{tab}=0}$

$$(C_{Lh(hf)})_{\delta_e=0, \delta_{tab}=0} = (C_{L\alpha})_{h(hf)} (\alpha_b - \bar{\epsilon}_h) \frac{\bar{q}_h}{\bar{q}_\infty}$$

Symbol	Description	Reference	Magnitude
$(C_{L\alpha})_{h(hf)}$	Lift-curve slope of tail with tail-fuselage intersection effects included, referenced to $S_h = 32.5$ sq ft	Table 4.10-1(a)	0.0746/deg
α_h^*	Limit of linearity, deg	Table 4.10-1(a)	10.6
$\bar{\epsilon}_h$	Downwash of the horizontal tail, deg	Figure 4.9.1-1	$f(\alpha_b)$
$\frac{\bar{q}_h}{\bar{q}_\infty}$	Dynamic-pressure ratio at the horizontal tail	Figure 4.9.1-1	1.00
Summary: $(C_{Lh(hf)})_{\delta_e=0, \delta_{tab}=0} = 0.0746 (\alpha_b - \bar{\epsilon}_h)$			

(b) Effect of tail deflection on lift ($\delta_{tab} = 0^\circ$), $(\Delta C_L)_{\delta_e}$

$$(\Delta C_L)_{\delta_e} = (C_{L\delta_e})_{\delta_{tab}=0} \delta_e \left(\frac{\bar{q}_h}{\bar{q}_\infty} \right) = (C_{L\alpha})_{h_e} (k_h(f) + k_f(h)) (\delta_e) \left(\frac{\bar{q}_h}{\bar{q}_\infty} \right) \frac{S_{he}}{S_h}$$

Symbol	Description	Reference	Magnitude
$(df)_h$	Fuselage width at horizontal tail, ft	Figure 3.2-2	1.25
b_h	Span of horizontal tail, ft	Table 3.2-1	12.5
$\frac{(df)_h}{b_h}$.10
$k_h(f)$	Ratio of lift on movable tail in presence of body to tail alone	Figure 4.13.1-1	.96
$k_f(h)$	Ratio of movable-tail lift carryover on body to tail alone	Figure 4.13.1-1	.11
$(C_{L\alpha})_{h_e}$	$C_{L\alpha}$ of exposed horizontal-tail panels referenced to S_{he} , per deg	Table 4.2-1	0.0700
S_{he}	Area of exposed horizontal-tail panels, sq ft	Table 3.2-1	28.73
S_h	Horizontal-tail area, sq ft	Table 3.2-1	32.5
$\frac{\bar{q}_h}{\bar{q}_\infty}$	Dynamic-pressure ratio at the horizontal tail	Figure 4.9.1-1	1.00
Summary: $(\Delta C_L)_{\delta_e} = 0.0662 \delta_e$ referenced to S_h and $\frac{\bar{q}_h}{\bar{q}_\infty} = 1.0$			

TABLE 4.13.1-1 (Continued)

(c) Effect of tab deflection on lift, $(C_{L\delta_{tab}} \delta_{tab}) \frac{\bar{q}_h}{\bar{q}_\infty}$

$$c_{l\delta_{tab}} = \frac{1}{\beta'} \left[\frac{c_{l\delta_{tab}}}{(c_{l\delta_{tab}})_{theory}} \right] (c_{l\delta_{tab}})_{theory} K'$$

$$(C_{L\alpha})_{h(f)} = (C_{L\alpha})_{he} k_{h(f)} \frac{S_{he}}{S_h}$$

$$C_{L\delta_{tab}} = c_{l\delta_{tab}} \frac{(C_{L\alpha})_{h(f)}}{(C_{L\alpha})_h} \left[\frac{(\alpha\delta_{tab}) C_L}{(\alpha\delta_{tab}) c_l} \right] K_b$$

Symbol	Description	Reference	Magnitude
M	Mach number	Wind-tunnel test conditions	0.083
β^1	$\sqrt{1 - M^2}$	-----	.997
$\frac{t}{c}$	Airfoil section thickness ratio of horizontal tail	NACA 0008	0.08
ϕ_{te}	Trailing-edge angle of horizontal tail, deg	Table 4.1-1	11.0
A_h	Aspect ratio of horizontal tail	Table 3.2-1	4.8
λ_h	Taper ratio of horizontal tail	Table 3.2-1	.515
S_h	Horizontal-tail area, sq ft	Table 3.2-1	32.5
S_{he}	Area of exposed horizontal-tail panels, sq ft	Table 3.2-1	28.73
$\frac{c_{tab}}{c_h}$	Ratio of tab chord to tail chord	Figure 3.2-2	.18
η_i	Distance from root chord of horizontal tail to inboard edge of tab as a fraction of horizontal-tail semispan	Figure 3.2-2	0
η_o	Distance from root chord of horizontal tail outboard edge of tab as a fraction of horizontal-tail semispan	Figure 3.2-2	.792
$(c_{l\alpha})_h$	Section lift-curve slope of horizontal tail (untabed), per deg	Table 4.1-1	0.109
$(c_{l\alpha})_{theory}$	Theoretical section lift-curve slope of horizontal tail, $(c_{l\alpha})_{theory} = \frac{1}{57.3} \left[6.28 + 4.7 \left(\frac{t}{c} \right) (1 + 0.00375 a_c) \right]$, per deg	Equation (4.1-1)	.1164
$\frac{(c_{l\alpha})_h}{(c_{l\alpha})_{theory}}$	-----	-----	.936
$(c_{l\delta_{tab}})_{theory}$	Theoretical section effectiveness of tab, $f\left(\frac{c_{tab}}{c_h}, \frac{1}{c}\right)$, per deg	Figure 4.13.1-4	{3.4 per rad .0593 per deg
$\frac{c_{l\delta_{tab}}}{(c_{l\delta_{tab}})_{theory}}$	Function of $\frac{c_{tab}}{c_h}$ and $\frac{(c_{l\alpha})_h}{(c_{l\alpha})_{theory}}$	Figure 4.13.1-5	.89
K'	Empirical correction for flap effectiveness, $f\left(\frac{c_{tab}}{c_h}, \delta_{tab}\right)$	From figure 4.13.1-6: For $\delta_{tab} = 6, 0, -7.5$: $K' = 1.00$ For $\delta_{tab} = -15$: $K' = 0.98$ For $\delta_{tab} = -21$: $K' = 0.83$	
$c_{l\delta_{tab}} = \frac{1}{\beta'} \left[\frac{c_{l\delta_{tab}}}{(c_{l\delta_{tab}})_{theory}} \right] (c_{l\delta_{tab}})_{theory} K'$ $c_{l\delta_{tab}} = 0.0529 \text{ per deg for } \delta_{tab} = 6^\circ, 0^\circ, -7.5^\circ$ $= 0.0518 \text{ per deg for } \delta_{tab} = -14^\circ$ $= 0.0439 \text{ per deg for } \delta_{tab} = -21^\circ$			

TABLE 4.13.1-1 (Concluded)

(c) Concluded

Symbol	Description	Reference	Magnitude
$(C_{L\alpha})_{h_e}$	$C_{L\alpha}$ of exposed horizontal-tail panels referenced to S_{h_e}	Table 4.2-1	0.0700 per deg
$k_{h(f)}$	Ratio of lift on movable tail in presence of body to tail alone	Figure 4.13.1-1	.96
S_{h_e}	Area of exposed horizontal-tail panels, sq ft	Table 3.2-1	28.73
S_h	Area of horizontal tail, sq ft	Table 3.2-1	32.50
$(C_{L\alpha})_{h(f)} = C_{L\alpha}$ of horizontal tail only in the presence of the body $= (C_{L\alpha})_{h_e} k_{h(f)} \frac{S_{h_e}}{S_h}$ referenced to S_h and $\frac{\bar{q}_h}{\bar{q}_\infty} = 1.0$ $= 0.0700 (0.96)(1) \left(\frac{28.73}{32.50} \right)$ $= 0.0594$ per deg			
Symbol	Description	Reference	Magnitude
$(\alpha_{\delta_{tab}})_{c_l}$	Section lift parameter, $f \left(\frac{c_{tab}}{c_h} \right)$	Figure 4.13.1-2	-0.530
$\frac{(\alpha_{\delta_{tab}})_{C_L}}{(\alpha_{\delta_{tab}})_{c_l}}$	Ratio of finite and section lift parameter, $f \left[A_h, (\alpha_{\delta_{tab}})_{c_l} \right]$	Figure 4.13.1-2	1.075
$\frac{(C_{L\alpha})_{h(f)}}{(C_{L\alpha})_h}$	$\frac{0.0594}{0.109}$	-----	.545
K_b	Span factor, $f(\eta_1, \eta_0, \lambda_h)$	Figure 4.13.1-3	.90
$C_{L\delta_{tab}} = c_{l\delta_{tab}} \frac{(C_{L\alpha})_{h(f)}}{(C_{L\alpha})_h} \left[\frac{(\alpha_{\delta_{tab}})_{C_L}}{(\alpha_{\delta_{tab}})_{c_l}} \right] K_b$ $= 0.527 c_{l\delta_{tab}}$ referenced to S_h and $\frac{\bar{q}_h}{\bar{q}_\infty} = 1.0$ $= 0.0279$ per deg for $\delta_{tab} = 6^\circ, 0^\circ, -7.5^\circ$ $= 0.0273$ per deg for $\delta_{tab} = -15^\circ$ $= 0.0231$ per deg for $\delta_{tab} = -21^\circ$			

(d) Lift contribution of the horizontal tail with tab-to-elevator gear ratio of 1.5

$$\bar{C}_{Lh(hf)} = \left[(C_{L\alpha})_{h(hf)} (\alpha_b - \bar{\epsilon}_h) + (C_{L\delta_e})_{\delta_{tab}=0} \delta_e + C_{L\delta_{tab}} \left(\frac{\delta_{tab}}{\delta_e} \right) \delta_e \right] \frac{\bar{q}_h}{\bar{q}_\infty}$$

$$= \left[(C_{L\alpha})_{h(hf)} (\alpha_b - \bar{\epsilon}_h) + C_{L\delta_e} \delta_e \right] \frac{\bar{q}_h}{\bar{q}_\infty}$$

Substitution of the calculated values of $(C_{L\alpha})_{h(hf)}$, $(C_{L\delta_e})_{\delta_{tab}=0}$, and $C_{L\delta_{tab}}$ — obtained in parts (a),(b), (c) of this table — into the above equation results in the specific formats listed below for the δ_e settings to be considered in the follow-on analysis.

δ_e settings to be considered in follow-on analysis	Corresponding δ_{tab} settings with $\left(\frac{\delta_{tab}}{\delta_e} \right) = 1.5$	$\bar{C}_{Lh(hf)} = \left[(C_{L\alpha})_{h(hf)} (\alpha_b - \bar{\epsilon}_h) + C_{L\delta_e} \delta_e \right] \frac{\bar{q}_h}{\bar{q}_\infty}$ referenced to S_h and $\frac{\bar{q}_h}{\bar{q}_\infty} = 1.0$
4 0 -5	6 0 -7.5	$0.0746(\alpha_b - \bar{\epsilon}_h) + 0.1080\delta_e$
-10	-15	$0.0746(\alpha_b - \bar{\epsilon}_h) + 0.1072\delta_e$
-14	-21	$0.0746(\alpha_b - \bar{\epsilon}_h) + 0.1008\delta_e$

TABLE 4.13.2-1
MAXIMUM LIFT COEFFICIENTS OF THE HORIZONTAL TAIL

(a) Pertinent parameters

Symbol	Description	Reference	Magnitude
$(\Delta c/4)_h$	Sweep of horizontal tail along $c/4$ line, deg	Figure 3.2-2	8.0
$(\frac{t}{c})_h$	Section thickness ratio of horizontal tail	NACA 0008	.08
$\frac{c_{tab}}{c_h}$	Tab chord as ratio of tail chord	Figure 3.2-2	.18
$(S_h)_{tab}$	Area of horizontal tail in front of and including tab, sq ft	Figure 3.2-2	27.4
S_h	Area of horizontal tail, sq ft	Table 3.2-1	32.5
K_A	Correction factor for wing planform	Figure 4.13.2-1	.907
$(\Delta c_{l_{max}})_{base}$	Section maximum lift increment for 25-percent-chord tab	Figure 4.13.2-2	.82
k_1	Factor accounting for $\frac{c_{tab}}{c_{ht}}$ other than 0.25	Figure 4.13.2-3	.885
k_2	Factor accounting for tab deflection other than reference value	Figure 4.13.2-4	Variable
k_3	Factor accounting for tab motion as a function of $\frac{\delta_{tab}}{(\delta_{tab})_{reference}}$	-----	1.0
$[(C_{L_{max}})_{h(hf)}]_{\delta_{tab}=0^\circ}$	Horizontal-tail maximum lift coefficient with $\delta_{tab} = 0^\circ$ in presence of the fuselage, based on $S_h = 32.5$ sq ft	Table 4.10-1	± 0.926
$[(\alpha C_{L_{max}})_{h(hf)}]_{\delta_{tab}=0^\circ}$	Horizontal-tail angle of attack at $[(C_{L_{max}})_{h(hf)}]_{\delta_{tab}=0^\circ}$, deg	Table 4.10-1	± 14.45

$$(b) (\bar{C}_{L_{max}})_{h(hf)} = [(C_{L_{max}})_{h(hf)}]_{\delta_{tab}=0} + (\Delta c_{l_{max}})_{tab} \frac{(S_h)_{tab}}{S_h} K_A = 0.926 + 0.765 (\Delta c_{l_{max}})_{tab}$$

①	②	③	④	⑤	⑥	⑦	⑧	⑨	⑩ (a)
δ_e , deg	$\delta_{tab} = 1.5 \delta_e$, deg	k_1	k_2 , figure 4.13.2-2	k_3	$k_1 k_2 k_3 =$ ③ \times ④ \times ⑤	$(\Delta c_{l_{max}})_{base}$	$(\Delta c_{l_{max}})_{tab} =$ ⑥ \times ⑦	$\Delta C_{L_{max}} =$ 0.765 ⑧	$(\bar{C}_{L_{max}})_{h(hf)} =$ -0.926 + ⑨, based on $S_h = 32.5$ sq ft
4	6	0.885	0.200	1.0	0.177	0.82	0.145	0.110	-0.816
0	0	.885	0	1.0	0	.82	0	0	-.926
-5	-7.5	.885	-.250	1.0	-.221	.82	-.181	-.138	-1.064
-10	-15	.885	-.46	1.0	-.407	.82	-.334	-.256	-1.182
-14	-21	.885	-.59	1.0	-.522	.82	-.428	-.327	-1.253

^a $(C_{L_{max}})_{h(hf)}$ for minus α_h range.

TABLE 4.13.4-1
EFFECT OF ELEVATOR DEFLECTION ON LIFT AND PITCHING MOMENTS OF THE AIRPLANE

$$\frac{\delta_{\text{tab}}}{\delta_c} = 1.5$$

①	②	③	④	⑤	⑥	⑦	⑧
Figure 1.9.1-7	Figure 1.9.1-7	Figure 1.9.1-7	Figure 1.9.1-7	Figure 1.13.3-1 based on $\frac{\bar{q}_h}{\bar{q}_c}$	Equation (4.13.4-1)	Table 4.5-2, figure 4.5-4	Equation (4.13.4-1)
α_D , deg	$\bar{\epsilon}_h$	α_h	$\frac{\bar{q}_h}{\bar{q}_c}$	$\bar{C}_{Lh(h)} \text{ referenced to } S_h = 32.5 \text{ sq ft}$	$\frac{S_h}{S_w} \frac{\bar{q}_h}{\bar{q}_c} \left(\bar{C}_{Lh(h)} \right) \text{ referenced to } S_w = 178 \text{ sq ft}$	$C_{Lwfn} \text{ referenced to } S_w = 178 \text{ sq ft}$	$C_L \text{ referenced to } S_w = 178 \text{ sq ft}$
		① - ②		δ_c , deg	δ_c , deg		δ_c , deg
				4 0 -5 -10 -14	4 0 -5 -10 -14	4 0 -5 -10 -14	4 0 -5 -10 -14
-4	0	-4.00	1.00	0.135 -0.298 -0.843 -1.180 -1.010	0.0247 -0.0544 -0.1539 -0.2155 -0.1844	0.0023 -0.0738 -0.1733 -0.2749 -0.2038	0.0023 -0.0738 -0.1733 -0.2749 -0.2038
-2	.96	-2.96	1.00	.213 -.220 -.764 -1.178 -1.033	.0349 -.0402 -.1395 -.2151 -.1846	.1759 -.0998 .0005 -.0751 -.0480	.1759 -.0998 .0005 -.0751 -.0480
0	1.90	-1.90	1.00	0.292 -0.140 -0.686 -1.155 -1.138	0.0333 -.0236 -.1253 -.2109 -.2078	0.3533 0.2744 0.1747 0.0591 0.0922	0.3533 0.2744 0.1747 0.0591 0.0922
2	2.93	-2.93	1.00	.362 -.070 -.614 -1.118 -1.232	.0661 -.0128 -.1121 -.2041 -.2250	.5261 -.4472 .3479 .2559 .2350	.5261 -.4472 .3479 .2559 .2350
4	3.87	0.13	1.00	0.446 0.013 -0.333 -1.024 -1.250	0.0814 0.0024 -0.0973 -0.1925 -0.2282	0.621 0.7024 0.6234 0.5237 0.4285	0.621 0.7024 0.6234 0.5237 0.4285
6	4.86	1.11	1.00	.518 .087 -.437 -.977 -1.235	.0946 -.0159 -.0834 -.1784 -.2235	.7979 .6986 .7979 .6986 .6036	.7979 .6986 .7979 .6986 .6036
8	5.77	2.23	1.00	0.599 0.167 -0.377 -0.898 -1.200	0.1094 0.0305 -0.0688 -0.1640 -0.2191	0.942 1.0514 0.9725 0.8732 0.7780	0.942 1.0514 0.9725 0.8732 0.7780
10	6.61	3.39	1.00	.685 .252 -.292 -.812 -1.147	.1251 .0460 -.0533 -.1483 -.2094	1.104 1.2291 1.1500 1.0307 .9557	1.104 1.2291 1.1500 1.0307 .9557
12	7.55	4.45	1.00	0.762 0.332 -0.212 -0.733 -1.068	0.1391 0.0606 -0.0387 -0.1338 -0.1950	1.230 1.3691 1.2906 1.1913 1.0962	1.230 1.3691 1.2906 1.1913 1.0962
13.8	8.30	5.50	1.00	0.840 0.410 -0.135 -0.655 -0.990	0.1534 0.0749 -0.0217 -0.1196 -0.1808	1.280 1.4334 1.3549 1.2553 1.1604	1.280 1.4334 1.3549 1.2553 1.1604

①	②	③	④	⑤	⑥	⑦	⑧
Figure 1.9.1-7	Figure 1.9.1-7	Figure 1.9.1-7	Figure 1.9.1-7	Equation (4.13.4-2)	Table 4.8.3-1	Equation (4.13.4-2)	Equation (4.13.4-2)
α_D , deg	$\bar{\epsilon}_h$	α_h	$\frac{\bar{q}_h}{\bar{q}_c}$	$\epsilon \left(\frac{\bar{\epsilon}_h - \bar{\epsilon}_h}{\bar{\epsilon}_w} \right) \left(\frac{S_h}{S_w} \frac{\bar{q}_h}{\bar{q}_c} \right) \left(\bar{C}_{Lh(h)} \right) \text{ referenced to } S_w = 178 \text{ sq ft}$	$C_{mwfn} \text{ referenced to } S_w = 178 \text{ sq ft}$	$C_m = \text{⑤} + \text{⑥}$ referenced to $S_w = 178 \text{ sq ft}$	$C_m = \text{⑤} + \text{⑥}$ referenced to $S_w = 178 \text{ sq ft}$
		① - ②		δ_c , deg	δ_c , deg		δ_c , deg
				4 0 -5 -10 -14	4 0 -5 -10 -14	4 0 -5 -10 -14	4 0 -5 -10 -14
-4	0	-4.00	1.00	-0.0722 0.1591 0.4500 0.6301 0.5401	-0.0457 -0.1179 0.1134 0.4043 0.5844	-0.1179 0.1134 0.4043 0.5844 0.4944	-0.1179 0.1134 0.4043 0.5844 0.4944
-2	.96	-2.96	1.00	-.1137 .1175 .4079 .6290 .5515	-.0386 -.1523 -.0789 .3693 .5129	-.1523 -.0789 .3693 .5129 .5129	-.1523 -.0789 .3693 .5129 .5129
0	1.90	-1.90	1.00	-0.1538 0.0749 0.3684 0.6167 0.6076	-0.0318 -.0318 -.0318 -.0318 -.0318	-0.1876 0.0431 0.3346 0.5849 0.5758	-0.1876 0.0431 0.3346 0.5849 0.5758
2	2.93	-2.93	1.00	-.1933 .0371 .3278 .5968 .6579	-.0255 -.0255 -.0255 -.0255 -.0255	-.2188 -.0119 .3023 .5713 .6324	-.2188 -.0119 .3023 .5713 .6324
4	3.87	0.13	1.00	-0.2380 -0.0070 0.2815 .5629 0.6673	-0.0198 -.0198 -.0198 -.0198 -.0198	-0.2578 -.0268 0.2647 0.5431 0.6475	-0.2578 -.0268 0.2647 0.5431 0.6475
6	4.86	1.11	1.00	-.2766 -.0465 .2439 .5316 .6394	-.0113 -.0113 -.0113 -.0113 -.0113	-.2909 -.0608 .2296 .5073 .6431	-.2909 -.0608 .2296 .5073 .6431
8	5.77	2.23	1.00	-0.3199 -0.0892 0.2012 0.4795 0.6106	-0.0093 -.0093 -.0093 -.0093 -.0093	-0.3292 -.0495 0.1919 0.4702 0.6313	-0.3292 -.0495 0.1919 0.4702 0.6313
10	6.61	3.39	1.00	-.3658 -.1345 .1558 .4336 .6123	-.0048 -.0048 -.0048 -.0048 -.0048	-.3706 -.1333 .1510 .4288 .6075	-.3706 -.1333 .1510 .4288 .6075
12	7.55	4.45	1.00	-0.4067 -0.1772 0.1132 0.3912 0.5702	-0.0044 -.0044 -.0044 -.0044 -.0044	-0.4111 -.0181 0.1088 0.3868 0.5658	-0.4111 -.0181 0.1088 0.3868 0.5658
13.8	8.30	5.50	1.00	-.4485 -.2190 .0722 .3488 .5287	-.0111 -.0111 -.0111 -.0111 -.0111	-.4596 -.2301 .0611 .3377 .5176	-.4596 -.2301 .0611 .3377 .5176

^aLimit of linearity.

^bStaff (propeller off).

^cFor the subject airplane, the distance from the center of gravity to the c/4 of the horizontal tail in terms of wing mean aerodynamic chord, for a center of gravity of 0.10c_{wp}, is $\frac{x_{cg} \cdot x_h}{c_w} = 2.924$ (table 4.11-1(a)).

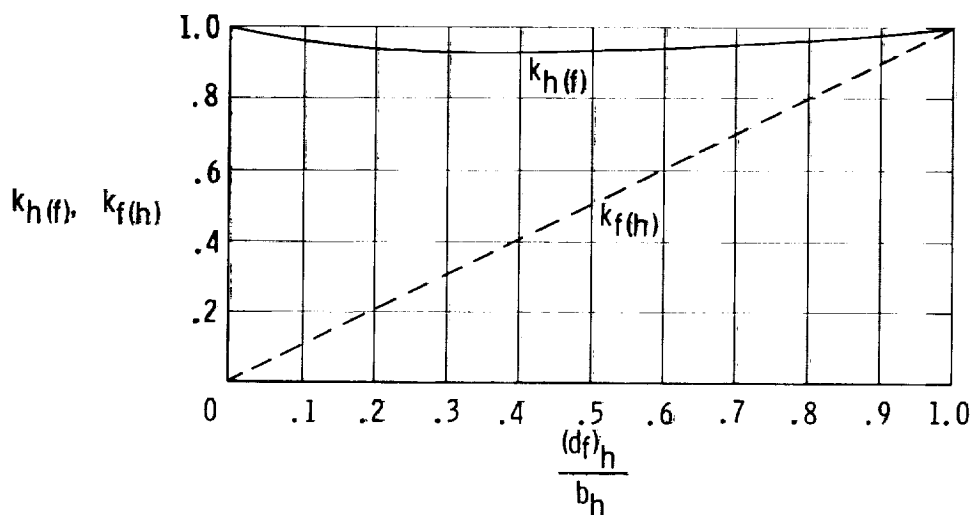


Figure 4.13.1-1. Lift ratios $k_h(f)$ and $k_f(h)$ based on slender-body theory variable incidence (ref. 11).

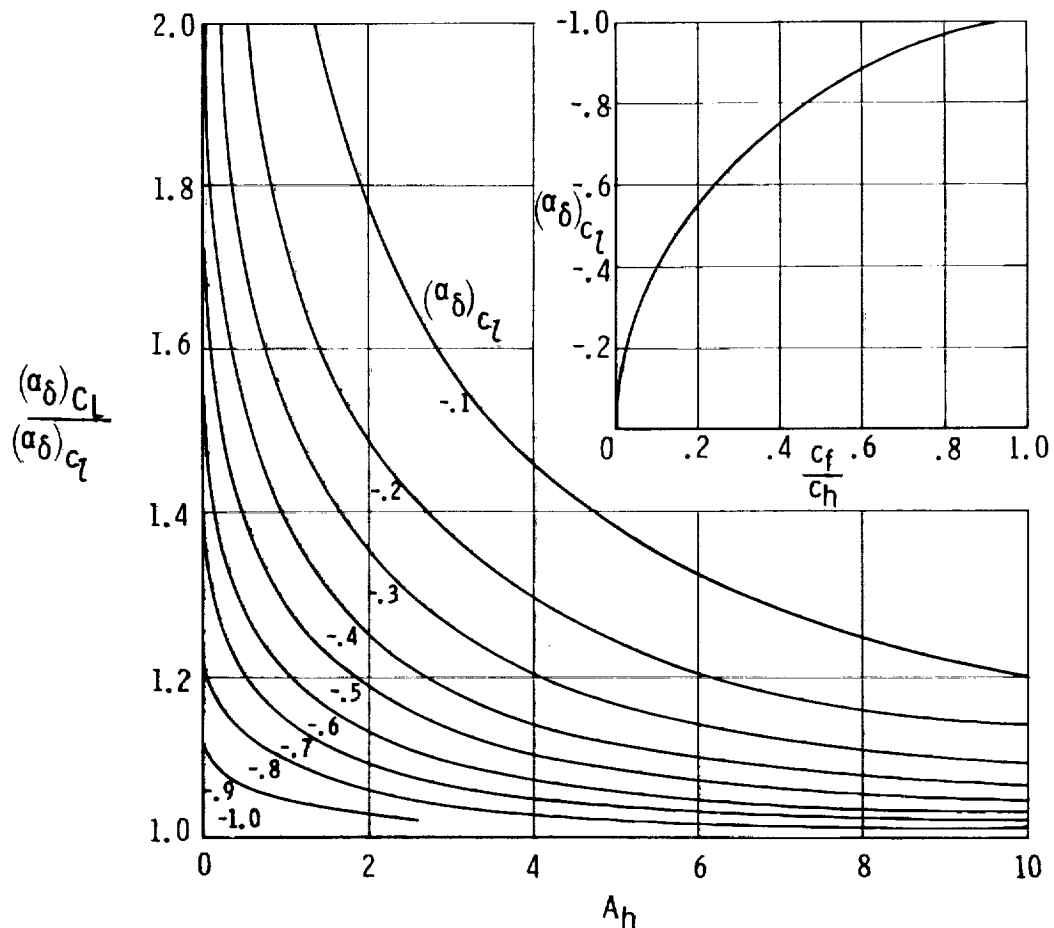


Figure 4.13.1-2. Tab-chord factor (ref. 8). Subsonic speeds; $(\alpha_\delta)_{c_l} = (\alpha_{\delta_{\text{tab}}})_{c_l}$.

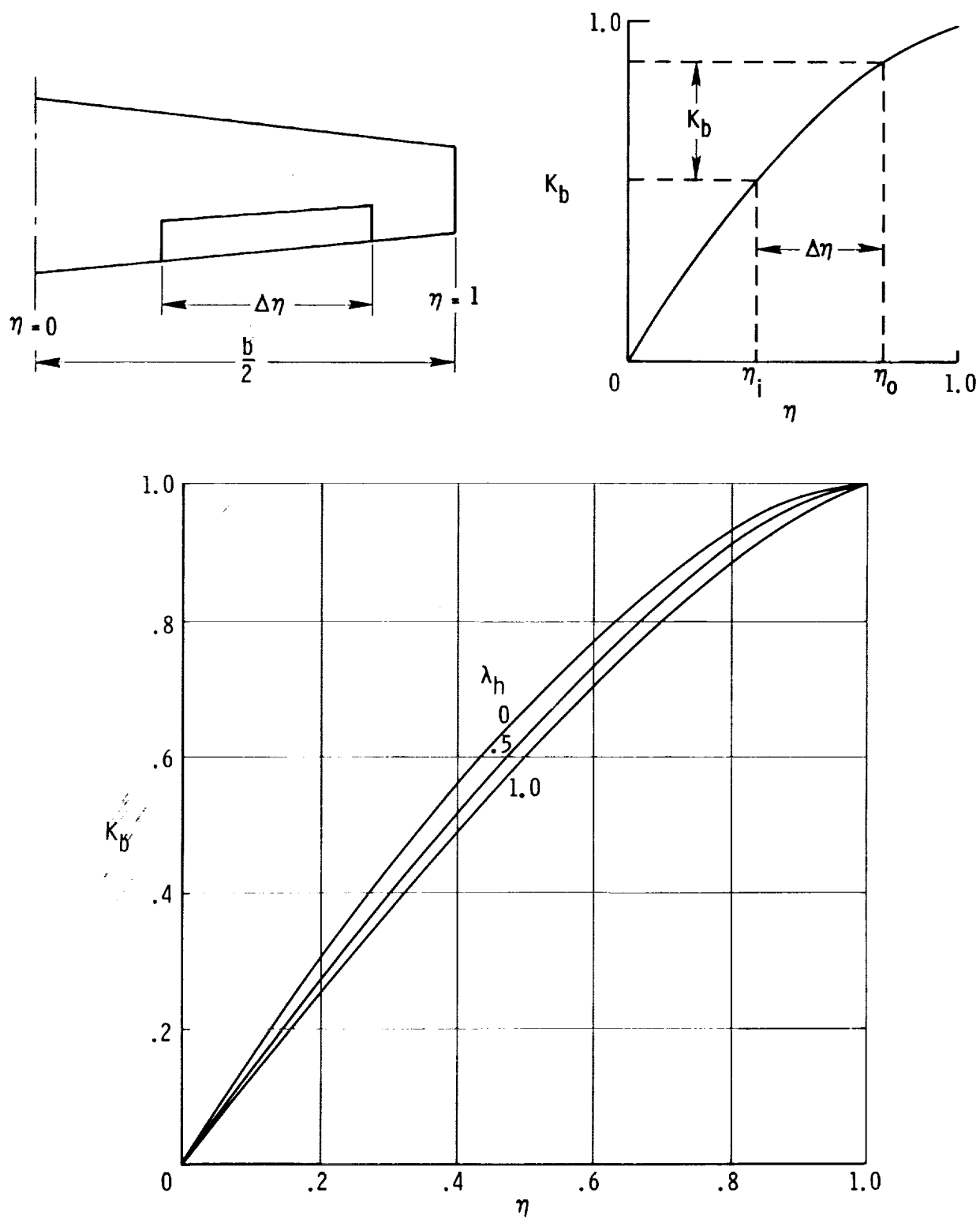


Figure 4.13.1-3. Span factor for inboard flaps (ref. 8).

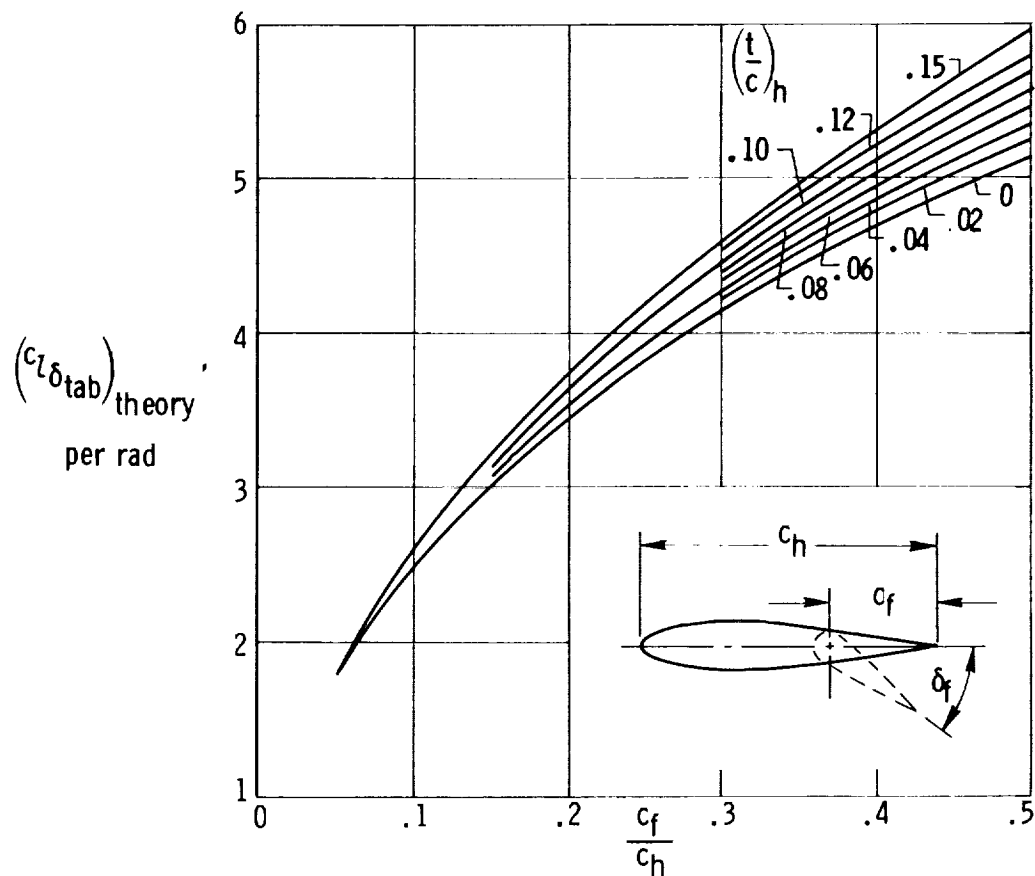


Figure 4.13.1-4. Theoretical lift effectiveness of plain trailing-edge flaps (ref. 1).
 $c_f = c_{tab}$.

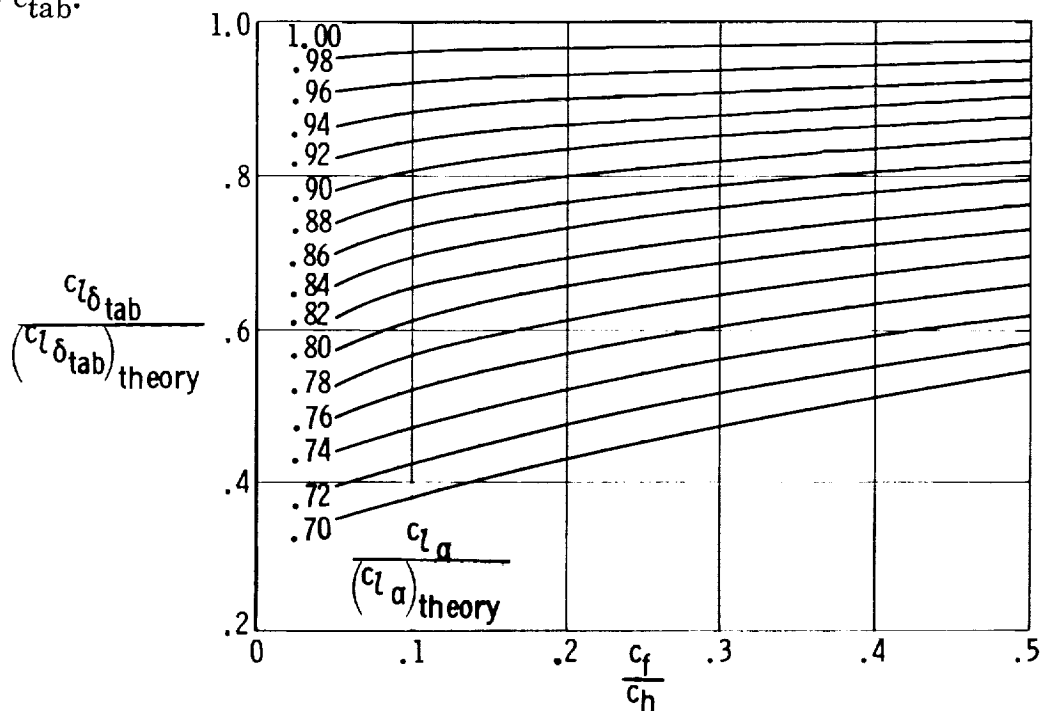


Figure 4.13.1-5. Empirical correction for lift effectiveness of plain trailing-edge flaps (ref. 1). $c_f = c_{tab}$.

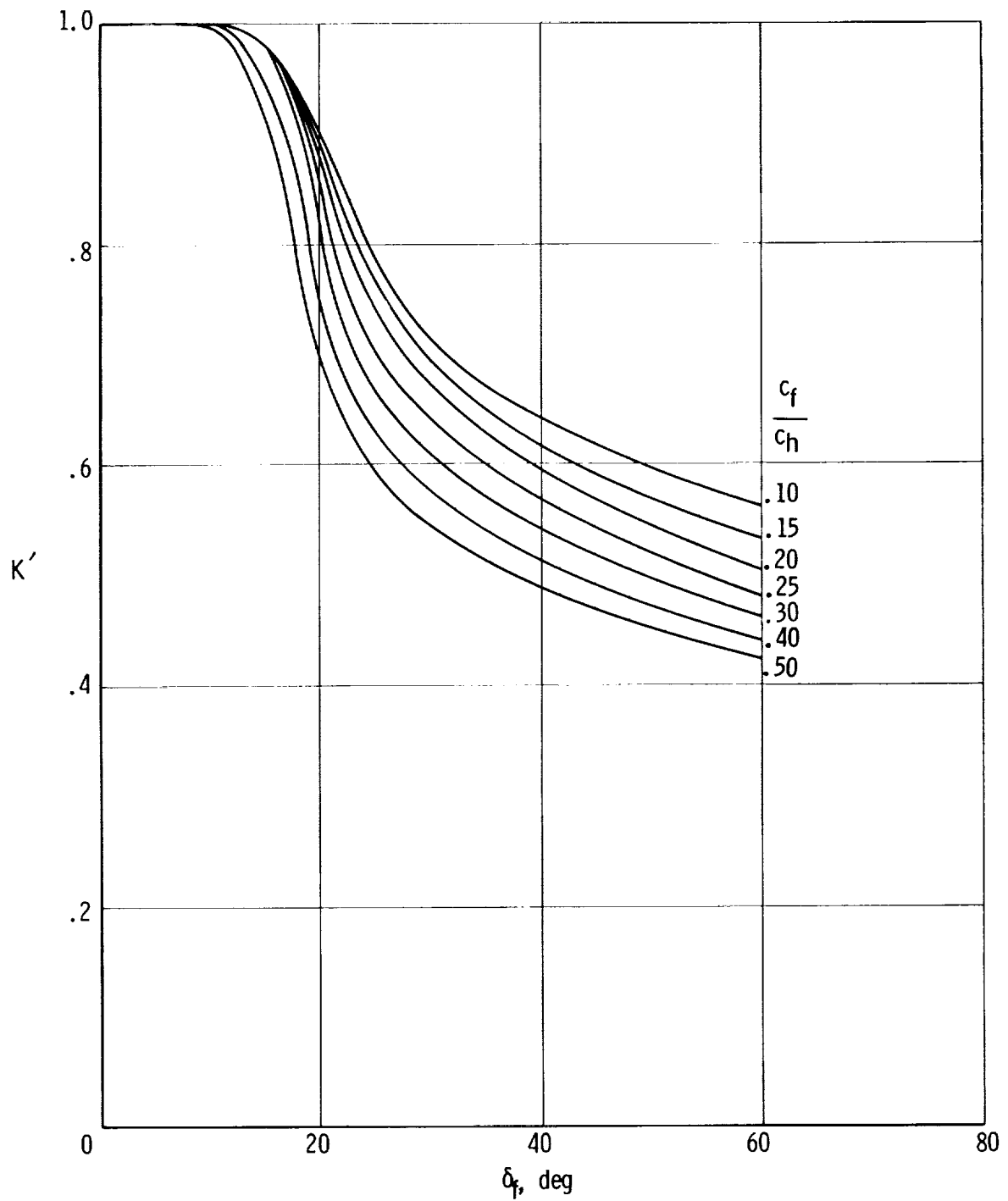


Figure 4.13.1-6. Empirical correction for lift effectiveness of plain trailing-edge flaps at high flap deflections (revised edition of ref. 1).

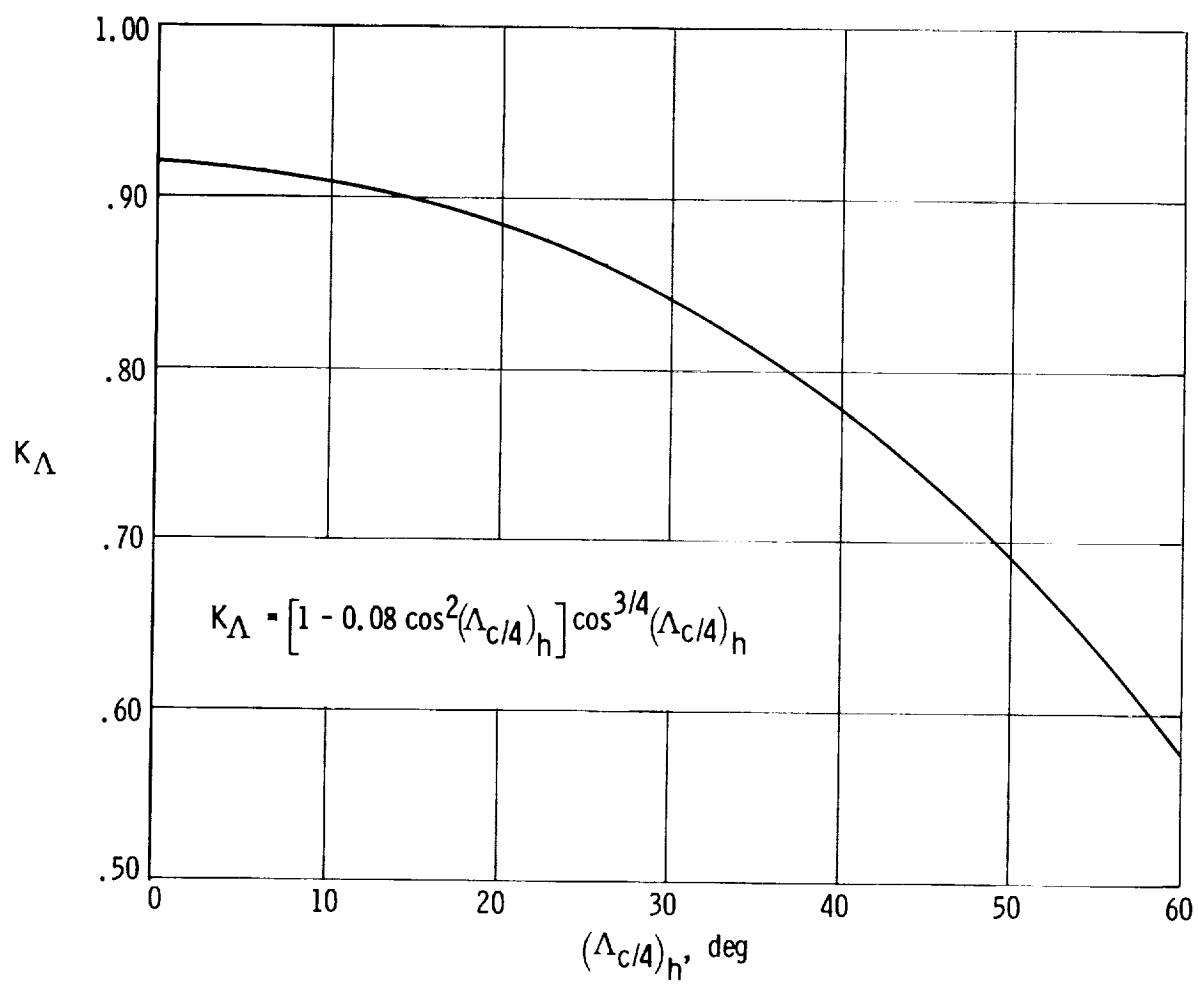


Figure 4.13.2-1. Planform correction factor (ref. 1). Trailing-edge flaps.

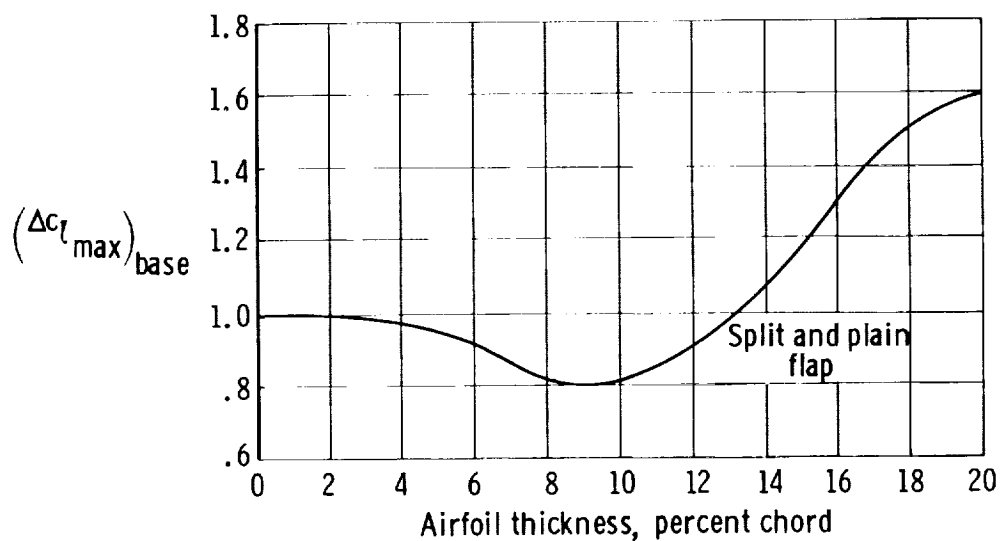


Figure 4.13.2-2. Maximum-lift increments of 25-percent-chord flaps at reference flap angle (ref. 1).

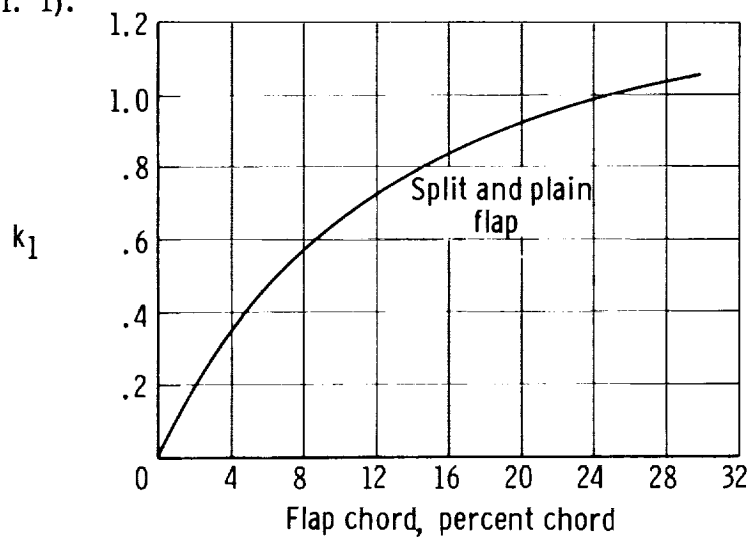


Figure 4.13.2-3. Flap-chord correction factor (ref. 1).

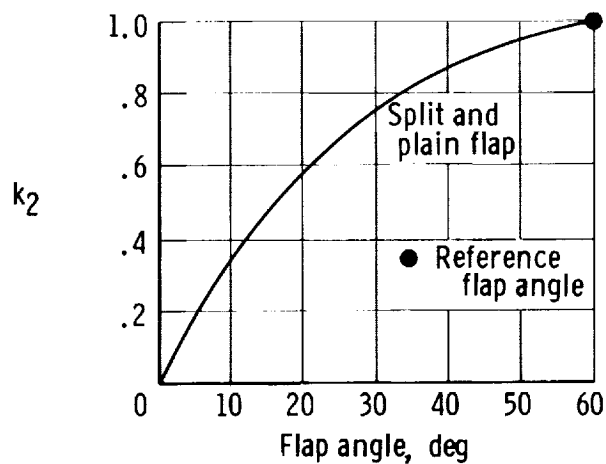


Figure 4.13.2-4. Flap angle correction factor (ref. 1).

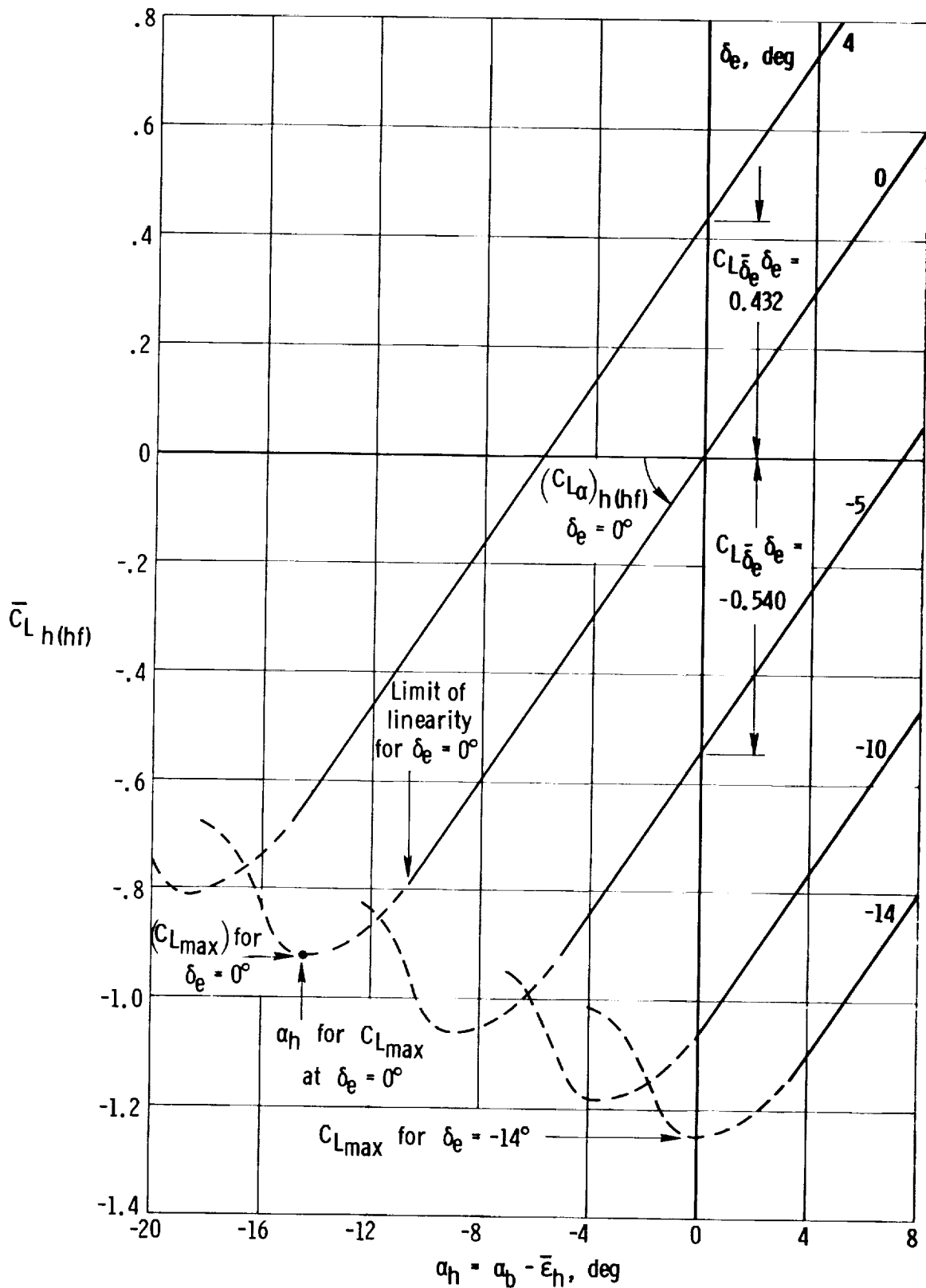
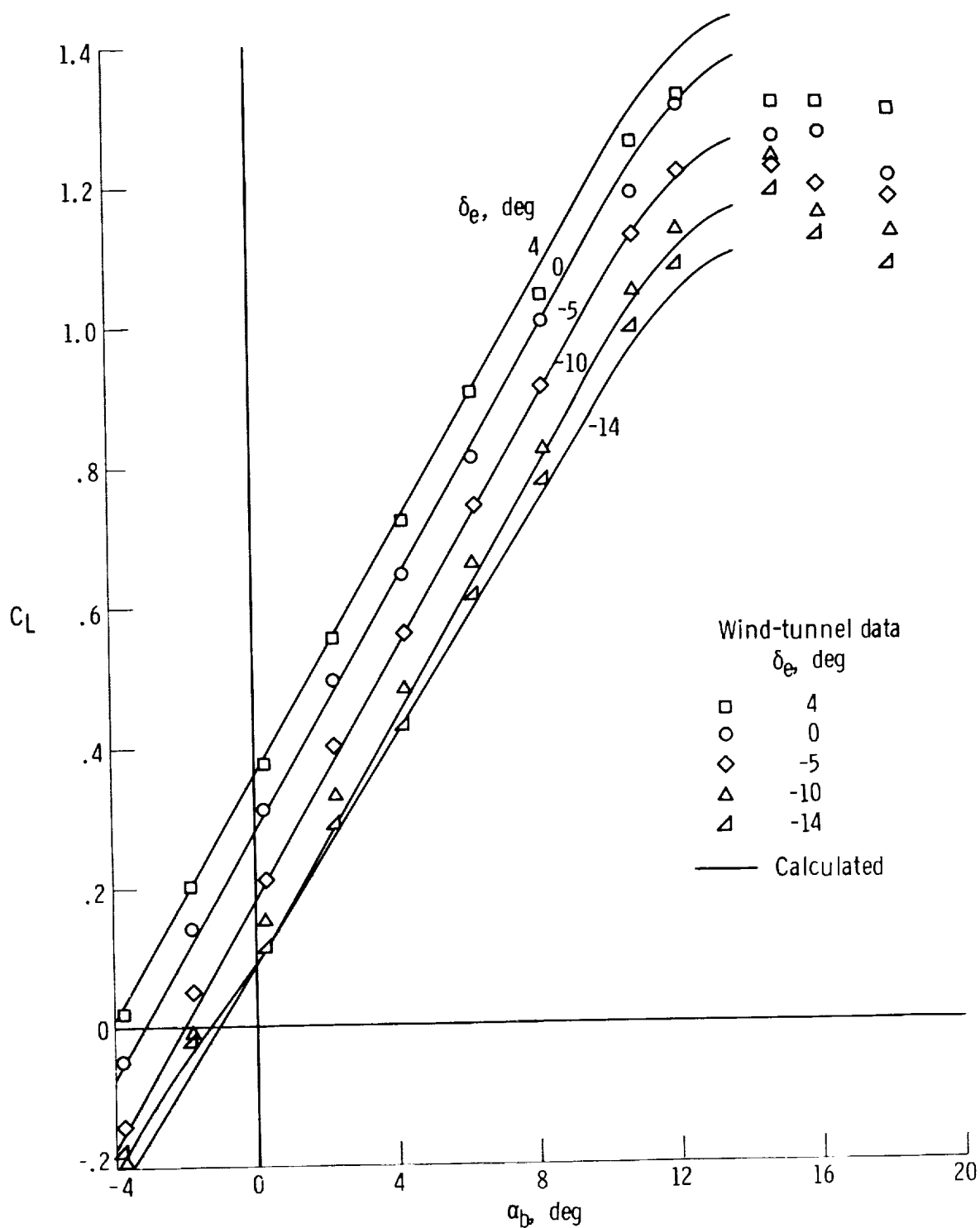
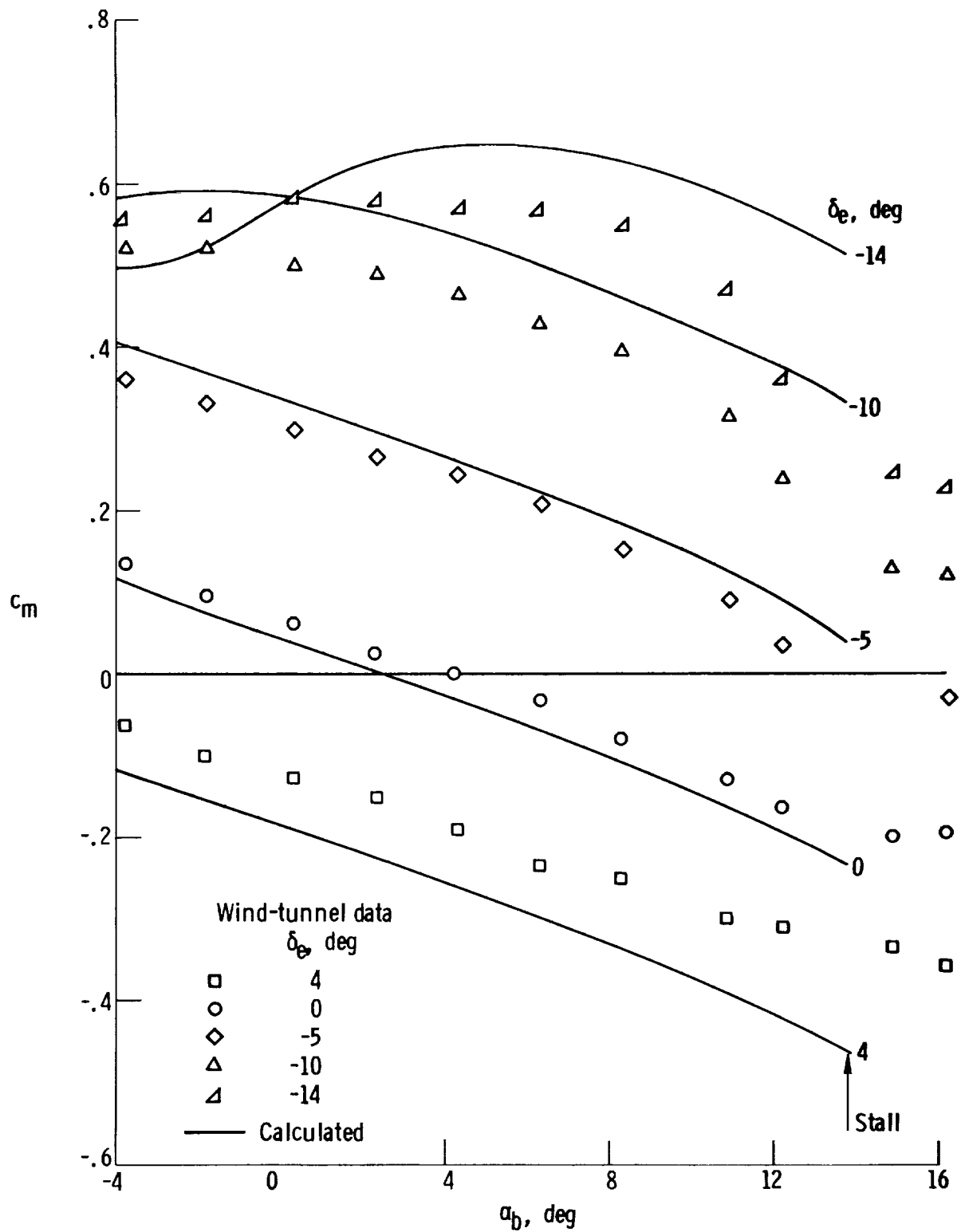


Figure 4.13.3-1. Calculated lift curves of the horizontal tail with tab geared to elevator. $\delta_{tab}/\delta_e = 1.5$; $S_h = 32.5$ sq ft; $\bar{q}_h/\bar{q}_\infty = 1.00$.



(a) Lift characteristics.

Figure 4.13.4-1. Comparison of predicted propeller-off lift and pitching-moment characteristics of the airplane with wind-tunnel data as a function of α_b and δ_e . $S_w = 178$ sq ft; $\delta_{tab}/\delta_e = 1.5$ (propeller-off wind-tunnel data obtained from propeller-on data at $T'_c = 0$ with propeller effects calculated out); center of gravity = $0.10\bar{c}_w$.



(b) Pitching-moment characteristics.

Figure 4.13.4-1. Concluded.

4.14 Horizontal-Tail Hinge Moments and Stick Forces

The procedure of reference 1 for determining pitching moments of wings having trailing-edge flaps was used to determine the hinge moments of an all-moving surface equipped with a tab or flap. It is based on the method of reference 31 for determining the pitching moments of wings having trailing-edge flaps. The method makes use of load distribution theory (ref. 32) for subsonic flow together with two-dimensional airfoil data adjusted for the effects of sweep. The method, as developed in reference 31, is limited to subsonic speeds.

4.14.1 Horizontal-Tail Hinge Moments

The hinge moments of an uncambered horizontal tail about its hinge line, referenced to the tail area, S_h , and a unity dynamic-pressure ratio, may be determined from the following equation:

$$C_{hh(f)} = (C_{Lh(f)})_{\delta_{tab}=0} \frac{(x_{hinge} - x_{ac})_h}{\bar{c}_h} + (\Delta C_L)_{\delta_{tab}} \frac{(x_{hinge} - \bar{x}_{\bar{c}}/4)_h}{\bar{c}_h} + (\Delta C'_m)_{\delta_{tab}} \quad (4.14.1-1)$$

where

$(C_{Lh(f)})_{\delta_{tab}=0}$ is the lift coefficient of the tail alone in the presence of the body as a function of $\alpha_h = \alpha_b - \bar{\epsilon}_h$ and δ_e only, with $\delta_{tab} = 0$, based on tail area

The following equation considers the lift of the stabilizer only, in the presence of the fuselage, due to α_h and δ_e . The lift on the fuselage due to carryover of tail lift onto the fuselage is not a factor at this time, because it does not enter into the hinge-moment calculations.

$$\begin{aligned} (C_{Lh(f)})_{\delta_{tab}=0} &= (C_{Lh(f)})_{\alpha_h} + (\Delta C_L)_{\delta_e} \\ &= (C_{L\alpha})_{h_e} \alpha_h K_{h(f)} \frac{S_{h_e}}{S_h} \frac{\bar{q}_h}{\bar{q}_\infty} + (C_{L\alpha})_{h_e} \delta_e k_{h(f)} \frac{S_{h_e}}{S_h} \frac{\bar{q}_h}{\bar{q}_\infty} \\ &= (C_{L\alpha})_{h_e} \left[K_{h(f)} \alpha_h + k_{h(f)} \delta_e \right] \frac{S_{h_e}}{S_h} \frac{\bar{q}_h}{\bar{q}_\infty} \end{aligned} \quad (4.14.1-2)$$

and

$(\Delta C_L)_{\delta_{tab}}$ is the increment of lift coefficient due to tab deflection, based on tail area, obtained from section 4.13

$\frac{(x_{\text{hinge}} - x_{\text{ac}})_h}{\bar{c}_h}$ is the distance from the aerodynamic center of the tail, with $\delta_{\text{tab}} = 0$, to the hinge line in terms of tail mean aerodynamic chord, measured on the tail mean aerodynamic chord

$\frac{(x_{\text{hinge}} - x_{\bar{c}/4})_h}{\bar{c}_h}$ is the distance from the quarter chord of the tail mean aerodynamic chord to the hinge line in terms of the tail mean aerodynamic chord

$(\Delta C'_m)_{\delta_{\text{tab}}}$ is the pitching moment of the tab about the quarter chord of the tail mean aerodynamic chord (The procedure for obtaining this quantity is discussed below.)

In instances where the center of pressure of the untabbed tail is at the quarter-chord point, as in the present case,

$$C_{h_{h(f)}} = \left[(C_{L_{h(f)}})_{\delta_{\text{tab}}=0} + (\Delta C_L)_{\delta_{\text{tab}}} \right] \frac{(x_{\text{hinge}} - x_{\bar{c}/4})_h}{\bar{c}_h} + (\Delta C'_m)_{\delta_{\text{tab}}} \quad (4.14.1-3)$$

When the tab is geared to the horizontal tail, the net tail lift in the above equation, on the basis of tail area, is obtained from

$$\begin{aligned} \bar{C}_{L_{h(f)}} = \left[(C_{L_{h(f)}})_{\delta_{\text{tab}}=0} + (\Delta C_L)_{\delta_{\text{tab}}} \right] = & \left\{ (C_{L_{\alpha}})_{h_e} \alpha_h K_{h(f)} \frac{S_{h_e}}{S_h} + \right. \\ & \left. \left[(C_{L_{\alpha}})_{h_e} k_{h(f)} \frac{S_{h_e}}{S_h} + C_{L_{\delta_{\text{tab}}}} \left(\frac{\delta_{\text{tab}}}{\delta_e} \right) \right] \delta_e \right\} \frac{\bar{q}_h}{\bar{q}_{\infty}} \end{aligned} \quad (4.14.1-4)$$

Applied to the subject airplane, the lift characteristics equations of the tail alone in the linear range in the presence of the body are shown in table 4.14.1-1(a). The stall conditions of the horizontal tail alone in the presence of the body are obtained by using the stall conditions calculated in table 4.13.2-1(b). For $\delta_e = 0^\circ$, the stall angle

$(\alpha C_{L_{\text{max}}})_{h(f)}$ is the same as $(\alpha C_{L_{\text{max}}})_{h(hf)}$ in the table. The maximum lift coefficients for the several elevator settings listed in the table are reduced by the ratio of $\frac{S_{h_e}}{S_h}$ to obtain $(\bar{C}_{L_{\text{max}}})_{h(f)}$, or

$$(\bar{C}_{L_{\text{max}}})_{h(f)} \approx (\bar{C}_{L_{\text{max}}})_{h(hf)} \frac{S_{h_e}}{S_h} \quad (4.14.1-5)$$

The results for stall conditions are summarized in table 4.14.1-1(b). The lift

characteristics of the horizontal tail alone in the presence of the body are plotted in figure 4.14.1-1 as a function of $\alpha_h = \alpha_b - \bar{\epsilon}_h$ and δ_e (with $\frac{\delta_{tab}}{\delta_e} = 1.5$) for a dynamic-pressure ratio of $\frac{\bar{q}_h}{\bar{q}_\infty} = 1.0$.

The determination of the pitching-moment contribution of the tab, $(\Delta C'_m)_{\delta_{tab}}$, requires the determination of the variation of the spanwise-loading coefficient, $\frac{G}{\delta}$, across the span of the tail per unit (radian) tab deflection, $\frac{G}{\delta}$, and the determination of the chordwise center-of-pressure location, x_{cp} , for stations across the span. The spanwise loading coefficient, G , at any one spanwise station is equal to $\frac{c_l c_h}{2b_h}$, where c_l is the local lift coefficient at the station per unit of span, c_h is the corresponding local chord, and b_h is the span of the tail. The determinations of $\frac{G}{\delta}$ and x_{cp} are followed by calculations, using an integration process, of incremental pitching moments due to the tab. The following outline is a detailed clarification of the procedures to be used to determine $(\Delta C'_m)_{\delta_{tab}}$. The outline is similar to that presented in reference 1.

(1) Obtain the span-loading coefficient per unit of tab deflection, $\frac{G}{\delta}$, from the design charts of reference 35 which are shown in figures 4.14.1-2(a) to 4.14.1-2(d) as a function of wing (or tail) semispan station, η , for several inboard flaps having semispans, η_f , of 0.195, 0.556, 0.831, and 1.00 for appropriate values of $\frac{\beta A}{k}$, Λ_β , and λ , where $k = \frac{c_l \alpha}{2\pi}$ (from section 4.2), $\beta = \sqrt{1 - M^2}$, and $\Lambda_\beta = \tan^{-1} \left(\frac{\tan \Lambda_c / 4}{\beta} \right)$. To arrive at the appropriate curves for the flapped surface being considered, interpolate each set of taper ratio curves for a constant η_f to obtain curves to conform to the taper ratio of the surface being considered. With the desired taper ratio for each η_f established, interpolate through several crossplots to obtain a net set of three curves ($\eta_f = 0.195, 0.556, 1.00$) which are now in accord with the design parameters $\frac{\beta A}{k}$, Λ_β , and λ for the surface being considered. Such a set of reduced load distribution curves is shown in figure 4.14.1-3 for a hypothetical case.

Cross-plot the net set of three curves, such as in figure 4.14.1-3(a), as in figure 4.14.1-3(b). (The circles are the crossplot points.) On the crossplot locate the inboard and outboard limits of the flap semispan under consideration ($\eta_f = 0.1$ and 0.75 in the specific illustration) and cross-plot again the span-load distribution curves for these two stations, as in figure 4.14.1-2(c). The two resulting span-load distribution curves in figure 4.14.1-3(c) are the operational curves for subsequent analysis to determine the incremental section lift coefficients as a function of span station, η .

(2) Determine the incremental section lift coefficient as a function of span station from

$$(c_{l\Lambda})_{\eta} = -\frac{2b_h}{57.3(c_h)_{\eta}} \left(\Delta \frac{G}{\delta}\right)_{\eta} (\alpha\delta)_{c_l} \delta'_{\text{tab}} \quad (4.14.1-6)$$

where

$(c_{l\Lambda})_{\eta}$ is the incremental section lift coefficient due to tab (flap) deflection at station η

$(c_h)_{\eta}$ is the chord of the tail at station η

b_h is the span of the tail

$\left(\Delta \frac{G}{\delta}\right)_{\eta}$ is the difference in span-load coefficients for the two bounding span-load distribution curves at station η (fig. 4.14.1-3(c), for example)

$(\alpha\delta)_{c_l}$ is the two-dimensional lift-effectiveness parameter obtained from $-\frac{c_l \delta_{\text{tab}}}{(c_{l\alpha})_h}$ as per section 4.13.1

δ'_{tab} is the streamwise tab deflection in degrees, which is related to the deflection δ_{tab} normal to the hinge line by the relationship

$$\delta'_{\text{tab}} = \tan^{-1}(\cos \Lambda_{hl} \tan \delta_{\text{tab}}) \quad (4.14.1-7)$$

For conventional tail surfaces, the difference between δ'_{tab} and δ_{tab} is negligible.

(3) The chordwise center-of-pressure location, x_{cp} , for the incremental section lift coefficient, due to tab deflection, for stations across the tail semispan depends upon three regions of the semispan, two of which are affected by the tab. These three regions, shown by the sketch in figure 4.14.1-4, consist of the following:

Semispan stations included in the tabbed section

Semispan stations adjacent to and within $\Delta\eta = 0.20$ of the ends of the tab

Semispan stations, not influenced by the tab, outboard of $\Delta\eta = 0.20$ from the ends of the tab

(a) For a semispan station included in the tabbed portion of the semispan,

$$\left(\frac{x_{cp}}{c_h}\right)_{\eta} = 0.25 - \frac{(\Delta c_{mf})_{\eta}}{(c_{l\Lambda=0})_{\eta}} \quad (4.14.1-8)$$

where

$(c_{l_{\Lambda=0}})_{\eta}$ is the increment of lift coefficient at station η referred to the basic load line, obtained from

$$(c_{l_{\Lambda=0}})_{\eta} = \frac{(c_{l_{\Lambda}})_{\eta}}{\cos^2 \Lambda_b} \quad (4.14.1-9)$$

where

$(c_{l_{\Lambda}})_{\eta}$ is obtained from equation (4.14.1-6)

Λ_b is the sweepback angle of the $(x_{cp})_b$ chordline which is the chordwise center-of-pressure position of the basic (effective camber type) loading due to tab deflection, deg, obtained from

$$\tan \Lambda_b = \tan \Lambda_{c/4} - \frac{4}{A} \left[\frac{(x_{cp})_b}{c_h} - 0.25 \right] \left(\frac{1 - \lambda}{1 + \lambda} \right) \quad (4.14.1-10)$$

and $\frac{(x_{cp})_b}{c_h}$ is obtained from figure 4.14.1-5.

$(\Delta c_{mf})_{\eta}$ is the section increment pitching-moment coefficient at semispan station, η , due to tab deflection about the quarter-chord point in the plane normal to the constant-percent chord line through $(x_{cp})_b$

For tab deflections up to approximately 6° $(\Delta c_{mf})_{\eta}$ may be obtained from

$$(\Delta c_{mf})_{\eta} = c_{m\delta''_{tab}} \delta''_{tab} \quad (4.14.1-11)$$

where, on the basis of lifting line theory,

$$c_{m\delta''_{tab}} = -\frac{2}{57.3} \sqrt{\left(\frac{c_{tab}}{c_h}\right)_{\eta} \left[1 - \left(\frac{c_{tab}}{c_h}\right)_{\eta}\right]^3} \text{ per deg} \quad (4.14.1-12)$$

and where

$$\delta''_{tab} = \tan^{-1} \left(\frac{\cos \Lambda_{hl} \tan \delta_{tab}}{\cos \Lambda_b} \right) \quad (4.14.1-13)$$

For large tab deflections, $(\Delta c_{mf})_{\eta}$ may be determined by using the empirical curves

of Δc_{mf} in figure 4.14.1-6 (from ref. 1) based on unpowered-model wind-tunnel data. Figure 4.14.1-7 compares the empirically determined variation of Δc_{mf} versus $\delta_{tab}(\delta_f)$ with lifting-line theory as applied to the subject airplane.

(b) For semispan stations adjacent to and within $\Delta\eta = 0.20$ from the ends of the tab,

$$\left(\frac{x_{cp}}{c_h}\right)_\eta = 0.25 - K \left[\frac{(\Delta c_{mf})_\eta}{(c_{l_{\Lambda=0}})_\eta} \right]_{\text{edge of tab}} \quad (4.14.1-14)$$

where

$$\left[\frac{(\Delta c_{mf})_\eta}{(c_{l_{\Lambda=0}})_\eta} \right]_{\text{edge of tab}} \quad \text{is the ratio of } (\Delta c_{mf})_\eta \text{ and } (c_{l_{\Lambda=0}})_\eta, \text{ determined in}$$

part (a), for span stations corresponding to the edge of the tab

K is a factor for estimating section center-of-pressure location for untabbed airfoil sections near the ends of the tab, obtained from figure 4.14.1-8

(c) For semispan stations outboard of $\Delta\eta = 0.20$ from the ends of the tab, $\left(\frac{x_{cp}}{c_h}\right)_\eta$ is considered to be 0.25.

(4) For wings with a swept quarter chord, the chordwise center-of-pressure position at each semispan station must be referred to the quarter chord of the tail mean aerodynamic chord by

$$\left(\frac{x}{\bar{c}_h}\right)_\eta = (\eta - \bar{\eta}) \frac{b_h/2}{\bar{c}_h} \tan \Lambda_{c/4} + \frac{(c_h)_\eta \left[\left(\frac{x_{cp}}{c_h}\right)_\eta - 0.25 \right]}{\bar{c}_h} \quad (4.14.1-15)$$

where

$\left(\frac{x}{\bar{c}_h}\right)_\eta$ is the distance to the center of pressure at the semispan station, η , aft of the quarter chord as a ratio of the tail mean aerodynamic chord

$\bar{\eta}$ is the lateral distance of the tail mean aerodynamic chord from the body centerline in semispans, obtained from section 3.2

(5) Obtain the pitching moment due to the tab deflection from the integral

$$(\Delta C'_m)_{\delta_{tab}} = - \int_0^{1.0} (c_{l_\Lambda})_\eta \frac{(c_h)_\eta}{(c_h)_{av}} \left(\frac{x}{\bar{c}_h}\right)_\eta d\eta \quad (4.14.1-16)$$

where

$\frac{(c_h)_\eta}{(c_h)_{av}}$ is the ratio of the tail chord at the semispan station, η , to the average chord, $\frac{S_h}{b_h}$

Tables 4.14.1-2, 4.14.1-3, and 4.14.1-4 summarize the calculations for determining the horizontal-tail hinge moments of the subject airplane, based on the foregoing procedures. Figure 4.14.1-9 shows the variation of the spanwise loading coefficient, $\frac{\Delta G}{\delta}$, due to the tab deflection, used in the calculations. The basic pertinent parameters and operational forms of the equations are listed in table 4.14.1-2. Horizontal-tail tab characteristics are summarized in table 4.14.1-3. The results from table 4.14.1-3 are applied to table 4.14.1-4 to obtain the hinge-moment characteristics for the condition where the tab is geared to the elevator in the ratio of $\frac{\delta_{tab}}{\delta_e} = 1.5$. It should be noted that in table 4.14.1-4 the calculations involving the non-linear portion (calculated) of the tail lift curve are identified by block outline and are not used. The calculated limit of linearity was obtained from a coordinated study of $\alpha_h = \alpha_b - \bar{\epsilon}_h$ and δ_e in table 4.14.1-4 with figure 4.14.1-1.

The calculated hinge-moment characteristics are compared with full-scale wind-tunnel data in figure 4.14.1-10. In general, correlation for $\delta_e = 4^\circ$, 0° , and -5° is reasonably good. At $\delta_e = -10^\circ$ and -14° , although good correlation exists at high α_b , the increasing discrepancy between wind-tunnel data and calculations with decreasing α_b indicates an earlier nonlinearity in tail characteristics (due to tab deflection) than calculated.

It is possible to arrive at a simple first approximation of the variation of the tail hinge moment with α_b at a constant δ_e for at least the first half of the nonlinear region of the tail hinge moments. The suggested empirical procedure is as follows:

(1) Obtain the tail hinge moment at tail stall for the δ_e considered. At tail stall, the center of pressure may be assumed to be at 50 percent of the tail mean aerodynamic chord. Thus at tail stall,

$$(C_{hh(f)})_{stall} \approx (\bar{C}_{Lmax})_{h(f)} \frac{(\bar{x}_{hinge} - \bar{x}_{\bar{c}}/2)_h}{\bar{c}_h} \frac{\bar{q}_h}{\bar{q}_\infty} \quad (4.14.1-17)$$

For the subject airplane at $\delta_e = -14^\circ$,

$$(C_{hh(f)})_{stall} \approx -1.107 \left(\frac{-6.94}{32.45} \right) (1.0) = 0.236$$

where

$$\frac{\bar{q}_h}{\bar{q}_\infty} = 1.0 \text{ from table 4.14.1-4}$$

$$\left. \begin{aligned} \bar{c}_h &= 32.45 \text{ inches} \\ (x_{\text{hinge}} - x_{\bar{c}/2})_h &= -6.94 \text{ inches} \end{aligned} \right\} \text{ from figure 3.2-2}$$

$$\left. \begin{aligned} (\bar{C}_{L_{\text{max}}})_{h(f)} &= -1.107 \\ (\alpha_h)_{\text{stall}} &= (\alpha_b - \bar{\epsilon}_h)_{\text{stall}} = 1.0^\circ \end{aligned} \right\} \text{ from figure 4.14.1-1}$$

(2) Obtain α_b corresponding to $(\alpha_h)_{\text{stall}}$ from the correlation of $(\alpha_h)_{\text{stall}}$ with columns 2 and 1 in table 4.14.1-4. For the subject airplane, with $(\alpha_h)_{\text{stall}} = 1.00$ at $\delta_e = -14^\circ$, $(\alpha_b)_{h\text{stall}} \approx 5.7^\circ$.

(3) Locate $(C_{hh(f)})_{\text{stall}}$ on the plot. For the subject airplane this is indicated by a solid symbol in figure 4.14.1-10 for $\delta_e = -14^\circ$.

(4) Assuming that, in general, nonlinearity due to the tab will be experienced earlier than predicted, spot a point on the calculated $C_{hh(f)}$ curve approximately one-fourth of its length from the linearity limit toward the calculated airplane stall point. From this plotted point, sweep a curve to $(C_{hh(f)})_{\text{stall}}$. This has been done for $\delta_e = -14^\circ$ for the subject airplane in figure 4.14.1-10.

4.14.2 Stick Forces

Control forces on the stick in a reversible control system are obtained from the following relation based on the principle that work input is equal to work output:

$$F_{\text{stick}} = (\text{Hinge moment}) \frac{\delta_e}{\bar{\delta}_{\text{stick}}} \quad (4.14.1-18)$$

$$\begin{aligned} &= \frac{1}{57.3} \left[C_{hh(f)} \bar{q}_\infty S_h \bar{c}_h \right] \frac{\delta_e}{\bar{\delta}_{\text{stick}}} \\ &= \frac{1}{57.3} \left[C_{hh(f)} \left(\frac{\delta_e}{\bar{\delta}_{\text{stick}}} \right) \right] \bar{q}_\infty S_h \bar{c}_h \end{aligned} \quad (4.14.1-19)$$

where

$C_{hh(f)}$ is the hinge-moment coefficient based on horizontal-tail dimensions and $\frac{\bar{q}_h}{\bar{q}_\infty}$

δ_e is the elevator deflection, degrees

δ_{stick} is the stick deflection at the grip point, feet

For the subject airplane

$$F_{\text{stick}} = 40.0 C_{hh(f)} \bar{q}_\infty \quad (4.14.1-20)$$

based on $\frac{\delta_e}{\delta_{\text{stick}}} = 26 \text{ deg/ft}$, $S_h = 32.5 \text{ sq ft}$, and $\bar{c}_h = 2.71 \text{ ft}$

4.14.3 Symbols

All lift and moment coefficients are referenced to the horizontal-tail area and the mean aerodynamic chord.

A	horizontal-tail aspect ratio
b_h	horizontal-tail span, ft
$C_{hh(f)}$	hinge-moment coefficient of the horizontal tail with fuselage effects on the tail included
$(C_{hh(f)})_{\text{stall}}$	value of $C_{hh(f)}$ at the tail stall angle
C_L	lift coefficient
$\bar{C}_{Lh(f)}$	net lift coefficient of the tail, due to α_h , δ_e , and δ_{tab} , with the fuselage effects included
$(C_{Lh(f)})_{\alpha_h}$	lift coefficient of the tail, with fuselage effects included, due to the tail angle of attack, $\alpha_h = \alpha_b - \bar{\epsilon}_h$, only
$(C_{Lh(f)})_{\delta_{\text{tab}}=0}$	lift coefficient of the tail due to α_h and δ_e (with $\delta_{\text{tab}} = 0^\circ$), with the fuselage effects included
$(\bar{C}_{L\text{max}})_{h(f)}$	maximum value of $\bar{C}_{Lh(f)}$ at stall
$(\bar{C}_{L\text{max}})_{h(hf)}$	maximum lift coefficient of the tail with interacting tail-fuselage effects included
$(\Delta C_L)_{\delta_e}$	increment of lift due to the elevator deflection
$(\Delta C_L)_{\delta_{\text{tab}}}$	increment of lift due to the tab deflection

$(C_{L\alpha})_{h_e}$	lift-curve slope of the exposed portion of the tail panels, referenced to the effective area of the exposed panels, per deg
$(\overline{C_{L\alpha}})_{h(f)} = \frac{\partial \overline{C_{Lh(f)}}}{\partial \alpha_h}$	
$C_{L\delta_e}$	elevator effectiveness with the tab geared to the elevator to deflect in the ratio of $\frac{\delta_{tab}}{\delta_e}$, per deg
$C_{L\delta_{tab}}$	tab effectiveness, $\frac{\partial C_L}{\partial \delta_{tab}}$, per deg
$(\Delta C'_m)_{\delta_{tab}}$	increment of pitching moment, about the quarter-chord of the tail mean aerodynamic chord, due to tab deflection
$c_1 = \frac{2b_h}{57.3} (\alpha\delta) c_l$	
c_f, c_{tab}	chord of the flap and tab, respectively, used synonymously in this section, ft
c_h	tail chord, ft
$(c_h)_{av}$	average tail chord, ft
$(c_h)_\eta$	tail chord at the semispan station, η , ft
\bar{c}_h	tail mean aerodynamic chord, ft
c_l	section lift coefficient
c_{l_α}	section lift-curve slope, $\frac{\partial c_l}{\partial \alpha}$, per deg
$(c_{l_\alpha})_h$	section lift-curve slope of the horizontal tail
$c_{l\delta_{tab}}$	section tab effectiveness, $\frac{\partial c_l}{\partial \delta_{tab}}$, per deg
$(c_{l_\Lambda})_\eta$	increment section-lift coefficient at semispan station, η , due to the tab (flap) deflection
$(c_{l_{\Lambda=0}})_\eta$	increment section-lift coefficient at semispan station, η , due to the tab deflection, referred to the constant-percent chord line through $(x_{cp})_b$, the basic loading line due to tab deflection

$c_{m\delta''_{\text{tab}}}$	rate of change of the section pitching-moment coefficient with δ''_{tab} about the quarter-chord point in the plane normal to the constant-percent chord line through $(x_{\text{cp}})_b$, per deg
Δc_{mf}	section increment pitching-moment coefficient, due to the flap (tab) deflection, about the quarter-chord point in the plane normal to the constant-percent chord line through $(x_{\text{cp}})_b$
$(\Delta c_{mf})_\eta$	Δc_{mf} at semispan station, η
$\left(\frac{c_{\text{tab}}}{c_h}\right)_\eta$	ratio of the tab to the tail chord at semispan station, η
F_{stick}	stick force, lb
G	spanwise loading coefficient
$\frac{G}{\delta}$	span loading coefficient due to the flap (tab) extending to the plane of symmetry
$\left(\Delta \frac{G}{\delta}\right)_\eta$	difference in span-load coefficients for two bounding span-load-distribution curves at semispan station, η (fig. 4.14.1-3(b), for example)
K	a factor for estimating the section center-of-pressure location for untabbed section near the ends of the tab, obtained from figure 4.14.1-8
$K_h(f)$	ratio of the lift on the fixed stabilizer, due to angle of attack, in the presence of the fuselage to the stabilizer alone, obtained from figure 4.4-1
$k = \frac{c_l \alpha}{2\pi}$	
$k_h(f)$	ratio of the lift on the stabilizer, due to the stabilizer deflection, in the presence of the fuselage to the stabilizer alone, obtained from figure 4.13.1-1
M	Mach number
\bar{q}_h	dynamic pressure at the horizontal tail, lb/sq ft
\bar{q}_∞	free-stream dynamic pressure, lb/sq ft
S_h	horizontal-tail area, sq ft

S_{h_e}	area of the exposed panels of the horizontal tail, sq ft
T'_c	thrust coefficient
$\left(\frac{x}{\bar{c}_h}\right)_\eta$	chordwise center-of-pressure location, at semispan station, η , aft of the quarter chord of and as a ratio of the horizontal-tail mean aerodynamic chord
x_{ac_h}	chordwise location of the aerodynamic center from the leading edge of the tail mean aerodynamic chord with $\delta_{tab} = 0^\circ$, in.
x_{cp}	chordwise center-of-pressure location, ft
$(x_{cp})_b$	chordwise section basic loading center of pressure, ft
$\frac{(x_{cp})_b}{c_h}$	chordwise section basic loading center of pressure, due to the tab deflection, from the leading edge of the tail as a ratio of the tail chord
$\left(\frac{x_{cp}}{c_h}\right)_\eta$	chordwise center-of-pressure location of the lift due to the tab deflection, at semispan station, η , from the leading edge of the tail as a ratio of the tail chord
$(x_{hinge} - x_{ac})_h$	distance from the aerodynamic center of the tail to the hinge line of the tab, in.
$(x_{hinge} - \bar{x}_c/4)_h$, $(x_{hinge} - \bar{x}_c/2)_h$	distance, on the tail mean aerodynamic chord, from the quarter-chord and half-chord point, respectively, to the tab hinge line, in.
y	lateral distance from the plane of symmetry, ft
$y_{\bar{c}_h}$	lateral distance to the tail mean aerodynamic chord, ft
α	angle of attack, deg
α_b	airplane angle of attack relative to the X-body axis, deg
$(\alpha_b)_{h_{stall}}$	airplane angle of attack corresponding to horizontal-tail stall at any one deflected position, deg
α_h	angle of attack of the tail, $\alpha_b - \bar{\epsilon}_h$, deg
$(\alpha_h)_{stall}$	stall α_h for any one δ_e setting, deg
$(\alpha_{C_{Lmax}})_{h(f)}, (\alpha_{C_{Lmax}})_{h(hf)}$	angle of attack of the tail at the maximum lift of the tail including fuselage effect on the tail and tail-fuselage interaction effects, respectively $((\alpha_{C_{Lmax}})_{h(f)})$ is the same as $(\alpha_h)_{stall}$

$\left[(\alpha_{CL_{\max}})_{h(f)} \right]_{\delta_{\text{tab}}=0}$	$(\alpha_h)_{\text{stall}}$ with the tab at zero setting
$(\alpha_\delta)_{c_l} = - \frac{c_l \delta_{\text{tab}}}{c_{l_\alpha}}$	
$\beta = (1 - M^2)^{1/2}$	
δ_e	elevator deflection, deg
δ_f	flap deflection, same as tab deflection, δ_{tab} , deg
δ_{stick}	stick deflection at the grip point, ft
δ_{tab}	tab deflection normal to the hinge line, deg
δ'_{tab}	streamwise tab deflection, deg
δ''_{tab}	tab deflection normal to the section basic-loading center-of-pressure line, deg
$\bar{\epsilon}_h$	average downwash across the horizontal tail, deg
η	semispan station, $\frac{2y}{b_h}$
η_i, η_o	semispan station of the inboard and outboard end of the tab, respectively
$\bar{\eta}$	semispan station of the tail mean aerodynamic chord
$\Delta\eta$	increment of spanwise distance as a ratio of the tail semispan
η_f	spanwise length of the flap (tab) from the plane of symmetry as a ratio of tail semispan
Λ_b	sweep of the section basic-loading center-of-pressure line, deg
$\Lambda_{c/4}$	sweep of the tail quarter-chord line, deg
Λ_{hl}	sweep of the tab hinge line, deg
$\Lambda_\beta = \tan^{-1} \left(\frac{\tan \Lambda_{c/4}}{\beta} \right)$, deg	
λ	horizontal-tail taper ratio

TABLE 4. 14. 1-1

LIFT CHARACTERISTICS OF HORIZONTAL TAIL ALONE IN THE PRESENCE OF THE BODY AS A FUNCTION OF α_h AND δ_e , WITH TAB GEARED IN RATIO OF $\frac{\delta_{tab}}{\delta_e} = 1.5$

(a) Linear range (referenced to S_h)

$$\begin{aligned}\bar{C}_{Lh(f)} &= (C_{Lh(f)})_{\delta_{tab}=0} + (\Delta C_L)_{\delta_{tab}} \\ &= \left\{ (C_{L\alpha})_{h_e} \alpha_h K_{h(f)} \frac{S_{h_e}}{S_h} + \left[(C_{L\alpha})_{h_e} k_{h(f)} \frac{S_{h_e}}{S_h} + C_{L\delta_{tab}} \left(\frac{\delta_{tab}}{\delta_e} \right) \right] \delta_e \right\} \frac{\bar{q}_h}{\bar{q}_\infty}\end{aligned}$$

Symbol	Description	Reference	Magnitude
$(C_{L\alpha})_{h_e}$	Lift-curve slope of exposed horizontal-tail panels, per deg	Table 4.2-1	0.0700
S_{h_e}	Area of exposed horizontal-tail panels, sq ft	Table 3.2-1	28.73
S_h	Reference horizontal-tail area, sq ft	Table 3.2-1	32.5
$K_{h(f)}$	Ratio of lift on tail in presence of fuselage to tail alone	Table 4.10-1	1.075
$k_{h(f)}$	Ratio of lift on movable tail in presence of fuselage to tail alone	Table 4.13.1-1(b)	.96
$\frac{\delta_{tab}}{\delta_e}$	Gearing ratio of tab to elevator	-----	1.5
$C_{L\delta_{tab}}$	Lift effectiveness of tab, referenced to S_h , per deg: for $\delta_{tab} = 6^\circ, 0^\circ, -7.5^\circ$ $\delta_{tab} = -15^\circ$ $\delta_{tab} = -21^\circ$	Table 4.13.1-1(c) Table 4.13.1-1(c) Table 4.13.1-1(c)	.0279 .0273 .0231
Summary: For $\delta_e = 4^\circ, 0^\circ, -5^\circ$: $\bar{C}_{Lh(f)} = (0.0665\alpha_h + 0.1013\delta_e) \frac{\bar{q}_h}{\bar{q}_\infty}$ $\delta_e = -10^\circ$: $\bar{C}_{Lh(f)} = (0.0665\alpha_h + 0.1004\delta_e) \frac{\bar{q}_h}{\bar{q}_\infty}$ $\delta_e = -14^\circ$: $\bar{C}_{Lh(f)} = (0.0665\alpha_h + 0.0941\delta_e) \frac{\bar{q}_h}{\bar{q}_\infty}$			

(b) $(\bar{C}_{Lmax})_{h(f)}$ (referenced to S_h)

Symbol	Description	Reference	Magnitude
$[(\alpha C_{Lmax})_{h(f)}]_{\delta_{tab}=0}$	Horizontal-tail angle of attack at $(\bar{C}_{Lmax})_{h(f)}$ with $\delta_{tab}=0^\circ$, deg	Table 4.13.2-1(a)	± 14.45

δ_e , deg	$\delta_{tab} = 1.5\delta_e$	$(\bar{C}_{Lmax})_{h(f)}$, from table 4.13.2-1(b)	$(\bar{C}_{Lmax})_{h(f)} = (\bar{C}_{Lmax})_{h(f)} \frac{S_{h_e}}{S_h}$
4	6	-0.816	-0.721
0	0	-.926	-.819
-5	-7.5	-1.064	-.941
-10	-15	-1.182	-1.045
-14	-21	-1.253	-1.108

TABLE 4.14.1-2
PERTINENT RELATIONS FOR HORIZONTAL-TAIL HINGE MOMENTS

(a) Pertinent parameters

Symbol	Description	Reference	Magnitude
M	Mach number	Wind-tunnel Mach number	0.083
β	$\sqrt{1 - M^2}$	-----	.997
b_h	Horizontal-tail span, ft	Table 3.2-1	12.5
A	Horizontal-tail aspect ratio	Table 3.2-1	4.8
λ	Horizontal-tail taper ratio	Table 3.2-1	.515
S_h	Horizontal-tail area, sq ft	Table 3.2-1	32.5
\bar{c}_h	Horizontal-tail mean aerodynamic chord, ft	Table 3.2-1	2.704
$y_{\bar{c}_h}$	Lateral position of \bar{c}_h , ft	Table 3.2-1	2.758
x_{ac_h}	Aerodynamic center relative to leading edge of mean aerodynamic chord	Table 4.5-1	.25 \bar{c}_h
$(x_{hinge} - x_{ac})_h$	Distance between aerodynamic center of mean aerodynamic chord and hinge line, in.	Figure 3.2-2	1.17
$(x_{hinge} - x_{\bar{c}/4})_h$	Distance between quarter chord of mean aerodynamic chord and hinge line, in.	Figure 3.2-2	1.17
$(c_h)_{av}$	$\frac{S_h}{b_h}$	-----	2.60
$\left(\frac{c_{tab}}{c_h}\right)_\eta$	Ratio of tab chord to tail chord	Figure 3.2-2	.18
$\frac{(x_{hinge} - x_{ac})_h}{\bar{c}_h}$	-----	-----	.0361
$\frac{(x_{hinge} - x_{\bar{c}/4})_h}{\bar{c}_h}$	-----	-----	.0361
$\frac{2y_{\bar{c}_h}}{b_h}$	-----	-----	.441
$\Lambda_{c/4}$	Sweep of quarter-chord line of horizontal tail, deg	Table 3.2-1	8.0
Λ_{hl}	Sweep of tab hinge line, deg	Figure 3.2-2	0
$\frac{(x_{cp})_b}{c_h}$	Chordwise center-of-pressure position of basic loading due to tab deflection	Figure 4.14.1-5	.66
Λ_b	Sweep of $(x_{cp})_b$ chordline = $\tan^{-1} \left\{ \tan \Lambda_{c/4} - \frac{4}{A} \left[\frac{(x_{cp})_b}{c_h} - 0.25 \right] \left(\frac{1-\lambda}{1+\lambda} \right) \right\}$, deg	Equation (4.14.1-10)	1.8
δ_{tab}	Tab deflection in plane normal to tab hinge line, deg	-----	-----
δ'_{tab}	Tab deflection in streamwise plane = $\tan^{-1} (\cos \Lambda_{hl} \tan \delta_{tab})$	Equation (4.14.1-7)	δ_{tab}
δ''_{tab}	Tab deflection in plane normal to $(x_{cp})_b = \tan^{-1} \left(\frac{\cos \Lambda_{hl} \tan \delta_{tab}}{\cos \Lambda_b} \right)$	Equation (4.14.1-13)	$\approx \delta_{tab}$
k	$\frac{c_l \alpha}{2\pi}$	Table 4.2-1	0.995
$(\alpha_\delta)_{c_l}$	$-\frac{c_l \delta_{tab}}{(c_l \alpha)_h}$	Table 4.13.1-1(c)	$\left. \begin{array}{l} -.485 \text{ for } \delta_{tab} = 6^\circ, 0^\circ, -7.5^\circ \\ -.475 \text{ for } \delta_{tab} = -15^\circ \\ -.403 \text{ for } \delta_{tab} = -21^\circ \end{array} \right\}$
λ	Horizontal-tail taper ratio	Table 3.2-1	0.515
$\frac{\beta A}{k}$	Design parameter for span-load distribution	-----	4.81
Λ_β	Design parameter for span-load distribution = $\tan^{-1} \left(\frac{\tan \Lambda_{c/4}}{\beta} \right)$, deg	-----	8.02
$\left(\Delta \frac{G}{\delta}\right)_\eta$	Spanwise loading coefficient due to tab deflection	Figure 4.14.1-2	See figure 4.14.1-9
$(c_{l_\Lambda})_\eta$	Incremental section lift coefficient	Equation (4.14.1-6)	See part (b)
$(c_{l_\Lambda=0})_\eta$	$(c_{l_\Lambda})_\eta$ referred to basic load line = $\frac{(c_{l_\Lambda})_\eta}{\cos^2 \Lambda_b}$	Equation (4.14.1-9)	$\approx (c_{l_\Lambda})_\eta$
For general reference - $c_{m\delta''_{tab}}$	$= -\frac{2}{57.3} \sqrt{\left(\frac{c_{tab}}{c_h}\right)_\eta} \left[\left(1 - \frac{c_{tab}}{c_h}\right)_\eta \right]^3$, per deg, based on lifting-line theory	Equation (4.14.1-12)	-0.0110

TABLE 4.14.1-2 (Concluded)

(b) Increment section lift coefficient $(c_{l\Lambda})_\eta$

$$\begin{aligned}
 (c_{l\Lambda})_\eta &= \frac{2b_h}{57.3(c_h)_\eta} \left(\frac{\Delta G}{\delta} \right) (\alpha_\delta)_{c_l} \delta'_{\text{tab}} & (4.14.1-6) \\
 &\approx 0.212 \left(\frac{\Delta G}{\delta} \right)_\eta \frac{\delta_{\text{tab}}}{(c_h)_\eta} \quad \text{for } \delta_{\text{tab}} = 6^\circ, -7.5^\circ \quad (\text{used in analysis}) \\
 &\approx 0.207 \left(\frac{\Delta G}{\delta} \right)_\eta \frac{\delta_{\text{tab}}}{(c_h)_\eta} \quad \text{for } \delta_{\text{tab}} = -15^\circ \quad (\text{used in analysis}) \\
 &\approx 0.176 \left(\frac{\Delta G}{\delta} \right)_\eta \frac{\delta_{\text{tab}}}{(c_h)_\eta} \quad \text{for } \delta_{\text{tab}} = -21^\circ
 \end{aligned}$$

(c) Chordwise center of pressure $(x_{cp})_\eta$ at increment section

For semispan stations included in the tabbed portion,

$$\left(\frac{x_{cp}}{c_h} \right)_\eta = 0.25 - \frac{(\Delta c_{mf})_\eta}{(c_{l\Lambda=0})_\eta} \quad (4.14.1-8)$$

where, from figure 4.14.1-7 (for $\frac{cf}{c_h} = 0.18$),

$$\begin{array}{cccc}
 \delta_{\text{tab}} & 6^\circ & -7.5^\circ & -15^\circ & -21^\circ \\
 \Delta c_{mf} & -0.060 & 0.070 & 0.125 & 0.160
 \end{array}$$

For semispan stations adjacent to and within $\Delta\eta = 0.20$ from the ends of the tabs,

$$\left(\frac{x_{cp}}{c_h} \right)_\eta = 0.25 - K \left[\frac{(\Delta c_{mf})_\eta}{(c_{l\Lambda=0})_\eta} \right]_{\text{edge of tab}} \quad (4.14.1-14)$$

where K is obtained from figure 4.14.1-8

(d) Chordwise center of pressure of increment section lift coefficient relative to quarter chord of tail mean aerodynamic chord

$$\begin{aligned}
 \left(\frac{x}{c_h} \right)_\eta &= (\eta - \bar{\eta}) \frac{b_h}{c_h} \tan \Lambda_{c/4} + \frac{(c_h)_\eta}{c_h} \left[\left(\frac{x_{cp}}{c_h} \right)_\eta - 0.25 \right] \\
 &= 0.325 (\eta - 0.441) + \frac{(c_h)_\eta}{2.704} \left[\left(\frac{x_{cp}}{c_h} \right)_\eta - 0.25 \right]
 \end{aligned} \quad (4.14.1-15)$$

(e) Pitching moment about the quarter chord of the tail mean aerodynamic chord due to tab deflection

$$\begin{aligned}
 (\Delta C'_m)_{\delta_{\text{tab}}} &= - \int_0^{1.0} (c_{l\Lambda})_\eta \frac{(c_h)_\eta}{(c_h)_{\text{av}}} \left(\frac{x}{c_h} \right)_\eta d\eta \\
 &= - \int_0^{1.0} (c_{l\Lambda})_\eta \frac{(c_h)_\eta}{2.60} \left(\frac{x}{c_h} \right)_\eta d\eta \quad \left(\text{referenced to } S_h = 32.5 \text{ sq ft and } \frac{\bar{q}_h}{\bar{q}_\infty} = 1.0 \right)
 \end{aligned} \quad (4.14.1-16)$$

(f) Hinge-moment coefficient of the horizontal tail

$$\begin{aligned}
 C_{h(f)} &= (C_{Lh(f)})_{\delta_{\text{tab}}=0} \frac{(x_{\text{hinge}} - x_{ac})_h}{\bar{c}_h} + (\Delta C_L)_{\delta_{\text{tab}}} \frac{(x_{\text{hinge}} - x_{c/4})_h}{\bar{c}_h} + (\Delta C'_m)_{\delta_{\text{tab}}} \\
 &= 0.0361 \left[(C_{Lh(f)})_{\delta_{\text{tab}}=0} + (\Delta C_L)_{\delta_{\text{tab}}} \right] + (\Delta C'_m)_{\delta_{\text{tab}}} \\
 &= 0.0361 \bar{C}_{Lh(f)} + (\Delta C'_m)_{\delta_{\text{tab}}} \quad \left(\text{referenced to } S_h = 32.5 \text{ sq ft and } \frac{\bar{q}_h}{\bar{q}_\infty} = 1.0 \right)
 \end{aligned} \quad (4.14.1-17)$$

where

 $\bar{C}_{Lh(f)}$ is obtained from figure 4.14.1-1

TABLE 4.14.1-3
HORIZONTAL-TAIL TAB CHARACTERISTICS

①	②	③	Increment section lift coefficient		Chordwise center-of-pressure location									
			④		⑤		⑥		⑦		⑧			
			Table 4.14.1-2 (b)		Table 4.14.1-2 (c)		Figure 4.14.1-8		Table 4.14.1-2 (c)		-----			
η , semispan station	$(c_h)_\eta$, local chord, ft	$\left(\frac{G}{S}\right)_\eta$, spanwise loading coefficient	$(c_{L_{A=0}})_\eta \approx (c_{L_N})_\eta = c_{L_1} \frac{\delta_{tab}}{\eta}$		$\left(\frac{x_{cp}}{c_h}\right)_\eta = 0.25 \frac{(\Delta c_{mf})_\eta}{(c_{L_{A=0}})_\eta}$		K		$\left(\frac{x_{cp}}{c_h}\right)_\eta =$ $0.25 - \textcircled{6} \left[\frac{(\Delta c_{mf})_\eta}{4} \right]$ at η_0		$\left(\frac{x_{cp}}{c_h}\right)_\eta$ summary = $\textcircled{5} + \textcircled{7}$			
			c_{L_1}		Δc_{mf}									
			δ_{tab} , deg		δ_{tab} , deg				δ_{tab} , deg		δ_{tab} , deg			
			6	-7.5	-15	-21	6	-7.5	-15	-21	6	-7.5	-15	-21
			0.207 .2068	-0.2509 -.2586	-0.4900 -.5049	-0.5832 -.6010	0.5490 .5401	0.5290 .5207	0.5051 .4976	0.5243 .5162	0.5490 .5401	0.5290 .5207	0.5051 .4976	0.5243 .5162
0.2	3.13	0.519	0.2109	-0.2636	-0.5149	-0.6129	0.5345	0.5156	0.4928	0.5111	0.5345	0.5156	0.4928	0.5111
0.3	2.93	.498	.2162	-.2702	-.5277	-.6282	.5275	.5091	.4869	.5047	.5275	.5091	.4869	.5047
0.4	2.78	0.473	0.2164	-0.2705	-0.5283	-0.6289	0.5273	0.5088	0.4866	0.5044	0.5273	0.5088	0.4866	0.5044
0.5	2.60	.437	.2138	-.2672	-.5219	-.6212	.5306	.5120	.4895	.5076	.5306	.5120	.4895	.5076
0.6	2.43	0.392	0.2052	-0.2565	-0.5009	-0.5962	0.5424	0.5229	0.4996	0.5184	0.5424	0.5229	0.4996	0.5184
0.7	2.25	.343	.1939	-.2424	-.4733	-.5634	.5594	.5388	.5141	.5340	.5594	.5388	.5141	.5340
$\eta_0 = 0.79$	2.10	0.288	0.1744	-0.2181	-0.4258	-0.5069	0.5390	0.5170	0.5436	0.5656	0.5390	0.5170	0.5436	0.5656
0.8	2.08	.282	-----	-----	-----	-----	-----	-----	-----	-----	0.5899	0.5661	0.5392	0.5609
0.9	1.92	0.160	-----	-----	-----	-----	-----	-----	-----	-----	0.3429	0.3367	0.3293	0.3352
1.0	1.78	0	-----	-----	-----	-----	-----	-----	-----	-----	.2500	.2500	.2500	.2500

^a $c_{L_1} = \frac{2b_h}{57.3} \left(\frac{G}{S}\right)_{c_1}$ with values for b_h and $(G/S)_{c_1}$ obtained from table 4.14.1-2 (c).

^bValues used in computing $\left(\frac{x_{cp}}{c_h}\right)_\eta$ in column 7 for stations adjacent to and outboard of η_0 .

TABLE 4.14.1-3 (Concluded)

Pitching moment due to tab deflection about quarter chord of tail mean aerodynamic chord ^a , $(\Delta C'_m)_{\delta_{tab}}$																
①	⑨	⑩	⑪	⑫	⑬	⑭										
-----	-----	-----	Table 4.14.1-2(d)													
η , semispan station	$\frac{(c_h)_{\eta}}{(c_h)_{av}} = \frac{(c_h)_{\eta}}{\bar{c}_h}$ ②/2.60	$\frac{(c_h)_{\eta}}{\bar{c}_h} \left[\left(\frac{x_{cp}}{\bar{c}_h} \right) - 0.25 \right] =$ ⑩ [⑧ - 0.25]	$.325(\eta - .441) =$ $.325 (1 - .441)$	$\left(\frac{x}{\bar{c}_h} \right)_{\eta} = ⑪ + ⑫$	$-(c'_{L_A})_{\eta} \frac{(c_h)_{\eta}}{(c_h)_{av}} \left(\frac{x}{\bar{c}_h} \right) \Delta \eta =$ $-(4) \times (9) \times (13) \times (0.1)$	$\delta_{tab}, \text{ deg}$										
							$\delta_{tab}, \text{ deg}$	$\delta_{tab}, \text{ deg}$								
								6	-7.5	-15	-21	6	-7.5	-15	-21	
								$\eta_1 = 0$	1.3308	1.2796	-0.1433	0.3826	0.3570	0.3264	0.3510	0.2393
.1	1.2654	1.2167	-.1108	.3530	.3294	.3013	.3239	.2422	.2186	.1905	.2131	-.00634	.00715	.01217	.01621	
.2	1.2038	1.1575	-0.0783	0.3293	0.3074	0.2810	0.3022	0.2510	0.2291	0.2027	0.2239	-0.00637	0.00727	0.01256	0.01652	
.3	1.1269	1.0836	-.0458	.3007	.2808	.2567	.2760	.2549	.2350	.2109	.2302	-.00621	.00716	.01254	.01630	
.4	1.0692	1.0281	-0.0133	0.2851	0.2661	0.2432	0.2615	0.2718	0.2528	0.2299	0.2482	-0.00629	0.00731	0.01299	0.01669	
.5	1.0000	.9615	.0192	.2698	.2519	.2303	.2477	.2890	.2711	.2495	.2669	-.00618	.00724	.01302	.01658	
.6	0.9346	0.8987	0.0517	0.2628	0.2453	0.2243	0.2412	0.3145	0.2970	0.2760	0.2929	-0.00603	0.00712	0.01292	0.01632	
.7	.8654	.8321	.0842	.2575	.2403	.2198	.2363	.3417	.3245	.3040	.3205	-.00573	.00681	.01245	.01563	
$\eta_0 = 0.79$	0.8077	0.7766	0.1134	-----	-----	-----	-----	-----	-----	-----	-----	-----	-----	-----	-----	
	.8000	.7692	.1167	0.2615	0.2431	0.2225	0.2391	0.3782	0.3598	0.3392	0.3558	-0.00522	0.00621	0.01142	0.01426	
.9	0.7385	0.7101	0.1492	0.0660	0.0616	0.0563	0.0605	0.2152	0.2108	0.2055	0.2087	-0.00168	0.00206	0.00393	0.00477	
1.0	.6846	.6583	.1817	0	0	0	0	.1817	.1817	.1817	.1817	0	0	0	0	
$(\Delta C'_m)_{\delta_{tab}} = \sum ⑭ =$													-0.05644	0.06547	0.11594	0.14940
*Referenced to $S_h = 32.5$ sq ft and $\dot{q}_h/\dot{q}_w = 1$.																

TABLE 4.14.1-4
HORIZONTAL-TAIL HINGE-MOMENT CHARACTERISTICS
[Tab geared to elevator in ratio of $\frac{\delta_{\text{tab}}}{\delta_e} = 1.5$]

①	②	③	④					⑤					⑥				
-----	Table 4.10-2	Table 4.9.2-2(b)	Figure 4.14.1-1					Table 4.14.1-2(f)					Table 4.14.1-3				
α_b , deg	$\alpha_h =$ $\alpha_b - \bar{\delta}_h$, deg	$\frac{\bar{q}_h}{\bar{q}_\infty}$	$\bar{C}_{Lh(f)}$ referenced to $S_h = 32.5$ sq ft and $\frac{\bar{q}_h}{\bar{q}_e} = 1.0$					$0.0361 \bar{C}_{Lh(f)} = 0.0361$ ④					$(\Delta C'_m)_{\delta_{tab}}$				
			δ_e , deg					δ_e , deg					δ_e , deg				
			4	0	-5	-10	-14	4	0	-5	-10	-14	4	0	-5	-10	-14
			δ_{tab} , deg					δ_{tab} , deg					δ_{tab} , deg				
			6	0	-7.5	-15	-21	6	0	-7.5	-15	-21	6	0	-7.5	-15	-21
-4	-4.00	1.00	0.135	-0.267	-0.775	-0.935	-----	0.00487	-0.00964	-0.02798	-0.03375	-----	-0.05644	0	0.06547	0.11594	0.14940
-2	-2.96	1.00	.205	-.197	-.704	-1.050	-----	.00740	-.00711	-.02541	-.03790	-----	-.05644	0	.06547	.11594	.14940
0	-1.90	1.00	0.277	-0.175	-0.632	-1.036	-0.851	0.01000	-0.00632	-0.02282	-0.03710	-0.03072	-0.05644	0	0.06547	0.11594	0.14940
2	-.93	1.00	.340	-.061	-.569	-1.012	-.895	.01227	-.00220	-.02054	-.03653	-.03231	-.05644	0	.06547	.11594	.14940
4	0.13	1.00	0.413	0.011	-0.495	-0.976	-1.049	0.01491	0.00040	-0.01787	-0.03523	-0.03787	-0.05644	0	0.06547	0.11594	0.14940
6	1.14	1.00	.480	.078	-.429	-.927	-1.100	.01733	.00282	-.01549	-.03346	-.03971	-.05644	0	.06547	.11594	.14940
8	2.23	1.00	0.553	0.151	-0.357	-0.858	-1.090	0.01996	0.00545	-0.01289	-0.03097	-0.03935	-0.05644	0	0.06547	0.11594	0.14940
10	3.39	1.00	.630	.230	-.280	-.782	-1.060	.02274	.00830	-.01011	-.02823	-.03827	-.05644	0	.06547	.11594	.14940
12	4.45	1.00	0.700	0.299	-0.208	-0.711	-1.014	0.02527	0.01079	-0.00751	-0.02567	-0.03661	-0.05644	0	0.06547	0.11594	0.14940
*13.8	5.50	1.00	.768	.368	-.138	-.633	-.951	.02772	.01328	-.00498	-.02285	-.03438	-.05644	0	.06547	.11594	.14940

Denotes tail to be in nonlinear region of its lift-curve slope on basis of figure 4.14.1-1.

①	⑦					⑧				
-----	Table 4.14.1-2(f)					-----				
α_b , deg	$C_{hh(f)} = ⑤ + ⑥$ with $\frac{\bar{q}_h}{\bar{q}_e} = 1$					$C_{hh(f)} = ③ \times ⑦$ with $\frac{\bar{q}_h}{\bar{q}_e}$ taken into account				
	δ_e , deg					δ_e , deg				
	4	0	-5	-10	-14	4	0	-5	-10	-14
	δ_{tab} , deg					δ_{tab} , deg				
	6	0	-7.5	-15	-21	6	0	-7.5	-15	-21
-4	-0.0516	-0.0096	0.0375	0.0822	-----	-0.0516	-0.0096	0.0375	0.0822	-----
-2	-.0490	-.0071	.0401	.0780	-----	-.0490	-.0071	.0401	.0780	-----
0	-0.0464	-0.0063	0.0426	0.0785	0.1168	-0.0464	-0.0063	0.0426	0.0785	0.1168
2	-.0442	-.0022	.0449	.0794	.1171	-.0442	-.0022	.0449	.0794	.1171
4	-0.0415	0.0004	0.0476	0.0807	0.1115	-0.0415	0.0004	0.0476	0.0807	0.1115
6	-.0391	.0028	.0500	.0825	.1097	-.0391	.0028	.0500	.0825	.1097
8	-0.0365	0.0054	0.0526	0.0850	0.1101	-0.0365	0.0054	0.0526	0.0850	0.1101
10	-.0337	.0083	.0554	.0877	.1111	-.0337	.0083	.0554	.0877	.1111
12	-0.0312	0.0108	0.0580	0.0903	0.1128	-0.0312	0.0108	0.0580	0.0903	0.1128
*13.8	-.0287	.0133	.0605	.0931	.1151	-.0287	.0133	.0605	.0931	.1151

*Stall of airplane.

Denotes tail to be in nonlinear region of its lift-curve slope on basis of figure 4.14.1-1.

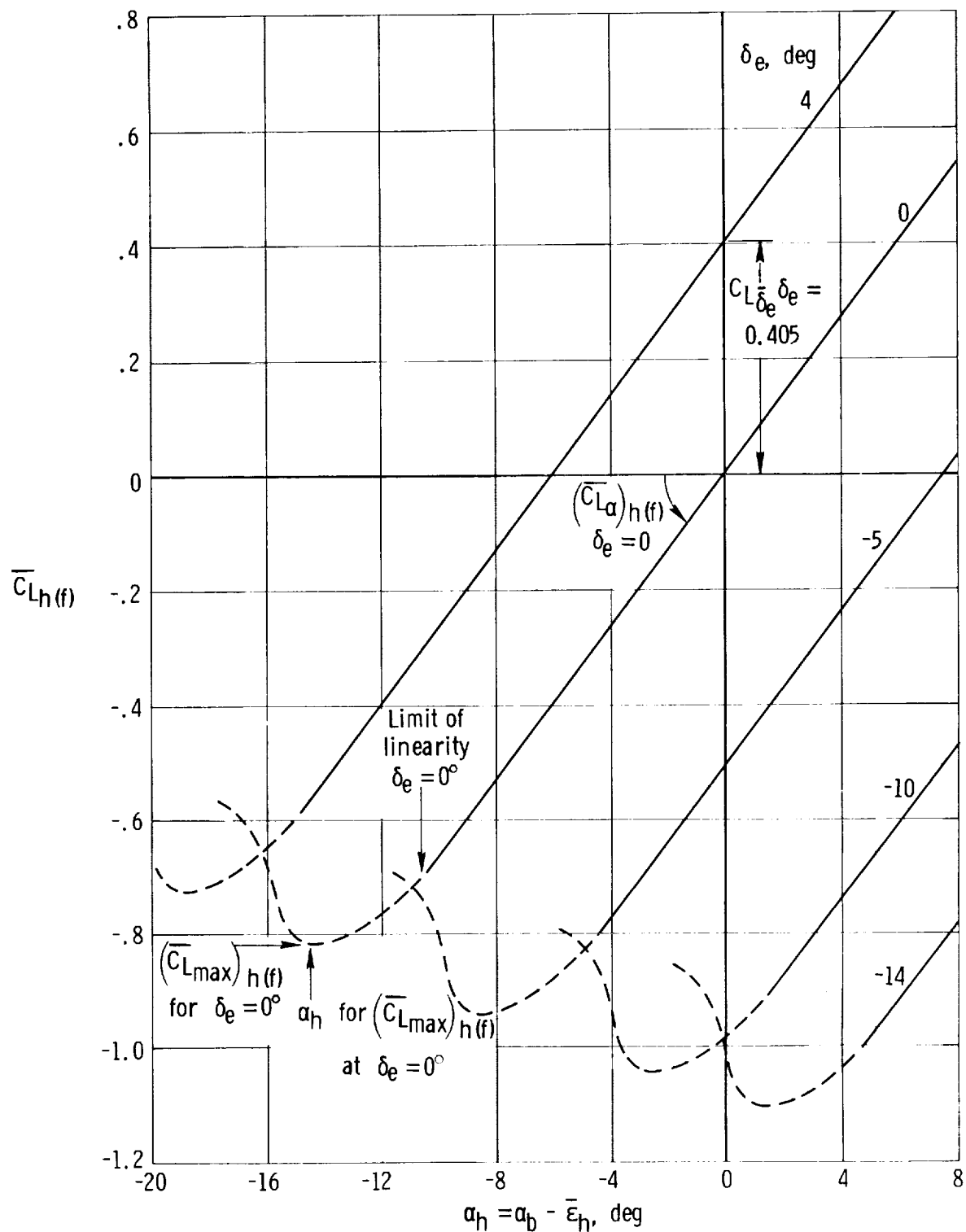
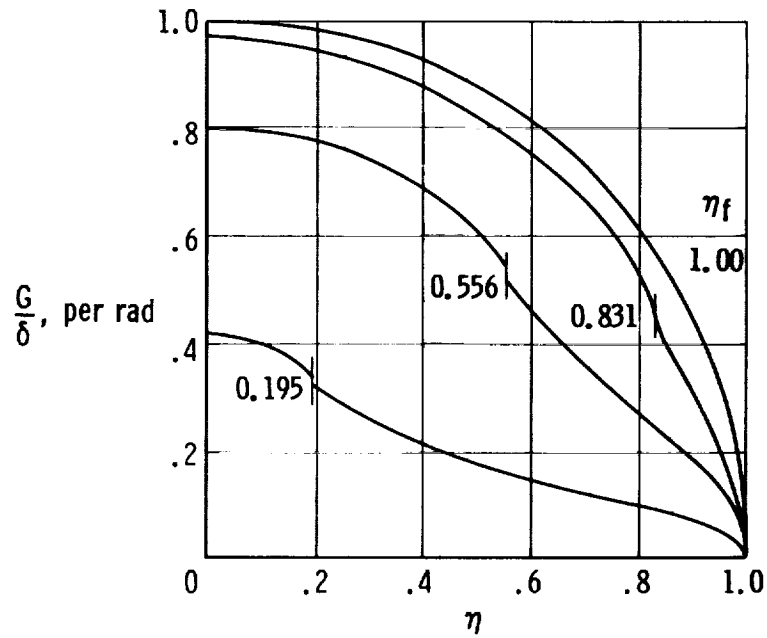
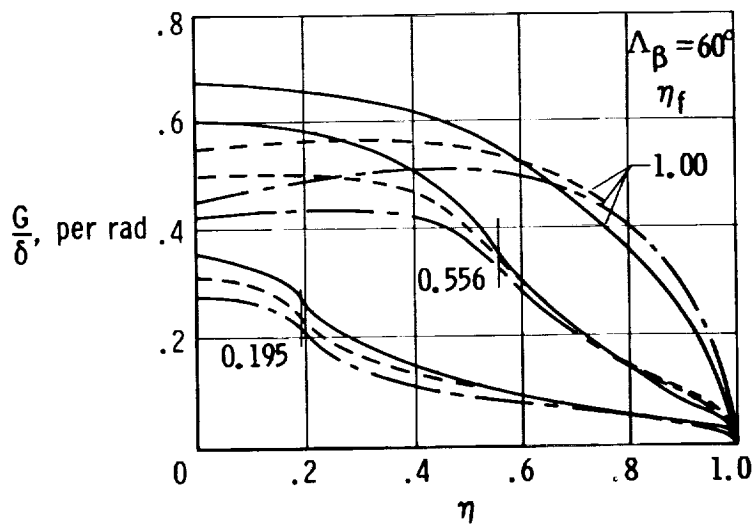
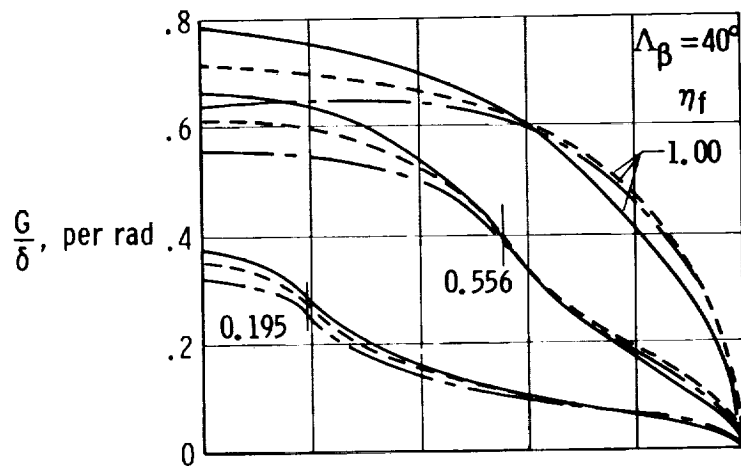
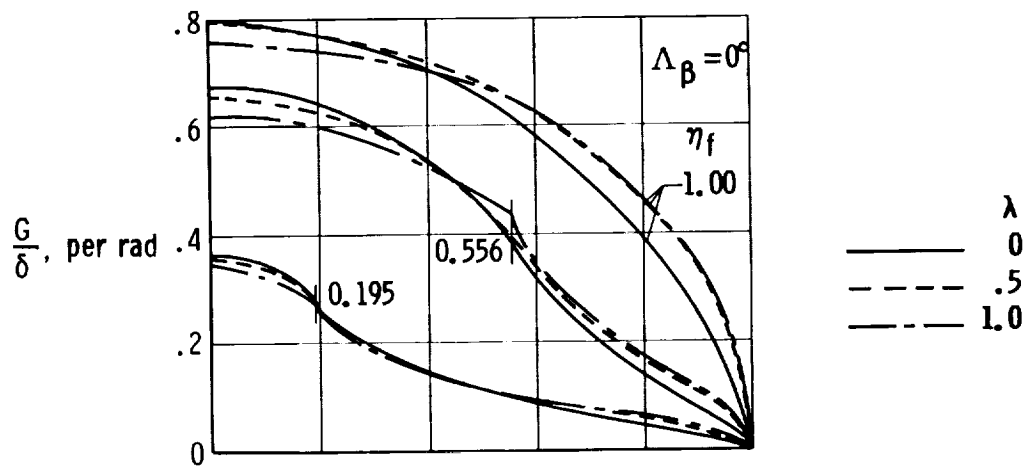


Figure 4.14.1-1. Calculated lift curves of the horizontal tail alone in the presence of the body with tab geared to elevator. $\frac{\delta_{tab}}{\delta_e} = 1.5$; $\frac{\bar{q}_h}{\bar{q}_\infty} = 1.0$; reference area, S_h , 32.5 sq ft.



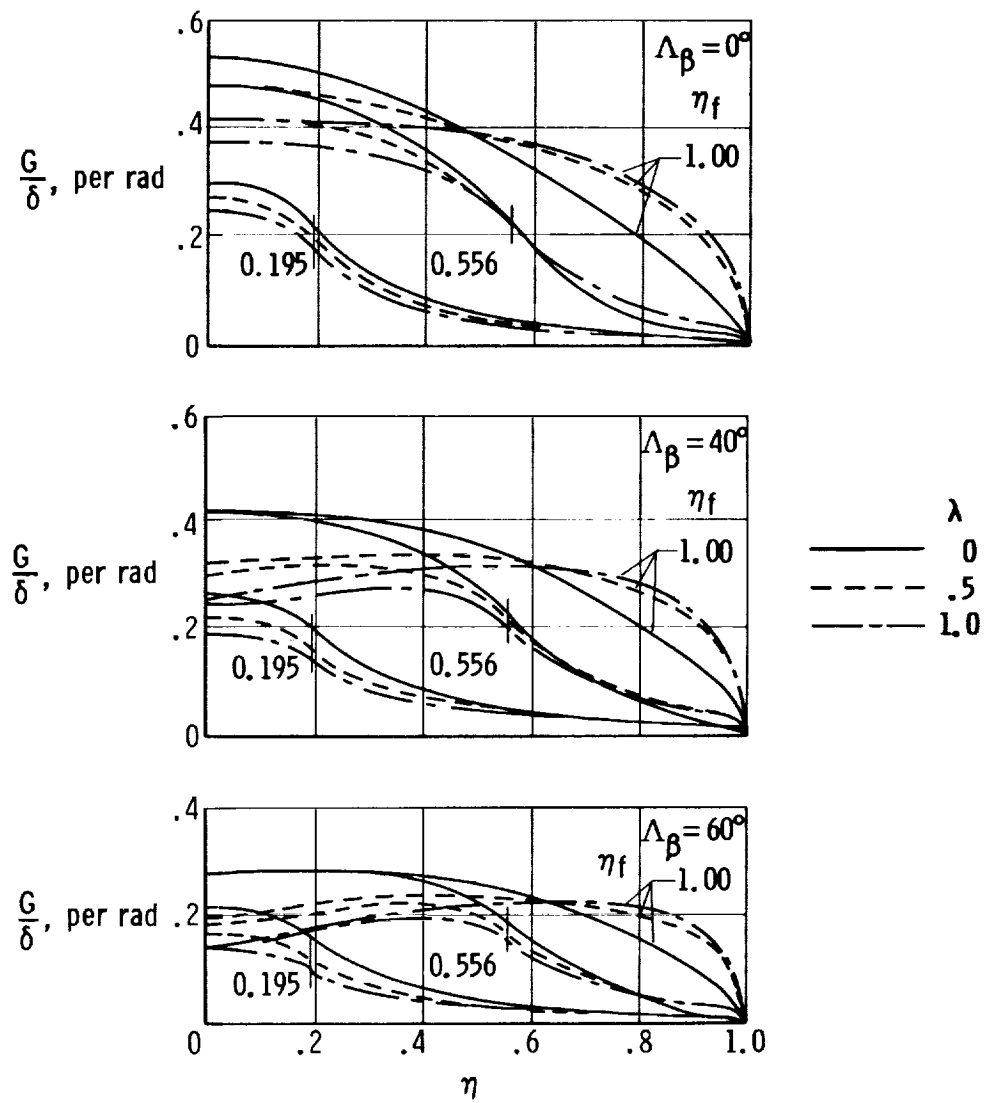
(a) $\frac{\beta A}{k} = 0$; inboard flaps.

Figure 4.14.1-2. Spanwise load distribution due to symmetric flap deflection for straight tapered wing (ref. 32). Subsonic speeds; $\frac{c_f}{c} = 1$.



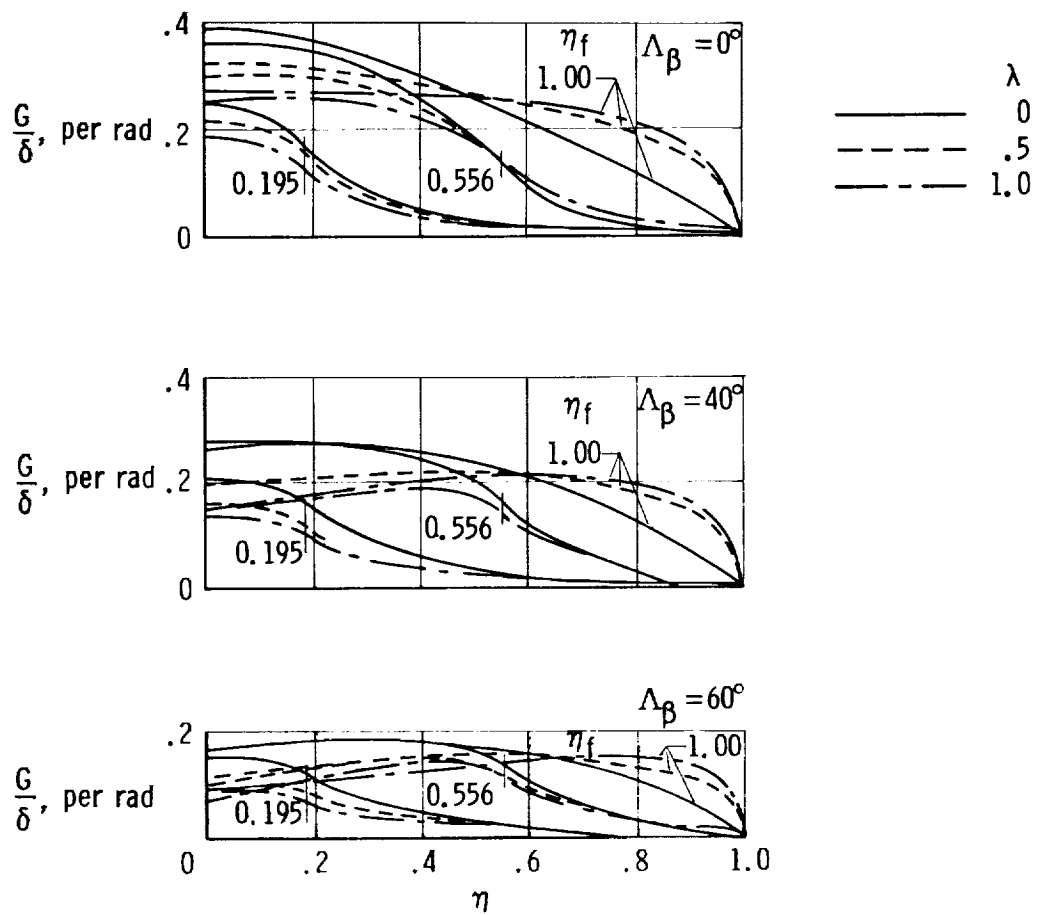
(b) $\frac{\beta A}{k} = 2.0$; inboard flaps.

Figure 4.14.1-2. Continued.



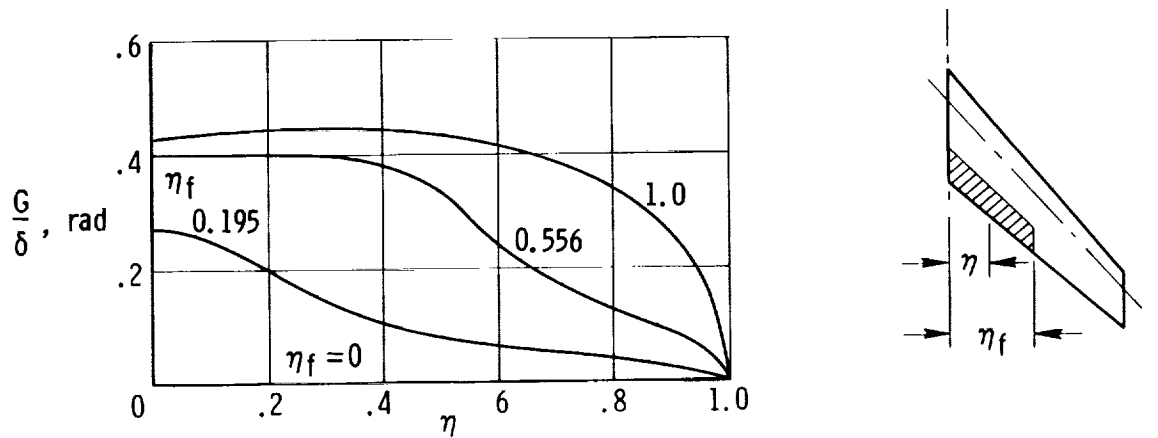
(c) $\frac{\beta A}{k} = 6.0$; inboard flaps.

Figure 4.14.1-2. Continued.

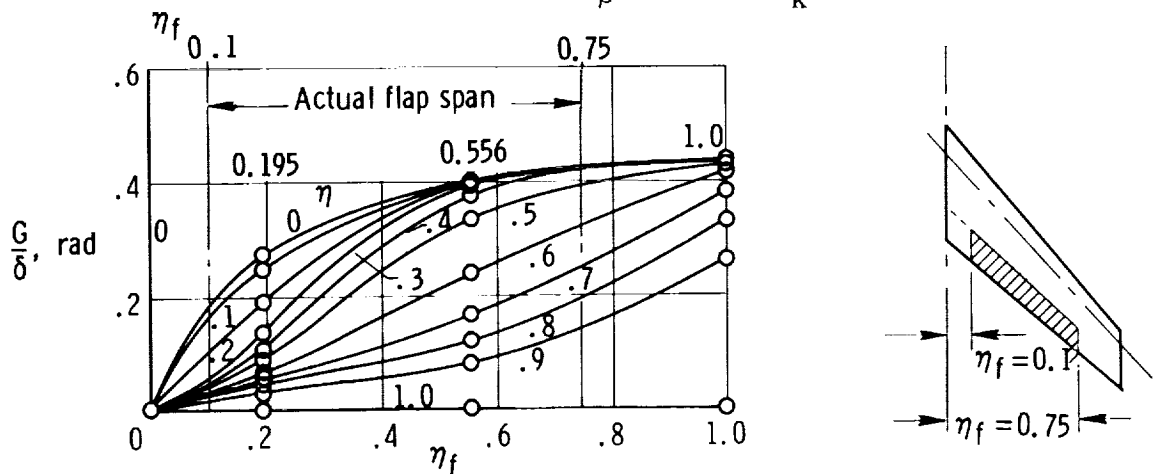


(d) $\frac{\beta A}{k} = 10.0$; inboard flaps.

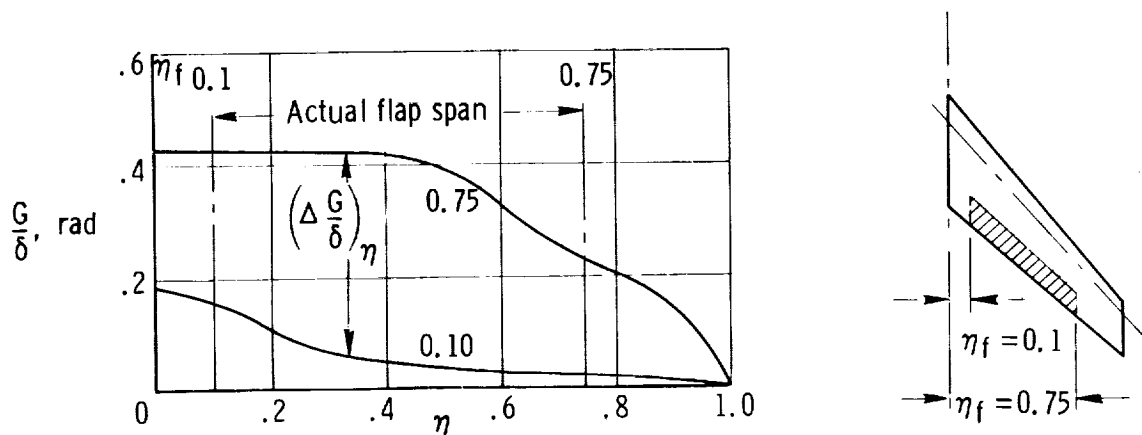
Figure 4.14.1-2. Concluded.



(a) General spanwise load distribution curves reduced to $\frac{\beta A}{k}$, Λ_β , and λ for specific design. $\lambda = 0.586$; $\Lambda_\beta = 47.35^\circ$; $\frac{\beta A}{k} = 3.87$.



(b) Crossplot of (a) to provide variation of loading coefficient with flap span for a specific flap configuration extending from η_f of 0.1 to 0.75.



(c) Variation of spanwise loading coefficient (from (b)) for flap configuration extending from $\eta_f = 0.1$ to 0.75.

Figure 4.14.1-3. Sketches showing reduction of spanwise loading design charts to specific design condition.

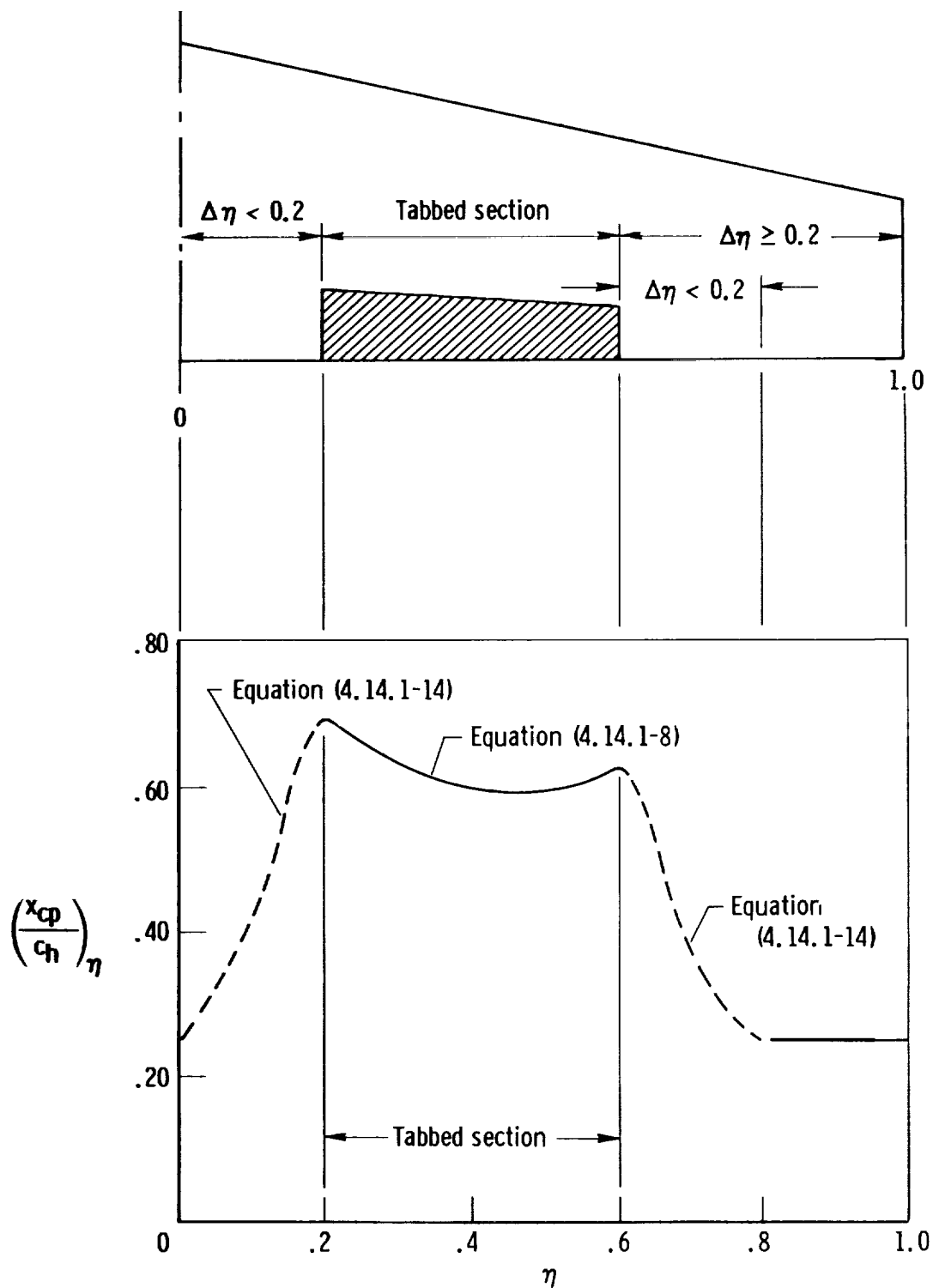


Figure 4.14.1-4. Sketch of typical variation of chordwise center-of-pressure location for stations across semispan.

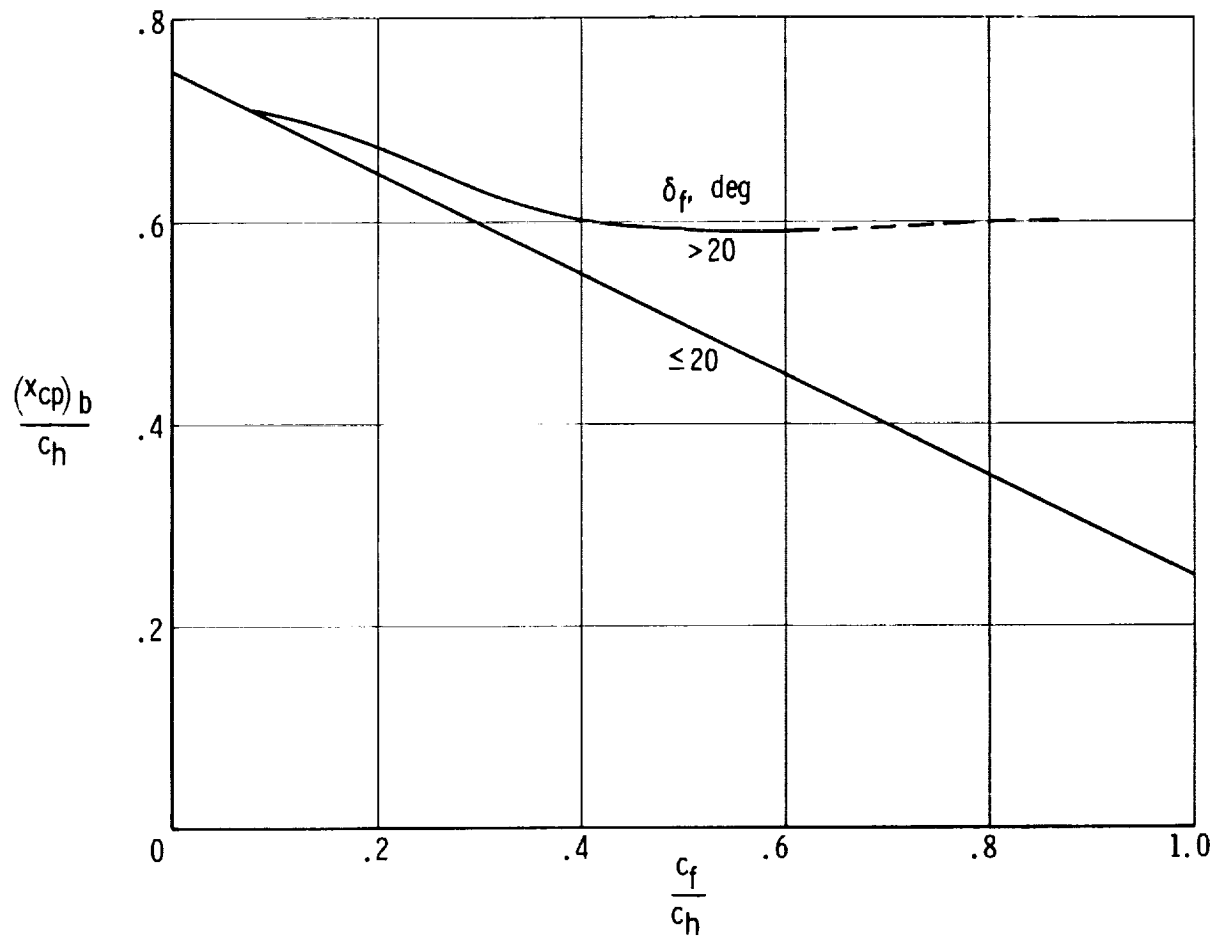


Figure 4.14.1-5. Variation of section-basic-loading center of pressure with flap-chord ratio (ref. 31).

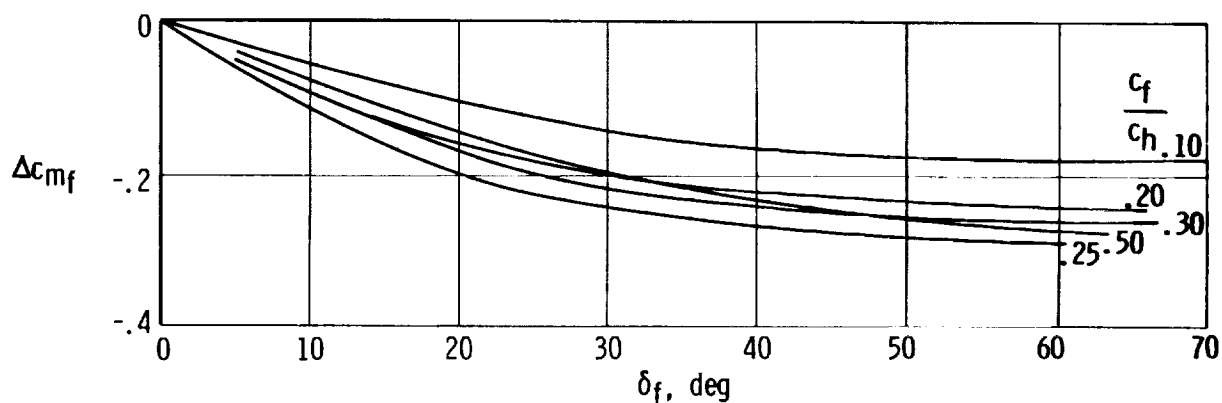


Figure 4.14.1-6. Effect of plain-flap deflection and flap-chord-to-wing-chord ratio on section incremental pitching moment. Based on unpowered-model wind-tunnel data (ref. 1).

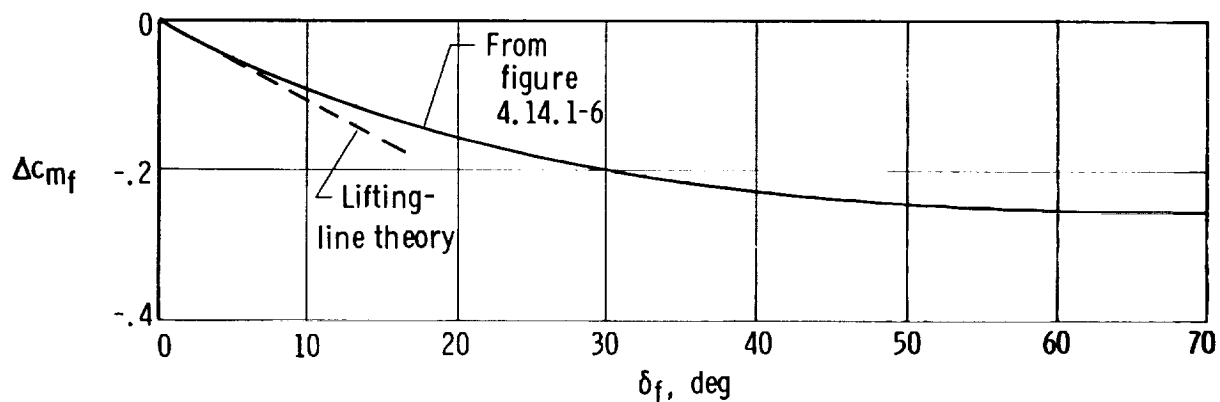


Figure 4.14.1-7. Comparison of effect of plain-flap deflection on section pitching moment calculated by lifting-line theory with empirically determined effects from figure 4.14.1-5 for $\frac{c_f}{c_h} = 0.18$.

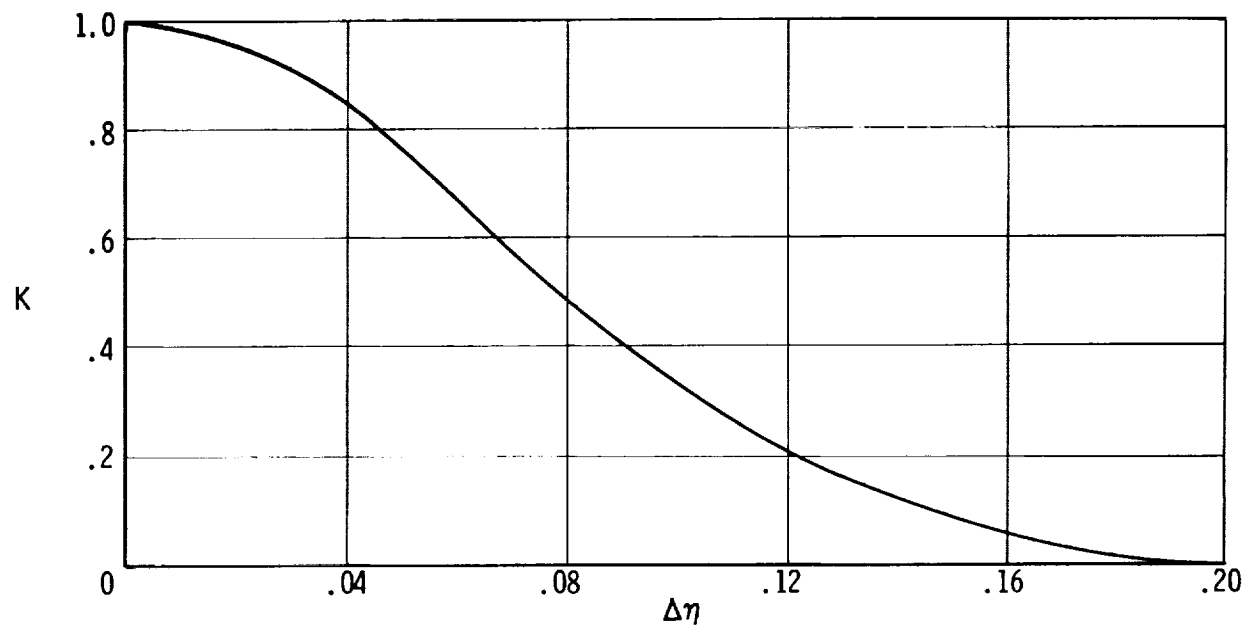


Figure 4. 14. 1-8. Factor for estimation of section center-of-pressure location for unflapped sections near end of flaps (ref. 31). Subsonic speeds.

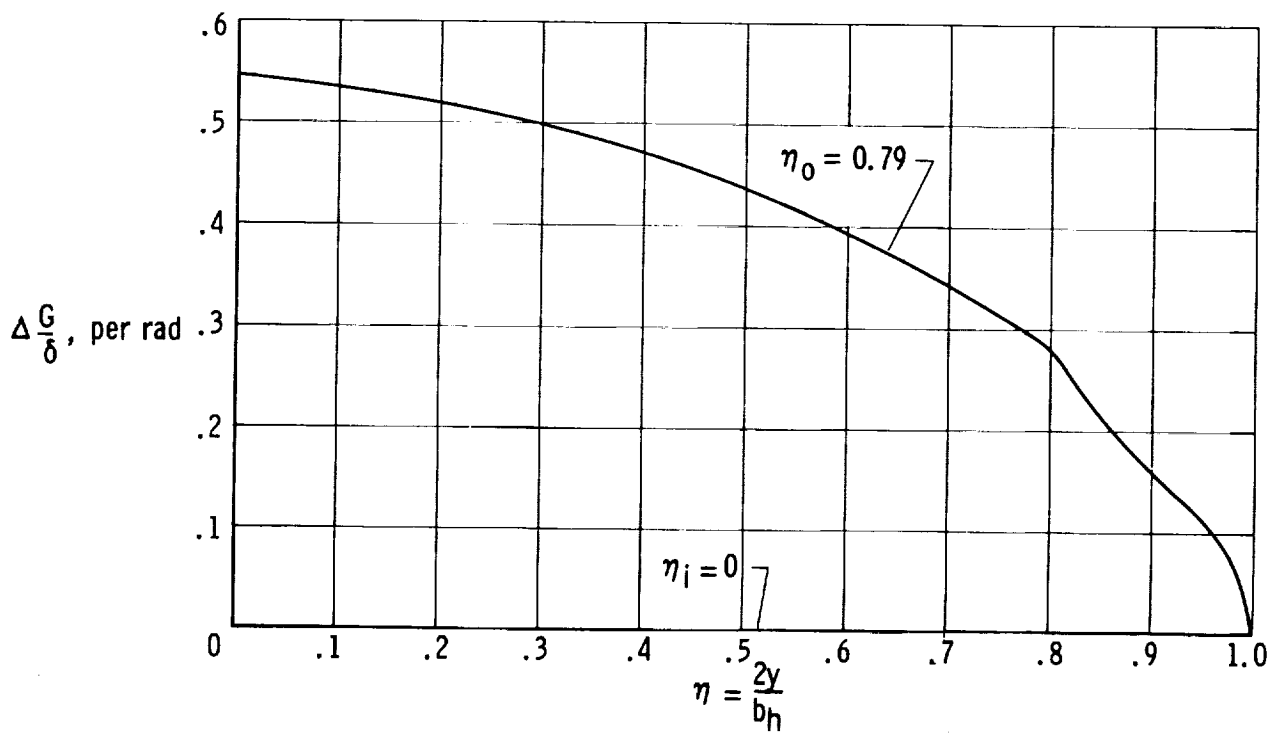


Figure 4.14.1-9. Variation of spanwise loading coefficient due to tab deflection on horizontal tail of subject airplane. $\frac{\beta A}{k} = 4.81$; $\Lambda_\beta = 8.02^\circ$; $\lambda = 0.515$.

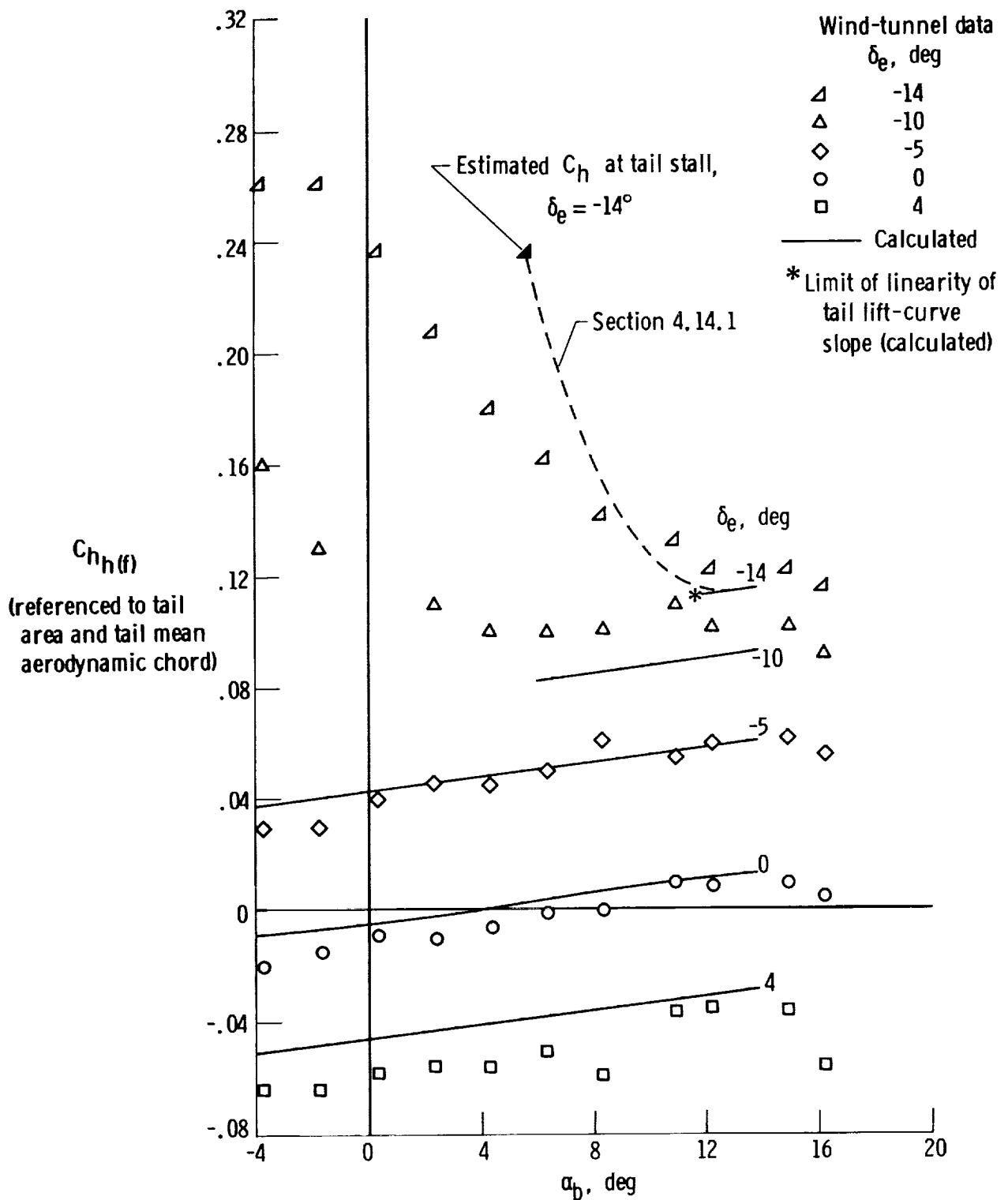


Figure 4.14.1-10. Comparison of calculated and wind-tunnel determined hinge-moment coefficients of the horizontal tail. $\frac{\delta_{tab}}{\delta_e} = 1.5$; wind-tunnel data at $T'_c = 0$ assumed equivalent to propeller-off condition.

5.0 PREDICTION OF POWER-ON AERODYNAMIC CHARACTERISTICS

The effects of power from propeller operation are generally significant on the stability and control characteristics of an airplane. Unfortunately, because the propeller slipstream usually interacts with the flow around several of the airplane components, a number of separate effects must be accounted for. Although some of the effects have been accounted for by theoretical analysis, many are usually estimated by empirical methods.

Successful analytical methods were developed in reference 33 for estimating propeller forces normal to the thrust axis and the effects of slipstream on wing-fuselage characteristics. A successful empirical method was developed in reference 19 for estimating the change in wing lift due to the change in slipstream dynamic pressure on the immersed portion of the wing. Less success has been achieved in providing a general technique to predict the complex changes in flow at the tail. It appears that an empirical technique for predicting power effects on the tail is generally based on experimental data of single-engine airplanes of similar configurations. Attempts to apply the technique to other configurations require some prior knowledge (gained through experience) of the empirical corrections to be applied to the prediction techniques used.

One of the more successful investigations to provide a semiempirical approach to the problem of determining the effects of power on the tail contribution to the stability of single-engine monoplanes is reported in reference 34. Some effects of power on elevator hinge moments are discussed in reference 35.

In the following sections, the effects of power on lift, pitching moments, drag, and elevator hinge moments are considered on the basis of methods presented in reference 1 which are, with some modifications, the methods of reference 19. The method of reference 19, in turn, utilizes the method of reference 33 and refines the method of reference 34. The procedures presented are applied to the subject airplane, sources of discrepancy are identified, and a modification is established for future guidance for similar aircraft.

To facilitate the presentation of nomenclature in the discussion of power effects, immersed surface areas and propeller slipstream are defined in figures 5-1 and 5-2, respectively. Figure 5-1(a) provides surface area definitions for a single-engine airplane, and figure 5-1(b) provides definitions for a two-engine airplane (the subject airplane). These definitions are supplemented by written definitions in section 5.1-3.

5.1 Power Effects on Lift

The effects of the propeller on the lift forces acting on the airplane may be divided into two groups, those due to the propeller forces and those due to the propeller slipstream. On this basis the lift of the airplane may be represented by

$$C_L = C_{L_{\text{prop off}}} + (\Delta C_L)_T + (\Delta C_L)_{N_p} + \overbrace{(\Delta C_L)_{\Delta \bar{q}_w} + (\Delta C_L)_{\epsilon_p}}^{\text{Wing}} + \overbrace{(\Delta C_{L_h})_{\Delta \bar{q}_h} + (\Delta C_{L_h})_{(\Delta \epsilon_h)_{\text{power}}}}^{\text{Horizontal tail}} \quad (5.1-1)$$

where

$(\Delta C_L)_T$ is the lift component of the propeller thrust vector

$(\Delta C_L)_{N_p}$ is the lift component of the propeller normal force, N_p (fig. 5-2)

$(\Delta C_L)_{\Delta \bar{q}_w}$ is the change in lift due to power-induced change in dynamic pressure over the portion of the wing immersed in the propeller slipstreams

$(\Delta C_L)_{\epsilon_p}$ is the change in lift of the immersed portion of the wing due to change in angle of attack of this portion resulting from propeller downwash, ϵ_p , shown in figure 5-2

$(\Delta C_{L_h})_{\Delta \bar{q}_h}$ is the change in lift contribution of the horizontal tail resulting from change in dynamic pressure at the tail due to power

$(\Delta C_{L_h})_{(\Delta \epsilon_h)_{\text{power}}}$ is the change in lift contribution of the horizontal tail resulting from change in downwash at the tail due to power

In the following discussion of power effects on lift, the airplane will be considered initially on the basis of tail-off lift characteristics, followed by horizontal-tail contributions to lift with tail-fuselage interaction effects included. This treatment is represented by the equation

$$C_L = \left[\overbrace{(\Delta C_{L_{\text{wfn}}})_{\text{power}}}^{\substack{\text{Direct propeller} \\ \text{force effects}} + \substack{\text{Propeller slip-} \\ \text{stream effects}}} + \overline{C}_{L_h(\text{hf})} \right] \quad (5.1-2)$$

5.1.1 Tail-Off Lift Characteristics With Power On

The propeller-off, tail-off lift characteristics were considered in section 4.5.

The contribution of the thrust vector to lift is obtained from

$$(\Delta C_L)_T = n (T'_c / \text{prop}) \sin \alpha_T = T'_c \sin \alpha_T \quad (5.1.1-1)$$

where

n is the number of propellers

$$T'_c / \text{prop} = \frac{\text{Thrust/propeller}}{\bar{q}_\infty S_w}$$

α_T is the angle of attack of the thrust axis relative to the free-stream velocity vector

The contribution of the propeller normal force to the lift is obtained from the following equation from reference 19:

$$(\Delta C_L)_{N_p} = n f (C_{N_\alpha})_p \frac{\alpha_p}{57.3} \left(\frac{S_p / \text{prop}}{S_w} \right) \cos \alpha_T \quad (5.1.1-2)$$

where

f is the propeller inflow factor from figure 5.1.1-1

$(C_{N_\alpha})_p$ is the propeller normal-force parameter at $T'_c = 0$, per radian given by

$$(C_{N_\alpha})_p = \left[(C_{N_\alpha})_p \right]_{K_N=80.7} \left[1 + 0.8 \left(\frac{K_N}{80.7} - 1 \right) \right] \quad (5.1.1-3)$$

where

K_N is the normal-force factor obtained from the propeller manufacturer or approximated by

$$K_N = 262 \left(\frac{b_p}{R_p} \right)_{0.3R_p} + 262 \left(\frac{b_p}{R_p} \right)_{0.6R_p} + 135 \left(\frac{b_p}{R_p} \right)_{0.9R_p} \quad (5.1.1-4)$$

where $\left(\frac{b_p}{R_p} \right)_{0.3R_p}$ is the ratio of the blade width, b_p , to the propeller radius, R_p , at $0.3R_p$ (similar ratios have the same connotation)

$\left[(C_{N\alpha})_p \right]_{K_N=80.7}$ is the propeller normal-force derivative given in figure 5.1.1-2 as a function of blade angle, β' , and type of propeller

α_p is the local angle of attack of the propeller plane (fig. 5-2), obtained from

$$\alpha_p = \alpha_T - \frac{\partial \epsilon_u}{\partial \alpha} (\alpha_w - \alpha_o) \quad (5.1.1-5)$$

where

$-\frac{\partial \epsilon_u}{\partial \alpha}$ is the upwash gradient at the propeller, obtained from figure 5.1.1-3

α_w is the angle of attack of the wing, $\alpha_b + i_w$

α_o is the zero-lift angle of the wing

S_p/prop is the disk area of the propeller, πR_p^2

The contribution of power to lift due to change in dynamic pressure on the immersed portion of the wing is obtained from the following equation from reference 19:

$$(\Delta C_L)_{\Delta \bar{q}_w} = nK_1 \frac{\Delta \bar{q}_w}{\bar{q}_\infty} (C_{L_w})_{\text{prop off}} \frac{(S_i/\text{prop})}{S_w} \quad (5.1.1-6)$$

where

K_1 is an empirical correlation parameter for additional wing lift due to the power effects on the wing, obtained from figure 5.1.1-4 as a function of $\frac{S_w(T'_c/\text{prop})}{8R_p^2}$ and aspect ratio, A_i , of the immersed portion of the wing (fig. 5-1)

$\frac{\Delta \bar{q}_w}{\bar{q}_\infty}$ is the increase in dynamic pressure due to propeller slipstream on the immersed portion of the wing:

$$\frac{\Delta \bar{q}_w}{\bar{q}_\infty} = \frac{S_w(T'_c/\text{prop})}{\pi R_p^2} \quad (5.1.1-7)$$

The portion of the wing, S_i , immersed in the propeller slipstream (per propeller) is obtained, on the basis of figures 5-1(b) and 5-2, from

$$S_i/\text{prop} = (b_i/\text{prop}) \bar{c}_i \quad (5.1.1-8)$$

where

$$b_i/\text{prop} = 2\sqrt{R_p^2 - (z_s - z_w)^2} \quad (5.1.1-9)$$

and

$$z_s = -x_p'(\alpha_b - \epsilon_u - \epsilon_p) + z_T \quad (5.1.1-10)$$

with

$$-\epsilon_u = -\frac{\partial \epsilon_u}{\partial \alpha} (\alpha_w - \alpha_o) \quad (5.1.1-11)$$

and

$$\epsilon_p = \frac{\partial \epsilon_p}{\partial \alpha_p} \alpha_p \quad (5.1.1-12)$$

The derivative $\frac{\partial \epsilon_p}{\partial \alpha_p}$ is given by

$$\frac{\partial \epsilon_p}{\partial \alpha_p} = C_1 + C_2 (C_{N\alpha})_p \quad (5.1.1-13)$$

where the constants C_1 and C_2 are obtained from figure 5.1.1-5 and $(C_{N\alpha})_p$ is obtained from equation (5.1.1-3).

The contribution of power to lift due to change in angle of attack resulting from propeller downwash, ϵ_p , is obtained from

$$(\Delta C_L)_{\epsilon_p} = n(1 + \frac{\Delta \bar{q}_w}{\bar{q}_\infty}) (C_{L\alpha})_{w_{\text{prop off}}} (\Delta \alpha)_{S_i} \frac{(S_i/\text{prop})}{S_w} \quad (5.1.1-14)$$

where $\frac{\Delta \bar{q}_w}{\bar{q}_\infty}$ and S_i/prop are defined by equations (5.1.1-7) and (5.1.1-8), respectively, and

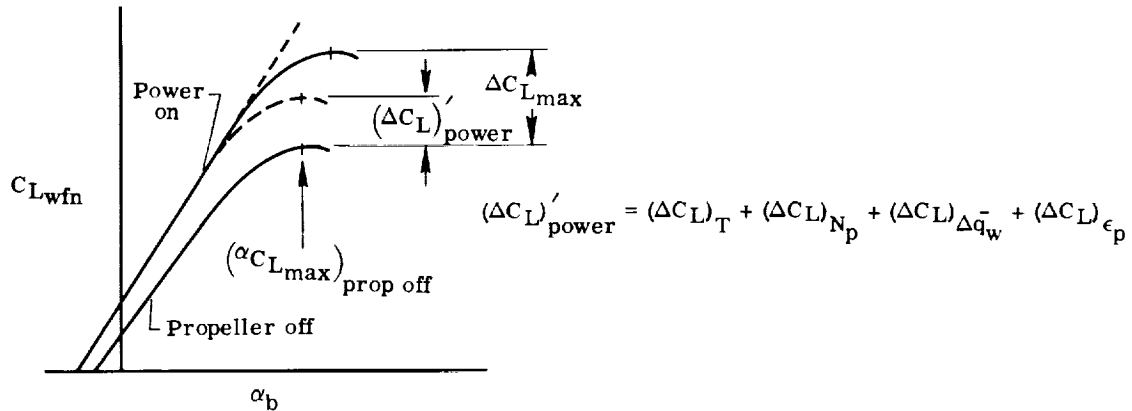
$$(\Delta \alpha)_{S_i} = -\frac{\epsilon_p}{1 - \frac{\partial \epsilon_u}{\partial \alpha}} \quad (5.1.1-15)$$

where

ϵ_p was defined in equation (5.1.1-12)

The contribution of power to the maximum lift must also be accounted for. The preceding contributions of power to lift were considered to occur at discrete angles of attack to be added to the power-off lift curve. However, because the angle of attack

for stall increases with power, depending primarily upon the ratio of immersed wing area to total wing area, an additional increase in power effect occurs at or near maximum lift due to the increase in stall angle. This is illustrated in the following sketch:



The increment in maximum lift due to the propeller power, $\Delta C_{L_{\max}}$, is obtained from the following empirical equation (from ref. 1):

$$\Delta C_{L_{\max}} = K (\Delta C_L)'_{\text{power}} \quad (5.1.1-16)$$

where

$(\Delta C_L)'_{\text{power}}$ is the increment in tail-off lift due to power at propeller-off, maximum-lift angle of attack

K is a correction for maximum lift due to power, a function of the ratio of total immersed wing area to total wing area, obtained from figure 5.1.1-6

The complete power-on lift curve is constructed by: (a) plotting the linear portion of the power-on curve, (b) drawing a horizontal line representing the power-on maximum lift coefficient, and (c) translating the nonlinear propeller-off portion of the lift curve to a tangency with (a) and (b). This construction not only shapes the power-on lift curve but also fixes the power-on stall angle.

By using the foregoing procedures, the tail-off lift characteristics of the subject airplane were determined and are summarized in tables 5.1.1-1 to 5.1.1-4 for three thrust conditions. In tables 5.1.1-1(c), 5.1.1-2(a)-3, 5.1.1-2(b), and 5.1.1-3, in which the power effects are computed as functions of angle of attack, α_b , the tables

are separated into three parts:

The first part provides for the calculation of power effects on lift from $\alpha_b = -4^\circ$ (essentially zero lift) to $\alpha_b = 12^\circ$. The results of these calculations for each thrust condition (table 5.1.1-3, column 7) are plotted as in figure 5.1.1-7 with the propeller-off, tail-off lift curves superimposed on the plots. These plots constitute the initial phase of construction plots for power-on curves and completion of the calculations.

The second part is an interjected line item used only to obtain $(\Delta C_L)'_{\text{power}}$ (summarized in column 5 of table 5.1.1-3) to be used in table 5.1.1-4 to obtain $\Delta C_{L\text{max}}$ due to power for each power condition. The $\Delta C_{L\text{max}}$ thus determined for each power condition is now added to the propeller-off $C_{L\text{max}}$ value in figure 5.1.1-7 to obtain power-on $C_{L\text{max}}$. With power-on $C_{L\text{max}}$ and the linear portion of power-on C_L determined, the power-on lift curves are completed as explained earlier in this section and as shown in figure 5.1.1-7.

With the power-on lift curves completed, the stall angle for each power condition is noted and used to extend the propeller-off, wing-alone and propeller-off, tail-off lift curves to the power-on stall angles as in figure 5.1.1-8. This figure is now used to provide the information required in column 12 of table 5.1.1-2(a) and column 6 in table 5.1.1-3 to complete the third part of the tables.

The power-on tail-off characteristics as summarized in column 7 of table 5.1.1-3 are now in tabular form ready for the consideration of net lift with tail on.

5.1.2 Horizontal-Tail Contribution to Lift

The addition of power alters the propeller-off lift contribution of the horizontal tail due to power-induced increments of downwash, $(\Delta \epsilon_h)_{\text{power}}$, and dynamic-pressure ratio, $\frac{\Delta q_h}{\bar{q}_\infty}$, at the tail. The determination of the power-induced downwash has been particularly troublesome, more so for multiengine than single-engine aircraft because of the variations in size, shape, and position of the nacelles relative to the wing, which appear to provide more variables and interference with flow over the wing than in single-engine installations. The errors in predicting the power effects on the lift contribution of the horizontal tail for normal configurations are not too significant in determining the net lift of an airplane. They are, however, very significant in determining the pitching-moment characteristics.

The power-induced change in downwash at the tail, $(\Delta \epsilon_h)_{\text{power}}$, may be estimated from figure 5.1.2-1 for single-engine airplanes and from figure 5.1.2-2 for multi-engine airplanes. These nomographs, developed in reference 19, are presented as functions of propeller-off downwash angle, $(\bar{\epsilon}_h)_{\text{props off}}$, thrust coefficient, T'_c/prop , and airplane geometry involving wing area, S_w , propeller radius, R_p , and distance

from thrust axis to the horizontal tail, z_{hT} .

The power-induced change in dynamic-pressure ratio at the tail, $\frac{\Delta \bar{q}_h}{\bar{q}_\infty}$, may be estimated from the nomograph in figure 5.1.2-3 with some reservation regarding the $T'_c = 0$ condition. This nomograph, obtained from reference 1, was originally developed in reference 19 and differs from the original in the vertical displacement of the ordinate, $\frac{\Delta \bar{q}_h}{\bar{q}_\infty}$. In the original development, the zero value of $\frac{\Delta \bar{q}_h}{\bar{q}_\infty}$ was aligned with the zero value of $S_w \frac{T'_c/\text{prop}}{8R_p^2}$. This is in contrast to the present alignment of $\frac{\Delta \bar{q}_h}{\bar{q}_\infty}$ with the zero value of $S_w \frac{T'_c/\text{prop}}{8R_p^2}$. No explanation is given in reference 1 for the shift of the ordinate. It is surmised that the shift was made to conform with a normally accepted assumption that the dynamic pressure at the tail is 90 percent of free-stream value in the absence of power effects (propeller off or $T'_c = 0$). For $T'_c = 0$ conditions and positive thrust conditions for which figure 5.1.2-3 provides values of dynamic-pressure ratio less than the values determined in section 4.9.2 for propeller-off conditions, it is recommended that the values obtained for propeller-off conditions be used.

For the subject airplane with the tab geared to the elevator to deflect in the ratio of $\frac{\delta_{\text{tab}}}{\delta_e} = 1.5$, the contribution of the horizontal tail to the lift of the airplane may be obtained from the following relation:

$$C_{Lh(hf)} = \left[(\bar{C}_{Lh(hf)})'_{S_h, \bar{q}_h/\bar{q}_\infty = 1.0} \left(\frac{S_h}{S_w} \right) \left(\frac{\bar{q}_h}{\bar{q}_\infty} \right)_{\text{prop off}} + \frac{\Delta \bar{q}_h}{\bar{q}_\infty} \right] \quad (5.1.2-1)$$

where

$(\bar{C}_{Lh(hf)})'_{S_h, \bar{q}_h/\bar{q}_\infty = 1.0}$ is the lift of the tail referenced to the tail area and a

dynamic-pressure ratio of 1.0, obtained from figure 4.13.3-1 as a function of $\alpha_h = \alpha_b - (\bar{\epsilon}_h)_{\text{prop off}} - (\Delta \epsilon_h)_{\text{power}}$ and δ_e ; downwash at the tail with propeller off,

$(\bar{\epsilon}_h)_{\text{props off}}$, obtained from figure 4.9.1-7; downwash increment due to power,

$(\Delta \epsilon_h)_{\text{power}}$, obtained from figure 5.1.2-2

$\left(\frac{\bar{q}_h}{\bar{q}_\infty} \right)_{\text{prop off}}$ is the propeller-off dynamic-pressure ratio at the tail, obtained

from figure 4.9.1-7

$\frac{\Delta \bar{q}_h}{\bar{q}_\infty}$ is the power-induced increment in dynamic-pressure ratio at the tail,

obtained from figure 5.1.2-3. When the increment obtained from the figure is negative for zero or positive thrust conditions, it is assumed to be zero

The effect of the horizontal tail, including elevator (with geared tab) deflections, on the lift of the subject airplane with power on is summarized in column 14 of table 5.1.2-1 as a function of α_b , δ_e , and T'_C . Calculated downwash characteristics are compared with those determined from experimental data (ref. 2) in figure 5.1.2-4. The downwash and dynamic-pressure ratio of the horizontal tail, calculated in columns 3 and 4 and column 11 of table 5.1.2-1(b), respectively, are shown in figure 5.1.2-5.

The downwash at the tail determined from experimental data, shown in figure 5.1.2-5, was determined in reference 2 for each power setting as a function of α_b by superimposing the wind-tunnel-determined tail-off C_m versus α_b plot on the tail-on C_m plot which included δ_e effects. At each α_b point considered, the downwash was considered to be equal to the δ_e at which C_m , tail on, was equal to C_m , tail off. Using this approach, the authors of reference 2 considered the downwash, thus determined, to be within 1° of the correct value at the high angles of attack.

Considering the accuracy of the experimentally determined downwash, the calculated downwash at high angle of attack for $T'_C = 0$ is believed to be within 1° . As is shown later, the pitching-moment curves, $C_m = f(\alpha_b, \delta_e)$, for $T'_C = 0$ show good correlation, thus implying fairly accurate calculated values for $T'_C = 0$. At total $T'_C = 0.20$ and 0.44 , it was found necessary to reduce the increment of downwash due to power by 40 percent to achieve correlation in pitching-moment curves (as a function of α_b and δ_e), as is discussed later. This 40-percent decrease in downwash due to power had only a slight effect on the calculated dynamic-pressure ratio at the tail (fig. 5.1.2-5).

5.1.3 Net Characteristics of the Subject Airplane

A comparison of the calculated (from column 16 of table 5.1.2-1(b)) and wind-tunnel-determined (ref. 2) lift characteristics for total $T'_C = 0, 0.20$, and 0.44 in figure 5.1.3-1 shows good correlation. At total $T'_C = 0.20$ and 0.44 , a 40-percent reduction in downwash due to power (discussed in the last paragraph of the previous section) improved the correlation.

It should be noted that the lift contributions of the tail include tail-lift carryover effects onto the body due to the angle of attack of the tail ($\delta_e = 0^\circ$) and elevator deflection as discussed in sections 4.10(a) and 4.13-1, respectively. These calculated tail-lift carryover effects for the tail-body configuration of the subject airplane are considered to be excessive, as shown in section 4.11 and section 4.13.4, and should

be neglected for this tail-body configuration. Neglect of these carryover effects would have an insignificant influence on the lift curves of figure 5.1.3-1 but not on the pitching-moment curves (as was shown in section 4.13.4).

5.1.4 Symbols

A	wing aspect ratio
A_i	aspect ratio of the portion of the wing immersed in the slipstream of one propeller, $\frac{b_i/\text{prop}}{\bar{c}_i}$
b_i	span of the total portion of the wing immersed in the slipstreams of the propellers, ft
b_i/prop	span of the portion of the wing immersed in the slipstream of one propeller, ft
$(b_i)_e$	span of the exposed portions of the wing panels immersed in the propeller slipstream of a single-engine airplane, ft
b_p	blade width of the propeller, ft
C_1, C_2	factors used in determining the propeller downwash, ϵ_p , obtained from figure 5.1.1-5
C_L	lift coefficient
$\bar{C}_{Lh(hf)}$	net lift coefficient of the horizontal tail due to α_h , δ_e , and δ_{tab} , with tail-fuselage interaction effects included, referenced to the wing area
$(\bar{C}_{Lh(hf)})'_{S_h, \frac{\bar{q}_h}{\bar{q}_\infty} = 1.0}$	net lift coefficient, $\bar{C}_{Lh(hf)}$, referenced to the horizontal-tail area and a dynamic-pressure ratio at the tail equal to 1.0
$C_{L_{\max}}$	maximum lift coefficient
$C_{L_{\text{prop off}}}$	lift coefficient at propeller-off conditions
$(C_{L_w})_{\text{prop off}}, (C_{L_{wfn}})_{\text{prop off}}$	lift coefficient of the wing alone and the tail-off configuration, respectively, at propeller-off conditions
$C_{L_{wfn}}$	lift coefficient of the tail-off configuration at power-on conditions, $(C_{L_{wfn}})_{\text{prop off}} + (\Delta C_{L_{wfn}})_{\text{power}}$
$(C_{L_{wfn}})_{\max}$	tail-off maximum lift coefficient

$\Delta C_{L_{\max}}$	increment of maximum lift coefficient due to power
$(\Delta C_L)_{N_p}$	increment of lift coefficient due to the lift component of the propeller normal force, N_p (fig. 5-2)
$(\Delta C_L)'_{\text{power}}$	increment of the tail-off lift due to power at the propeller-off maximum-lift angle of attack
$(\Delta C_L)_{\Delta \bar{q}_w}$	increment of lift coefficient due to the power-induced change in dynamic pressure over the portion of the wing immersed in the propeller slipstreams
$(\Delta C_L)_T$	increment of lift coefficient due to the lift-component propeller thrust vector
$(\Delta C_L)_{\epsilon_p}$	increment of lift coefficient due to the change in angle of attack, resulting from propeller downwash, ϵ_p , of the portions of the wing immersed in the propeller slipstreams
$(\Delta C_{L_h})_{\Delta \bar{q}_h}$	increment of horizontal-tail contribution to the lift coefficient resulting from the power-induced change in dynamic pressure at the tail
$(\Delta C_{L_h})_{(\Delta \epsilon_h)_{\text{power}}}$	increment of horizontal-tail contribution to the lift coefficient resulting from the power-induced change in downwash at the tail
$(\Delta C_{L_{\text{wfn}}})_{\text{power}}$	increment of tail-off lift coefficient due to power
$(C_{L_\alpha})_{\text{wprop off}}$	lift-curve slope of the wing alone at propeller-off conditions, per deg
C_m	pitching-moment coefficient
$(C_{N_\alpha})_p$	normal-force derivative of the propeller based on the propeller disk area, per rad
$[(C_{N_\alpha})_p]_{K_N=80.7}$	reference normal-force derivative of a propeller having a normal-force factor, K_N , equal to 80.7, per rad
\bar{c}	mean aerodynamic chord
\bar{c}_i	mean aerodynamic chord of the portion of the wing immersed in the propeller slipstream (figs. 5-1(a) and 5-1(b)), ft
$(c_{r_i})_e$	root chord of the exposed portion of the wing panel immersed in the propeller slipstream of a single-engine airplane, ft

c_{t_i}	tip chord of the portion of the wing immersed in the propeller slipstream, ft
f	propeller inflow factor, ratio of the propeller normal-force coefficient at power-on to power-off ($T'_C = 0$) conditions
i_T	incidence of the thrust axis relative to the X-body axis, deg
i_w	incidence of the wing relative to the X-body axis, deg
K	correction factor for maximum lift due to power
K_1	correlation parameter for additional wing lift due to power effects on the wing
K_N	propeller normal-force factor
l_h, l'_h	distance from the center of gravity and the quarter chord of the mean aerodynamic chord of the immersed portion of the wing, respectively, to the quarter chord of the horizontal-tail mean aerodynamic chord, ft
N_p	normal force of a propeller, lb
n	number of propellers
\bar{q}_∞	free-stream dynamic pressure, lb/sq ft
$\frac{\bar{q}_h}{\bar{q}_\infty}, \left(\frac{\bar{q}_h}{\bar{q}_\infty}\right)_{\text{prop off}}$	dynamic pressure at the horizontal tail for power-on and propeller-off conditions, respectively, as a ratio of the free-stream dynamic pressure
$\frac{\Delta\bar{q}_h}{\bar{q}_\infty}, \frac{\Delta\bar{q}_w}{\bar{q}_\infty}$	increment of power-induced dynamic pressure acting on the horizontal tail and the portions of the wing immersed in the propeller slipstream, respectively, as a ratio of the free-stream dynamic pressure
R_p	propeller radius, ft
S_h, S_w	horizontal-tail and wing area, respectively, sq ft
S_i, S_{h_i}	area of the portions of the wing and horizontal tail, respectively, immersed in the propeller slipstreams (fig. 5-1(b)), sq ft

S_{hi}/prop	horizontal-tail area immersed in the slipstream of one propeller, sq ft
S_i/prop	wing area immersed in the slipstream of one propeller, sq ft
S_p/prop	disk area of one propeller, sq ft
T	thrust of the propellers, lb
$T'_c = \frac{T}{\bar{q}_\infty S_w}$	
T'_c/prop	thrust coefficient due to one propeller
V	airspeed, ft/sec
X_b, Z_b	x- and z-coordinate axis, respectively, of the body-axes system
x_p, x'_p	distance from the center of gravity and the quarter chord of the mean aerodynamic chord of the immersed portion of the wing, respectively, to the propeller, positive forward, ft
x_w	distance from the aerodynamic center of the mean aerodynamic chord of the immersed portion of the wing area to the center of gravity, positive forward, in. or ft
y_{ci}	lateral distance from the root chord of the exposed portion of an immersed wing panel on a single-engine airplane to the mean aerodynamic chord of the immersed panel, ft
z_h	distance, parallel to the Z-body axis, from the X-body axis to the quarter chord of the horizontal-tail mean aerodynamic chord, positive down, ft
z_{heff}	effective distance, parallel to the Z-body axis, from the quarter chord of the horizontal-tail mean aerodynamic chord to the centerline of the propeller slipstream, positive down, ft
z_{hT}	distance, parallel to the Z-body axis, from the thrust axis to the quarter chord of the horizontal-tail mean aerodynamic chord, positive down, ft

z_s	distance, parallel to the Z-body axis, from the X-body axis to the centerline of the propeller slipstream at the longitudinal station of the quarter chord of the mean aerodynamic chord of the immersed portion of the wing, positive down, ft
z_T	distance, parallel to the Z-body axis, from the X-body axis to the thrust axis, positive down, ft
z_w	distance, parallel to the Z-body axis, from the X-body axis to the quarter chord of the mean aerodynamic chord of the immersed portion of the wing, positive down, ft
α	angle of attack, deg
α_b	airplane angle of attack relative to the X-body axis, deg
$(\alpha_{C_{L_{\max}}})_{\text{prop off}}$	angle of attack, α_b , at stall with the propellers off, deg
α_p	angle of attack of the propeller plane, includes the effect of the wing upwash, deg
α_T	angle of attack of the thrust axis, deg
α_w	angle of attack of the wing relative to its chord line, deg
α_o	angle of attack of the wing zero-lift line relative to its chord line, deg
$(\Delta\alpha)_{S_i}$	change in angle of attack of the portion of the wing immersed in the propeller slipstream due to the propeller, deg
β'	propeller blade angle at $0.75 R_p$, deg
δ_e	elevator deflection, deg
δ_{tab}	tab deflection, deg
$\epsilon_h = (\bar{\epsilon}_h)_{\text{props off}} + (\Delta\epsilon_h)_{\text{power}}$	
$(\Delta\epsilon_h)_{\text{power}}$	increment of downwash at the horizontal tail due to power, deg
$(\bar{\epsilon}_h)_{\text{props off}}$	average downwash at the horizontal tail with the propellers off, obtained from section 4.9.1, deg

$\epsilon_{\text{power on}}$	downwash at the horizontal tail for power-on conditions, deg
ϵ_p	downwash angle behind the propeller, deg
$\frac{\partial \epsilon_p}{\partial \alpha}$	downwash gradient behind the propeller
$-\epsilon_u$	upwash angle at the propeller, deg
$-\frac{\partial \epsilon_u}{\partial \alpha}$	upwash gradient at the propeller
λ_{ie}	taper ratio of the exposed portion of the immersed wing panel on a single-engine airplane (fig. 5-1(a))

TABLE 5.1.1-1
LIFT DUE TO DIRECT ACTION OF THE PROPELLER FORCES

(a) Contribution of thrust vector to lift, $(\Delta C_L)_T$

$$(\Delta C_L)_T = n(T'_c/\text{prop}) \sin \alpha_T$$

(a)-1

Symbol	Description	Magnitude
n	Number of propellers	2
T'_c/prop	<u>Thrust/propeller</u> $\bar{q}_\infty S_w$	As selected
i_T	Incidence of thrust line to reference X_b -axis, deg	0
α_T	$\alpha_b + i_T$, deg	α_b

(a)-2

T'_c/prop	$n(T'_c/\text{prop})$	$(\Delta C_L)_T^1$
0	0	0
.10	.20	.20 $\sin \alpha_b$
.22	.44	.44 $\sin \alpha_b$

¹On basis of $S_w = 178$ sq ft.

(b) Contribution of propeller normal force, $(\Delta C_L)_{N_p}$

$$(\Delta C_L)_{N_p} = n f(C_{N\alpha})_p \frac{\alpha_p}{57.3} \frac{(S_p/\text{prop})}{S_w} \cos \alpha_T$$

(b)-1

Symbol	Description	Reference	Magnitude
R_p	Propeller radius, ft	Table 3-1	3.0
S_p/prop	Propeller disk area, πR_p^2 , sq ft	-----	28.27 per propeller
S_w	Reference wing area for comparison with wind-tunnel and flight data, sq ft	Table 3-1	178
$\frac{S_w(T'_c/\text{prop})}{8R_p^2}$	Power parameter for obtaining correlation functions	-----	2.47 (T'_c/prop)
f	Propeller inflow factor, function of $\frac{S_w(T'_c/\text{prop})}{8R_p^2}$	Figure 5.1.1-1	Depends on T'_c/prop
b_p	Width of propeller blade, ft	Manufacturer	0.416 at 0.3 R_p .492 at .6 R_p .409 at .9 R_p
K_N	Normal-force factor, $262 \left(\frac{b_p}{R_p} \right)_{0.3R_p} + 262 \left(\frac{b_p}{R_p} \right)_{0.6R_p} + 135 \left(\frac{b_p}{R_p} \right)_{0.9R_p}$	Equation (5.1.1-4)	97.7
β'	Propeller blade angle, function of $\frac{V}{(rps)2R_p}$ and T_c , deg	Propulsion group Figure 5.1.1-2	As selected
$[(C_{N\alpha})_p]_{K_N=80.7}$	Propeller normal-force parameter, function of β'		Depends on β'
$(C_{N\alpha})_p$	Propeller normal-force derivative, $[(C_{N\alpha})_p]_{K_N=80.7} \left[1 + 0.8 \left(\frac{K_N}{80.7} - 1 \right) \right]$	Equation (5.1.1-3)	1.17 $[(C_{N\alpha})_p]_{K_N=80.7}$

TABLE 5.1.1-1 (Concluded)

(b)-1 (Concluded)

Symbol	Description	Reference	Magnitude
\bar{c}_i	Effective chord of immersed wing area, ft	Figure 5-1(b)	5.50
x'_p	Distance of propeller forward of quarter-chord point of c_i , ft	Figure 5-2	6.0
$\frac{x'_p}{\bar{c}_i}$			1.09
Λ	Aspect ratio of wing	Table 3.2-1	7.5
$-\frac{\partial \epsilon_u}{\partial \alpha}$	Upwash gradient at propeller	Figure 5.1.1-3	.195
α_w	Angle of attack of wing relative to wing chord, $\alpha_b + i_w$, deg	Table 3-1	$\alpha_b + 2$
α_o	Wing zero-lift angle relative to wing chord, deg	Table 4.2-1	-2
α_T	Angle of attack of thrust line, $\alpha_b + i_T$, deg		α_b
α_p	Angle of attack of propeller plane, $\alpha_T - \frac{\partial \epsilon_u}{\partial \alpha}(\alpha_w - \alpha_o)$, deg	Equation (5.1.1-5)	$1.20 \alpha_b + .78$

(b)-2

①	②	③	④	⑤	⑥	⑦
T'_c/prop	$\frac{S_w(T'_c/\text{prop})}{8R_p^2}$ $2.47(T'_c/\text{prop})$	i , figure 5.1.1-1	β'_T as in wind-tunnel test of the subject air- plane, deg	$[(C_{N\alpha})_p]_{KN=80.7}$ figure 5.1.1-2	$(C_{N\alpha})_p$ = 1.17 ⑤	$(\Delta C_L)_{N_p}$ for two propellers = 0.00554 ③ ⑥ $\alpha_p \cos \alpha_b$
0	0	1.00	14.8	0.080	0.0936	0.000519(1.2 α_b + 0.78) $\cos \alpha_b$
.10	.247	1.19	19.3	.098	.1147	.000756(1.2 α_b + .78) $\cos \alpha_b$
.22	.543	1.37	21.5	.104	.1217	.000924(1.2 α_b + .78) $\cos \alpha_b$

(c) Summary of lift due to direct action of propeller forces

①	②	③	④	⑤	⑥	⑦
			Table 5.1.1-1(b)-1	Table 5.1.1-1(a)-2	Table 5.1.1-1(b)-2	
				$(\Delta C_L)_T = T'_c$ ②	$(\Delta C_L)_{N_p} = c_1$ ③ ④	$(\Delta C_L)_T + (\Delta C_L)_{N_p} = ⑤ + ⑥$
α_b , deg	$\sin \alpha_b$ = \sin ①	$\cos \alpha_b$ = \cos ①	α_p , deg = 1.2 ① + 0.78	T'_c	T'_c	T'_c
				0 0.2 0.44	0 0.2 0.44	0 0.2 0.44
				0 0.00519 0.000756 0.000924	0 0.00519 0.000756 0.000924	0 0.00519 0.000756 0.000924
-1	-0.0698	0.9976	-4.0	0 -0.0140 -0.0309	-0.00207 -0.00302 -0.00369	-0.00207 -0.01702 -0.03459
-2	-.0349	.9994	-1.6	0 -.0070 -.0154	-.00083 -.00121 -.00148	-.00083 -.00821 -.01688
0	0	1.000	0.8	0 0 0	0.00042 0.00060 0.00074	0.00042 0.00060 0.00074
2	.0349	.9994	3.2	0 .0070 .0154	.00166 .00242 .00296	.00166 .00942 .01836
4	0.0698	0.9976	5.6	0 0.0140 0.0307	0.00290 0.00422 0.00516	0.00290 0.01822 0.03586
6	.1045	.9945	8.0	0 .0209 .0460	.00413 .00601 .00735	.00413 .02691 .05335
8	0.1392	0.9903	10.4	0 0.0278 0.0612	0.00535 0.00779 0.00952	0.00535 0.03559 0.07072
10	.1736	.9848	12.8	0 .0347 .0764	.00654 .00953 .01165	.00654 .04423 .08805
12	0.2079	0.9781	15.2	0 0.0416 0.0915	0.00772 0.01124 0.01374	0.00772 0.05284 0.10524
^a 13.8	0.2385	0.9711	17.3	0 0.0477 0.1049	0.00872 0.01270 0.01552	0.00872 0.06040 0.12042
^b 13.8	0.2385	0.9711	17.3	0 0.0477 0.1049	0.00872 0.01270 0.01552	0.00872 0.06040 0.12042
^c 14.1	.2436	.9699	17.7	- .0487 .1072	----- .01298 .01586	----- .06168 .12306
^d 14.4	0.2487	0.9686	18.1	- ----- 0.1094	----- 0.01620	----- 0.12560

^aStall angle for $(C_{L_{wfn}})_{\text{max}}$ propeller off (used only to obtain $(C_{L_{\text{max}}})_{\text{power on}}$).^{b,c,d}Stall angles for tail-off configuration at $T'_c = 0, 0.20, 0.44$, respectively.

TABLE 5.1.1-2
WING-LIFT INCREMENTS DUE TO PROPELLER SLIPSTREAM EFFECTS

(a) Wing-lift increments due to change in dynamic pressure on immersed portion of the wing, $(\Delta C_L) \Delta \bar{q}_w$

$$(\Delta C_L) \Delta \bar{q}_w = n K_1 \frac{\Delta \bar{q}_w}{\bar{q}_\infty} (C_{L_w})_{\text{prop off}} \frac{S_i/\text{prop}}{S_w}$$

(a)-1

Symbol	Description	Reference	Magnitude
$(C_{L_w})_{\text{prop off}}$	C_L of wing alone (The C_L curve of figure 4.2-1(a), based on $S_w = 172.3$ sq ft, was re-referenced to $S_w = 178$ sq ft in figure 5.1.1-7 and its nonlinear portion approaching stall was translated, along its linear portion, to the stall angles for power-on conditions.)	Figure 5.1.1-8	Function of α_b
n	Number of propellers	-----	2
S_w	Reference wing area for comparison with wind-tunnel and flight data, sq ft	Table 3-1	178
R_p	Propeller radius, ft	Table 3-1	3.0
T'_c/prop	Net thrust per propeller $\bar{q}_\infty S_w$	-----	As selected
$\frac{\Delta \bar{q}_w}{\bar{q}_\infty}$	Change in dynamic-pressure ratio on immersed portion of wing, $\frac{S_w (T'_c/\text{prop})}{\pi R_p^2}$	Equation (5.1.1-7)	Function of (T'_c/prop)
$\frac{S_w (T'_c/\text{prop})}{\pi R_p^2}$	Power parameter for obtaining correlating functions	-----	$2.47 (T'_c/\text{prop})$
C_1	Factor for determining propeller downwash, ϵ_p	Figure 5.1.1-5	Function of (T'_c/prop)
C_2	Factor for determining propeller downwash, ϵ_p	Figure 5.1.1-5	Function of (T'_c/prop)
$(C_{N_{\alpha_p}})$	Propeller normal-force derivative	Table 5.1.1-1(b)-2	Function of (T'_c/prop)
$\frac{\partial \epsilon_p}{\partial \alpha_p}$	$C_1 + C_2 (C_{N_{\alpha_p}})$	Equation (5.1.1-13)	Function of (T'_c/prop)
α_p	Angle of attack of propeller plane, deg	Table 5.1.1-1(c)	$1.2 \alpha_b + .78$
ϵ_p	Propeller downwash behind propeller, $\frac{\partial \epsilon_p}{\partial \alpha_p} \alpha_p$, deg	Equation (5.1.1-12)	$f(\alpha_b, T'_c/\text{prop})$
$-\epsilon_u$	Wing upwash at propeller plane, $-\frac{\partial \epsilon_u}{\partial \alpha} (\alpha_w - \alpha_0)$, deg	Table 5.1.1-1(b)-1	$0.2 \alpha_b + 0.78$
x'_p	Distance from quarter chord of \bar{c}_i to propeller, ft	Figure 5-2	6.0
z_T	Distance from X_b -axis to thrust axis at propeller, ft	Figure 5-2	- .869
z_s	$-\frac{x'_p}{57.3} (\alpha_b - \epsilon_u - \epsilon_p) + z_T$, ft	Equation (5.1.1-10)	$f(\alpha_b, T'_c/\text{prop})$
z_w	Distance from X_b -axis to quarter-chord immersed wing mean aerodynamic chord	Figure 5-2	-.020
$z_s - z_w$	Distance from centerline slipstream to quarter-chord immersed wing mean aerodynamic chord at the quarter chord	Figure 5-2	$f(\alpha_b, T'_c/\text{prop})$
b_i/prop	$2 \sqrt{R_p^2 - (z_s - z_w)^2}$, ft	Figure 5-1(a)	$f(\alpha_b, T'_c/\text{prop})$
\bar{c}_i	Effective immersed mean chord, ft	Figure 5-1(b)	5.5
A_i	$\frac{(b_i/\text{prop})}{\bar{c}_i}$	Figure 5-1(a)	$\frac{(b_i/\text{prop})}{5.5}$
K_1	Correlation parameter for added lift due to power	Figure 5.1.1-4	$f(\lambda_1, T'_c/\text{prop})$
S_i/prop	Immersed wing area per propeller, $(b_i/\text{prop}) \bar{c}_i$, sq ft	Figure 5-1(a)	$5.5 (b_i/\text{prop})$

TABLE 5.1.1-2 (Concluded)

(b) Wing-lift increments due to change in angle of attack induced by propeller downwash, $(\Delta C_L)_{\epsilon_p}$

$$(\Delta C_L)_{\epsilon_p} = n \left(1 + \frac{\Delta \bar{q}_w}{\bar{q}_\infty} \right) (C_{L\alpha})_{w \text{ prop off}} \frac{S_i / \text{prop}}{S_w} (\Delta \alpha)_{S_i}$$

(b)-1

Symbol	Description	Reference	Magnitude
n	Number of propellers	-----	2
S_w	Reference wing area for comparison with wind-tunnel and flight data, sq ft	Table 3-1	178
$\frac{S_i}{S_w}$	Ratio of immersed wing area per propeller to total area	Table 5.1.1-2(a)-3	$f(\alpha_b, T'_c / \text{prop})$
$\frac{\Delta \bar{q}_w}{\bar{q}_\infty}$	Change in dynamic-pressure ratio on immersed wing	Table 5.1.1-2(a)-2	$f(T'_c / \text{prop})$
$(C_{L\alpha})_{w \text{ prop off}}$	Lift-curve slope of wing referenced to $S_w = 178$ sq ft	Table 4.2-1	.0759 referenced to $S_w = 172.3$ sq ft .0735 referenced to $S_w = 178$ sq ft
ϵ_p	Propeller downwash behind propeller, deg	Table 5.1.1-2(a)-3	$f(\alpha_b, T'_c / \text{prop})$
$\frac{\partial \epsilon_u}{\partial \alpha}$	Upwash gradient at propeller	Figure 5.1.1-3	0.195
$(\Delta \alpha)_{S_i}$	$-\frac{\epsilon_p}{1 - \frac{\partial \epsilon_u}{\partial \alpha}}$	Equation (5.1.1-15)	$-\frac{\epsilon_p}{1.20}$

$$(\Delta C_L)_{\epsilon_p} = -0.123 \epsilon_p \left(1 + \frac{\Delta \bar{q}_w}{\bar{q}_\infty} \right) \frac{S_i / \text{prop}}{S_w}, \text{ referenced to } S_w = 178 \text{ sq ft}$$

(b)-2

①	②			③			④			⑤		
-----	Table 5.1.1-2(a)-3, column 4			Table 5.1.1-2(a)-2, column 7			Table 5.1.1-2(a)-3, column 10			Table 5.1.1-2(b)-1		
α_b , deg	ϵ_p , deg			$1 + \frac{\Delta \bar{q}_w}{\bar{q}_\infty}$			$\frac{S_i / \text{prop}}{S_w}$			$(\Delta C_L)_{\epsilon_p} = -0.123 \text{ ② ③ ④}$		
	T'_c / prop			T'_c / prop			T'_c / prop			T'_c		
	0	0.10	0.22	0	0.10	0.22	0	0.10	0.22	0	0.20	0.44
-4	-0.0936	-0.7948	-1.1584	1.000	1.6295	2.385	0.1834	0.1827	0.1822	0.00211	0.02919	0.06192
-2	-.0374	-.3179	-.4634	1.000	1.6295	2.385	.1805	.1801	.1798	.00083	.01148	.02444
0	0.0187	0.1590	0.2317	1.000	1.6295	2.385	0.1762	0.1765	0.1767	-0.00041	-0.00561	-0.0120
2	.0749	.6358	.9267	1.000	1.6295	2.385	.1706	.1721	.1728	-.00157	-.02193	-.04700
4	0.1310	1.1127	1.6218	1.000	1.6295	2.385	0.1633	0.1665	0.1681	-0.00263	-0.03713	-0.08000
6	.1872	1.5896	2.3168	1.000	1.6295	2.385	.1541	.1598	.1625	-.00355	-.05091	-.11044
8	0.2434	2.0665	3.0118	1.000	1.6295	2.385	0.1428	0.1518	0.1559	-0.00428	-0.06287	-0.13774
10	.2995	2.5434	3.7069	1.000	1.6295	2.385	.1288	.1423	.1478	-.00474	-.07254	-.16072
12	0.3557	3.0202	4.4019	1.000	1.6295	2.385	0.1110	0.1309	0.1393	-0.00486	-0.07924	-0.17990
^a 13.8	0.4048	3.4375	5.0101	1.000	1.6295	2.385	0.0905	0.1190	0.1302	-0.00451	-0.08199	-0.19136
^b 13.8	0.4048	3.4375	5.0101	1.000	1.6295	2.385	0.0905	0.1190	0.1302	-0.00451	-0.08199	-0.19136
^c 14.1	-----	3.5170	5.1259	-----	1.6295	2.385	-----	.1165	.1283	-----	-.08212	-.19293
^d 14.4	-----	-----	5.2418	-----	-----	2.385	-----	-----	0.1264	-----	-----	-0.19437

^aStall angle for $(C_{L_{wfn}})_{\text{max}}$ propeller off (used only to obtain $(C_{L_{\text{max}}})_{\text{power on}}$).^{b,c,d}Stall angles for tail-off configuration at total $T'_c = 0, 0.20, 0.44$, respectively.

TABLE 5.1.1-3
TAIL-OFF LIFT CHARACTERISTICS WITH POWER ON
 $C_{L_{wfn}} = (C_{L_{wfn}})_{\text{prop off}} + (\Delta C_{L_{wfn}})_{\text{power}}$ referenced to $S_w = 178 \text{ sq ft}$

①	②			③			④			⑤			⑥			⑦		
	Table 5.1.1-1(c)			Table 5.1.1-2(a)-3			Table 5.1.1-2(b)-2			Figure 5.1.1-8			Figure 5.1.1-8			Figure 5.1.1-8		
	$(\Delta C_L)_T + (\Delta C_L)_{N_p}$			$(\Delta C_L)_{\Delta \bar{q}_w}$			$(\Delta C_L)_{\epsilon_p}$			$(\Delta C_L)_{wfn} \text{ power} =$ $② + ③ + ④$			$(C_{L_{wfn}})_{\text{prop off}}$			$C_{L_{wfn}} = ⑤ + ⑥$		
$\alpha_B, \text{ deg}$	T'_c			T'_c			T'_c			T'_c			T'_c			T'_c		
	0	0.20	0.44	0	0.20	0.44	0	0.20	0.44	0	0.20	0.44	0	0.20	0.44	0	0.20	0.44
-4	-0.00207	-0.01702	-0.03439	0	0	0	0.00211	0.02910	0.06194	0.00004	0.01208	0.02755	-0.0194	-0.0194	-0.0194	-0.01936	-0.00732	0.00815
-2	-0.00083	-0.00821	-0.01688	0	0.0308	0.0623	0.00083	0.01148	0.02445	0	0.03407	0.06987	0.1400	0.1400	0.1400	0.14000	0.17407	0.20987
0	0.00042	0.00060	0.00074	0	0.0602	0.1217	0	0.00042	-0.00361	-0.01201	0	0.05519	0.11043	0.3000	0.3000	0.30000	0.35519	0.41043
2	0.00166	0.00942	0.01836	0	0.0874	0.1775	-0.00157	-0.02193	-0.04700	0.00009	0.07489	0.14886	0.4600	0.4600	0.4600	0.46009	0.53489	0.60886
4	0.00290	0.01822	0.03586	0	0.1124	0.2287	-0.00263	-0.03713	-0.08001	0.00027	0.09349	0.18455	0.6200	0.6200	0.6200	0.62027	0.71319	0.80455
6	0.00413	0.02691	0.05335	0	0.1348	0.2763	-0.00355	-0.05091	-0.11049	0.00058	0.11080	0.21916	0.7810	0.7810	0.7810	0.78158	0.89180	1.00016
8	0.00535	0.03539	0.07072	0	0.1533	0.3157	-0.00428	-0.06287	-0.13780	0.00011	0.12602	0.24862	0.9420	0.9420	0.9420	0.94211	1.06802	1.19062
10	0.00654	0.04423	0.08805	0	0.1659	0.3481	-0.00474	-0.07254	-0.16079	0.00180	0.13759	0.27536	1.1040	1.1040	1.1040	1.10580	1.24139	1.37936
12	0.00772	0.05284	0.10524	0	0.1709	0.3669	-0.00486	-0.07924	-0.17996	0.00286	0.14450	0.29218	1.2400	1.2400	1.2400	1.24286	1.38450	1.53218
a _{13.8}	0.00872	0.06040	0.12042	0	0.1659	0.3653	-0.00451	-0.08199	-0.19136	0.00421	0.14431	0.29436	-----	-----	-----	-----	-----	-----
b _{13.8}	0.00872	0.06040	0.12042	0	0.1687	0.3762	-0.00451	-0.08199	-0.19136	0.00421	0.14431	0.29436	1.2800	1.2800	1.2800	1.28421	1.44631	1.63031
c _{14.1}	-----	0.06168	0.12306	-	0.1657	0.3716	-----	-0.08212	-0.19293	-----	0.14526	0.30177	-----	-----	-----	-----	1.44826	1.62977
d _{14.4}	-----	-----	0.12560	-	-----	0.3658	-----	-----	-0.19437	-----	-----	0.29700	-----	-----	1.3300	-----	-----	1.62700

*Stall angle for $(C_{L_{wfn}})_{\text{max}}$ propeller off (used only to obtain $(C_{L_{wfn}})_{\text{max}}$ power on).
b.c.d. all angles for tail-off configurations at $T'_c = 0, 0.20, 0.44$, respectively.

TABLE 5.1.1-4
POWER EFFECTS ON MAXIMUM LIFT

$$\Delta C_{L_{\max}} = K(\Delta C_L)'_{\text{power}}$$

Symbol	Description	Reference	Magnitude
K	Correlation factor, function of $\frac{S_i}{S_w}$ (a function of T'_C) at angle of attack of propeller-off $(C_{L_{wfn}})_{\max}$	Figure 5.1.1-6	$f\left(\frac{S_i}{S_w}\right)$
$\frac{S_i}{S_w}$	$n\left(\frac{S_i/\text{prop}}{S_w}\right) = 2\left(\frac{S_i/\text{prop}}{S_w}\right)$	Table 5.1.1-2(a)-3, column 10 at $\alpha_b = 13.8^\circ$	
$(\Delta C_L)'_{\text{power}}$	Increment in lift due to power at angle of attack of propeller-off $(C_{L_{wfn}})_{\max}$	Table 5.1.1-3, column 5 at $\alpha_b = 13.8^\circ$	

①	②	③	④	⑤
-----	Table 5.1.1-2(a)-3, column 10, at $\alpha_b = 13.8^\circ$	Figure 5.1.1-6	Table 5.1.1-3, column 5, at $\alpha_b = 13.8^\circ$	-----
T'_C/prop	$\frac{S_i}{S_w} = 2\left(\frac{S_i/\text{prop}}{S_w}\right)$	K	$(\Delta C_L)'_{\text{power}}$	$(\Delta C_L)_{\max} = \textcircled{3}\textcircled{4}$
0	0.1810	1.07755	0.00421	0.00454
.10	.2380	1.12857	.14431	.16286
.22	.2604	1.15918	.29436	.34112

TABLE 5.1.2-1
EFFECT OF ELEVATOR DEFLECTION ON LIFT WITH POWER ON

$$C_L = C_{Lwfn} + \left[(C_{Lh(h)})' S_h \frac{\bar{q}_h}{\bar{q}_\infty} - 1 \right] \left(\frac{S_h}{S_w} \right) \left(\frac{\bar{q}_h}{\bar{q}_\infty} \right)_{\text{prop off}} + \frac{\Delta \bar{q}_h}{\bar{q}_\infty}$$

(a)

Symbol	Description	Reference	Magnitude
S_w	Reference wing area, sq ft	Table 3-1	178
S_h	Horizontal-tail area, sq ft	Table 3.2-1	32.5
z_{hT}	Vertical distance from thrust axis to horizontal tail, ft	Figure 5-2	~.80
R_p	Propeller radius, ft	Table 3-1	3.0
$\frac{z_{hT}}{2R_p}$	Parameter for determining $(\Delta \epsilon_h)_{\text{power}}$	-----	-0.133
$\frac{S_w(T'_c/\text{prop})}{8R_p^2}$	Thrust parameter for determining $(\Delta \epsilon_h)_{\text{power}}$ and $\frac{\Delta \bar{q}_h}{\bar{q}_\infty}$	-----	$2.47(T'_c/\text{prop})$
$(\bar{\epsilon}_h)_{\text{props off}}$	Downwash at horizontal tail with propellers off, deg	Figure 4.9.1-7	Function of α_b
$(\Delta \epsilon_h)_{\text{power}}$	Downwash increment at horizontal tail due to power, deg	Figure 5.1.2-2	$f\left(\frac{z_{hT}}{2R_p}, \frac{S_w(T'_c/\text{prop})}{8R_p^2}, (\bar{\epsilon}_h)_{\text{props off}}\right)$
$\alpha_b = \epsilon_u - \epsilon_p$	Inclination of slipstream centerline behind propeller relative to X-body axis	Table 5.1.1-2(a)-3, column 5	Variable
S_{hi}	Total immersed horizontal-tail area, sq ft	Figure 5-1(b)	15.26
$\frac{S_{hi}}{S_h}$	Parameter for determining $\frac{\Delta \bar{q}_h}{\bar{q}_\infty}$	-----	.470
z_s	Vertical distance from X-body axis to slipstream centerline at $\frac{\bar{c}_l}{4}$ station of immersed portion of wing, as shown in figure 5-2	Table 5.1.1-2(a)-3, column 6	Variable
z_h	Vertical distance from X-body axis to horizontal tail, ft	Figure 5-2	-1.67
l'_h	Distance along X-body axis from $\frac{\bar{c}_l}{4}$ of immersed wing area to $\frac{\bar{c}_h}{4}$, ft	Figure 5-2	13.76
z_{heff}	Vertical distance from $\frac{\bar{c}_h}{4}$ to slipstream centerline, $z_{heff} = z_s - \frac{l'_h}{57.3} [\alpha_b - \epsilon_u - \epsilon_p - (\bar{\epsilon}_h)_{\text{props off}} - (\Delta \epsilon_h)_{\text{power}}] - z_h$ $= z_s - 0.241 [\alpha_b - \epsilon_u - \epsilon_p - (\bar{\epsilon}_h)_{\text{props off}} - (\Delta \epsilon_h)_{\text{power}}] + 1.67$	Figure 5-2	Variable
$\frac{\Delta \bar{q}_h}{\bar{q}_\infty}$	Dynamic-pressure increment at horizontal tail due to power as a ratio of free-stream dynamic pressure	Figure 5.1.2-3	$f\left(\frac{z_{heff}}{R_p}, \frac{S_w(T'_c/\text{prop})}{8R_p^2}, \frac{S_{hi}}{S_h}\right)$
$\left(\frac{\bar{q}_h}{\bar{q}_\infty}\right)_{\text{prop off}}$	Propeller-off dynamic-pressure ratio at horizontal tail as a ratio of free-stream dynamic pressure	Figure 4.9.1-7	Function of α_b
$\left(\frac{C_{Lh(hn)}}{S_h} \frac{\bar{q}_h}{\bar{q}_\infty}\right)'_{\bar{q}_\infty=1.0}$	C_L of horizontal tail referenced to tail area and a dynamic-pressure ratio of 1.0	Figure 4.13.3-1	$f(\alpha_h, \delta_c)$
C_{Lwfn}	Tail-off C_L with power on referenced to $S_w = 178$ sq ft	Table 5.1.1-3, column 7	Variable

TABLE 5.1.2-1 (Continued)

(b) Summary of effect of elevator deflection on lift with power on

$$(b)-1: T'_c = 0; \frac{\delta_{lab}}{\delta_e} = 1.5$$

①	②	③	④	⑤	⑥	⑦	⑧	⑨	⑩	⑪	⑫
	Table 5.1.1-2(a)-3, column 5	Figure 4.9.1-7	Figure 5.1.2-2	-----	Table 5.1.2-1(a)	Table 5.1.2-3, column 6	Table 5.1.2-1(a)	Figure 5.1.2-3	Figure 4.9.1-7	-----	-----
α_b , deg	$\alpha_b - \epsilon_u - \epsilon_p$, deg	$\bar{\epsilon}_h$ props off', deg	$(\Delta \epsilon)_p$ power', deg	② - ③ - ④	L'_h 57.3	z_s	$\frac{z_{heff}}{R_p} = \frac{⑥ + ⑦}{3}$	$\frac{\Delta \bar{q}_h}{\bar{q}_\infty}$	$\left(\frac{\bar{q}_h}{\bar{q}_\infty}\right)$ prop off	$\left(\frac{\bar{q}_h}{\bar{q}_\infty}\right)$ power	① - ③ - ④
			(a)	-0.241 ⑤ + 1.67				(b)		$= ⑨ + ⑩$	
-4	-3.9064	0	0	-3.91	2.61	-0.4600	0.7167	0	1.0	1.0	-4.00
-2	-1.5626	.962	0	-2.52	2.28	-.7054	-.5249	0	1.0	1.0	-2.96
0	0.7813	1.900	0	-1.12	1.94	-0.9508	0.3297	0	1.0	1.0	-1.90
2	3.1251	2.930	0	.20	1.62	-1.1962	.1413	0	1.0	1.0	-.93
4	5.4690	3.870	0	1.60	1.28	-1.4416	-0.0539	0	1.0	1.0	0.13
6	7.8128	4.860	0	2.95	.96	-1.6870	-.2423	0	1.0	1.0	1.14
8	10.1566	5.770	0	4.39	0.61	-1.9324	-0.4408	0	1.0	1.0	2.23
10	12.5005	6.610	0	5.89	.25	-2.1778	-.6426	0	1.0	1.0	3.39
12	14.8443	7.550	0	7.29	-0.09	-2.4232	-0.8371	0	1.0	1.0	4.45
13.8	16.8952	8.300	0	8.60	-.40	-2.6379	-1.0126	0	1.0	1.0	5.50

①	⑬	⑭	⑮
	Figure 4.13.3-1	Equation (5.1.2-1)	Table 5.1.2-3, column 7
α_b , deg	$(\bar{C}_{LH}(\alpha))'$ $S_h, \bar{q}_h/\bar{q}_\infty = 1.0$	$\bar{C}_{LH}(\alpha) = \frac{S_h}{S_w}$	C_{LWfn}
	δ_e , deg	δ_e , deg	$S_w = 178$ sq ft
	4 0 -5 -10 -14	4 0 -5 -10 -14	4 0 -5 -10 -14
-4	0.135 -0.298 -0.843 -1.180 -1.010	0.0247 -0.0544 -0.1539 -0.2155 -0.1844	-0.01336 -0.0738 -0.1733 -0.2349 -0.2038
-2	.213 -.220 -.764 -1.178 -1.033	-.0389 -.0402 -.1395 -.2151 -.1886	.14000 .1789 .0998 .0005 -.0751
0	0.292 -0.140 -0.686 -1.135 -1.138	0.0533 -0.0256 -0.1253 -0.2109 -0.2078	0.30000 0.3533 0.2744 0.1747 0.0891
2	.362 -.070 -.614 -1.118 -1.232	.0661 -.0128 -.1121 -.2041 -.2250	.16009 .5262 .4473 .3450 .2560
4	0.446 0.013 -0.533 -1.054 -1.250	0.0814 0.0024 -0.0973 -0.1925 -0.2282	0.62027 0.7017 0.6227 0.5280 0.4278
6	.518 .087 -.457 -.977 -1.235	.0946 .0159 -.0834 -.1784 -.2255	.78158 .8762 .7975 .6982 .5561
8	0.589 0.167 -0.377 -0.898 -1.200	0.1094 0.0305 -0.0688 -0.1640 -0.2191	0.94210 1.0515 0.9726 0.8733 0.7781
10	.685 .252 -.292 -.812 -1.147	.1251 .0460 -.0533 -.1483 -.2094	1.10380 1.2309 1.1518 1.0525 .9575
12	0.762 0.332 -0.212 -0.733 -1.068	0.1391 0.0606 -0.0387 -0.1338 -0.1950	1.24286 1.3820 1.3035 1.2042 1.1091
13.8	.840 .410 -.135 -.655 -0.990	.1534 .0749 -.0217 -.1196 -.1808	1.28420 1.4376 1.3591 1.2595 1.1646

$$^a \frac{z_{heff}}{2R_p} = 0.133; \frac{S_w(T'_c/prop)}{8R_p^2} = 0; \text{column 3.}$$

$$^b \frac{S_w(T'_c/prop)}{8R_p^2} = 0; \frac{S_h}{S_w} = 0.470; \text{column 8}$$

TABLE 5.1.2-1 (Continued)

(b)-2: $T'_c = 0.20$; $\frac{\delta_{tab}}{T'_c} = 1.5$

①	②	③	④	⑤	⑥	⑦	⑧	⑨	⑩	⑪	⑫
Table 5.1.2-1(a)-3, Figure 4.9.1-7, column 5											
α_b , deg	$\alpha_b - \epsilon_b - \epsilon_p$, deg	$(\bar{\epsilon}_b)_{\text{props off.}}$, deg	$(\Delta \epsilon_b)$, power, deg	$\frac{\bar{\epsilon}_b}{57.3}$, ⑤ - ④	$\frac{\bar{\epsilon}_b}{57.3}$, ⑤ - ④	z , ft	$\frac{z_{\text{eff}}}{R_p} = \frac{⑥ + ⑦}{3}$	$\frac{\Delta \bar{\epsilon}_b}{q_\infty}$, (b)	$\left(\frac{\bar{\epsilon}_b}{q_\infty}\right)$, power off	$\left(\frac{\bar{\epsilon}_b}{q_\infty}\right)$, power = ⑨ + ⑩	$\gamma_h = \frac{⑪ - ⑫ - ⑬}{\text{deg}}$
-4	-3.2052	0	0	-3.21	2.44	-0.5334	0.6355	0.0868	1.0	1.0868	-4.00
-2	-1.2821	.982	.72	-2.96	2.38	-0.7348	.5484	.1028	1.0	1.1028	-3.68
0	0.6410	1.900	1.33	-2.56	2.29	-0.9361	0.4513	0.1167	1.0	1.1167	-3.23
2	2.5642	2.930	1.90	-2.27	2.22	-1.1375	.3608	.1222	1.0	1.1222	-2.83
4	4.4873	3.870	2.46	-1.84	2.11	-1.3388	0.2571	0.1333	1.0	1.1333	-2.33
6	6.4104	4.860	2.88	-1.33	1.99	-1.5402	.1499	.1889	1.0	1.1389	-1.71
8	8.3335	5.770	3.23	-0.67	1.83	-1.7415	0.0295	0.1444	1.0	1.1444	-1.00
10	10.2566	6.610	3.52	-.13	1.64	-1.9429	-.1010	.1417	1.0	1.1417	-.13
12	12.1798	7.550	3.80	0.83	1.47	-2.1442	-0.2247	0.1361	1.0	1.1361	0.65
13.8	13.8625	8.300	3.98	1.58	1.29	-2.3204	-.3435	.1278	1.0	1.1278	1.52
14.1	14.1830	8.400	4.02	1.76	1.25	-2.3540	-0.3680	0.1222	1.0	1.1222	1.68

①	⑬	⑭	⑮	⑯
Figure 4.13.3-1				
Equation (5.1.2-1)				
α_b , deg	$(\bar{\epsilon}_b)_{\text{tab}} S_h, \bar{q}_b/q_\infty = 1.0$	$\bar{C}_{Lb}(\alpha_b) = \frac{S_h}{S_w} \frac{13}{11} = 0.1826 \frac{13}{11}$	$C_{L_{wfn}}$, $S_w = 178$ sq ft	$C_L = ⑬ + ⑭$ referenced to $S_w = 178$ sq ft
	δ_e , deg	δ_e , deg	δ_e , deg	
	4	4	4	4
-4	0.135	-0.298	-0.843	-0.195
-2	0.158	-0.275	-0.820	.2059
0	0.194	-0.237	-0.786	0.3948
2	0.223	-0.209	-0.753	.5806
4	0.261	-0.170	-0.718	0.7675
6	0.303	-0.130	-0.676	.9548
8	0.358	-0.072	-0.617	1.1428
10	0.420	-0.011	-0.554	1.3292
12	0.480	0.047	-0.495	1.5159
13.8	.542	.112	-.432	1.7017
14.1	0.560	0.128	-0.417	1.8810

$\frac{S_h(T'_c/\text{prop})}{2R_p} = 0.133$; $\frac{S_h(T'_c/\text{prop})}{8R_p^2} = 0.247$; column 3

$\frac{S_h(T'_c/\text{prop})}{8R_p^2} = 0.247$; $\frac{S_h}{S_w} = 0.470$; column 8.

TABLE 5.1.2-1(Concluded)

(b)-3: $T'_c = 0.44$; $\frac{\delta_{tab}}{\delta_c} = 1.5$

①	②	③	④	⑤	⑥	⑦	⑧	⑨	⑩	⑪	⑫
	Table 3.1.1-2(a)-3, column 5	Figure 4.9.1-7	Figure 5.1.2-2	-----	Table 5.1.2-1(a)	Table 5.1.2-1(a) column 6	Table 5.1.2-1(a)	Figure 5.1.2-3	Figure 4.9.1-7	-----	-----
α_b , deg	$\alpha_b - \epsilon_u - \epsilon_p$, deg	$(\bar{\epsilon}_b)_{prop off}$, deg	$(\Delta \epsilon_b)_{power}$, deg	$\textcircled{2} - \textcircled{3} - \textcircled{4}$	$\textcircled{5} - \textcircled{6} = \frac{I'_b}{57.3}$ $-0.241 \textcircled{5} + 1.67$	z_s	$\frac{z_{heff} = \textcircled{6} + \textcircled{7}}{R_p}$	$\frac{\Delta \bar{\epsilon}_b}{\bar{\epsilon}_\infty}$	$\left(\frac{\bar{\epsilon}_b}{\bar{\epsilon}_\infty}\right)_{prop off}$	$\left(\frac{\bar{\epsilon}_b}{\bar{\epsilon}_\infty}\right)_{power}$ $\textcircled{9} + \textcircled{10}$	$\alpha_b = \textcircled{1} - \textcircled{3} - \textcircled{4}$, deg
-4	-2.8416	0	0	-2.84	2.35	-0.5715	0.5928	0.2027	1.0	1.2027	-4.00
-2	-1.1366	.962	1.12	-3.22	2.45	-.7500	.5667	.2108	1.0	1.2108	-4.08
0	0.5683	1.900	2.09	-3.42	2.49	-0.9285	0.5205	0.2216	1.0	1.2216	-3.99
2	2.2733	2.830	2.96	-3.62	2.54	-1.1070	.4777	.2324	1.0	1.2324	-3.89
4	3.9782	3.870	3.72	-3.61	2.54	-1.2855	0.4182	0.2432	1.0	1.2432	-3.59
6	5.6832	4.860	4.46	-3.64	2.55	-1.4640	.3620	.2541	1.0	1.2541	-3.32
8	7.3882	5.770	5.06	-3.44	2.50	-1.6425	0.2858	0.2622	1.0	1.2622	-2.83
10	9.0931	6.610	5.44	-2.96	2.38	-1.8210	.1863	.2676	1.0	1.2676	-2.05
12	10.7981	7.550	5.84	-2.38	2.29	-1.9996	0.0968	0.2757	1.0	1.2757	-1.39
13.8	12.2899	8.300	6.11	-2.12	2.18	-2.1538	.0081	.2811	1.0	1.2811	-.61
14.1	12.5741	8.400	6.13	-1.96	2.14	-2.1855	-0.0152	0.2811	1.0	1.2811	-0.43
14.4	12.8582	8.500	6.16	-1.80	2.10	-2.2153	-.0384	.2784	1.0	1.2784	-.26

①	⑬	⑭	⑮	⑯
	Figure 4.13.3-1	Equation (5.1.2-1)	Table 5.1.1-3, column 1	-----
α_b , deg	$(\bar{\epsilon}_b)_{prop off}$, $\bar{\epsilon}_b/\bar{\epsilon}_\infty = 1.0$	$\bar{\epsilon}_{LH}(hf) = \frac{\bar{\epsilon}_b}{S_w} \textcircled{13} \textcircled{11} = 0.1826 \textcircled{13} \textcircled{11}$	C_{Lwf} ($S_w = 178$)	$C_L = \textcircled{14} + \textcircled{15}$ referenced to $S_w = 178$ sq ft
	δ_c , deg	δ_c , deg	δ_c , deg	δ_c , deg
	4 0 -5 -10 -14	4 0 -5 -10 -14	4 0 -5 -10 -14	4 0 -5 -10 -14
-4	0.135 -0.298 -0.843 -1.180 -1.010	0.0296 -0.0654 -0.1851 -0.2591 -0.2219	0.00815	0.0578 -0.0572 -0.1770 -0.2510 -0.2138
-2	.130 -.304 -.850 -1.178 -1.010	.0287 -.0672 -.1879 -.2604 -.2233	.20987	.2386 -.1427 .0220 -.0505 -.0134
0	0.134 -0.297 -0.842 -1.180 -1.011	0.0299 -0.0662 -0.1878 -0.2632 -0.2255	0.41043	0.4403 0.3442 0.2226 0.1472 0.1849
2	.144 -.289 -.835 -1.180 -1.013	.0324 -.0650 -.1879 -.2655 -.2260	.60886	.6413 .5439 .4210 .3434 .3809
4	0.165 -0.267 -0.813 -1.180 -1.020	0.0375 -0.0606 -0.1846 -0.2679 -0.2315	0.80455	0.8420 0.7440 0.6200 0.5366 0.5730
6	.189 -.245 -.790 -1.180 -1.030	.0433 -.0561 -.1809 -.2702 -.2359	1.00016	1.0435 .9441 .8193 .7300 .7643
8	0.222 -0.207 -0.754 -1.175 -1.054	0.0512 -0.0477 -0.1737 -0.2708 -0.2429	1.19062	1.2418 1.1429 1.0169 0.9198 0.9477
10	.283 -.150 -.697 -1.159 -1.124	.0655 -.0655 -.1613 -.2683 -.2602	1.37936	1.4449 1.3447 1.2181 1.1111 1.1192
12	0.330 -0.103 -0.649 -1.136 -1.194	0.0769 -0.0240 -0.1512 -0.2646 -0.2781	1.53218	1.6091 1.5082 1.3810 1.2676 1.2541
13.8	.390 -.045 -.590 -1.100 -1.244	.0912 -0.0106 -0.1389 -.2573 -.2910	1.63031	1.7215 1.6197 1.4923 1.3730 1.3393
14.1	0.402 -0.030 -0.575 -1.091 -1.248	0.0940 -0.0070 -0.1345 -0.2552 -0.2919	1.62977	1.7238 1.6228 1.4953 1.3746 1.3379
14.4	.414 -.015 -.560 -1.080 -1.250	.0966 -.0035 -.1307 -.2521 -.2918	1.62700	1.7236 1.6235 1.4963 1.3749 1.3352

 $\frac{z_{LH}}{2R_p} = 0.133$; $\frac{S_w(T'_c/prop)}{8R_p^2} = 0.543$; column 3

 $\frac{S_w(T'_c/prop)}{8R_p^2} = 0.543$; $\frac{S_{b1}}{S_{b2}} = 0.470$; column 8

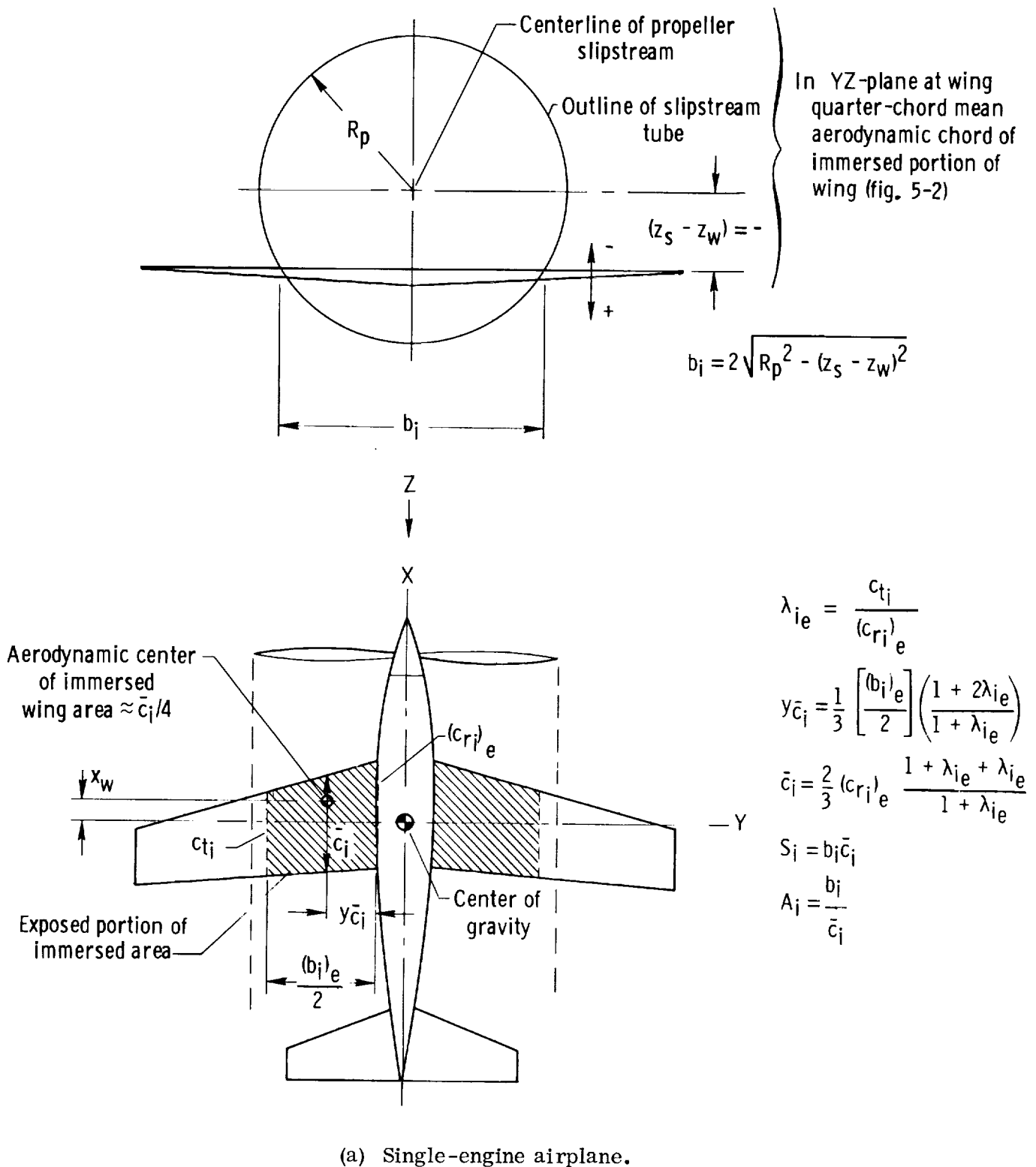


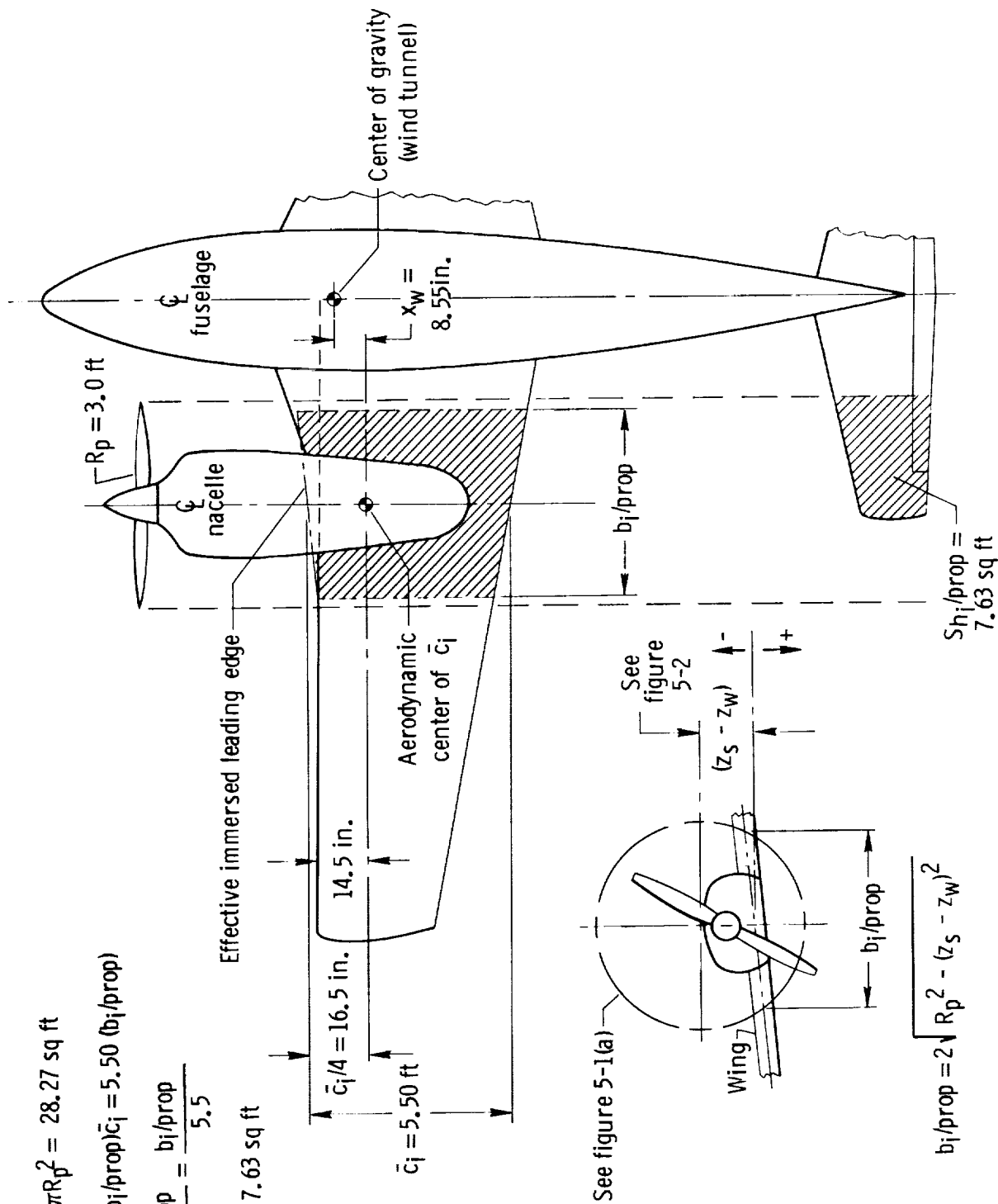
Figure 5-1. Definition sketches for calculation of immersed wing areas.

$$S_p/\text{prop} = \pi R_p^2 = 28.27 \text{ sq ft}$$

$$S_i/\text{prop} = (b_i/\text{prop})\bar{c}_i = 5.50 (b_i/\text{prop})$$

$$A_i = \frac{b_i/\text{prop}}{\bar{c}_i} = \frac{b_i/\text{prop}}{5.5}$$

$$S_{H_i}/\text{prop} = 7.63 \text{ sq ft}$$



(b) Twin-engine airplane (subject airplane).

Figure 5-1. Concluded.

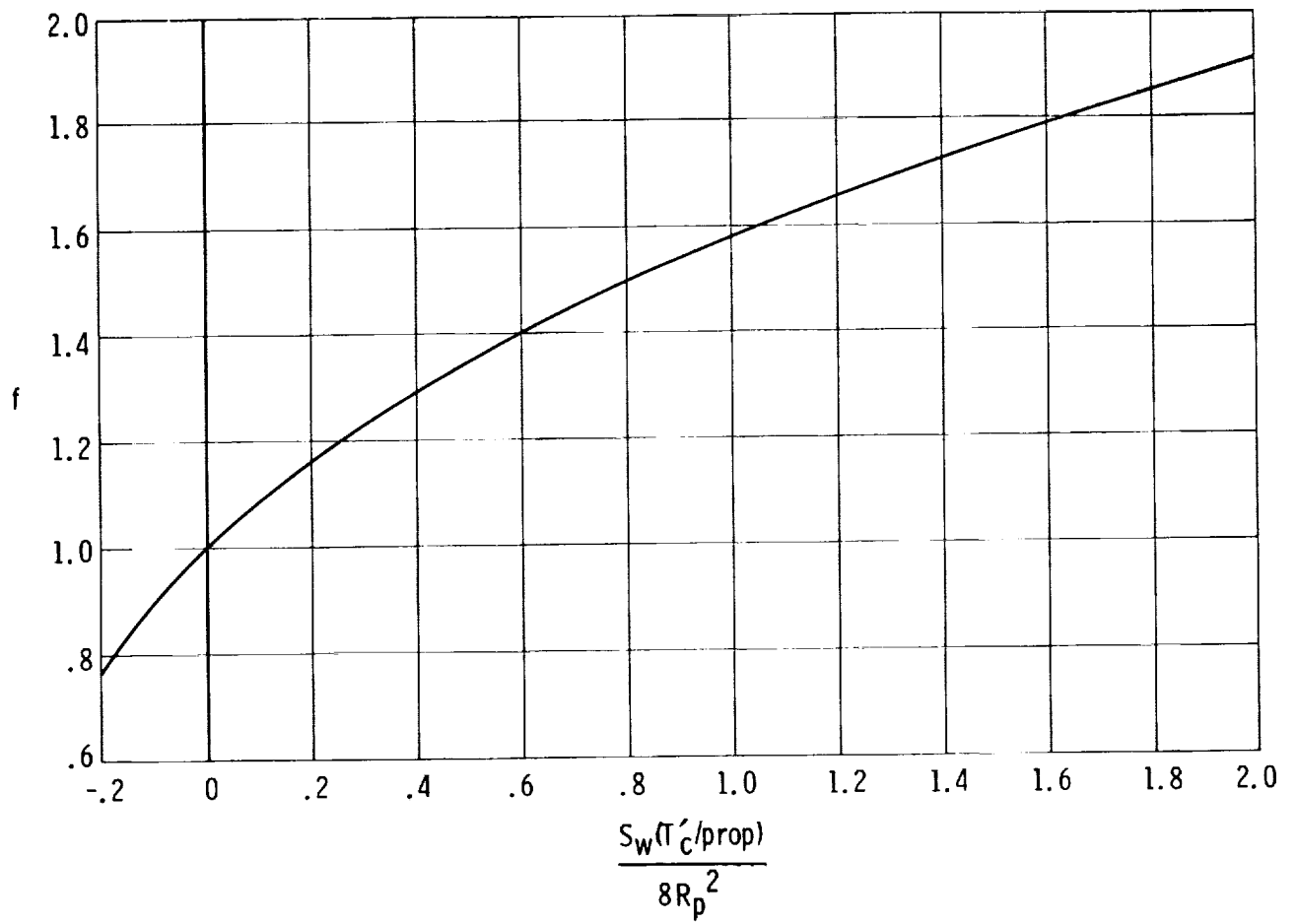


Figure 5.1.1-1. Propeller inflow factor (ref. 33).

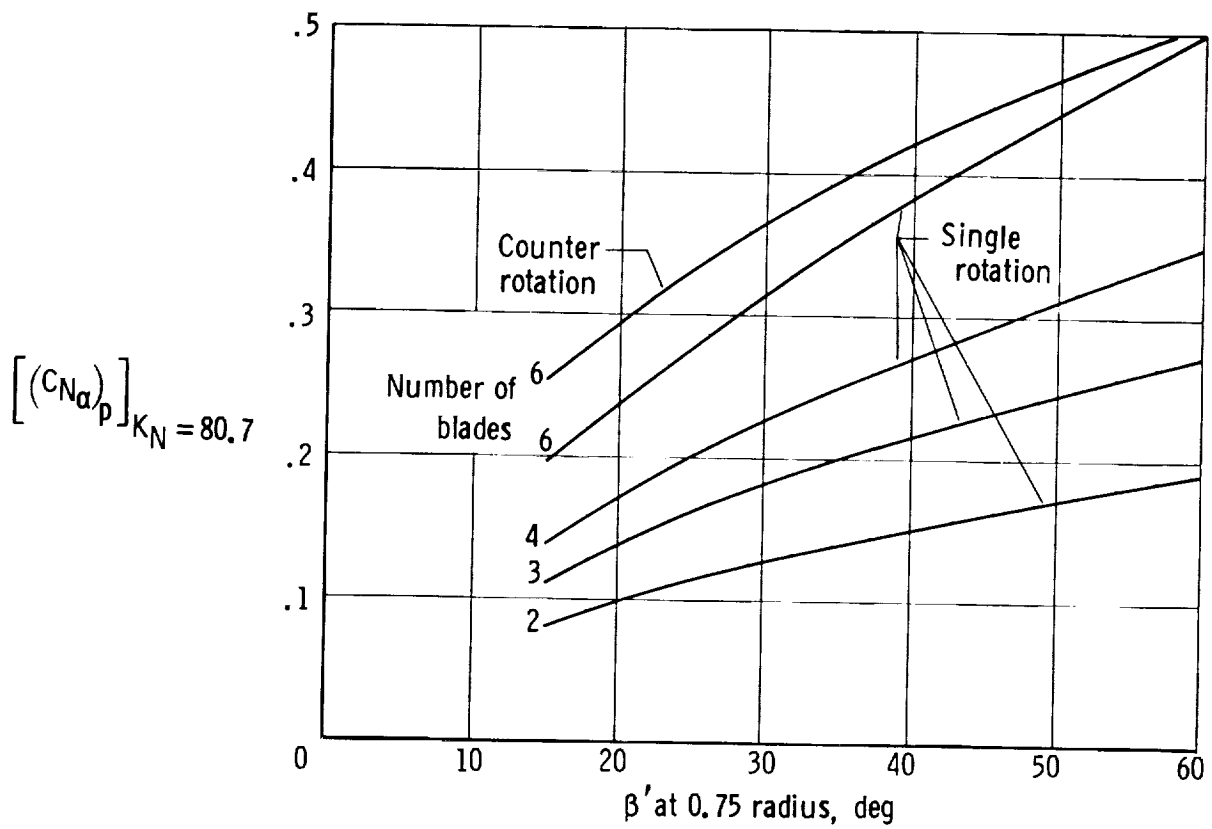


Figure 5.1.1-2. Propeller normal-force parameter (ref. 33).

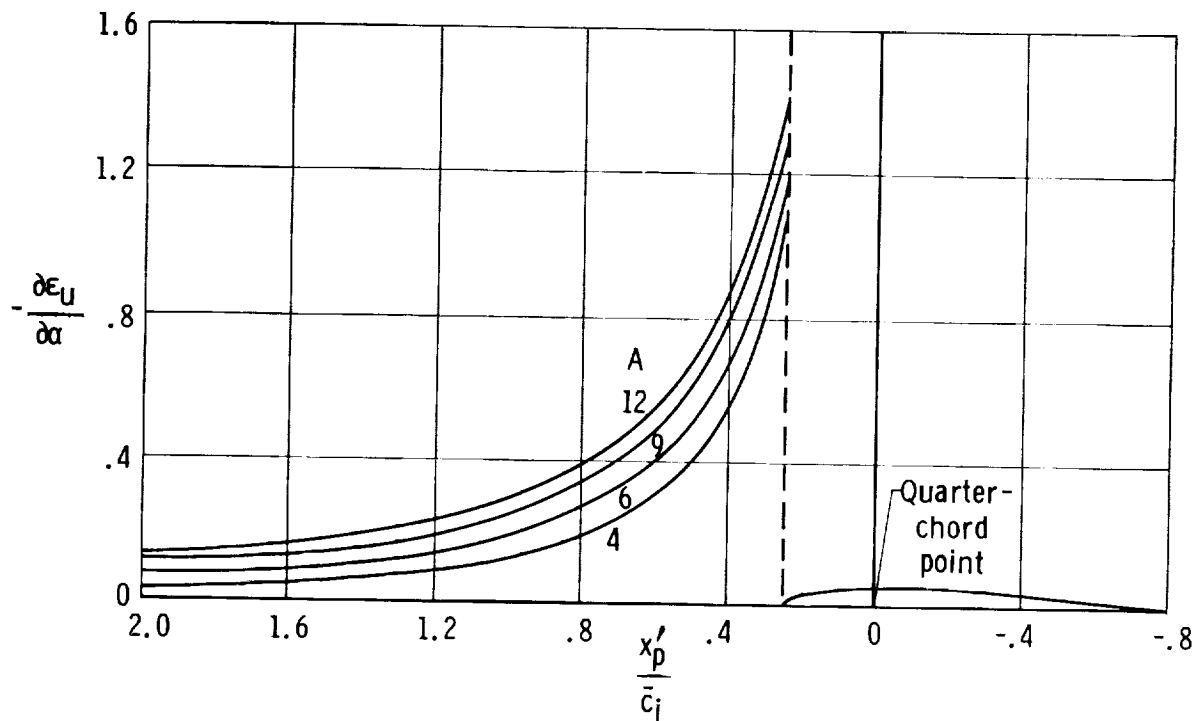


Figure 5.1.1-3. Upwash gradient at plane of symmetry for unswept wings (ref. 1).

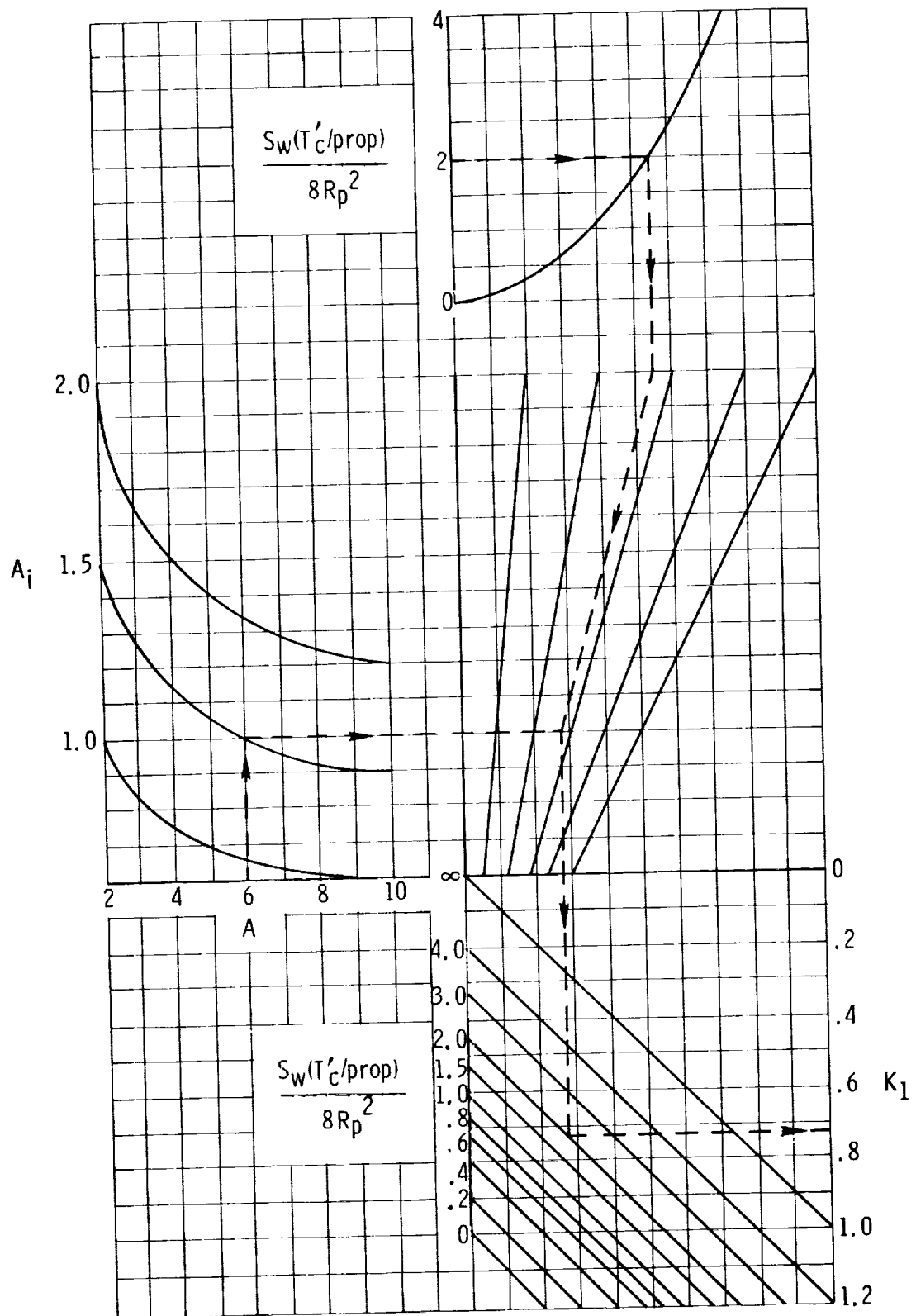


Figure 5.1.1-4. Correlation parameter for additional wing lift due to propeller power (ref. 19).

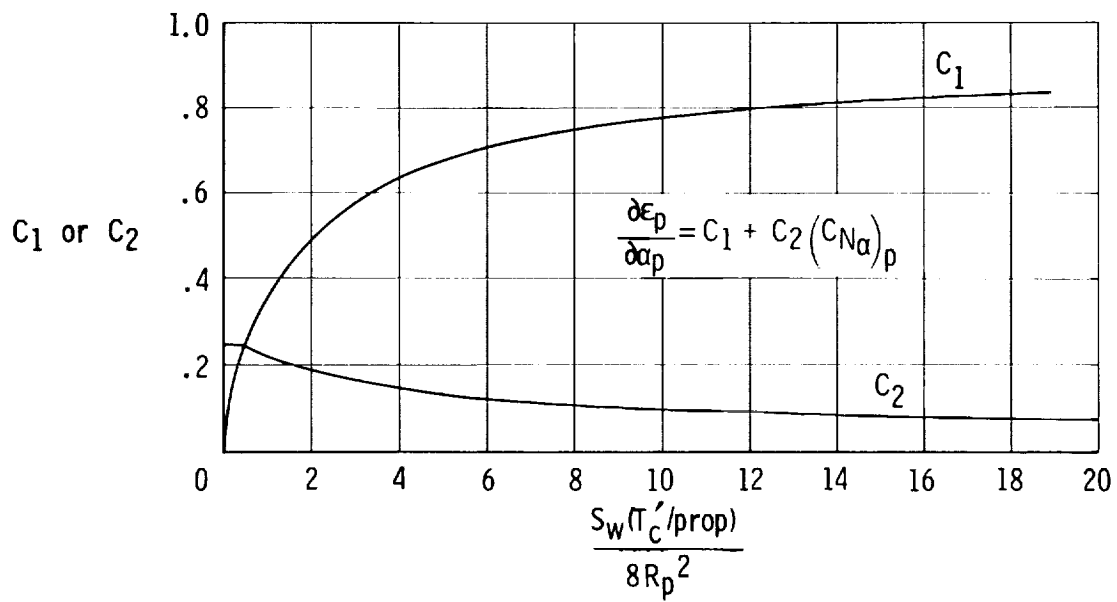


Figure 5.1.1-5. Factors for determining propeller downwash (ref. 19).

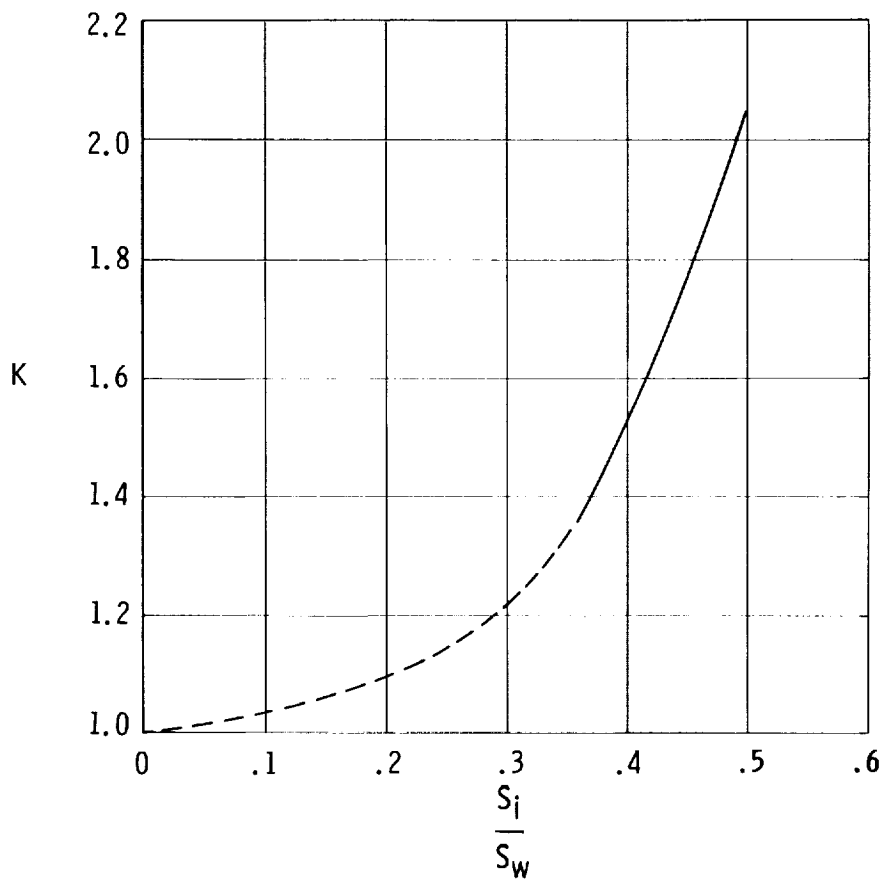
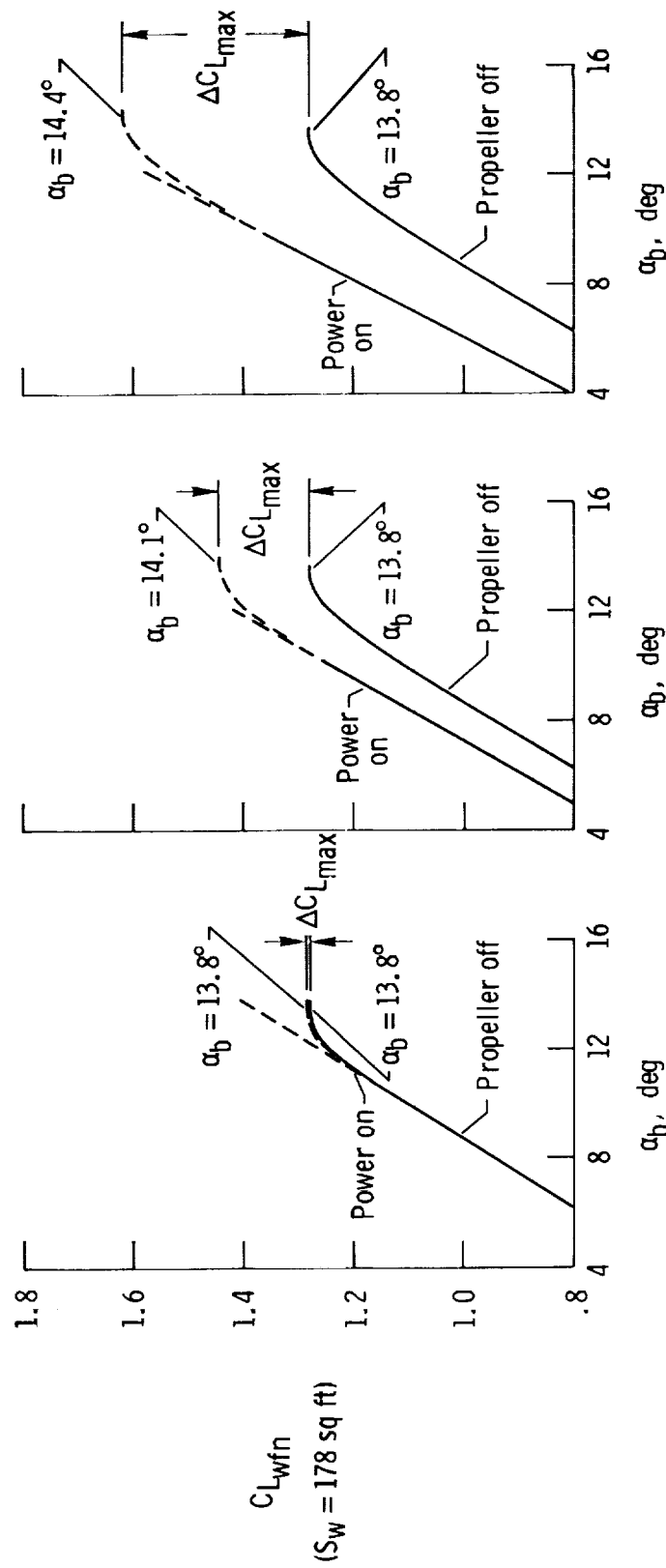


Figure 5.1.1-6. Correction factor for maximum lift due to power (ref. 1).



(a) $T'_C = 0$.

(b) $T'_C = 0.20$.

(c) $T'_C = 0.44$.

Figure 5.1.1-7. Working plots of tail-off lift characteristics of subject airplane used to obtain stall angles of attack due to power. $\Delta C_{L_{max}}$ obtained from table 5.1.1-4.

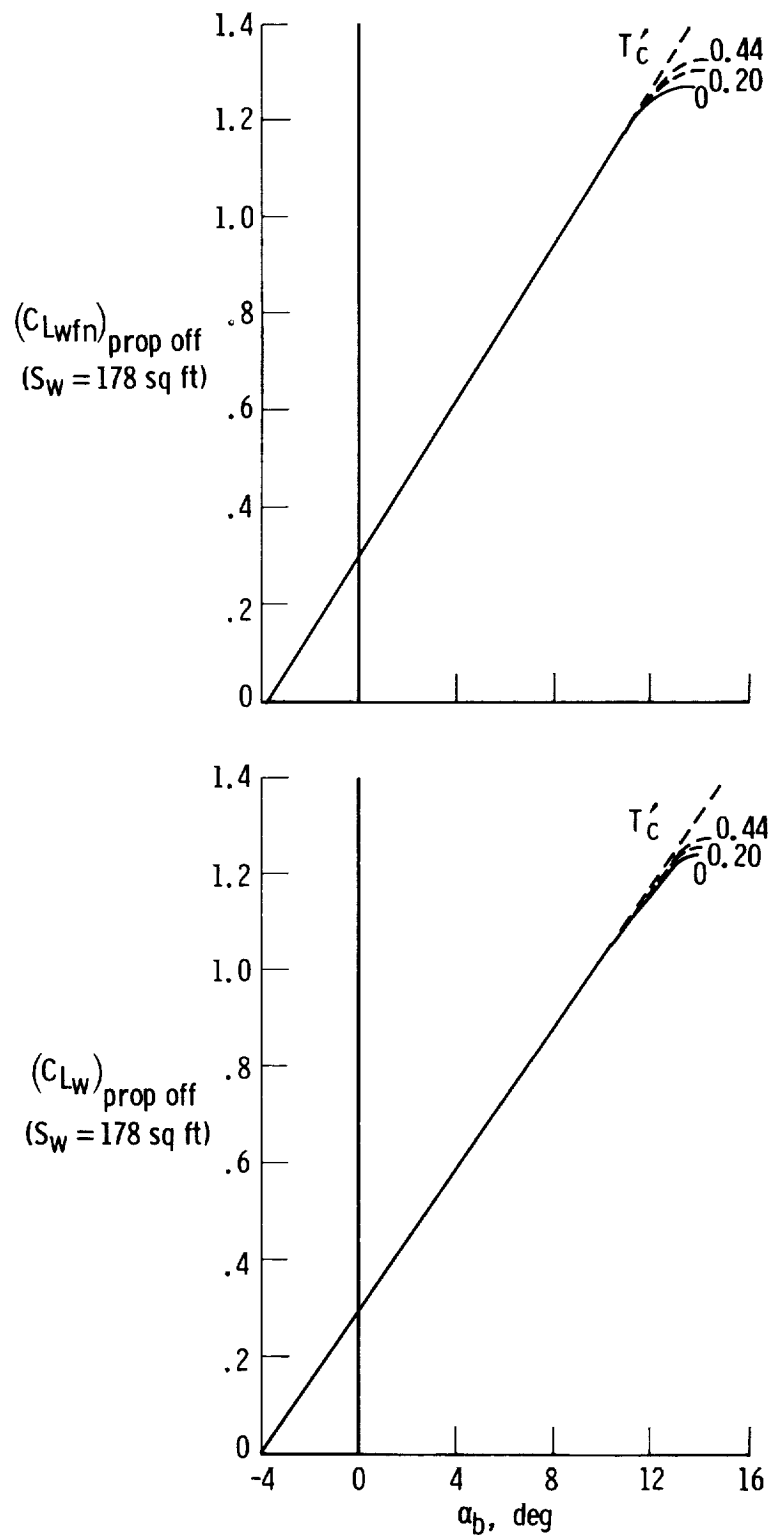


Figure 5.1.1-8. Propeller-off lift characteristics of subject airplane for wing alone and tail-off conditions with stall extended to power-on stall angles. (Power-on stall angles obtained from fig. 5.1.1-7.)

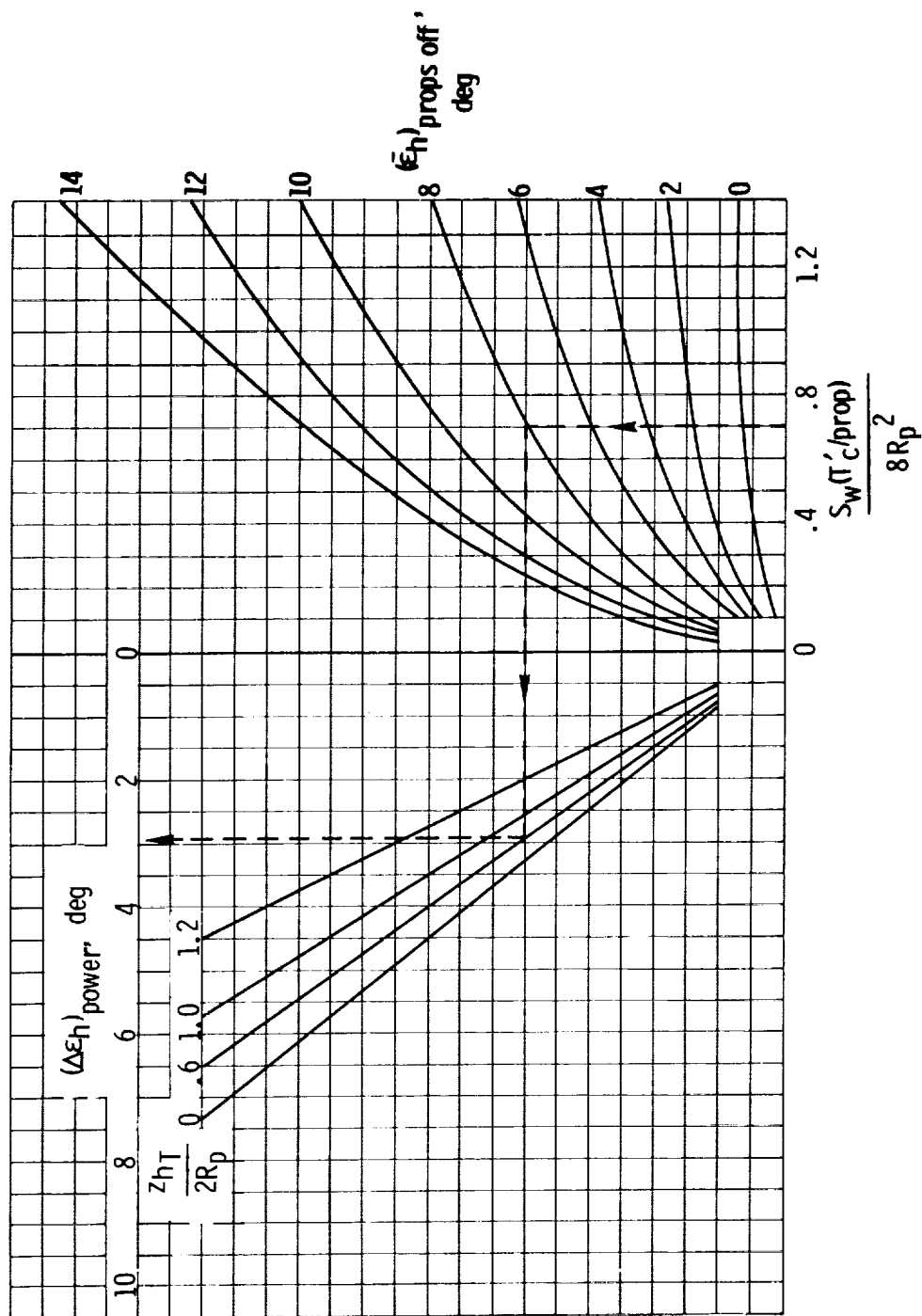


Figure 5.1.2-1. Increment in downwash due to propeller power for single-engine airplanes (ref. 19).

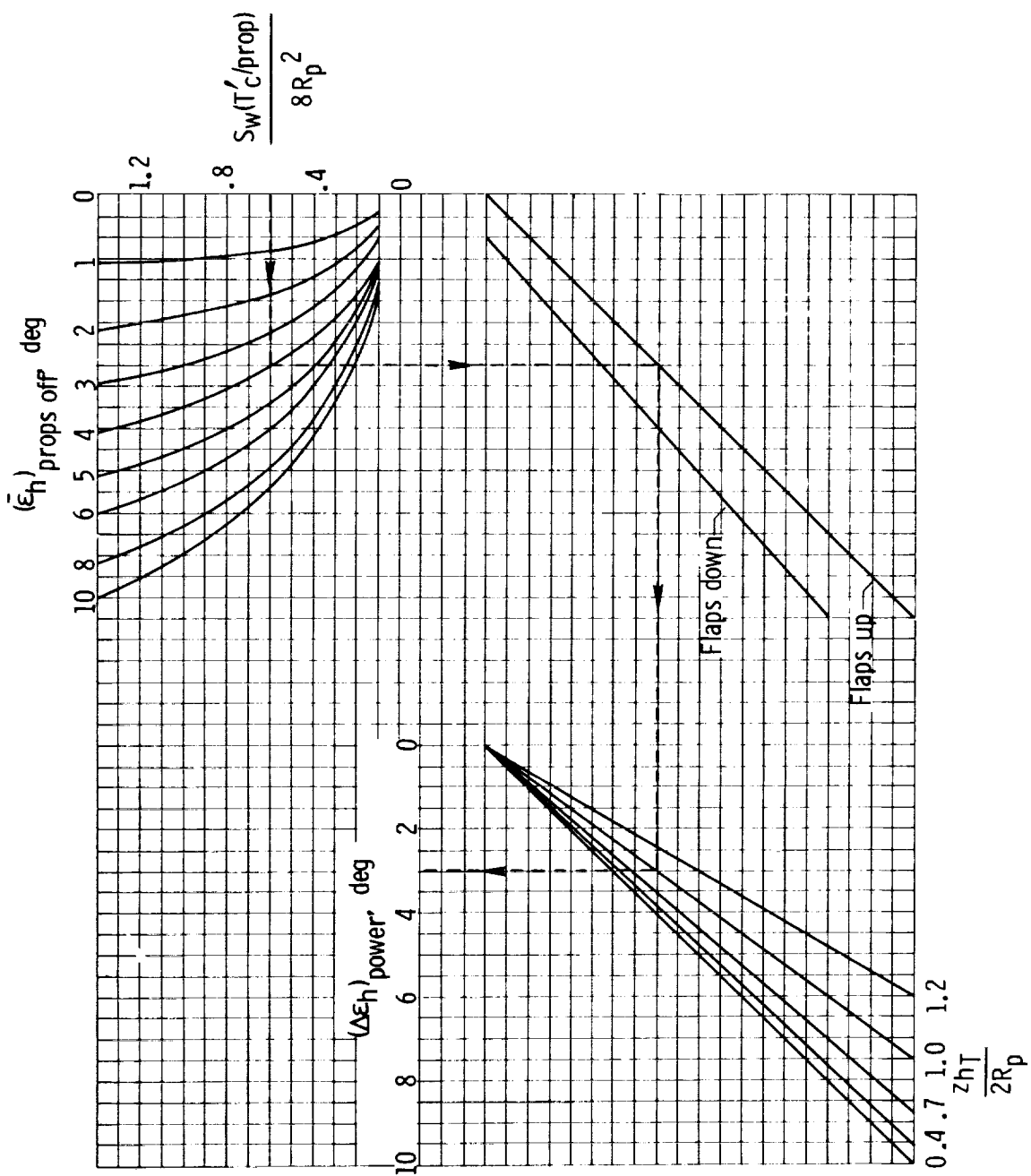


Figure 5.1.2-2. Increment in downwash due to propeller power for multiengine airplanes (ref. 19).

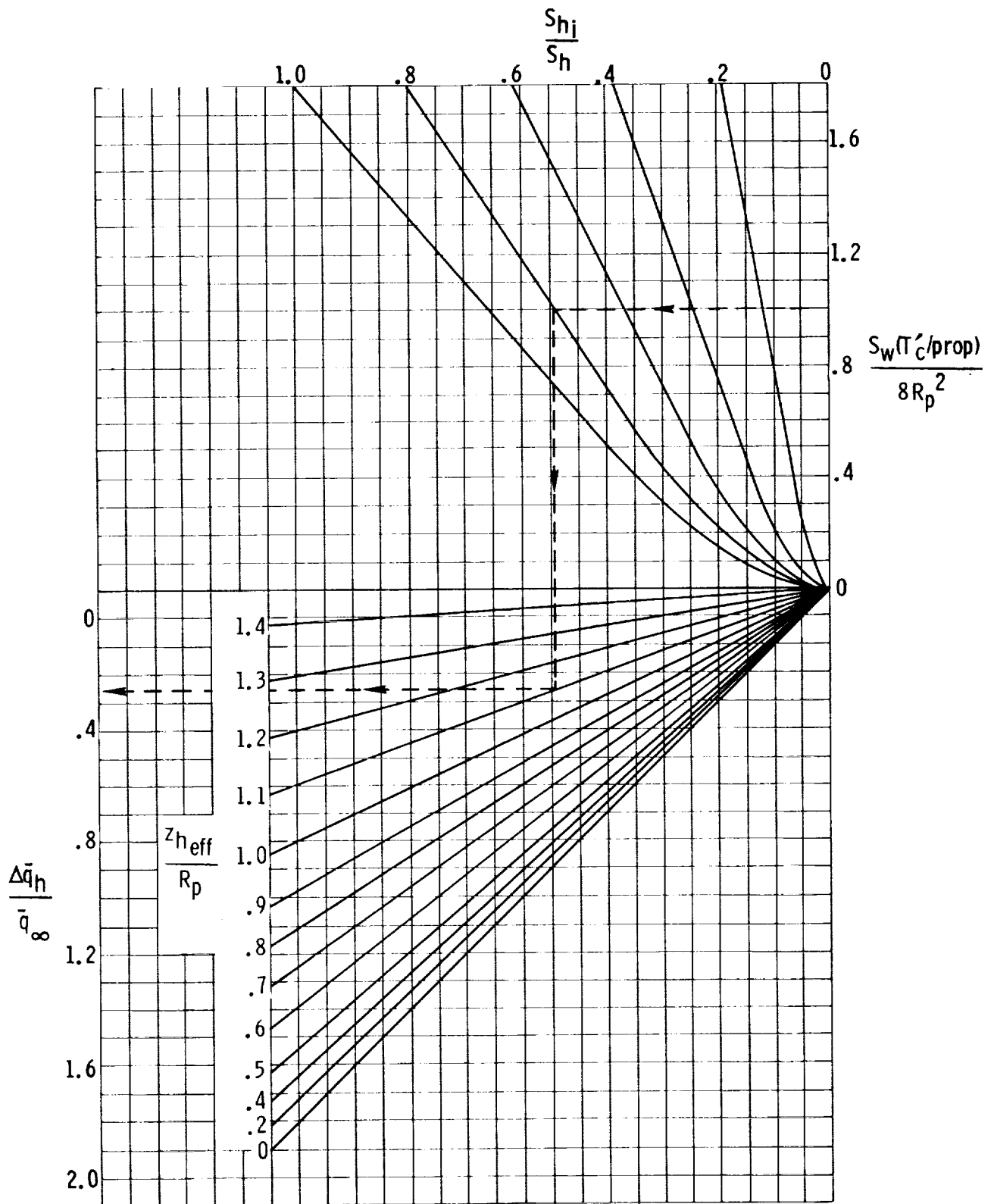


Figure 5.1.2-3. Effect of propeller power on the dynamic-pressure ratio at the horizontal tail (ref. 1).

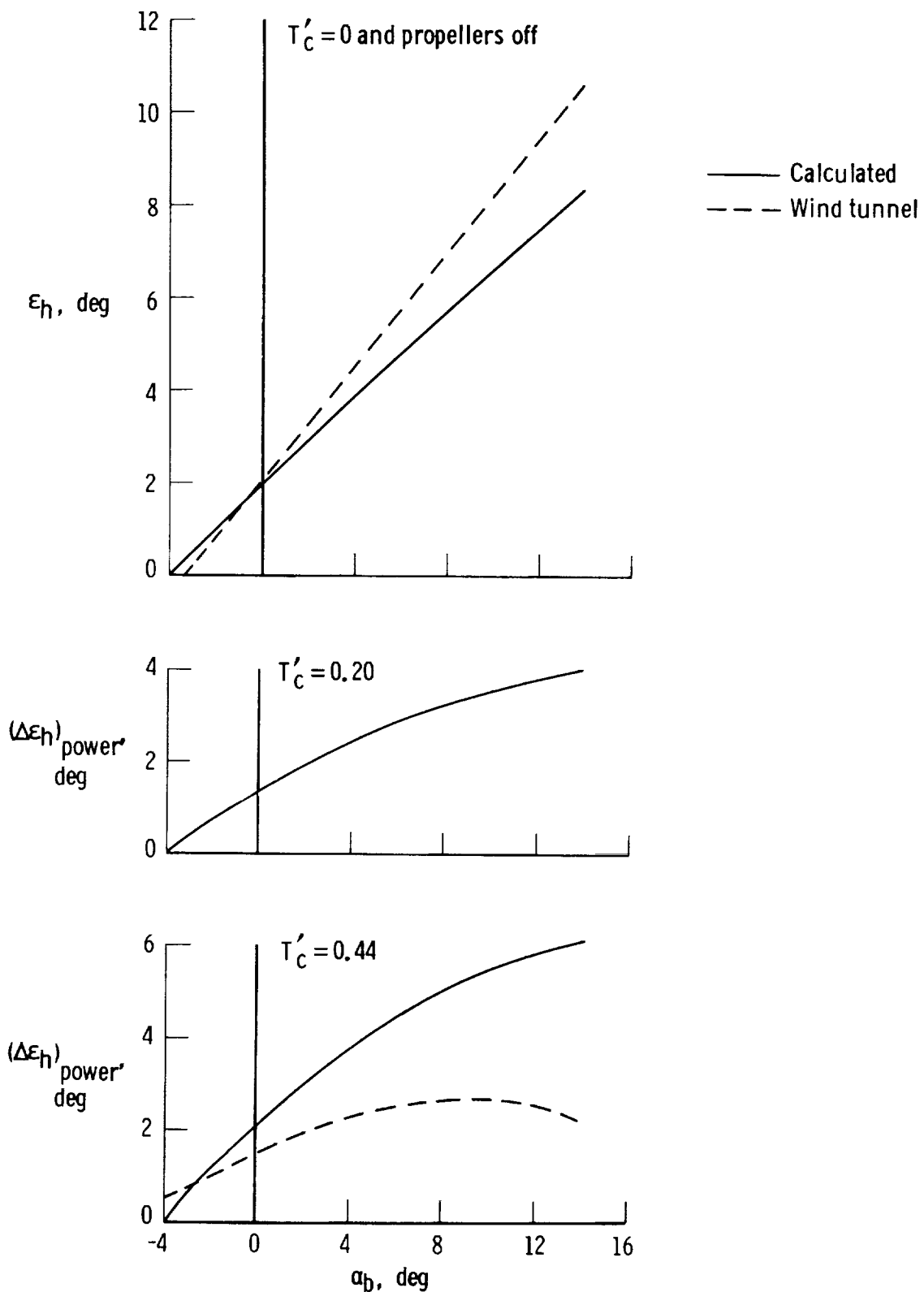


Figure 5.1.2-4. Comparison of calculated and experimentally determined (ref. 2) downwash at the horizontal tail of the subject airplane at several power settings.

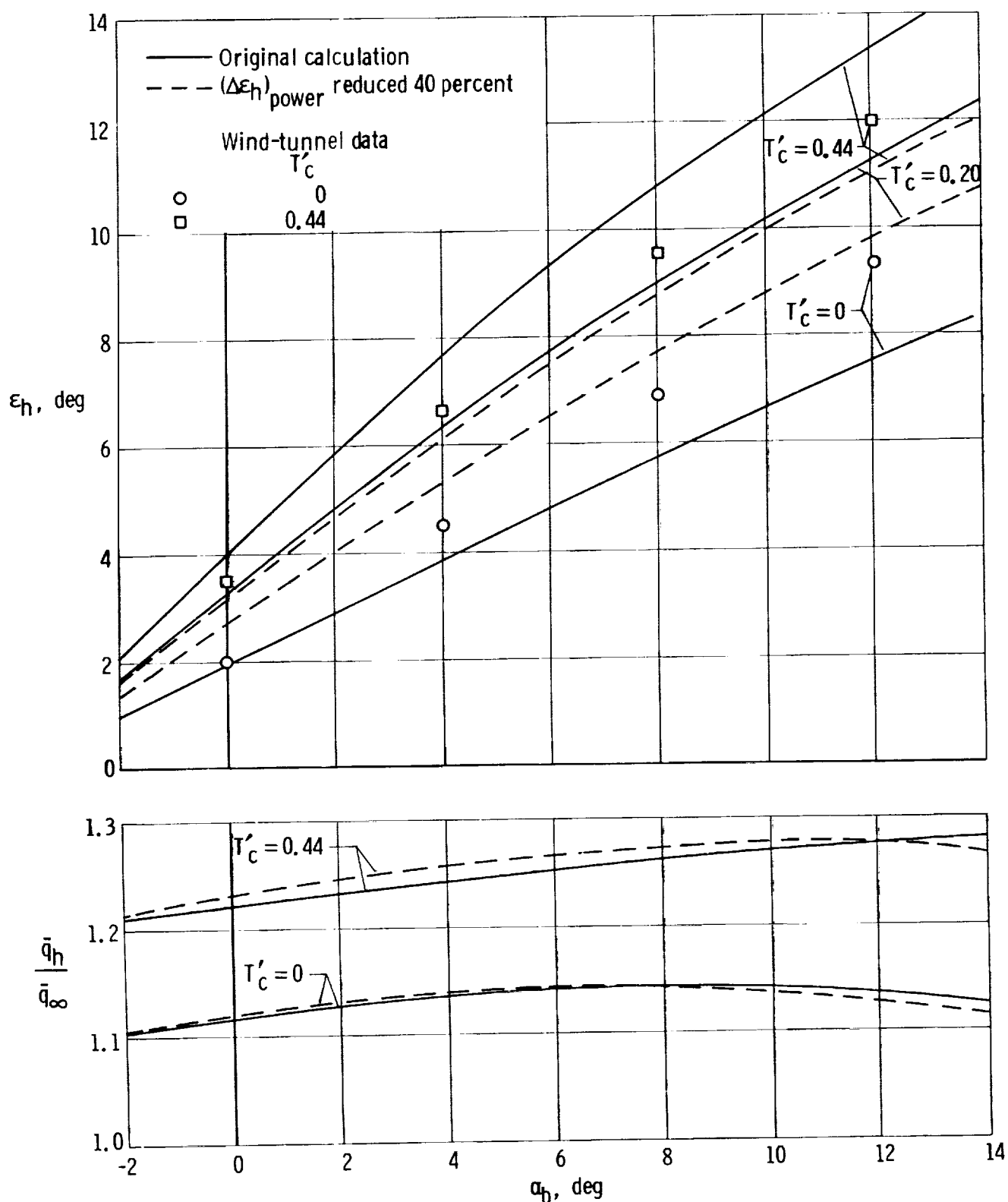


Figure 5.1.2-5. Variation of calculated downwash and dynamic-pressure ratio of horizontal tail with airplane angle of attack and total thrust coefficient, including wind-tunnel data for downwash at $T'_c = 0$ and $T'_c = 0.44$.

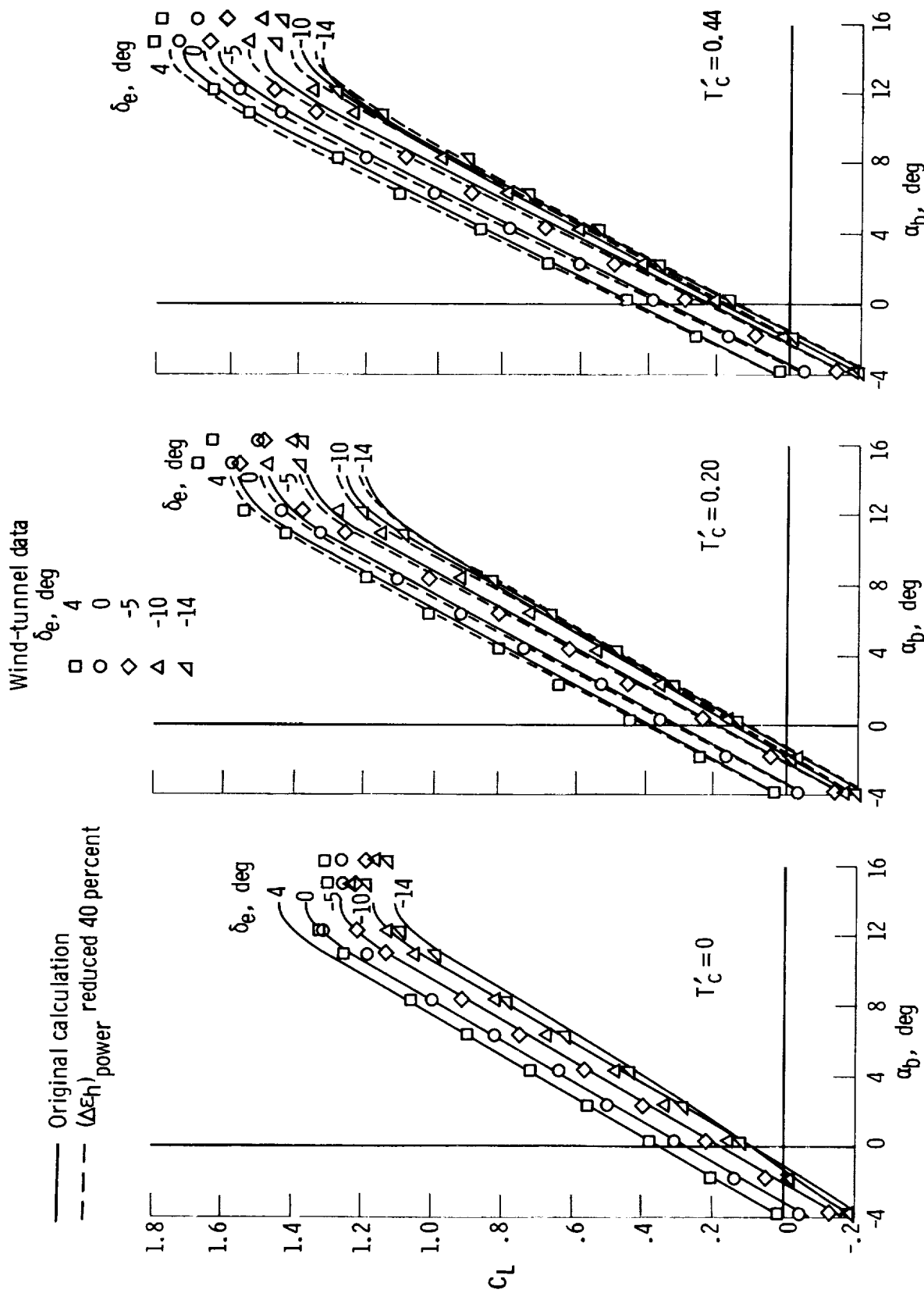


Figure 5.1.3-1. Comparison of calculated and wind-tunnel-determined variation of C_L with α_b at different power conditions and elevator deflections.

5.2 Power Effects on Pitching Moments

Power effects of propellers introduce increments of pitching moments due to direct action of the propeller forces offset from the center of gravity and propeller-induced slipstream effects on the wing, nacelles (or body), and the horizontal tail. Although all the increments of lift due to power (section 5.1) contribute to power-induced increments of pitching moment, several additional contributions must be considered. These additional contributions include the propeller slipstream dynamic-pressure effect on C_{m_0} and nacelle (or body) free moments.

The pitching moments of the subject airplane, as considered in the following calculations, can be represented by

$$C_m = \overbrace{(C_{m_{wfn}})_{\text{prop off}}}^{\text{Propeller forces}} + (\Delta C_m)_T + (\Delta C_m)_{N_p} + \overbrace{(\Delta C_{m_0})_{\Delta \bar{q}_w} + (\Delta C_m)_{w_L} + (\Delta C_m)_{n_p} + [(\Delta C_m)_h + (\bar{C}_{m_h(hf)})_{\text{props off}}]}^{\text{Propeller slipstream effects}} \quad (5.2-1a)$$

or

$$C_m = (C_{m_{wfn}})_{\text{prop off}} + (\Delta C_m)_T + (\Delta C_m)_{N_p} + \overbrace{(\Delta C_{m_0})_{\Delta \bar{q}_w} + (\Delta C_m)_{w_L} + (\Delta C_m)_{n_p}}^{(\Delta C_{m_{wfn}})_{\text{power}}} + \bar{C}_{m_h(hf)} \quad (5.2-1b)$$

where

$(C_{m_{wfn}})_{\text{prop off}}$ is the propeller-off, tail-off pitching moment obtained from section 4.8.3

$(\Delta C_m)_T$ is the pitching moment due to offset (distance z_T in fig. 5-2) of thrust from the center of gravity

$(\Delta C_m)_{N_p}$ is the pitching moment due to offset (distance x_p in fig. 5-2) of propeller normal force from the center of gravity

$(\Delta C_{m_0})_{\Delta \bar{q}_w}$ is the effect of propeller slipstream dynamic-pressure increment on zero-lift pitching moment

$(\Delta C_m)_{w_L}$ is the net effect on pitching moments due to change in wing lift resulting from propeller slipstream-induced dynamic-pressure and angle-of-attack changes on the wing, $(\Delta C_m)_{w_L} = [(\Delta C_m)_{\Delta \bar{q}_w} + (\Delta C_m)_{\epsilon_p}]$

$(\Delta C_m)_{n_p}$ is the effect of propeller slipstream on nacelle free moments

$(\Delta C_m)_h$ is the net effect of propeller slipstream on dynamic pressure and downwash on the horizontal tail

$\overline{C_{m_{h(hf)}}} = \left(\overline{C_{m_{h(hf)}}} \right)_{\text{prop off}} + (\Delta C_m)_h$ is the net pitching-moment contribution of the horizontal tail for power-on conditions (the tail is considered on a net power-on basis rather than on a summation of propeller-off and power-on increment basis)

The pitching-moment increment, $(\Delta C_m)_T$, due to propeller thrust is obtained from

$$(\Delta C_m)_T = n (T'_c / \text{prop}) \frac{z_T}{\bar{c}_w} \quad (5.2-2)$$

where

n is the number of propellers

z_T is the moment arm of the thrust relative to the center of gravity (fig. 5-2)

\bar{c}_w is the wing mean aerodynamic chord

The pitching-moment increment, $(\Delta C_m)_{N_p}$, due to the propeller normal force is obtained from

$$(\Delta C_m)_{N_p} = (\Delta C_L)_{N_p} \frac{x_p}{\bar{c}_w} \frac{1}{\cos \alpha_T} \quad (5.2-3)$$

where

$(\Delta C_L)_{N_p}$ is the increment of lift coefficient due to the normal force of the propeller, obtained from equation (5.1.1-2)

x_p is the moment arm of the propeller normal force relative to the center of gravity (fig. 5-2)

α_T is the angle of attack of the thrust axis

The zero-lift pitching-moment increment, $(\Delta C_{m_o})_{\Delta \bar{q}_w}$, due to propeller slip-stream effects on immersed portions of the wing-body or wing-nacelles at zero-lift conditions is accounted for by the following equation from reference 1:

$$(\Delta C_{m_o})_{\Delta \bar{q}_w} = \frac{\Delta \bar{q}_w}{\bar{q}_\infty} \frac{S_i}{S_w} \frac{\bar{c}_i}{\bar{c}_w} (C_{m_o})_{i_{\text{prop off}}} \quad (5.2-4)$$

where

$\frac{\Delta \bar{q}_w}{\bar{q}_\infty \frac{S_w(T'_C/\text{prop})}{\pi R_p^2}}$ is the increase in dynamic-pressure ratio of the immersed portion of the wing,

S_i is the immersed portion of the wing area, $n(b_i/\text{prop})\bar{c}_i$ (fig. 5.1(b))

\bar{c}_i is the mean chord of the immersed wing area (fig. 5-1(b))

S_w is the reference wing area

\bar{c}_w is the reference wing mean aerodynamic chord

For twin-engine airplanes, $(C_{m_o})_{i\text{prop off}}$ may be approximated by

$$(C_{m_o})_{i\text{prop off}} = (C_{m_o})_{wn\text{prop off}} - (C_{m_o})_{\text{area not immersed}} \quad (5.2-5)$$

where

$(C_{m_o})_{wn\text{prop off}}$ is the propeller off C_{m_o} of the wing and nacelles, obtained from section 4.6

and

$$(C_{m_o})_{\text{area not immersed}} \approx (C_{m_o})_{w\text{prop off}} \frac{S_w - S_i}{S_w} \frac{\bar{c}_{\text{not immersed}}}{\bar{c}_w} \quad (5.2-6)$$

where

$(C_{m_o})_{w\text{prop off}}$ is obtained from section 4.5

$$\bar{c}_{\text{not immersed}} \approx \frac{S_w - S_i}{b_w - b_i} \quad (5.2-7)$$

For a single-engine airplane, $(C_{m_o})_{wn\text{prop off}}$ is replaced by $(C_{m_o})_{wf\text{prop off}}$, which is the propeller-off C_{m_o} of the wing and fuselage obtained from section 4.6.

The pitching-moment increment, $(\Delta C_m)_{w_L}$, due to change in the lift of the wing resulting from power effects is obtained from

$$(\Delta C_m)_{wL} = - \left[(\Delta C_L)_{\Delta \bar{q}_w} + (\Delta C_L)_{\epsilon_p} \right] \frac{x_w}{\bar{c}_w} \quad (5.2-8)$$

where

x_w is the distance from the aerodynamic center of the immersed wing area to the center of gravity (fig. 5-1)

$(\Delta C_L)_{\Delta \bar{q}_w}$ and $(\Delta C_L)_{\epsilon_p}$ are obtained from equations (5.1.1-6) and (5.1.1-14), respectively, or table 5.1.1-2(a)-3 and table 5.1.1-2(b)-2, respectively

The pitching-moment increment, $(\Delta C_m)_{np}$, due to propeller slipstream effects on nacelle free moments (for twin-engine installations) is accounted for by calculations similar to those in section 4.8.1 which considered the free moments due to wing-induced flows with the propeller off. To account for the free-moment increments due to power effects on wing-induced flows,

$$\begin{aligned} (\Delta C_m)_{np} &= - \frac{n}{36.5 S_w \bar{c}_w} \int w_n^2 (\epsilon_p + \epsilon_u) \left(1 + \frac{\Delta \bar{q}_w}{\bar{q}_\infty} \right) dx \\ &= - \frac{n(\epsilon_p + \epsilon_u)}{36.5 S_w \bar{c}_w} \left(1 + \frac{\Delta \bar{q}_w}{\bar{q}_\infty} \right) \int w_n^2 dx \end{aligned} \quad (5.2-9)$$

where

$(\epsilon_p + \epsilon_u)$ are propeller-induced changes in flow inclination on the nacelle (fig. 5-2), obtained from equations (5.1.1-12) and (5.1.1-11), respectively, or table 5.1.1-2(a)-3

$$\frac{\Delta \bar{q}_w}{\bar{q}_\infty} \text{ is equal to } \frac{S_w (T'_c / \text{prop})}{\pi R_p^2}$$

$$\int w_n^2 dx \text{ is obtained from table 4.8.1-2(b)}$$

For single-engine installations, the effect of power on the free moments of the fuselage should be accounted for. The procedure is identical to that described for power effects on nacelle free moments.

— The net pitching-moment contribution of the horizontal tail for power-on conditions, $\overline{C_{mh(hf)}}$, is obtained from

$$\overline{C_{mh(hf)}} = - \frac{l_h}{\bar{c}_w} \overline{C_{Lh(hf)}} \quad (5.2-10)$$

where

l_h is the distance from the center of gravity to the quarter-chord point of the mean aerodynamic chord of the horizontal tail (fig. 5-2)

$\bar{C}_{Lh(hf)}$ is the lift of the horizontal tail, based on S_w , as a function of $\alpha_h = \alpha_b - (\bar{\epsilon}_h)_{\text{prop off}} - (\Delta\epsilon_h)_{\text{power}}$, δ_e , and $\frac{\bar{q}_h}{\bar{q}_\infty}$ obtained from table 5.1.2-1, column 14

The calculations for the power-on pitching-moment characteristics of the subject airplane are summarized in tables 5.2-1 to 5.2-6 as a function of α_b , δ_e , and T'_C with the elevator tab geared to the elevator in the ratio of $\frac{\delta_{\text{tab}}}{\delta_e} = 1.5$.

Tables 5.2-1 to 5.2-4 account for the pitching-moment increments due to the direct propeller forces and power-induced slipstream effects on the wing and nacelles. These increments are summarized and added to the propeller-off, tail-off pitching moments in table 5.2-5 to provide power-on, tail-off characteristics. These characteristics are added to the power-on horizontal-tail contributions in table 5.2-6 to provide the pitching-moment characteristics of the complete airplane. The horizontal-tail contributions include tail-lift carryover effects onto the body which, in accordance with the discussion in section 4.13.4, should have been considered negligible because of the tail-body configuration of the subject airplane.

The propeller-off, tail-off pitching-moment characteristics in column 8 of table 5.2-5 were obtained from figure 5.2-1, which is basically the propeller-off, tail-off curve of figure 4.8.3-1 with the stalling portion extended to the stall angle for each power condition considered. This extension procedure is identical to that used in section 5.1.1 to extend the stall regions for C_{Lw} and C_{Lwfn} in figure 5.1.1-8.

Calculated tail-off pitching-moment characteristics for the largest thrust condition available ($T'_C = 0.44$) are plotted and compared with wind-tunnel data in figure 5.2-2.

The tail-off pitching-moment and lift coefficients in the figure were obtained from tables 5.2-5 and 5.1.2-1(b), respectively. In figure 5.2-2 excellent correlation is evident for the lift characteristics throughout the angle-of-attack range and for the pitching-moment characteristics at the low and high angles of attack. For some unknown reason, the wind-tunnel pitching-moment data dip at an angle of attack of 3° to 4° . This dip, although significant in magnitude, does not appear in the tail-on wind-tunnel data (figs. 5.2-3 and 5.2-4). If the dip can be charged to erroneous data, and thus discounted, the calculated tail-off pitching moments can be considered to be in good agreement with the tunnel data.

Calculated tail-on pitching-moment characteristics for total $T'_C = 0, 0.20$, and 0.44 are compared with wind-tunnel data in figures 5.2-3 and 5.2-4. The incremental change in pitching moments due to elevator deflection shows calculated $C_{m\delta_e}$ to be larger than wind-tunnel values for all power conditions. This discrepancy is attributed primarily to the inclusion of a tail-lift carryover effect onto the body in the

pitching-moment contributions of the tail. As indicated earlier, particularly in section 4.13.4, the tail-lift carryover onto the fuselage should have been considered to be similar to zero because of the tail-body configuration of the subject airplane and the gap between the tail and the fuselage.

For $T'_C = 0$, the correlation of pitching-moment slopes C_{m_α} and $C_{m_{C_L}}$ is generally good. However, for $T'_C = 0.20$ and 0.44 , the correlations, as indicated by the solid lines, deteriorate with increasing power at increasing angles of attack. Several facts were considered in attempting to locate in the predicted pitching-moment characteristics the source of the deterioration in correlation with increasing power:

(1) Tail-off pitching moments, excluding the dip in the wind-tunnel data, correlated well with wind-tunnel data throughout the angle-of-attack range.

(2) Tail-on pitching moments generally would have correlated well with wind-tunnel data for all power conditions at zero lift, where the downwash due to power, $(\Delta\epsilon_h)_{\text{power}}$, was essentially zero, had tail-lift carryover effects onto the body been considered to be similar to zero (section 4.13.4).

(3) Pitching-moment increments between constant δ_e curves correlated consistently with wind-tunnel data through the angle-of-attack range within the linear region of the tail-lift characteristics. An error in dynamic-pressure ratio as a function of angle of attack would have spread the curves with increasing angle of attack if the pressure ratio had been excessive and would have converged the curves if the pressure ratio had been deficient.

(4) An error in downwash due to power as a function of angle of attack would result in an angular rotation of curves on the C_m plot.

On the basis of the preceding facts, it was surmised that the deterioration in slope correlation between calculated and wind-tunnel pitching moments with increasing power at increasing angles of attack was caused primarily by inaccurate determination of downwash increments due to power, as obtained from figure 5.1.2-2. The large, wide, faired-into-the-wing nacelles of the subject airplane are undoubtedly not representative of configurations dealt with in correlating experimental data to arrive at the nomograph of figure 5.1.2-2 used to obtain $(\Delta\epsilon_h)_{\text{power}}$.

When the downwash increment due to power, $(\Delta\epsilon_h)_{\text{power}}$, was decreased by 40 percent for all power conditions and the calculations affected by the change were redone, the resulting modified pitching-moment characteristics showed good slope correlation with wind-tunnel data. The modified calculated pitching-moment characteristics are shown in figures 5.2-3 and 5.2-4 as dashed lines. The reduction in downwash increment due to power, $(\Delta\epsilon_h)_{\text{power}}$, shown in figure 5.1.2-5, also improved the correlation of the calculated tail-on lift curves with wind-tunnel lift data, as shown in figure 5.1.2-6.

The stick-fixed neutral-point characteristics of the subject airplane determined from the wind-tunnel data and the modified calculated data of figure 5.2-4 are compared

in figure 5.2-5 for the three power conditions. The neutral points, determined by the method 1 technique of reference 36, show a decrease in static margin with increase in power.

Pitch-control effectiveness, $C_{m\bar{\delta}_e}$, determined from modified calculated data is compared with that based on wind-tunnel data in figure 5.2-6 as a function of thrust coefficient and trim angle of attack. Both calculated (based on a 40-percent decrease in power-induced downwash) and wind-tunnel-based values of $C_{m\bar{\delta}_e}$ show some increase in effectiveness with increasing power. Throughout the thrust range, the $C_{m\bar{\delta}_e}$ based on modified calculated data shows smaller angle-of-attack effects and larger control effectiveness than reflected in the wind-tunnel data. Had tail-lift carryover effects onto the body been omitted from the calculations (as mentioned previously), the calculated $C_{m\bar{\delta}_e}$ would have correlated better with the wind-tunnel-based data.

Flight-determined pitch stability, C_{m_α} , and pitch-control effectiveness, $C_{m\bar{\delta}_e}$, are compared in figure 5.2-7 with their counterparts determined from the modified calculated and wind-tunnel-determined pitch data of figure 5.2-1. At low angles of attack it appears that the modified calculated values of C_{m_α} correlate better with flight data than with wind-tunnel data. It is possible that the slight scatter of the wind-tunnel data is a factor. Modified calculated values of $C_{m\bar{\delta}_e}$ show poorer correlation with flight data than with wind-tunnel data. Deletion of the calculated tail-lift carryover effect onto the body improved the correlation of the calculated $C_{m\bar{\delta}_e}$ with flight and wind-tunnel data (fig. 5.2-7). The flight values of $C_{m\bar{\delta}_e}$ were determined from the initial portion of a pullup or rapid-pulse maneuver, as described in reference 37. Flight values of C_{m_α} were obtained by using the natural frequency determined by the technique of reference 38 in the simple C_{m_α} expression of reference 37.

Flight-determined C_L , α_b , and δ_e characteristics for trim level flight are shown in figure 5.2-8 as a function of calibrated airspeed for an altitude of 6000 feet. Included for comparison are the characteristics based on wind-tunnel and modified calculated data. Close correlation is shown between flight, wind-tunnel, and modified calculated data.

5.2.1 Symbols

b_i	span of the total portion of the wing immersed in the slipstreams of the propellers, ft
b_w	wing span, ft
C_L	lift coefficient

$\overline{C}_{Lh(hf)}$	net lift coefficient of the horizontal tail due to α_h , δ_e , and δ_{tab} , with tail-fuselage interaction effects included, referenced to the wing area
C_{Lw}	lift coefficient of the wing alone
C_{Lwfn}	lift coefficient of the tail-off configuration
$(C_{Lwfn})_{prop\ off}$	C_{Lwfn} at propeller-off conditions
$(\Delta C_L)_{N_p}$	increment of lift coefficient due to the lift component of the propeller normal force, N_p
$(\Delta C_L)_{\Delta \bar{q}_w}$	increment of lift coefficient due to the power-induced change in dynamic pressure over the portion of the wing immersed in the propeller slipstreams
$(\Delta C_L)_{\epsilon_p}$	increment of lift coefficient due to the change in angle of attack, resulting from propeller downwash, ϵ_p , of the portions of the wing immersed in the propeller slipstreams
C_m	pitching-moment coefficient
$C_m C_L$	static-margin parameter, $\frac{\partial C_m}{\partial C_L}$
C_{mwfn}	pitching-moment coefficient of the tail-off configuration
$(C_{mwfn})_{prop\ off}$	C_{mwfn} at propeller-off conditions
$\overline{C}_{mh(hf)}$	contribution of $\overline{C}_{Lh(hf)}$ to the pitching-moment coefficient
$(\overline{C}_{mh(hf)})_{props\ off}$	propeller-off contribution of $\overline{C}_{Lh(hf)}$ to the pitching-moment coefficient
C_{m_0}	zero-lift pitching-moment coefficient
$(C_{m_0})_{area\ not\ immersed}$	zero-lift pitching-moment coefficient of that portion of the wing not immersed in the propeller slipstreams
$(C_{m_0})_{i\ prop\ off}$	zero-lift pitching-moment coefficient of the portions of the wing-fuselage or wing-nacelles immersed in the propeller slipstreams for propeller-off conditions
$(C_{m_0})_{w\ prop\ off}$	zero-lift pitching-moment coefficient of the wing alone at propeller-off conditions
$(C_{m_0})_{wf\ prop\ off}$	zero-lift pitching-moment coefficient of the wing-fuselage at propeller-off conditions

$(C_{m_0})_{\text{wnprop off}}$	zero-lift pitching-moment coefficient of the wing and nacelle at propeller-off conditions
C_{m_α}	static-stability parameter, $\frac{\partial C_m}{\partial \alpha}$, per deg
$C_{m_{\bar{\delta}_e}}$	pitch-control effectiveness, $\frac{\partial C_m}{\partial \bar{\delta}_e}$, with the elevator-tab geared to elevator, per deg
$(\Delta C_m)_h$	increment of tail contribution to the pitching-moment coefficient due to the propeller-induced increments of dynamic pressure and downwash at the tail
$(\Delta C_m)_{N_p}$	increment of pitching-moment coefficient due to the propeller normal force, N_p
$(\Delta C_m)_{n_p}$	increment of pitching-moment coefficient due to the propeller effects on the nacelles
$(\Delta C_m)_T$	increment of pitching-moment coefficient due to the thrust of the propellers
$(\Delta C_m)_{wL}$	increment of pitching-moment coefficient due to the net change in the wing lift coefficient resulting from propeller-slipstream-induced dynamic pressure and angle-of-attack changes on the wing
$(\Delta C_m)_{\epsilon_p}$	change in the pitching-moment coefficient of the wing due to the propeller-slipstream-induced change in angle of attack
$(\Delta C_{m_0})_{\Delta \bar{q}_w}$	increment of zero-lift pitching-moment coefficient due to the increase in dynamic pressure induced by the propeller slipstreams on the immersed portions of the wing
$(\Delta C_{m_{wfn}})_{\text{power}}$	power-induced change in the pitching-moment coefficient of the tail-off configuration
\bar{c}_i	mean aerodynamic chord of the portion of the wing immersed in the propeller slipstream (fig. 5-1), ft
$\bar{c}_{\text{not immersed}}$	mean chord of the portion of the wing not immersed in the slipstreams of the propellers, ft
\bar{c}_w	mean aerodynamic chord of the wing, ft
l_h	distance from the center of gravity to the quarter chord of the horizontal-tail mean aerodynamic chord, ft
n	number of propellers
\bar{q}_∞	free-stream dynamic pressure, lb/sq ft

$\frac{\bar{q}_h}{\bar{q}_\infty}$	dynamic pressure at the tail as a ratio of the free-stream dynamic pressure
$\frac{\Delta \bar{q}_w}{\bar{q}_\infty}$	increment of power-induced dynamic pressure acting on the portions of the wing immersed in the propeller slipstreams as a ratio of the free-stream dynamic pressure
R_p	propeller radius, ft
S_i	area of the portions of the wing immersed in the propeller slipstreams, sq ft
S_w	wing area, sq ft
T	thrust of the propellers, lb
$T'_c = \frac{T}{\bar{q}_\infty S_w}$	
V_c	calibrated airspeed, knots
x_p	distance from the center of gravity to the propeller, positive forward, ft
x_w	distance from the aerodynamic center of the mean aerodynamic chord of the immersed portion of the wing area to the center of gravity (fig. 5-1), positive forward, in. or ft
w_n	mean width of a nacelle planform segment of Δx length, ft
z_T	distance, parallel to the Z-body axis, from the X-body axis to the thrust axis, positive down, ft
α	angle of attack, deg
α_b	airplane angle of attack relative to the X-body axis, deg
α_h	local angle of attack of the horizontal tail with the elevator setting equal to zero, $\alpha_b - (\bar{\epsilon}_h)_{\text{prop off}} - (\Delta \epsilon_h)_{\text{power}}$, deg
α_{stall}	stall value of α_b , deg
α_T	angle of attack of the thrust axis, deg
$\delta_e, \delta_{\text{tab}}$	elevator and tab deflection, respectively, deg
$(\bar{\epsilon}_h)_{\text{prop off}}$	average downwash at the horizontal tail with the propellers off, deg

$(\Delta\epsilon_h)_{\text{power}}$	increment of downwash at the horizontal tail due to power, deg
ϵ_p	downwash angle behind the propeller, deg
$-\epsilon_u$	upwash angle at the propeller, deg

TABLE 5.2-1
PITCHING-MOMENT INCREMENTS DUE TO PROPELLER FORCES

$$(\Delta C_m)_T = n(T'_c/\text{prop}) \frac{z_T}{\bar{c}_w}$$

$$(\Delta C_m)_{N_p} = \frac{N_p}{\bar{c}_w} \frac{(\Delta C_L)_{N_p}}{\cos \alpha_T}$$

(a-1)

Symbol	Description	Reference	Magnitude
n	Number of propellers	-----	2
\bar{c}_w	Wing mean aerodynamic chord, ft	Table 3.2-1	4.96
z_T	Distance from thrust axis to the center of gravity, ft	Figure 5-2	-0.869
x_p	Distance from propeller plane to the center of gravity, ft	Figure 5-2	5.26
α_T	Angle of attack of thrust axis, deg	-----	α_b
T'_c/prop	Thrust coefficient per propeller	-----	0, 0.10, 0.22
$(\Delta C_L)_{N_p}$	Normal-force coefficients of the propellers	Table 5.1.1-1(c)	$f(\alpha_b, T'_c)$

Summary: $(\Delta C_m)_T = -0.3504(T'_c/\text{prop})$
 $(\Delta C_m)_{N_p} = \frac{1.06(\Delta C_L)_{N_p}}{\cos \alpha_T}$

(a-2)

①	②	③	④	⑤	⑥
		Table 5.1.1-1(c), column 6	Table 5.2-1(a)-1	Table 5.2-1(a)-1	-----
α_b , deg	$\cos \alpha_T = \cos \text{①}$	$(\Delta C_L)_{N_p}$	$(\Delta C_m)_T =$ -0.3504 T'_c/prop T'_c/prop	$(\Delta C_m)_{N_p} = 1.06 \frac{\text{③}}{\text{②}}$	$(\Delta C_m)_T + (\Delta C_m)_{N_p} = \text{④} + \text{⑤}$
		T'_c	T'_c	T'_c	T'_c
		0 0.20 0.44	0 0.20 0.44	0 0.20 0.44	0 0.20 0.44
-4	0.9976 -.9994	-0.00207 -0.00369 -.00121 -.00148	0 -0.03504 -.07709 -.07709	-0.00220 -0.00321 -.00125 -.00157	-0.00220 -0.00321 -.00125 -.00157
-2					
0	1.0000 .9994	0.00042 .00166 -.00242 .00296	0 -0.03504 -.07709 -.07709	0.00045 0.00064 0.00078 0.00176	0.00045 0.00064 0.00078 0.00176
2					
4	0.9976 .9945	0.00290 -.00413 .00601 .00735	0 -0.03504 -.07709 -.07709	0.00306 .00448 0.00548 .00783	-0.00308 -.00440 -.00548 -.00783
6					
8	0.9903 .9848	0.00533 -.00654 .00953 .01165	0 -0.03504 -.07709 -.07709	0.00573 .00704 0.00837 .01026	0.00573 .00704 0.00837 .01026
10					
12	0.9781 .9711	0.00772 -.00872 .01270 .01552	0 -0.03504 -.07709 -.07709	0.01218 0.01489 0.01694 .01866	-0.01218 -0.01489 -0.01694 -.01866
13.8					
14.1	0.9699 -.9686	0.01298 -.01586 -.01620 -.01620	0 -0.03504 -.07709 -.07709	0.01419 0.01733 .01773 .01773	-0.01419 -0.01733 -.01773 -.01773
14.4					

a,b: Stall angles at $T'_c = 0, 0.20, 0.44$, respectively.

TABLE 5.2-2
ZERO-LIFT PITCHING-MOMENT INCREMENT DUE TO POWER

$$(\Delta C_{m_o})_{\Delta \bar{q}_w} = \frac{\Delta \bar{q}_w}{\bar{q}_\infty} \frac{S_i}{S_w} \frac{\bar{c}_i}{\bar{c}_w} (C_{m_o})_{i \text{ prop off}}$$

where

$$(C_{m_o})_{i \text{ prop off}} \approx (C_{m_o})_{w \text{ n prop off}} - (C_{m_o})_{\text{area not immersed}}$$

and

$$(C_{m_o})_{\text{area not immersed}} = (C_{m_o})_{w \text{ prop off}} \left(1 - \frac{S_i}{S_w} \right)^2 \frac{S_w}{\bar{c}_w} \frac{1}{(b_w - n(b_i/\text{prop}))}$$

(a)-1

Symbol	Description	Reference	Magnitude
n	Number of propellers	-----	2
R _p	Propeller radius, ft	Table 3-1	3.0
S _w	Reference wing area for comparison with wind-tunnel data, sq ft	Table 3-1	178.0
b _w	Wing span, ft	Table 3.2-1	36.0
\bar{c}_w	Wing mean aerodynamic chord, ft	Table 3.2-1	4.96
$\frac{S_i}{S_w}$	Ratio of total immersed to reference wing area, sq ft	Table 5.1.1-2(a)-3, column 10	2 x (col. 10)
n(b _i /prop)	2(b _i /prop) = total immersed span, ft	Table 5.1.1-2(a)-3, column 8	2 x (col. 8)
\bar{c}_i	Chord of immersed wing area, ft	Figure 5-1(b)	5.50
(C _{m_o}) _{w prop off}	Zero-lift pitching moment of wing, propellers off	Table 4.5-1	-0.0240
(C _{m_o}) _{w n prop off}	Zero-lift pitching moment of wing plus nacelles, propellers off	Table 4.6-1	-.0240
$\frac{\Delta \bar{q}_w}{\bar{q}_\infty}$	Power-induced change in dynamic-pressure ratio on immersed portion of wing, $\frac{S_w(T'_c/\text{prop})}{\pi R_p^2}$	Equation (5.1.1-7)	6.30(T' _c /prop)
<p>Summary: $(C_{m_o})_{\text{area not immersed}} = -0.861 \frac{(1 - \frac{S_i}{S_w})^2}{b_w - 2(b_i/\text{prop})}$</p> <p>$(C_{m_o})_{i \text{ prop off}} = -0.0240 - (C_{m_o})_{\text{area not immersed}}$</p> <p>$(\Delta C_{m_o})_{\Delta \bar{q}_w} = 6.99(T'_c/\text{prop}) \left(\frac{S_i}{S_w} \right) (C_{m_o})_{i \text{ prop off}}$</p>			

TABLE 5.2-2 (Concluded)

①	②			③			④			⑤			⑥			⑦			⑧		
	Table 5.1.1-2(a)-3, column 10			-----			Table 5.1.1-2(a)-3, column 8			b _w - 2(b _l /prop) = 36.0 - ④			Table 5.2-2(a)-1 (C _{m0}) _{area not immersed} = -0.861 ③ ⑤			Table 5.2-2(a)-1 (C _{m0}) _l prop off = -0.0240 - ⑥			Table 5.2-2(a)-1 (ΔC _{m0})Δδ _w = 6.99(T _c '/prop) ② ⑦		
α _b , deg	S _l S _w = 2(ref. column 10)			(1 - S _l ² / S _w) ² = (1 - ②) ²			2(ref. column 8)			T _c '			T _c '			T _c '			T _c '		
	0	0.20	0.44	0	0.20	0.44	0	0.20	0.44	0	0.20	0.44	0	0.20	0.44	0	0.20	0.44	0	0.20	0.44
-4	0.3668	0.3654	0.3644	0.40094	0.40272	0.40399	11.8702	11.8230	11.7954	24.1298	24.1770	24.2046	-0.01431	-0.01434	-0.01437	-0.00969	-0.00966	-0.00963	0	-0.00247	-0.00540
-2	0.3610	0.3602	0.3596	0.40832	0.40934	0.41011	11.6826	11.6544	11.6394	24.3174	24.3456	24.3606	-0.01446	-0.01448	-0.01449	-0.00954	-0.00952	-0.00951	0	-0.00240	-0.00526
0	0.3524	0.3530	0.3534	0.41989	0.41861	0.41809	11.4076	11.4268	11.4366	24.5924	24.5732	24.5634	-0.01468	-0.01467	-0.01465	-0.00932	-0.00933	-0.00935	0	-0.00230	-0.00508
2	0.3412	0.3442	0.3456	0.43402	0.43007	0.42824	11.0392	11.1364	11.1846	24.9608	24.8636	24.8134	-0.01497	-0.01489	-0.01510	-0.00903	-0.00911	-0.00914	0	-0.00219	-0.00486
4	0.3266	0.3330	0.3362	0.45347	0.44489	0.44063	10.5672	10.7784	10.8800	25.4328	25.2216	25.1200	-0.01535	-0.01519	-0.01574	-0.00865	-0.00881	-0.00890	0	-0.00205	-0.00460
6	0.3082	0.3196	0.3250	0.47859	0.46294	0.45562	9.9768	10.3452	10.5184	26.0232	25.6548	25.4816	-0.01583	-0.01554	-0.01539	-0.00817	-0.00846	-0.00861	0	-0.00189	-0.00430
8	0.2856	0.3036	0.3118	0.51037	0.48497	0.47362	9.2458	9.8276	10.0936	26.7542	26.1724	25.9064	-0.01642	-0.01595	-0.01574	-0.00758	-0.00805	-0.00826	0	-0.00171	-0.00396
10	0.2576	0.2846	0.2956	0.55116	0.51180	0.49618	8.3368	9.2108	9.5678	27.6632	26.7892	26.4322	-0.01715	-0.01645	-0.01616	-0.00685	-0.00755	-0.00784	0	-0.00150	-0.00356
12	0.2220	0.2618	0.2786	0.60528	0.54494	0.52042	7.1828	8.4738	9.0166	28.8172	27.5262	26.9834	-0.01808	-0.01705	-0.01661	-0.00592	-0.00685	-0.00739	0	-0.00127	-0.00317
13.8	0.1810	0.2380	0.2604	0.67076	0.58064	0.54701	5.8606	7.7026	8.4270	30.1394	28.2974	27.5730	-0.01916	-0.01767	-0.01708	-0.00484	-0.00633	-0.00692	0	-0.00103	-0.00277
14.1	0.2330	0.2566	0.2528	0.58829	0.55264	0.53631	7.5392	8.3048	8.3048	27.6352	27.6352	27.6352	-----	-----	-----	-----	-----	-----	-----	-----	-----
14.4	0.2528	0.2528	0.2528	0.55831	0.55831	0.55831	8.1786	8.1786	8.1786	27.8214	27.8214	27.8214	-----	-----	-----	-----	-----	-----	-----	-----	-----

a,b*Small angles at T_c' = 0, 0.20, 0.44, respectively.

TABLE 5.2-3
PITCHING-MOMENT INCREMENT DUE TO POWER-INDUCED CHANGE IN WING LIFT

$$(\Delta C_m)_{w_L} = - \left[(\Delta C_L)_{\Delta \bar{q}_w} + (\Delta C_L)_{\epsilon_p} \right] \frac{x_w}{\bar{c}_w}$$

(a)-1

Symbol	Description	Reference	Magnitude
x_w	Distance from aerodynamic center of immersed wing area to the center of gravity, ft	Figure 5-1(b)	0.712
\bar{c}_w	Wing mean aerodynamic chord, ft	Table 3.2-1	4.96
$(\Delta C_L)_{\Delta \bar{q}_w}$	Change in wing lift due to power-induced change in dynamic pressure on wing	Table 5.1.1-2(a)-3, column 13	$f(\alpha_b, T'_c/\text{prop})$
$(\Delta C_L)_{\epsilon_p}$	Change in wing lift due to power-induced change in flow direction on wing	Table 5.1.1-2(b)-2, column 5	$f(\alpha_b, T'_c/\text{prop})$

$$(\Delta C_m)_{w_L} = -0.144 \left[(\Delta C_L)_{\Delta \bar{q}_w} + (\Delta C_L)_{\epsilon_p} \right]$$

(a)-2

①	②			③			④		
-----	Table 5.1.1-2(a)-3, column 13			Table 5.1.1-2(b)-2, column 5			Table 5.2-3(a)-1		
α_b , deg	$(\Delta C_L)_{\Delta \bar{q}_w}$			$(\Delta C_L)_{\epsilon_p}$			$(\Delta C_m)_{w_L} = -0.144 (\textcircled{2} + \textcircled{3})$		
	T'_c			T'_c			T'_c		
	0	0.20	0.44	0	0.20	0.44	0	0.20	0.44
-4	0	0	0	0.00211	0.02910	0.06192	-0.000304	-0.004190	-0.008916
-2	0	.0308	.0623	.00083	.01148	.02444	-.000120	-.006088	-.012490
0	0	0.0602	0.1217	-0.00042	-0.00561	-0.01201	0.000060	-0.007861	-0.015795
2	0	.0874	.1775	-.00157	-.02193	-.04700	.000226	-.009428	-.018792
4	0	0.1124	0.2287	-0.00263	-0.03713	-0.08000	0.000379	-0.010839	-0.021413
6	0	.1348	.2763	-.00355	-.05091	-.11044	.000511	-.012080	-.023884
8	0	0.1533	0.3157	-0.00428	-0.06287	-0.13774	0.000616	-0.013022	-0.025626
10	0	.1659	.3481	-.00474	-.07254	-.16072	.000682	-.013444	-.026983
12	0	0.1709	0.3669	-0.00486	-0.07924	-0.17990	0.000700	-0.013199	-0.026928
^a 13.8	0	.1687	.3762	-.00451	-.08199	-.19136	.000649	-.012486	-.026617
^b 14.1	-	0.1657	0.3716	-----	-0.08212	-0.19293	-----	-0.012036	-0.025728
^c 14.4	-	-----	.3658	-----	-----	-.19437	-----	-----	-.024686

^{a,b,c}Stall angles at $T'_c = 0, 0.20, 0.44$, respectively.

TABLE 5.2-4
PITCHING-MOMENT INCREMENT DUE TO POWER EFFECT ON NACELLE FREE MOMENTS

$$(\Delta C_m)_{n_p} = -\frac{n(\epsilon_u + \epsilon_p)}{36.5 S_w c_w} \left(1 + \frac{\Delta \bar{q}_w}{\bar{q}_\infty} \right) \int w_n^2 dx$$

(a)-1

Symbol	Description	Reference	Magnitude
n	Number of nacelles	-----	2
S_w	Reference wing area, sq ft	Table 3-1	178
\bar{c}_w	Wing mean aerodynamic chord, ft	Table 3.2-1	4.96
$-\epsilon_u$	Upwash at propeller, deg	Table 5.1.1-2(a)-3, column 3	As per reference
ϵ_p	Propeller-induced downwash behind propeller, deg	Table 5.1.1-2(a)-3, column 4	As per reference
$\frac{\Delta \bar{q}_w}{\bar{q}_\infty}$	Power-induced change in dynamic-pressure ratio on immersed portion of nacelles (and wing)	Equation (5.1.1-7)	6.30 (T'_c/prop)
$\int w_n^2 dx$	Integral of square of mean width of nacelle planform segments of Δx length, cu ft	Table 4.8.1-2(c), summation of fifth column	33.55 per nacelle

$$(\Delta C_m)_{n_p} = -0.00209 [1 + 6.30(T'_c/\text{prop})](\epsilon_u + \epsilon_p)$$

(a)-2

①	②	③			④			⑤		
-----	Table 5.1.1-2(a)-3, column 3	Table 5.1.1-2(a)-3, column 4			-----			Table 5.2-4(a)-1		
α_b , deg	ϵ_u , deg	ϵ_p , deg			$(\epsilon_u + \epsilon_p) = \textcircled{2} + \textcircled{3}$, deg			$(\Delta C_m)_{n_p} = -0.00209 [1 + 6.30(T'_c/\text{prop})]\textcircled{4}$		
		T'_c/prop			T'_c/prop			T'_c		
		0	0.10	0.22	0	0.10	0.22	0	0.20	0.44
-1	0	-0.0936	-0.7948	-1.1584	-0.0936	-0.7948	-1.1584	0.000196	0.002708	0.005777
-2	-.4	-.0374	-.3179	-.4634	-.4374	-.7179	-.8634	.000914	.002446	.004306
0	-0.8	0.0187	0.1590	0.2317	-0.7813	-0.6410	-0.5683	0.001633	0.002184	0.002834
2	-1.2	.0749	.6358	.9267	-1.1251	-.5642	-.2733	.002351	.001922	.001363
4	-1.6	0.1310	1.1127	1.6218	-1.4690	-0.4873	-0.0218	0.003070	0.001660	0.000109
6	-2.0	.1872	1.5896	2.3168	-1.8128	-.4104	.3168	.003789	.001398	-.001580
8	-2.4	0.2434	2.0665	3.0118	-2.1568	-0.3335	0.6118	0.004508	0.001136	-0.003051
10	-2.8	.2995	2.5434	3.7069	-2.5005	-.2660	.9069	.005226	.000906	-.004522
12	-3.2	0.3557	3.0202	4.4019	-2.8443	-0.1798	1.2019	0.005945	0.000613	-0.005994
^a 13.8	-3.5	.4048	3.4375	5.0101	-3.0952	-.0625	1.5101	.006469	.000210	-.007530
^b 14.1	-3.6	-----	3.5170	5.1259	-----	-0.0830	1.5259	-----	0.000283	-0.007609
^c 14.4	-3.7	-----	-----	5.2418	-----	-----	1.5418	-----	-----	-.007688

^{a,b,c}Stall angles at $T'_c = 0, 0.20, 0.44$, respectively.

TABLE 5.2-5
TAIL-OFF PITCHING-MOMENT CHARACTERISTICS WITH POWER ON

$$C_{m_{wfm}} = (C_{m_{wfm}})_{prop\ off} + (\Delta C_m)_T + (\Delta C_m)_{N_p} + (\Delta C_m)_{N_p} + (\Delta C_m)_{\Delta \bar{q}_w} + (\Delta C_m)_{\Delta \bar{q}_w} + (\Delta C_m)_{h_p}$$

①	②				③				④				⑤				⑥				⑦			
	Table 5.2-1(a)-2, column 8				Table 5.2-2(a)-2, column 8				Table 5.2-3(a)-2, column 4				Table 5.2-4(a)-2, column 5				-----				Table 5.1.1-3, column 6			
σ_b , deg	$(\Delta C_m)_T + (\Delta C_m)_{N_p}$				$(\Delta C_m)_{\Delta \bar{q}_w}$				$(\Delta C_m)_{w_L}$				$(\Delta C_m)_{h_p}$				$(\Delta C_m)_{wfm}$ power ② + ③ + ④ + ⑤				$(C_{L_{wfm}})_{prop\ off}$			
	T_c				T_c				T_c				T_c				T_c				T_c			
	0	0.20	0.44	0	0.20	0.44	0	0.20	0.44	0	0.20	0.44	0	0.20	0.44	0	0.20	0.44	0	0.20	0.44	0	0.20	0.44
-4	-0.00220	-0.03825	-0.08101	0	-0.00247	-0.00540	-0.008916	0.000186	0.002708	0.005777	-0.002308	-0.049714	-0.095949	-0.0194	-0.0194	-0.0194	-0.0194	-0.0194	-0.0194	-0.0194	-0.0194	-0.0194	-0.0194	-0.0194
-2	-0.00088	-0.03632	-0.07866	0	-0.00120	-0.00526	-0.012490	-0.000914	-0.002446	0.004306	-0.000986	-0.042362	-0.092104	-0.01400	-0.01400	-0.01400	-0.01400	-0.01400	-0.01400	-0.01400	-0.01400	-0.01400	-0.01400	-0.01400
0	0.00045	-0.03440	-0.07631	0	-0.00230	-0.00508	0.000660	-0.007861	-0.015795	0.001633	0.002184	-0.042928	-0.094351	0.3000	0.3000	0.3000	0.3000	0.3000	0.3000	0.3000	0.3000	0.3000	0.3000	0.3000
2	0.00176	-0.03247	-0.07395	0	-0.00219	-0.00486	0.002226	-0.009428	-0.018792	0.002351	0.001922	-0.042166	-0.096239	0.4600	0.4600	0.4600	0.4600	0.4600	0.4600	0.4600	0.4600	0.4600	0.4600	0.4600
4	0.00308	-0.03056	-0.07161	0	-0.00205	-0.00460	0.003379	-0.010839	-0.021413	0.003070	0.001660	-0.041789	-0.0957514	0.6200	0.6200	0.6200	0.6200	0.6200	0.6200	0.6200	0.6200	0.6200	0.6200	0.6200
6	0.00440	-0.02863	-0.06926	0	-0.00189	-0.00430	0.003511	-0.012080	-0.023854	0.003789	0.001398	-0.041202	-0.099024	0.7810	0.7810	0.7810	0.7810	0.7810	0.7810	0.7810	0.7810	0.7810	0.7810	0.7810
8	0.00573	-0.02670	-0.06690	0	-0.00171	-0.00396	0.003616	-0.013022	-0.025626	0.004508	0.001136	-0.040522	-0.099539	0.9420	0.9420	0.9420	0.9420	0.9420	0.9420	0.9420	0.9420	0.9420	0.9420	0.9420
10	0.00704	-0.02478	-0.06455	0	-0.00150	-0.00356	0.003682	-0.013444	-0.026952	0.005226	0.000906	-0.038818	-0.099614	1.1040	1.1040	1.1040	1.1040	1.1040	1.1040	1.1040	1.1040	1.1040	1.1040	1.1040
12	0.00837	-0.02286	-0.06220	0	-0.00127	-0.00317	0.003700	-0.013199	-0.026928	0.005945	0.000613	-0.036716	-0.098292	1.240	1.240	1.240	1.240	1.240	1.240	1.240	1.240	1.240	1.240	1.240
13.8	0.00952	-0.02118	-0.06015	0	-0.00105	-0.00277	0.003649	-0.012486	-0.026617	0.006469	0.000213	-0.034503	-0.097067	1.325	1.325	1.325	1.325	1.325	1.325	1.325	1.325	1.325	1.325	1.325
14.1	0.00952	-0.02085	-0.05976	0	-0.00101	-0.00269	0.003649	-0.012036	-0.025728	0.006469	0.000213	-0.033613	-0.095787	1.303	1.303	1.303	1.303	1.303	1.303	1.303	1.303	1.303	1.303	1.303
14.4	0.00952	-0.02085	-0.05936	0	0.000649	-0.00261	0.003649	-0.012036	-0.024686	0.006469	0.000213	-0.033613	-0.094344	1.280	1.280	1.280	1.280	1.280	1.280	1.280	1.280	1.280	1.280	1.280

a,b,c: Scaled angles at $T_c = 0, 0.20, 0.44$, respectively.

①	②				③				④				⑤				⑥				⑦			
	Figure 5.2-1				-----				-----				-----				-----				-----			
σ_b , deg	$(C_{m_{wfm}})_{prop\ off}$				$C_{m_{wfm}} =$ ⑥ + ⑦				$C_{m_{wfm}} =$ ⑥ + ⑦				$C_{m_{wfm}} =$ ⑥ + ⑦				$C_{m_{wfm}} =$ ⑥ + ⑦				$C_{m_{wfm}} =$ ⑥ + ⑦			
	T_c				T_c				T_c				T_c				T_c				T_c			
	0	0.20	0.44	0	0.20	0.44	0	0.20	0.44	0	0.20	0.44	0	0.20	0.44	0	0.20	0.44	0	0.20	0.44	0	0.20	0.44
-4	-0.0456	-0.0456	-0.0456	-0.0479	-0.0933	-0.1351	-0.0456	-0.0456	-0.0456	-0.0479	-0.0933	-0.1351	-0.0456	-0.0456	-0.0456	-0.0479	-0.0933	-0.1351	-0.0456	-0.0456	-0.0456	-0.0479	-0.0933	-0.1351
-2	-0.0387	-0.0387	-0.0387	-0.0387	-0.0811	-0.1308	-0.0387	-0.0387	-0.0387	-0.0387	-0.0811	-0.1308	-0.0387	-0.0387	-0.0387	-0.0387	-0.0811	-0.1308	-0.0387	-0.0387	-0.0387	-0.0387	-0.0811	-0.1308
0	-0.0320	-0.0320	-0.0320	-0.0299	-0.0749	-0.1264	-0.0320	-0.0320	-0.0320	-0.0299	-0.0749	-0.1264	-0.0320	-0.0320	-0.0320	-0.0299	-0.0749	-0.1264	-0.0320	-0.0320	-0.0320	-0.0299	-0.0749	-0.1264
2	-0.0256	-0.0256	-0.0256	-0.0236	-0.0678	-0.1218	-0.0256	-0.0256	-0.0256	-0.0236	-0.0678	-0.1218	-0.0256	-0.0256	-0.0256	-0.0236	-0.0678	-0.1218	-0.0256	-0.0256	-0.0256	-0.0236	-0.0678	-0.1218
4	-0.0196	-0.0196	-0.0196	-0.0196	-0.0614	-0.1171	-0.0196	-0.0196	-0.0196	-0.0196	-0.0614	-0.1171	-0.0196	-0.0196	-0.0196	-0.0196	-0.0614	-0.1171	-0.0196	-0.0196	-0.0196	-0.0196	-0.0614	-0.1171
6	-0.0141	-0.0141	-0.0141	-0.0141	-0.0553	-0.1131	-0.0141	-0.0141	-0.0141	-0.0141	-0.0553	-0.1131	-0.0141	-0.0141	-0.0141	-0.0141	-0.0553	-0.1131	-0.0141	-0.0141	-0.0141	-0.0141	-0.0553	-0.1131
8	-0.0090	-0.0090	-0.0090	-0.0090	-0.0493	-0.1085	-0.0090	-0.0090	-0.0090	-0.0090	-0.0493	-0.1085	-0.0090	-0.0090	-0.0090	-0.0090	-0.0493	-0.1085	-0.0090	-0.0090	-0.0090	-0.0090	-0.0493	-0.1085
10	-0.0048	-0.0048	-0.0048	-0.0048	-0.0436	-0.1044	-0.0048	-0.0048	-0.0048	-0.0048	-0.0436	-0.1044	-0.0048	-0.0048	-0.0048	-0.0048	-0.0436	-0.1044	-0.0048	-0.0048	-0.0048	-0.0048	-0.0436	-0.1044
12	-0.0049	-0.0049	-0.0049	-0.0049	-0.0402	-0.1009	-0.0049	-0.0049	-0.0049	-0.0049	-0.0402	-0.1009	-0.0049	-0.0049	-0.0049	-0.0049	-0.0402	-0.1009	-0.0049	-0.0049	-0.0049	-0.0049	-0.0402	-0.1009
13.8	-0.0110	-0.0110	-0.0110	-0.0110	-0.0430	-0.1051	-0.0110	-0.0110	-0.0110	-0.0110	-0.0430	-0.1051	-0.0110	-0.0110	-0.0110	-0.0110	-0.0430	-0.1051	-0.0110	-0.0110	-0.0110	-0.0110	-0.0430	-0.1051
14.1	-0.0100	-0.0100	-0.0100	-0.0100	-0.0436	-0.1048	-0.0100	-0.0100	-0.0100	-0.0100	-0.0436	-0.1048	-0.0100	-0.0100	-0.0100	-0.0100	-0.0436	-0.1048	-0.0100	-0.0100	-0.0100	-0.0100	-0.0436	-0.1048
14.4	-0.0100	-0.0100	-0.0100	-0.0100	-0.0436	-0.1043	-0.0100	-0.0100	-0.0100	-0.0100	-0.0436	-0.1043	-0.0100	-0.0100	-0.0100	-0.0100	-0.0436	-0.1043	-0.0100	-0.0100	-0.0100	-0.0100	-0.0436	-0.1043

TABLE 5.2-6
EFFECT OF ELEVATOR DEFLECTION ON PITCHING MOMENTS WITH POWER ON

$$C_m = C_{m_{wfn}} - \frac{l_h}{c_w} \bar{C}_{L_h}(\delta_n)$$

$$= C_{m_{wfn}} - 2.92 C_{L_h}(\delta_n)$$

where $l_h = 14.5 \text{ ft}$; $c_w = 4.96 \text{ ft}$

①	②					③					④					⑤				
	Table 5.1.2-1(b), column 14					Equation (5.2-10)					Table 5.2-5, column 9					-----				
	$\bar{C}_{L_h}(\delta_n)$					$\bar{C}_{m_h}(\delta_n) = -2.92 \text{ } \bar{C}_{L_h}(\delta_n)$					$C_{m_{wfn}}$					$C_m = \text{③} + \text{④}$				
σ_b , deg	δ_n , deg					δ_n , deg					δ_n , deg					δ_n , deg				
	4	0	-5	-10	-14	4	0	-5	-10	-14	4	0	-5	-10	-14	4	0	-5	-10	-14
$T_C = 0$																				
-4	0.0247	-0.0544	-0.1539	-0.2155	-0.1844	-0.07212	0.15885	0.44939	0.62926	0.53845	-0.0479	0.1200	0.1110	0.4015	0.5814	0.4906				
-2	0.0389	-0.0402	-0.1395	-0.2151	-0.1886	-0.11359	0.11738	0.40734	0.62809	0.55071	-0.0388	-0.1524	0.0786	0.3685	0.5893	0.5119				
0	0.0533	-0.0256	-0.1253	-0.2109	-0.2078	-0.15564	0.07475	0.36588	0.61583	0.60678	-0.0299	-0.1855	0.0449	0.3360	0.5839	0.5769				
2	0.0661	-0.0128	-0.1121	-0.2041	-0.2250	-0.19301	0.03738	0.32733	0.59597	0.65700	-0.0213	-0.2143	0.0161	0.3060	0.5747	0.6337				
4	0.0814	0.0024	-0.0973	-0.1925	-0.2282	-0.23769	-0.00701	0.28412	0.56210	0.66634	-0.0131	-0.2508	-0.0201	0.2710	0.5490	0.6532				
6	0.0946	0.0159	-0.0834	-0.1784	-0.2255	-0.27623	-0.04643	0.24353	0.52093	0.65846	-0.0054	-0.2816	-0.0518	0.2381	0.5155	0.6531				
8	0.1094	0.0305	-0.0688	-0.1640	-0.2191	-0.31945	-0.08906	0.20090	0.47888	0.63977	0.0019	-0.3176	-0.0872	0.2028	0.4808	0.6417				
10	0.1251	0.0460	-0.0533	-0.1483	-0.2094	-0.36529	-0.13432	0.15364	0.43304	0.61143	0.0081	-0.3572	-0.1262	0.1637	0.4411	0.6195				
12	0.1391	0.0606	-0.0387	-0.1338	-0.1950	-0.40617	-0.17695	0.11300	0.39070	0.56940	0.0101	-0.3961	-0.1668	0.1231	0.4008	0.5795				
*13.8	0.1534	0.0749	-0.0247	-0.1196	-0.1808	-0.44793	-0.21871	0.07212	0.34923	0.52794	0.0056	-0.4423	-0.2131	0.0777	0.3548	0.5335				
$T_C = 0.20$																				
-4	0.0268	-0.0591	-0.1673	-0.2342	-0.2004	-0.07826	0.17257	0.48652	0.68386	0.58517	-0.0953	-0.1736	0.0773	0.3932	0.5886	0.4899				
-2	0.0318	-0.0554	-0.1651	-0.2376	-0.2048	-0.09286	0.16177	0.48209	0.69379	0.59802	-0.0811	-0.1740	0.0807	0.4010	0.6127	0.5169				
0	0.0396	-0.0483	-0.1603	-0.2406	-0.2100	-0.11563	0.14104	0.46808	0.70255	0.61320	-0.0749	-0.1905	0.0661	0.3932	0.6276	0.5383				
2	0.0457	-0.0428	-0.1543	-0.2406	-0.2160	-0.13944	0.12498	0.45056	0.70555	0.63072	-0.0678	-0.2012	0.0572	0.3828	0.6348	0.5629				
4	0.0540	-0.0352	-0.1486	-0.2413	-0.2272	-0.15768	0.10278	0.43391	0.70460	0.66342	-0.0614	-0.2191	0.0414	0.3725	0.6432	0.6020				
6	0.0630	-0.0270	-0.1406	-0.2392	-0.2392	-0.18396	0.07884	0.41055	0.69446	0.69846	-0.0553	-0.2393	0.0235	0.3552	0.6432	0.6432				
8	0.0748	-0.0150	-0.1291	-0.2340	-0.2564	-0.21842	0.04380	0.37637	0.68328	0.74869	-0.0493	-0.2677	0.0055	0.3277	0.6340	0.6994				
10	0.0876	-0.0023	-0.1155	-0.2239	-0.2606	-0.25579	0.00672	0.33726	0.65379	0.76095	-0.0436	-0.2994	-0.0369	0.2937	0.6102	0.7174				
12	0.0996	0.0098	-0.1027	-0.2118	-0.2585	-0.29083	-0.02462	0.29988	0.61846	0.75432	-0.0402	-0.3310	-0.0688	0.2597	0.5783	0.7146				
13.8	0.1116	0.0231	-0.0890	-0.1965	-0.2523	-0.32587	-0.06745	0.25988	0.57378	0.73672	-0.0430	-0.3689	-0.1104	0.2169	0.5308	0.6937				
*14.1	0.1147	0.0262	-0.0854	-0.1922	-0.2498	-0.33492	-0.07650	0.24937	0.56122	0.72942	-0.0436	-0.3785	-0.1201	0.2058	0.5176	0.6858				
$T_C = 0.44$																				
-4	0.0296	-0.0654	-0.1851	-0.2591	-0.2219	-0.08643	0.19097	0.54049	0.75657	0.64795	-0.1351	-0.2215	0.0559	0.4054	0.6215	0.5129				
-2	0.0287	-0.0672	-0.1879	-0.2694	-0.2233	-0.08380	0.19622	0.54867	0.76037	0.65204	-0.1308	-0.2146	0.0654	0.4179	0.6296	0.5212				
0	0.0299	-0.0662	-0.1878	-0.2632	-0.2255	-0.08731	0.19330	0.54838	0.76654	0.65846	-0.1264	-0.2137	0.0669	0.4220	0.6421	0.5321				
2	0.0324	-0.0650	-0.1879	-0.2655	-0.2280	-0.09461	0.18980	0.54867	0.77526	0.66576	-0.1218	-0.2164	0.0680	0.4269	0.6535	0.5440				
4	0.0375	-0.0606	-0.1846	-0.2679	-0.2315	-0.10950	0.17695	0.53903	0.78227	0.67598	-0.1171	-0.2266	0.0598	0.4219	0.6652	0.5589				
6	0.0433	-0.0561	-0.1809	-0.2702	-0.2359	-0.12644	0.16381	0.52823	0.78898	0.68863	-0.1131	-0.2395	0.0507	0.4151	0.6759	0.5757				
8	0.0512	-0.0477	-0.1737	-0.2708	-0.2429	-0.14950	0.13928	0.50720	0.79074	0.70927	-0.1085	-0.2550	0.0308	0.3987	0.6822	0.6008				
10	0.0655	-0.0347	-0.1613	-0.2683	-0.2602	-0.19126	0.10132	0.47100	0.78344	0.75978	-0.1044	-0.2857	-0.0031	0.3666	0.6790	0.6534				
12	0.0769	-0.0240	-0.1512	-0.2646	-0.2781	-0.22455	0.07008	0.44150	0.77263	0.81205	-0.1009	-0.3254	-0.0308	0.3406	0.6717	0.7112				
13.8	0.0912	-0.0106	-0.1380	-0.2573	-0.2910	-0.26630	0.03095	0.40286	0.75132	0.84972	-0.1051	-0.3714	-0.0742	0.2979	0.6462	0.7446				
14.1	0.0940	-0.0070	-0.1345	-0.2552	-0.2919	-0.27448	0.02044	0.39274	0.74518	0.85235	-0.1048	-0.3793	-0.0844	0.2879	0.6404	0.7476				
*14.4	0.0966	-0.0035	-0.1307	-0.2521	-0.2918	-0.28207	0.01022	0.38164	0.73613	0.85206	-0.1043	-0.3864	-0.0941	0.2773	0.6318	0.7478				

^a Stall angles of $T_C = 0$ and 0.20, respectively.

^b Stall angle at $T_C = 0.44$.

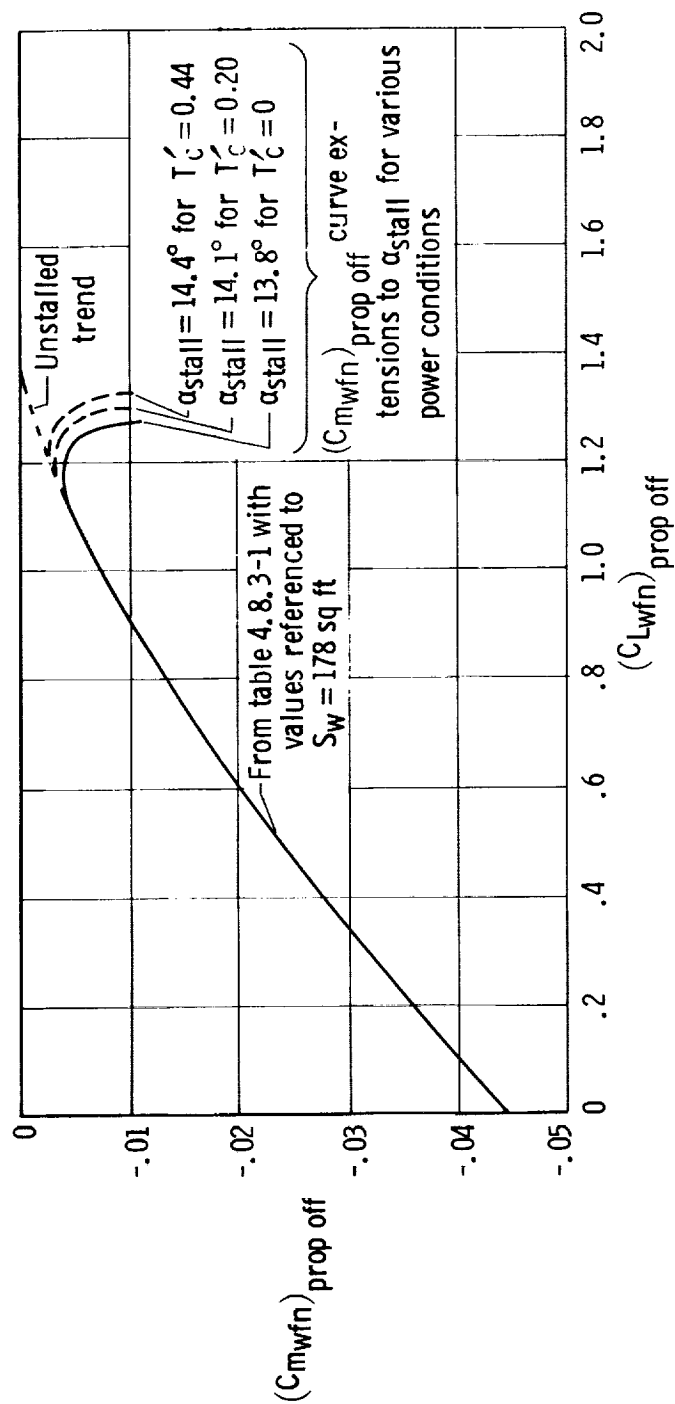


Figure 5.2-1. Propeller-off pitching-moment characteristics of subject airplane for tail-off conditions with characteristics extended to power-on stall angles obtained from figure 5.1.1-7. Center of gravity = $0.10 \bar{c}_w$.

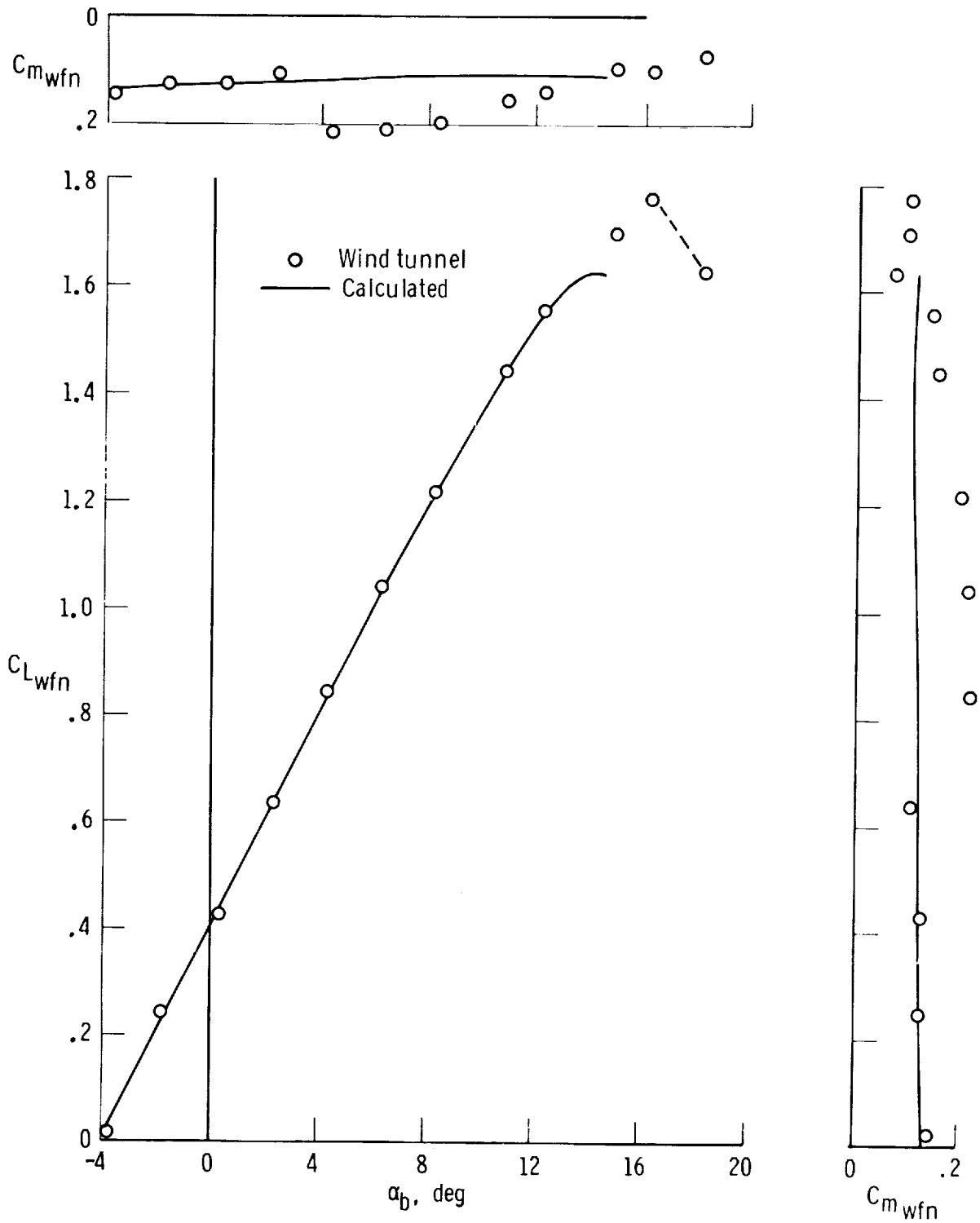


Figure 5.2-2. Comparison of calculated and wind-tunnel-determined tail-off lift and pitching-moment characteristics at $T'_c = 0.44$ and center of gravity = $0.10 \bar{c}_w$.

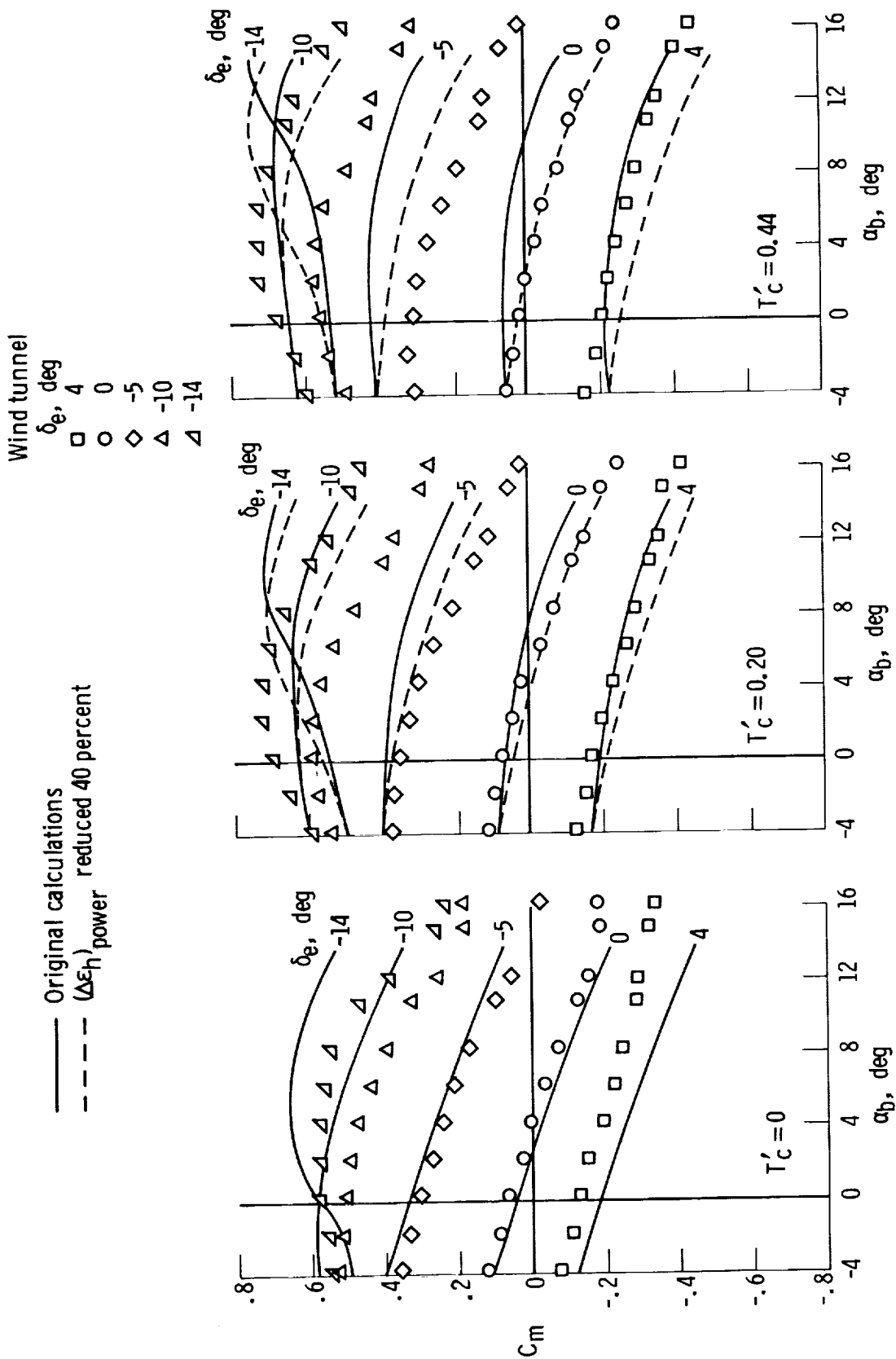


Figure 5.2-3. Comparison of calculated and wind-tunnel-determined variation of C_m with α_b at different power conditions and elevator deflections. Center of gravity = $0.10C_w$.

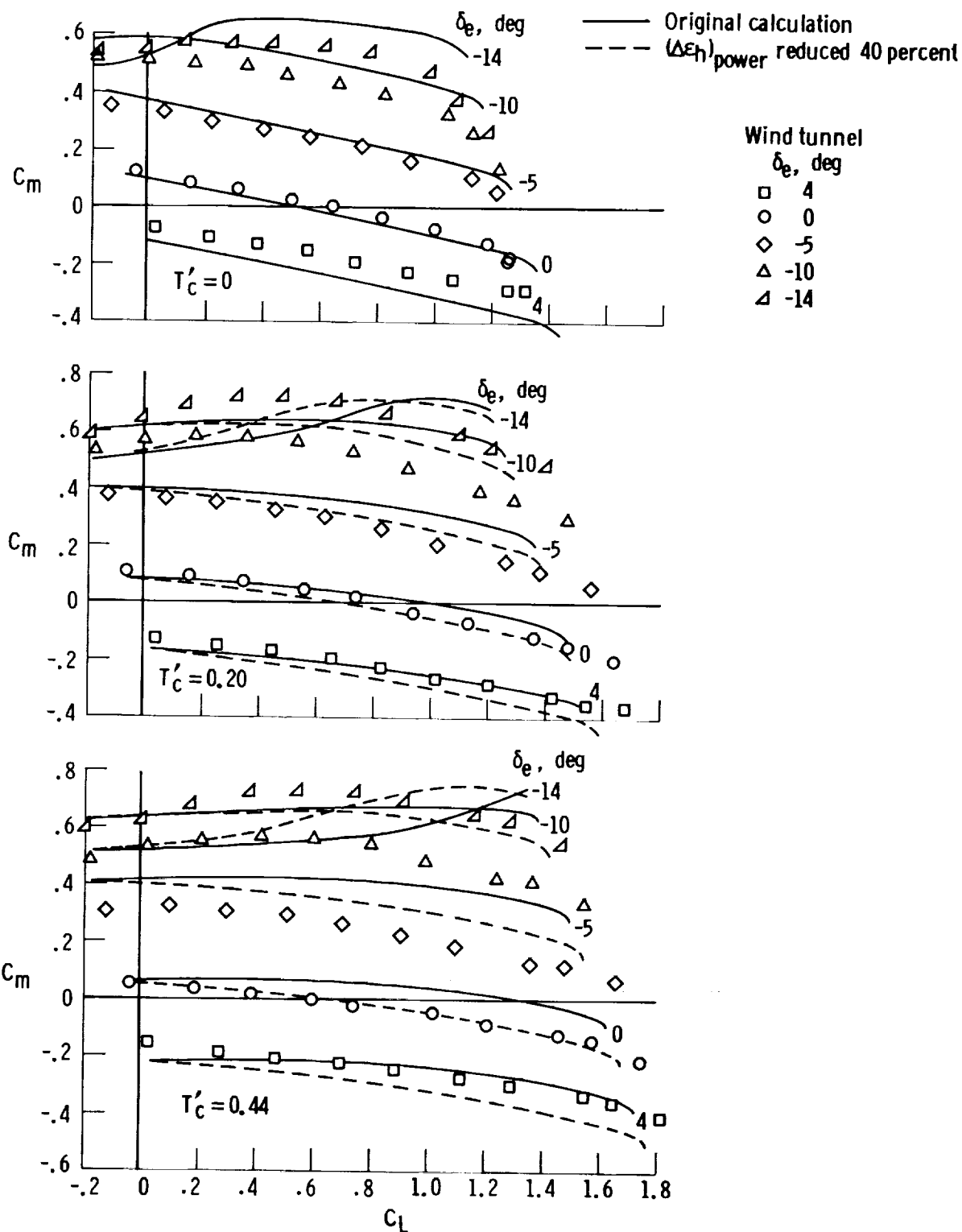


Figure 5.2-4. Comparison of calculated and wind-tunnel-determined variation of C_m with C_L at different power conditions and elevator deflections. Center of gravity = $0.10 \bar{c}_w$.

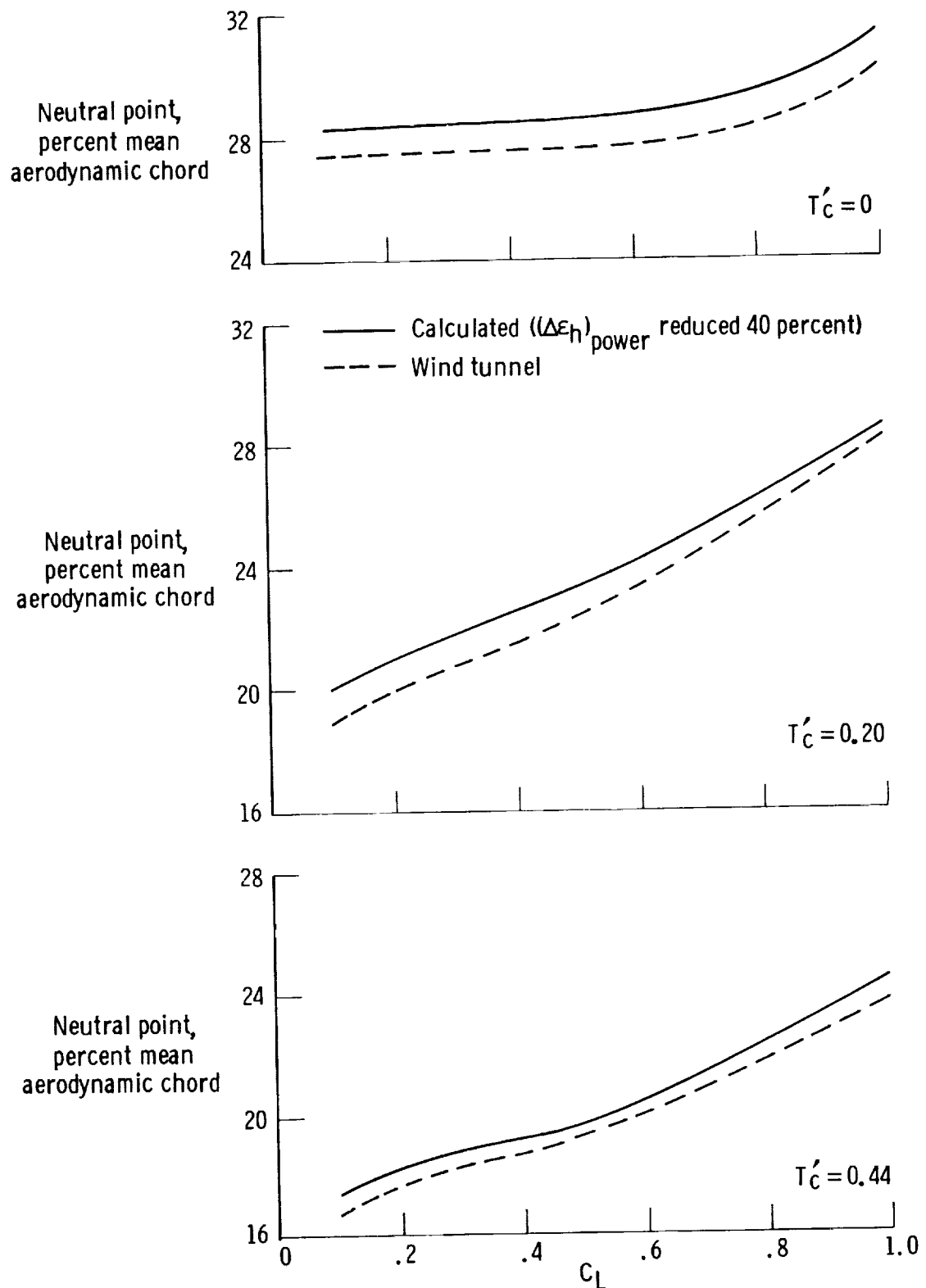


Figure 5.2-5. Comparison of neutral-point characteristics determined from modified calculated and wind-tunnel pitching-moment characteristics. Center of gravity = $0.10 \bar{c}_w$.

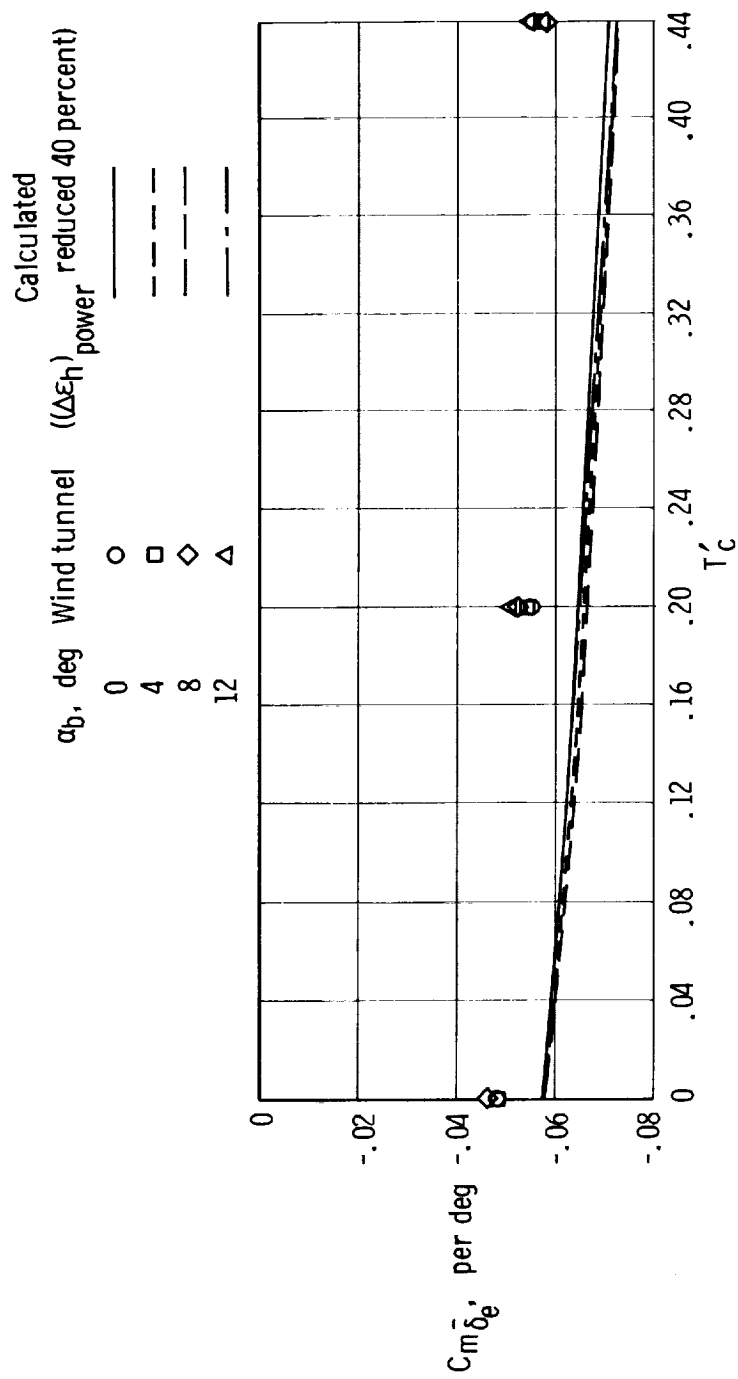


Figure 5.2-6. Comparison of the variation of calculated and wind-tunnel-determined pitch-control effectiveness with thrust coefficient and angle of attack.

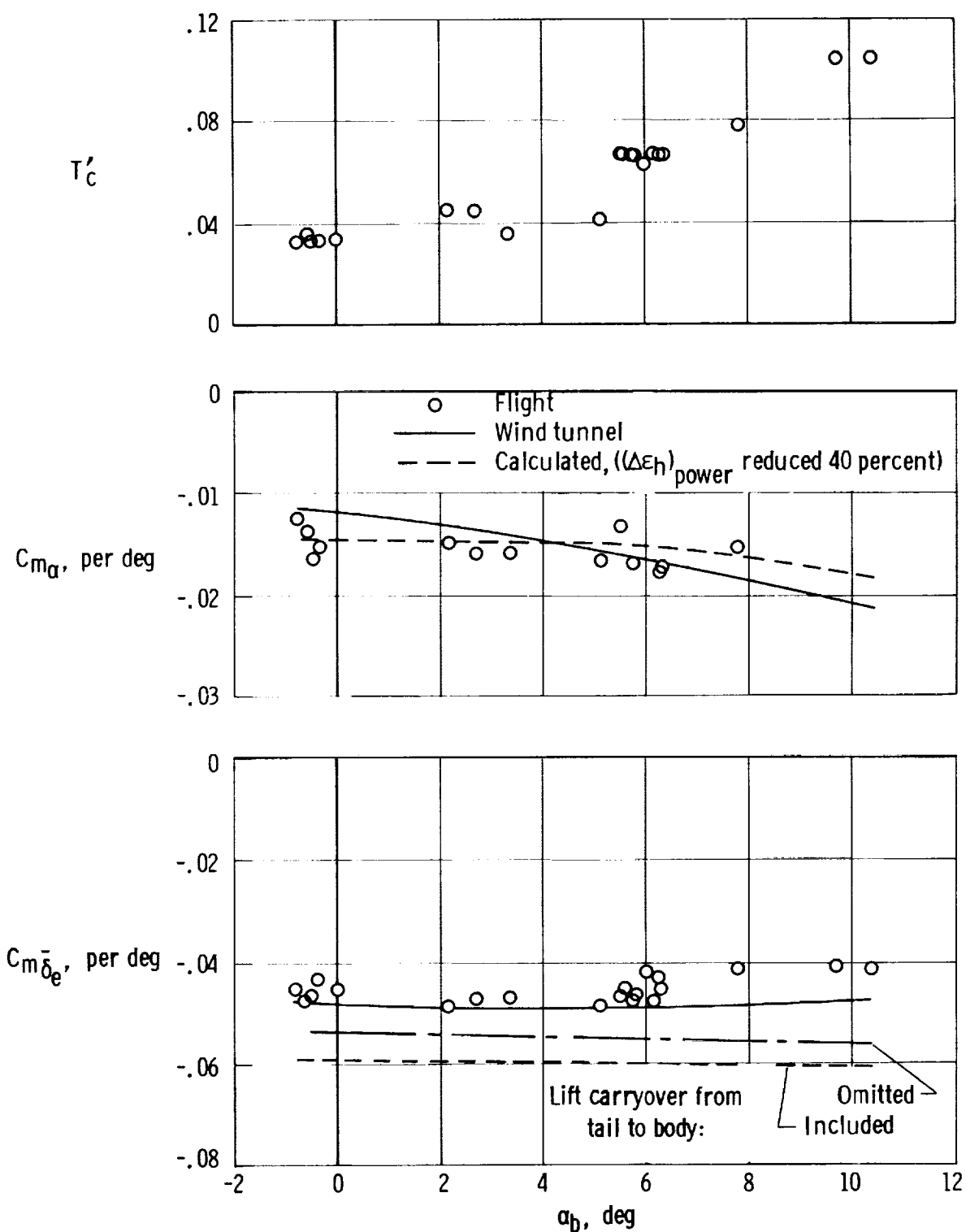


Figure 5.2-7. Comparison of calculated static pitch, C_{m_α} , and control effectiveness, $C_{m_{\delta_e}}$, with wind-tunnel and flight-determined values as a function of angle of attack. Center of gravity = $0.12 \bar{c}_w$.

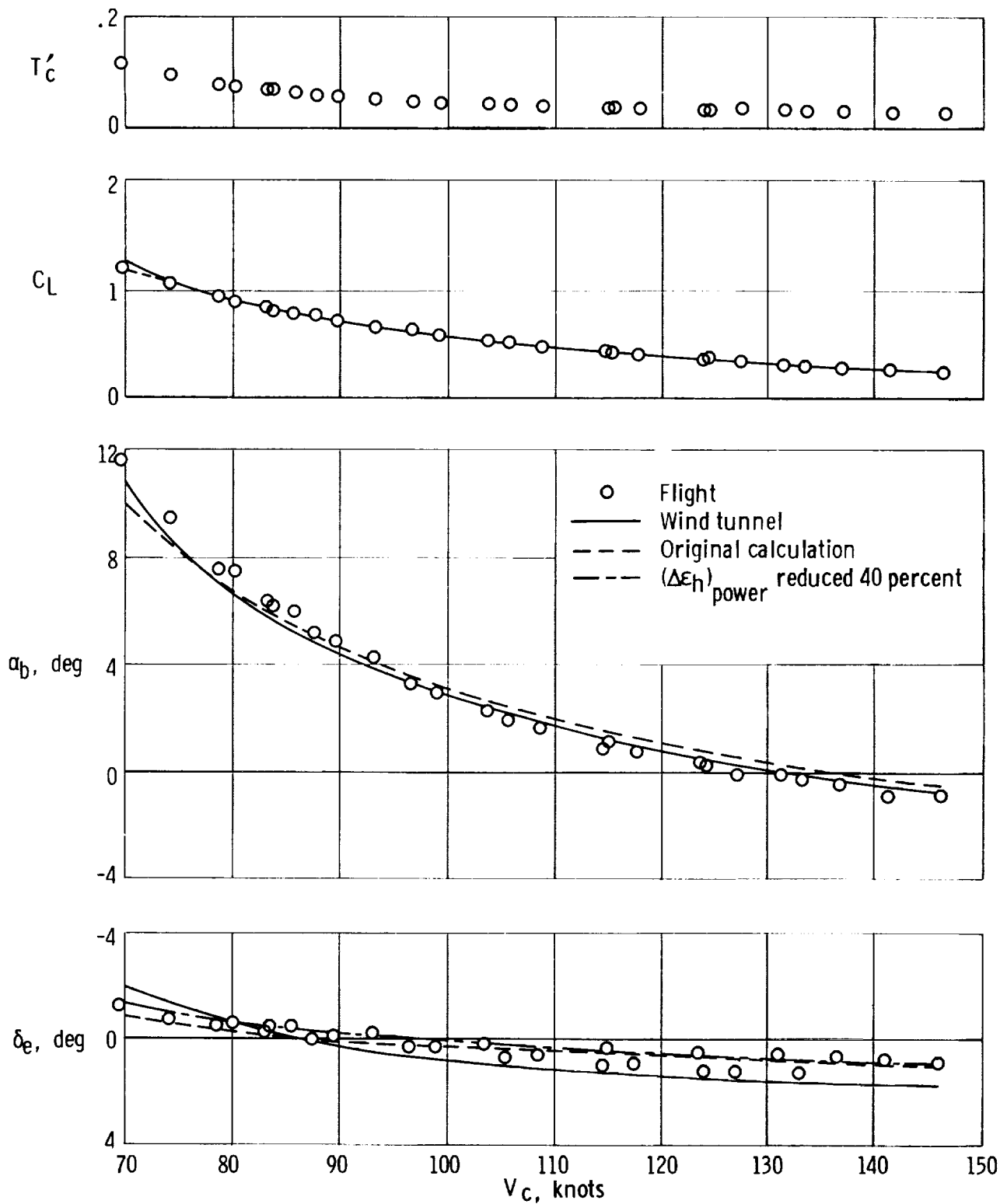


Figure 5.2-8. Comparison of calculated C_L , α_b , and δ_e characteristics for trim level flight conditions with those obtained from wind-tunnel and flight data as a function of calibrated airspeed. Center of gravity = $0.12 \bar{c}_w$.

5.3 Power Effects on Drag

The net drag change of the airplane due to propeller power results from: (1) the component of propeller thrust parallel to the X-stability axis; (2) the change in slipstream dynamic pressure on the profile drag of those portions of the aircraft immersed in the propeller slipstream; (3) the change in induced drag due to the lift component of the direct propeller forces and the change in angle of attack of the immersed portions of the wing; and (4) the change in cooling drag due to the power-induced change in dynamic pressure acting on the immersed cooling system.

For the subject airplane, where the propeller slipstream immerses the nacelle as well as a portion of the wing and the horizontal tail, the drag with power on can be summarized by the following expression:

$$C_D = C_{D_{\text{prop off}}} - n(T'_c/\text{prop}) \cos \alpha_T + \overbrace{\left[(\Delta C_{D_o})_w + (\Delta C_{D_o})_h + (\Delta \overline{C_{D_o}})_n + \Delta C_{D_i} + (\Delta C_D)_{\text{cooling system}} \right]}^{(\Delta C_D)_{\text{power}}, \text{ change in drag due to power}} \quad (5.3-1)$$

where

$C_{D_{\text{prop off}}}$ is the propeller-off drag of the complete airplane (obtained from section 4.12)

$-n(T'_c/\text{prop}) \cos \alpha_T$ is the component of total thrust parallel to the velocity vector, a positive thrust is equal to a negative drag contribution

ΔC_{D_o} is the change in profile drag coefficient due to power

ΔC_{D_i} is the change in induced drag coefficient due to power

$(\Delta C_D)_{\text{cooling system}}$ is the change in the cooling system drag coefficient due to power

The change in profile drag coefficient, ΔC_{D_o} , due to power effects on the wing, horizontal tail, and nacelles is accounted for by

$$\begin{aligned} \Delta C_{D_o} &= (\Delta C_{D_o})_w + (\Delta C_{D_o})_h + (\Delta \overline{C_{D_o}})_n \\ &= n(C_{D_o})_{w_{\text{prop off}}} \frac{S_i/\text{prop}}{S_w} \frac{\Delta \bar{q}_w}{\bar{q}_\infty} + n(C_{D_o})_{h_{\text{prop off}}} \frac{S_{h_i}/\text{prop}}{S_w} \frac{\Delta \bar{q}_h}{\bar{q}_\infty} + (\overline{C_{D_o}})_{n_{\text{prop off}}} \frac{\Delta \bar{q}_w}{\bar{q}_\infty} \end{aligned} \quad (5.3-2)$$

where

n is the number of propellers

$(C_{D0})_{w_{prop\ off}}, (C_{D0})_{h_{prop\ off}}$ are the propeller-off zero-lift drag coefficients of the wing and horizontal tail, respectively, determined from equation (4.12.1-1), per square foot of the respective areas

$(\bar{C}_{D0})_{n_{prop\ off}}$ is the propeller-off zero-lift drag coefficient of the two nacelles with nacelle-wing interference effects included and referenced to the wing area

$S_i/prop$ is the immersed wing area per propeller, obtained from section 5.1.1 and figure 5-1(b)

$Sh_i/prop$ is the immersed horizontal-tail area per propeller, obtained from figure 5-1(b)

$\frac{\Delta \bar{q}_w}{\bar{q}_\infty}$ is the increment in dynamic-pressure ratio, due to power, at the wing and nacelle, obtained from equation (5.1.1-7)

$\frac{\Delta \bar{q}_h}{\bar{q}_\infty}$ is the increment in dynamic-pressure ratio, due to power, at the horizontal tail, obtained from section 5.1.2

The induced drag increment, ΔC_{Di} , of the wing due to propeller slipstream modification of the downwash over portions of the wing can be accounted for by the following equation based on the empirical equation for power-on induced drag in reference 19:

$$\Delta C_{Di} = (C'_{Di})_{w_{prop\ off}} n \left\{ \frac{[(C_{Di})_{w/prop}]_{power\ on}}{(C'_{Di})_{w_{prop\ off}}} - 1 \right\} \quad (5.3-3)$$

where, from reference 19, on a per propeller basis

$$\frac{[(C_{Di})_{w/prop}]_{power\ on}}{(C'_{Di})_{w_{prop\ off}}} = \left(\frac{C_{Lw_{prop\ off}}}{C''_L} \right)^2 \left[1 + \frac{\pi^2 A_w \bar{c}}{180 C_{Lw_{prop\ off}}} \right] + K \left[\frac{h_w}{2R_p} \left(\frac{\Delta C_L}{C''_L} \right)_{T/prop} + \left(\frac{\Delta C_L}{C''_L} \right)_{N_p/prop} \right]^2 \quad (5.3-4)$$

and where

n is the number of propellers

$(C'_{Di})_{w_{prop\ off}}$ is equal to $\frac{(C_{Lw_{prop\ off}})^2}{\pi A_w} (1 + \delta_1 \delta_2)$, obtained from section 4.12.4

$C_{Lw_{prop\ off}}$ is the lift of the wing alone with no power effects, obtained from plots similar to figure 5.1.1-8 having stall angles extended to power-on stall angles

$(\Delta C_L)_T / \text{prop}$ is the lift component of thrust per propeller, obtained from equation (5.1.1-1) on a per propeller basis

$(\Delta C_L)_{N_p} / \text{prop}$ is the lift component of the propeller normal force per propeller, obtained from equation (5.1.1-2) on a per propeller basis

$$C''_L = C_{Lw_{prop\ off}} + (\Delta C_L)_T / \text{prop} + (\Delta C_L)_{N_p} / \text{prop} \quad (5.3-5)$$

A_w, b_w are the wing aspect ratio and span, respectively, obtained from table 3.2-1

R_p is the propeller radius

K is a propeller drag factor, obtained from figure 5.3-1 as a function of $\frac{S_w(T'_c / \text{prop})}{R_p^2}$

$\bar{\epsilon}$ is the effective propeller downwash angle averaged over the entire wing, equal to

$$\bar{\epsilon} = \left(\frac{\bar{\epsilon}}{\epsilon_p} \right) \left(\frac{\partial \epsilon_p}{\partial \alpha_p} \right) \alpha_T \quad (5.3-6)$$

where

$\frac{\partial \epsilon_p}{\partial \alpha_p}$ is obtained from equation (5.1.1-13) and figure 5.1.1-5

$\frac{\bar{\epsilon}}{\epsilon_p}$ is obtained from figure 5.3-2 or figure 5.3-3

α_T is the propeller angle of attack relative to the free stream

The change in drag coefficient of the cooling system, $(\Delta C_D)_{\text{cooling system}}$, due to the power-induced change in dynamic pressure behind the propeller acting on the cooling system immersed in the propeller slipstream is accounted for, to a first order of approximation, by

$$(\Delta C_D)_{\text{cooling system}} \approx (C_{D \text{ cooling system}})_{\text{prop off}} \frac{\Delta \bar{q}_w}{\bar{q}_\infty} \quad (5.3-7)$$

where

$(C_{D \text{ cooling system}})_{\text{prop off}}$ is the contribution of the cooling system to the drag of the airplane for propeller-off conditions, obtained from figure 4.12.7-1 for the cooling systems of both nacelles of the subject airplane

$\frac{\Delta \bar{q}_w}{\bar{q}_\infty}$ is the increase in dynamic pressure behind the propeller, due to power, as a ratio of free-stream dynamic pressure, obtained from equation (5.1.1-7)

Calculations for power-on net-drag characteristics of the subject airplane are summarized in tables 5.3-1 to 5.3-4 as functions of α_b and T'_C . Table 5.3-1

summarizes the zero-lift increments of drag due to power, table 5.3-2 the induced drag increments due to power, and table 5.3-3 the change in cooling-system drag due to power. Table 5.3-4 summarizes all the power effects on drag and lists the power-on net drag.

The calculated power-on drag results, compared with wind-tunnel data (from ref. 2) in figures 5.3-4 and 5.3-5, show good correlation at $T'_C = 0$ and an increasing discrepancy with increasing power at the higher angles of attack. When the increments of induced drag due to power, ΔC_{D_i} , were omitted from the calculations (after a study of table 5.3-4), the correlation improved significantly.

It is surmised that the large, wide, built-in nacelles of the subject airplane interfere with the power-induced slipstream in the immersed area of the wing and, consequently, affect the magnitude of the power-induced increments of induced drag. As in the case of the power-induced downwash at the tail, $(\Delta \epsilon_h)_{\text{power}}$, discussed in section 5.2, it appears that the nacelle-wing configuration of the subject airplane is not representative of the configurations used in correlating experimental data to arrive at the empirical relations used in calculations, in this instance, to arrive at the empirical equation for ΔC_{D_i} .

5.3.1 Symbols

A_w	wing aspect ratio
b_w	wing span, ft
C_D	airplane drag coefficient
$(C_{D \text{ cooling system}})_{\text{prop off}}$	contribution of the cooling system to the drag of the airplane for power-off conditions

$C_{D_{\text{power on}}}$	power-on drag coefficient of the airplane
$C_{D_{\text{prop off}}}$	airplane drag coefficient, propellers off
$(\Delta C_D)_{\text{cooling system}}$	increment of airplane drag coefficient due to the cooling system
$(\Delta C_D)_{\text{power}}$	increment of airplane drag coefficient due to power
$(C'_{Di})_{w_{\text{prop off}}} = \frac{(C_{L_{w_{\text{prop off}}}})^2}{\pi A_w} (1 + \delta_1 \delta_2)$	
$[(C_{Di})_{w/\text{prop}}]_{\text{power on}}$	induced drag coefficient of the wing with power effects, due to one propeller, included
ΔC_{Di}	increment of drag coefficient due to power effects on induced drag
$(C_{Do})_{h_{\text{prop off}}}$ $(C_{Do})_{w_{\text{prop off}}}$	propeller-off zero-lift drag coefficient of the horizontal tail and wing, respectively, per sq ft of the respective areas
$(\overline{C_{Do}})_{n_{\text{prop off}}}$	propeller-off zero-lift drag coefficient of the two nacelles of the subject airplane with nacelle-wing interference effects included, referenced to the wing area
ΔC_{Do}	increment of zero-lift drag coefficient due to power
$(\Delta C_{Do})_h, (\Delta \overline{C_{Do}})_n, (\Delta C_{Do})_w$	contribution of the horizontal tail, nacelles (including nacelle-wing interference effects), and wing, respectively, to ΔC_{Do}
C_f	skin friction coefficient of a flat plate
C_L	lift coefficient of the airplane
$C_{L_{w_{\text{prop off}}}}$	lift coefficient of an isolated wing, propellers off
$C''_L = C_{L_{w_{\text{prop off}}}} + (\Delta C_L)_{T/\text{prop}} + (\Delta C_L)_{N_p/\text{prop}}$	
$(\Delta C_L)_{N_p/\text{prop}}$	increment of lift coefficient due to the normal force of one propeller
$(\Delta C_L)_{T/\text{prop}}$	increment of lift coefficient due to the lift component of one propeller

K	propeller drag factor
k	surface roughness height, in.
l	reference length used in obtaining the Reynolds number of a lifting surface and skin-friction coefficient, C_f , of a flat plate, mean aerodynamic chord of surface, in.
N_{Re}	Reynolds number
n	number of propellers
\bar{q}_∞	free-stream dynamic pressure, lb/sq ft
$\frac{\Delta \bar{q}_h}{\bar{q}_\infty}, \frac{\Delta \bar{q}_w}{\bar{q}_\infty}$	change in dynamic pressure on an immersed portion of the horizontal tail and wing, respectively, as a ratio of the free-stream dynamic pressure
R_p	propeller radius, ft
$S_{l/prop}, S_{h_l/prop}$	portion of the wing and horizontal-tail area, respectively, immersed in the slipstream of one propeller, sq ft
S_w	wing area, sq ft
T	thrust of propellers, lb
$T'_c = \frac{T}{\bar{q}_\infty S_w}$	
$T'_c/prop$	thrust coefficient of one propeller
$\frac{t}{c}$	thickness ratio
α_b	airplane angle of attack relative to the X-body axis, deg
α_T	angle of attack of the thrust axis, deg
δ_1, δ_2	correction factor for the taper ratio and sweep angle of the quarter-chord line, respectively, in calculating the propeller-off induced drag coefficient of the wing and horizontal tail
$\bar{\epsilon}$	effective propeller downwash angle averaged over the entire wing, deg
$\frac{\bar{\epsilon}}{\epsilon_p}$	ratio of $\bar{\epsilon}$ to the downwash angle, ϵ_p , of the propeller slipstream behind the propeller

$$\frac{\partial \epsilon_p}{\partial \alpha_p}$$

rate of change of the propeller downwash angle, ϵ_p ,
with the propeller angle of attack

$$(\Delta \epsilon_h)_{\text{power}}$$

change in the downwash angle at the horizontal tail
due to power

TABLE 5.3-1
ZERO-LIFT DRAG INCREMENTS DUE TO POWER

$$\Delta C_{D_o} = n(C_{D_o})_{w \text{ prop off}} \frac{S_l / \text{prop}}{S_w} \frac{\Delta \bar{q}_w}{\bar{q}_\infty} + n(C_{D_o})_{h \text{ prop off}} \frac{S_{h_l} / \text{prop}}{S_w} \frac{\Delta \bar{q}_h}{\bar{q}_\infty} + (\overline{C_{D_o}})_{n \text{ prop off}} \frac{\Delta \bar{q}_w}{\bar{q}_\infty}$$

(a)

Symbol	Description	Reference	Magnitude		
			Wing	Horizontal tail	Nacelles
n	Number of propellers	-----	2	2	2
$\frac{S_l / \text{prop}}{S_w}$	Reference wing area, sq ft	Table 3-1	178	-----	-----
$\frac{S_{h_l} / \text{prop}}{S_w}$	Immersed wing area per propeller as ratio of S_w	Table 5.1.1-2(a)-3, column 10	Column 10 of reference	-----	-----
	Immersed horizontal-tail area per propeller, sq ft	Figure 5-1	-----	7.63 per prop	-----
k	Surface roughness height, in.	Table 4.12.1-2	0.25×10^{-3} , smooth matte finish		
l	Reference length, mean aerodynamic chord of surface, in.	Table 3.2-1	59.50	32.45	-----
$\frac{l}{k}$	-----	-----	2.38×10^5	1.30×10^5	-----
N_{Re}	Reynolds number at 63.4 mph, sea level = $\frac{l}{12} (0.65 \times 10^6)$	Wind-tunnel test conditions	3.22×10^6	1.75×10^6	-----
C_f	Skin-friction coefficient of flat plate	Figure 4.12.1-1	3.65×10^{-3}	4.08×10^{-3}	-----
$\frac{t}{c}$	Thickness ratio of surface	Table 4.1-1	.15	.08	-----
$(C_{D_o})_{w \text{ prop off}}$	$2 C_f \left[1 + 2 \left(\frac{t}{c} \right) + 120 \left(\frac{t}{c} \right)^4 \right]$	Equation (4.12.1-1)	.00993 per sq ft of wing	.00951 per sq ft of horizontal tail	-----
$(C_{D_o})_{h \text{ prop off}}$					
$(\overline{C_{D_o}})_{n \text{ prop off}}$	Propeller-off zero-lift drag coefficient of both nacelles referenced to $S_w = 178$ sq ft	Table 4.12.3-1(c)	-----	-----	0.00827 per two nacelles
$\frac{\Delta \bar{q}_w}{\bar{q}_\infty}$	$\frac{S_w (T'_c / \text{prop})}{\pi R_p^2}$ where $R_p = 3.0$ ft	Equation (5.1.1-7)	$6.30 (T'_c / \text{prop})$	-----	$6.30 (T'_c / \text{prop})$
$\frac{\Delta \bar{q}_h}{\bar{q}_\infty}$	Change in dynamic-pressure ratio at the horizontal tail due to power	Table 5.1.2-1(b), column 9	-----	Column 9 of reference	-----
Summary: $\Delta C_{D_o} = 0.125 \left(\frac{S_l / \text{prop}}{S_w} \right) (T'_c / \text{prop}) + 0.0008 \frac{\Delta \bar{q}_h}{\bar{q}_\infty} + 0.052 (T'_c / \text{prop})$ $\approx \left[0.125 \left(\frac{S_l / \text{prop}}{S_w} \right) + 0.052 \right] (T'_c / \text{prop})$					

(b)

①	②			③		
-----	Table 5.1.1-2(a)-3, column 10			Table 5.3-1(a)		
α_b , deg	$\frac{S_l / \text{prop}}{S_w}$			$\Delta C_{D_o} = [0.125 \text{ ②} + 0.052] \times (T'_c / \text{prop})$		
	T'_c / prop			T'_c / prop		
	0	0.10	0.22	0	0.10	0.22
-4	0.1834	0.1827	0.1822	0	0.007484	0.016450
-2	.1805	.1801	.1798	0	.007451	.016384
0	0.1762	0.1765	0.1767	0	0.007406	0.016299
2	.1706	.1721	.1728	0	.007351	.016192
4	0.1633	0.1665	0.1681	0	0.007281	0.016063
6	.1541	.1598	.1625	0	.007198	.015909
8	0.1428	0.1518	0.1559	0	0.007098	0.015727
10	.1288	.1423	.1478	0	.006979	.015504
12	0.1110	0.1309	0.1393	0	0.006836	0.015271
^a 13.8	.0905	.1190	.1302	0	.006688	.015020
^b 14.1	-----	0.1165	0.1283	-	0.006656	0.014968
^c 14.4	-----	-----	.1264	-	-----	.014916

^{a,b,c} Stall angles for total $T'_c = 0, 0.20, 0.44$, respectively.

TABLE 5.3-2
INDUCED-DRAG INCREMENT DUE TO POWER

$$\Delta C_{D_i} = (C_{D_i}')_{w_{prop\ off}} \left\{ \left(\frac{C_{L_{w_{prop\ off}}}}{C_L''} \right)^2 \left(1 + \frac{\pi^2 A_w \bar{\epsilon}}{180 C_{L_{w_{prop\ off}}}} \right) + K \left[\frac{b_w}{2R_p} \left(\frac{(\Delta C_L)_T / prop + (\Delta C_L)_{N_p} / prop}{C_L''} \right)^2 \right] - 1 \right\}$$

Symbol	Description	Reference	Magnitude
n α_T	Number of propellers Angle of attack of thrust axis and propeller plane, deg	----- -----	2 Same as α_b
b_w A_w R_p	Wing span, ft Wing aspect ratio Propeller radius, ft	Table 3.2-1 Table 3.2-1 Table 3-1	36.0 7.5 3.0
$C_{D_{prop\ off}}$ ΔC_{D_0}	Drag of airplane with propeller off Zero-lift drag increment due to power	Table 4.12.8-1, column 9 Table 5.3-1(b), column 3	Column 9 of reference Column 3 of reference
$(C_{D_i}')_{w_{prop\ off}}$ $C_{L_{w_{prop\ off}}}$ $(\Delta C_L)_T / prop + (\Delta C_L)_{N_p} / prop$ C_L''	$\frac{(C_{L_{w_{prop\ off}}})^2}{\pi A_w} (1 + \delta_1 \delta_2)$ Lift coefficient of wing alone with propeller off Lift contribution of direct propeller forces/propeller $C_{L_{w_{prop\ off}}} + (\Delta C_L)_T / prop + (\Delta C_L)_{N_p} / prop$	Table 4.12.4-1 Figure 5.1.1-8 Table 5.1.1-1(c), column 7 -----	$0.0432 C_{L_{w_{prop\ off}}}^2$ $f(\alpha_b)$ $\frac{\text{Column 7 of reference}}{2}$ $f(\alpha_b, T_c' / prop)$
$\frac{\partial \epsilon_p}{\partial \alpha_p}$ $\bar{\epsilon}$ $\bar{\epsilon}_p$	Rate of change of propeller downwash with propeller angle of attack Averaged propeller downwash over wing span as a ratio of propeller downwash behind propeller, $f\left(\frac{R_p}{b_w}, \frac{S_w(T_c' / prop)}{R_p^2}\right)$ $\bar{\epsilon}_p \left(\frac{\partial \epsilon_p}{\partial \alpha_p} \right) \alpha_T$	Table 5.1.1-2(a)-2, column 6 Figure 5.3-3 Equation (5.3-6)	See part (b) of table
K	Propeller drag factor, $f\left(\frac{S_w(T_c' / prop)}{R_p^2}\right)$	Figure 5.3-1	

①	②	③	④	⑤	⑥	⑦	⑧
-----	-----	-----	-----	Figure 5.3-1	Table 5.1.1-2(a)-2, column 6	Figure 5.3-3	Equation (5.3-6)
Total T_c'	$T_c' / prop$	$\frac{S_w(T_c' / prop)}{R_p^2}$	$\frac{R_p}{b_w}$	K	$\frac{\partial \epsilon_p}{\partial \alpha_p}$	$\frac{\bar{\epsilon}}{\epsilon_p}$	$\bar{\epsilon} =$ $⑥ \times ⑦ \times \alpha_T$
0 .20 .44	0 .10 .22	0 1.978 4.350	0.0833 .0833 .0833	4.00 3.43 2.90	0.0234 .1987 .2896	0.052 .153 .246	0.00122 α_b .0304 α_b .07124 α_b

TABLE 5.3-2 (Continued)

(c)-1 $T'_c = 0$

①	②	③	④	⑤	⑥	⑦	⑧	⑨	⑩	⑪
	Table 5.3-2(b)			Table 5.1.1-1(c), column 7	Figure 5.1.1-8					
α_b , deg	$\cos \alpha_b =$ $\cos ①$	$\bar{\epsilon} =$ $0.00122 \times ①$	$\frac{\pi^2 A_w \bar{\epsilon}}{180} =$ $0.411 ③$	$(\Delta C_L)_T / \text{prop} +$ $(\Delta C_L)_{N_p} / \text{prop}$ (Column 7 of reference) $\frac{2}{2}$	$C_{Lw} \text{prop off}$	$C_L'' =$ $⑤ + ⑥$	$\frac{(C_{Lw} \text{prop off})^2}{C_L''}$ $= (⑤ / ⑦)^2$	$\frac{(\Delta C_L)_T / \text{prop} + (\Delta C_L)_{N_p} / \text{prop}}{C_L''}$ $= ⑤ / ⑦$	$1 + \frac{④}{⑥}$	$\left(\frac{C_{Lw} \text{prop off}}{C_L''} \right)^2 \left(1 + \frac{\pi^2 A_w \bar{\epsilon}}{180 C_{Lw} \text{prop off}} \right)$ $= ⑧ \times ⑩$
-4	0.9976	-0.00488	-0.00201	-0.00104	0	0.00104	0	1.0	0.99308	0
-2	.9994	-.00244	-.00100	-.00041	.145	.14459	1.00575	-.00287	.99879	.99879
2	1.0000	0	0	0.00021	0.290	0.29021	0.99855	0.00072	1.0	0.99855
4	.9994	.00244	.00100	.00083	.440	.44083	.99624	.00188	1.00228	.99851
6	0.9976	0.00488	0.00201	0.00145	0.586	0.58745	0.99507	0.00247	1.00342	0.99847
8	.9945	.00732	.00301	.00206	.734	.73607	.99410	.00280	1.00410	.99848
10	0.9903	0.00976	0.00401	0.00268	0.879	0.88168	0.99394	0.00303	1.00456	0.99832
12	.9848	.01220	.00501	.00327	1.026	1.02927	.99366	.00318	1.00489	.99832
13.8	0.9781	0.01464	0.00502	0.00386	1.164	1.16786	0.99340	0.00331	1.00517	0.99854
	.9711	.01684	.00692	.00436	1.230	1.23436	.99295	.00353	1.00563	.99854

①	⑫	⑬	⑭	⑮	⑯
	Table 5.3-2(a)	Table 5.3-2(b)	Table 5.3-2(a)	Equation (5.3-3)	
α_b , deg	$b_w \times ③ =$ $6 \times ③$	$\left[\frac{b_w (\Delta C_L)_T / \text{prop} + (\Delta C_L)_{N_p} / \text{prop}}{K \frac{2}{2R_p} C_L''} \right]^2$ $= 4.0 \times ⑫^2$	$(C_{D1})_{w \text{prop off}}$ $⑬ + ⑭ - 1$	$\Delta C_{D1} =$ $n(⑬) ⑮ =$ $2 ⑬ ⑮$	
-4	6.0	144.00	143.00	0	0
-2	-.01722	.00119	-.00002	.00091	0
2	0.00434	0.00084	-0.00138	0.00362	-0.00001
4	.01130	.00051	-.00098	.00834	-.00002
6	0.01481	0.00088	-0.00065	0.01480	-0.00002
8	.01682	.00113	-.00039	.02322	-.00002
10	0.01820	0.00133	-0.00015	0.03330	-0.00001
12	.01906	.00145	-.00003	.04537	0
13.8	0.01983	0.00157	0.00011	0.05840	0.00001
	.02119	.00180	.00034	.06521	.00004

^aStall angle for total $T'_c = 0$.

TABLE 5.3-2 (Continued)

①	②	③	④	⑤	⑥	⑦	⑧	⑨	⑩	⑪
		Table 5.3-2(b)		Table 5.1.1-1(c), column 7	Figure 5.1.1-8					
α_b , deg	$\cos \alpha_b =$ $\cos ①$	$\bar{\epsilon} =$ $0.0304 \times ①$	$\frac{\pi^2 A_w \bar{\epsilon}}{180}$ $=$ $0.411 ③$	$(\Delta C_L)_T / \text{prop} +$ $(\Delta C_L)_{N_p} / \text{prop} =$ (Column 7 of reference) $\frac{2}{2}$	$C_{Lw} \text{prop off}$	$C_L'' =$ $⑤ + ⑥$	$\left(\frac{C_{Lw} \text{prop off}}{C_L''} \right)^2$ $= (⑥ / ⑦)^2$	$\frac{(\Delta C_L)_T / \text{prop} + (\Delta C_L)_{N_p} / \text{prop}}{C_L''}$ $= ⑤ / ⑦$	$1 + \frac{④}{⑥}$	$\left(\frac{C_{Lw} \text{prop off}}{C_L''} \right)^2 \left(1 + \frac{\pi^2 A_w \bar{\epsilon}}{180 C_{Lw} \text{prop off}} \right)$ $= ⑧ \times ⑩$
-4	0.9976	-0.1216	-0.0498	-0.00801	0	-0.00801	0	1.0	0	0
-2	.9994	-.0608	-.02499	-.00411	.145	.14090	1.05912	-.02914	0.82766	.87659
0	1.0000	0	0	0.00030	0.290	0.29030	0.99793	0.00103	1.00000	0.99793
2	.9994	.0608	.02499	.00471	.440	.44471	.97993	.01059	1.05679	1.03452
4	0.9976	0.1216	0.0498	0.00911	0.586	0.59511	0.96962	0.01531	1.08529	1.05232
6	.9945	.1824	.07497	.01346	.734	.74746	.96432	.01800	1.10213	1.06281
8	0.9903	0.2432	0.09996	0.01780	0.879	0.89680	0.96071	0.01984	1.11371	1.06985
10	.9848	.3040	.12494	.02212	1.026	1.04812	.95825	.02110	1.12178	1.07495
12	0.9781	0.3648	0.14993	0.02642	1.170	1.19642	0.95632	0.02208	1.12815	1.07887
13.8	.9711	.4195	.17242	.03020	1.251	1.28120	.95341	.02337	1.13783	1.08482
*14.1	0.9699	0.4286	0.17617	0.03084	1.255	1.28584	0.95261	0.02398	1.14038	1.08634

①	⑫	⑬	⑭	⑮	⑯
	Table 5.3-2(a)	Table 5.3-2(b)	Table 5.3-2(a)	Equation (5.3-3)	
α_b , deg	$\frac{b_w}{2R_p} \times ⑤ =$ $6 \times ⑤$	$\frac{b_w}{K} \left[\frac{(\Delta C_L)_T / \text{prop} + (\Delta C_L)_{N_p} / \text{prop}}{C_L''} \right]^2$ $= 3.43 \times ⑩^2$	$① + ⑬ - 1$	$(C_{D1})_{w \text{prop off}} =$ $① + ⑬ - 1$	$\Delta C_{D1} =$ $n ⑭ ⑮ =$ $2 ⑭ ⑮$
-4	6.0	123.48	122.48	0	0
-2	-0.17481	.10482	-.01859	.00091	-0.00003
0	0.00620	0.00013	-0.00194	0.00362	-0.00001
2	.06354	.01385	.04837	.00834	.00081
4	0.09186	0.02894	0.08126	0.01480	0.00241
6	.10800	.04001	.10282	.02322	.00477
8	0.11904	0.04861	0.11856	0.03330	0.00790
10	.12660	.05498	.12992	.04537	.01179
12	0.13248	0.06020	0.13907	0.05900	0.01641
13.8	.14142	.06860	.15342	.06752	.02072
*14.1	0.14388	0.07101	0.15735	0.06788	0.02136

*Sail angle for total $T'_c = 0.20$.

TABLE 5.3-2 (Concluded)

(c)-3 T'_c 0.44

①	②	③	④	⑤	⑥	⑦	⑧	⑨	⑩	⑪
		Table 5.3-2(b)		Table 5.1.1-1(c), column 7	Figure 5.1.1-8					
α_b , deg	$\cos \alpha_b$ $\cos ①$	$\bar{\epsilon} =$ $0.07124 \times ①$	$\frac{\pi^2 A_w \bar{\epsilon}}{180}$ $=$ $0.411 ③$	$(\Delta C_L)_T / \text{prop} +$ $(\Delta C_L)_{N_p} / \text{prop}$ $(\text{Column 7 of reference})^2$	$C_{L_w} \text{ prop off}$	$C_L'' =$ $⑤ + ⑥$	$\left(\frac{C_{L_w} \text{ prop off}}{C_L''} \right)^2$ $= (⑥ / ⑦)^2$	$\frac{(\Delta C_L)_T / \text{prop} + (\Delta C_L)_{N_p} / \text{prop}}{C_L''}$ $= ⑤ / ⑦$	$1 + \frac{④}{⑥}$	$\left(\frac{C_{L_w} \text{ prop off}}{C_L''} \right)^2 \left(1 + \frac{\pi^2 A_w \bar{\epsilon}}{180 C_{L_w} \text{ prop off}} \right)$ $= ⑧ \times ⑩$
-4	0.9976	-0.28496	-0.11712	-0.01730	0	-0.01730	0	1.0	0	0
-2	.9994	-.14248	-.05856	-.00844	.145	.13656	1.12743	-.06180	0.59614	.67211
0	1.0000	0	0	0.00037	0.290	0.29037	0.99745	0.00127	1.00000	0.99745
2	.9994	.14248	.05856	.00918	.440	.44918	.93834	.02044	1.13309	1.08725
4	0.9976	0.28496	0.11712	0.01793	0.536	0.60393	0.94150	0.02969	1.19986	1.12967
6	.9945	.42744	.17568	.02668	.734	.76068	.93109	0.03507	1.23934	1.13394
8	0.9903	0.56992	0.23424	0.03536	0.879	0.91436	0.92415	0.03867	1.26648	1.17042
10	.9848	.71240	.29280	.04403	1.026	1.07002	.91941	.04114	1.28538	1.18179
12	0.9781	0.85488	0.35136	0.05202	1.170	1.22262	0.91577	0.04304	1.30030	1.19078
14.1	.9711	.98311	.40406	.06021	1.267	1.32721	.91133	.04537	1.31891	1.20196
14.4	0.9699	1.00448	0.41284	0.06153	1.270	1.33153	0.90972	0.04621	1.32507	1.20544
	.9688	1.02586	.42163	.06280	1.272	1.33480	.90812	.04705	1.33147	1.20913

①	②	③	④	⑤	⑥	⑦	⑧	⑨	⑩	⑪
		Table 5.3-2(a)	Table 5.3-2(b)	Table 5.3-2(c)	Equation (5.3-3)					
α_b , deg	$\frac{b_w}{2R_p} \times ③ =$ $\frac{②}{6 \times ③}$	$\frac{b_w}{K \frac{2R_p}{K}} =$ $\frac{②}{K \frac{2R_p}{K}}$ $= 2.90 \times ③^2$	$\left(\frac{(\Delta C_L)_T / \text{prop} + (\Delta C_L)_{N_p} / \text{prop}}{C_L''} \right)^2$ $= ① + ③ - 1$	$(C_{D1})_{w \text{ prop off}}$ $= 0.0432 ⑥^2$	$\Delta C_{D1} =$ $n ④ ⑤$ $= 2 ④ ⑤$					
-4	6.0	104.00	103.00	0	0	0	0	0	0	0
-2	-.37080	.39873	.07084	.00091	.00013	.00013	.00013	.00013	.00013	.00013
0	0.00762	0.00017	-.00238	0.00362	0.00834	0.00834	-.00002	-.00002	-.00002	-.00002
2	.12264	.04362	.13087	.13087	.00834	.00834	.00218	.00218	.00218	.00218
4	0.17814	0.09203	0.22170	0.22170	0.01480	0.01480	0.00656	0.00656	0.00656	0.00656
6	.21042	.12840	.28234	.28234	.02322	.02322	.01311	.01311	.01311	.01311
8	0.23202	0.15612	0.32654	0.32654	0.03330	0.03330	0.02175	0.02175	0.02175	0.02175
10	.24684	.17670	.35849	.35849	.04537	.04537	.03253	.03253	.03253	.03253
12	0.25824	0.19340	0.38418	0.38418	0.05900	0.05900	0.04533	0.04533	0.04533	0.04533
13.8	.27222	.21490	.41686	.41686	.06919	.06919	.05768	.05768	.05768	.05768
14.1	0.27726	0.22293	0.42837	0.42837	0.06952	0.06952	0.05956	0.05956	0.05956	0.05956
14.4	.28230	.23111	.43655	.43655	.06974	.06974	.06089	.06089	.06089	.06089

*Stall angles for total $T'_c = 0.44$.

TABLE 5.3-3
CHANGE IN COOLING-SYSTEM DRAG DUE TO POWER

$$(\Delta C_D)_{\text{cooling system}} \approx (C_{D\text{cooling system}})_{\text{prop off}} \frac{\Delta \bar{q}_w}{\bar{q}_\infty}$$

Symbol	Description	Reference	Magnitude
$(C_{D\text{cooling system}})_{\text{prop off}}$	Cooling drag coefficient with propellers off	Figure 4.12.7-1	$f(\alpha_b)$
S_w	Reference wing area, sq ft	Table 3-1	178
R_p	Propeller radius, ft	Table 3-1	3
$\frac{\Delta \bar{q}_w}{\bar{q}_\infty}$	$\frac{S_w(T'_c/\text{prop})}{\pi R_p^2}$	Equation (5.1.1-7)	$6.30(T'_c/\text{prop})$
Summary: $(\Delta C_D)_{\text{cooling system}} = 6.30(T'_c/\text{prop})(C_{D\text{cooling system}})_{\text{prop off}}$			

①	②	③			④		
-----	Figure 4.12.7-1	Equation (5.1.1-7)			Equation (5.3-7)		
α_b , deg	$(C_{D\text{cooling system}})_{\text{prop off}}$	$\frac{\Delta \bar{q}_w}{\bar{q}_\infty} = 6.30(T'_c/\text{prop})$			$(\Delta C_D)_{\text{cooling system}} \approx ② \times ③$		
		T'_c/prop			T'_c		
		0	0.10	0.22	0	0.20	0.44
-4	0.00200	0	0.630	1.386	0	0.00126	0.00277
-2	.00340	0	.630	1.386	0	.00214	.00471
0	0.00333	0	0.630	1.386	0	0.00210	0.00462
2	.00280	0	.630	1.386	0	.00176	.00388
4	0.00224	0	0.630	1.386	0	0.00141	0.00310
6	.00185	0	.630	1.386	0	.00117	.00256
8	0.00166	0	0.630	1.386	0	0.00105	0.00230
10	.00310	0	.630	1.386	0	.00195	.00430
12	≈ 0.00740	0	0.630	1.386	0	0.00466	0.01026
^a 13.8	≈ 0.0090 (assumed)	0	.630	1.386	0	≈ 0.00567	≈ 0.01247
^b 14.1	≈ 0.0090	-	0.630	1.386	-	≈ 0.00567	≈ 0.01247
^c 14.4	≈ 0.0090 (assumed)	-	-----	1.386	-	-----	≈ 0.01247

^{a,b,c}Stall angles for total $T'_c = 0, 0.20, 0.44$, respectively.

TABLE 5.3-4
POWER-ON DRAG OF THE COMPLETE AIRPLANE

$$C_{D_{\text{power on}}} = C_{D_{\text{prop off}}} - n(T'_c/\text{prop}) \cos \alpha_T + \Delta C_{D_0} + \Delta C_{D_1} + (\Delta C_D)_{\text{cooling system}}$$

①	②	③	④	⑤	⑥	⑦	⑧
-----	----	Table 4.12.8-1, column 10	-----	Table 5.3-1(b), column 3	Table 5.3-2, column 16	Table 5.3-3, column 4	Equation (5.3-1)
α_b , deg	$\cos \alpha_T$ = \cos ①	$C_{D_{\text{prop off}}}$	$-n(T'_c/\text{prop}) \times$ $\cos \alpha_T$ = $-2(T'_c/\text{prop})$ ②	ΔC_{D_0}	ΔC_{D_1}	$(\Delta C_D)_{\text{cooling system}}$	$C_{D_{\text{power on}}} =$ ③+④+⑤+⑥+⑦
$T'_c = 0, T'_c/\text{prop} = 0, n = 2$ (propellers)							
-4	0.9976	0.0320	0	0	≈ 0	0	0.0320
-2	.9994	.0327	0	0	≈ 0	0	.0327
0	1.0000	0.0345	0	0	≈ 0	0	0.0345
2	.9994	.0408	0	0	≈ 0	0	.0408
4	0.9976	0.0526	0	0	≈ 0	0	0.0526
6	.9945	.0697	0	0	≈ 0	0	.0697
8	0.9903	0.0914	0	0	≈ 0	0	0.0914
10	.9848	.1203	0	0	≈ 0	0	.1203
12	0.9781	0.1586	0	0	≈ 0	0	0.1586
13.8	.9711	.1840	0	0	≈ 0	0	.1840
$T'_c = 0.20, T'_c/\text{prop} = 0.10, n = 2$ (propellers)							
-4	0.9976	0.0320	-0.1995	0.0075	0	0.0013	-0.1587
-2	.9994	.0327	-.1999	.0075	≈ 0	.0021	-.1576
0	1.0000	0.0345	-0.2000	0.0074	≈ 0	0.0021	-0.1560
2	.9994	.0408	-.1999	.0074	.0008	.0018	-.1491
4	0.9976	0.0526	-0.1995	0.0073	0.0024	0.0014	-0.1358
6	.9945	.0697	-.1989	.0072	.0048	.0012	-.1160
8	0.9903	0.0914	-0.1981	0.0071	0.0079	0.0011	-0.0907
10	.9848	.1203	-.1970	.0070	.0118	.0020	-.0559
12	0.9781	0.1586	-0.1956	0.0068	0.0164	0.0047	-0.0091
13.8	.9711	.1840	-.1942	.0067	.0207	.0057	.0229
14.1	0.9699	-----	-0.1939	0.0067	0.0214	0.0057	-----
$T'_c = 0.44, T'_c/\text{prop} = 0.22, n = 2$ (propellers)							
-4	0.9976	0.0320	-0.4389	0.0164	0	0.0028	-0.3877
-2	.9994	.0327	-.4397	.0164	.0001	.0047	-.3858
0	1.0000	0.0345	-0.4400	0.0163	≈ 0	0.0046	-0.3846
2	.9994	.0408	-.4397	.0162	.0022	.0039	-.3766
4	0.9976	0.0526	-0.4389	0.0161	0.0066	0.0031	-0.3605
6	.9945	.0697	-.4376	.0159	.0131	.0026	-.3363
8	0.9903	0.0914	-0.4357	0.0157	0.0217	0.0023	-0.3046
10	.9848	.1203	-.4333	.0155	.0325	.0043	-.2607
12	0.9781	0.1586	-0.4304	0.0153	0.0453	0.0103	-0.2009
13.8	.9711	.1840	-.4273	.0150	.0577	.0125	-.1581
14.1	0.9699	-----	-0.4268	0.0150	0.0596	0.0125	-----
14.4	.9686	-----	-.4262	.0149	.0609	.0125	-----

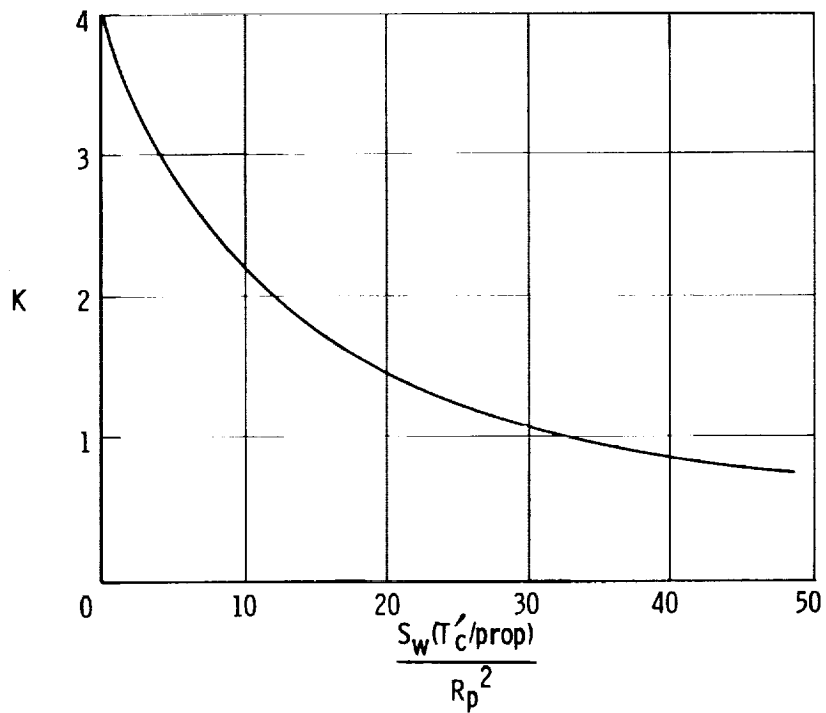


Figure 5.3-1. Propeller drag factor (from ref. 1, based on ref. 19).

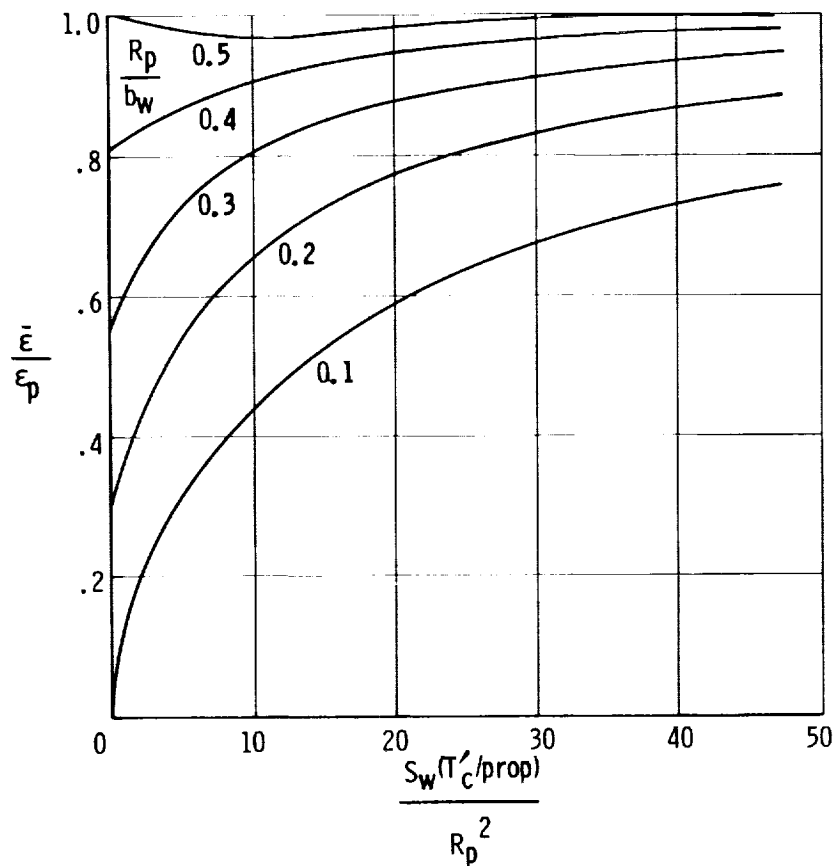


Figure 5.3-2. Average propeller downwash (from ref. 1, based on ref. 19).

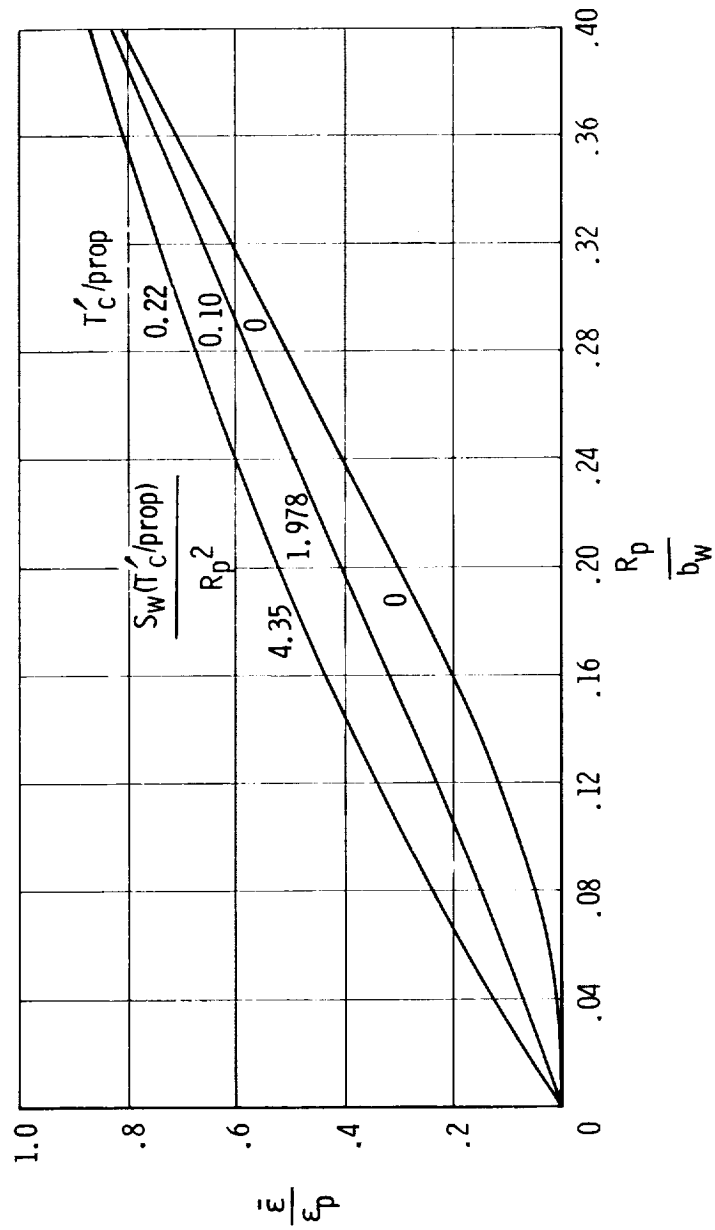


Figure 5.3-3. Average propeller downwash for analyzed thrust conditions of subject airplane (obtained from crossplot of fig. 5.3-2).

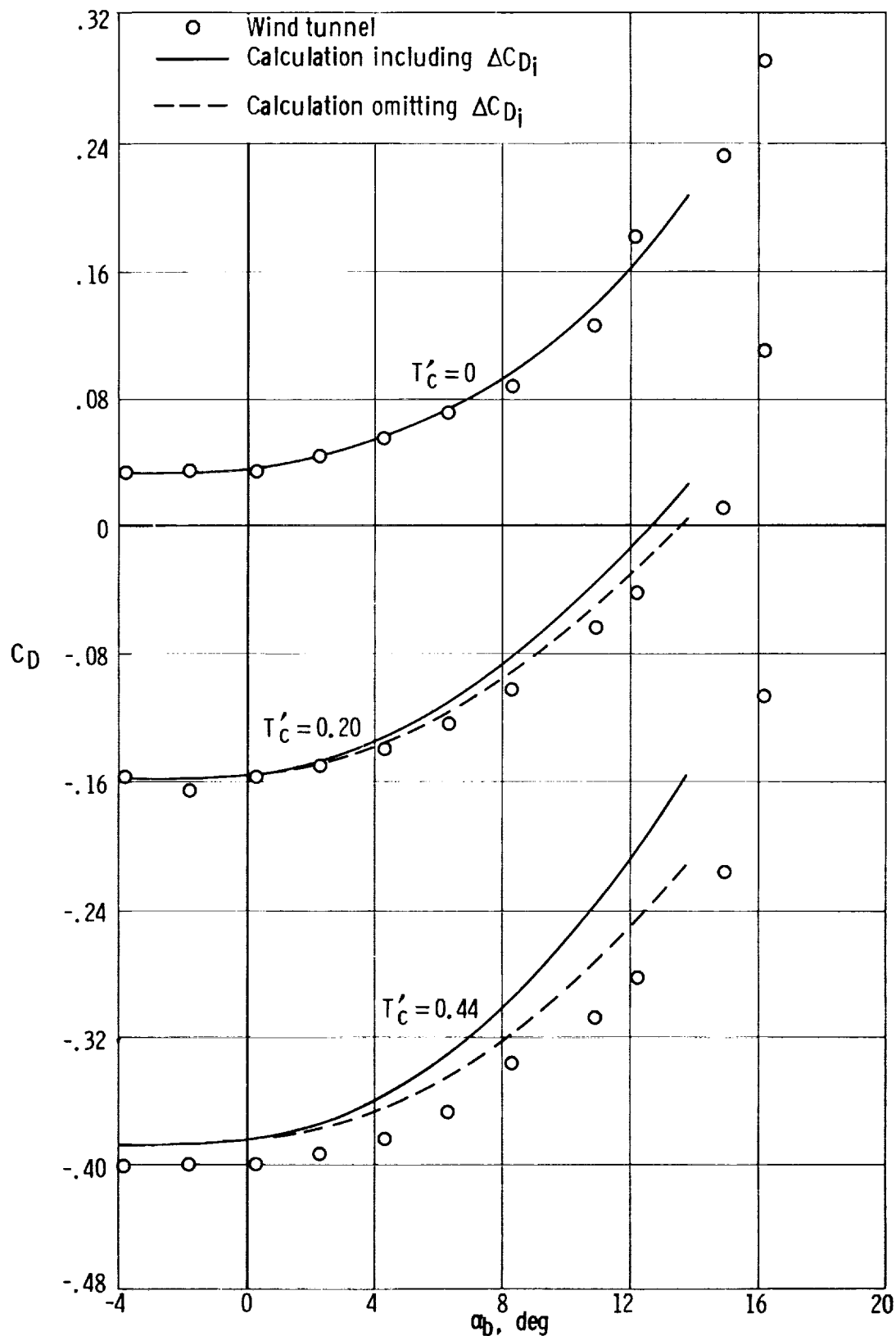


Figure 5.3-4. Comparison of calculated and wind-tunnel-determined variation of C_D with α_b at different power conditions. $\delta_e = 0^\circ$.

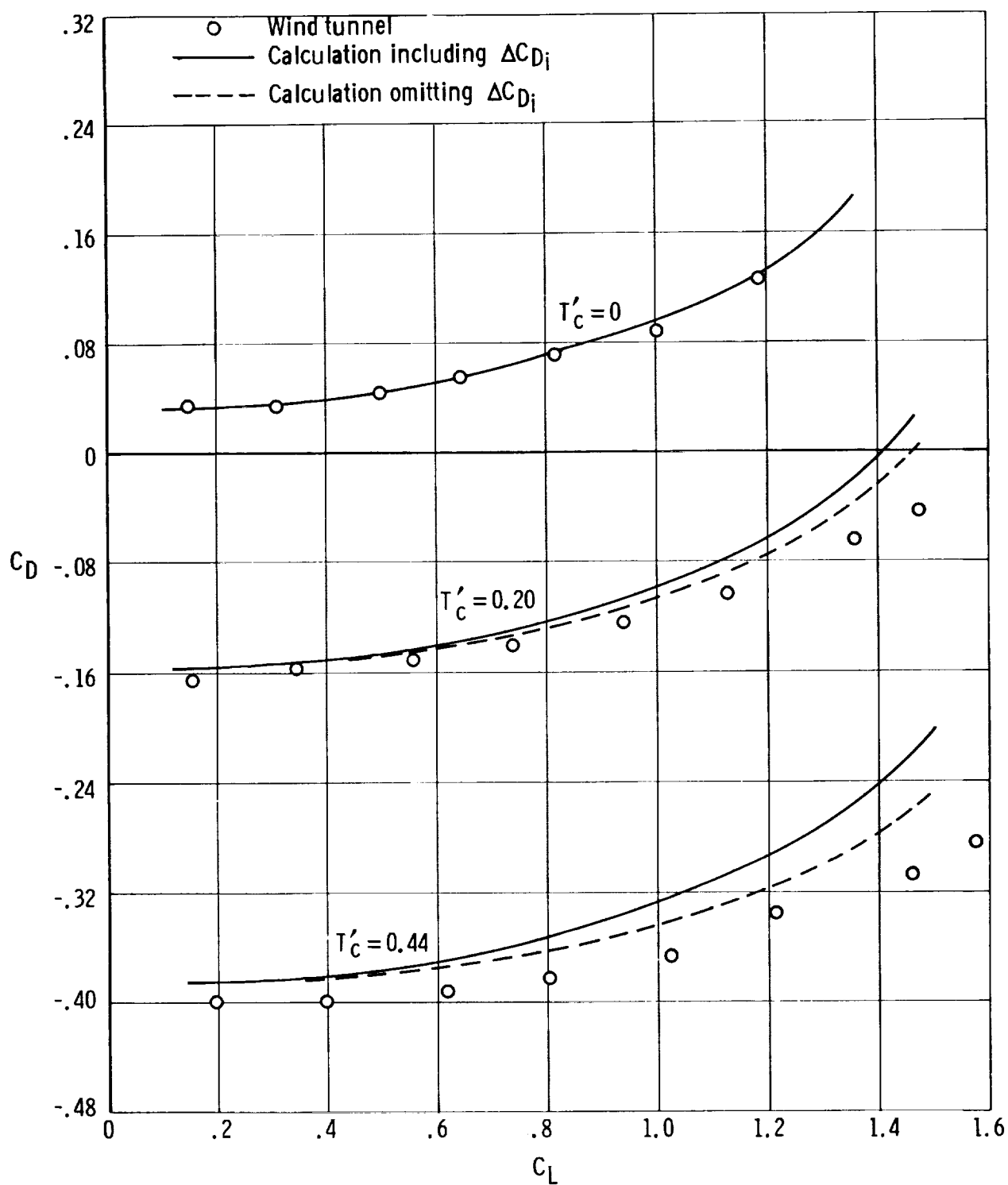


Figure 5.3-5. Comparison of calculated and wind-tunnel-determined variation of C_D with C_L at different power conditions. $\delta_e = 0^\circ$.

5.4 Power Effects on Horizontal-Tail Hinge Moments and Stick Forces

The procedures for determining the horizontal-tail hinge moments for power-on conditions are essentially identical to those used in section 4.14 for propeller-off conditions. Quantities affected by power include the tail lift, as a result of power-induced changes in downwash and dynamic pressure at the tail, and the section increment pitching-moment coefficient for larger tab deflections.

The effect of power on the lift of the tail was accounted for in section 5.1.2. The effect of power on the section increment pitching-moment coefficient, $(\Delta c_{mf})_\eta$, has not been defined quantitatively. In section 4.14.1, in relation to equations (4.14.1-11) and (4.14.1-12) involving $(\Delta c_{mf})_\eta$, it was indicated that for propeller-off conditions the empirical curves of $(\Delta c_{mf})_\eta$ in figure 4.14.1-6 should be used for large tab deflections in lieu of the following equation based on lifting-line theory:

$$(\Delta c_{mf})_\eta = -\frac{2}{57.3} \sqrt{\left(\frac{c_{tab}}{c_h}\right)_\eta \left[1 - \left(\frac{c_{tab}}{c_h}\right)_\eta\right]^2} \delta''_{tab} \text{ per deg} \quad (5.4-1)$$

where

$$\delta''_{tab} = \tan^{-1} \left(\frac{\cos \Lambda_{hl} \tan \delta_{tab}}{\cos \Lambda_b} \right) \quad (4.14.1-13)$$

However, because a significant amount of thrust will increase the dynamic pressure on the portion of the horizontal tail immersed in the propeller slipstream, the added energy at the tail will tend to maintain full tab effectiveness to higher tab deflections than for propeller-off conditions. Thus, for significant power-on thrust conditions, it is suggested that equation (5.4-1) be used in place of figure 4.14.1-6 to determine $(\Delta c_{mf})_\eta$

for tab deflections up to about 21° . Beyond this magnitude of tab deflection, the effectiveness of the tab may be approximated by empirically extending the results of the lifting-line theory on a trend of decreasing effectiveness tending to parallel the propeller-off experimental curves. For $T'_C = 0$, the propeller-off curves of figures 4.14.1-6 and 4.14.1-7 should still be used; that is, the $T'_C = 0$ and propeller-off calculated hinge moments are the same.

The calculations for the power-on hinge-moment characteristics of the horizontal tail for the subject airplane are summarized in tables 5.4-1 and 5.4-2. The magnitudes of the section increment pitching-moment coefficient, $(\Delta c_{mf})_\eta$, used in columns 5 and

7 of table 5.4-1 were obtained from equations (5.4-1) and (4.14.1-13) which reduced to

$$(\Delta c_{mf})_\eta = -0.0110 \delta_{tab} \quad (5.4-2)$$

on the basis of supporting configuration data in table 4.14.1-2(a).

Figure 5.4-1 shows the correlation of the calculated hinge moments with wind-tunnel data for total $T'_C = 0, 0.20, \text{ and } 0.44$. The calculated hinge moments for $T'_C = 0$ are the same as those for propeller-off conditions. The calculated hinge moments for total $T'_C = 0.20$ and 0.44 include the results obtained when using the originally determined tail lift coefficients as well as the results obtained when using the lift coefficients based on a 40-percent reduction in power-induced downwash discussed in section 5.2. The calculated hinge moments based on the modified power-induced downwash at the tail show better correlation with wind-tunnel data than do the original results. At total $T'_C = 0.20$, the discrepancy between calculated results and wind-tunnel data at $\delta_e = 4^\circ$ is unexplained. On the basis of the correlations at $T'_C = 0$ and 0.44 , however, it appears that there may be an error in the tunnel data.

Figure 5.4-2 shows the correlation of flight-determined stick forces with the stick forces based on calculated and wind-tunnel stability and control trim characteristics for 1-g flight over a calibrated velocity range of 70 knots to 146 knots at 6000 feet altitude. Calculated stick forces as well as calculated angle of attack and elevator deflection show reasonably good correlation with the flight data. The stick forces were obtained by using the following relation derived in section 4.14.1 for the subject airplane:

$$F_{\text{stick}} = 40 C_{hh(f)} \bar{q}_\infty \quad (4.14.1-20)$$

5.4.1 Symbols

All lift and moment coefficients are referenced to the horizontal-tail area and mean aerodynamic chord unless noted otherwise.

b_h	horizontal-tail span, ft
$C_{hh(f)}$	hinge-moment coefficient of the horizontal tail with fuselage effects on the tail included
C_L	airplane lift coefficient referred to the wing area
$\bar{C}_{Lh(f)}$	net lift coefficient of the horizontal tail due to α_h , δ_e , and δ_{tab} , with fuselage effects included
$(\Delta C'_m)_{\delta_{\text{tab}}}$	increment of tail pitching-moment coefficient, about the quarter chord of the tail mean aerodynamic chord, due to the tab deflection
$(c_h)_{\text{av}}$	average tail chord, ft
$(c_h)_\eta$	tail chord at semispan station, η , ft

$(c_{l\Lambda})_\eta$	increment section-lift coefficient due to the tab deflection, at semispan station, η
$(c_{l\Lambda=0})_\eta$	increment section-lift coefficient due to the tab deflection, at semispan station, η , referred to the constant-percent-chord basic loading line of the tab deflection
$(\Delta c_{mf})_\eta$	section increment pitching-moment coefficient due to the tab (flap) deflection, at semispan station, η , about the quarter-chord point in the plane normal to the constant-percent-chord basic loading line of the tab deflection
c_{tab}	tab chord, ft
\bar{c}_h	tail mean aerodynamic chord, ft
\bar{c}_w	wing mean aerodynamic chord, ft
F_{stick}	stick force, lb
$(\Delta \frac{G}{\delta})_\eta$	difference in span-load coefficients for two bounding span-load distribution curves at semispan station, η (fig. 4.14.1-3(b), for example)
K	a factor for estimating the section center-of-pressure location for the untabbed section near the ends of the tab
$\bar{q}_h, \bar{q}_\infty$	dynamic pressure at the horizontal tail and in the free stream, respectively, lb/sq ft
S_h	horizontal-tail area, sq ft
T'_c	thrust coefficient
V_c	calibrated airspeed, knots
$(\frac{x}{c_h})_\eta$	chordwise center-of-pressure location, at semispan station, η , aft of the quarter chord of and as a ratio of the horizontal-tail mean aerodynamic chord
$(\frac{x_{cp}}{c_h})_\eta$	chordwise center-of-pressure location of the lift due to the tab deflection, at semispan station, η , from the leading edge of the tail as a ratio of the tail chord at the station
y	lateral distance from the plane of symmetry, ft
α_b	airplane angle of attack relative to the X-body axis, deg
α_h	angle of attack of the tail relative to its chord line, deg
δ_e	elevator deflection, deg

δ_{tab}	tab deflection normal to the hinge line, deg
δ''_{tab}	tab deflection normal to the section basic loading center-of-pressure line, deg
$(\Delta\epsilon_h)_{\text{power}}$	change in downwash at the tail due to power, deg
η	semispan station, $\frac{2y}{b_h}$
η_i, η_o	semispan station of the inboard and the outboard end of the tab, respectively
$\Delta\eta$	increment of the spanwise distance as a ratio of the tail semi-span
Λ_b	sweep of the section basic loading center-of-pressure line, deg
Λ_{hl}	sweep of the tab hingeline, deg

TABLE 5.4-1
HORIZONTAL-TAIL TAB CHARACTERISTICS
For $T_c = 0.20, 0.44$

			Increment section lift coefficient				Chordwise center-of-pressure location			
①	②	③	Table 4.14.1-3, column 4				Figure 4.14.1-8			
			④				⑤			
			Equation (4.14.1-3, column 4)				Equation (4.14.1-8)			
			$(c_{l_{A=0}})_\eta = (c_l)_\eta$				$(\frac{x_{cp}}{c_h})_\eta = 0.25 - \frac{(\Delta C_{mf})_\eta}{(c_{l_{A=0}})_\eta}$			
			$(\Delta \frac{G}{D})_\eta$				$0.25 - \frac{(\Delta C_{mf})_\eta}{(c_{l_{A=0}})_\eta}$			
			$\delta_{tab}, \text{ deg}$				$\delta_{tab}, \text{ deg}$			
			6	-7.5	-15	-21	6	-7.5	-15	-21
η	η_0	0	0.2007	-0.2509	-0.1900	-0.5832	0.3788	0.3788	0.3788	0.3788
	.1	3.29	0.2068	-0.2586	-0.1949	-0.6010	0.3788	0.3788	0.3788	0.3788
	.2	3.13	0.2109	-0.2636	-0.1949	-0.6129	0.3788	0.3788	0.3788	0.3788
	.3	2.93	0.2162	-0.2702	-0.1949	-0.6282	0.3788	0.3788	0.3788	0.3788
	.4	2.78	0.2164	-0.2705	-0.1949	-0.6289	0.3788	0.3788	0.3788	0.3788
η	.5	2.60	0.2138	-0.2672	-0.1949	-0.6212	0.3788	0.3788	0.3788	0.3788
	.6	2.43	0.2052	-0.2565	-0.1949	-0.5962	0.3788	0.3788	0.3788	0.3788
	.7	2.25	0.1939	-0.2424	-0.1949	-0.5634	0.3788	0.3788	0.3788	0.3788
	.8	2.08	0.1744	-0.2181	-0.1949	-0.5069	0.3788	0.3788	0.3788	0.3788
	.9	1.92	0.1517	-0.1949	-0.1949	-0.4444	0.3788	0.3788	0.3788	0.3788
η	1.0	1.78	0.1274	-0.1744	-0.1949	-0.3788	0.3788	0.3788	0.3788	0.3788

Pitching moment due to tab deflection about quarter chord of tail mean aerodynamic chord, $b(\Delta C'_m)_{\delta_{tab}}$										
①	②	③	④	⑤	⑥	⑦	⑧	⑨	⑩	⑪
Table 4.14.1-2(d)										
η	$\frac{(c_h)_{\eta}}{(c_h)_{av}}$	$\frac{(c_h)_{\eta}}{\bar{c}_h}$	$\frac{(c_h)_{\eta}}{\bar{c}_h} \left[\frac{x_{cp}}{c_h} - 0.25 \right]$	$\delta_{tab}, \text{ deg}$	$\delta_{tab}, \text{ deg}$	$\delta_{tab}, \text{ deg}$	$\delta_{tab}, \text{ deg}$	$\delta_{tab}, \text{ deg}$	$\delta_{tab}, \text{ deg}$	$\delta_{tab}, \text{ deg}$
	$\frac{(c_h)_{\eta}}{(c_h)_{av}}$	$\frac{(c_h)_{\eta}}{\bar{c}_h}$	$\frac{(c_h)_{\eta}}{\bar{c}_h} \left[\frac{x_{cp}}{c_h} - 0.25 \right]$	6	-7.5	-15	-21	6	-7.5	-15
	$\frac{(c_h)_{\eta}}{(c_h)_{av}}$	$\frac{(c_h)_{\eta}}{\bar{c}_h}$	$\frac{(c_h)_{\eta}}{\bar{c}_h} \left[\frac{x_{cp}}{c_h} - 0.25 \right]$	0.4207	0.4308	0.4308	0.4308	0.4207	0.4308	0.4308
	$\frac{(c_h)_{\eta}}{(c_h)_{av}}$	$\frac{(c_h)_{\eta}}{\bar{c}_h}$	$\frac{(c_h)_{\eta}}{\bar{c}_h} \left[\frac{x_{cp}}{c_h} - 0.25 \right]$	0.4207	0.4308	0.4308	0.4308	0.4207	0.4308	0.4308
	$\frac{(c_h)_{\eta}}{(c_h)_{av}}$	$\frac{(c_h)_{\eta}}{\bar{c}_h}$	$\frac{(c_h)_{\eta}}{\bar{c}_h} \left[\frac{x_{cp}}{c_h} - 0.25 \right]$	0.4207	0.4308	0.4308	0.4308	0.4207	0.4308	0.4308
η	$\frac{(c_h)_{\eta}}{(c_h)_{av}}$	$\frac{(c_h)_{\eta}}{\bar{c}_h}$	$\frac{(c_h)_{\eta}}{\bar{c}_h} \left[\frac{x_{cp}}{c_h} - 0.25 \right]$	$\delta_{tab}, \text{ deg}$	$\delta_{tab}, \text{ deg}$	$\delta_{tab}, \text{ deg}$	$\delta_{tab}, \text{ deg}$	$\delta_{tab}, \text{ deg}$	$\delta_{tab}, \text{ deg}$	$\delta_{tab}, \text{ deg}$
0	1.3108	1.2786	-0.1433	0.4207	0.4308	0.4308	0.4308	0.4207	0.4308	0.4308
1	1.2054	1.2167	-0.1108	0.4207	0.4308	0.4308	0.4308	0.4207	0.4308	0.4308
2	1.2038	1.1575	-0.0783	0.4207	0.4308	0.4308	0.4308	0.4207	0.4308	0.4308
3	1.1269	1.0636	-0.0458	0.4207	0.4308	0.4308	0.4308	0.4207	0.4308	0.4308
4	1.0692	1.0281	-0.0133	0.4207	0.4308	0.4308	0.4308	0.4207	0.4308	0.4308
5	1.0000	0.9615	0.0182	0.4207	0.4308	0.4308	0.4308	0.4207	0.4308	0.4308
6	0.9346	0.8987	0.0517	0.4207	0.4308	0.4308	0.4308	0.4207	0.4308	0.4308
7	0.8634	0.8321	0.0842	0.4207	0.4308	0.4308	0.4308	0.4207	0.4308	0.4308
8	0.79	0.7766	0.1184	0.4207	0.4308	0.4308	0.4308	0.4207	0.4308	0.4308
9	0.7385	0.7101	0.1492	0.4207	0.4308	0.4308	0.4308	0.4207	0.4308	0.4308
1.0	0.6846	0.6583	0.1817	0.4207	0.4308	0.4308	0.4308	0.4207	0.4308	0.4308

*The values of $(c_h)_{\eta}$ in column 4 for η_0 (shown boxed in) are used in computing $(c_h)_{\eta}$ in column 7 for stations adjacent to and outboard of η_0 .

$(\Delta C'_m)_{\delta_{tab}} = \sum (\Delta C'_m)_{\delta_{tab}} = -0.06253 \text{ } 0.07817 \text{ } 0.13659 \text{ } 0.22155$

*The values of $(c_{l_{A=0}})_\eta$ in column 4 for η_0 (shown boxed in) are used in computing $(x_{cp})_\eta$ in column 7 for stations adjacent to and outboard of η_0 .

Referenced to $S_R = 32.55 \text{ sq ft}$ and $q_\infty/\rho_\infty = 1$.

$$(\Delta C_m')_{\eta_{tab}} = \sum (\Delta C_m')_{\eta_{tab}} = -0.06253 \quad 0.07817 \quad 0.13659 \quad 0.22155$$

TABLE 5.4-2
HORIZONTAL-TAIL HINGE-MOMENT CHARACTERISTICS

[Tab geared to elevator in ratio of $\frac{\delta_{tab}}{\delta_e} = 1.5$]

(a) $T'_c = 0$									
①	②	③	④	⑤				⑥	
-----	Table 5.1.2-(b), column 12	Table 5.1.2-(b), column 11	Figure 4.14.1-1	Table 4.14.1-2(f)				Table 4.14.1-3, column 14 ^a	
α_b , deg	α_h , deg	$\frac{\bar{q}_h}{\bar{q}_\infty}$	$\bar{C}_{L_h}(\theta)$ referenced to $S_h = 32.5$ sq ft and $\frac{\bar{q}_h}{\bar{q}_\infty} = 1.0$	$0.0361 \bar{C}_{L_h}(\theta) = 0.0361$ ④				$(\Delta C'_m)_{\delta_{tab}}$	
				δ_e , deg				δ_e , deg	
				δ_{tab} , deg				δ_{tab} , deg	
				4	0	-5	-10	-14	4
-4	-4.00	1.0	-0.775	-15	-21	0	-7.5	-15	-21
-2	-2.96	1.0	-0.775	-15	-21	0	-7.5	-15	-21
0	-1.90	1.0	-0.775	-15	-21	0	-7.5	-15	-21
2	-.93	1.0	-0.775	-15	-21	0	-7.5	-15	-21
4	0.13	1.0	-0.775	-15	-21	0	-7.5	-15	-21
6	1.14	1.0	-0.775	-15	-21	0	-7.5	-15	-21
8	2.23	1.0	-0.775	-15	-21	0	-7.5	-15	-21
10	3.39	1.0	-0.775	-15	-21	0	-7.5	-15	-21
12	4.45	1.0	-0.775	-15	-21	0	-7.5	-15	-21
b _{13.8}	5.50	1.0	-0.775	-15	-21	0	-7.5	-15	-21

(b) $T'_c = 0$		⑦	⑧
-----		Table 4.14.1-2(f)	-----
α_b , deg	$C_{hh}(\theta) = \textcircled{5} + \textcircled{6}$ with $\frac{\bar{q}_h}{\bar{q}_\infty} = 1.0$	$C_{hh}(\theta) = \textcircled{3} \times \textcircled{7}$ with $\frac{\bar{q}_h}{\bar{q}_\infty}$ taken into account	
		δ_e , deg	
		δ_{tab} , deg	
		δ_{tab} , deg	
-4	-0.0516	0.0375	0.0822
-2	-.0490	-.0071	.0401
0	-0.0464	0.0426	0.0785
2	-.0442	-.0002	.0449
4	-0.0415	0.0004	0.0807
6	-.0391	.0028	.0500
8	-0.0365	0.0054	0.0850
10	-.0337	.0083	.0554
12	-0.0312	0.0108	0.0903
b _{13.8}	-.0287	.0133	.0605

^aFor propeller off and $T'_c = 0$ only.

^bStall angle for total $T'_c = 0$.

Denotes tail to be in nonlinear region of its lift-curve slope on basis of figure 4.14.1-1. Not applicable to final figure.

TABLE 5.4-2 (Continued)

(b) $T'_c = 0.20$

①	②	③	④	⑤					⑥								
-----	Table 5.1.2-1(b), column 12	Table 5.1.2-1(b), column 11	Figure 4.14.1-1	Table 4.14.1-2(f)					Table 5.4-1, column 14								
α_b , deg	α_h , deg	$\frac{\bar{q}_h}{\bar{q}_\infty}$	$\bar{C}_{Lh}(\eta)$ referenced to $S_h = 32.5$ sq ft and $\frac{\bar{q}_h}{\bar{q}_\infty} = 1.0$					$0.0361 \bar{C}_{Lh}(\eta) = 0.0361$ ④					$(\Delta C'_m)_{\delta_{tab}}$				
			δ_e , deg					δ_e , deg					δ_e , deg				
			δ_{tab} , deg					δ_{tab} , deg					δ_{tab} , deg				
			4	0	-5	-10	-14	4	0	-5	-10	-14	4	0	-5	-10	-14
			6	0	-7.5	-15	-21	6	0	-7.5	-15	-21	6	0	-7.5	-15	-21
-4	-4.00	1.087	0.135	-0.267	-0.775	-0.935	-----	0.00487	-0.00964	-0.03375	-----	-----	-0.06253	0	0.07817	0.15659	0.22155
-2	-3.68	1.103	.158	-.244	-.753	-1.000	-----	.00570	-.00881	-.02718	-.03610	-----	-.06253	0	-.07817	.15659	-.22155
0	-3.23	1.117	0.187	-0.216	-0.722	-1.028	-----	0.00675	-0.00780	-0.02606	-0.03711	-----	-0.06253	0	0.07817	0.15659	0.22155
2	-2.83	1.122	.215	-.187	-.695	-1.041	-----	.00776	-.00675	-.02509	-.03758	-----	-.06253	0	-.07817	.15659	-.22155
4	-2.33	1.133	0.247	-0.154	-0.660	-1.041	-----	0.00892	-0.00556	-0.03283	-0.03738	-----	-0.06253	0	0.07817	0.15659	0.22155
6	-1.74	1.139	.289	-.114	-.623	-1.034	-0.855	-0.0412	-.02249	-0.03733	-0.03087	-0.03087	-0.06253	0	-.07817	.15659	-.22155
8	-1.00	1.144	0.335	-0.065	-0.574	-1.015	-0.888	0.01209	-0.00235	-0.02072	-0.03664	-0.03206	-0.06253	0	0.07817	0.15659	0.22155
10	-.13	1.142	.394	-.007	-.517	-.986	-.995	.01422	-.00025	-.01866	-.03559	-.03592	-0.06253	0	-.07817	.15659	-.22155
12	0.65	1.136	0.448	0.045	-0.463	-0.933	-1.088	0.01617	0.00162	-0.01671	-0.03440	-0.03928	-0.06253	0	0.07817	0.15659	0.22155
13.8	1.52	1.128	.502	.103	-.405	-.904	-1.100	.01812	.00372	-.01462	-.03263	-.03971	-0.06253	0	-.07817	.15659	-.22155
*14.1	1.68	1.122	0.517	0.117	-0.394	-0.893	-1.100	0.01866	0.00422	-0.01422	-0.03224	-0.03971	-0.06253	0	0.07817	0.15659	0.22155

①	⑦	⑧
-----	Table 4.14.1-2(f)	-----
α_b , deg	$C_{Lh}(f) = \textcircled{5} + \textcircled{6}$ with $\frac{\bar{q}_h}{\bar{q}_\infty} = 1.0$	$C_{Lh}(f) = \textcircled{3} \times \textcircled{7}$ with $\frac{\bar{q}_h}{\bar{q}_\infty}$ taken into account
	δ_e , deg	δ_e , deg
	4 0 -5 -10 -14	4 0 -5 -10 -14
	δ_{tab} , deg	δ_{tab} , deg
	6 0 -7.5 -15 -21	6 0 -7.5 -15 -21
-4	-0.05766 -0.00964 0.05019 0.12284	----- -0.0627 -0.0105 0.0546 0.1335
-2	-.05683 -.00881 .05039 .12049	----- -.0627 -.0097 .0562 .1329
0	-0.05578 -0.00078 0.05211 0.11948	----- -0.0623 -0.0087 0.0582 0.1335
2	-.05477 -.00675 .05308 .11901	----- -.0615 -.0076 .0596 .1335
4	-0.05361 -0.00556 0.05434 0.11901	----- -0.0607 -0.0063 0.0616 0.1348
6	-.05210 -.00412 .05568 .11926	----- -0.0593 -.0047 .0634 .1358 0.2172
8	-0.05044 -0.00235 0.05745 0.11995	----- -0.0577 -0.0027 0.0657 0.1372 0.2168
10	-.04831 -.00025 .05951 .12100	----- -0.0552 -.0003 .0680 .1382 .2120
12	-0.04636 0.00162 0.06146 0.12219	----- -0.0527 0.0018 0.0698 0.1388 0.2071
13.8	-.04441 -.00372 .06355 .12396	----- -0.0501 .0042 .0717 .1398 .2051
*14.1	-0.04387 0.00422 0.06395 0.12435	----- -0.0492 0.0047 0.0718 0.1395 0.2040

*Stall angle for total $T'_c = 0.20$.

Denotes tail to be in nonlinear region of its lift-curve slope on basis of figure 4.14.1-1. Not applicable to final figure.

(c) $T'_c = 0.44$

TABLE 5.4-2 (Concluded)

①	②	③	④	⑤										⑥				
-----	Table 5.1.2-(b), column 12	Table 5.1.2-(b), column 11	Figure 4.14.1-1	Table 4.14.1-2(f)										Table 5.4-1, column 14				
α_b , deg	α_h , deg	$\frac{\bar{q}_h}{\bar{q}_\infty}$	$\bar{C}_{Lh(f)}$ referenced to $S_h = 32.5$ sq ft and $\frac{\bar{q}_h}{\bar{q}_\infty} = 1.0$	$0.0361 C_{Lh(f)} = 0.0361$ ④										$(\Delta C'_m) \delta_{lab}$				
				δ_e , deg										δ_e , deg				
				δ_{tab} , deg										δ_{tab} , deg				
				1	0	-5	-10	-14	4	0	-5	-10	-14	1	0	-5	-10	-14
-4	-4.00	1.203	0.135	-0.267	-0.775	-0.935	-1.106	-1.281	6	0	-7.5	-15	-21	6	0	-7.5	-15	-21
-2	-4.08	1.211	0.130	-0.274	-0.778	-0.938	-1.109	-1.284	0.00487	-0.00964	-0.02798	-0.05375	-----	-0.06253	0	0.7817	0.15659	0.22155
0	-3.99	1.222	0.137	-0.266	-0.773	-0.937	-1.106	-1.281	0.00469	-0.00989	-0.02809	-0.05378	-----	-0.06253	0	0.7817	0.15659	0.22155
2	-3.89	1.232	0.144	-0.258	-0.767	-0.925	-1.094	-1.269	0.00495	-0.00960	-0.02791	-0.05378	-----	-0.06253	0	0.7817	0.15659	0.22155
4	-3.59	1.243	0.163	-0.238	-0.748	-0.906	-1.076	-1.249	0.00520	-0.00931	-0.02769	-0.05348	-----	-0.06253	0	0.7817	0.15659	0.22155
6	-3.32	1.254	0.182	-0.219	-0.726	-0.884	-1.046	-1.211	0.00588	-0.00859	-0.02700	-0.05322	-----	-0.06253	0	0.7817	0.15659	0.22155
8	-2.83	1.262	0.215	-0.187	-0.695	-0.851	-1.041	-1.206	0.00657	-0.00791	-0.02621	-0.03704	-----	-0.06253	0	0.7817	0.15659	0.22155
10	-2.05	1.268	0.267	-0.136	-0.643	-0.807	-1.037	-1.197	0.00776	-0.00675	-0.02509	-0.03758	-----	-0.06253	0	0.7817	0.15659	0.22155
12	-1.39	1.276	0.310	-0.092	-0.600	-0.764	-1.027	-1.182	0.00964	-0.00491	-0.02321	-0.03744	-----	-0.06253	0	0.7817	0.15659	0.22155
13.8	-0.61	1.281	0.364	-0.038	-0.547	-0.703	-1.003	-1.164	0.01119	-0.00332	-0.02166	-0.03707	-0.03137	-0.06253	0	0.7817	0.15659	0.22155
14.1	-0.43	1.281	0.376	-0.029	-0.536	-0.694	-1.000	-1.164	0.01357	-0.00105	-0.01935	-0.03610	-0.03393	-0.06253	0	0.7817	0.15659	0.22155
14.4	-0.26	1.278	0.390	-0.015	-0.522	-0.689	-0.989	-1.148	0.01408	-0.00054	-0.01884	-0.03570	-0.03538	-0.06253	0	0.7817	0.15659	0.22155

①	⑦										⑧							
Table 4, 14, 1-2(f)																		
$C_{bh}(f) = ⑤ + ⑥$ with $\frac{\bar{q}_h}{\bar{q}_\infty} = 1.0$																		
$C_{bh}(f) = ③ \times ⑦$ with $\frac{\bar{q}_h}{\bar{q}_\infty}$ taken into account																		
α_b , deg	δ_e , deg										δ_e , deg							
	δ_{tab} , deg										δ_{tab} , deg							
	δ_{tab} , deg										δ_{tab} , deg							
	4	0	-5	-10	-14	4	0	-5	-10	-14	6	0	-5	-10	-14			
-4	-0.05766	-0.00964	0.05019	-0.12284	-0.0694	-0.0116	0.0604	0.1478	0.21	-	-	-	-	-				
-2	-0.05784	-0.00989	0.05008	-0.12381	-0.0700	-0.0112	0.0606	0.1499	0.21	-	-	-	-	-				
0	-0.05758	-0.00960	0.05026	-0.12276	-0.0704	-0.0117	0.0614	0.1500	0.21	-	-	-	-	-				
2	-0.05733	-0.00931	0.05048	-0.12211	-0.0706	-0.0115	0.0622	0.1504	0.21	-	-	-	-	-				
4	-0.05665	-0.00859	0.05117	-0.12027	-0.0704	-0.0108	0.0636	0.1495	0.21	-	-	-	-	-				
6	-0.05596	-0.00791	0.05196	-0.11955	-0.0702	-0.0099	0.0632	0.1499	0.21	-	-	-	-	-				
8	-0.05477	-0.00675	0.05308	-0.11001	-0.0691	-0.0085	0.0670	0.1502	0.21	-	-	-	-	-				
10	-0.05289	-0.00491	0.05496	-0.11915	-0.0671	-0.0062	0.0697	0.1511	0.21	-	-	-	-	-				
12	-0.05134	-0.00332	0.05651	-0.11952	-0.0651	-0.0042	0.0721	0.1525	0.21	-	-	-	-	-				
13.8	-0.04939	-0.00137	0.05842	-0.12038	-0.0633	-0.0018	0.0748	0.1542	0.21	-	-	-	-	-				
14.1	-0.04896	-0.00105	0.05882	-0.12049	-0.0627	-0.0013	0.0753	0.1543	0.2403	-	-	-	-	-				
14.4	-0.04845	-0.00054	0.05933	-0.12089	-0.0619	-0.0007	0.0758	0.1545	0.2379	-	-	-	-	-				

^aStall angle for total $T'_c = 0.44$.

Denotes tail to be in nonlinear region of its lift-curve slope on basis of figure 4.14.1-1. Not applicable to final figure.

Wind tunnel

δ_e , deg
 \square 4
 \circ 0
 \diamond -5
 \triangle -10
 ∇ -14

— Original calculation
 --- (ΔE_h) power reduced 40 percent

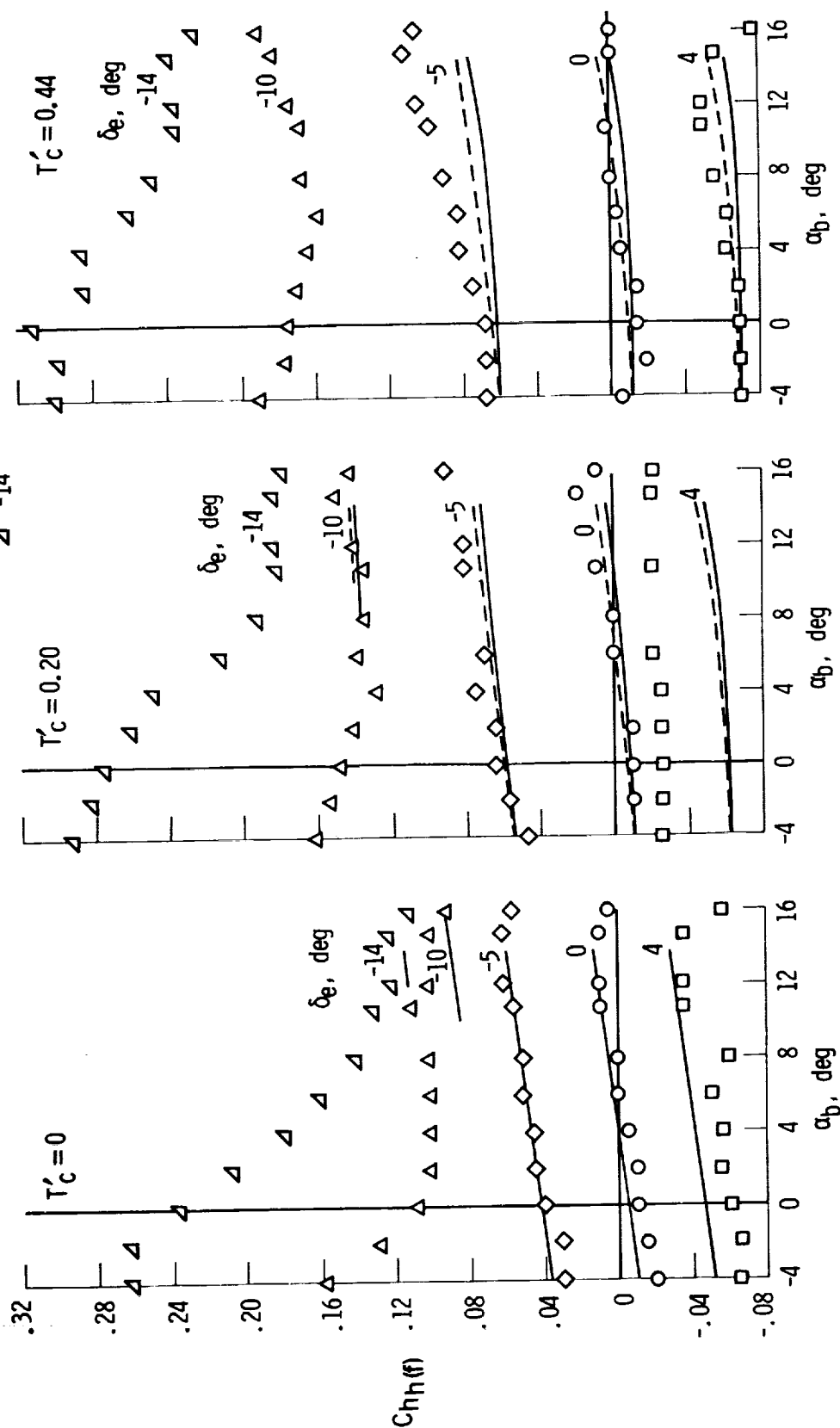


Figure 5.4-1. Comparison of calculated and wind-tunnel-determined variation of hinge moment, $Ch_h(f)$, with angle of attack at different power conditions and elevator deflections.

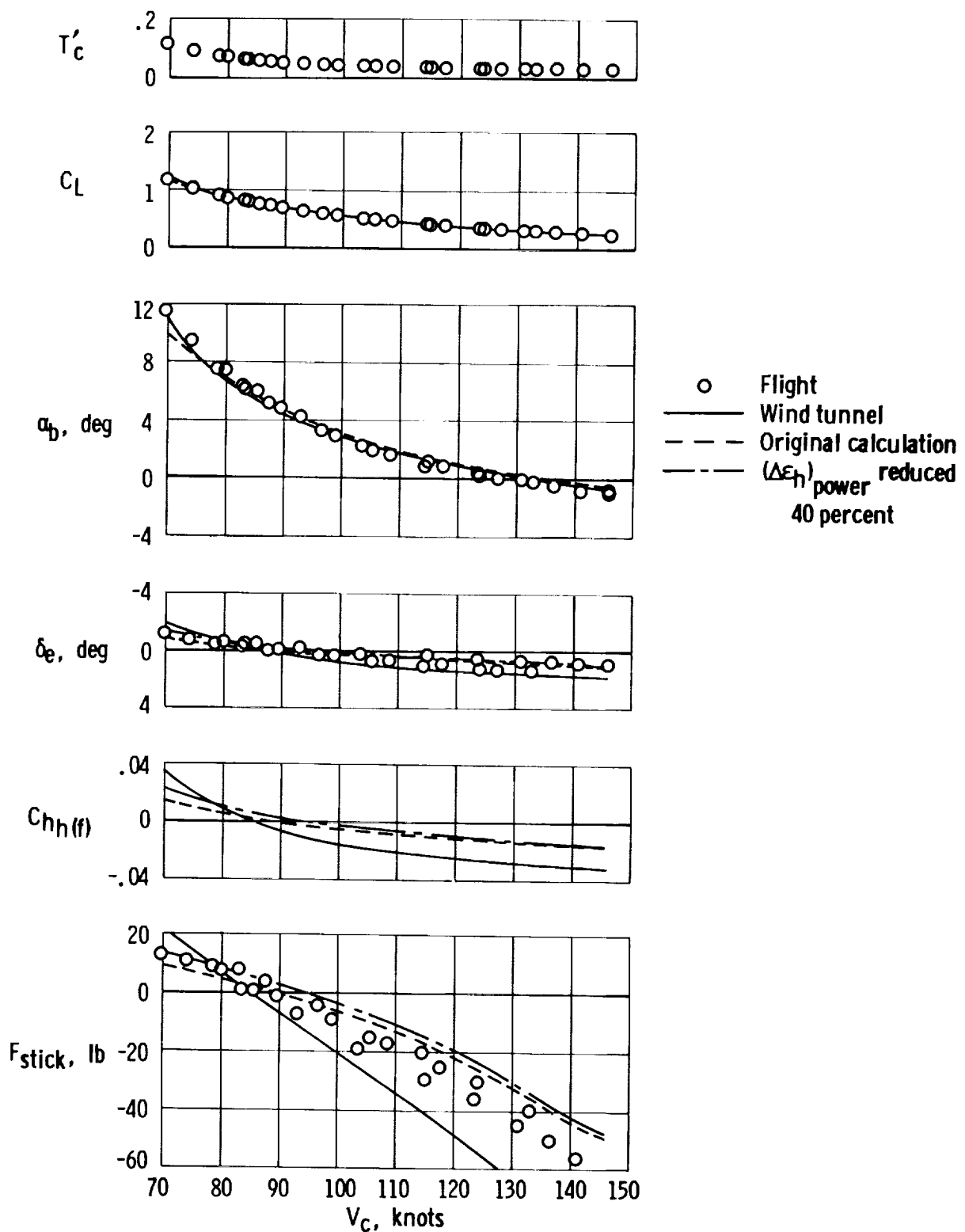


Figure 5.4-2. Comparison of calculated hinge-moment and stick-force characteristics in level flight with those obtained from wind-tunnel and flight data as a function of air-speed. Altitude = 6000 ft; center of gravity = $0.12 \bar{c}_w$.

6.0 DYNAMIC CHARACTERISTICS

The preceding considerations dealt with the static characteristics of general aviation airplanes. Since longitudinal dynamic characteristics are associated with the aerodynamic forces and pitching moments caused by the pitch velocity, q , and normal linear acceleration, \dot{w} (considered in the form of $\dot{\alpha}$), it is essential that aerodynamic parameters accounting for the effects of these two variables be determined.

Consideration is given in the following discussions to the determination of the dynamic derivatives C_{Lq} , $C_{L\dot{\alpha}}$, C_{mq} , and $C_{m\dot{\alpha}}$ and to the appropriate application of the derivatives to the determination of windup-turn and short-period oscillatory characteristics. Although the derivatives C_{Lq} and $C_{L\dot{\alpha}}$ are generally taken to be negligible, C_{Lq} will be applied to the windup-turn considerations to provide a quantitative insight into its influence. The derivative $C_{L\dot{\alpha}}$, although not used, is determined for completeness.

The methods to be presented for determining the dynamic derivatives are based on theories which assume attached-flow conditions and are thus not frequency dependent. Fortunately, attached-flow conditions prevail for the high-aspect-ratio wings normally used on general aviation aircraft and the methods are applicable over the linear lift range of the subject airplane.

It is assumed throughout the following discussions that the dynamic motions, q and $\dot{\alpha}$, negligibly influence the effects of power on lift and pitching moments.

In the absence of appropriate wind-tunnel data, but with the availability of appropriate flight data, all calculated characteristics are referenced to a center of gravity of $0.12 \bar{c}_w$ to conform to the flight data.

6.1 Lift Due to Dynamic Motions

6.1.1 Lift Due to Pitch Rate, C_{Lq}

The lift contributions of the wing, fuselage, nacelles, and horizontal tail due to pitch rate can be summarized by the following expression in which the individual terms are referenced to the wing area:

$$C_{Lq} = (C_{Lq})_{w(wf)} + (C_{Lq})_f + (C_{Lq})_n + (C_{Lq})_{h(hf)} \quad (6.1.1-1)$$

(a) The lift contribution of the wing due to pitch rate can be obtained from the following expressions which take into account the mutual wing-fuselage interference effects:

$$(C_{Lq})_{w(wf)} = \left[K_{w(f)} + K_{f(w)} \right] \left(\frac{S_{we}}{S_w} \right) \left(\frac{\bar{c}_{we}}{\bar{c}_w} \right) (C_{Lq})_{we} \quad (6.1.1-2)$$

where, on the basis of reference 39,

$$(C_{Lq})_{we} = \left(\frac{1}{2} + 2 \frac{\bar{x}}{\bar{c}_{we}} \right) (C_{L\alpha})_{we} \quad (6.1.1-3)$$

In the preceding equations

$K_{w(f)}, K_{f(w)}$ are wing-body interference factors, obtained from section 4.5

S_{we}, \bar{c}_{we} are the wing area and the mean aerodynamic chord of the exposed portion of the wing, respectively, obtained from section 3.2

$(C_{L\alpha})_{we}$ is the lift-curve slope of the exposed portion of the wing per radian, obtained from section 4.2

$$\frac{\bar{x}}{\bar{c}_{we}} = \frac{x_{ac}}{\bar{c}_{we}} - \frac{x_{cg}}{\bar{c}_{we}} \quad (6.1.1-4)$$

$\frac{x_{ac}}{\bar{c}_{we}}$ is the distance to the aerodynamic center of the exposed wing panel from the leading edge and as a fraction of the exposed panel mean aerodynamic chord, obtained from table 4.5-1

$\frac{x_{cg}}{\bar{c}_{we}}$ is the distance to the center of gravity of the airplane from the leading edge

and as a fraction of the exposed panel mean aerodynamic chord

(b) The lift contributions of the fuselage and nacelles, $(C_{Lq})_f + (C_{Lq})_n$, due to pitch rate are not as explicitly accounted for as for the wing. No explicit method is available for obtaining body or nacelle dynamic derivatives for general planforms. The following method, used herein, is the method of reference 1 which considers the body contribution to C_{Lq} to be a product of the body lift-curve slope, $(C_{L\alpha})_B$, and the expression for the ratio of slender-body derivatives, $\left(\frac{C_{Lq}}{C_{L\alpha}}\right)_{\text{slender-body theory}}$, as obtained from reference 40. The fuselage and nacelles contribution to C_{Lq} , based on wing area and wing mean aerodynamic chord and referred to the center of gravity, is thus given by

$$(C_{Lq})_f + (C_{Lq})_n = 2(C_{L\alpha})_f \left(1 - \frac{x_{mf}}{l_f}\right) \frac{l_f}{\bar{c}_w} + 2(C_{L\alpha})_n \left(1 - \frac{x_{mn}}{l_n}\right) \frac{l_n}{\bar{c}_w} \quad (6.1.1-5)$$

where

$(C_{L\alpha})_f, (C_{L\alpha})_n$ are the lift-curve slopes of the fuselage and nacelles, respectively, obtained from section 4.3 on the basis of potential flow terms only, per radian

x_{mf}, x_{mn} are the distances from the nose of the fuselage and nacelle, respectively, to the center of gravity of the airplane, obtained from figure 3.2-1

l_f, l_n are the lengths of the fuselage and nacelles, respectively, obtained from table 4.3-1

(c) The lift contributions of the horizontal tail, $(C_{Lq})_{h(hf)}$, due to pitch rate are obtained from the following derivation which takes into account the tail-fuselage interaction effects on the lift-curve slope of the horizontal tail. Because a change in pitch rate will result in a change in tail angle of attack, in radians, of

$$(\Delta\alpha)_h = \frac{q l_h}{V} \quad (6.1.1-6)$$

where l_h is the distance from the center of gravity to the quarter chord of the horizontal-tail mean aerodynamic chord

$$(\Delta C_{Lh(hf)})_q = 57.3 (C_{L\alpha})_{h(hf)} (\Delta\alpha)_h = 57.3 (C_{L\alpha})_{h(hf)} \left(\frac{q l_h}{V}\right) \quad (6.1.1-7)$$

From the preceding

$$(C_{Lq})_{h(hf)} = \frac{\partial C_{Lh(hf)}}{\partial \frac{q\bar{c}_w}{2V}} = 2(57.3) \frac{l_h}{\bar{c}_w} (C_{L\alpha})_{h(hf)} \quad (6.1.1-8)$$

where $(C_{L\alpha})_{h(hf)}$ is the elevator-fixed lift-curve slope of the horizontal tail, in degrees, with tail-fuselage interaction effects accounted for and is obtained from equation (4.10-2) as

$$(C_{L\alpha})_{h(hf)} = [K_{h(f)} + K_{f(h)}] (C_{L\alpha})_{h_e} \left(\frac{\bar{q}_h}{\bar{q}_\infty} \right) \frac{S_{h_e}}{S_w} \quad (6.1.1-9)$$

In the present application of the equation (6.1.1-9), $(C_{L\alpha})_{h_e}$ is the propeller-off value of the tail lift-curve slope, based on the exposed tail panels, obtained from table 4.2-1, and $\frac{\bar{q}_h}{\bar{q}_\infty}$ is the power-on dynamic-pressure ratio at the tail, as obtained in sec-

tion 5.1.2. Although the preceding equation was applied to the subject airplane as presented, the caution given in section 4.11 is reiterated: For the geometric tail-fuselage configuration of the subject airplane, the lift carryover from the tail to the fuselage (represented by $K_{f(h)}$) may be insignificant because of the location of the tail on the fuselage and the air gap between the tail and the fuselage. It is suggested that $K_{f(h)}$ be considered to be similar to zero for tail-fuselage configurations similar to that of the subject airplane.

(d) By applying the preceding methods to the subject airplane, the lift due to pitch rate, C_{Lq} , was calculated and is presented in table 6.1.1-1 as a function of angle of attack and power condition on the basis of original downwash calculations. The results are plotted in figure 6.1.1-1. Included in the figure are the results of calculations which included a 40-percent decrease in power-induced downwash on the tail. No experimental data were available for comparison. Because of the inclusion of the lift carryover from the tail to the fuselage, which is undoubtedly small or nil in accordance with the preceding cautionary remarks, the calculated C_{Lq} is, in all likelihood, about 10 percent larger than it should be.

6.1.2 Lift Due to Vertical Acceleration, $C_{L\dot{\alpha}}$

The wing, fuselage, nacelles, and horizontal-tail contributions to the lift due to vertical acceleration, $\dot{\alpha}$, are summarized by the following expression in which the individual terms are referenced to the wing area:

$$C_{L\dot{\alpha}} = (C_{L\dot{\alpha}})_w + (C_{L\dot{\alpha}})_f + (C_{L\dot{\alpha}})_n + (C_{L\dot{\alpha}})_{h(hf)} \quad (6.1.2-1)$$

(a) The lift contribution of the wing, $(C_{L\dot{\alpha}})_w$, due to the vertical acceleration, $\dot{\alpha}$, cannot be accounted for because explicit expressions for the subsonic region are not available except for triangular wings. Because the wing contribution is relatively small for conventional aircraft, the omission of the wing contribution would not seem to significantly affect the net $C_{L\dot{\alpha}}$.

(b) The lift contributions of the fuselage and nacelles, $(C_{L\dot{\alpha}})_f + (C_{L\dot{\alpha}})_n$, due to vertical acceleration, $\dot{\alpha}$, are accounted for by the following approximate equation, which was arrived at in a manner synonymous to the derivation of the equation for body contribution to C_{Lq} (section 6.1.1(b)). Referenced to the wing area and the wing mean aerodynamic chord,

$$(C_{L\dot{\alpha}})_f + (C_{L\dot{\alpha}})_n = 2 (C_{L\alpha})_f \frac{l_f}{\bar{c}_w} + 2 (C_{L\alpha})_n \frac{l_n}{\bar{c}_w} \quad (6.1.2-2)$$

The individual terms in the equation have the same definitions as the terms in equation (6.1.1-5)

(c) The lift contribution of the horizontal tail, $(C_{L\dot{\alpha}})_{h(hf)}$, due to vertical acceleration, $\dot{\alpha}$, is based on the concept of the "lag of the downwash." The downwash at the tail does not respond instantaneously to changes in wing angle of attack. Because the trailing vortex is convected with the airstream, a change in circulation at the wing is not felt as a change in downwash at the tail until a time, $\Delta t = \frac{l_h}{V}$, has elapsed (l_h is the distance from the center of gravity to the tail). The lag in change in downwash and, therefore, the lag in change in angle of attack, in radians, of the horizontal tail is accounted for by

$$(\Delta\alpha)_h = \Delta\epsilon_h = \frac{\partial\epsilon_h}{\partial\alpha_b} (\dot{\alpha}\Delta t) = \frac{\partial\epsilon_h}{\partial\alpha_b} \dot{\alpha} \frac{l_h}{V} \quad (6.1.2-3)$$

The correction to the tail-lift coefficient to account for the lag in downwash change is obtained from

$$(\Delta C_{Lh(hf)})_{\dot{\alpha}} = 57.3 (C_{L\alpha})_{h(hf)} (\Delta\alpha)_h = 57.3 (C_{L\alpha})_{h(hf)} \frac{\partial\epsilon_h}{\partial\alpha_b} \frac{l_h}{V} \dot{\alpha} \quad (6.1.2-4)$$

from which

$$(C_{L\dot{\alpha}})_{h(hf)} = \frac{\partial C_{Lh(hf)}}{\partial \frac{\dot{\alpha} \bar{c}_w}{2V}} = 2(57.3) (C_{L\alpha})_{h(hf)} \frac{l_h}{\bar{c}_w} \frac{\partial\epsilon_h}{\partial\alpha_b} \quad (6.1.2-5)$$

Comparison of this equation with the equation for $(C_{Lq})_{h(hf)}$ (eq. (6.1.1-8)) shows

the two equations to be identical except for the $\frac{\partial \epsilon_h}{\partial \alpha_b}$ term. Thus

$$(C_{L\dot{\alpha}})_{h(hf)} = (C_{Lq})_{h(hf)} \frac{\partial \epsilon_h}{\partial \alpha_b} \quad (6.1.2-6)$$

where

$(C_{Lq})_{h(hf)}$ is obtained from equation (6.1.1-8)

$\frac{\partial \epsilon_h}{\partial \alpha_b}$ is the rate of change of tail downwash with airplane angle of attack, obtained from figure 5.1.2-4 as a function of α_b and power condition being analyzed

(d) By applying the preceding methods to the subject airplane, the lift due to the vertical acceleration was calculated and is presented in table 6.1.2-1 as a function of angle of attack and power condition on the basis of original downwash calculations. The results are plotted in figure 6.1.2-1. Included are the results of calculations which included a 40-percent decrease in power-induced downwash at the tail. No experimental data were available for comparison.

6.1.3 Symbols

All lift coefficients and their derivatives are referenced to the wing area unless noted otherwise.

C_L	lift coefficient
$C_{Lh(hf)}$	lift coefficient of the horizontal tail with the tail-fuselage interaction effects included
$(\Delta C_{Lh(hf)})_q, (\Delta C_{Lh(hf)})_{\dot{\alpha}}$	increment of lift coefficient due to the pitch rate and angle-of-attack rate, respectively
$C_{Lq}, C_{L\dot{\alpha}} = \frac{\partial C_L}{\partial \frac{q\bar{c}_w}{2V}} \text{ and } \frac{\partial C_L}{\partial \frac{\dot{\alpha}\bar{c}_w}{2V}}, \text{ respectively, per rad}$	
$(C_{Lq})_f, (C_{L\dot{\alpha}})_f$	contribution of the fuselage to C_{Lq} and $C_{L\dot{\alpha}}$, respectively, per rad
$(C_{Lq})_{h(hf)}, (C_{L\dot{\alpha}})_{h(hf)}$	contribution of the horizontal tail to C_{Lq} and $C_{L\dot{\alpha}}$, respectively, with tail-fuselage interaction effects included, per rad
$(C_{Lq})_n, (C_{L\dot{\alpha}})_n$	contribution of the nacelles to C_{Lq} and $C_{L\dot{\alpha}}$, respectively, per rad
$(C_{Lq})_{w_e}$	contribution of the exposed wing panels to C_{Lq} , per rad

$(C_{Lq})_{w(wf)}$	contribution of the wing to C_{Lq} with wing-fuselage interaction effects accounted for, per rad
$\left(\frac{C_{Lq}}{C_{L\alpha}}\right)_{\text{slender-body theory}}$	ratio of C_{Lq} and $C_{L\alpha}$ of a body obtained from slender-body theory, used in the form of its mathematical equivalence to obtain $(C_{Lq})_f$ and $(C_{Lq})_n$ (eq. (6.1.1-5))
$(C_{L\alpha})_B$	lift-curve slope of a body, per rad
$(C_{L\alpha})_f, (C_{L\alpha})_n$	lift-curve slope of the fuselage and nacelles, respectively, per rad
$(C_{L\alpha})_{he}$	lift-curve slope of the exposed horizontal-tail panels, referenced to the area of the exposed panels, per deg
$(C_{L\alpha})_h(hf)$	lift-curve slope of the horizontal tail with tail-fuselage interaction effects included, per deg
$(C_{L\alpha})_{we}$	lift-curve slope of the exposed wing panels, referenced to the area of the exposed panels, per rad
$(C_{L\dot{\alpha}})_w$	wing contribution to $C_{L\dot{\alpha}}$, per rad
C_m	pitching-moment coefficient
$C_{mq} = \frac{\partial C_m}{\partial \frac{q\bar{c}_w}{2V}}$, per rad	
$C_{m\dot{\alpha}} = \frac{\partial C_m}{\partial \frac{\dot{\alpha}\bar{c}_w}{2V}}$, per rad	
\bar{c}_w	mean aerodynamic chord of the wing, in. when used in ratio of two dimensions, ft when used in derivatives
\bar{c}_{we}	mean aerodynamic chord of the exposed wing panels, in.
$K_{h(f)}, K_{f(h)}$	ratio of the lift on the horizontal tail in the presence of the fuselage and the lift carryover from the tail onto the fuselage, respectively, to the lift on the tail alone
$K_{w(f)}, K_{f(w)}$	ratio of the lift on the wing in the presence of the fuselage and the lift carryover from the wing onto the fuselage, respectively, to the lift on the wing alone

l_f, l_n	length of the fuselage and nacelle, respectively, in.
l_h	distance from the center of gravity to the quarter chord of the horizontal-tail mean aerodynamic chord, in.
q	pitch rate, rad/sec
$\bar{q}_h, \bar{q}_\infty$	dynamic pressure at the horizontal tail and the free stream, respectively, lb/sq ft
S_{he}, S_{we}	area of the exposed panels of the horizontal tail and the wing, respectively, sq ft
S_w	wing area, sq ft
T'_c	thrust coefficient
t	time, sec
Δt	increment of time, sec
$\frac{x_{ac}}{\bar{c}_{we}}$	distance to the aerodynamic center of the exposed wing panels from the leading edge of the wing as a fraction of the exposed panel mean aerodynamic chord
$\frac{x_{cg}}{\bar{c}_w}, \frac{x_{cg}}{\bar{c}_{we}}$	distance to the center of gravity of the airplane from the leading edge of the wing as a fraction of the complete wing mean aerodynamic chord and the exposed panel mean aerodynamic chord, respectively
$\frac{\bar{x}}{\bar{c}_{we}} = \frac{x_{ac}}{\bar{c}_{we}} - \frac{x_{cg}}{\bar{c}_{we}}$	
x_{mf}, x_{mn}	distance from the nose of the fuselage and nacelle, respectively, to the airplane center of gravity, in.
V	airspeed, ft/sec
α_b	airplane angle of attack relative to the X-body axis, deg
$\dot{\alpha}$	time rate of change of α_b , $\frac{\partial \alpha_b}{\partial t}$, rad/sec
$(\Delta \alpha)_h$	change in the angle of attack of the horizontal tail, rad
$\Delta \epsilon_h$	change in the downwash at the tail, rad
$(\Delta \epsilon_h)_{\text{power}}$	change in the downwash at the tail due to power, rad or deg

$$\frac{\partial \epsilon_h}{\partial \alpha_b}$$

rate of change of the downwash at the tail with airplane
angle of attack

TABLE 6.1.1-1
LIFT DUE TO PITCH RATE, C_{Lq}
[Flight center of gravity = $0.12 \bar{c}_w$]
(a) Contribution of wing, $(C_{Lq})_{w(wf)}$

$$(C_{Lq})_{w(wf)} = \left\{ \left[K_w(f) + K_f(w) \right] \left(\frac{S_{we}}{S_w} \right) \left(\frac{\bar{c}_{we}}{\bar{c}_w} \right) \right\} \left\{ \left(1 + 2 \frac{\bar{x}}{\bar{c}_{we}} \right) (C_{L\alpha})_{we} \right\}$$

Symbol	Description	Reference	Magnitude
$K_w(f)$	Ratio of lift on wing in presence of fuselage to wing alone	Table 4.4-1	1.09
$K_f(w)$	Ratio of wing-lift carryover on fuselage to wing alone	Table 4.4-1	.14
S_{we}	Exposed wing panels area, sq ft	Table 3.2-1	148
S_w	Reference wing area, sq ft	Table 3-1	178
\bar{c}_{we}	Mean aerodynamic chord of exposed wing panels, in.	Table 3.2-1	57.1
\bar{c}_w	Mean aerodynamic chord of complete wing, in.	Table 3.2-1	59.5
$\frac{x_{cg}}{\bar{c}_w}$	Center of gravity of the airplane from leading edge of wing mean aerodynamic chord as a fraction of the wing aerodynamic chord	Flight data	0.12
$\frac{x_{cg}}{\bar{c}_{we}}$	Center of gravity of the airplane from leading-edge exposed-panel mean aerodynamic chord as a fraction of mean aerodynamic center of the exposed panel	$\left(\frac{x_{cg}}{\bar{c}_w} \right) \frac{\bar{c}_w}{\bar{c}_{we}}$.125
$\frac{x_{ac}}{\bar{c}_{we}}$	Aerodynamic center of exposed wing panels from leading edge and as a fraction of exposed-panel mean aerodynamic chord	Table 4.5-1	.249
$\frac{\bar{x}}{\bar{c}_{we}}$	$\frac{x_{ac}}{\bar{c}_{we}} - \frac{x_{cg}}{\bar{c}_{we}}$	Equation (6.1.1-4)	.124
$(C_{L\alpha})_{we}$	Lift-curve slope of exposed wing panels referenced to S_{we} , per rad	Table 4.2-1	4.28
Summary: $(C_{Lq})_{w(wf)} = 3.14$ per rad			

(b) Contributions of fuselage and nacelles, $(C_{Lq})_f + (C_{Lq})_n$

$$(C_{Lq})_f + (C_{Lq})_n = 2(C_{L\alpha})_f \left(1 - \frac{x_{mf}}{l_f} \right) \frac{l_f}{\bar{c}_w} + 2(C_{L\alpha})_n \left(1 - \frac{x_{mn}}{l_n} \right) \frac{l_n}{\bar{c}_w}$$

Symbol	Description	Reference	Magnitude
S_w	Reference wing area, sq ft	Table 3-1	178
\bar{c}_w	Wing mean aerodynamic chord, in.	Table 3.2-1	59.5
$(C_{L\alpha})_f$	Lift-curve slope of fuselage based on potential flow only, referenced to $S_w = 178$ sq ft, per rad	Table 4.3-1	0.121
$(C_{L\alpha})_n$	Lift-curve slope of nacelles based on potential flow only, referenced to $S_w = 178$ sq ft, per rad	Table 4.3-1	.089
x_{mf}	Distance from nose of fuselage to flight center of gravity of the airplane, in.	Figure 3.2-1	100.33
x_{mn}	Distance from nose of nacelles to flight center of gravity of the airplane, in.	Figure 3.2-1	60.14
l_f	Fuselage length, in.	Figure 4.3-5(a)	290
l_n	Nacelle length, in.	Figure 4.3-5(b)	106
Summary: $(C_{Lq})_f + (C_{Lq})_n = 0.9087$ per rad			

TABLE 6.1.1-1 (Concluded)

(c) Contribution of horizontal tail, $(C_{Lq})_{h(hf)}$

$$(C_{Lq})_{h(hf)} = 114.6 \frac{l_h}{\bar{c}_w} (C_{L\alpha})_{h(hf)}$$

Symbol	Description	Reference	Magnitude
S_w	Reference wing area, sq ft	Table 3-1	178
\bar{c}_w	Wing mean aerodynamic chord, in.	Table 3.2-1	59.5
$(C_{L\alpha})_{h(hf)}$	Lift-curve slope of horizontal tail, referenced to $S_w = 178$ sq ft, per deg	Table 4.10-1(a)	$0.01361 \left(\frac{\bar{q}_h}{\bar{q}_\infty} \right)$
$\frac{\bar{q}_h}{\bar{q}_\infty}$	Dynamic-pressure ratio at the tail with power on	Table 5.1.2-1(b), column 11	Table 5.1.2-1(b), as per column 11
l_h	Distance from reference (flight) center of gravity to the quarter chord of the tail, in.	Figure 3.2-2	172.75
Summary: $(C_{Lq})_{h(hf)} = 4.53 \left(\frac{\bar{q}_h}{\bar{q}_\infty} \right)$ per rad			

(d) Lift due to pitch rate, C_{Lq}

$$\begin{aligned}
 C_{Lq} &= (C_{Lq})_{w(wf)} + (C_{Lq})_f + (C_{Lq})_n + (C_{Lq})_{h(hf)} \\
 &= 3.14 + 0.9087 + 4.53 \left(\frac{\bar{q}_h}{\bar{q}_\infty} \right) \\
 &= 4.049 + 4.53 \left(\frac{\bar{q}_h}{\bar{q}_\infty} \right)
 \end{aligned}$$

①	②			③		
-----	Table 5.1.2-1(b), column 11			-----		
α_b , deg	$\frac{\bar{q}_h}{\bar{q}_\infty}$			$C_{Lq} = 4.049 + 4.53$ ②		
	T'_c			T'_c		
	0	0.20	0.44	0	0.20	0.44
-4	1.0	1.0868	1.2027	8.579	8.972	9.497
-2	1.0	1.1028	1.2108	8.579	9.045	9.534
0	1.0	1.1167	1.2216	8.579	9.108	9.583
2	1.0	1.1222	1.2324	8.579	9.133	9.632
4	1.0	1.1333	1.2432	8.579	9.183	9.681
6	1.0	1.1389	1.2541	8.579	9.208	9.730
8	1.0	1.1444	1.2622	8.579	9.233	9.767
10	1.0	1.1417	1.2676	8.579	9.221	9.791
12	1.0	1.1361	1.2757	8.579	9.196	9.828
^a 13.8	1.0	1.1278	1.2811	8.579	9.158	9.852
^b 14.1	---	1.1222	1.2811	-----	9.133	9.852
^c 14.4	---	-----	1.2784	-----	-----	9.840

^{a,b,c}Stall angles for $T'_c = 0, 0.20, 0.44$ power conditions, respectively.

TABLE 6.1.2-1
LIFT DUE TO VERTICAL ACCELERATION, $C_{L\dot{\alpha}}$
[Flight center of gravity = $0.12 \bar{c}_w$]

(a) Contribution of wing, $(C_{L\dot{\alpha}})_w$

In accordance with discussion in section 6.1.2(a),

$$(C_{L\dot{\alpha}})_w \approx 0$$

(b) Contributions of fuselage and nacelles, $(C_{L\dot{\alpha}})_f + (C_{L\dot{\alpha}})_n$

$$(C_{L\dot{\alpha}})_f + (C_{L\dot{\alpha}})_n = 2(C_{L\alpha})_f \frac{l_f}{\bar{c}_w} + 2(C_{L\alpha})_n \frac{l_n}{\bar{c}_w}$$

Symbol	Description	Reference	Magnitude
S_w	Reference wing area, sq ft	Table 3-1	178
\bar{c}_w	Wing mean aerodynamic chord, in.	Table 3.2-1	59.5
$(C_{L\alpha})_f$	Lift-curve slope of fuselage based on potential flow only, referenced to $S_w = 178$ sq ft, per rad	Table 6.1.1-1(b)	.121
$(C_{L\alpha})_n$	Lift-curve slope of nacelles based on potential flow only, per rad	Table 6.1.1-1(b)	.089
l_f	Fuselage length, in.	Figure 4.3-5(a)	290
l_n	Nacelle length, in.	Figure 4.3-5(b)	106
Summary: $(C_{L\dot{\alpha}})_f + (C_{L\dot{\alpha}})_n = 1.497$ per rad			

(c) Contribution of horizontal tail, $(C_{L\dot{\alpha}})_{h(hf)}$

$$(C_{L\dot{\alpha}})_{h(hf)} = (C_{Lq})_{h(hf)} \frac{\partial \epsilon_h}{\partial \alpha_b}$$

Symbol	Description	Reference	Magnitude
S_w	Reference wing area, sq ft	Table 3-1	178
$(C_{Lq})_{h(hf)}$	Tail contribution to C_{Lq} with tail-fuselage interaction effects included, per radian	Table 6.1.1-1(c)	$4.53 \frac{\bar{q}_h}{\bar{q}_\infty}$
$\frac{\partial \epsilon_h}{\partial \alpha_b}$	Rate of change of downwash at tail with α_b	Figure 5.1.2-5	$f(\alpha_b, T'_c)$
$\frac{\bar{q}_h}{\bar{q}_\infty}$	Dynamic-pressure ratio at tail with power on	Table 6.1.1-1(d), column 2	$f(\alpha_b, T'_c)$
Summary: $(C_{L\dot{\alpha}})_{h(hf)} = 4.53 \left(\frac{\bar{q}_h}{\bar{q}_\infty} \right) \frac{\partial \epsilon_h}{\partial \alpha_b}$ per rad			

TABLE 6.1.2-1 (Concluded)

(d) Lift due to vertical acceleration, $C_{L\dot{\alpha}}$

$$C_{L\dot{\alpha}} = (C_{L\dot{\alpha}})_w + (C_{L\dot{\alpha}})_f + (C_{L\dot{\alpha}})_n + (C_{L\dot{\alpha}})_{h(hf)}$$

$$= 0 + 1.497 + 4.53 \left(\frac{\bar{q}_h}{\bar{q}_\infty} \right) \frac{\partial \epsilon_h}{\partial \alpha_b}$$

$$= 1.497 + 4.53 \left(\frac{\bar{q}_h}{\bar{q}_\infty} \right) \left(\frac{\partial \epsilon_h}{\partial \alpha_b} \right)$$

①	②			③			④		
-----	Table 6.1.1-1(d) column 2			Figure 5.1.2-5			-----		
α_b , deg	$\frac{\bar{q}_h}{\bar{q}_\infty}$			$\frac{\partial \epsilon_h}{\partial \alpha_b}$			$C_{L\dot{\alpha}} =$ 1.497 + 4.53 ② ③		
	T'_c			T'_c			T'_c		
	0	0.20	0.44	0	0.20	0.44	0	0.20	0.44
-4	1.0	1.0868	1.2027	-----	-----	-----	-----	-----	-----
-2	1.0	1.1028	1.2108	0.475	0.785	0.915	3.649	5.419	6.516
0	1.0	1.1167	1.2216	0.475	0.775	0.920	3.649	5.417	6.588
2	1.0	1.1222	1.2324	.475	.760	.905	3.649	5.361	6.549
4	1.0	1.1333	1.2432	0.475	0.730	0.865	3.649	5.245	6.368
6	1.0	1.1389	1.2541	.475	.680	.810	3.649	5.005	6.099
8	1.0	1.1444	1.2622	0.470	0.640	0.740	3.626	4.815	5.728
10	1.0	1.1417	1.2676	.450	.600	.670	3.536	4.600	5.344
12	1.0	1.1361	1.2757	0.425	0.530	0.589	3.332	4.225	4.901
^a 13.8	1.0	1.1278	1.2811	.405	.475	.500	-----	3.924	4.399
^b 14.1	---	1.1222	1.2811	-----	0.470	0.470	-----	3.886	4.225
^c 14.4	---	-----	1.2784	-----	-----	.450	-----	-----	4.103

^{a,b,c}Stall angles for $T'_c = 0, 0.20, 0.44$ power conditions, respectively.

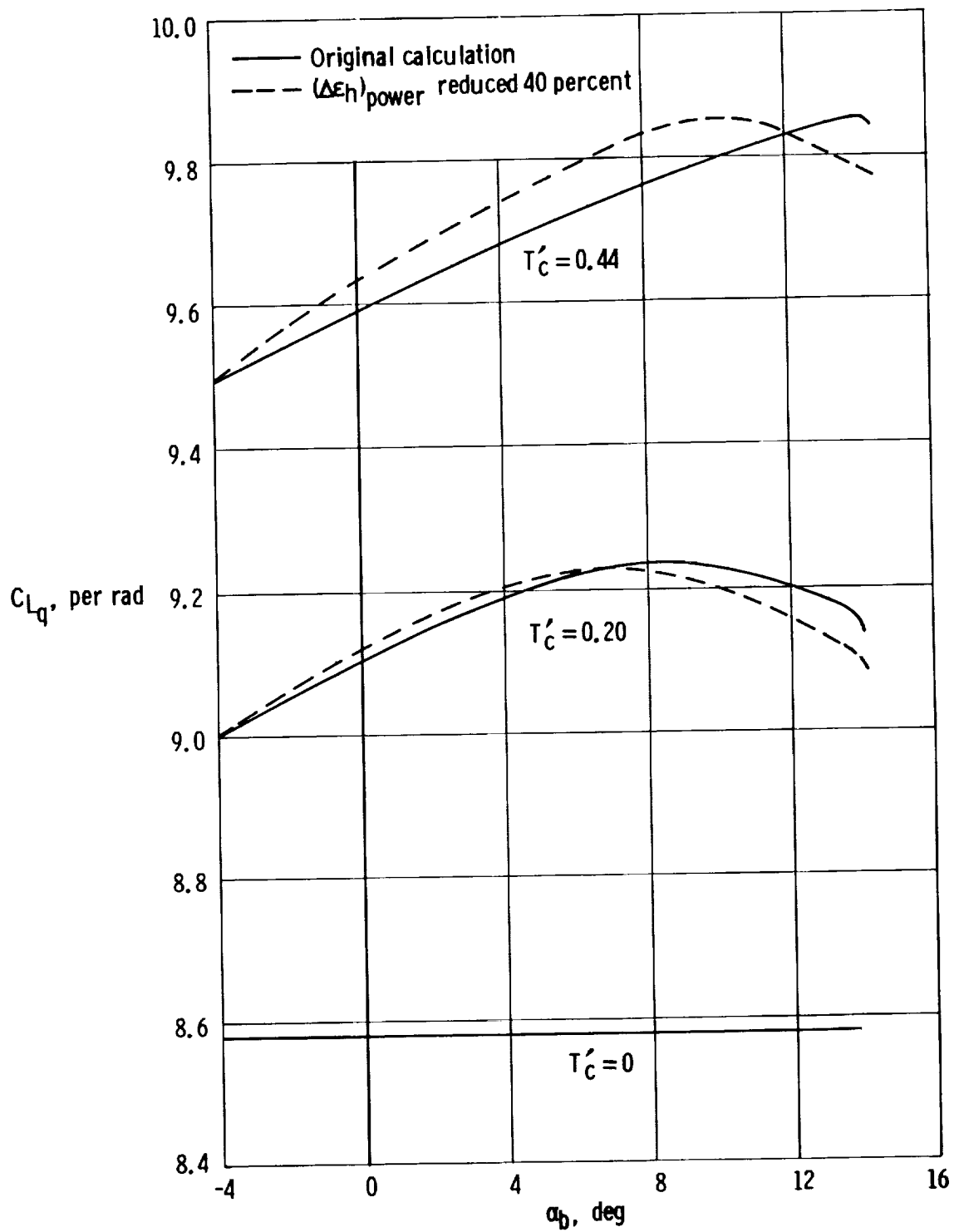


Figure 6.1.1-1. Variation of calculated lift due to pitching moment, C_{Lq} , with angle of attack and power conditions.

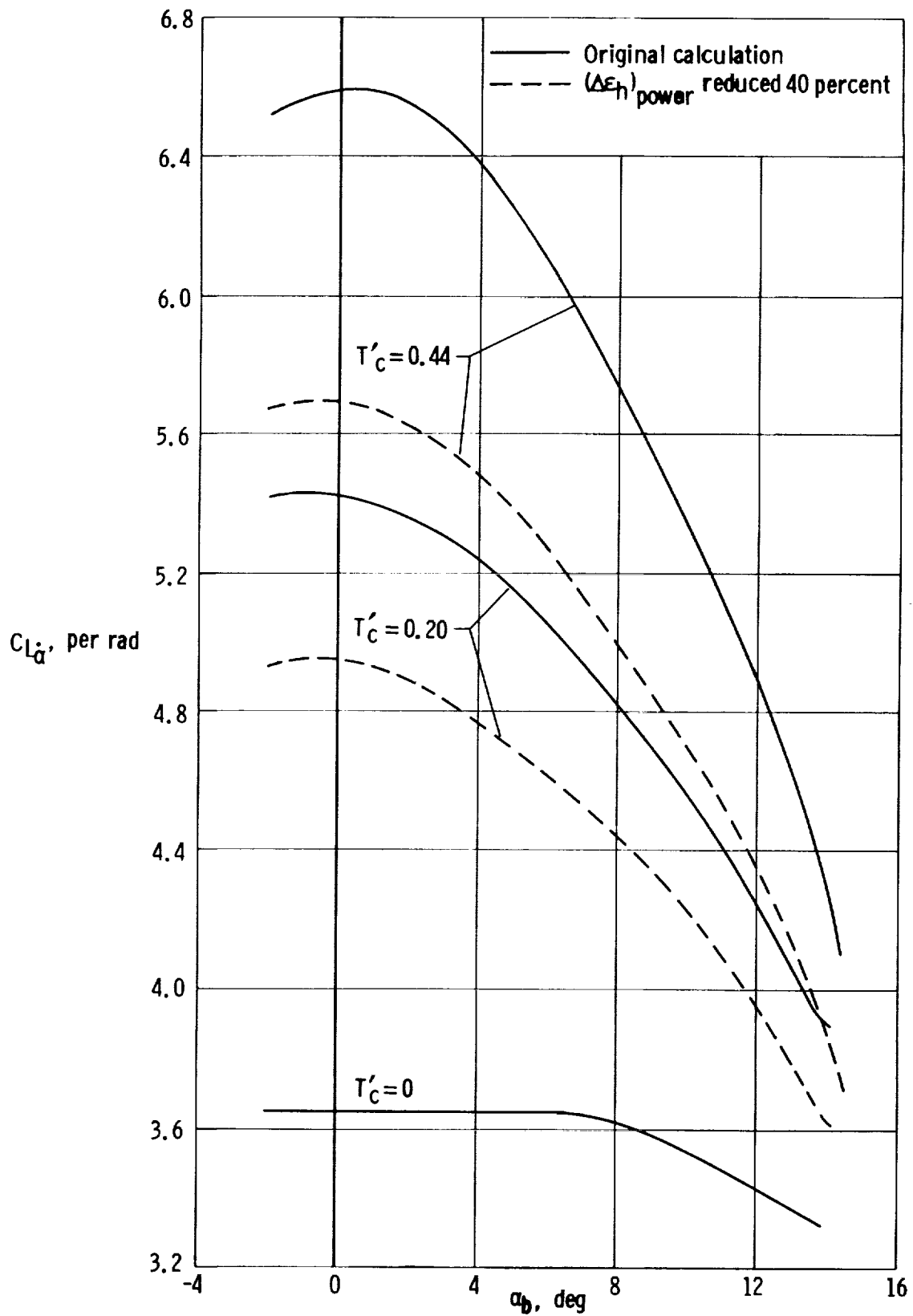


Figure 6.1.2-1. Variation of calculated lift due to vertical acceleration, $C_{L\dot{\alpha}}$, with angle of attack and power.

6.2 Pitching Moments Due to Dynamic Motions

6.2.1 Pitching Moments Due to Pitch Rate, C_{mq}

The contributions of the wing, fuselage, nacelles, and horizontal tail to the pitching moment due to pitch rate can be summarized by

$$C_{mq} = (C_{mq})_{w(wf)} + (C_{mq})_f + (C_{mq})_n + (C_{mq})_{h(hf)} \quad (6.2.1-1)$$

(a) The contribution of the wing, including the mutual wing-fuselage interference effects, to the pitching moments due to pitch rate, C_{mq} , can be accounted for by

$$(C_{mq})_{w(wf)} = \left[K_{w(f)} + K_{f(w)} \right] \left(\frac{S_{we}}{S_w} \right) \left(\frac{\bar{c}_{we}}{\bar{c}_w} \right)^2 (C_{mq})_{we} \quad (6.2.1-2)$$

in which the individual terms, with the exception of $(C_{mq})_{we}$, were previously defined (eq. (6.1.1-2)). For low-speed incompressible conditions ($M \lesssim 0.2$), $(C_{mq})_{we}$ is obtained from the following equation, which was derived in reference 39 and modified in reference 41 by the inclusion of the factor k :

$$\left[(C_{mq})_{we} \right]_{M \approx 0.2} = -k (57.3 c_{l_\alpha}) \cos \Lambda_{c/4} \left\{ \frac{A_{we} \left[\frac{1}{2} \frac{\bar{x}}{\bar{c}_{we}} + 2 \left(\frac{\bar{x}}{\bar{c}_{we}} \right)^2 \right]}{A_{we} + 2 \cos \Lambda_{c/4}} + \frac{1}{24} \left(\frac{A_{we}^3 \tan^2 \Lambda_{c/4}}{A_{we} + 6 \cos \Lambda_{c/4}} \right) + \frac{1}{8} \right\} \quad (6.2.1-3)$$

where

c_{l_α} is the section lift-curve slope, in degrees, obtained from section 4.2

A_{we} is the aspect ratio of the exposed portion of the wing, obtained from table 3.2-1

$\frac{\bar{x}}{\bar{c}_{we}}$ is the distance from the aerodynamic center to the center of gravity as a fraction of the exposed panel mean aerodynamic chord

The factor k is empirical, having been obtained by correlating equation (6.2.1-3) with dynamic model data (ref. 41). For an aspect ratio between 1 and 6, k was determined to be of the order of 0.7. No experimental data were obtained in reference 41 for higher aspect ratios; however, for very high aspect ratios, k approaches 1.0. Reference 1 suggests that for aspect ratios of about 10 or 12, k should be approximately 0.9. Although no experimental data are available to show how k should vary for intermediate aspect ratios, reference 1 suggests that a smooth fairing be used.

For subsonic speeds involving compressibility effects, $(C_{mq})_{we}$ is obtained by applying an approximate compressibility correction factor, derived in reference 42, to the results of equation (6.2.1-3). Thus

$$[(C_{mq})_{we}]_{M>0.2} = \left(\frac{\frac{A_{we}^3 \tan^2 \Lambda_{c/4}}{A_{we} B_2 + 6 \cos \Lambda_{c/4}} + \frac{3}{B_2}}{\frac{A_{we}^3 \tan^2 \Lambda_{c/4}}{A_{we} + 6 \cos \Lambda_{c/4}} + 3} \right) [(C_{mq})_{we}]_{M<0.2} \quad (6.2.1-4)$$

where

A_{we} is the aspect ratio of the exposed wing panels (table 3.2-1)

$$B_2 = \sqrt{1 - M^2 \cos^2 \Lambda_{c/4}} \quad (6.2.1-5)$$

$\Lambda_{c/4}$ is the sweepback of the wing quarter-chord line

(b) The pitching-moment contributions of the fuselage and nacelles due to pitch rate, $(C_{mq})_f + (C_{mq})_n$, as for lift due to pitch rate, are not explicitly accounted for.

The contributions of the fuselage and nacelles were obtained on the basis of equation (6.2.1-6), from reference 1, which was derived in a manner synonymous to the derivation of equation (6.1.1-5) using slender-body theory. Referred to body base area, S_b , body length, l_B , and a selected center of rotation (the center of gravity of the airplane),

$$(C_{mq})_{BS_b l_B} = 2 \left[57.3 (C_{m\alpha})_{BS_b l_B} \right] \left[\frac{\left(1 - \frac{x_{mB}}{l_B} \right)^2 - \frac{V_B}{S_b l_B} \left(\frac{x_{cB}}{l_B} - \frac{x_{mB}}{l_B} \right)}{\left(1 - \frac{x_{mB}}{l_B} \right) - \frac{V_B}{S_b l_B}} \right] \quad (6.2.1-6)$$

where

$(x_m)_B$ is the distance from the nose of the body to the center of gravity of the airplane

$(x_c)_B$ is the distance from the nose of the body to the centroid of the body volume

$(C_{m\alpha})_{BS_b l_B}$ is the $C_{m\alpha} = \frac{\partial C_m}{\partial \alpha_b}$ of the body referenced to $S_b l_B$

Because the base area of the subject airplane is essentially zero, equation (6.2.1-6) can be reduced to

$$(C_{mq})_{BS_b l_B} = 2 \left[57.3 (C_{m\alpha})_{BS_b l_B} \right] \left(\frac{x_{cB}}{l_B} - \frac{x_{mB}}{l_B} \right) \quad (6.2.1-7)$$

Referencing $(C_{mq})_B$ and $(C_{m\alpha})_B$ to the wing area, S_w , and the wing mean aerodynamic chord, \bar{c}_w ,

$$(C_{mq})_B = 2 \left[57.3 (C_{m\alpha})_B \right] \left(\frac{x_{cB}}{\bar{c}_w} - \frac{x_{mB}}{\bar{c}_w} \right) \quad (6.2.1-8)$$

Considering that $(C_{m\alpha})_B$, when obtained from equation (4.7-1) and applied to the fuselage and nacelle components of the subject airplane, was referred to the leading edge of the wing mean aerodynamic chord, conversion to airplane center of gravity requires that

$$(C_{m\alpha})_B = (C_{m\alpha})_{B_{le}} + (C_{L\alpha})_B \frac{x_{cg}}{\bar{c}_w} \quad (6.2.1-9)$$

Hence, relative to the center of gravity of the airplane,

$$(C_{mq})_B = 2(57.3) \left[(C_{m\alpha})_{B_{le}} + (C_{L\alpha})_B \frac{x_{cg}}{\bar{c}_w} \right] \left(\frac{x_{cB}}{\bar{c}_w} - \frac{x_{mB}}{\bar{c}_w} \right) \quad (6.2.1-10)$$

Applied specifically to the fuselage and nacelles of the subject airplane, the net contribution of the fuselage and nacelles to C_{mq} is obtained from

$$(C_{mq})_{fn} = 2(57.3) \left[(C_{m\alpha})_{f_{le}} + (C_{L\alpha})_f \frac{x_{cg}}{\bar{c}_w} \right] \left(\frac{x_{cf}}{\bar{c}_w} - \frac{x_{mf}}{\bar{c}_w} \right) + 2(57.3) \left[(C_{m\alpha})_{n_{le}} + (C_{L\alpha})_n \frac{x_{cg}}{\bar{c}_w} \right] \left(\frac{x_{cn}}{\bar{c}_w} - \frac{x_{mn}}{\bar{c}_w} \right) \quad (6.2.1-11)$$

where

$(C_{m\alpha})_{f_{le}}$ and $(C_{m\alpha})_{n_{le}}$ are obtained from section 4.7 relative to the leading edge of the wing mean aerodynamic chord, per deg (to a practical degree of approximation, only the potential flow term of equation (4.7-1) need be considered)

x_{cg} is the distance from the leading edge of the wing mean aerodynamic chord to the center of gravity of the airplane

$(C_{L\alpha})_f, (C_{L\alpha})_n$ are the lift-curve slopes of the fuselage and nacelles, respectively, obtained from section 4.3 on the basis of potential-flow terms only, per deg

x_{mf}, x_{mn} are the distances from the nose of the fuselage and nacelle, respectively, to the center of gravity of the airplane, obtained from figure 3.2-1, in.

x_{cf} is the distance from the nose of the fuselage to the centroid of the fuselage volume, in.,

$$x_{cf} = \frac{\int_0^{l_f} S_x x \, dx}{12V_f} \quad (6.2.1-12)$$

x_{cn} is the distance from the nose of the nacelle to the centroid of the nacelle volume, in.,

$$x_{cn} = \frac{\int_0^{l_n} S_x x \, dx}{12V_n} \quad (6.2.1-13)$$

(c) The pitching-moment contribution of the horizontal tail due to pitch rate, $(C_{mq})_{h(hf)}$, with tail-fuselage interaction effects included, is accounted for by

$$(C_{mq})_{h(hf)} = -\frac{l_h}{\bar{c}_w} (C_{Lq})_{h(hf)} \quad (6.2.1-14)$$

where $(C_{Lq})_{h(hf)}$ and l_h are defined in section 6.1.1(c).

(d) By applying the preceding methods to the subject airplane, the pitching moments due to pitch rate, C_{mq} , were calculated and are presented in table 6.2.1-1 as a function of angle of attack and power condition on the basis of the original downwash calculations. The results are plotted in figure 6.2.1-1. Included are the results of calculations which included a 40-percent decrease in power-induced downwash at the tail. No experimental data were available for comparison.

6.2.2 Pitching Moment Due to Vertical Acceleration, $C_{m\dot{\alpha}}$

The contributions of the wing, fuselage, nacelles, and horizontal tail to the pitching moments due to vertical acceleration can be summarized in terms of reference wing area and wing mean aerodynamic chord by

$$C_{m\dot{\alpha}} = (C_{m\dot{\alpha}})_{w(wf)} + (C_{m\dot{\alpha}})_f + (C_{m\dot{\alpha}})_n + (C_{m\dot{\alpha}})_{h(hf)} \quad (6.2.2-1)$$

(a) The pitching-moment contribution of the wing due to vertical acceleration, $(C_{m\dot{\alpha}})_{w(wf)}$, with wing-fuselage interactions included, would normally be accounted for by an equation identical to equation (6.2.1-2) except for the substitution of $(C_{m\dot{\alpha}})_{we}$ for $(C_{mq})_{we}$. However, in the subsonic region, with the exception of triangular wing planforms, no explicit expression for $(C_{m\dot{\alpha}})_{we}$ is available. In the absence of suitable procedural information, $(C_{m\dot{\alpha}})_{w(wf)}$ is assumed to be zero. This assumption is acceptable as an approximation because, as pointed out in reference 1, tests indicate that this contribution for conventional configurations in subsonic flow is small.

(b) The pitching-moment contributions of the fuselage and nacelles due to vertical acceleration, $(C_{m\dot{\alpha}})_f + (C_{m\dot{\alpha}})_n$, are accounted for by the use of the following equation, which was arrived at in a manner synonymous to the derivation of the equation for body contribution to C_{Lq} (section 6.1.1(b)). Referenced to body base area, S_b , and body length, l_B , and a selected center of rotation (the center of gravity of the airplane),

$$(C_{m\dot{\alpha}})_{BS_b l_B} = 2(57.3) (C_{m\alpha})_{BS_b l_B} \frac{\frac{V_B}{S_b l_B} \left(\frac{x_{cB}}{l_B} - \frac{x_{mB}}{l_B} \right)}{\left[\left(1 - \frac{x_{mB}}{l_B} \right) - \frac{V_B}{S_b l_B} \right]} \quad (6.2.2-2)$$

Because the base area, S_b , is essentially zero in most general aviation aircraft, and particularly for the subject airplane, the preceding equation can be readily modified to express $(C_{m\dot{\alpha}})_B$ and $(C_{m\alpha})_B$ in terms of S_w and \bar{c}_w (as was done in equation (6.2.1-6) for $(C_{mq})_B$). With the modification accomplished and $(C_{m\alpha})_B$, which was obtained in section 4.7 about the leading edge of the mean aerodynamic chord, transferred to the center of gravity (eq. (6.2.1-9)), the following format is arrived at which, except for sign, is identical to equation (6.2.1-10):

$$(C_{m\dot{\alpha}})_B = -2(57.3) \left[(C_{m\alpha})_{B l_e} + (C_{L\alpha})_B \frac{x_{cg}}{\bar{c}_w} \right] \left(\frac{x_{cB}}{\bar{c}_w} - \frac{x_{mB}}{\bar{c}_w} \right) \quad (6.2.2-3)$$

Applied specifically to the fuselage and nacelles of the subject airplane, equation (6.2.2-3) becomes identical to equation (6.2.1-11), except for sign, or

$$(C_{m\dot{\alpha}})_f + (C_{m\dot{\alpha}})_n = -(C_{mq})_f - (C_{mq})_n \quad (6.2.2-4)$$

This result is interesting, inasmuch as, under certain conditions, such as short-period transient oscillations where both quantities appear in the working equation, the above

result indicates that the two quantities cancel each other.

(c) The pitching-moment contribution of the horizontal tail due to vertical acceleration, $(C_{m\dot{\alpha}})_{h(hf)}$, with the tail-fuselage interaction effects included, is accounted for by

$$(C_{m\dot{\alpha}})_{h(hf)} = -\frac{l_h}{\bar{c}_w} (C_{L\dot{\alpha}})_{h(hf)} \quad (6.2.2-5)$$

or, upon substitution for $(C_{L\dot{\alpha}})_{h(hf)}$ from equation (6.1.2-6),

$$(C_{m\dot{\alpha}})_{h(hf)} = -\frac{l_h}{\bar{c}_w} (C_{Lq})_{h(hf)} \frac{\partial \epsilon_h}{\partial \alpha_b} \quad (6.2.2-6)$$

An additional substitution from equation (6.2.1-14) results in

$$(C_{m\dot{\alpha}})_{h(hf)} = (C_{mq})_{h(hf)} \frac{\partial \epsilon_h}{\partial \alpha_b} \quad (6.2.2-7)$$

where $\frac{\partial \epsilon_h}{\partial \alpha_b}$ is as defined for equation (6.1.2-6).

(d) By applying the preceding methods to the subject airplane, the pitching moments due to the vertical acceleration were calculated and are presented in table 6.2.2-1 as a function of angle of attack and power condition. The results are plotted in figure 6.2.2-1. No experimental data were available for comparison.

6.2.3 Pitching Moments Due to Pitch Rate and Vertical Acceleration in Short-Period Transient Oscillations, $(C_{mq} + C_{m\dot{\alpha}})$

Although C_{mq} and $C_{m\dot{\alpha}}$ have been calculated as individual quantities, it is not simple to obtain experimental values of these individual quantities for comparison purposes.

In flight-test investigations, it is generally not practical to attempt to determine C_{mq} and $C_{m\dot{\alpha}}$ as individual quantities. To do so requires a well-conditioned maneuver and very accurate instrumentation. In this respect, an accurate determination of $\dot{\alpha}$ is generally not feasible and proper conditioning of a maneuver is difficult. As a result of these problems, flight test utilizes a control-fixed, short-period transient response maneuver to obtain a combined pitch-damping derivative, $C_{mq} + C_{m\dot{\alpha}}$.

In control-fixed, short-period transient response maneuvers, the pitch rate, q , and the vertical acceleration, $\dot{\alpha}$, are approximately in phase and are similar in magnitude. As a result, for this maneuver, the pitching moments due to pitch rate, q , and vertical acceleration, $\dot{\alpha}$, may be represented by the single combined derivative

$C_{m_q} + C_{m_{\dot{\alpha}}}$ as obtained from

$$\Delta C_m = C_{m_q} \frac{q\bar{c}_w}{2V} + C_{m_{\dot{\alpha}}} \frac{\dot{\alpha}\bar{c}_w}{2V} \approx (C_{m_q} + C_{m_{\dot{\alpha}}}) \frac{q\bar{c}_w}{2V} \quad (6.2.3-1)$$

Figure 6.2.3-1 compares flight-determined and calculated $C_{m_q} + C_{m_{\dot{\alpha}}}$ as a function of angle of attack and flight power condition. The flight-determined values were obtained by using the flight-determined damping ratio and frequency of oscillatory transient response, obtained by the methods of reference 38 and equation (143) in reference 37. The calculated values are based on the conditions where the power-induced downwash at the tail, $(\Delta\epsilon_h)_{\text{power}}$, was reduced 40 percent. Considering the scatter of flight-determined $C_{m_q} + C_{m_{\dot{\alpha}}}$, obtained from heavily damped transient responses, the calculated values reflect somewhat larger negative values than the flight values but show reasonably good correlation.

It should be noted that the calculated values of $C_{m_q} + C_{m_{\dot{\alpha}}}$ include the tail-lift carryover effects onto the fuselage. As indicated in sections 4.13-4 and 5.2, all evidence indicates that the tail-lift carryover onto the fuselage should have been considered to be similar to zero for the tail-fuselage configuration of the subject airplane. Had this been done in the present instance, the tail contribution would have been approximately 11 percent less and the calculated values of $C_{m_q} + C_{m_{\dot{\alpha}}}$ would have been, in general, approximately 11 percent smaller in magnitude than shown. This would have resulted in an improved correlation with the flight data.

6.2.4 Symbols

A_{we}	aspect ratio of the exposed portion of the wing
$B_2 = (1 - M^2 \cos^2 \Lambda_{c/4})^{1/2}$	
C_L	lift coefficient
$(C_{L\alpha})_B$	lift-curve slope of the body, referenced to the wing area, per deg
$(C_{L\alpha})_f, (C_{L\alpha})_n$	$(C_{L\alpha})_B$ applied specifically to the fuselage and the nacelle, respectively
$C_{L_{\dot{\alpha}}}, C_{L_q}$	$\frac{\partial C_L}{\partial \frac{\dot{\alpha}\bar{c}_w}{2V}}$ and $\frac{\partial C_L}{\partial \frac{q\bar{c}_w}{2V}}$, respectively, referenced to the wing area, per rad
$(C_{L_{\dot{\alpha}}})_{h(hf)}, (C_{L_q})_{h(hf)}$	contribution of the horizontal tail to $C_{L_{\dot{\alpha}}}$ and C_{L_q} , respectively, with tail-fuselage interaction effects included, per rad

C_m	pitching-moment coefficient
ΔC_m	increment of the pitching-moment coefficient about the center of gravity, referenced to wing area
$(C_{mq})_{fn}$	net contribution of the fuselage and nacelles to C_{mq}
$\left[(C_{mq})_{we} \right]_{M \approx 0.2}$, $\left[(C_{mq})_{we} \right]_{M > 0.2}$	$(C_{mq})_{we}$ at incompressible and compressible flow conditions, respectively
$C_{m_\alpha} = \frac{\partial C_m}{\partial \alpha_b}$, per deg	
$(C_{m_\alpha})_B$	C_{m_α} of the body about the center of gravity, referenced to the wing area, per deg
$(C_{m_\alpha})_{B_{le}}$	C_{m_α} of the body about the leading edge of the wing mean aerodynamic chord, referenced to the wing area, per deg
$(C_{m_\alpha})_{B_{sb}l_B}$	C_{m_α} of the body about the center of gravity referenced to the volume parameter, $S_b l_B$, per deg
$(C_{m_\alpha})_{f_{le}}, (C_{m_\alpha})_{n_{le}}$	$(C_{m_\alpha})_{B_{le}}$ applied specifically to the fuselage and nacelles, respectively
$C_{m_{\dot{\alpha}}}, C_{m_q}$	$\frac{\partial C_m}{\partial \frac{\dot{\alpha} \bar{c}_w}{2V}}$ and $\frac{\partial C_m}{\partial \frac{q \bar{c}_w}{2V}}$, respectively, about the center of gravity, referenced to the wing area, per rad
$(C_{m_{\dot{\alpha}}})_B, (C_{m_q})_B$	contribution of the body to $C_{m_{\dot{\alpha}}}$ and C_{m_q} , respectively
$(C_{m_{\dot{\alpha}}})_{B_{sb}l_B}, (C_{m_q})_{B_{sb}l_B}$	contribution of the body to $C_{m_{\dot{\alpha}}}$ and C_{m_q} , respectively, referenced to the body base area, S_b , and body length, l_B
$(C_{m_{\dot{\alpha}}})_f, (C_{m_q})_f$	$(C_{m_{\dot{\alpha}}})_B$ and $(C_{m_q})_B$, respectively, applied specifically to the fuselage
$(C_{m_{\dot{\alpha}}})_{h(hf)}, (C_{m_q})_{h(hf)}$	contribution of the horizontal tail to $C_{m_{\dot{\alpha}}}$ and C_{m_q} , respectively, with tail-fuselage interaction effects accounted for

$(C_{m\dot{\alpha}})_n, (C_{mq})_n$	$(C_{m\dot{\alpha}})_B$ and $(C_{mq})_B$, respectively, applied specifically to the nacelles
$(C_{m\dot{\alpha}})_{we}, (C_{mq})_{we}$	contribution of the exposed wing panels to $C_{m\dot{\alpha}}$ and C_{mq} , respectively, referenced to the area of the exposed panels
$(C_{m\dot{\alpha}})_{w(wf)}, (C_{mq})_{w(wf)}$	contribution of the wing to $C_{m\dot{\alpha}}$ and C_{mq} , respectively, with wing-fuselage interaction effects accounted for
c_{l_α}	section lift-curve slope, per deg
\bar{c}_w	mean aerodynamic chord of the wing, in. when used in ratio of dimensions, ft when used in derivatives
\bar{c}_{we}	mean aerodynamic chord of the exposed wing panels, in.
$K_{w(f)}, K_{f(w)}$	ratio of the lift on the wing in the presence of the fuselage and the lift carryover from the wing onto the fuselage, respectively, to the lift on the wing alone
k	a factor used in equation (6.2.1-3) to modify the theoretical equation for $[(C_{mq})_{we}]_{M \approx 0.2}$ to correlate with dynamic model data
l_B	length of the body, in. (ft when used with S_b in $S_b l_B$)
l_f, l_n	l_B applied specifically to the fuselage and the nacelles, respectively
l_h	distance from the center of gravity to the quarter chord of the tail mean aerodynamic chord, in.
M	Mach number
q	pitch rate, rad/sec
$\frac{\bar{q}_h}{\bar{q}_\infty}$	ratio of the dynamic pressure at the horizontal tail to the free-stream dynamic pressure
S_b	body base area, sq ft
$S_b l_B$	product of the body base area and body length, cu ft
S_w	wing area, sq ft
S_{we}	area of the exposed portion of the wing panels, sq ft

S_x	cross-section area of the body at distance x from the nose of the body, sq ft
T'_c	thrust coefficient
t	time, sec
x	distance from the nose of the body to the cross-sectional area, S_x , in.
x_{cB}	distance from the nose of body to the centroid of the body volume, in.
x_{cf}, x_{cn}	x_{cB} applied specifically to the fuselage and nacelle, respectively, in.
x_{cg}	distance from the leading edge of the wing mean aerodynamic chord to the center of gravity of the airplane, in.
x_{mB}	distance from the nose of the body to the center of gravity of the airplane, in.
x_{mf}, x_{mn}	x_{mB} applied specifically to the fuselage and nacelles, respectively, in.
$\frac{\bar{x}}{\bar{c}_{we}}$	distance from the wing aerodynamic center to the center of gravity of the airplane as a fraction of the exposed panel mean aerodynamic chord, positive forward, in.
V	airspeed, ft/sec
V_B	volume of the body, cu ft
V_f, V_n	V_B applied specifically to the fuselage and nacelle, respectively
α_b	airplane angle of attack, deg
$\dot{\alpha} = \frac{\partial \alpha_b}{\partial t}$	
ϵ_h	downwash angle at the horizontal tail, deg
$(\Delta \epsilon_h)_{\text{power}}$	increment of the downwash angle at the horizontal tail due to power, deg
$\Lambda_{c/4}$	sweep of the quarter-chord line, deg

TABLE 6.2.1-1
PITCHING MOMENTS DUE TO PITCH RATE, C_{mq}

[Flight center of gravity = $0.12 \bar{c}_w$]

(a) Contribution of wing, $(C_{mq})_{w(wf)}$

$$(C_{mq})_{w(wf)} = [K_{w(f)} + K_{f(w)}] \left(\frac{\bar{c}_{we}}{\bar{c}_w} \right) \left(\frac{\bar{c}_{we}}{\bar{c}_w} \right)^2 (C_{mq})_{we}$$

where

$$(C_{mq})_{we} = -0.7(57.3 c_{l\alpha}) \cos \Lambda_{c/4} \left\{ \frac{A_{we} \left[\frac{1}{2} \frac{\bar{x}}{\bar{c}_{we}} + 2 \left(\frac{\bar{x}}{\bar{c}_{we}} \right)^2 \right]}{A_{we} + 2 \cos \Lambda_{c/4}} + \frac{1}{24} \left(\frac{A_{we}^3 \tan^2 \Lambda_{c/4}}{A_{we} + 6 \cos \Lambda_{c/4}} \right) + \frac{1}{8} \right\}$$

Symbol	Description	Reference	Magnitude
$c_{l\alpha}$	Section lift-curve slope, per deg	Table 4.1-1	0.095
A_{we}	Aspect ratio of exposed portion of wing	Table 3.2-1	6.9
$\Lambda_{c/4}$	Sweepback of wing quarter-chord line, deg	Table 3.2-1	-2.5
$\frac{\bar{x}}{\bar{c}_{we}}$	Distance of the center of gravity from the aerodynamic center of the exposed wing panels mean aerodynamic chord as a fraction of \bar{c}_{we}	Table 6.1.1-1(a)	.124
$(C_{mq})_{we}$	Per radian for flight center of gravity of $0.12 \bar{c}_w$	Equation (6.2.1-3)	-0.757
$K_{w(f)}$	Ratio of lift on wing in presence of body to wing alone	Table 4.4-1	1.09
$K_{f(w)}$	Ratio of wing-lift carryover on body to wing alone	Table 4.4-1	.14
S_{we}	Area of exposed wing panels, sq ft	Table 3.2-1	148
S_w	Reference wing area, sq ft	Table 3-1	178
\bar{c}_{we}	Mean aerodynamic chord of exposed wing panels, in.	Table 3.2-1	57.1
\bar{c}_w	Mean aerodynamic chord of complete wing, in.	Table 3.2-1	59.5
Summary: $(C_{mq})_{w(wf)} = -0.743$ per rad			

(b) Contributions of fuselage and nacelles, $(C_{mq})_f + (C_{mq})_n$

$$(C_{mq})_f + (C_{mq})_n = 2(57.3) \left[(C_{m\alpha})_{f_{le}} + (C_{L\alpha})_f \frac{x_{cg}}{\bar{c}_w} \right] \left(\frac{x_{cf}}{\bar{c}_w} - \frac{x_{mf}}{\bar{c}_w} \right) + 2(57.3) \left[(C_{m\alpha})_{n_{le}} + (C_{L\alpha})_n \frac{x_{cg}}{\bar{c}_w} \right] \left(\frac{x_{cn}}{\bar{c}_w} - \frac{x_{mn}}{\bar{c}_w} \right)$$

Symbol	Description	Reference	Magnitude	
			Fuselage	Nacelles
S_w	Reference wing area, sq ft	Table 3-1	178	178
\bar{c}_w	Mean aerodynamic chord of the wing, in.	Table 3.2-1	59.5	59.5
$(C_{m\alpha})_{B_{le}}$	$C_{m\alpha}$ of body about leading edge of wing mean aerodynamic chord, based on potential flow only, referenced to $S_w = 178$ sq ft	Table 4.7-1	0.00216 per deg	0.00147 per deg
$(C_{L\alpha})_B$	Lift-curve slope of body based on potential flow only; referenced to $S_w = 178$ sq ft, per deg	Table 4.3-1	.00212	.00155
$\frac{x_{cg}}{\bar{c}_w}$	Distance of the center of gravity from the leading edge of the wing mean aerodynamic chord as ratio of the mean aerodynamic chord	Flight data	0.12	0.12
x_{cB}	Distance from nose of body to centroid of body volume, $\frac{\int_0^{l_B} S_x x dx}{12V_B}$, in.	-----	≈ 147.7	-----
x_{mB}	Distance from nose of body to the center of gravity of the airplane, in.	Figure 3.2-1	100.33	60.14
Summary: $(C_{mq})_f + (C_{mq})_n = 0.220 - 0.088 = 0.132$ per rad				

TABLE 6.2.1-1 (Concluded)

(c) Contribution of horizontal tail, $(C_{mq})_{h(hf)}$

$$(C_{mq})_{h(hf)} = -\frac{l_h}{\bar{c}_w} (C_{Lq})_{h(hf)}$$

Symbol	Description	Reference	Magnitude
S_w	Reference wing area, sq ft	Table 3-1	178
\bar{c}_w	Wing mean aerodynamic chord, in.	Table 3.2-1	59.5
l_h	Distance from reference (flight) center of gravity to the quarter chord of the tail, in.	Figure 3.2-2	172.75
$(C_{Lq})_{h(hf)}$	Rate of change of tail lift with pitch rate, $\frac{\partial C_L}{\partial \frac{q \bar{c}_w}{2V}}$ per rad	Table 6.1.1-1(c)	$4.53 \left(\frac{\bar{q}_h}{\bar{q}_\infty} \right)$
$\frac{\bar{q}_h}{\bar{q}_\infty}$	Dynamic-pressure ratio at tail with power on	Table 6.1.1-1(d), column 2	As per table 6.1.1-1(d), column 2
Summary: $(C_{mq})_{h(hf)} = -13.152 \left(\frac{\bar{q}_h}{\bar{q}_\infty} \right)$ per rad			

(d) Pitching moment due to pitch rate, C_{mq}

$$\begin{aligned}
 C_{mq} &= (C_{mq})_{w(wf)} + (C_{mq})_f + (C_{mq})_n + (C_{mq})_{h(hf)} \\
 &= -0.743 + 0.132 - 13.152 \left(\frac{\bar{q}_h}{\bar{q}_\infty} \right) \\
 &= -0.611 - 13.152 \left(\frac{\bar{q}_h}{\bar{q}_\infty} \right)
 \end{aligned}$$

①	②			③		
-----	Table 6.1.1-1(d), column 2			-----		
α_b , deg	$\frac{\bar{q}_h}{\bar{q}_\infty}$			$C_{mq} = -0.611 - 13.152 \text{ ②}$		
	T'_c			T'_c		
	0	0.20	0.44	0	0.20	0.44
-4	1.0	1.0868	1.2027	-13.76	-14.90	-16.43
-2	1.0	1.1028	1.2108	-13.76	-15.12	-16.54
0	1.0	1.1167	1.2216	-13.76	-15.30	-16.68
2	1.0	1.1222	1.2324	-13.76	-15.37	-16.82
4	1.0	1.1333	1.2432	-13.76	-15.52	-16.96
6	1.0	1.1389	1.2541	-13.76	-15.60	-17.10
8	1.0	1.1344	1.2622	-13.76	-15.66	-17.21
10	1.0	1.1417	1.2676	-13.76	-15.63	-17.28
12	1.0	1.1361	1.2757	-13.76	-15.55	-17.39
^a 13.8	1.0	1.1278	1.2811	-13.76	-15.44	-17.46
^b 14.1	---	1.1222	1.2811	-----	-15.37	-17.46
^c 14.4	---	-----	1.2784	-----	-----	-17.42

^{a,b,c}Stall angles for $T'_c = 0, 0.20, 0.44$ power conditions, respectively.

TABLE 6.2.2-1
PITCHING MOMENT DUE TO VERTICAL ACCELERATION, $C_{m\dot{\alpha}}$
[Flight center of gravity = $0.12 \bar{c}_w$]

(a) Contribution of wing, $(C_{m\dot{\alpha}})_{w(wf)}$

In accordance with discussion in section 6.2.2(a),

$$(C_{m\dot{\alpha}})_{w(wf)} = 0$$

(b) Contributions of fuselage and nacelles, $(C_{m\dot{\alpha}})_f + (C_{m\dot{\alpha}})_n$

Since, in accordance with equation (6.2.2-4),

$$(C_{m\dot{\alpha}})_f + (C_{m\dot{\alpha}})_n = -[(C_{mq})_f + (C_{mq})_n]$$

then, from table 6.2.1-1(b)

$$(C_{m\dot{\alpha}})_f + (C_{m\dot{\alpha}})_n = -0.132 \text{ per rad}$$

(c) Contribution of horizontal tail, $(C_{m\dot{\alpha}})_{h(hf)}$

Since, in accordance with equation (6.2.2-7),

$$(C_{m\dot{\alpha}})_{h(hf)} = (C_{mq})_{h(hf)} \frac{\partial \epsilon_h}{\partial \alpha_b}$$

then, on the basis of the calculated value of $(C_{mq})_{h(hf)}$ in table 6.2.1-1(c),

$$(C_{m\dot{\alpha}})_{h(hf)} = -13.152 \left(\frac{\bar{q}_h}{\bar{q}_\infty} \right) \frac{\partial \epsilon_h}{\partial \alpha_b}$$

where

$$\left(\frac{\bar{q}_h}{\bar{q}_\infty} \right) \frac{\partial \epsilon_h}{\partial \alpha_b} \text{ are obtained from table 6.1.2-1(d)}$$

(d) Pitching moments due to vertical acceleration, $C_{m\dot{\alpha}}$

$$C_{m\dot{\alpha}} = (C_{m\dot{\alpha}})_{w(wf)} + (C_{m\dot{\alpha}})_f + (C_{m\dot{\alpha}})_n + (C_{m\dot{\alpha}})_{h(hf)}$$

$$= 0 - 0.132 - 13.152 \left(\frac{\bar{q}_h}{\bar{q}_\infty} \right) \frac{\partial \epsilon_h}{\partial \alpha_b}$$

$$= -0.132 - 13.152 \left(\frac{\bar{q}_h}{\bar{q}_\infty} \right) \frac{\partial \epsilon_h}{\partial \alpha_b}$$

①	②			③			④		
-----	Table 6.1.2-1(d), column 2			Table 6.1.2-1(d), column 3			-----		
α_b , deg	$\frac{\bar{q}_h}{\bar{q}_\infty}$			$\frac{\partial \epsilon_h}{\partial \alpha_b}$			$C_{m\dot{\alpha}} = -0.132$ $- 13.152 \text{ ②③}$		
	T'_c			T'_c			T'_c		
	0	0.20	0.44	0	0.20	0.44	0	0.20	0.44
-4	1.0	1.0868	1.2027	-----	-----	-----	-----	-----	-----
-2	1.0	1.1028	1.2108	0.475	0.785	0.915	-6.38	-11.52	-14.70
0	1.0	1.1167	1.2216	0.475	0.775	0.920	-6.38	-11.51	-14.91
2	1.0	1.1222	1.2324	.475	.760	.905	-6.38	-11.35	-14.80
4	1.0	1.1333	1.2432	0.475	0.730	0.865	-6.38	-11.01	-14.28
6	1.0	1.1389	1.2541	.475	.680	.810	-6.38	-10.32	-13.49
8	1.0	1.1444	1.2622	0.470	0.640	0.740	-6.31	-9.76	-12.42
10	1.0	1.1417	1.2676	.450	.600	.670	-6.05	-9.14	-11.30
12	1.0	1.1361	1.2757	0.425	0.530	0.589	-5.72	-8.05	-10.01
^a 13.8	1.0	1.1278	1.2811	.405	.475	.500	-5.46	-7.18	-8.56
^b 14.1	---	1.1222	1.2811	-----	0.470	0.470	-----	-7.07	-8.05
^c 14.4	---	-----	1.2784	-----	-----	.450	-----	-----	-7.70

^{a,b,c} Stall angles for $T'_c = 0, 0.20, 0.44$ power conditions, respectively.

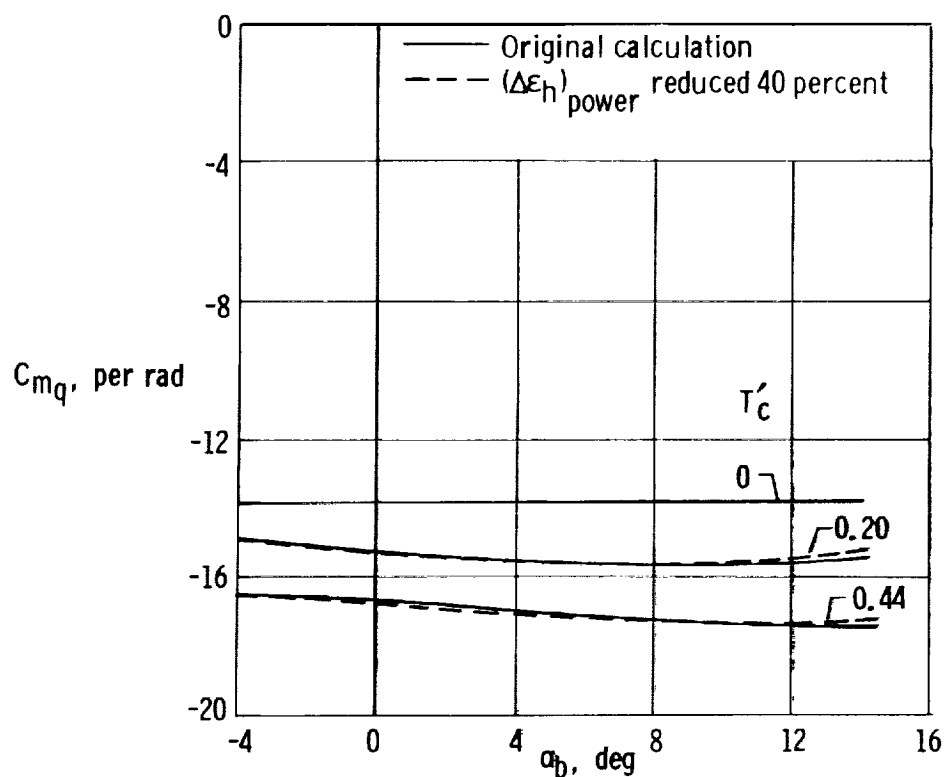


Figure 6.2.1-1. Variation of calculated pitching moment due to pitch rate, C_{m_q} , with angle of attack and power. Center of gravity = $0.12 \bar{c}_w$.

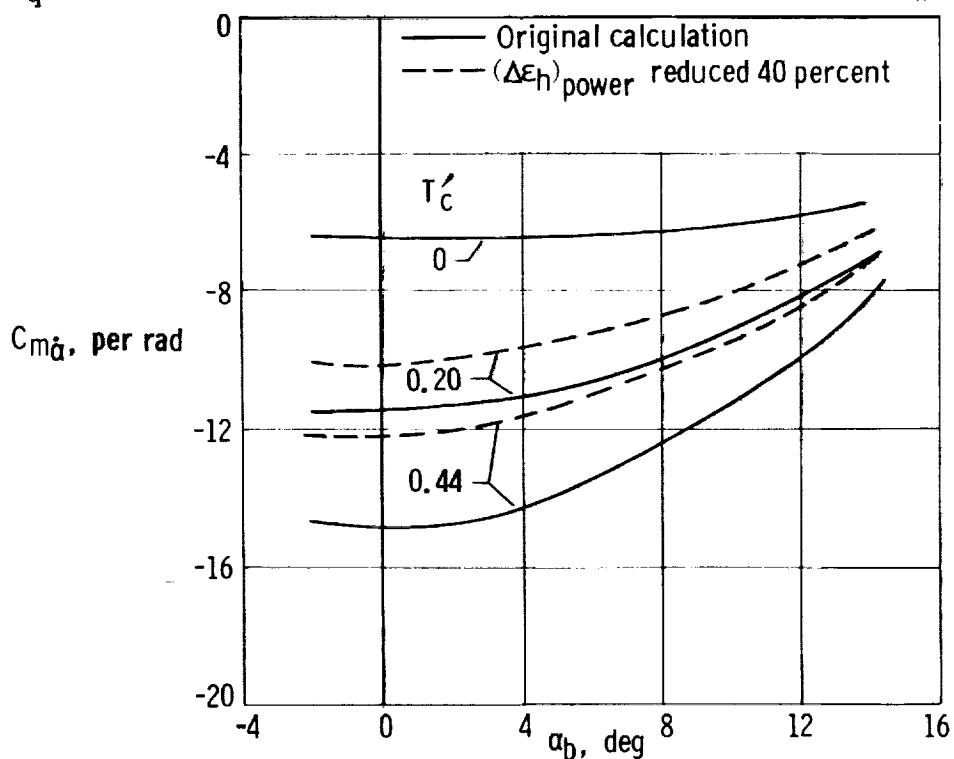


Figure 6.2.2-1. Variation of calculated pitching moment due to vertical acceleration, $C_{m_{\dot{\alpha}}}$, with angle of attack and power. Center of gravity = $0.12 \bar{c}_w$.

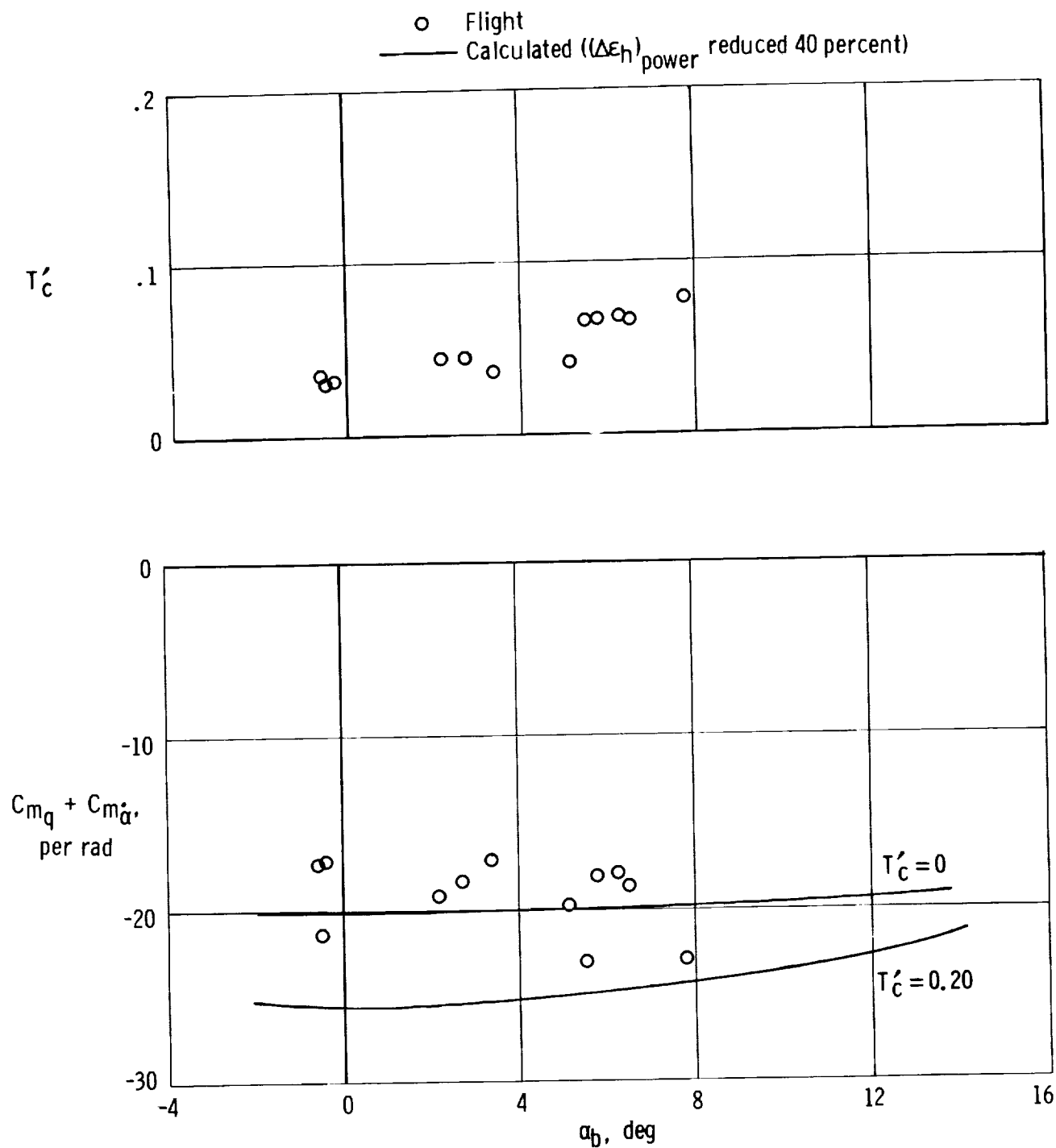


Figure 6.2.3-1. Comparison of calculated $C_{m_q} + C_{m_{\dot{\alpha}}}$ with flight-determined values obtained from transient short-period pulse maneuvers. Center of gravity = $0.12 \bar{c}_w$.

6.3 Short-Period Transient Oscillation Characteristics

During control-fixed longitudinal short-period transient oscillations, the airplane is presumed to be oscillating at a constant velocity, V . It is thus considered to be constrained to two degrees of freedom represented by the following small-perturbation equations:

Lift

$$W(\Delta a_n) = mV(\Delta q - \Delta \dot{\alpha}) = \left(C_{L\alpha} \Delta \alpha + C_{Lq} \Delta q \frac{\bar{c}_w}{2V} + C_{L\dot{\alpha}} \Delta \dot{\alpha} \frac{\bar{c}_w}{2V} \right) \bar{q} S_w \quad (6.3-1)$$

Moment

$$I_Y \Delta \dot{q} = \left(C_{m\alpha} \Delta \alpha + C_{mq} \Delta q \frac{\bar{c}_w}{2V} + C_{m\dot{\alpha}} \Delta \dot{\alpha} \frac{\bar{c}_w}{2V} \right) \bar{q} S_w \bar{c}_w \quad (6.3-2)$$

where, for present purposes, all derivatives and motions are in radians.

Differentiating equation(6.3-1) with respect to time and substituting for $\Delta \dot{q}$ and Δq in equation (6.3-2) provides the following result (after removing negligible quantities):

$$\Delta \ddot{\alpha} + \frac{1}{2\tau} \left[C_{L\alpha} - \frac{m \bar{c}_w^2}{2I_Y} (C_{mq} + C_{m\dot{\alpha}}) \right] \Delta \dot{\alpha} - \left(C_{m\alpha} + \frac{C_{mq} C_{L\alpha}}{4\mu_c} \right) \frac{\bar{q} S_w \bar{c}_w}{I_Y} \Delta \alpha = 0 \quad (6.3-3)$$

where

m is the mass density of the airplane $\left(\frac{W}{g}\right)$, slugs

I_Y is the moment of inertia about the Y-axis, slug-ft²

τ is a time parameter equal to $\frac{m}{\rho V S_w}$, seconds

μ_c is the relative aircraft density, $\frac{m}{\rho S_w \bar{c}_w}$

ρ is the mass density of the air, slugs/cubic foot

V is the airspeed, feet/second

Because equation (6.3-3) is a second-order differential equation of the form

$$\Delta \ddot{\alpha} + 2\zeta \omega_n \Delta \dot{\alpha} + \omega_n^2 \Delta \alpha = 0 \quad (6.3-4)$$

then undamped natural frequency

$$\omega_n = \sqrt{\frac{\bar{q} S_w \bar{c}_w}{I_Y} \left(C_{m_\alpha} + \frac{C_{m_q} C_{L_\alpha}}{4 \mu_c} \right)} \quad (6.3-5)$$

and damping ratio

$$\xi = \frac{(\omega_n \xi)}{\omega_n} = \frac{1}{2\tau\omega_n} \left[C_{L_\alpha} - \frac{m \bar{c}_w^2}{2I_Y} (C_{m_q} + C_{m_{\dot{\alpha}}}) \right] \quad (6.3-6)$$

The damped natural frequency can be obtained from

$$\omega_{nd} = \omega_n \sqrt{1 - \xi^2} \quad (6.3-7)$$

When the short-period transient oscillatory characteristics are to be expressed in terms of period of damped oscillations and the time-to-damp-to-one-half amplitude,

$$P = \frac{2\pi}{\omega_{nd}} \quad (6.3-8)$$

and

$$T_{1/2} = \frac{0.693}{\xi \omega_n} \quad (6.3-9)$$

The preceding relations were applied to the calculation of the short-period P and $T_{1/2}$ characteristics of the subject airplane at an altitude of 6000 feet and a nominal weight of 3380 pounds. The derivatives C_{L_α} , C_{m_α} , and $C_{m_{\dot{\alpha}}}$ were based on calculated data in which the power-induced downwash at the horizontal tail, $\Delta\epsilon_h$ power, was reduced 40 percent. The calculated P and $T_{1/2}$ characteristics show good correlation with flight data in figure 6.3-1. The consistency of the flight data points reflects the care exercised in applying the technique of reference 38 to the flight time histories, which involved damping ratios of the order of 0.7.

Figure 6.3-2 shows a typical flight time history used in the analysis. The figure also shows comparative calculated time-histories based on flight-determined and calculated derivatives using equations (6.3-1) and (6.3-2) to which $C_{L_{\delta_e}} \Delta\delta_e$ and $C_{m_{\delta_e}} \Delta\delta_e$, respectively, were added. The $\Delta\delta_e$ input shown in figure 6.3-2 was used in both calculated time histories. The calculated time histories were obtained from a computerized solution of the standard linearized equations of motion.

6.3.1 Symbols

$a_n, \Delta a_n$ load factor and perturbed value of the load factor, respectively, g units

C_L	lift coefficient referenced to the wing area
$C_{L\alpha} = \frac{\partial C_L}{\partial \alpha_b}$, per rad	
$C_{L\dot{\alpha}} = \frac{\partial C_L}{\partial \frac{\dot{\alpha} \bar{c}_w}{2V}}$, per rad	
$C_{Lq} = \frac{\partial C_L}{\partial \frac{q \bar{c}_w}{2V}}$, per rad	
$C_{L\bar{\delta}_e}$	$\frac{\partial C_L}{\partial \bar{\delta}_e}$ with the elevator tab geared to move with the elevator and accounted for, per rad
C_m	pitching-moment coefficient referenced to the wing area and mean aerodynamic chord of the wing
$C_{m\alpha} = \frac{\partial C_m}{\partial \alpha_b}$, per rad	
$C_{m\dot{\alpha}} = \frac{\partial C_m}{\partial \frac{\dot{\alpha} \bar{c}_w}{2V}}$, per rad	
$C_{mq} = \frac{\partial C_m}{\partial \frac{q \bar{c}_w}{2V}}$, per rad	
$C_{m\bar{\delta}_e}$	$\frac{\partial C_m}{\partial \bar{\delta}_e}$ with the elevator tab geared to move with the elevator and accounted for, per rad
\bar{c}_w	mean aerodynamic chord of the wing, ft
g	gravitational acceleration, ft/sec ²
I_Y	mass moment of inertia of the airplane about the Y-body axis (pitch axis), slug-ft ²
m	airplane mass, $\frac{W}{g}$, slugs
P	period of the short-period transient oscillations, sec
q	pitch rate, rad/sec

\bar{q}	free-stream dynamic pressure, lb/sq ft
$q, \Delta q$	pitch rate and perturbed value of pitch rate, respectively, rad/sec unless indicated otherwise
$\dot{q}, \Delta \dot{q}$	pitch acceleration and perturbed value of pitch acceleration, respectively, rad/sec ² unless indicated otherwise
S_w	wing area, sq ft
T'_c	thrust coefficient
$T_{1/2}$	time for the short-period transient oscillation to damp to half amplitude, sec
t	time, sec
V	airspeed, ft/sec
V_c	calibrated airspeed, knots
W	airplane weight, lb
α, α_b	airplane angle of attack relative to the X-body axis, rad unless indicated otherwise
$\Delta \alpha$	perturbed value of α_b , rad
$\Delta \dot{\alpha}$	perturbed value of the time rate of change of α_b , rad/sec
$\Delta \ddot{\alpha}$	perturbed value of the acceleration of α_b , rad/sec ²
$\delta_e, \Delta \delta_e$	elevator deflection and perturbed value of elevator deflection, respectively, rad unless indicated otherwise
$(\Delta \epsilon_h)_{\text{power}}$	increment of downwash at the horizontal tail due to power, deg
ζ	damping ratio of the short-period transient oscillation
μ_c	relative airplane density, $\frac{m}{\rho S_w \bar{c}_w}$
ρ	mass density of the air, slugs/cu ft
τ	time parameter, $\frac{m}{\rho V S_w}$, sec
ω_n	undamped natural frequency of the short-period transient oscillation, rad/sec
ω_{nd}	damped natural frequency

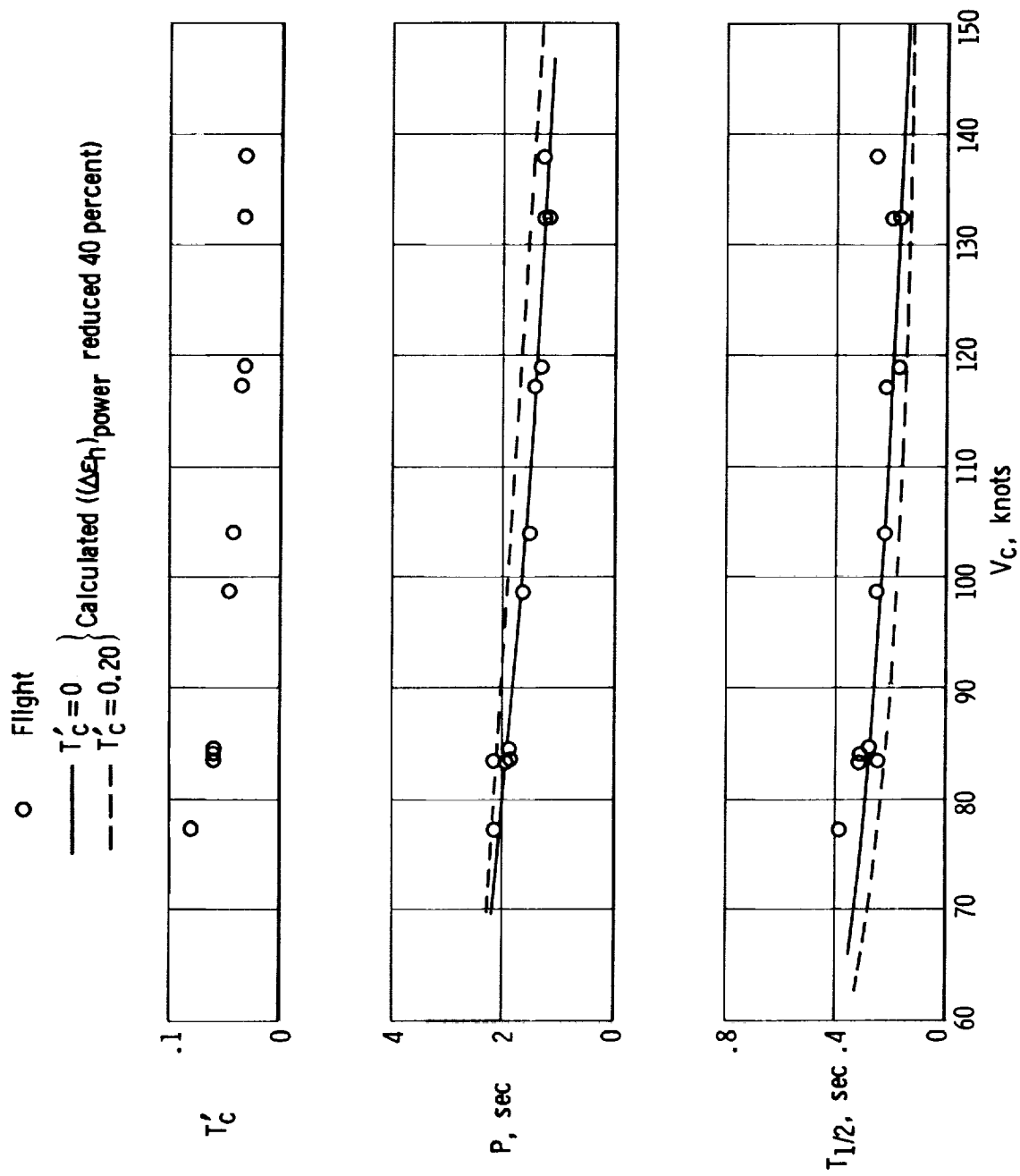


Figure 6.3-1. Comparison of calculated short-period frequency and damping characteristics with flight-determined values as a function of airspeed. Center of gravity = $0.12\bar{c}_w$.

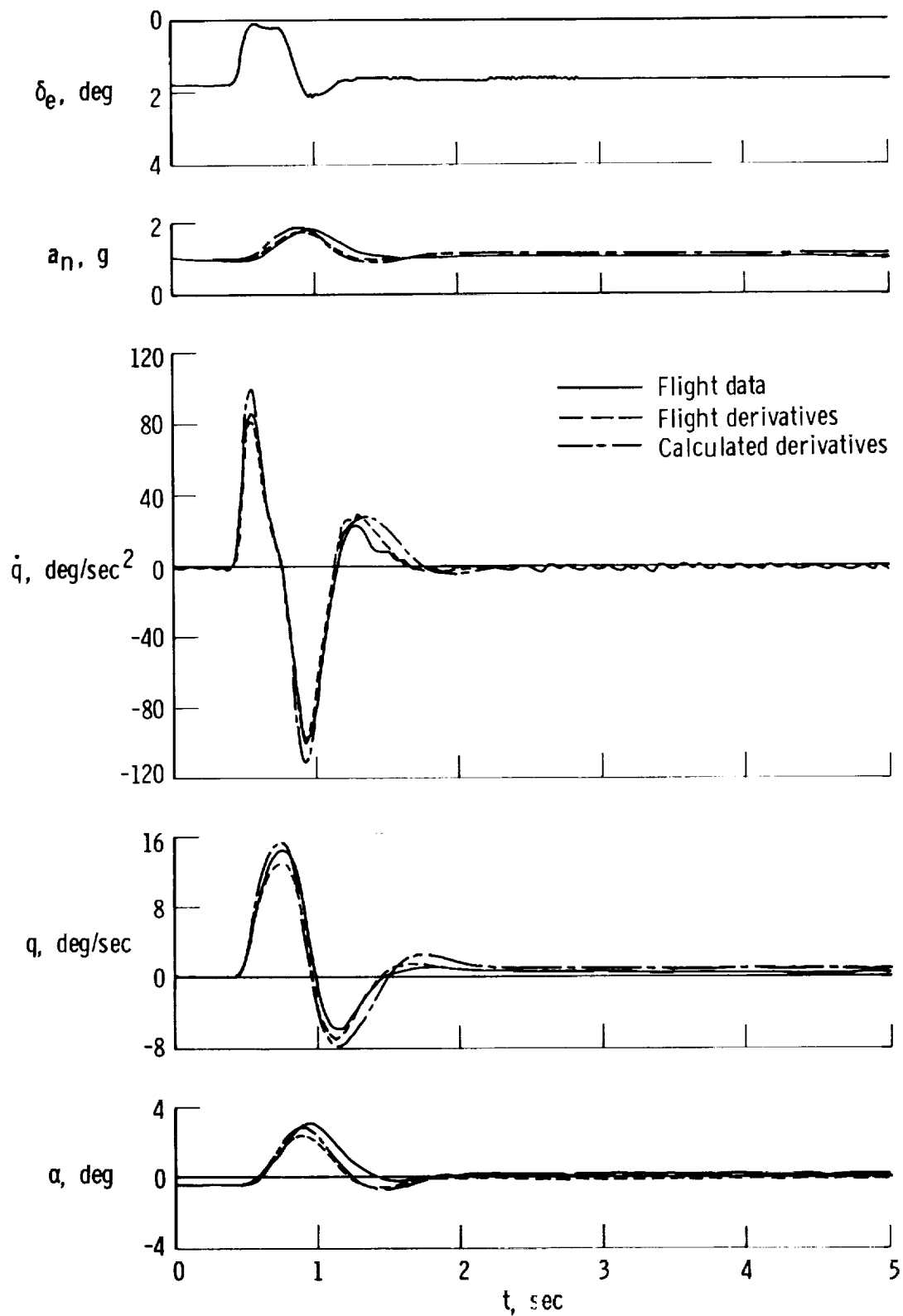


Figure 6.3-2. Comparison of calculated and flight-determined time histories of airplane response to pulse-type input. Center of gravity = $0.12\bar{c}_w$.

6.4 Windup-Turn Characteristics

In considering the calculation of the windup-turn characteristics (expressed as the variation of elevator displacement and stick force as a function of load factor), the airplane is normally assumed to be maneuvering at constant weight, center of gravity, altitude, and velocity. In addition, the maneuver is considered to be performed in steps rather than as a steadily tightening turn, thereby eliminating pitching acceleration, \dot{q} , and vertical acceleration, \dot{a}_n , from consideration. As a result of these constraints, the windup turn is represented by the following two equations when the maneuver is initiated from trim level flight:

$$C_L = C_{L\alpha}(\alpha_b - \alpha_o) + C_{Lq} \frac{q\bar{c}_w}{2V} + C_{L\bar{\delta}_e} \delta_e \left(\frac{\bar{q}_h}{\bar{q}_\infty} \right) + C_{L\delta_{tab}} (\delta_{tab})_o \frac{S_h}{S_w} \left(\frac{\bar{q}_h}{\bar{q}_\infty} \right) \quad (6.4-1)$$

$$C_m = C_{m_o} + C_{m\alpha}(\alpha_b - \alpha_o) + C_{mq} \frac{q\bar{c}_w}{2V} + C_{m\bar{\delta}_e} \delta_e \left(\frac{\bar{q}_h}{\bar{q}_\infty} \right) - C_{L\delta_{tab}} (\delta_{tab})_o \frac{l_h}{\bar{c}_w} \frac{S_h}{S_w} \left(\frac{\bar{q}_h}{\bar{q}_\infty} \right) \quad (6.4-2)$$

where

$$C_L = \frac{a_n W}{\bar{q}_\infty S_w} \quad (6.4-3)$$

and, from reference 43,

$$q = \frac{g}{V} \left(a_n - \frac{1}{a_n} \right) \quad (6.4-4)$$

$C_{L\bar{\delta}_e}$ and $C_{m\bar{\delta}_e}$ are control-effectiveness terms including the effect of the tab geared to the elevator as determined in section 4.13, based on wing area

$C_{L\delta_{tab}} (\delta_{tab})_o$ is the lift due to the trim setting of the tab when $\delta_e = 0^\circ$, based on horizontal-tail area, S_h , obtained from section 4.13

l_h is the distance from the center of gravity to the quarter-chord point of the tail mean aerodynamic chord, obtained from figure 3.2-2

6.4.1 Variation of α_{trim} and $\delta_{e_{trim}}$ With Load Factor

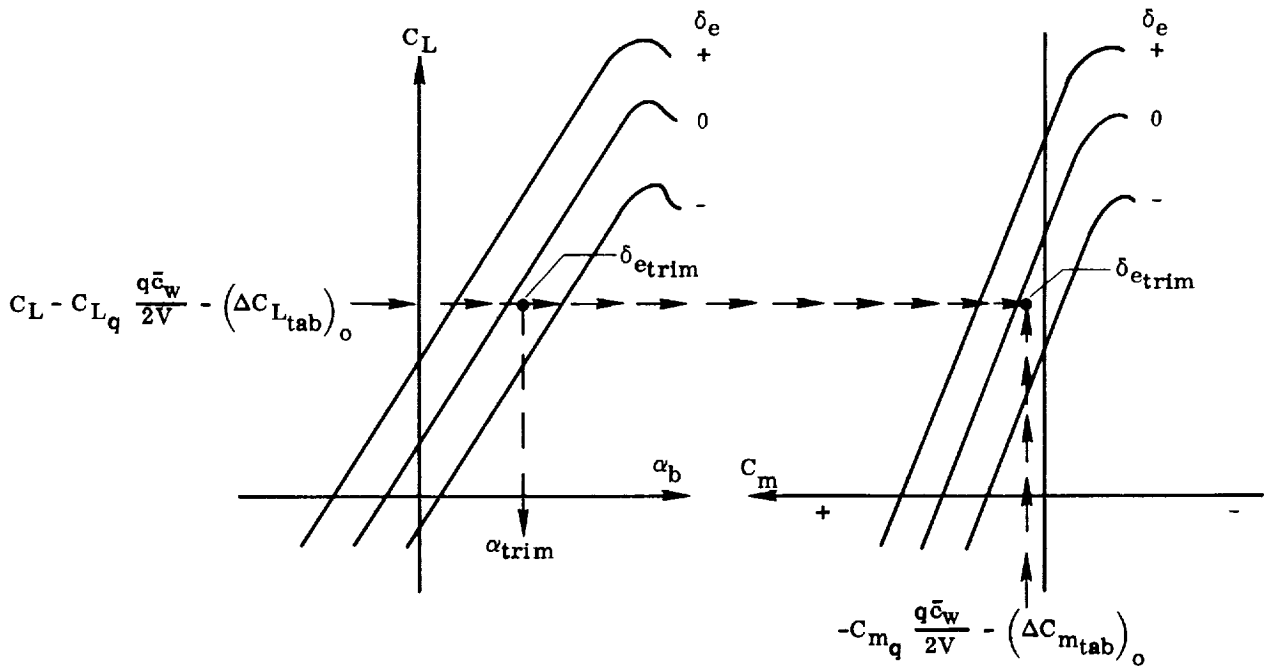
To obtain the variation of α_{trim} and $\delta_{e_{trim}}$ with load factor, a_n , equations (6.4-1) and (6.4-2) are transposed to the following format:

$$C_L - C_{Lq} \frac{q\bar{c}_w}{2V} - (\Delta C_{L_{tab}})_0 = C_{L\alpha}(\alpha_b - \alpha_0) + C_{L\delta_e} \delta_e \left(\frac{\bar{q}_h}{\bar{q}_\infty} \right) \quad (6.4.1-1)$$

$$- C_{mq} \frac{q\bar{c}_w}{2V} - (\Delta C_{m_{tab}})_0 = C_{m_0} + C_{m\alpha}(\alpha_b - \alpha_0) + C_{m\delta_e} \delta_e \left(\frac{\bar{q}_h}{\bar{q}_\infty} \right) \quad (6.4.1-2)$$

The right-hand side of equations (6.4.1-1) and (6.4.1-2) are the static-lift and pitching-moment equations, respectively, with trim tab at zero setting when $\delta_e = 0^\circ$, represented by the lift curves of figure 5.1.3-1 and the pitching-moment curves of figures 5.2-3 and 5.2-4.

The left-hand side of equations (6.4.1-1) and (6.4.1-2) can be considered as the equivalent net static lift and pitching moments to be applied to the C_L versus α and C_m versus C_L plots (figs. 5.1.3-1 and 5.2-4), as shown in the following sketch, to obtain α_{trim} and $\delta_{e_{trim}}$. The $\delta_{e_{trim}}$ obtained from the point of intersection of the left-hand quantities (of eqs. (6.4.1-1) and (6.4.1-2)) on the C_m versus C_L plot is used to obtain α_{trim} on the C_L versus α_b plot.



In applying this procedure, the curves on the C_m versus C_L plot are oriented to be representative of the center-of-gravity condition being analyzed. Also, when the power condition being analyzed is between two plotted power conditions, the α_{trim}

and $\delta_{e\text{trim}}$ are obtained for the two bracketing power conditions and interpolated for the desired power condition.

There still remains the problem of determining the equivalent net static lift and pitching moment (the left-hand side of eqs. (6.4.1-1) and (6.4.1-2)). Considering that the altitude and velocity of the windup turn would be known, and α_{trim} and $\delta_{e\text{trim}}$ are to be determined for selected load factors, a_n , it remains to determine the thrust coefficient and the dynamic derivatives, C_{Lq} and C_{mq} , which are functions of α_{trim} and T'_c . The dynamic-pressure ratio of the horizontal tail is also required to be used in the increments of lift and pitching moments due to the trim setting of the tab, $(\Delta C_{L\text{tab}})_0$ and $(\Delta C_{m\text{tab}})_0$. The determination of these quantities involves an iteration procedure to arrive at trim conditions. The procedure is best explained by tracing its application in table 6.4-1 to the subject airplane as follows:

(a) The calculations to be performed are for altitude, velocity, weight, and load-factor conditions of actual flight data for the purpose of comparing the degree of correlation between calculated and flight characteristics. In the absence of flight data, the velocity, weight, and altitude would be considered to be constant.

(b) Table 6.4.1-1(a) lists pertinent known and required parameters.

(c) In table 6.4.1-1(b) columns 1 to 4 list the stipulated conditions for the analysis. Columns 5 and 7 list the corresponding calculated pitch rates and lift coefficients in accordance with equations (6.4-4) and (6.4-3), respectively.

(d) Using C_L determined in column 7, obtain the first estimate of total T'_c from figure 5.3-5 for a drag coefficient of zero.

(e) Using C_L and total T'_c from columns 7 and 8, and considering C_m to be equal to zero, obtain the first approximation of α_{trim} and $\delta_{e\text{trim}}$ from figures 5.1.3-1 and 5.2-4. Figure 5.2-4 must be oriented to the center of gravity being considered.

(f) Using total T'_c and α_{trim} from columns 8 and 9, obtain the first estimate of C_{Lq} , C_{mq} , and $\frac{\bar{q}_h}{\bar{q}_\infty}$ from figures 6.1.1-1, 6.2.1-1, and 5.1.2-5, respectively.

(g) The results of the first approximations are now used to obtain equivalent net static lift and pitching moments (columns 14 and 16, respectively) which are now used to obtain the first iterated values of total T'_c , α_{trim} , $\delta_{e\text{trim}}$, C_{Lq} , C_{mq} , and $\frac{\bar{q}_h}{\bar{q}_\infty}$, in columns 15 and columns 17 to 21.

(h) The iteration procedure is repeated, as indicated in table 6.4.1-1(b), until

satisfactory convergence is achieved. Two iterations will normally be sufficient.

The predicted variations of total T'_c , α_{trim} , and $\delta_{e_{trim}}$, obtained from preceding calculations based on calculated characteristics, are compared with flight data in figure 6.4.2-1. Also shown in the figure are the predicted variations, based on wind-tunnel data, obtained by using the foregoing procedure.

6.4.2 Variation of Hinge Moments and Stick Forces With Load Factor

The equation for stick forces was derived in section 4.14.1. For the subject airplane the stick forces are represented by

$$F_{stick} = 40 C_{hh(f)} \bar{q}_\infty \quad (4.14.1-20)$$

The hinge moment of the horizontal tail referenced to the tail area, S_h , and a dynamic-pressure ratio of 1.0 were shown, in section 4.14.1, to be represented by

$$C_{hh(f)} = \bar{C}_{Lh(f)} \frac{(x_{hinge} - x_{\bar{c}}/4)h}{\bar{c}_h} + (\Delta C'_m)_{\delta_{tab}} \quad (4.14.1-3)$$

where

$\bar{C}_{Lh(f)}$ is the net lift coefficient of the tail in the presence of the body as a function of α_h , δ_e , and δ_{tab}

$(\Delta C'_m)_{\delta_{tab}}$ is the pitching moment about the quarter-chord point of the tail mean aerodynamic chord due to tab deflection

For the subject airplane where the tab was geared to the elevator in the ratio of $\frac{\delta_{tab}}{\delta_e} = 1.5$ and was also used as a trim tab, the above equation (4.14.1-3), with dynamic-pressure ratio included, can be modified to

$$C_{hh(f)} = \left\{ \left[\bar{C}_{Lh(f)} \right]_{(\delta_{tab})_0=0} + C_{L\delta_{tab}}(\delta_{tab})_0 \right\} \frac{(x_{hinge} - x_{\bar{c}}/4)h}{\bar{c}_h} + C'_{m\delta_{tab}} \left[\left(\frac{\delta_{tab}}{\delta_e} \right) \delta_e + (\delta_{tab})_0 \right] \frac{\bar{q}_h}{\bar{q}_\infty} \quad (6.4.2-1)$$

where

$(\delta_{tab})_0$ is the trim setting of the tab when $\delta_e = 0^\circ$

$\left(\frac{\delta_{tab}}{\delta_e} \right)$ is the tab-elevator gearing ratio

$(x_{\text{hinge}} - x_{\bar{c}/4})_h$ is the distance between the quarter chord of the horizontal-tail mean aerodynamic chord and the hinge line, obtained from table 3.2-2 or table 4.14.1-2(a)

\bar{c}_h is the horizontal-tail mean aerodynamic chord, obtained from table 3.2-1

$\left(\frac{\bar{q}_h}{\bar{q}_\infty}\right)$ is the dynamic-pressure ratio at the horizontal tail, obtained from figure 5.1.2-5

$C_{L\delta_{\text{tab}}}$ is the lift effectiveness of the tab, based on horizontal-tail area, S_h , obtained from equation (4.13.1-2) or table 4.13.1-1(c)

$C'_{m\delta_{\text{tab}}}$ is the pitching-moment effectiveness of the tab about the quarter chord of the tail mean aerodynamic chord, based on tail area, obtained from table 4.14.1-3, column 14, as an average for $\delta_{\text{tab}} = 6^\circ, -7.5^\circ, -15^\circ$

$$C'_{m\delta_{\text{tab}}} = \frac{(\Delta C'_m)\delta_{\text{tab}}}{\delta_{\text{tab}}} \quad (6.4.2-2)$$

$(\bar{C}_{Lh(f)})_{(\delta_{\text{tab}})_0=0}$ is the net lift coefficient of the horizontal tail in the presence of the body as a function of α_h , δ_e , and δ_{tab} with the trim setting of the tab equal to 0 when $\delta_e = 0^\circ$, referenced to tail area, S_h , and dynamic-pressure ratio of 1.0, obtained from figure 4.14.1-1 for tab-elevator ratio of 1.5

The angle of attack of the horizontal tail, required to determine $(\bar{C}_{Lh(f)})_{(\delta_{\text{tab}})_0=0}$, is obtained from

$$\alpha_h = \alpha_{\text{trim}} - \epsilon_h + (\Delta\alpha_h)_q \quad (6.4.2-3)$$

where

α_{trim} is the airplane angle of attack in the turn for the load factor, a_n , considered, obtained from table 6.4.1-1(b)

ϵ_h is the downwash at the horizontal tail, obtained from figure 5.1.2-5 as a function of α_{trim} and total T'_c

$(\Delta\alpha_h)_q$ is the increment of angle of attack at the tail due to pitching rate, q , obtained from

$$(\Delta \alpha_h)_q = 57.3 \frac{q l_h}{V} \quad (6.4.2-4)$$

where

l_h is the distance from the center of gravity to the quarter chord of the tail mean aerodynamic chord obtained from figure 3.2-2

The procedure for obtaining the predicted variation of hinge moment and stick force as a function of load factor in a windup turn was applied to the subject airplane. The summary calculations are presented in table 6.4.2-1. The predicted hinge moments and stick forces are compared with flight data in figure 6.4.2-1. Also shown in the figure are the predicted variations based on wind-tunnel data.

6.4.3 Symbols

a_n	load factor, g units
$C_{hh(f)}$	hinge-moment coefficient of the horizontal tail with fuselage effects on the tail included, referenced to the area and mean aerodynamic chord of the tail
C_L	lift coefficient
$(\Delta C_{L_{tab}})_o$	increment of airplane lift coefficient due to the trim setting of the tab when $\delta_e = 0^\circ$, equal to $C_{L_{\delta_{tab}}}(\delta_{tab})_o \left(\frac{S_h}{S_w} \right) \left(\frac{\bar{q}_h}{\bar{q}_\infty} \right)$, referenced to the wing area
$\bar{C}_{L_h(f)}$	net lift coefficient of the tail due to α_h , δ_e , and δ_{tab} , with fuselage effects included, referenced to the tail area
$(\bar{C}_{L_h(f)})_{(\delta_{tab})_o=0}$	net lift coefficient, $\bar{C}_{L_h(f)}$, with trim setting of the tab equal to zero when $\delta_e = 0^\circ$
C_{L_α}	airplane lift-curve slope, referenced to the wing area, per deg
C_{L_q}	$\frac{\partial C_L}{\partial \frac{q \bar{c}_w}{2V}}$, referenced to the wing area, per rad
$C_{L_{\delta_e}}$	elevator effectiveness, $\frac{\partial C_L}{\partial \delta_e}$, with the elevator tab geared to move with the elevator, referenced to the wing area, dynamic-pressure ratio equal to 1.0, per deg
$C_{L_{\delta_{tab}}}$	tab effectiveness, $\frac{\partial C_L}{\partial \delta_{tab}}$, with the dynamic-pressure ratio equal to 1.0, referenced to the horizontal-tail area, per deg

C_m	pitching-moment coefficient
C_{m_0}	airplane pitching-moment coefficient at zero lift with the elevator and tab at zero setting, referenced to the area and mean aerodynamic chord of the wing
$(\Delta C'_m)_{\delta_{tab}}$	increment of pitching-moment coefficient about the quarter-chord point of the tail mean aerodynamic chord due to the tab deflection, referenced to the area and the mean aerodynamic chord of the horizontal tail
$(\Delta C_{m_{tab}})_0$	increment of the airplane pitching-moment coefficient due to the trim setting of the tab when $\delta_e = 0^\circ$, referenced to the area and mean aerodynamic chord of the wing
C_{m_α}	airplane static pitch-stability parameter, $\frac{\partial C_m}{\partial \alpha_b}$, referenced to the area and mean aerodynamic chord of the wing, per deg
C_{m_q}	airplane pitch-damping parameter, $\frac{\partial C_m}{\partial \frac{q\bar{c}_w}{2V}}$, referenced to the area and mean aerodynamic chord of the wing, per rad
$C_{m_{\bar{\delta}_e}}$	airplane pitch-control effectiveness, $\frac{\partial C_m}{\partial \bar{\delta}_e}$, with the elevator tab geared to move with the elevator, referenced to the area and mean aerodynamic chord of the wing, per deg
$C'_{m_{\bar{\delta}_{tab}}}$	pitching-moment effectiveness of the tab about the quarter-chord point of the tail mean aerodynamic chord, referenced to the area and mean aerodynamic chord of the horizontal tail, per deg
\bar{c}_h	tail mean aerodynamic chord, in.
\bar{c}_w	wing mean aerodynamic chord, ft
F_{stick}	stick force, lb
g	acceleration of gravity, ft/sec ²
h_p	pressure altitude, ft
l_h	distance from the center of gravity to the quarter chord of the tail mean aerodynamic chord, ft
q	pitching rate, rad/sec
\dot{q}	pitching acceleration, rad/sec ²
\bar{q}_h	dynamic pressure at the horizontal tail, lb/sq ft

\bar{q}_∞	free-stream dynamic pressure, lb/sq ft
S_h, S_w	area of the horizontal tail and wing, respectively, sq ft
T'_c	thrust coefficient
t	time, sec
V	airspeed, ft/sec
W	airplane weight, lb
$(x_{\text{hinge}} - x_{\bar{c}}/4)_h$	distance, on the tail mean aerodynamic chord, from the quarter-chord point to the hinge line, in.
α_b	airplane angle of attack relative to the X-body axis, deg
α_h	angle of attack of the horizontal tail (with $\delta_e = 0^\circ$), deg
$(\Delta\alpha_h)_q$	increment of α_h due to the pitching rate, deg
α_o	airplane angle of attack at zero lift (with $\delta_e = 0^\circ$), deg
α_{trim}	α_b at constant load factor, a_n , in the turn, deg
$\dot{\alpha} = \frac{\partial\alpha_b}{\partial t}$	
δ_e	elevator deflection, deg
$\delta_{e\text{trim}}$	elevator position for α_{trim} , deg
δ_{tab}	tab deflection, deg
$(\delta_{\text{tab}})_o$	tab setting when $\delta_e = 0^\circ$, deg
ϵ_h	downwash angle at the horizontal tail, deg
$(\Delta\epsilon_h)_{\text{power}}$	increment of ϵ_h due to power, deg

Flight Research Center,
National Aeronautics and Space Administration,
Edwards, Calif., July 30, 1971.

TABLE 6.4, 1-1
WINDUP-TURN VARIATION OF α_{trim} AND $\delta_{e_{trim}}$ WITH LOAD FACTOR

(a) Pertinent parameters

Symbol	Description	Reference	Magnitude
----- h_p	Airplane center of gravity Pressure altitude, ft	Flight data Flight data	$0.12 \bar{c}_w$ 6000
V \bar{q}_∞ W a_n	True airspeed, ft/sec Free-stream dynamic-pressure ratio, lb/sq ft Airplane weight, lb Load factor, g units	Flight data Flight data Flight data Flight data	Flight data Flight data Flight data Flight data
T'_c	Airplane thrust coefficient, function of $C_L - C_{Lq} \frac{q\bar{c}_w}{2V} - (\Delta C_{L_{tab}})_0$	Figure 5.3-5	See "Description"
S_w \bar{c}_w	Reference wing area, sq ft Wing mean aerodynamic chord, ft	Table 3.2-1 Table 3.2-1	178 4.96
$C_{L\delta_{tab}}$ $(\delta_{tab})_0$ l_h \bar{q}_h \bar{q}_∞	Lift effectiveness of tab, $\frac{\partial C_L}{\partial \delta_{tab}}$, based on horizontal-tail area, $S_h = 32.5$ sq ft Trim setting of tab when $\delta_e = 0^\circ$, deg Distance from the center of gravity to the quarter chord of the tail mean aerodynamic chord, ft Dynamic-pressure ratio at horizontal tail	Table 4.13.1-1(c) Flight data Figure 3.2-2 Figure 5.1.2-5	0.0279 per deg 2.0 14.40 $f(T'_c, \alpha_{trim})$
$(\Delta C_{L_{tab}})_0$ $(\Delta C_{m_{tab}})_0$	$C_{L\delta_{tab}} (\delta_{tab})_0 \frac{S_h}{S_w} \left(\frac{\bar{q}_h}{\bar{q}_\infty} \right)$, referenced to S_w Airplane pitching-moment increment due to $(\delta_{tab})_0 = -(\Delta C_{L_{tab}})_0 \frac{l_h}{\bar{c}_w}$	Equations (6.4-1) and (6.4.1-1) Equations (6.4-1) and (6.4.1-1)	$0.0102 \left(\frac{\bar{q}_h}{\bar{q}_\infty} \right)$ $-.0296 \left(\frac{\bar{q}_h}{\bar{q}_\infty} \right)$
C_L	$\frac{a_n W}{\bar{q}_\infty S_w}$	Equation (6.4-3)	$\frac{a_n W}{178 \bar{q}_\infty}$
C_{Lq} C_{mq}	$\frac{\partial C_L}{\partial \frac{q\bar{c}_w}{2V}}$, per rad $\frac{\partial C_m}{\partial \frac{q\bar{c}_w}{2V}}$, per rad	Figure 6.1.1-1 Figure 6.2.1-1	$f(\alpha_{trim}, T'_c)$ $f(\alpha_{trim}, T'_c)$
q	$\frac{g}{V} (a_n - \frac{1}{a_n})$, rad/sec	Equation (6.4-4)	$f(V, a_n)$
α_{trim} , $\delta_{e_{trim}}$	Obtained from C_L versus α_b plot (fig. 5.1.3-1) and C_m versus C_L plot (fig. 5.2-4) rotated to flight center of gravity using equivalent net static lift $(C_L - C_{Lq} \frac{q\bar{c}_w}{2V} - (\Delta C_{L_{tab}})_0)$ on the lift curve and $(-C_{mq} \frac{q\bar{c}_w}{2V} - (\Delta C_{m_{tab}})_0)$ on the C_m versus C_L plot, as per sketch in section 6.4.1	-----	-----

TABLE 6.4.1-1 (Concluded)

(b) α_{trim} and δ_{etrim} using calculated characteristics with $(\Delta c_h)_{power}$ reduced 40 percent

First approximation												
①	②	③	④	⑤	⑥	⑦	⑧	⑨	⑩	⑪	⑫	⑬
Flight data				Equation (6.4-4)	-----	Equation (6.4-3)	Figure 5.3-5	Figures 5.1.3-1 and 5.2-4	Figure 6.1.1-1	Figure 6.2.1-1	Figure 5.1.2-5	
a_n , g, units	V , ft/sec	\bar{q}_∞ , lb/sq ft	W , lb	$q = \frac{1}{2} \rho V^2$, rad/sec	$\frac{q \bar{c}_w}{2V} = \frac{1}{178} \frac{W}{V}$	$C_L = \frac{1}{178} \frac{W}{V}$	$T'_c = f(\frac{7}{1})$, $C_D = 0$	α'_{trim} , $f(\frac{7}{1})$, deg	δ'_{etrim} , $f(\frac{7}{1})$, deg	C'_{Lq} , $f(\frac{8}{1})$, rad	C'_{mq} , $f(\frac{8}{1})$, rad	$\frac{\bar{q}_h}{\bar{q}_\infty}$, $f(\frac{8}{1})$
1.00	216	46.5	3383	0	0	0.409	0.038	1.34	0.457	8.684	-14.072	1.029
1.25	211	44.4	3380	.0687	.000807	.535	.044	2.84	.188	8.708	-14.132	1.037
1.50	213	45.5	3376	.1260	.001467	.625	.051	3.88	-.011	8.734	-14.216	1.045
1.75	220	48.3	3374	.1725	.001945	.687	.057	4.58	-.122	8.756	-14.277	1.051
2.00	226	51.2	3372	.2137	.002345	.740	.063	5.18	-.342	8.778	-14.333	1.057

First iteration									
⑭	⑮	⑯	⑰	⑱	⑲	⑳	㉑	㉒	㉓
Equation (6.4.1-1) and table 6.4.1-1(a)	Figure 5.3-5	Equation (6.4.1-2) and table 6.4.1-1(a)	Figures 5.1.3-1 and 5.2-4	Figure 6.1.1-1	Figure 6.2.1-1	Figure 5.1.2-5	Figure 6.1.1-1	Figure 6.2.1-1	Figure 5.1.2-5
$C_L - C_{Lq} \frac{q \bar{c}_w}{2V} - (\Delta C_{Ltab})_0$ ⑦ - ⑭⑥ - 0.0102 ⑬	$T'_c = f(\frac{14}{1})$	$\frac{q \bar{c}_w}{2V} - (\Delta C_{Ltab})_0 =$ ⑭⑥ + 0.0296 ⑬	α'_{trim} , $f(\frac{14}{1})$, deg	δ'_{etrim} , $f(\frac{14}{1})$, deg	C'_{Lq} , $f(\frac{15}{1})$, rad	C'_{mq} , $f(\frac{15}{1})$, rad	$\frac{\bar{q}_h}{\bar{q}_\infty}$, $f(\frac{15}{1})$	$\frac{\bar{q}_h}{\bar{q}_\infty}$, $f(\frac{15}{1})$	$\frac{\bar{q}_h}{\bar{q}_\infty}$, $f(\frac{15}{1})$
0.398 .517 .602 .659 .709	0.036 .043 .049 .054 .058	0.0307 .0421 .0518 .0589 .0649	1.38 2.84 3.88 4.56 5.16	-0.23 -.84 -1.30 -1.61 -1.89	8.679 8.706 8.728 8.747 8.762	-14.06 -14.12 -14.20 -14.25 -14.29	1.023 1.029 1.034 1.038 1.041	1.023 1.029 1.034 1.038 1.041	1.023 1.029 1.034 1.038 1.041

Second iteration									
㉔	㉕	㉖	㉗	㉘	㉙	㉚	㉛	㉜	㉝
-----	-----	-----	Figure 5.1.3-1 and 5.2-4	Figure 6.1.1-1	Figure 6.2.1-1	Figure 5.1.2-5	Figure 6.1.1-1	Figure 6.2.1-1	Figure 5.1.2-5
$C_L - C_{Lq} \frac{q \bar{c}_w}{2V} - (\Delta C_{Ltab})_0$ ⑦ - ⑭⑥ - 0.0102 ㉑	$T'_c = f(\frac{22}{1})$	$\frac{q \bar{c}_w}{2V} - (\Delta C_{Ltab})_0 =$ ㉑⑥ + 0.0296 ㉑	α'_{trim} , $f(\frac{22}{1})$, deg	δ'_{etrim} , $f(\frac{22}{1})$, deg	C'_{Lq} , $f(\frac{23}{1})$, rad	C'_{mq} , $f(\frac{23}{1})$, rad	$\frac{\bar{q}_h}{\bar{q}_\infty}$, $f(\frac{23}{1})$	$\frac{\bar{q}_h}{\bar{q}_\infty}$, $f(\frac{23}{1})$	$\frac{\bar{q}_h}{\bar{q}_\infty}$, $f(\frac{23}{1})$
0.399 .517 .602 .659 .709	0.036 .043 .049 .054 .058	0.0303 .0419 .0514 .0584 .0643	1.38 2.84 3.88 4.56 5.16	-0.23 -.84 -1.30 -1.61 -1.89	8.679 8.706 8.728 8.747 8.762	-14.06 -14.12 -14.20 -14.25 -14.29	1.023 1.029 1.034 1.038 1.041	1.023 1.029 1.034 1.038 1.041	1.023 1.029 1.034 1.038 1.041

TABLE 6.4.2-1
VARIATION OF HINGE MOMENTS AND STICK FORCES WITH LOAD FACTOR IN WINDUP TURN

(a) Pertinent parameters

Symbol	Description	Reference	Magnitude
----- h_p	Airplane center of gravity Pressure altitude, ft	Flight data Flight data	$0.12\bar{c}_w$ 6000
$\frac{a_n}{V}$ $\frac{\bar{q}}{\bar{q}_\infty}$	Load factor, g units Airspeed, ft/sec Free-stream dynamic pressure, ft/sec	Selected flight data, table 6.4.1-1(b), columns 1, 2, and 3	
$\frac{q}{T_c}$ α_{trim} $\delta_{e,trim}$ $\frac{\bar{q}_h}{\bar{q}_\infty}$	Pitch rate, rad/sec Airplane thrust coefficient Airplane angle of attack in turn, deg Elevator angle in turn, deg Dynamic-pressure ratio at tail	Column 5 Column 23 Column 25 Column 26 Column 29	Table 6.4.1-1(b)
S_h \bar{c}_h	Horizontal-tail area, sq ft Horizontal-tail mean aerodynamic chord, in.	Table 3.2-1 Table 3.2-1	32.5 32.45
$(\delta_{tab})_0$ $\frac{\delta_{tab}}{\delta_e}$	Trim setting of tab when $\delta_e = 0^\circ$, deg Tab-elevator gearing ratio	Flight data Section 3	2.0 1.5
$(x_{hinge} - \bar{x}_c/4)_h$ l_h	Distance between hinge line and tail quarter chord, in. Distance from the center of gravity to the tail quarter chord, ft	Table 4.14.1-2(a) Table 6.4.1-1(a)	1.17 14.40
α_h ϵ_h	$\alpha_{trim} - \epsilon_h + 57.3 \frac{q l_h}{V}$, deg Downwash at horizontal tail, deg	Equation (6.4.2-3) Figure 5.1.2-5	Variable $f(\alpha_{trim}, T'_c)$
$(\bar{C}_{Lh(f)})_{(\delta_{tab})_0=0}$ $C_{L\delta_{tab}}$	Net lift coefficient of horizontal tail only in presence of body as function of α_h , δ_e , and $\delta_{tab} = \left(\frac{\delta_{tab}}{\delta_e}\right)\delta_e = 1.5\delta_e$, trim tab setting = 0, referenced to $S_h = 32.5$ sq ft Lift effectiveness of tab, $\frac{\partial C_L}{\partial \delta_{tab}}$, referenced to $S_h = 32.5$ sq ft	Figure 4.14.1-1 Table 6.4.1-1(a)	$f(\alpha_h, \delta_e)$ 0.0279 per deg
$C'_{m\delta_{tab}}$	Pitching effectiveness of tab about quarter chord of tail mean aerodynamic chord, $\frac{(\Delta C'_m)\delta_{tab}}{\delta_{tab}}$, per deg	Table 4.14.1-3, column 14 Table 5.4-1, column 14	For $T'_c = 0$: $C'_{m\delta_{tab}} = -0.00908$ average value for $\delta_{tab} = 6.0^\circ$ to -7.5° For $T'_c = 0.20$: $C'_{m\delta_{tab}} = -0.0104$ average value for $\delta_{tab} = 6.0^\circ$ to -7.5°
Summary: From equation (6.4.2-1) and above parameters, $C_{hh(f)} = \left\{ \left[(\bar{C}_{Lh(f)})_{(\delta_{tab})_0=0} + 0.0558 \right] 0.0361 + C_{m\delta_{tab}} (1.5\delta_e + 2) \right\} \frac{\bar{q}_h}{\bar{q}_\infty}$			

TABLE 6.4.2-1 (Concluded)

$$(b) \quad C_{h(f)} = \left\{ \left[\frac{C_{Lh(f)}}{q_\infty} + 0.0558 \right] 0.0361 + C' m \delta_{tab} (1.5 \delta_e + 2) \right\} \frac{q_h}{q_\infty}$$

$$F_{stick} = 40 C_{h(f)} \bar{q}_\infty$$

①	②	③	④	⑤	⑥	⑦	⑧	⑨	⑩	⑪
Flight data, table 6.4.1-1(b)										
Column 1	Column 2	Column 3	Column 23	Column 5	Column 25	Column 26	Column 29	Figure	Equation	Equation
a_h , g units	V , ft/sec	\bar{q}_∞ , lb/sq ft	T'_c	q , rad/sec	α_{trim} , deg	$\delta_{e(trim)}$, deg	$\frac{q_h}{q_\infty}$	ϵ_h , f (4)(6)	$(\Delta \alpha)_q = 57.3 \frac{q L_h}{V}$ $= 825.1 \frac{(5)}{(2)}$	$\alpha_h =$ $(6) - (9) + (10)$, deg
1.00	216	46.5	0.036	0	1.38	-0.23	1.023	2.79	0	-1.41
1.25	211	44.4	.043	.0687	2.84	-.84	1.029	3.60	.2686	-.49
1.50	213	45.5	.049	.1260	3.88	-1.30	1.034	4.15	.4881	.22
1.75	220	48.3	.054	.1725	4.56	-1.61	1.038	4.54	.6470	.67
2.00	226	51.2	.058	.2137	5.16	-1.89	1.041	4.88	.7802	1.06

⑫	⑬	⑭	⑮	⑯	⑰	⑱
Figure 4.14.1-1						
Interpolated from table 6.4.2-1(a)						
$(C_{Lh(f)}) (\delta_{tab})_0 = 0$ f (7), (1)	0.0361 ((12) + 0.0558)	$C' m \delta_{tab}$	$\delta_{tab} = (1.5 \delta_e + 2)$ $= 1.5 (7) + (2)$	$C' m \delta_{tab} \delta_{tab} =$ (14) (15)	$C_{h(f)} = (8) / (13) + (19)$	Equation (4.14.1-20) $F_{stick} = 40 (17) (3)$
-0.1144	-0.002115	-0.00932	1.655	-0.01542	-0.01754	-32.6
-.1162	-.002180	-.00936	.74	-.00693	-.00937	-16.6
-.1163	-.002184	-.00940	.05	-.00047	-.00274	-5.0
-.1186	-.002267	-.00944	.415	.00392	.00172	3.3
-.1194	-.002296	-.00946	-.835	.00790	.00583	11.9

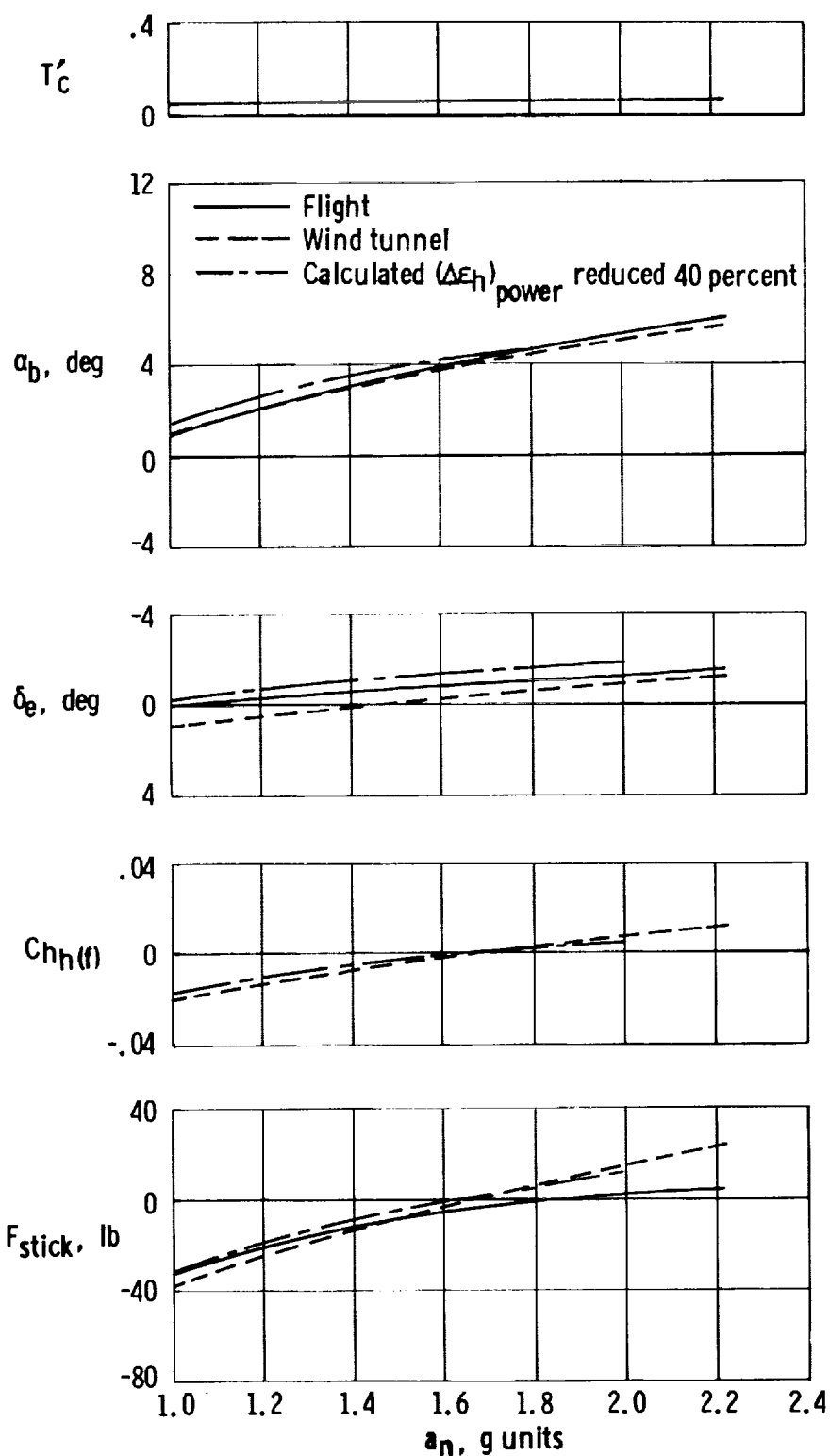


Figure 6.4.2-1. Comparison of calculated hinge-moment and stick-force characteristics in a windup turn with those obtained from wind-tunnel and flight data as a function of load factor. Altitude = 6000 ft; center of gravity = $0.12 \bar{c}_w$; $V = 220$ ft/sec.

REFERENCES

1. Anon.: USAF Stability and Control Datcom. Air Force Flight Dynamics Lab., Wright-Patterson Air Force Base, Oct. 1960 (rev. Aug. 1968).
2. Fink, Marvin P.; and Freeman, Delma C., Jr.: Full-Scale Wind-Tunnel Investigation of Static Longitudinal and Lateral Characteristics of a Light Twin-Engine Airplane. NASA TN D-4983, 1969.
3. Abbott, Ira H.; von Doenhoff, Albert E.; and Stivers, Louis S., Jr.: Summary of Airfoil Data. NACA Rep. 824, 1945.
4. Loftin, Lawrence K., Jr.; and Smith, Hamilton A.: Aerodynamic Characteristics of 15 NACA Airfoil Sections at Seven Reynolds Numbers From 0.7×10^6 to 9.0×10^6 . NACA TN 1945, 1949.
5. Stack, John; and von Doenhoff, Albert E.: Tests of 16 Related Airfoils at High Speeds. NACA Rep. 492, 1934.
6. Gault, Donald E.: A Correlation of Low-Speed, Airfoil-Section Stalling Characteristics With Reynolds Number and Airfoil Geometry. NACA TN 3963, 1957.
7. DeYoung, John; and Harper, Charles W.: Theoretical Symmetric Span Loading at Subsonic Speeds for Wings Having Arbitrary Plan Form. NACA Rep. 921, 1948.
8. Lowry, John G.; and Polhamus, Edward C.: A Method for Predicting Lift Increments Due to Flap Deflection at Low Angles of Attack in Incompressible Flow. NACA TN 3911, 1957.
9. Silverstein, Abe; and Katzoff, S.: Aerodynamic Characteristics of Horizontal Tail Surfaces. NACA Rep. 688, 1940.
10. Hopkins, Edward J.: A Semiempirical Method for Calculating the Pitching Moment of Bodies of Revolution at Low Mach Numbers. NACA RM A51C14, 1951.
11. Pitts, William C.; Nielsen, Jack N.; and Kaattari, George E.: Lift and Center of Pressure of Wing-Body-Tail Combinations at Subsonic, Transonic, and Supersonic Speeds. NACA Rep. 1307, 1957.
12. Etkin, Bernard: Dynamics of flight. John Wiley & Sons, Inc., c.1959, p. 479.
13. Multhopp, H.: Aerodynamics of the Fuselage. NACA TM 1036, 1942.
14. Silverstein, Abe; and Katzoff, S.: Design Charts for Predicting Downwash Angles and Wake Characteristics Behind Plain and Flapped Wings. NACA Rep. 648, 1939.
15. DeYoung, John; and Barling, Walter H., Jr.: Prediction of Downwash Behind Swept-Wing Airplanes at Subsonic Speed. NACA TN 3346, 1955.

16. Decker, James L.: Prediction of Downwash at Various Angles of Attack for Arbitrary Tail Locations. *Aeron. Eng. Rev.*, vol. 15, no. 8, Aug. 1956, pp. 22-27, 61.
17. Spreiter, John R.; and Sacks, Alvin H.: The Rolling Up of the Trailing Vortex Sheet and Its Effect on the Downwash Behind Wings. *J. Aeron. Sci.*, vol. 18, no. 1, Jan. 1951, pp. 21-32, 72.
18. Silverstein, Abe; Katzoff, S.; and Bullivant, W. Kenneth: Downwash and Wake Behind Plain and Flapped Airfoils. NACA Rep. 651, 1939.
19. Anon.: USAF Stability and Control Handbook. Wright Air Dev. Div., Flight Control Lab., Aug. 1956.
20. Hoggard, H. Page, Jr.; and Hagerman, John R.: Downwash and Wake Behind Untapered Wings of Various Aspect Ratios and Angles of Sweep. NACA TN 1703, 1948.
21. Lange, Roy H.; and Fink, Marvin P.: Studies of the Flow Field Behind a Large Scale 47.5° Sweptback Wing Having Circular-Arc Airfoil Sections and Equipped with Drooped-Nose and Plain Flaps. NACA RM L51L12, 1952.
22. Johnson, Ben H., Jr.; and Rollins, Frances W.: Investigation of a Thin Wing of Aspect Ratio 4 in the Ames 12-Foot Pressure Wind Tunnel. V - Static Longitudinal Stability and Control Throughout the Subsonic Speed Range of a Semispan Model of a Supersonic Airplane. NACA RM A9I01, 1949.
23. Foster, Gerald V.; and Griner, Roland F.: Low-Speed Longitudinal and Wake Airflow Characteristics at a Reynolds Number of 5.5×10^6 of a Circular-Arc 52° Sweptback Wing With a Fuselage and a Horizontal Tail at Various Vertical Positions. NACA RM L51C30, 1951.
24. Bandettini, Angelo; and Selan, Ralph: The Effects of Horizontal-Tail Height and a Partial-Span Leading-Edge Extension on the Static Longitudinal Stability of a Wing-Fuselage-Tail Combination Having a Sweptback Wing. NACA RM A53J07, 1954.
25. Furlong, G. Chester; and Bollech, Thomas V.: Downwash, Sidewash, and Wake Surveys Behind a 42° Sweptback Wing at a Reynolds Number of 6.8×10^6 With and Without a Simulated Ground. NACA RM L8G22, 1948.
26. Woods, Robert L.; and Spooner, Stanley H.: Effects of High-Lift and Stall-Control Devices, Fuselage, and Horizontal Tail on a Wing Swept Back 42° at the Leading Edge and Having Symmetrical Circular-Arc Airfoil Sections at a Reynolds Number of 6.9×10^6 . NACA RM L9B11, 1949.
27. Hoerner, Sighard F.: Fluid-Dynamic Drag. Pub. by the author (148 Busted Dr., Midland Park, N. J.), 1965.
28. Benepe, David B.; Kouri, Bobby G.; and Webb, J. Bert: Aerodynamic Characteristics of Non-Straight-Taper Wings. Tech. Rep. AFFDL-TR-66-73, Air Force Flight Dynamics Laboratory, Wright-Patterson Air Force Base, Oct. 1966.

29. Frost, Richard C.; and Rutherford, Robbie: Subsonic Wing Span Efficiency. AIAA J., vol. 1, no. 4, April 1963, pp. 931-933.
30. Furlong, G. Chester; and McHugh, James G.: A Summary and Analysis of the Low-Speed Longitudinal Characteristics of Swept Wings at High Reynolds Number. NACA Rep. 1339, 1957.
31. James, Harry A.; and Hunton, Lynn W.: Estimation of Incremental Pitching Moments Due to Trailing-Edge Flaps on Swept and Triangular Wings. NACA TN 4040, 1957.
32. DeYoung, John: Theoretical Symmetric Span Loading Due to Flap Deflection for Wings of Arbitrary Plan Form at Subsonic Speeds. NACA Rep. 1071, 1952.
33. Ribner, Herbert S.: Notes on the Propeller and Slipstream in Relation to Stability. NACA WR L-25, 1944. (Formerly NACA ARR L4I12a.)
34. Weil, Joseph; and Sleeman, William C., Jr.: Prediction of the Effects of Propeller Operation on the Static Longitudinal Stability of Single-Engine Tractor Monoplanes With Flaps Retracted. NACA Rep. 941, 1949.
35. Pass, H. R.: Wind-Tunnel Study of the Effects of Propeller Operation and Flap Deflection on the Pitching Moments and Elevator Hinge Moments of a Single-Engine Pursuit-Type Airplane. NACA WR L-411, 1942. (Formerly NACA ARR.)
36. Schuldenfrei, Marvin: Some Notes on the Determination of the Stick-Fixed Neutral Point From Wind-Tunnel Data. NACA WR L-344, 1943. (Formerly NACA RB 3I20.)
37. Wolowicz, Chester H.: Considerations in the Determination of Stability and Control Derivatives and Dynamic Characteristics From Flight Data. AGARD Rep. 549-Part 1, 1966.
38. Neal, T. Peter: Frequency and Damping from Time Histories: Maximum-Slope Method. J. Aircraft, vol. 4, no. 1, Jan.-Feb., 1967, p. 76.
39. Toll, Thomas A.; and Queijo, M. J.: Approximate Relations and Charts for Low-Speed Stability Derivatives of Swept Wings. NACA TN 1581, 1948.
40. Sacks, Alvin H.: Aerodynamic Forces, Moments, and Stability Derivatives for Slender Bodies of General Cross Section. NACA TN 3283, 1954.
41. MacLachlan, Robert; and Fisher, Lewis R.: Wind-Tunnel Investigation at Low Speeds of the Pitching Derivatives of Untapered Swept Wings. NACA RM L8G19, 1948.
42. Fisher, Lewis R.: Approximate Corrections for the Effects of Compressibility on the Subsonic Stability Derivatives of Swept Wings. NACA TN 1854, 1949.
43. Seckel, Edward: Stability and Control of Airplanes and Helicopters. Academic Press Inc., c.1964, p. 95.

